Establishing a detailed tephrochronological framework for Japan to aid the synchronisation of palaeoenvironmental records across the Asian/Pacific region

DANIELLE MCLEAN

Jesus College
Research Laboratory for Archaeology & the History of Art
School of Archaeology, University of Oxford



Submitted to the University of Oxford for the degree
Doctor of Philosophy in Archaeological Science
Michaelmas Term 2018

Supervised by
Associate Professor Victoria Smith
& Dr Paul Albert

Establishing a detailed tephrochronological framework for Japan to aid the synchronisation of palaeoenvironmental records across the Asian/Pacific region

Danielle McLean, Jesus College
Submitted to the University of Oxford for the degree *Doctor of Philosophy* in *Archaeological Science*
Michaelmas Term 2018

Abstract

Tephra (volcanic ash) layers have the potential to synchronise palaeoenvironmental archives across regional to hemispheric scales. Highly productive arc regions, like those in East Asia, offer a considerable number of widespread isochrons, but before records can be confidently correlated using these layers, a refined and integrated tephrochronological framework is required. The Lake Suigetsu sequence, obtained from a small tectonic lake in central Honshu, is the most precisely dated sedimentary record for Japan. Here, the sediments are examined for the presence of thin (sub-millimetre in thickness) and 'non-visible' (cryptotephra) layers in order to provide a comprehensive record of East Asian volcanism, and a linchpin site for correlating sequences.

On average, cryptotephra layers are identified four times more frequently than visible markers in the studied sediments of Lake Suigetsu, providing an unprecedented record of ash fall events that reached the densely populated regions of central Honshu. Major and trace element glass geochemistry obtained from these tephra layers is compared to new and published datasets to pinpoint their volcanic source. The cryptotephra were erupted from sources that span the length of Japan, and volcanoes further west, including Ulleungdo (South Korea) and Changbaishan (North Korea/China).

Constrained eruption ages are modelled for the tephra layers identified in the sequence, which can be transferred into other sedimentary records that contain these markers. Cryptotephra identifications show that many eruptions dispersed ash more widely than previously anticipated, and are able to synchronise palaeoclimate records over hemispheric scales. For example, the archive provides the most southerly tephra occurrence of the B-Tm tephra, synchronising this mid-latitude record to the Greenland ice cores. The augmented Lake Suigetsu eruption archive is established as a key node within the tephrostratigraphic framework for Japan, and provides an important resource for volcanological research, with constraints on the frequency, reoccurrence intervals and dispersal of numerous eruption events.

ACKNOWLEDGEMENTS

This research would not have been possible without the support and kindness of many people. I have to thank my supervisors Victoria Smith and Paul Albert for their dedicated involvement and endless encouragement throughout this project.

I am very grateful for the opportunity to build on the work of the Suigetsu Project and the chance to join the SG14 drilling campaign, and for this I thank the generosity and continuous support of Takeshi Nakagawa. I would also like to express my sincere gratitude for the guidance from Takehiko Suzuki and for sharing his expertise so willingly. Even though I have not worked directly with Professor Machida, the impact of their work is obvious through this project. Richard Staff has also been both a great friend and source of advice.

I would like to thank the Japan Society for the Promotion of Science for providing the opportunity to collaborate with Professor Jun-Ichi Kimura, and to everyone at JAMSTEC for their assistance and very kind welcome. I am grateful to NERC and the Oxford Doctoral Training Programme for funding this project and the research possibilities it has provided. Jesus College and the Institute of Archaeology have also offered funding for travel expenses and the opportunity to present this work in the UK and overseas.

I am grateful to Christopher Bronk Ramsey and Karen Fontijn for their insightful suggestions throughout this project, which gave me the incentive to widen this research. I also thank my fellow lab-mates including Steven Crabb, Nora Farber, Rebecca Kearney, Elisabeth Thompson, Patrick Roberts, Rebecca Smith and Maciej Wencel for their friendship and support.

I would also like to thank Simon Blockley for encouraging me to embark on a doctorate degree and for assigning me a tephra paper to read in my first undergraduate tutorial at Royal Holloway University.

Last but not least, I am grateful for the love and support of my family and friends, particularly my parents, Hayley McLean and my Grandma. I thank Spencer Lawes for his endless encouragement, and for celebrating with me on good days, and helping me through the bad. I also thank Andrea, Gary, Chris and Nic for their support and kindness over the course of this project.

TABLE OF CONTENTS

Abstract i
Acknowledgements ii
Table of Contents iii
List of Figures viii
List of Tables xii

CHAPTER 1: Introduction

1.1. Resolving palaeoclimate variability 1
1.2. Tephra as time-stratigraphic markers 3
1.2.1. Principles of tephrochronology 3
1.2.2. Identifying primary ash fall events 4
1.2.3. Geochemical fingerprinting eruption events 6
1.2.4. Absolute eruption ages 7
1.3. Tephrochronological frameworks 8
1.3.1. Building tephrochronological frameworks 8
1.3.2. A tephrochronological framework for Japan 10
1.4. Research aims and objectives 11
1.5. Guide to this thesis 13

CHAPTER 2: Tephrostratigraphy and tephrochronology in Japan

Overview 17
2.1. Tephra dispersal in and around Japan 18
2.1.1. Key sources of ash dispersal 18
2.1.2. Key tephra archives in East Asia 22
2.2. Geochemically discriminating tephra 25
2.3. Lake Suigetsu, Honshu Island 29
2.3.1. Geological background 29
2.3.2. SG93, SG06 and SG14 coring campaigns 31
2.3.3. Tephra preserved in the Suigetsu cores 35
2.4. Summary 37

CHAPTER 3: Identification of the Changbaishan 'Millennium' (B-Tm) eruption deposit in the Lake Suigetsu (SG06) sedimentary archive, Japan

Author List and Highlights 39
Abstract 40
3.1. Introduction 41
3.2. Background 42
3.2.1. The B-Tm tephra 42
3.2.2. The Lake Suigetsu (SG06) archive 44
3.3. Materials and Methods 45
3.3.1. Sampling and laboratory procedures 45
3.3.2. Compositional analysis 46
3.4. Results and discussion 47
3.4.1. Geochemical results 47
3.4.2. Age-depth modelling 51
3.5. Implications 53
3.5.1. Palaeoenvironmental potential for the B-Tm tephra 53
3.5.2. Future potential 53
Acknowledgements 54

CHAPTER 4: Integrating the Holocene tephrostratigraphy for East Asia using a high-resolution cryptotephra study from Lake Suigetsu (SG14 core), central Japan

Author List and Highlights 55
Abstract 56
4.1. Introduction 57
4.1.1. Tephra dispersal in and around Japan 61
4.1.2. Constraining Holocene climate intervals using tephra layers 62
4.2. Study Site 64
4.2.1. Lake Suigetsu sedimentary record 64
4.2.2. Geology of the Lake Suigetsu catchment 65
4.2.3. Coring campaigns 66
4.2.4. Lake Suigetsu tephrostratigraphy 68
4.3. Materials and Methods 69
4.3.1. Tephra identification 69
4.3.2. Glass geochemical analysis 70

4.3.3. Chronology 71
4.4. Tephrostratigraphy Results 73
4.4.1. Discriminating primary tephra layers 73
4.4.2. Overview of Lake Suigetsu Holocene tephrostratigraphy 75
4.4.3. Zone 3 80
4.4.4. Zone 2 81
4.4.5. Zone 1 82
4.5. Glass geochemistry results 83
4.6. Source of the tephra layers 88
4.6.1. Changbaishan tephra layers (SG14-1058 and SG14-0226) 88
4.6.2. Ulleungdo tephra layers (SG06-1288, SG14-1091, SG14-0803 and SG14-0433) 91
4.6.3. Towada (SG14-0840) and Mashu (SG14-0221) tephra layers 93
4.6.4. Kawagodaira (SG14-0490) and Kozushima (SG14-0239) tephra layers 97
4.6.5. Kikai tephra layers (SG06-0967 and SG14-0704) 99
4.6.6. Tephra layers pending further analysis for correlation 101
4.7. Discussion 102
4.7.1. An integrated tephrostratigraphic framework 102
4.7.2. Resolving the tempo of East Asian volcanism 105
4.7.3. Layers for synchronising palaeoclimate records 107
4.8. Conclusions 108
Acknowledgements 109

CHAPTER 5: An improved eruption chronology for explosive volcanism in East Asia (Aso and Aira) between 50 and 30 ka

Author List and Highlights 110
Abstract 111
5.1. Introduction 112
5.2. Study site 114
5.2.1. Lake Suigetsu 114
5.2.2. Sources of tephra dispersed to Lake Suigetsu 116
5.3. Materials and methods 118
5.3.1. Cryptotephra extraction techniques 118
5.3.2. Major element glass compositions 119

5.3.3. Trace element analysis of the glass shards 120
5.3.4. Chronology of the Lake Suigetsu sediment cores 121
5.4. Results 122
5.4.1. Tephrostratigraphy 122
5.4.2. Geochemical composition 125
5.5. Provenance for Suigetsu cryptotephras between 50 and 30 ka 133
5.5.1. Group 1: Ulleungdo and Changbaishan 137
5.5.2. Group 2: Aso, central Kyushu 139
5.5.3. Group 3: Aira and other sources south of Suigetsu 143
5.5.4. Group 4: Uncorrelated tephra from central and northern Japan 147
5.6. Discussion 148
5.6.1. Tempo and origin of eruptions reaching central Honshu 148
5.6.2. Further insights into pre- (Aira) and post- (Aso) caldera forming activity 150
5.7. Conclusions 152
Acknowledgements 153

CHAPTER 6: Refining the eruptive history of Ulleungdo and Changbaishan volcanoes (East Asia) over the last 86 ka using distal records

Author List and Highlights 154
Abstract 155
6.1. Introduction 156
6.2. Regional setting 159
6.2.1. Ulleungdo Island, South Korea 159
6.2.2. Changbaishan, North Korea/China border 162
6.2.3. Marine and lacustrine tephra archives 165
6.3. Tephra identification and analytical methods 168
6.3.1. Tephra identification in Lake Suigetsu 169
6.3.2. Major and trace element analysis of the glass shards 170
6.4. Results 171
6.4.1. Suigetsu tephrostratigraphy 171
6.4.2. Glass geochemistry 174
6.5. Review of eruption framework 180

6.5.1. Post 86 ka (Aso-4) Ulleungdo eruptions 180
6.5.2. Post 86 ka (Aso-4) Changbaishan eruptions 184
6.5.3. Holocene Ulleungdo eruptions 185
6.5.4. Holocene Changbaishan eruptions 187
6.6. Conclusions 188
Acknowledgements 190

CHAPTER 7: General Discussion
Overview 192
7.1. Establishing a detailed tephrochronological framework for Japan 193
7.1.1. Context and rationale 193
7.1.2. A tephrochronological framework for Japan 194
7.1.3. Key isochrons for palaeoclimate investigations 201
7.1.4. Synchronising records using the AT tephra 209
7.2. Building eruption records for hazard assessments 213
7.2.1. Context and rationale 213
7.2.2. Frequency of ash fall events to central Honshu 214

CHAPTER 8: Conclusions 220

Consolidated List of References 224

Supplementary Material

Appendix A: Supplementary Material for Article 1 255
Appendix B: Supplementary Material for Article 2 263
Appendix C: Supplementary Material for Article 3 291
Appendix D: Supplementary Material for Article 4 328

LIST OF FIGURES

CHAPTER 1: Introduction

1.1. The $\delta^{18}O$ record from the North GRIP ice core. 2

1.2. Schematic illustration of possible shard distribution profiles. 6

1.3. The RESET tephra lattice. 10

CHAPTER 2: Tephrostratigraphy and tephrochronology in Japan

2.1. Volcanoes in Japan, North Korea/China and South Korea known to have been active during the Quaternary. 19

2.2. Key tephra layers that were dispersed across Japan and the surrounding regions during the Late Pleistocene. 21

2.3. Marker tephra beds in southern Kyushu erupted over the last ca. 30 ka and their stratigraphic position to the $\delta^{18}O$ record from the NGRIP ice core. 25

2.4. Major element glass compositions of large magnitude Japanese eruptions over the last ~150 ka. 27

2.5. Trace elements which are useful for discriminating vitreous tephra erupted from different sources along the Japanese arcs. 28

2.6. Location of Lake Suigetsu and coring positions of the SG93, SG06 and SG14 campaigns. 30

2.7. Location the five Mikata lakes ('Mikata-goko') adjacent to the Sea of Japan coast and Wakasa Bay. 30

2.8. The atmospheric circulation around Japan. 32

2.9. Photo of Lake Suigetsu core segment A-22 that contains annually laminated sediments (varves). 32

2.10. Example of using event layers (e.g., clay-rich flood layers) to construct the master SG06 sequence. 34

2.11. The Lake Suigetsu (SG06) visible tephrostratigraphy. 36

CHAPTER 3: Identification of the B-Tm eruption deposit from Changbaishan (North Korea/China border) in the Lake Suigetsu record

3.1. Location of Changbaishan volcano, Lake Suigetsu and other sites that preserve the B-Tm tephra. 43

3.2. Major element glass compositions of the SG06-0226 tephra and the B-Tm type-site locality from Tomakomai Port. 49

3.3. The age-depth model for the upper 5 m of the SG06 core. 52

CHAPTER 4: Integrating the Holocene tephrostratigraphy for East Asia using a high-resolution cryptotephra study from Lake Suigetsu (SG14 core), central Japan

4.1. Volcanoes in Japan, North Korea/China and South Korea known to have been active during the Holocene. 60

4.2. Schematic representation of the end member glass morphologies observed in the Lake Suigetsu sequence. 70

4.3. Criteria used to decipher primary ash fall events within the Lake Suigetsu sedimentary sequence. 76

4.4. Glass shard concentrations in the Holocene sediments of the Lake Suigetsu SG14 core. 77

4.5. Photographs of the typical glass shards preserved in the SG14 Holocene tephra layers. 78

4.6. Major element compositions of the tephra layers within the Holocene sediments of the Lake Suigetsu SG14 core**.** 85

4.7. SiO_2 and K_2O glass compositions of the SG14 tephra layers. 87

4.8. Glass shard major element compositions of tephra layers compared to Changbaishan (B-Tm) and Ulleungdo (U-Oki) glasses. 90

4.9. Glass shard major element compositions of tephra layers compared to proximal glass compositions from Towada and Mashu volcano 95

4.10. Glass shard major element compositions of tephra layers compared to proximal glass compositions from Kawagodaira, Kozushima, Ulleungdo, Aira and Changbaishan. 99

4.11. Summary of the Lake Suigetsu Holocene tephrostratigraphy, and the positioning of isochrons against the Greenland ice core (NGRIP) $\delta^{18}O$ record. 103

4.12. Holocene sections of sedimentary archives situated in eastern China and Japan that can be integrated using the widespread Holocene tephra layers. 104

CHAPTER 5: An improved eruption chronology for explosive volcanism in East Asia (Aso and Aira) between 50 and 30 ka

5.1. Volcanoes in Japan, North Korea/China and South Korea known to have been active during the Quaternary 115

5.2. Glass shard concentrations in the laminated sediments (50 to 30 ka) of the Lake Suigetsu SG14 core. 123

5.3. Major element compositions of the tephra layers preserved between 50 to 30 ka. 129

5.4. Average Primitive Mantle normalised glass compositions of the tephra layers preserved between 50 to 30 ka. 131

5.5. Major and trace element compositions of the SG14 cryptotephra layers (50 to 30 ka) in comparison to those established for major eruptive centres in Japan. 135

5.6. Major element glass compositions of compositional Group 2 (Aso derived tephra layers) in comparison to other proximal deposits. 141

5.7. Summary of the augmented Lake Suigetsu tephrostratigraphy spanning 50 to 30 ka. 149

CHAPTER 6: Refining the eruptive history of Ulleungdo and Changbaishan volcanoes (East Asia) over the last 86 ka using distal records

6.1. Location of Ulleungdo and Changbaishan volcanoes and the sedimentary archives that contain distal ash deposits. 157

6.2. Sedimentological and stratigraphic characteristics of the intra- and extra-caldera outcrops on Ulleungdo Island. 161

6.3. The composite Lake Suigetsu tephrostratigraphy and stratigraphic position of Ulleungdo and Changbaishan tephra layers. 172

6.4. Glass shard concentrations preserved in the SG14 E-35 core and photograph of visible tephra layer SG14-3216. 173

6.5. Glass shard major and trace element compositions of Ulleungdo and Changbaishan preserved in the Lake Suigetsu sediments. 176

6.6. Primitive mantle normalised trace element glass compositions of Ulleungdo and Changbaishan tephra layers in the Lake Suigetsu sequence. 178

6.7. Summary tephrostratigraphy of proximal and distal archives that contain ash erupted from Ulleungdo (blue boxes) and Changbaishan. 181

6.8. Glass shard major and trace element compositions of Ulleungdo and Changbaishan tephra layers preserved in the Lake Suigetsu archive compared to other proximal and distal occurrences. 183

CHAPTER 7: General Discussion

7.1. Tephrostratigraphic framework for Japan constructed for the past 100 ka (i.e., Late Pleistocene and Holocene). 195

7.2. Key sedimentary records used to construct the tephrostratigraphic framework for Japan. 196

7.3. Late Holocene proxy data from East Asia. 205

7.4. Comparison of proxy data showing the 8.2 ka cooling event and positioning of the B-Sg-8 tephra. 207

7.5. Synchronisation of Lake Sihailongwan, Lake Biwa and marine core MD179-3312 using the AT tephra. 211

7.6. Population density map of Japan showing the sources of tephra to Lake Suigetsu, position of nuclear power plants and key international airports. 214

7.7. Summary of the Lake Suigetsu tephrostratigraphy and tephra research presented in this thesis. 216

LIST OF TABLES

CHAPTER 3: Identification of the B-Tm eruption deposit from Changbaishan (North Korea/China border) in the Lake Suigetsu record

3.1. Results of the WDS-EPMA normalised glass compositions of the SG06-0226 tephra layer and the B-Tm distal type-site deposits at Tomakomai Port. 48

CHAPTER 4: Integrating the Holocene tephrostratigraphy for East Asia using a high-resolution cryptotephra study from Lake Suigetsu (SG14 core), central Japan

4.1. Summary table of the Holocene tephras within the Lake Suigetsu SG06 and SG14 sediment cores**.** 79

4.2. Glass compositions (normalised) of the SG14 Holocene tephra layers identified in this study. 84

CHAPTER 5: An improved eruption chronology for explosive volcanism in East Asia (Aso and Aira) between 50 and 30 ka

5.1. Summary of the tephra layers identified the sediments of the Lake Suigetsu (SG14 core) between 50 and 30 ka. 124

5.2. Major and trace element glass compositions of the newly identified ash layers preserved in the SG14 core between 50 and 30 ka 126

CHAPTER 6: Refining the eruptive history of Ulleungdo and Changbaishan volcanoes (East Asia) over the last 86 ka using distal records

6.1. Summary of the Ulleungdo and Changbaishan tephra layers identified in the Lake Suigetsu (SG06 & SG14) sequence. 173

6.2. Average glass compositions of the Ulleungdo and Changbaishan tephra layers in the Lake Suigetsu sequence. 175

CHAPTER 7: General Discussion

7.1. Key isochrons for palaeoenvironmental investigations. 202

CHAPTER 1: INTRODUCTION

1.1. Resolving palaeoclimate variability

The geological record provides insight into the timing and magnitude of past climate variability, and is used to understand more about causal mechanisms, and societal impacts of environmental transitions. High-resolution archives (e.g., ice cores, marine and lake sediments) around the globe indicate that the Late Quaternary was a period of climatic instability, and was punctuated by a number of abrupt, high-amplitude cooling and warming episodes that occurred within several decades (i.e., within a human life-span) (Figure 1.1; Wang et al., 2001; Steffensen et al., 2008; Rasmussen et al., 2014). A key research aim for the palaeoclimate community is to determine how these episodes were expressed around the globe (e.g., assessing potential leads and lags in the climate system), and ultimately climate drivers and modifiers (e.g., Björck et al., 1998; Walker et al., 1999; Charman et al., 2009; Blockley et al., 2014; Lowe et al., 2015).

The annually dated isotopic signal recorded in the Greenland ice cores indicates that at least twenty-five significant warming and cooling episodes occurred during the Last Glacial cycle alone (ca. 100 – 11 ka; NGRIP members, 2004; Figure 1.1.). These are widely referred to as Dansgaard-Oeschger (D-O) events, and are characterised by an abrupt warm phase followed by gradual cooling, and are often reflected in proxy records by a distinctive saw-tooth pattern (Dansgaard et al., 1993; Alley et al., 1993; NGRIP members, 2004;

Steffensen et al., 2008; Rasmussen et al., 2014). There are also several distinct severe cold periods, which are marked by layers of ice-rafted debris in the North Atlantic marine sediments (Hemming, 2004; Andersen et al., 2004), and are referred to as Heinrich (H) events (Figure 1.1; Heinrich, 1988).

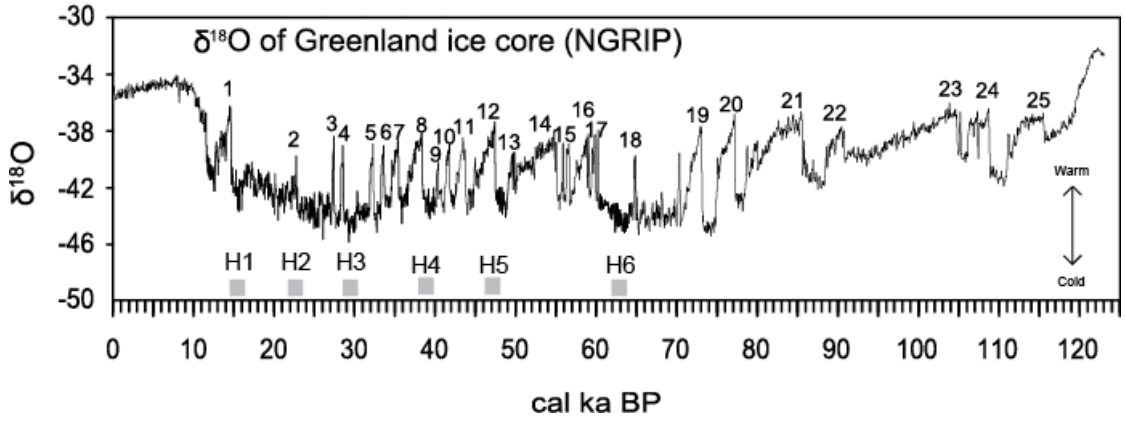


Figure 1.1. The $\delta^{18}O$ record from the North GRIP ice core, which shows rapid cooling and warming (numbered) transitions that are termed Dansgaard-Oeschger (D-O) events (NGRIP members, 2004). The approximate timing of Heinrich (H) events are marked with grey boxes (Heinrich, 1988).

It is not yet clear how representative our benchmark records, like the Greenland ice cores, are of climate variability that was experienced around the globe. It has been demonstrated that climate transitions may be spatially and temporally time-transgressive (e.g., Nakagawa et al., 2003; Lane et al., 2013; Shanahan et al., 2015; Schlolaut et al., 2017). However, regional disparities are very difficult to test since high-resolution and well-resolved records of past climatic change are rare, and the rapidity of these changes (e.g., sub- to multi-decadal), mean that the majority of regional records do not possess a sufficient chronology to be precisely compared (Lowe et al., 2008). Numerous dating techniques are applied within palaeoclimate research, and each of these possess different

levels of chronological uncertainty (e.g., sometimes the precision is equal to the length of the climatic transition; Blockley et al., 2004); are only suitable for specific time periods (e.g., only records in the last 50 ka can be radiocarbon dated); and are not possible in all geological contexts (see Brauer et al., 2014). For example, marine sediments are often not suitable for radiocarbon dating due to inherent uncertainties associated with temporal variations in marine reservoir offsets (Reimer and Reimer, 2001), and thus are often tuned to global benchmark records (see Blaauw, 2012). These tuned records cannot be used to assess the relative timing of environmental transitions unless they can be synchronised to other records using time-parallel stratigraphic markers.

1.2. Tephra as time-stratigraphic markers

1.2.1. Principles of tephrochronology

Time-stratigraphic (isochronous) markers can provide an invaluable way of overcoming problems of comparing palaeoenvironmental records on independent time-scales, which have different accuracies and precisions. Widely dispersed volcanic ash (tephra) layers can provide ideal isochronous layers that can be used to permit precise correlations (tephrostratigraphy) and transfer of absolute ages (tephrochronology) across a range of sedimentary sequences (e.g., Lowe et al., 2001; Davies et al., 2002; Turney et al., 2006; Lane et al*.,* 2014). The term ‘tephra’ encompasses all pyroclastic material (quenched melt and crystals) ejected during a volcanic eruption (Thórarinsson, 1944), however in medial and distal regions (e.g., > 100 km from source),

tephra is typically ash (particles < 2mm) or lapilli (2 – 64 mm) in size, and is predominantly composed of volcanic glass.

It is widely considered that there are three basic pre-requisites for using tephra layers as chronological markers (Davies et al., 2012; Lane et al., 2014; Lowe et al., 2015): it must be possible to identify the primary ash fall event within the region of interest; markers must be robustly correlated to a specific event; and an age estimate is required for the eruption. The challenges of these three conditions are outlined in the following sections.

1.2.2. Identifying primary ash fall events

The usefulness of volcanic ash as a time stratigraphic marker is reliant on tephra being quickly deposited following the eruption and remaining as a discrete, *in situ* horizon. Reworking processes (e.g., bioturbation, site re-occupation, high-energy floods) can obscure the primary ash-fall event, either by moving/skewing the stratigraphic positioning, or re-depositing older units (e.g., Wåstegard et al., 2006). It is therefore essential that all possible taphonomic processes are considered, and that secondary reworking events can be discounted. This criterion is usually achieved on a site-specific basis and best accomplished by considering several lines of reworking evidence (e.g., visual features of the unit such as grading, microscopic components of mineral and glass, and the geochemical consistency (Guðmundsdóttir et al., 2011; Abbott et al., 2018a).

Tephra can also be preserved as non-visible (cryptotephra) layers, where the concentration of glass shards is diluted and does not form a clear macroscopic unit (e.g., Dugmore et al., 1992; Davies 2015). Cryptotephra layers are almost exclusively composed of volcanic glass (Figure 1.2.) and shards are typically < 125 μm in distal settings. In order to identify the primary stratigraphic position of cryptotephra layers, sequences are continuously scanned to identify a peak in glass shard concentrations. This can be achieved by non-destructive techniques, such as X-ray fluorescence (XRF) continuous scanning (e.g., Lim et al., 2008; Kylander et al., 2012; McCanta et al., 2015), but findings can be inconsistent and it is difficult to assess the possibility of reworking**.** Arguably the most successful techniques for identifying non-visible markers are by isolating the volcanic glass from the host sediment using destructive techniques, but these methods can be very labour intensive. Density separation techniques can be used effectively to extract the glass from lighter (typically organic) and denser (minerogenic) components, and the number of glass shards can be counted using an optical microscope, to approximate the concentration per gram of dried sediment (see Turney, 1998; Blockley et al., 2005).

Although cryptotephra identifications have revolutionised the possibilities of dating and correlating records (see Davies, 2015), there are numerous other complexities that need to be considered when identifying such low primary inputs of glass, since even moderate reworking and taphonomic biases can easily skew or obscure the shard distribution profile (see Davies, 2015; Figure 1.2.).

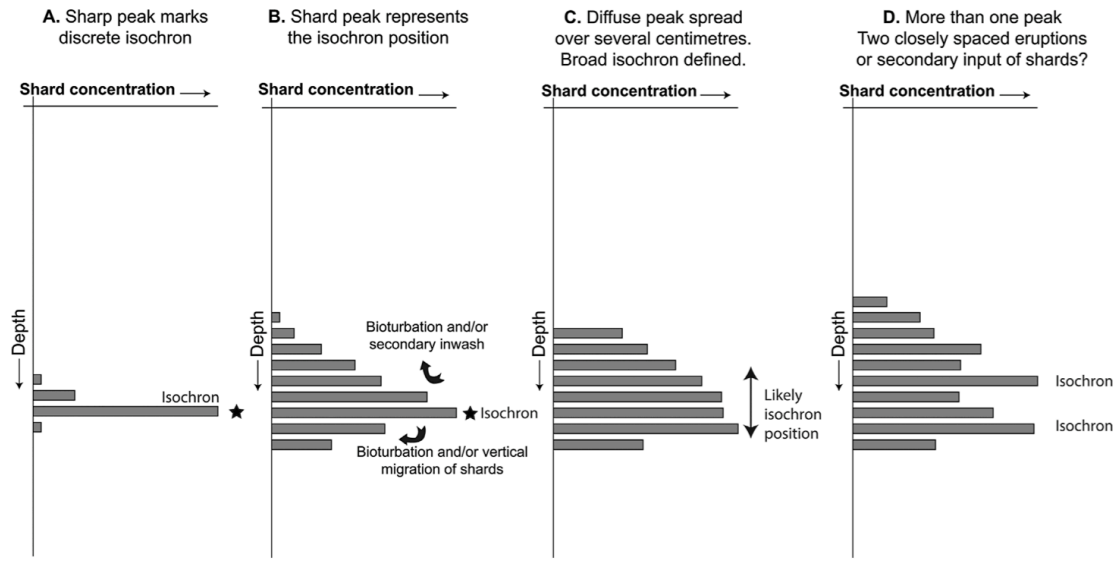


Figure 1.2. Schematic examples of possible glass shard concentration distribution profiles preserved in sedimentary records (from Davies, 2015). The primary ash input may be identified by a sharp increase in volcanic glass (as shown in A), but bioturbation processes may skew or obscure the isochron positioning (as shown in B, C and D).

For instance, taphonomic processes caused by inflows to the lake have been shown to affect the preservation of cryptotephra layers (Pyne-O'Donnell, 2011), weathering of the local geology can cause secondary in-wash events (MacLeod and Davies, 2016), and patchy tephra distribution can be caused by fallout on snow (Bergman et al., 2004).

1.2.3. Geochemical fingerprinting eruption events

Tephra can be 'fingerprinted' using the geochemical composition of the glass shards, which approximates the composition of the melt at the time of the eruption. Within tephra studies, Electron Probe Micro-Analysis (EPMA) forms the key technique for determining the precise major and minor element

compositions of individual glass shards (Hunt and Hill, 1993). The concentrations of these elements are used to robustly identify tephra from different tectonic settings, and to correlate the ash deposit to a known source, or specific eruption event. Since some centres erupt geochemically similar compositions through time (e.g., Lane et al., 2012; Bourne et al., 2013), to supplement these data, trace element compositions can be determined by laser ablation-inductively coupled plasma-mass spectrometry (LA-ICP-MS) (e.g., Pearce et al., 2007; 2011; Tomlinson et al., 2010). Improvements in the spatial resolution (e.g., spot size) and machine sensitivity (e.g., precision and accuracy) allows this technique to be applied to increasingly small shard sizes (e.g., Pearce et al., 2007; 2011; Tomlinson et al., 2010). Useful isochrons for palaeoenvironmental research ultimately need to have a geochemically distinct composition within a particular time period, to ensure robust correlations in the proximal and distal realm.

1.2.4. Absolute eruption ages

In addition to providing a valuable relative dating technique, once the eruption age is constrained it may be imported into other archives that contain the distal tephra, to improve or independently test the existing chronology. Eruptions can be dated directly using radiometric-dating methods, (e.g., $^{40}Ar/^{39}Ar$ dating or fission track; see Brauer et al., 2014), but these techniques often rely on knowing the source volcano to obtain large quantities of minerals from the deposits which are suitable for dating. For example, $^{40}Ar/^{39}Ar$ dating requires

measurable quantities of radiogenic argon, formed from the decay of potassium, and therefore K-rich deposits are required for precise ages.

Some of the most precise eruption ages are obtained indirectly, and are constrained in the medial or distal setting by sedimentary archives that have detailed age models (e.g., OxCal Bayesian age-models; Bronk Ramsey, 2008; Staff et al., 2013), and/or are underpinned by incremental chronologies (e.g., annually laminated varves; Smith et al., 2013).

1.3. Tephrostratigraphic frameworks

1.3.1. Building tephrostratigraphic frameworks

The increasing number of distal archives found to contain cryptotephra isochrons, and a better understanding of the values and complexities of tephrochronology, has led to the development of regional tephrostratigraphic frameworks (also referred to as lattices) (e.g., Shane, 2005; Curzio et al., 2008; Blockley et al., 2014; Davies et al., 2014; Bourne et al., 2015; Lowe et al., 2015; Matthews et al., 2015; Fontijn et al., 2016; Mackay et al., 2016; Nakamura, 2016; Abbott et al., 2018b). These frameworks can be constructed using the sequence of ash layers preserved in the geological record to create a network of sites that are bound by co-located markers. These are necessary to: grasp a comprehensive understanding of the number and frequency of eruption events; generate constrained eruption chronologies; and to build geochemical fingerprints for correlation purposes. Regional frameworks are usually underpinned by key reference sites (often termed *tephrostratotypes*), which

offer both detailed tephrostratigraphic sequences, and a precise chronology of eruptive events, usually from a range of volcanic sources (e.g., the Greenland ice cores; Abbott and Davies, 2012; Bourne et al*.,* 2015).

These frameworks are able to: i) incorporate new and lower magnitude events, ii) help resolve the stratigraphic positioning of eruption sources that are closely spaced in time, iii) establish which eruptions have a diagnostic geochemical signature or reliable tephra correlations, and iv) extend the known geographical footprint of ash fallout from individual eruptions, and therefore widen the area over which the key isochrons could be used.

An event framework for the North Atlantic region was generated by the International Working Group known as INTIMATE (INTegration of Ice-core, Marine and TErrestrial records), who outlined a tephra-based framework based on the GRIP ice core (e.g., Lowe et al., 2008; Blockley et al., 2012; Davies et al., 2012, 2014). As part of further work, the research project 'Response of Humans to Abrupt Environmental Transitions' (RESET) used tephra layers to tie together and synchronise chronologies of stratigraphic records at archaeological and environmental sites (Figure 1.3.). As a result of these frameworks, it has been possible to test long-standing questions that were previously hindered by chronological uncertainties (e.g., Rohling et al., 2009; Grant et al., 2012; Lowe et al., 2012; Barton et al., 2015).

Cryptotephra studies on the peripheral borders of these frameworks have shown widespread ash dispersal has occurred over long distances, increasing

the geographical area for synchronisation enormously (e.g., Lane et al., 2013; Mackay et al., 2016; van der Bilt et al., 2017; Lane et al., 2017; Cook et al., 2018). For instance, Pyne-O'Donnell et al. (2012) identified that Alaskan ash had been dispersed 7000 km to Newfoundland. Ash derived from Pacific arc volcanoes has also been identified in Greenland (Bourne et al., 2016), showing that there is potential to integrate records across intercontinental scales.

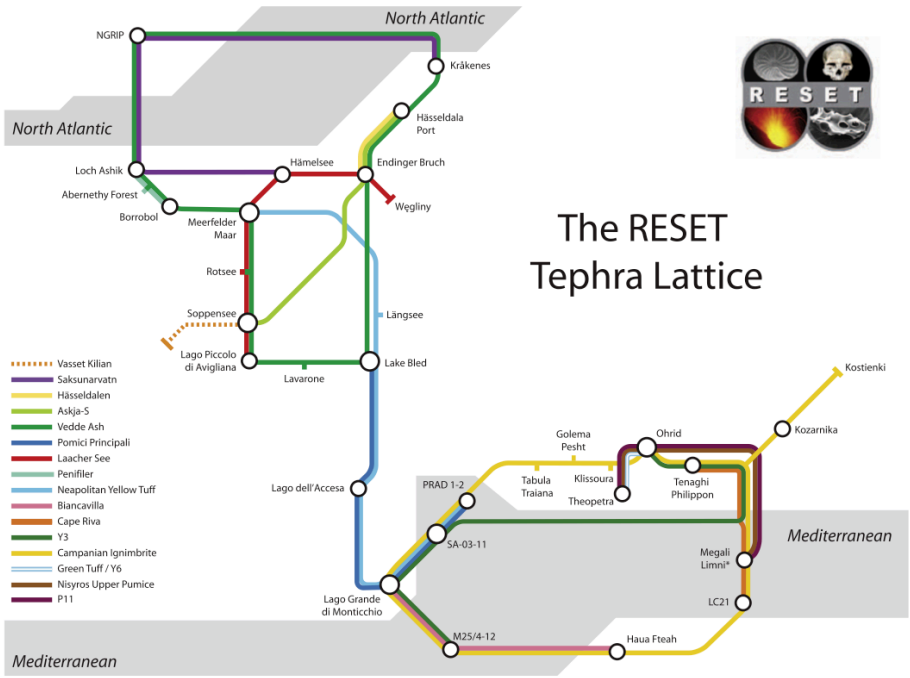


Figure 1.3. A schematic representation of the RESET ('Response of Humans to Abrupt Environmental Transitions') tephra lattice, which shows the sedimentary archives in Europe and the Mediterranean that can be precisely correlated using co-located isochrons (from Lowe et al., 2015).

1.3.2. A tephrochronological framework for Japan

Almost no detailed cryptotephra investigations have been undertaken to explore the true dispersal potential of key ash layers in Japan, however tephra from

East Asia has been transported and deposited as isochrons across the Northern Hemisphere, with recent discoveries in the Greenland ice cores (Sun et al., 2014a; Bourne at al. 2016), and possibly as far as the North American east coast (Mackay et al., 2016). This provides substantial encouragement that cryptotephra investigations in the East Asian/Pacific region will resolve new ash markers suitable for regional and hemispheric-scale correlations. Despite the abundance of high-resolution palaeoenvironmental archives across Japan, few have adequate chronologies enabling them to be precisely tied to other regional or global stratotype climate records. This prevents the evaluation of several outstanding palaeoclimate questions including the spatiotemporal variability of environmental change and the identification of high-magnitude, short-lived changes, as caused by the East Asian Monsoon (EAM). The EAM is of major socioeconomic importance for the 30% of the global population that reside in East Asia, yet its driving complexities are poorly understood and climatically modelled, partly due to limited long-term observations and records with detailed proxy information and chronology (Cook et al., 2010).

1.4. Research aims and objectives

This thesis aims to improve the tephrochronological framework for Japan to enable the synchronisation of palaeoclimate records across the Asian/Pacific region. The Lake Suigetsu sedimentary archive (central Honshu) is the most precisely dated palaeoenvironmental record for Japan, and pilot investigations indicate that the archive is suitable for detailed cryptotephra investigations (Smith et al., 2013). Augmenting the Lake Suigetsu tephrostratigraphy would

provide a detailed tephrostratotype for correlating and dating records in this region, and provide new insight into the frequency and origin of ash fall events dispersed over the densely populated regions of central Honshu. These concepts fall within the following research objectives:

- Augment the Lake Suigetsu tephrostratigraphy by identifying cryptotephra layers through key time periods of sedimentation.
- Devise suitable techniques to identify primary and secondary reworking events in the lake sediments.
- Chemically characterise the volcanic glass of the new tephra layers. Use the glass (major and trace element) compositions of the tephra layers to determine their source regions, and specific eruptions. Where possible, assess correlations to other key archives in the East Asian/Pacific region (or beyond).
- Classify key isochrons suitable to investigate palaeoenvironmental questions and build a framework for future correlations.
- Review the implications of this record for hazard assessments and the role of cryptotephra studies for volcanology in this region.

Cryptotephra will be identified by processing contiguous samples taken from U-channels spanning the composite sequence of the Lake Suigetsu sediments (cores SG06 and SG14). The volcanic glass shards will be extracted using density separation techniques as outlined by Blockley et al. (2005). Once the tephra layers have been identified the shards will be mounted for compositional analysis using a wavelength-dispersive electron microprobe (major elements) at the University of Oxford and, shard size permitting, laser ablation inductively

coupled mass spectrometer (trace elements) at the Japan Agency for Marine-Earth Science and Technology (JAMSTEC). Full analytical and research methods are outlined within each of the following research articles.

1.5. Guide to this thesis

This introductory chapter has outlined the value of time-stratigraphic markers for the precise comparisons of palaeoenvironmental archives. Volcanic ash (tephra) layers can synchronise sedimentary archives over hemispheric scales, but is it essential that three basic pre-requisites for tephrochronology are met. The value of building regional tephrostratigraphic frameworks has been explored, as well as the significant potential to expand tephrochronology (via cryptotephra analysis) in the East Asian/Pacific region. Improving the tephrochronological framework for Japan is possible using the research objectives listed, namely by utilising the high-resolution sediments of Lake Suigetsu (central Honshu) to provide a key tephrostratotype for Japan. To explore these research aims, this thesis is divided into six further chapters:

Chapter 2: Tephrostratigraphic and tephrochronological research in Japan

This chapter provides an introductory history of tephra research in Japan, the key sources of ash dispersal across the Asian/Pacific region, and the suitability of the study site Lake Suigetsu to meet the project objectives.

Chapter 3: Identification of the Changbaishan 'Millennium' (B-Tm) eruption deposit in the Lake Suigetsu (SG06) sedimentary archive, Japan

This article outlines the first direct tephra tie-point between a high-resolution mid-latitude palaeoclimate archive (Lake Suigetsu) and the Greenland ice cores, a major goal of research communities examining palaeoenvironmental change. The Greenland ice core derived age for the B-Tm tephra is used here to help constrain the chronology of the late Holocene sediments of Lake Suigetsu. This discovery provided significant encouragement for future cryptotephra investigations through the Holocene sediments of Late Suigetsu. This article was published in 2016 as a *Short Communication* paper in *Quaternary Science Reviews* (150: 301-307).

Chapter 4: Integrating the Holocene tephrostratigraphy for East Asia using a high-resolution cryptotephra study from Lake Suigetsu

This article provides the first detailed Holocene (< 10 ka) cryptotephra study for the East Asia/Pacific region, which recognises that it is possible to detect non-visible ash layers in a productive arc setting. The Lake Suigetsu tephrostratigraphy is extended from four to twenty ash layers using cryptotephra extraction techniques, which integrates deposits from volcanoes in North Korea/China, South Korea and along the Japanese arcs. The Lake Suigetsu tephrostratigraphy is established as the most comprehensive record of East Asian volcanism from multiple sources, and the linchpin site for correlating sequences across this region. This article was published in 2018 in *Quaternary Science Reviews* (183: 36-58).

Chapter 5: Improved eruption chronology for explosive volcanism in East Asia (Aso and Aira) between 50 and 30 ka.

This study reveals that four times more non-visible ash layers than visible tephras are preserved in the varved Suigetsu sediments between 50 and 30 ka, providing an unprecedented record of eruption events that were dispersed to central Honshu. Explosive activity from Aso and Aira are most frequently recorded in the record, which indicates that these calderas were very active between 35 to 30 ka. Aso erupted compositionally different magmas through time, producing eight widespread events over 20 ka. This study highlights that distal sedimentary records have a very important role to play in constraining the tempo and frequency of eruptions in East Asia, and to identify the medium to large magnitude events missing from the geological record.

Chapter 6: Refining the eruptive history of Ulleungdo and Changbaishan volcanoes (East Asia) over the last 86 ka using distal records

In order to provide new insight into the eruptive histories of Ulleungdo and Changbaishan, this study provides a review of the distal occurrences of alkaline ash deposits preserved in sedimentary records (marine and lacustrine cores) that span the last 86 ka (i.e., following the deposition of the widespread Aso-4 tephra, ca. 86.4 ka; Albert et al., accepted). The intensely-dated Lake Suigetsu archive (central Honshu, Japan) provides the most comprehensive eruption record for both centres, despite being located 600 km E of Ulleungdo and 1000 km SSE of Changbaishan, and is used to establish the stratigraphic framework of these tephra layers, and integrate other reported eruption events. Notably, a previously unreported explosive event from Changbaishan (ca. 41.8 ka), is

identified as a cryptotephra deposit in the Lake Suigetsu sediments and herein named the B-Sg-42 tephra.

Chapter 7: General Discussion

This chapter brings together a discussion over the overarching aim of this research project and the insights that can be gleaned from building very detail dossiers of eruption events. A comprehensive tephrostratigraphic framework for Japan is presented which is constructed using 24 key tephra archives that are distributed across Japan, North Korea/China and South Korea. In order to focus future research efforts, key East Asian isochrons, that are suitable to answer palaeoenvironmental questions are presented and discussed. The AT tephra is also used to synchronise three key palaeoenvironmental archives in Japan and China, demonstrating the possibility to overcome dating uncertainties and better assess the sensitivity of different climate proxies. This chapter closes with a review of the augmented Lake Suigetsu tephrostratigraphy, which can be used to provide insight into the frequency and origin of ash fall events that have been dispersed to the densely populated regions of central Honshu.

Chapter 8: Conclusions

This chapter provides a summary of the key conclusions of this research project and the potential of tephrochronology in the East Asian/Pacific region.

CHAPTER 2: TEPHROSTRATIGRAPHY AND TEPHROCHRONOLOGY IN JAPAN

Overview

This chapter provides an introduction to the volcanic arc systems distributed along the length of Japan, and the key sources of widespread ash dispersal in the East Asian/Pacific region. A brief history of tephra research is outlined, including key tephra archives (marine and lacustrine) that are used to underpin Japanese tephrostratigraphy and chronology. As part of these comprehensive marine and land-based studies, very detailed glass geochemical datasets (major and trace elements) have been established, which can permit robust distal to proximal tephra correlations. These datasets will be utilised and supplemented throughout this research project, as new visible and cryptotephra layers are identified. This chapter also provides an introduction to the study site Lake Suigetsu (Honshu Island, Japan), and its suitability to meet the project objectives. The previous coring campaigns (named SG93, SG06 and SG14) are outlined, as well as the other studies that have focused on characterising and correlating the visible ash deposits preserved within the Lake Suigetsu sediments. Several of these topics are explored further where relevant in the subsequent four articles (Chapters 3 – 6).

2.1. Tephra dispersal in and around Japan

2.1.1. Key sources of ash dispersal

Over 130 volcanic centres are distributed across the islands of Japan and are known to have been active during the Late Pleistocene and Holocene (Machida and Arai, 2003; Crosweller et al., 2012; Figure 2.1.). These centres are clustered along arc subduction zones situated in the east (i.e., Kurile, NE Japan, central Japan and the Izu-Bonin arc) and west (i.e., SW Japan and Ryukyu-Kyushu arc) (Figure 2.1; Sugimura, 1960; Machida, 1999). The Philippine Sea plate subducts beneath the Ryukyu-Kyushu and SW Japan arc, and hosts some of the most active calderas and volcanic complexes. Calderas on the Ryukyu-Kyushu arc are typically classified into the Southern (SVR; e.g., Kikai, Ata, Ikeda and Aira) and the Central Volcanic Region (CVR; e.g., Aso, and the Hohi Volcanic Zone that includes Kuju volcanic complex) (Figure 2.1; Mahony et al., 2011; Albert et al., accepted). The Pacific plate subducts beneath NE Hokkaido, where several other large calderas are situated (e.g., Kutcharo, Mashu). Key Late Quaternary calderas on the NE Japan arc include Towada (northern Honshu), Shikotsu and Toya (Hokkaido). In comparison, the Japanese back-arc is dominated by stratovolcanoes and monogenic centres (Suzuki, 1996; Machida and Arai, 2003; Crosweller et al., 2012). Furthermore, west of Japan, intraplate volcanoes Ulleungdo (South Korea) and Changbaishan (North Korea/China border) have been very productive throughout the Quaternary and are also of significance for Japanese tephra studies.

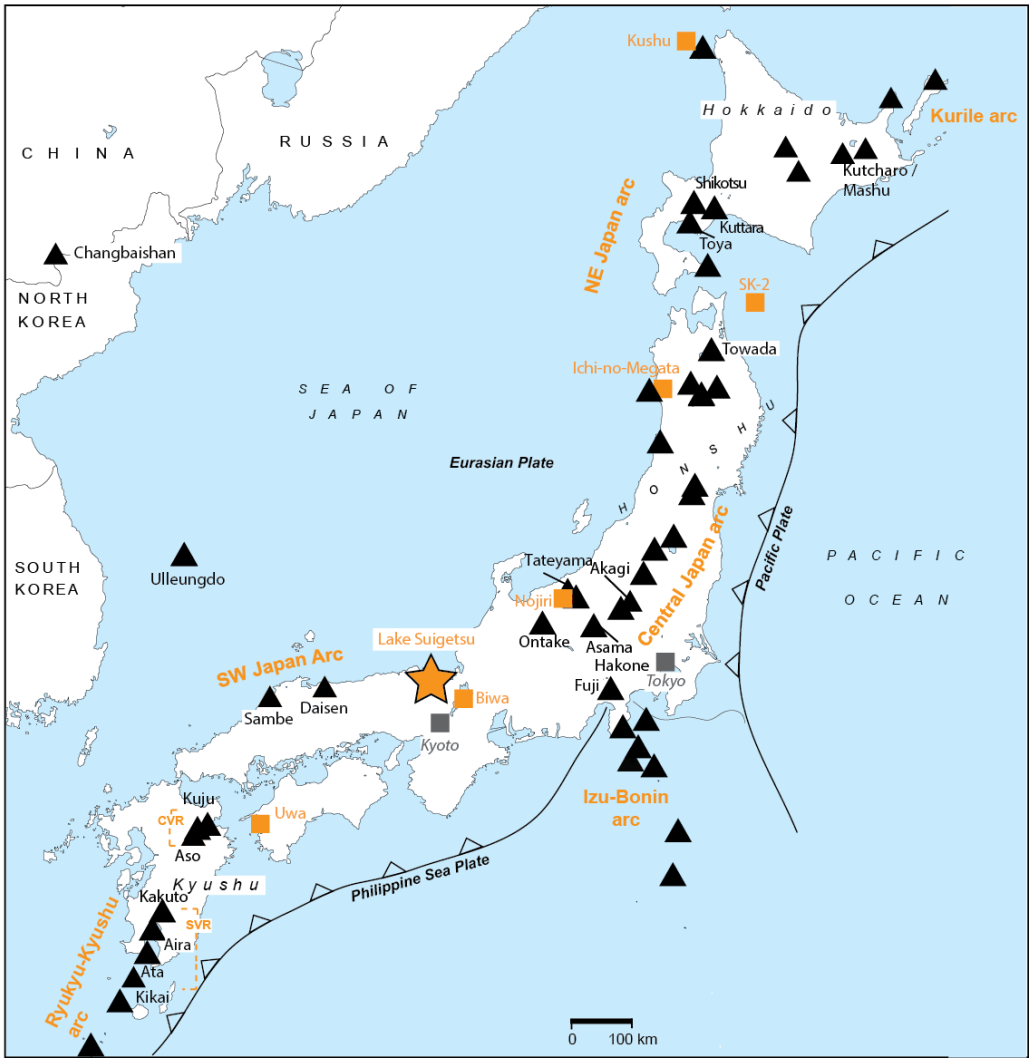


Figure 2.1. Volcanoes in Japan, North Korea/China (Changbaishan) and South Korea (Ulleungdo) (black triangles) known to have been active during the Quaternary (data from Machida and Arai, 2003). Large caldera volcanoes are concentrated on the Ryukyu-Kyushu arc (south) and the NE Japan arc in Hokkaido (north), associated with the areas of largest magma production (Kimura et al., 2015). In contrast, only two Quaternary volcanoes (Sambe and Daisen) are found on the SW Japan arc. Key tephra archives mentioned in Chapter 2 are marked with an orange square, and the study site Lake Suigetsu is marked with a star.

Pioneering investigations by researchers such as Machida and Arai (1983) provide the foundation for Japanese tephrochronology and have established a complex catalogue (via detailed mapping of visible ash deposits) of the succession and dispersal characteristics of the large explosive eruptions that occurred during the Quaternary (compiled in Machida and Arai, 2003; Figure

2.2.). This catalogue provides fundamental data for correlating Quaternary sequences, and showed that the six active and buried calderas on the SVR and CVR were the foci of some of the largest (Volcanic Explosivity Index (VEI) 7 – 8; Newhall and Self, 1982) caldera-forming eruptions during this period (Machida and Arai, 2003). Extensive land and sea-based mapping of these deposits indicate that ash plumes were predominantly dispersed towards the east (via the prevailing westerly winds), and can be traced several hundred kilometers downwind of their source (Machida and Arai, 2003; Figure 2.2.).

Several key widespread marker beds are commonly identified in Late Quaternary sedimentary sequences in and around Japan (Figure 2.2.), which are named using their source volcano and distal tephra type-site, a common practice in Japanese tephrostratigraphic studies. Of these, Kikai caldera (Kyushu SVR) is responsible for two key ash fall events (VEI 6 – 7), including the Kikai-Akahoya (K-Ah tephra; ca. 7.3 ka) and the Kikai-Tozurahara (K-Tz; ca. 96 ka) eruptions (Machida 1999; Machida and Arai, 2003; Smith et al., 2013). The Aira-Tanzawa (AT; 30 ka) tephra was erupted during the enormous VEI 7 eruption of Aria caldera (SVR), that ejected approximately 463 km^3 of bulk tephra (Machida, 1999). The AT ash was dispersed over the Japanese islands, the Sea of Japan and the Pacific Ocean (Figure 2.2; Machida and Aria, 2003). Aso (Kyushu CVR) is one of the largest active volcanoes in the world, and the caldera was formed by a series of at least four VEI 6 - 7 eruptions (oldest to youngest): Aso-1 (ca. 270 ka), Aso-2 (ca. 140 ka), Aso-3 (ca. 112-134 ka) and Aso-4 (ca. 84 ka) (Ono and Watanabe, 1985; Matsumoto et al., 1991; Albert et al., accepted), that also dispersed ash across vast regions of East Asia.

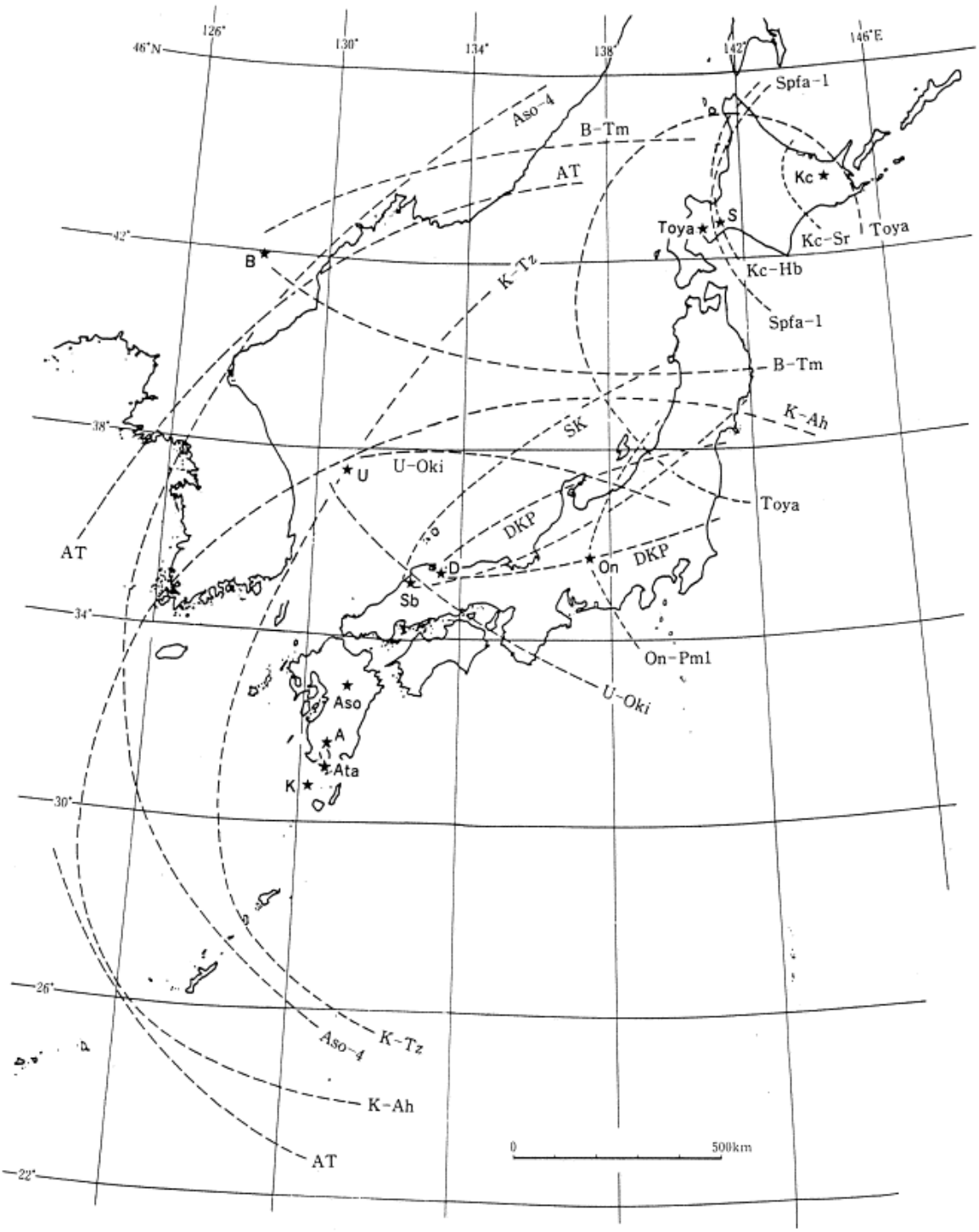


Figure 2.2. Key tephra layers that were dispersed across Japan and the surrounding regions during the Late Quaternary (from Machida, 1999). Six active and buried calderas on Kyushu Island (south) were the foci of some of the largest caldera-forming eruptions during the Quaternary (Machida and Arai, 2003).

Due to the prevailing westerly winds, tephra erupted from intraplate volcanoes Ulleungdo (South Korea) and Changbaishan (North Korea/China border) were also dispersed across the Sea of Japan (East Sea) (Arai et al., 1981; Chun et al., 1997, 2007; Ikehara, 2003; Machida and Arai, 2003; Ikehara et al., 2004; Lim et al., 2013) to the coastal regions of Japan (e.g., Nagahashi et al., 2004; Smith et al., 2013). The most widespread tephra layer erupted from Changbaishan is associated with the caldera-forming 'Millennium Eruption' (ME; VEI 7) which ejected ca. 100 km^3 of tephra (Dense Rock Equivalent ca. 25 km^3), blanketing at least the northernmost regions of Japan in ash (Horn and Schmincke, 2000; Zou et al., 2010; Wei et al., 2013; Sun et al., 2014b). The ash is distally named the Baegdusan-Tomakomai (B-Tm tephra), and glass shards from this eruption have been identified almost 9,000 km from source in the Greenland ice cores (Sun et al. 2014a). The largest known Plinian eruption from Ulleungdo generated the U-Oki tephra layer that is dated to 10,230 – 10,171 cal. yrs BP (95.4 % confidence interval; Smith et al., 2011a). The U-Oki ash is found in several high-resolution palaeoenvironmental archives in Japan, including Lake Biwa (BT-4; Nagahashi et al., 2004) and Lake Suigetsu (SG06-1288; Smith et al., 2011a).

2.1.2. Key tephra archives in East Asia

Ash deposits are routinely identified in medial and distal sedimentary archives in and around Japan, and are used to understand more about the magnitude, tempo and dispersal of past volcanic eruptions in East Asia. There is a high-density of scientific drilling (e.g., IODP; International Ocean Drilling Program)

cores that have been extracted from marine basins that surround Japan (e.g., the Sea of Japan/East Sea). These archives provide a detailed sequence of the high-magnitude silicic eruptions derived from the Japanese Islands and the Korean Peninsula (e.g., Arai et al., 1981; Machida and Arai, 1983; Furuta et al., 1986; Kutterolf et al., 2014; Ikehara, 2015, Schindlebeck et al., 2017; Sagawa et al., 2018). Since marine cores are not particularly suited to high-precision dating techniques, age-models are often orbitally tuned, or correlated to other records using the dark and light oxygenation layers present in the sediments (Tada, 1999). This means that tephra layers preserved in marine sediments are often not precisely dated using these age-models, and the assessment of climate sychroniety is not possible. Where the age of a tephra layer has been previously established (e.g., via $^{40}Ar/^{39}Ar$ dating or varve chronology), these isochrons can provide critical chronological constraints to the host marine sediments. For example, Sagawa et al. (2014) import the precise age of the B-Tm tephra (Changbaishan) to constrain the chronology of the Late Holocene sediments of marine core SK-2 (obtained from the northeastern part of the Japanese islands; Figure 2.1.), and use the Towada-Chuseri tephra (To-Cu) (Towada, ca. 6 ka) to independently test the age-model accuracy.

Lacustrine records from low energy environments provide arguably the most detailed and comprehensive records of eruption events, often resolving thinner or finer ash fall events that cannot be identified in the marine realm. There are numerous high-resolution lacustrine sedimentary sequences that have been obtained from Japan, including Lake Suigetsu (Smith et al., 2013), Lake Biwa (Nagahashi et al., 2004), Ichi-no-Megata (Okuno et al., 2011) and Lake Nojiri

(Kumon et al., 2003) (Figure 2.1.), which provide some of the most robust and stratigraphically constrained evidence of Japanese and Korean eruptions. These distal archives have proven increasingly important for building more detailed inventories of ash fall events, and provide insight to the lower magnitude and/or local eruption events. For example, the Lake Suigetsu sedimentary record (central Honshu) captures two periods of intense activity at Daisen volcano, which is situated downwind of the lake (Figure 2.1.), and was able to revolve and precisely date eruption events that occurred as little as 6 years apart (Albert et al., 2018).

Several key studies have constructed regional Japanese tephrostratigraphic frameworks, building on the earlier studies by Machida and Arai (2003), in order to provide an integrated sequence of local and regional eruption events. Nakamura (2016) mapped the distribution of thirty-one Holocene tephra layers dispersed across Hokkaido and central Honshu, and characterised these deposits using their mineral assemblages, refractive indices and major element glass compositions. In southern Japan, Nakamura (2016) proposed a regional tephra-based framework for the past ca. 30 ka, which included more than ninety visible ash beds derived from centres on the Ryukyu-Kyushu arc (e.g., Kakuto, Aira, Ata, Kikai), and showed their relationship to distinct palaeoenvironmental and cultural events (Figure 2.3.). These frameworks highlight that despite the significant number of ash fall events, to date, relatively very few layers have been identified geographically widespread, or have been precisely dated.

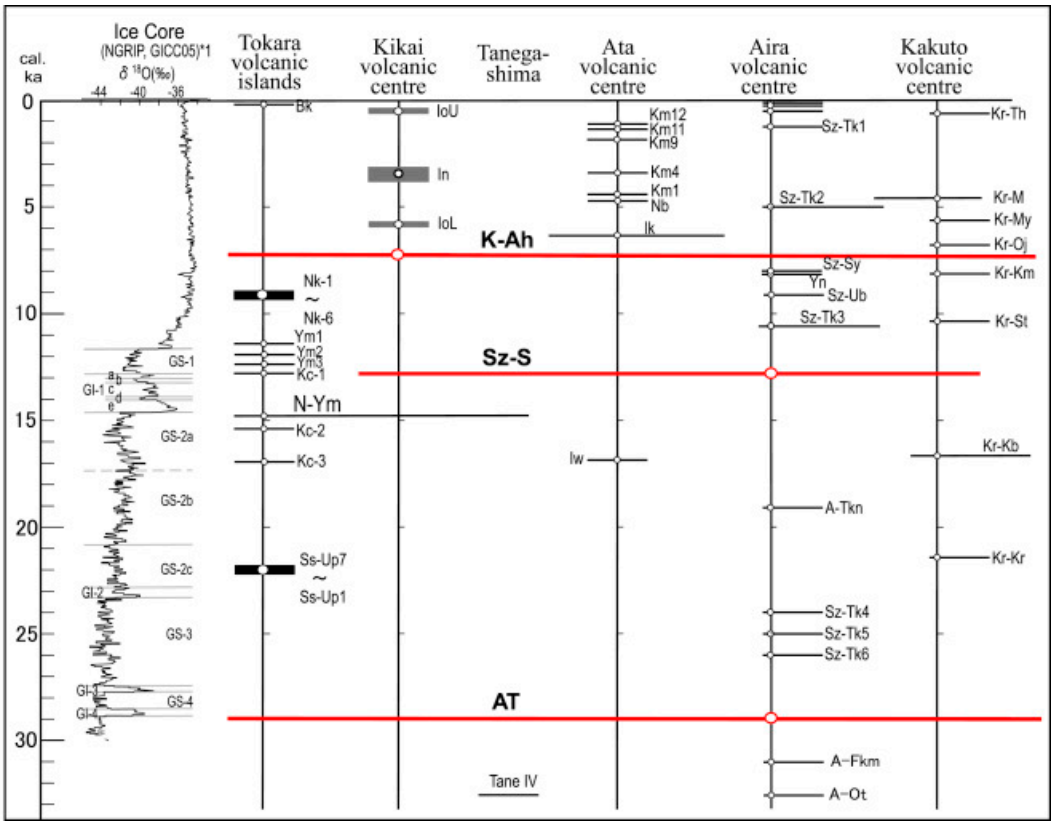


Figure 2.3. Marker tephra beds in southern Kyushu erupted over the last ca. 30 ka and their stratigraphic position to the $\delta^{18}O$ record from the NGRIP ice core (NGRIP members, 2004) (from Moriwaki et al., 2016). Eruption records can be integrated using key widespread marker layers (marked in red), which include the AT, Sz-S (Aira volcano) and K-Ah (Kikai) tephra.

2.2. Geochemically discriminating tephra deposits

Before the electron microprobe was used to analyse glass, Japanese tephra studies typically used the glass refractive indices to characterise the geological material (e.g., Arai, 1972; Furuta et al., 1986; Ahn et al., 2006). However, these values are not often unique, and do not allow precise comparisons to other distal ash occurrences across the globe. Glass compositional datasets (major and minor elements) for most widespread ash layers in East Asia are now well established (e.g., Machida and Arai, 2003; Aoki and Machida, 2006; Furukawa and Nanayama. 2006; Smith et al., 2013; Kimura et al., 2015; Nagahashi et al.,

2013; Nakamura, 2016; Albert et al., accepted) and can be used to robustly provenance tephra preserved in distal sequences.

It is relatively straightforward to distinguish tephra erupted from different arc sources distributed along length of Japan, which can often be discriminated by their SiO_2 to K_2O ratios (Figure 2.4.). For instance, Late Quaternary glasses erupted from the CVR and SVR typically contain Medium to High-K compositions, and are different for most major elements to those on the SW and NE Japan arc (typically Medium to Low-K; Kimura et al., 2015; Albert et al., accepted). Tephra erupted from Aso has the highest known K_2O for Japan (> 3 wt. % at 66 wt. SiO_2, and the most evolved glasses extend to 6 wt. % in K_2O), and are some of the most compositionally distinct. Source regions which are responsible for numerous low magnitude (e.g., VEI <4) monotonous eruptions (i.e., Holocene eruptions from Fuji; Kobayashi et al., 2007) are generally more poorly geochemically fingerprinted, which prevent unequivocal correlations to specific eruption events.

Some centres (e.g., Kikai, Ata and Aira) erupt very compositionally similar tephra over tens to hundreds of thousands of years, with only slight major element variances (Machida and Arai, 2003; Figure 2.4.). Therefore, trace element compositions, that reflect more subtle magmatic processes (e.g., Allan et al., 2008; Tomlinson et al., 2010), are required to discriminate these sources. When normalised to the primitive mantle, vitreous tephra derived from all sources in Japan are enriched in Large Ion Lithophile Elements (LILE) (e.g., Rb, Ba, K), relative to Rare Earth Elements (REE; e.g., LA to Yb) (Kimura et al.,

2015; Albert et al., accepted) as expected due to their subduction genesis. Since, LILE concentrations are linked to K_2O, these elements are very useful discriminators between different arc sources.

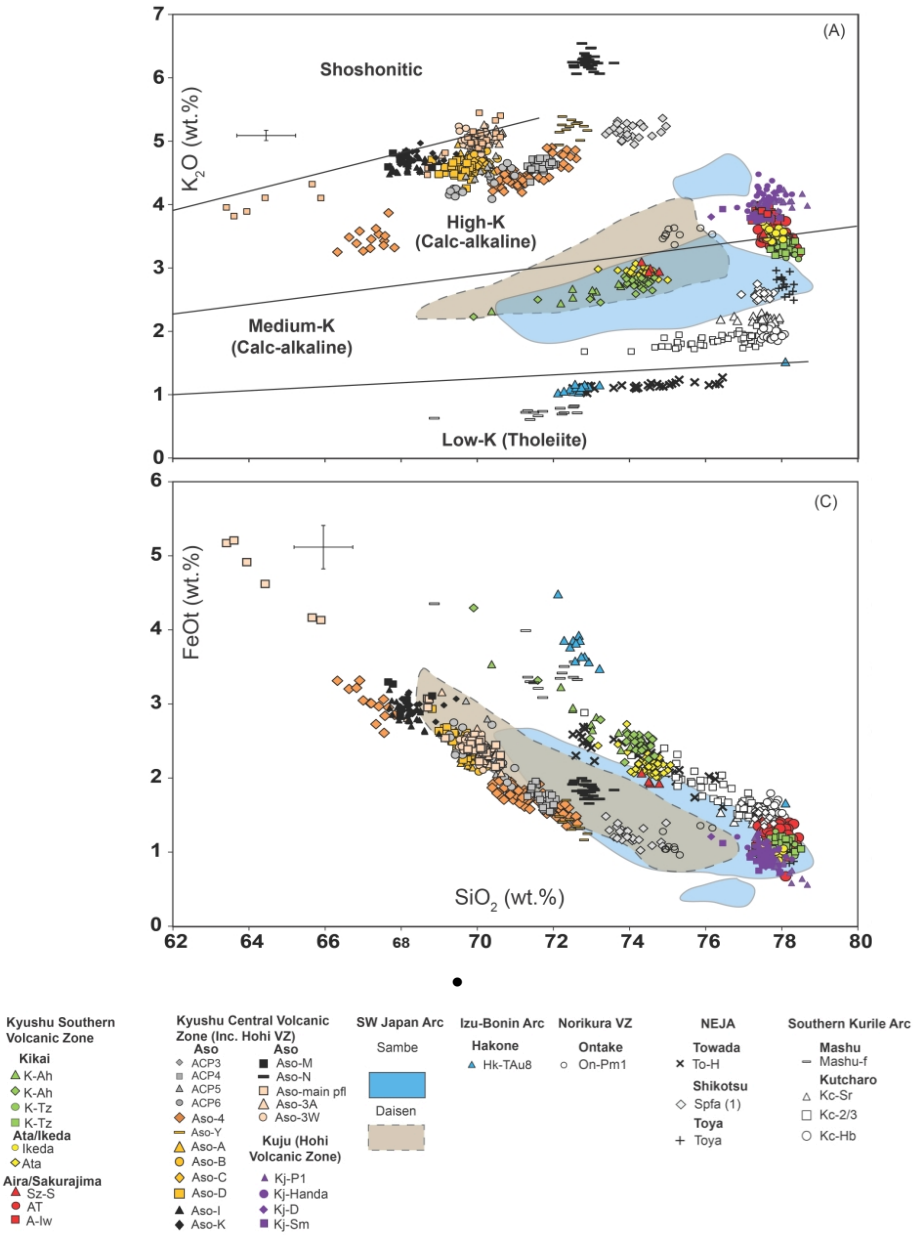


Figure 2.4. Major element glass compositions (SiO_2, K_2O and FeO^T) of large magnitude Japanese eruptions obtained (last 150 ka) from near source (proximal) deposits (from Albert et al., accepted). Glasses are plotted on the whole rock classification scheme of Peccerillo and Taylor (1976) in Figure 2.4a. and range from Low-K (Tholeiitic) to High-K (Calc-alkaline)/Shoshonitic affinities. Error bars on plots represent repeat analysis of MPI-DING StHs6/80-G.

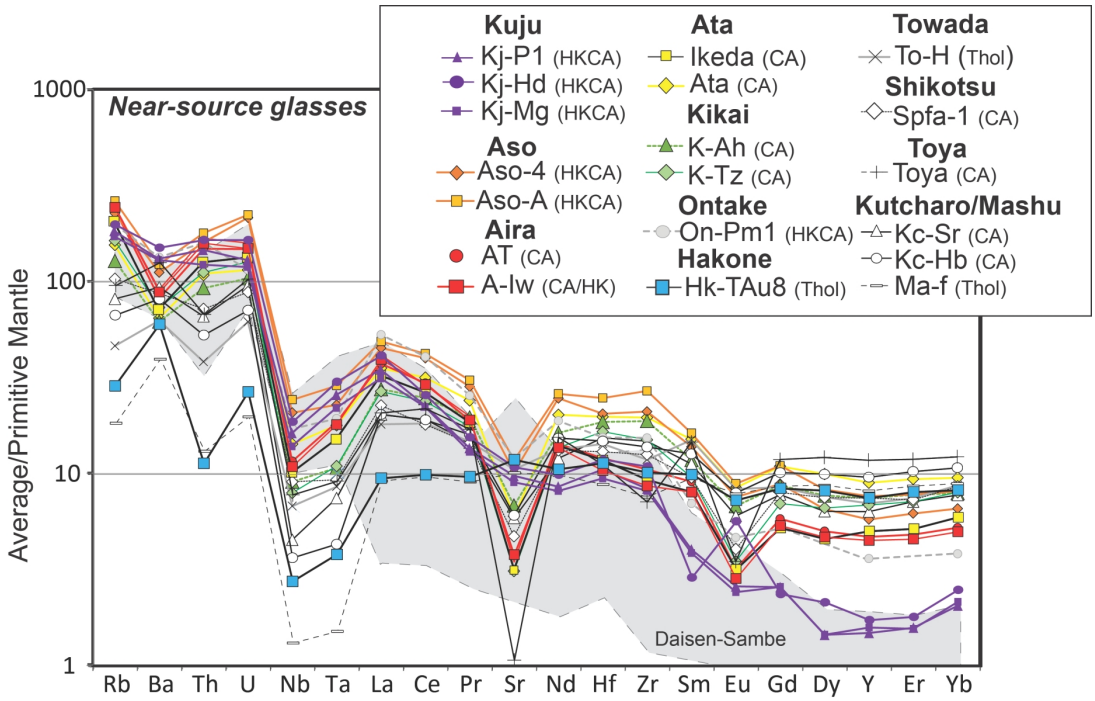


Figure 2.5. Average primitive mantle normalised volcanic glass compositions for representative near source (proximal) large magnitude eruption deposits. Primitive mantle values used for normalisation follow Sun and McDonough (1989) (from Albert et al., accepted).

Ulleungdo and Changbaishan are the only sources known to have dispersed alkaline tephra across Japan (Machida and Arai, 2003; Kimura et al., 2015; Albert et al., accepted), and their distal deposits can be easily discriminated from other intra-plate sources in the back-arc (e.g., Doki and Jeju volcanoes; Brenna et al., 2014) (see Chapter 6). For example, Ulleungdo derived tephra contain ca. 10 wt. % lower SiO_2 and much higher Al_2O_3 and K_2O compared to the Kyushu derived tephra. Glass erupted from Ulleungdo and Changbaishan are also easily distinguished by the absence of Nb and Ta depletions in their trace element profiles, when normalised to primitive mantle compositions.

2.3. Lake Suigetsu, Honshu Island

This section provides an introduction to the study site Lake Suigetsu (central Honshu, Japan) and its suitability to meet the project objectives. The previous coring campaigns (named SG93, SG06 and SG14) are outlined, as well as the studies that have focused on characterising and correlating the visible ash deposits preserved within the Suigetsu sediments.

2.3.1. Geological background

Lake Suigetsu is situated in Honshu Island (35°35'0''N, 135°53'0''E) and is located in a small tectonic basin situated on the western side of the Mikata fault line, adjacent to Wakasa Bay (Figure 2.6, 2.7). It forms the largest of the 'Mikata Five Lakes' and is located in the Wakasa Wan Quasi-National Park. Lake Suigetsu covers an area of ca. 4.3 km^2 (with a perimeter of ca. 10 km and diameter of ca. 2 km) and has a water depth of ca. 34 m (Kitagawa and van der Plicht, 1998a). The lake has a small catchment area, vegetated by warm mixed-forest and is surrounded by a ring of Palaeozoic hills (maximum elevation 400 m) (Nakagawa et al., 2005). The main tributary feeding the five Mikata lakes is the River Hasu (ca. 10 km in length), which enters on the southeast side of Lake Mikata and flows through the Seto Channel into Lake Suigetsu (Figure 2.7). This channel is particularly shallow (ca. 2 m in depth), meaning coarse sediment is deposited or trapped in Lake Mikata before reaching Lake Suigetsu (Nakagawa et al., 2005). The fine-grain sedimentation is often interrupted by deposits of coarse volcanic ash, which fall through the water column. Due to

this natural filter, sedimentation in Lake Suigetsu is predominantly autochthonous and authigenic material (Schlolaut et al., 2012).

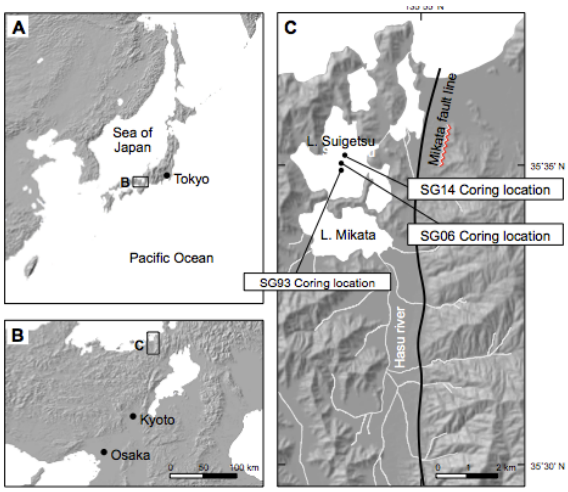


Figure 2.6. Location of Lake Suigetsu and coring positions of the SG93, SG06 and SG14 campaigns (modified after Nakagawa et al., 2005).



Figure 2.7. Location the five Mikata lakes ('Mikata-goko') adjacent to the Sea of Japan coast and Wakasa Bay.

Lake Suigetsu is located in the mid-latitude western Pacific region, where the East Asian Monsoon (EAM) annually migrates. The seasonal force of this system and the westerly jets heavily influence the climate (Liu et al., 1995). During the summer, the preferential heating of continental Eurasia (which warms more rapidly than the Pacific Ocean) forms an atmospheric pressure

gradient driving south-easterly winds and intense precipitation to Japan (Figure 2.8a). This phenomenon is reversed in winter, as the Eurasian continent begins to cool quicker than the Pacific Ocean, forcing a pressure gradient to drive cold northwesterly winds across the Japanese archipelago (Figure 2.8b). Since Lake Suigetsu is situated to the north of the front in winter and to the south in summer, its location is ideal to investigate the past dynamics and behaviour of the EAM.

2.3.2. SG93, SG06 and SG14 coring campaigns

The lake has been studied for over two decades, with the first ca. 4 m piston cores extracted in 1991 (Takemura et al., 1994; Kitagawa et al., 1995; Yasuda et al., 2004). Further interest sparked in 1993, following the 'SG93' drilling campaign, which obtained a 72.4 m piston core from the lake basal sediments (Kitagawa and van der Plicht, 1998a). This revealed much of the sequence contained varved (*nenko* in Japanese) laminations, with alternations of diatom-rich (lighter-coloured) and mineral rich (darker-coloured) layers (Figure 2.9; Fukusawa, 1995; Kitagawa et al., 1995; Kitagawa and van der Plicht, 1998b).

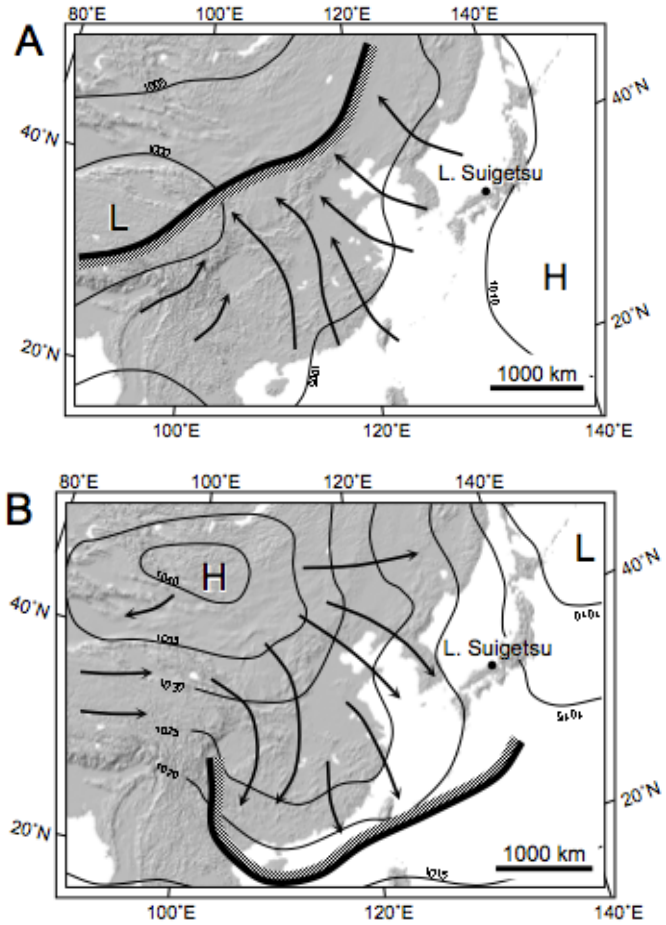


Figure 2.8. The atmospheric circulation around Japan in (a) summer, (b) winter (from Nakagawa et al., 2012, modified after Porter and An, 1995).



Figure 2.9. Photo of Lake Suigetsu core segment A-22 that contains annually laminated sediments (varves). These varves indicate that the lake basin was extremely stable, with anoxic conditions preventing bioturbation of the sediments.

The SG93 core was extensively radiocarbon dated, with over 250 accelerator mass spectrometry (AMS) radiocarbon (^{14}C) dates obtained from terrestrial plant macrofossils that were preserved in the sediments. An assessment of the SG93 age-model (radiocarbon and varve chronology) suggested that varved sediments were missing between core segments (Staff et al., 2010), and therefore two additional cores (15 m in length) were obtained to provide overlapping sediments for the upper section (Nakagawa et al., 2003).

Lake Suigetsu was re-drilled (using a hydro-pressure thin-walled piston corer) in the summer of 2006 as part of the 'Lake Suigetsu Varved Sediment Project'. This location was ca. 250 m north of the SG93 coring site and the master core (named SG06) was obtained from four parallel boreholes (A, B, C and D, that were located ca. 20 m apart). This meant that the overlapping sediments could be consistently monitored, and any disturbed sections could be substituted from the master sequence. Key marker horizons (e.g., flood horizons and tephra layers) were used to create a composite, overlapping master sequence (Figure 2.10.).

The SG06 campaign had two overarching project aims:

1. To provide high-resolution, quantitatively reconstructed palaeoenvironmental data for the East Asian monsoon region across the entirety of the last glacial/interglacial cycle
2. To establish a purely terrestrial radiocarbon calibration dataset across the complete radiocarbon dating range (ca. 60 ka)

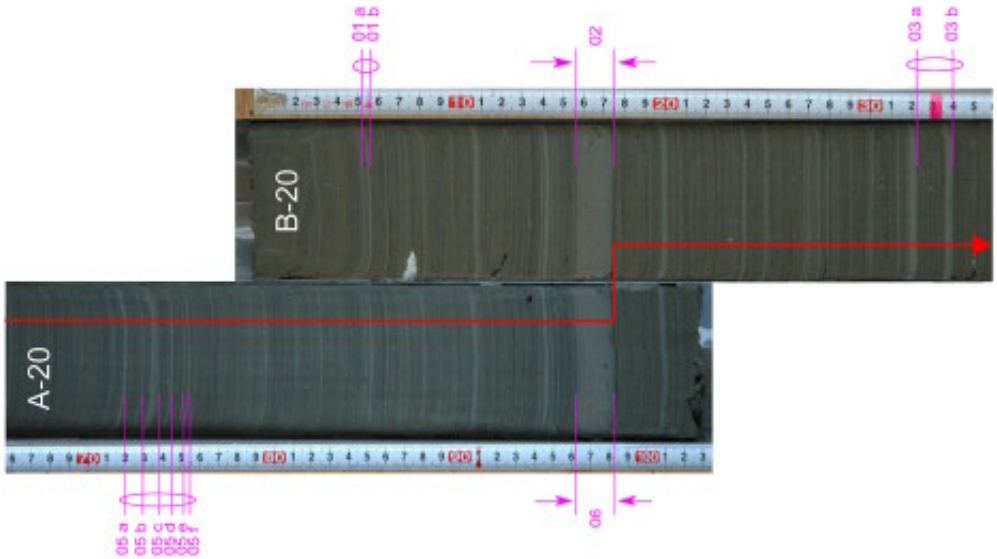


Figure 2.10. Example of using event layers (e.g., clay-rich flood layers) to construct the master SG06 sequence (photographs of cores A-20 to B-20).

The SG06 sediments were further radiocarbon dated between 11.2 and 52.8 kyr BP, and integrated with improved varve counting techniques (i.e., using thin-section microscopy and ultra-high x-ray fluorescence (XRF); Marshall et al., 2012; Schlolaut et al., 2012). This allowed the SG06 core to be precisely pinned against the SG93 profile, permitting the integration of both chronologies (Bronk Ramsey et al., 2012). As such, the Lake Suigetsu dataset is composed of 808 individual ^{14}C determinations, and providing an integral component of the International ^{14}C Calibration (IntCal) dataset (Bronk Ramsey et al., 2012; Reimer et al., 2013; Staff et al., 2013).

In the summer of 2014, an additional coring campaign was undertaken at Lake Suigetsu in order to obtain more material for analysis, and to generate thin-sections for a display at a purpose-built museum in Fukui Prefecture. The coring site was located ca. 320 m east of the SG06 boreholes and was obtained using a hydro-pressure piston sampler, and a triple sampler for deeper parts. This

campaign retrieved a composite overlapping sedimentary sequence from four boreholes (E, F, G and H) and spans ca. 98 m, (ca. 25 m of extra sedimentation compared to SG06), reaching a thick basal gravel. This composite master sequence, named 'Fukui-SG14' ('SG14' in short) has been precisely tied to the SG06 composite core using 361 common marker layers (which include visible tephra layers), permitting the high-precision SG06 chronology to be transferred to the SG14 core.

2.3.3. Tephra preserved in the Suigetsu cores

Thirty-one visible ash layers (named using their SG06 Composite Depths (CD)) were originally identified in the SG06 core (Smith et al., 2011a, 2013) most of which originate from arc volcanoes south of Suigetsu and were dispersed via the prevailing westerly winds (Figure 2.11). The thickest tephra beds preserved in the Lake Suigetsu sediments are therefore correlated to well-known caldera forming eruptions (VEI 6 – 7) of the four active or buried volcanoes situated on the Kyushu CVR and SVR (Kikai, Aira, Aso and Ata). These include the K-Ah and K-Tz (Kikai caldera), AT (Aria caldera), Aso-4 and Aso-A (Aso) and Ata tephra markers (Figure 2.11; Smith et al., 2013; Albert et al., accepted). Many of the thinnest visible ash layers preserved in the SG06 core possess overlapping rhyolitic heterogeneous glass chemistries, and are correlated using trace element analysis to activity of the two most local volcanoes Daisen and Sambe volcanoes, situated on the SW Japan arc (Albert et al., 2018; Figure 2.11).

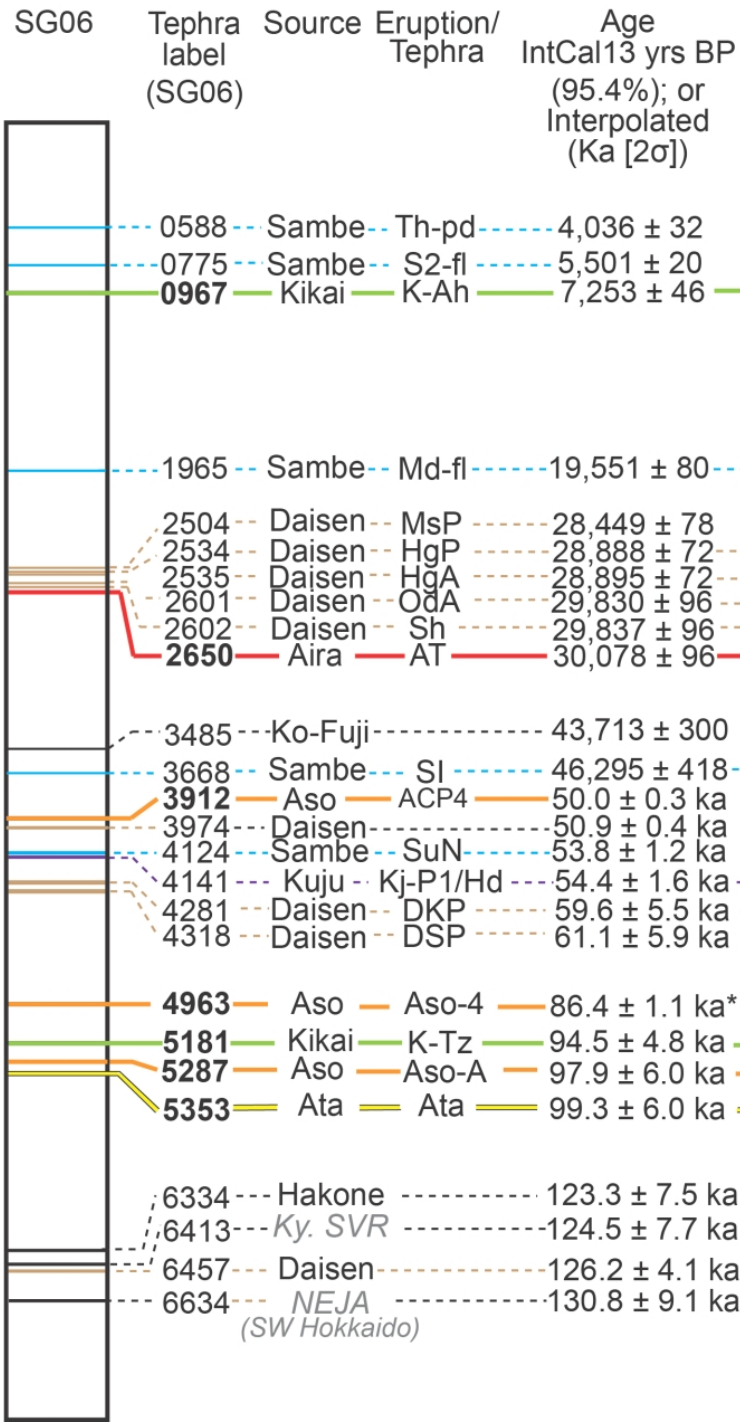


Figure 2.11: The Lake Suigetsu (SG06) visible tephrostratigraphy (Smith et al., 2013; Albert et al., 2018, accepted) (modified from Albert et al., accepted). The SG06 tephra layers are shown as IntCal13 yrs BP in the radiocarbon timeframe (95.4 % confidence interval). Beyond the annually laminated and ^{14}C dated portion of the sequence (ca. 50 k), the age-depth model is based on a linear interpolation that is anchored using an $^{40}Ar/^{39}Ar$ age of the Aso-4 eruption deposit (e.g., SG06-4963). All ages reported that are outside the ^{14}C timeframe are provided in ka with 2σ errors (equivalent to 95.4% confidence interval).

The visible tephra layers preserved in the SG06 core are dated using the Lake Suigetsu chronology presented in Bronk Ramsey et al. (2012). The sequence was modelled on to the IntCal13 timescale (Reimer et al., 2013) implementing three successive cross-referenced Poisson-process ('P_Sequence') depositional models using OxCal (ver. 4.3; Bronk Ramsey, 2008, 2017). These include 775 AMS ^{14}C dates obtained from terrestrial plant macrofossils from the upper 38 m (SG06-CD) of the SG93 and SG06 cores (Kitagawa and Van der Plicht, 1998a; 1998b, 2000; Staff et al., 2011, 2013a, 2013b) and varve counting between 12.88 and 31.67 m SG06 CD (Marshall et al., 2012; Schlolaut et al., 2012). Beyond the annually laminated and ^{14}C dated portion of the sequence the age-depth model of SG06 is based on a linear extrapolation which is anchored by deeper chronological tie points, which more recently includes the ^{40}Ar/^{39}Ar age of the Aso-4 (86.4 ± 1.1 ka; Albert et al., accepted). SG06 event-free depth(s) (EFD, ver. 29th Jan '11) are used within the age model, which excludes instantaneous deposits >5 mm in thickness, (i.e., event layers including floods, and tephra deposits) (Staff et al., 2011; Scholaut et al., 2012). All ^{14}C ages presented in this thesis, including those from the published literature (eruption ages) have been calibrated using IntCal13, and are reported with the 95.4 % probability range, unless stated otherwise.

2.4. Summary

There is significant potential for tephrochronology in the East Asian/Pacific region due to the number and widespread distribution of ash fall events across Japan. Pioneering investigations by researchers such as Machida and Arai

(1983) provide the foundation for Japanese tephrochronology, and showed that six active and buried calderas on the SVR and CVR (e.g., Kikai, Ata, Aira) were the foci of some of the largest (VEI 7 – 8) caldera-forming eruptions during the Late Quaternary. It is relatively straightforward to distinguish tephra erupted from different arc sources distributed along length of Japan using the major element glass compositions of the distal ash, however trace element compositions are required to discriminate successive eruptions of some centres. The Lake Suigetsu sedimentary archive (central Honshu) is the most precisely dated palaeoenvironmental record for Japan, and cryptotephra layers that are subsequently identified in the radiocarbon timeframe can be precisely dated using this detailed Bayesian age model.

CHAPTER 3: FIRST ARTICLE

IDENTIFICATION OF THE CHANGBAISHAN 'MILLENNIUM' (B-TM) ERUPTION DEPOSIT IN THE LAKE SUIGETSU (SG06) SEDIMENTARY ARCHIVE, JAPAN: SYNCHRONISATION OF HEMISPHERIC-WIDE PALAEOCLIMATE ARCHIVES

DANIELLE MCLEAN[a], PAUL G. ALBERT[a], TAKESHI NAKAGAWA[b,c], RICHARD A. STAFF[a], TAKEHIKO SUZUKI[d], SUIGETSU 2006 PROJECT MEMBERS[e] AND VICTORIA C. SMITH[A]

[a] *Research Laboratory for Archaeology and the History of Art, University of Oxford, Oxford, OX1 3QY, UK*

[b] *Department of Geography, University of Newcastle, Newcastle Upon Tyne, NE1 7RU, UK*

[c] *Research Centre for Palaeoclimatology, Ritsumeikan University, Kyoto, 603-8577, Japan*

[d] *Department of Geography, Tokyo Metropolitan University, Tokyo, 192-0397, Japan*

[e] www.suigetsu.org

Highlights:

- East Asian palaeoclimate record synchronised to the Greenland ice cores using tephra
- Suggests more ash layers that are common to both archives will be discovered
- Lake Suigetsu records, to date, the most southerly occurrence of the B-Tm tephra
- Identification of the B-Tm helps constrain the Holocene chronology of the SG06 core.

Abstract

The B-Tm tephra, dispersed during the highly explosive Changbaishan 'Millennium' eruption (ca. AD 940 – 950) and a key marker layer within the Greenland ice cores, has now been identified in the Lake Suigetsu (SG06) sedimentary sequence, central Japan. The major element geochemistry of the volcanic glasses within this tephra layer are compared to a new glass dataset from the distal type-locality (Tomakomai Port, Hokkaido) and other published 'Millennium' eruption/B-Tm deposits, to verify this correlation. The discovery of the B-Tm tephra in the Lake Suigetsu record provides, to date, the most southerly identification of this ash and, crucially, the first direct tie-point between this high-resolution, mid-latitude palaeoclimate archive and the Greenland ice cores. These findings present significant encouragement for on-going research into the tephrostratigraphy of East Asia, focusing on the identification of widely-dispersed tephra layers which can facilitate the synchronisation of disparate palaeoclimate archives and thus enable the assessment of spatio-temporal variations in past climatic change.

Keywords: Tephrochronology, Changbaishan 'Millennium' eruption; B-Tm tephra; Lake Suigetsu; Bayesian age-modelling

3.1. Introduction

Our understanding of past climate systems and environmental change is formed through the comparison of numerous multi-proxy palaeoenvironmental archives. Volcanic ash (tephra) horizons have proved extremely valuable for such studies as they allow disparate sedimentary records to be precisely correlated and dated (e.g., Lane et al., 2014; Albert et al., 2015; Lowe et al., 2015; Abbott et al., 2016). Such isochronous tie-points are essential to assessing the spatio-temporal variability of major climatic events and to assess abrupt and short-lived fluctuations, controlled by driving systems such as the East Asian monsoon (EAM). The EAM is of major socioeconomic importance for the ca. 30% of the global population that reside in East Asia, yet its driving complexities are poorly understood and climatically modelled, partly due to limited long-term observations (Liu and Ding, 1998; Cook et al., 2010; Ha et al., 2012). In addition, high-resolution palaeoenvironmental archives, such as the sediments of Lake Suigetsu in central Japan (Nakagawa et al., 2003; 2005), indicate that the magnitude and timing of major palaeoclimatic events do not necessarily occur synchronously with those reported in the polar and high-latitude regions. The identification of more widely-dispersed tephra layers, particularly connecting to key climate stratotypes including the Greenland ice cores, are fundamental to assessing the interplay between these regions and the forcing mechanisms of palaeo-monsoon variability.

Here we outline the recent discovery of the Baegdusan-Tomakomai (B-Tm) tephra layer within the sediments of Lake Suigetsu, and thus the first direct

tephra tie-point between this high-resolution, mid-latitude lacustrine palaeoclimate archive and the Greenland ice cores. This hemispheric-wide tephrostratigraphic marker is precisely dated using the Greenland (NS1-2011) chronology (Sigl et al., 2015) and therefore contributes a robust constraint to the Late Holocene sedimentation at Lake Suigetsu.

3.2. Background

3.2.1. The B-Tm tephra

The B-Tm tephra was dispersed during the highly explosive 'Millennium' eruption of Changbaishan (also referred to as Tianchi or Baitoushan) volcano, situated on the border between China and North Korea (128°03'E, 41°00'N) (Machida et al., 1990) (Figure 3.1.). This was one of the most violent eruptions of the past 2000 years, with a volcanic explosivity index (VEI) (Newhall and Self, 1982) of 7 (i.e., comparable to the 1815 eruption of Tambora, Indonesia).

The eruption had two explosive phases, with the initial main phase (ca. 95 % by volume) associated with a ca. 25 km-high Plinian column, producing a widespread pumice fall unit (Machida et al., 1990; Horn and Schmincke, 2000). This fall unit is overlain by partially-welded pyroclastic density current (PDC) deposits attributed to the partial collapse of the Plinian column. These deposits associated with the Plinian column and its associated PDC are comenditic in composition. Trachytic magma was erupted in a late phase of the eruption,

forming moderately welded PDC units, that post-date the comenditic fall and PDC deposits (Horn and Schmincke, 2000).

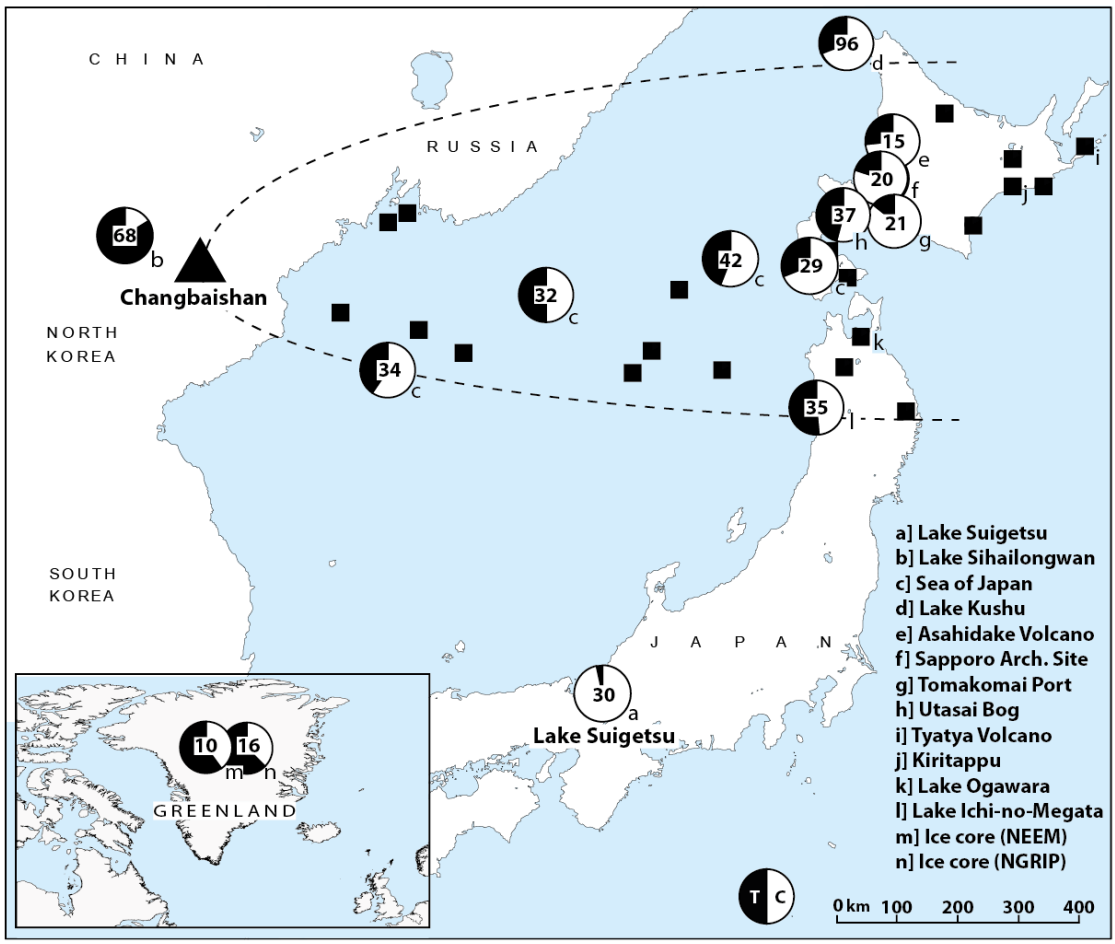


Figure 3.1. Location of Changbaishan volcano (China/North Korea border), Lake Suigetsu (central Japan) and other sites that preserve the B-Tm tephra. Pie charts indicate the proportion of trachytic (black) and comenditic (white) glasses in sites where there is sufficient major element glass data published to form a meaningful assessment of correlation (n > 10; shown in the middle of each chart; n=number of shards). Squares represent sites that report the B-Tm tephra, based on physical characteristics of the unit, but with limited or no glass geochemical data. Dispersal boundaries (dashed line) for the B-Tm as previously mapped by Machida and Arai (1983). References: (a) this study; (b) Sun et al., (2015); (c) Furuta et al., (1986); Machida and Arai, (1983); (d) Chen et al., (2016); (e) Wada et al., (2001); (f) Nakamura, (2016); (g) this study; (h) Hughes et al., (2013); (i) Nakagawa et al., (2002); (j) Nanayama et al., (2003); (k) Fukusawa et al., (1998); (l) Okuno et al., (2011); (m) Sun et al., (2014b); (n) Coulter et al., (2012).

The B-Tm tephra was named and characterised (using glass refractive indices and major element compositions) at a distal type-locality in Tomakomai Port, Hokkaido (42°37’57’’N, 141°37’47’’E; 53 km SSE of Sapporo City), where it was identified above the Tarumai-c (ca. 50 BC) and below the Tarumai-b (AD 1667) tephra layers (from the nearby Tarumae volcano) (Machida and Arai, 1983). The B-Tm tephra has since been identified in numerous marine, lacustrine and archaeological sequences across northern Japan, northeast China and coastal regions of Russia (Figure 3.1.). Moreover, a recent study found B-Tm glass shards in the Greenland ice cores, which provided a precise ice core-derived eruption age of AD 941 ± 1 (Sun et al., 2014b). ^{10}Be and ^{14}C tree-ring markers have since shown that there is a seven-year offset in the Greenland ice core (GICC05) timescale, so this age for the B-Tm eruption has been corrected to AD 946-947 (NS1-2011; Sigl et al., 2015).

3.2.2. Lake Suigetsu (SG06) archive

The Lake Suigetsu (Figure 3.1; 35°35'0"N; 135°53'0"E) SG06 sediment core provides a high-resolution palaeoenvironmental record from Honshu Island, central Japan (e.g. Tyler et al., 2010; Kossler et al., 2011; Saito-Kato et al., 2013; Schlolaut et al., 2014). The 73.19 m-long composite core was extracted as part of the ‘Suigetsu Varves 2006’ project, and provides a continuous record of sedimentation spanning the last ca. 150 ka (Nakagawa et al., 2012). The sequence is annually laminated (varved) between ca.10 and 70 ka and has been extensively radiocarbon (^{14}C) dated and varve counted to generate a high-

resolution chronology (Staff et al., 2011; Bronk Ramsey et al. 2012; Marshall et al. 2012; Schlolaut et al. 2012) for this palaeoenvironmental record.

Hitherto, 31 visible tephra layers from SG06 have been identified and characterised (using major element geochemical analysis), and provide a detailed record of Japanese and Korean eruption events (Smith et al., 2013). Due to the prevailing westerlies, tephra is largely dispersed northeast across this region. As Changbaishan is located northwest of Lake Suigetsu, coupled with the strong easterly dispersal of the eruptive plume implied from ash thicknesses (Figure 3.1.), the presence of a B-Tm ash layer in the sediments was previously considered unlikely. However, given its widespread distribution and recent ultra-distal identification in the Greenland ice cores (Figure 3.1.), the Lake Suigetsu sediments were carefully re-examined in order to attempt to identify this key tephra marker.

3.3. Materials and Methods

3.3.1. Sampling and laboratory procedures

A new, thin ash layer (<1 mm) was observed within overlapping core sections of the SG06 sequence at a composite depth (CD) of 225.5 cm (the CD was determined using the 20 April 2015 version of the correlation model; see Nakagawa et al., 2012 for more details). Herein, this tephra is labelled as SG06-0226. A subsample was extracted from core section D-01-104.7 cm and wet sieved using distilled water through a 25 μm mesh. Microscopic examination identified an abundant concentration of colourless glass shards with a distinct,

highly vesicular morphology. These were handpicked using a micromanipulator (Lane et al. 2014) and mounted in epoxy resin for geochemical analysis. To identify the stratigraphic positioning of the peak, cryptotephra analysis was performed in sediments above and below the layer. A sample of the B-Tm tephra from its type-locality at Tomakomai Port was also prepared for geochemical analysis to verify the correlation.

3.3.2. Compositional analysis

Major and minor element glass compositions were measured using a JEOL-8600 wavelength-dispersive electron microprobe (WDS-EPMA) at the Research Laboratory for Archaeology and History of Art, University of Oxford. All analyses were performed using an accelerating voltage of 15kV, beam current of 6nA and 10 μm-diameter beam. The electron microprobe was calibrated using a suite of mineral standards, and the PAP absorption correction method was used for quantification. Analyses of these secondary standards lie within the standard deviation of the preferred values and are presented in the Supplementary Material (Appendix A).

3.4. Results and Discussion

3.4.1. Geochemical results

The geochemical analyses of glass shards from the SG06-0226 layer and from the B-Tm type-locality (Tomakomai Port) are shown in Table 3.1 and selected bi-plots in Figure 3.2. Volcanic glasses erupted from Changbaishan volcano can be easily discriminated from those originating from volcanic centres in Russia (Kamchatka), South Korea and along the Japanese arc (Figure 3.2a). The eruption that produced the B-Tm tephra tapped both comenditic and trachytic magma batches, with particularly alkali-enriched compositions. The SG06-0226 dataset includes two outliers, which have the same composition as other shards present in low concentrations throughout the core and are considered to be background material. These outlier glass compositions are chemically distinct from the B-Tm tephra and clearly erupted from a Japanese volcano (Figure 3.2a), so are therefore not discussed further.

The SG06-0226 glasses are compositionally heterogeneous, with SiO_2 ranging from 65.14 to 75.49 wt.%, CaO from 0.18 to 1.48 wt.%, FeO^T (all Fe as FeO) from 3.72 to 4.55 wt.% and K_2O from 4.21 to 6.15 wt.% (n = 30). The deposit is dominated by a comenditic glass component (Figure 3.2.), with a single glass shard showing a trachytic composition. The comenditic glasses contain a lower Al_2O_3 (ca. 10 wt.%) and FeOt (ca. 4.0 wt.%) content compared to the single trachytic glass shard (Figure 3.2b).

Table 3.1. Results of the WDS-EPMA normalised glass compositions of the SG06-0226 tephra layer and of the B-Tm distal type-site deposits at Tomakomai Port.

Sample	SiO_2	TiO_2	Al_2O_3	FeO	MnO	MgO	CaO	Na_2O	K_2O	P_2O_5	Cl	Analytical total
SG06-0226	74.96	0.18	10.23	3.99	0.12	0.00	0.22	5.34	4.46	0.00	0.51	97.99
	74.95	0.26	10.14	3.97	0.09	0.00	0.24	5.43	4.40	0.00	0.52	97.90
	74.83	0.26	10.30	4.20	0.00	0.00	0.23	5.29	4.41	0.00	0.48	98.03
	75.14	0.19	10.17	4.02	0.06	0.02	0.23	5.34	4.35	0.02	0.46	97.31
	75.06	0.18	10.18	4.02	0.04	0.00	0.22	5.45	4.33	0.02	0.50	97.38
	74.89	0.23	10.32	3.97	0.14	0.00	0.23	5.51	4.21	0.01	0.49	97.36
	75.17	0.24	10.18	3.95	0.06	0.07	0.23	5.19	4.43	0.00	0.48	96.97
	74.84	0.21	10.22	3.92	0.06	0.00	0.18	5.71	4.40	0.00	0.46	97.35
	74.57	0.19	10.28	4.27	0.04	0.00	0.18	5.51	4.44	0.02	0.50	97.59
	74.85	0.19	10.53	3.90	0.12	0.00	0.21	5.33	4.38	0.02	0.47	97.15
	74.84	0.19	10.22	4.05	0.09	0.03	0.21	5.53	4.31	0.00	0.50	96.91
	74.65	0.28	10.28	4.19	0.17	0.01	0.20	5.42	4.27	0.01	0.52	96.88
	75.20	0.23	10.19	4.19	0.11	0.00	0.24	5.12	4.22	0.01	0.49	96.17
	74.87	0.29	10.39	3.98	0.13	0.00	0.29	5.19	4.35	0.01	0.50	96.56
	74.67	0.23	10.31	4.10	0.04	0.00	0.24	5.49	4.43	0.00	0.48	96.72
	74.96	0.19	10.22	3.99	0.13	0.08	0.19	5.48	4.25	0.00	0.50	96.33
	74.89	0.23	10.28	4.06	0.06	0.06	0.22	5.42	4.30	0.00	0.48	96.39
	74.80	0.24	10.30	4.27	0.04	0.00	0.23	5.33	4.27	0.00	0.50	96.42
	75.04	0.17	10.19	4.20	0.09	0.03	0.21	5.20	4.41	0.00	0.46	95.89
	75.49	0.20	10.20	3.72	0.08	0.05	0.22	5.09	4.44	0.01	0.48	95.12
	74.80	0.23	10.39	3.91	0.11	0.06	0.24	5.46	4.27	0.00	0.52	95.83
	74.94	0.25	10.25	4.28	0.09	0.01	0.21	5.26	4.21	0.00	0.52	95.38
	75.08	0.20	10.24	4.05	0.09	0.00	0.19	5.27	4.45	0.00	0.44	94.53
	75.06	0.20	10.25	4.20	0.01	0.01	0.21	5.17	4.42	0.00	0.47	94.55
	74.61	0.27	10.43	3.73	0.09	0.00	0.23	5.62	4.44	0.02	0.56	94.93
	74.55	0.26	10.30	4.13	0.17	0.00	0.22	5.36	4.50	0.00	0.51	94.98
	74.61	0.23	10.49	4.06	0.11	0.02	0.23	5.16	4.55	0.00	0.54	94.05
	74.88	0.18	10.23	4.02	0.00	0.03	0.23	5.45	4.48	0.00	0.51	93.48
	74.73	0.20	10.16	4.17	0.09	0.05	0.23	5.34	4.48	0.03	0.52	93.22
	65.14	0.57	16.10	4.55	0.15	0.28	1.48	5.41	6.15	0.08	0.10	96.87
Average (n = 30)	**74.57**	**0.23**	**10.47**	**4.07**	**0.09**	**0.03**	**0.26**	**5.36**	**4.43**	**0.01**	**0.48**	
σ	**1.79**	**0.07**	**1.07**	**0.17**	**0.05**	**0.05**	**0.23**	**0.15**	**0.34**	**0.02**	**0.08**	
SG06-0226 outliers	77.50	0.18	12.61	1.22	0.10	0.12	1.11	3.75	3.27	0.02	0.12	94.00
	73.86	0.48	12.97	2.45	0.11	0.50	1.95	3.08	4.35	0.09	0.14	98.28
Tomakomi Port	74.80	0.18	10.46	3.98	0.07	0.02	0.25	5.36	4.31	0.00	0.59	93.49
	75.27	0.22	10.65	3.92	0.05	0.00	0.25	4.80	4.31	0.01	0.52	96.91
	74.51	0.23	10.65	4.08	0.06	0.00	0.31	5.29	4.36	0.04	0.47	97.88
	75.13	0.18	10.51	4.08	0.08	0.05	0.27	4.98	4.26	0.00	0.47	99.41
	67.33	0.44	15.00	4.65	0.15	0.12	1.20	5.90	4.98	0.06	0.19	98.78
	74.88	0.21	10.51	3.87	0.12	0.02	0.25	5.28	4.37	0.00	0.50	97.90
	74.97	0.23	10.58	3.98	0.04	0.02	0.23	5.25	4.19	0.03	0.48	97.73
	74.41	0.25	10.86	3.85	0.11	0.00	0.30	5.07	4.62	0.02	0.52	97.82
	74.47	0.23	11.08	3.90	0.05	0.01	0.33	5.09	4.31	0.01	0.50	98.54
	75.08	0.20	10.59	3.97	0.05	0.00	0.23	5.10	4.21	0.01	0.55	96.35
	74.67	0.17	10.35	4.26	0.07	0.01	0.32	5.29	4.29	0.00	0.59	95.24
	74.10	0.28	10.90	4.14	0.00	0.01	0.28	5.34	4.44	0.03	0.47	98.96
	74.53	0.26	10.72	3.99	0.05	0.04	0.22	5.20	4.49	0.02	0.49	97.22
	74.46	0.25	10.54	4.11	0.06	0.00	0.30	5.31	4.41	0.02	0.56	93.69
	67.05	0.36	15.02	4.62	0.18	0.06	1.05	6.04	5.43	0.03	0.17	98.60
	69.91	0.30	13.66	4.26	0.04	0.00	0.59	5.81	5.12	0.00	0.31	94.54
	73.95	0.19	10.68	4.09	0.10	0.01	0.29	5.82	4.37	0.00	0.51	97.36
	75.01	0.18	10.40	4.05	0.09	0.03	0.26	5.08	4.41	0.01	0.48	96.71
	74.68	0.20	10.42	4.11	0.09	0.01	0.24	5.27	4.51	0.00	0.46	97.60
	74.62	0.20	10.35	3.96	0.07	0.04	0.24	5.51	4.50	0.00	0.51	96.90
	74.20	0.25	10.71	4.12	0.04	0.01	0.29	5.44	4.49	0.00	0.47	97.79
Average (n = 21)	**73.72**	**0.24**	**11.17**	**4.09**	**0.07**	**0.02**	**0.37**	**5.34**	**4.49**	**0.01**	**0.47**	
σ	**2.43**	**0.07**	**1.45**	**0.21**	**0.04**	**0.03**	**0.26**	**0.32**	**0.31**	**0.02**	**0.11**	

The data have been filtered to remove analyses of a <93% analytical total; see supplementary material for raw dataset and secondary standards

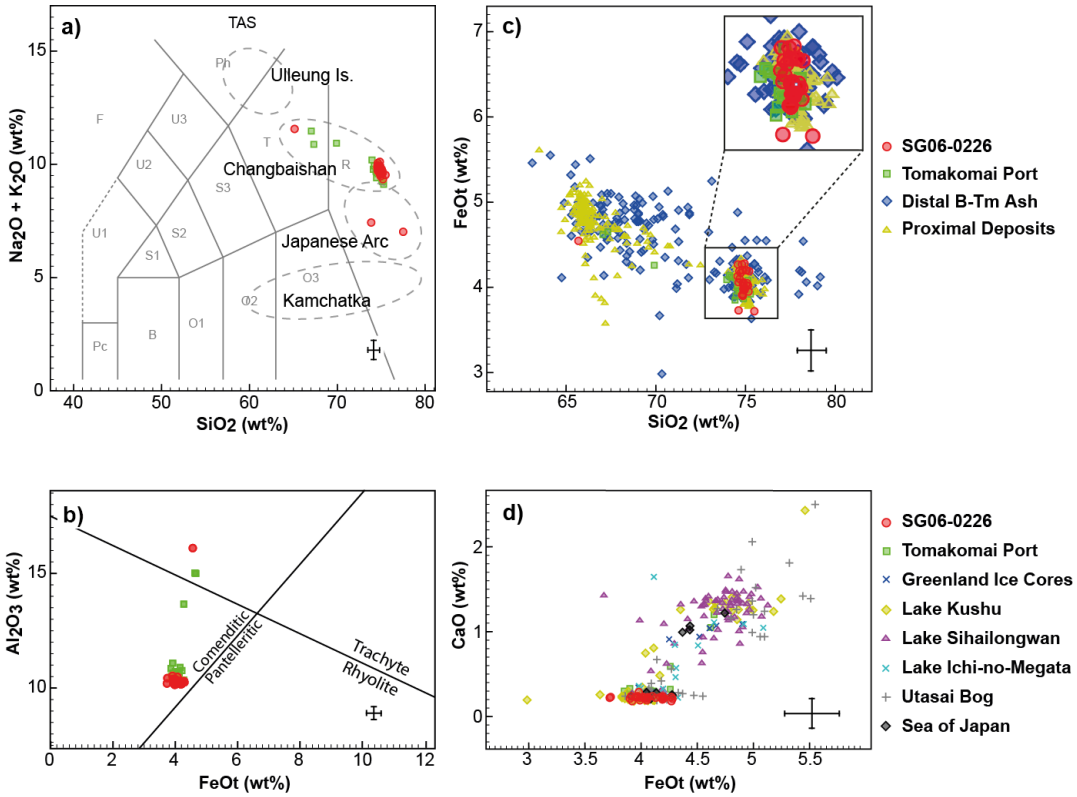


Figure 3.2. Major element glass compositions of the SG06-0226 tephra (red circles) and the B-Tm type-locality from Tomakomai Port (green squares) (a) Total alkalis versus silica plot (TAS; Le Bas et al., 1989) showing the glass composition of Changbaishan tephra relative to those from Ulleung Island (Smith et al., 2013), volcanoes in the Japanese arc (Smith et al., 2013), and Kamchatka (Kyle et al. 2011); (b) peralkaline classification diagram (McDonald, 1974); (c) the composition of glass shards from proximal Changbaishan 'Millennium' eruption deposits (Guo et al., 2002; Zou et al., 2010; Sun et al., 2014b; 2015; Chen et al, 2016*)* and composite published distal B-Tm data (Furuta et al., 1986; Okuno et al., 2011; Coulter et al., 2012; Hughes et al., 2013; Sun et al., 2014b; 2015; Chen et al., 2016); (d) the glass composition of distal B-Tm units compared to that of the SG06-0226 glasses. Error bars represent 2 x standard deviation of repeat analyses of the StHs6/80-G MPI-DING standard glass.

The glass compositions of SG06-0226 are consistent with the new glass data from the B-Tm type-locality at Tomakomai Port, confirming they are the same tephra. The new Tomakomai Port dataset also contains compositions that lie on a mixing line between the comenditic and trachytic end members of the SG06-

0226 tephra, which suggests that the two distinct magma batches were in contact before the eruption.

The geochemistry of the SG06-0226 and Tomakomai Port glasses are also consistent with published data for proximal Changbaishan 'Millennium' eruption deposits (Figure 3.2c) and other distal/ultra-distal B-Tm glass compositions, including those preserved in the Greenland ice cores (Figure 3.2d). The glass compositions of the tephra at these distal sites provide information on the spatial distribution of the different phases of the Changbaishan 'Millennium' eruption (Figure 3.1.). Given that the trachytic compositions were erupted in the late PDC phase of the eruption, the dispersal of glass with such compositions to the distal sites must have been via the plume that lofted off the top of the PDCs, i.e., a co-PDC plume. The compositions from the sites directly to the east of Changbaishan are predominately comenditic (ca. 50 – 80 %), and therefore mostly associated with the Plinian column or the co-PDC plume associated with the PDC generated during the collapse of the Plinian column, or both. These sites also have a trachytic component (ca. 15 – 50 %) implying that the dispersal axis for the late co-PDC plume was also to the east. The compositions of glass shards from sites northwest of the vent are mostly trachytic, implying that these glasses were deposited from the co-PDC plume. Glass shards in SG06-0226 are almost entirely comenditic in composition and associated with the Plinian column and the co-PDC associated with its collapse, and indicate that the late phase trachytic co-PDC plume did not disperse tephra towards the south. The trachytic compositions are more dominant in the Greenland ice cores implying that the tephra was mostly transported ultra-distally (ca. 7,000

km from vent) via the co-PDC plume. This inference is consistent with some studies of other large explosive eruptions that show that the ultra-distal transport of tephra is largely associated with co-PDC plumes (e.g., Campanian Ignimbrite eruption, Smith et al. 2016; Younger Toba Tuff, Costa et al., 2014).

3.4.2. Age-depth modelling

The age model for the SG06 sedimentary sequence (Staff et al., 2011) was constructed using a Bayesian Poisson-process '*P_Sequence'* depositional model in OxCal (ver. 4.2; Bronk Ramsey 2008; 2016), and the IntCal13 calibration curve (Reimer et al., 2013) (Figure 3.3.). This model includes 124 AMS ^{14}C dates obtained from terrestrial plant macrofossils from the non-varved Holocene part of the core (Staff et al., 2011). An age of (cal.) AD 880-956 (95.4% confidence) was obtained for the SG06-0226 tephra, consistent with other published dates for the 'Millennium' eruption (see Sun et al., 2014a). The lack of varved sedimentation throughout the late Holocene means that this SG06-derived age is not as precise as those reported elsewhere.

We are, however, able to import the NS1-2011 age of AD 947 ± 1 (Sigl et al., 2015) into the Lake Suigetsu age model using tephrochronology, thus further constraining the chronology of the upper part of SG06. This imported ice-core-based age will significantly improve the chronological analysis of proxy palaeoenvironmental data and any subsequent cryptotephra layers identified in the Suigetsu sediments within this timeframe.

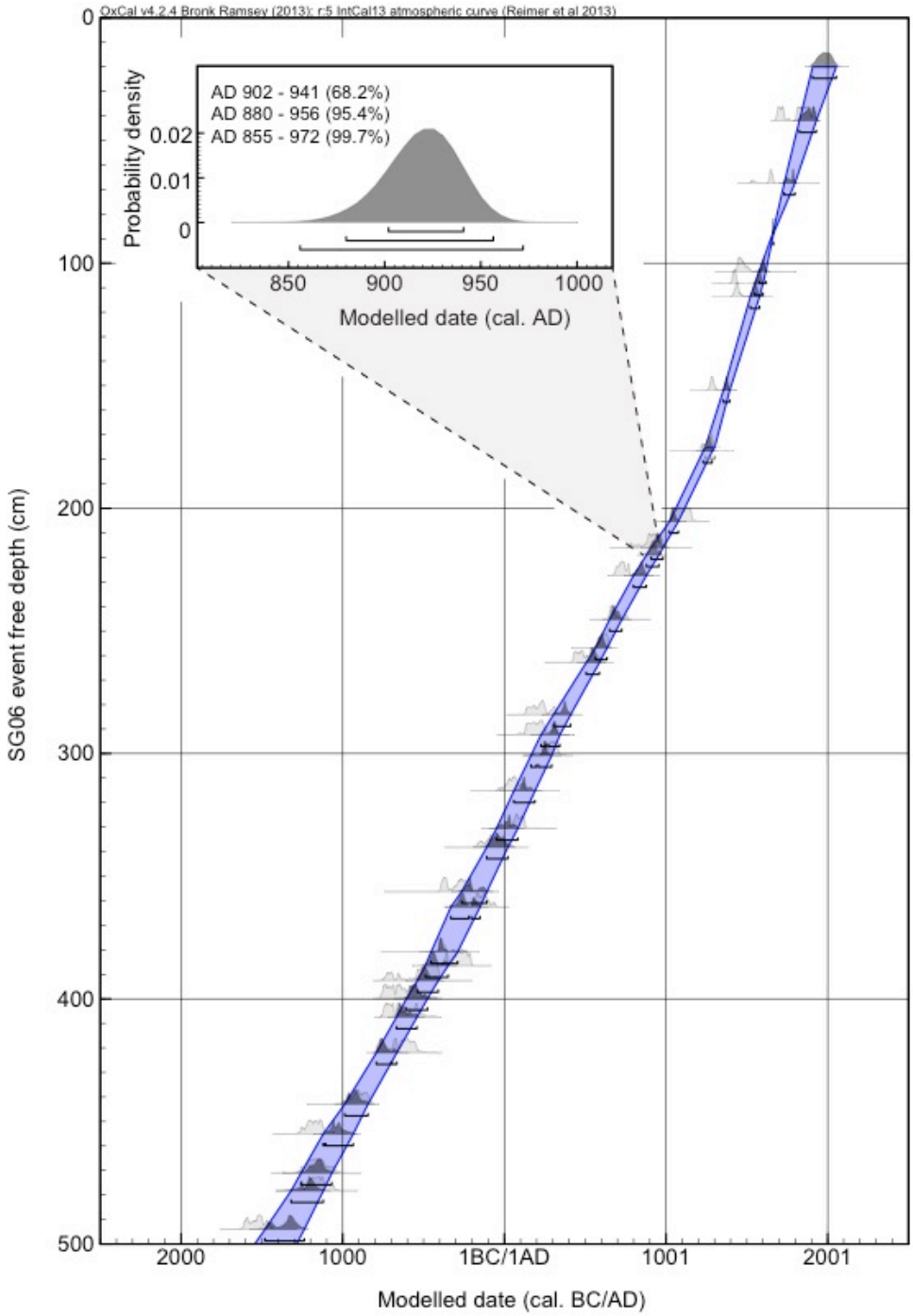


Figure 3.3. The age-depth model for the upper 5 m of the SG06 core (Staff et al., 2011). The blue envelope represents the 95.4% probability range. Inset: posterior probability density function (PDF) generated for the deposition of the SG06-0226 tephra, located at 219.1 cm event-free CD (determined using 29 Jan. 2011 version of the event-free depth model). The bars underlying the PDF represent the 68.2%, 95.4% and 99.7% probability ranges, respectively.

3.5. Implications

3.5.1. Palaeoenvironmental potential for the B-Tm tephra

The stratigraphic positioning of the B-Tm tephra holds significant potential to help constrain late Holocene climatic variations, such as the onset of the Medieval Warm Period (ca. AD 900 – 1300). Although this warming episode has been identified in numerous global paleoclimate proxy records, its spatio-temporal variability and regional magnitude is intensely debated (Broecker, 2001; Hunt, 2006). Once high-resolution palaeoenvironmental proxy data from Lake Suigetsu are obtained from this interval, the dynamics of such rapid and short-lived climatic episodes can be evaluated. Our discovery may also encourage others to look for the B-Tm tephra in other key palaeoenvironmental records, including sites further south.

3.5.2. Future potential

This study provides the first direct tephra tie-point between a high-resolution, mid-latitude palaeoclimate archive (Lake Suigetsu sediments) and the Greenland ice cores, a major goal of research communities examining palaeoenvironmental change (e.g. INTIMATE; Lowe et al. 2015; Blockley et al., 2014). This discovery therefore provides significant encouragement for the on-going research into refining the tephrostratigraphy of East Asia, research which aims to establish more hemispheric-wide tephra tie-points suitable for the synchronisation of key palaeoclimate archives.

Acknowledgements

This work was supported by the UK Natural Environmental Research Council (NERC; grants: NE/D00289/1 and NE/F003048/1), the Deutsche Forschungsgemeinschaft (DFG; grant: TA-540/3-1) and MEXT-Japan KAKENHI (grant: 21101002 and 15H02143), which funded the Suigetsu Varves 2006 Project. DM is funded by NERC (grant: NE/L002612/1) and part of the Environmental Research Doctoral Training Program at the University of Oxford. PGA and RAS are supported by Early Career Fellowships from the Leverhulme Trust. The authors would like to thank: Professor Hiroshi Machida for providing the B-Tm type-locality sample from Tomakomai Port; and David Lowe and an anonymous reviewer for comments.

See Appendix A for Supplementary Material

CHAPTER 4: SECOND ARTICLE

INTEGRATING THE HOLOCENE TEPHROSTRATIGRAPHY FOR EAST ASIA USING A HIGH-RESOLUTION CRYPTOTEPHRA STUDY FROM LAKE SUIGETSU (SG14 CORE), CENTRAL JAPAN

DANIELLE MCLEAN[a], PAUL G ALBERT[a], TAKESHI NAKAGAWA[b], TAKEHIKO SUZUKI[c], RICHARD A STAFF[a,d], KEITARO YAMADA[e], IKUKO KITABA[b], TSUYOSHI HARAGUCHI[f], JUNKO KITAGAWA[g], SG14 PROJECT MEMBERS[h] AND VICTORIA C SMITH[a]

[a] *Research Laboratory for Archaeology and the History of Art, University of Oxford, Oxford, OX1 3TG, UK*

[b] *Research Centre for Palaeoclimatology, Ritsumeikan University, Kyoto, 603-8577*

[c] *Department of Geography, Tokyo Metropolitan University, Tokyo, 192-0397, Japan*

[d] *Scottish Universities Environmental Research Centre, University of Glasgow, East Kilbride, G75 0QF, UK*

[e] *Institute for Geothermal Sciences, Kyoto University, Kusatsu, 525-8577, Japan*

[f] *Osaka City University, Osaka, 558-8585, Japan*

[g] *Fukui Prefectural Satoyama-Satoumi Research Institute, Wakasa, 919-1331 Japan*

[h] *www.suigetsu.org*

Highlights:

- First detailed Holocene cryptotephra study in a productive volcanic arc setting
- Integrated Holocene tephrostratigraphic record of key East Asian isochrons
- Improved chronology of many widespread tephra layers
- New constraints on volcanism from back-arc volcanoes (Changbaishan & Ulleungdo)
- Reveals isochrons than can be used to synchronise to the SG14 record

Abstract

Tephra (volcanic ash) layers have the potential to synchronise disparate palaeoenvironmental archives on regional to hemispheric scales. Highly productive arc regions, like those in East Asia, offer a considerable number of widespread isochrons, but before records can be confidently correlated using these layers, a refined and integrated framework of these eruptive events is required. Here we present the first high-resolution Holocene cryptotephra study in East Asia, using the Lake Suigetsu sedimentary archive in central Japan. The Holocene tephrostratigraphy has been extended from four to twenty ash layers using cryptotephra extraction techniques, which integrates the deposits from explosive eruptions from North Korea/China, South Korea and along the Japanese arc. This Lake Suigetsu tephrostratigraphy is now the most comprehensive record of East Asian volcanism, and the linchpin site for correlating sequences across this region. Major element glass geochemical compositions are presented for the tephra layers in the sequence, which have been compared to proximal datasets to correlate them to their volcanic source and specific eruptions. This study has significantly extended the ash dispersal of many key Holocene marker layers, and has identified the first distal occurrence of isochrons from Ulleungdo and Changbaishan volcanoes. Utilising the high-precision Lake Suigetsu chronology, we are able to provide constrained eruption ages for the tephra layers, which can be transferred into other site-specific age models containing these markers. This new framework indicates that several isochrons stratigraphically bracket abrupt climate intervals

in Japan, and could be used to precisely assess the regional and hemispheric synchronicity of these events.

Keywords: Tephrochronology, Cryptotephra, Lake Suigetsu, Japan, Eastern Asia, Changbaishan, Ulleungdo, Holocene, Palaeoclimatology, Lacustrine

4.1. Introduction

The importance of palaeoenvironmental archives for our understanding of abrupt climate change is well recognised, but it is essential that these records can be precisely integrated and dated to assess their ultimate drivers operating across large regional scales (e.g., the East Asian Monsoon; EAM). Widely dispersed volcanic ash (tephra) layers preserved in sedimentary sequences can provide ideal isochronous markers to facilitate high-precision correlations (tephrostratigraphy) and transfer absolute ages (tephrochronology) across palaeoclimate records (e.g., Albert et al*.,* 2013; Lane et al*.,* 2014; Abbott et al*.,* 2016; Alloway et al*.,* 2017). These markers can facilitate the assessment of the spatio-temporal variability of abrupt climate change, particularly when they bracket the onset or duration of these events (e.g., Lane et al*.,* 2013). Deciphering the regional and global synchronicity of these changes is fundamental for our understanding of the forcing mechanisms and interplay between large-scale oceanic and atmospheric systems.

In order to integrate and compare palaeoenvironmental records, regional tephrostratigraphic frameworks are established, which connect sites using

widespread, and well-characterised marker layers (e.g., Shane et al., 2006; Davies et al., 2014; Lowe et al., 2015). These regional frameworks are underpinned by key reference sites (often termed *tephrostratotypes*), which offer both detailed tephrostratigraphic sequences, and a precise chronology of eruptive events, usually from a range of volcanic sources (e.g., the Greenland ice cores; Abbott and Davies, 2012; Bourne et al., 2015). Both the number and geographical footprint of these visible ash layers can be significantly extended by examining sedimentary successions for the presence of non-visible (cryptotephra) ash layers (e.g., Wastegard, 2002; Lane et al., 2015; Albert et al., 2015; Mackay et al., 2016), which are essential to identify smaller magnitude and/or more distal occurrences of the largest eruptions.

Pioneering investigations by researchers such as Machida and Arai (1983) provide the foundation for Japanese tephrochronology, and have established a complex catalogue (via detailed mapping of visible ash deposits) of the succession and dispersal characteristics of the large explosive eruptions that occurred during the Quaternary (compiled in Machida and Arai, 2003). In other parts of the world, studies like those undertaken by the RESET ('Response of Human to Abrupt Environmental Transitions') project, centred in continental Europe and across the Mediterranean Sea (see Lowe et al., 2015), have further refined tephrostratigraphic frameworks through detailed analysis of key eruption sequences and at distal sites. In the RESET project, all tephra deposits were sampled and geochemically fingerprinted from proximal eruptive units close to their source, and detailed cryptotephra studies were undertaken in distal sedimentary sequences. These analyses were able to: i) incorporate new and

lower magnitude events into the master European tephrostratigraphic framework (e.g., Albert et al., 2013), ii) resolve the stratigraphic position of eruptions from different volcanic sources that were closely spaced in time (e.g., Karkanas et al., 2015), iii) establish which eruptions have a diagnostic geochemical signature for reliable tephra correlations (e.g., Smith et al., 2011b), (iv) identify erroneous tephra correlations (e.g., Albert et al., 2015), and v) extend the known geographical footprint of ash fallout from individual eruptions, and therefore widen the area over which the key isochrons could be used. This detailed work has revised and verified a comprehensive framework (Lowe et al., 2015) that can be used to robustly integrate key palaeoenvironmental and archaeological archives across the region surrounding the Mediterranean Sea, and test long-standing questions using the high-resolution chronology (e.g., Rohling et al., 2009; Grant et al., 2012; Lowe et al., 2012; Barton et al., 2015).

This project aimed to refine and augment the Holocene tephrostratigraphic framework for the East Asian/Pacific region using a similar methodology to that employed by the RESET project (outlined above). Here, the sediments of Lake Suigetsu (SG14 core; Figure 4.1.) were targeted for detailed cryptotephra analysis, since it currently provides the most precisely dated Holocene sedimentary record from Japan (see Nakagawa et al., 2012; Staff et al., 2011). The objectives of this research were to: i) verify the successful application of cryptotephra analysis from a lake located along the highly productive volcanic arc, ii) chemically characterise and date identified tephra isochrons in order to correlate them to their volcanic source and, where possible, specific eruptions,

and iii) use the Holocene tephrostratigraphic record from Lake Suigetsu to develop an integrated framework for the East Asian/Pacific region.

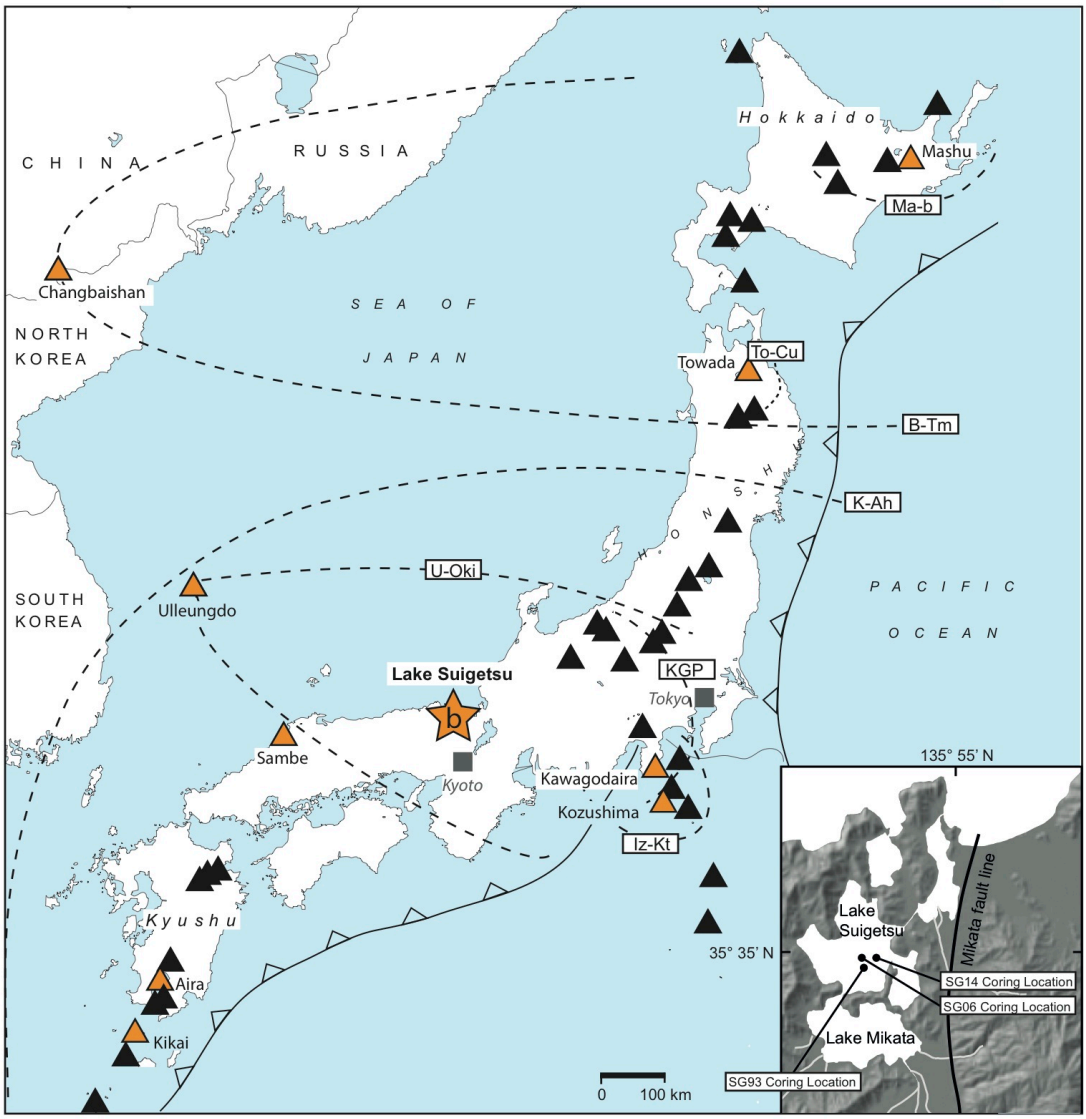


Figure 4.1. (a) Volcanoes in Japan, North Korea/China (Changbaishan volcano) and South Korea (Ulleungdo volcano) known to have been active during the Holocene (data obtained from VOGRIPA, 2016). Large caldera volcanoes in Japan, which are the sources of the most explosive eruptions, are concentrated on the island of Kyushu (south) and Hokkaido (north). Volcanoes mentioned within the text are coloured orange, and a star denotes the location of the study site, Lake Suigetsu. Dispersal boundaries (dashed lines) are shown for Holocene visible tephra layers (white boxes) Ma-b (Mashu volcano), B-Tm (Changbaishan), Iz-Kt (Kozushima), KGP (Kawagodaira), To-Cu (<10 cm isopach, Towada), K-Ah (Kikai) and U-Oki (Ulleungdo), as mapped by Machida and Arai, 1983. (b) Location of the five Mikata lakes, including the study site Lake Suigetsu, which are situated west of the Mikata fault line. The positions of coring campaigns SG93, SG06 and SG14 are also marked on Lake Suigetsu (modified after Nakagawa et al., 2005).

4.1.1. Tephra dispersal in and around Japan

Over 130 volcanic centres are distributed along the length of the Japanese arc (Figure 4.1.). These centres have been highly productive during the Late Quaternary, with numerous large caldera-forming eruptions (particularly on Hokkaido and the Kyushu Islands; Figure 4.1.) producing widespread tephra dispersal across the East Asian/Pacific region (Machida and Arai, 2003). Due to the prevailing westerly winds, ash from the explosive back-arc volcanism in South Korea (Ulleungdo volcano) and North Korea/China (Changbaishan) has also blanketed Japan and the surrounding seas numerous times over the Quaternary (Machida and Arai, 2003; Lim et al., 2013; Figure 4.1.).

During the Holocene three key widespread marker beds are commonly identified in sedimentary sequences in and around Japan, and are named using their source volcano and distal tephra type-site, a common practice in Japanese tephrostratigraphy studies. These include the Baegdusan-Tomakomai (B-Tm), Kikai-Akahoya (K-Ah) and Ulleungdo-Oki (U-Oki) ash (Machida and Arai, 1983). The B-Tm is the tephra deposit from the 'Millennium' eruption of Changbaishan, and has been recently dated to AD 946 (Oppenheimer et al., 2017; Hakozaki et al., 2017). The K-Ah tephra was dispersed from the now largely sub-marine Kikai caldera, located 50 km south of Kyushu. The most precise date for this eruption (7,303 – 7,165 cal. yrs BP) was obtained from the Lake Suigetsu SG06 sediment core (Smith et al., 2013). The U-Oki tephra is from Ulleungdo Island (South Korea), which is located in the Sea of Japan, and corresponds to the U-4 proximal eruptive unit (Smith et al., 2011a). Lake Suigetsu, situated in central

Japan, is the only archive to currently record all three of these key Holocene marker beds (Figure 4.1; Smith et al., 2011a; Smith et al., 2013; McLean et al., 2016).

In the past, the majority of tephra correlations in and around Japan are based on the physical characteristics of the deposit, i.e., refractive indices, layer thickness, grain-size and modal mineralogy. However, it is essential that tephra layers are geochemically characterised as accurately as possible to ensure unequivocal correlations across the proximal and distal settings. Volcanic glass compositions are routinely employed for robust tephra correlation around the world, including New Zealand (e.g., Froggat, 1983; Shane and Smith, 2000), Europe (e.g., Tomlinson et al., 2015), North America (e.g., Smith and Westgate, 1968; Sarna-Wojcicki et al*.,* 1987) and South America (e.g., Fontijn et al., 2016), but are only recently being utilised in Japan (e.g., Moriwaki et al., 2011; Okuno et al., 2011; Smith et al., 2013; Chen et al., 2016). Comprehensive glass datasets are yet to be obtained from many eruptive centres in this region, particularly those in central and southern Japan, which means that many distal correlations remain unconfirmed (e.g., Smith et al., 2013).

4.1.2. Constraining Holocene climate intervals using tephra layers

Palaeoenvironmental change during the Holocene can provide an improved perspective upon the causal mechanisms and drivers of climate change across the globe (Wanner et al., 2008). In the East Asian/Pacific region, the Holocene climate has been shown to vary considerably, with several abrupt (centennial-

scale) warming and cooling phases, likely caused by fluctuations in the behaviour of the East Asian Monsoon (EAM; Wang et al., 2005; Sagawa et al., 2014; Tada and Murray, 2016). Despite the regional and global importance of this climate system, its causal relationship to both external (e.g., orbital, solar and volcanic) and internal forcing remains poorly understood (Morrill et al., 2002; Park, 2017). This is partly due to the inherent difficulties in precisely comparing the distant and diverse palaeoclimate archives across the monsoon region.

Tephra layers can be used to precisely integrate disparate palaeoenvironmental records across the migration paths of the EAM (e.g., B-Tm tephra), and develop a more comprehensive picture of the spatio-temporal changes of this system. Visible ash layers are commonly recognised in key marine (e.g., Furuta et al., 1986; Park et al., 2003; Sagawa et al., 2014; Chun et al., 2007; Aoki et al., 2008; Ikehara et al., 2011) and terrestrial (e.g., Domitsu et al., 2002; Kumon et al., 2003; Nagahashi et al., 2004; Okuno et al., 2011; Smith et al., 2013) sedimentary archives across this region, but very few have thus far been detected over wide areas, prohibiting the synchronisation of these records, and few are adequately dated to improve site-specific age models. No detailed cryptotephra investigations have been undertaken to explore the true dispersal potential of key ash layers in Japan, however tephra from East Asia has been transported and deposited as isochrons across the northern hemisphere, with recent discoveries in the Greenland ice cores (Sun et al., 2015a; Bourne at al. 2016), and possibly as far as the North American east coast (Mackay et al., 2016). This provides substantial encouragement that additional cryptotephra

investigations in the East Asian/Pacific region will resolve new isochrons suitable for regional and hemispheric-scale correlations.

4.2. Study site

4.2.1. Lake Suigetsu sediment record

The Lake Suigetsu sedimentary archive, central Japan (Figure 4.1.) has numerous characteristics that make it suitable for detailed cryptotephra analysis and to provide a comprehensive Holocene tephrostratigraphic framework for the East Asian/Pacific region.

1. The visible tephrostratigraphic record (spanning ca. 150 ka) confirms that the lake is ideally situated to record explosive eruptions from multiple volcanic sources from across Japan, South Korea and North Korea/China (Smith et al., 2011a; Smith et al., 2013; McLean et al., 2016).
2. Suigetsu is a tectonic lake, adequately situated away from the large calderas in Hokkaido and Kyushu, so is unlikely to be inundated with locally sourced volcanic products (i.e., background glasses) that could obscure the cryptotephra record.
3. No rivers flow directly into Lake Suigetsu, which mean that the basal sediments are rarely disturbed by inflows from the immediate lake surroundings. The sedimentation is relatively fast with the accumulation of ca. 12 m of fine-grained sediment through the Holocene (Nakagawa et

al., 2012), which is ideal for high-resolution tephra investigations and palaeoenvironmental proxy analysis.

4. A detailed Bayesian age-model has been generated for the Holocene section of the sediment sequence (Staff et al., 2011) from a high resolution radiocarbon dataset (124 measurements of terrestrial plant macrofossil remains), and provides precise and well-constrained age estimates for identified eruption events. Since the Holocene sediments do not contain visible varves and the chronology is reliant on the ^{14}C dating, identifying precisely dated tephra layers can help improve the Lake Suigetsu chronology at their respective depths.
5. The lake is located in the mid-latitude western Pacific region where the EAM front annually migrates, and thus records the past behaviour of this sensitive climate system.
6. The archive is a key global palaeoenvironmental record (e.g., Nakagawa et al., 2005; Nakagawa et al., 2012), with the lake currently recognised as an auxiliary stratotype for the onset of the Holocene (Walker et al., 2009).

4.2.2. Geology of the Lake Suigetsu catchment

Lake Suigetsu, Honshu Island (35°35'0''N, 135°53'0''E) is located in a small tectonic basin situated on the western side of the Mikata fault line, adjacent to Wakasa Bay (Figure 4.1.). It forms the largest of the 'Mikata Five Lakes' and is located in the Wakasa Wan Quasi-National Park. Lake Suigetsu covers an area of ca. 4.3 km^2 (with a perimeter of ca. 10 km and diameter of ca. 2 km) and has

an average water depth of ca. 34 m (Kitagawa and van der Plicht, 1998a).

The lake has a small catchment area that is vegetated by warm mixed-forest and is surrounded by a ring of Palaeozoic hills (maximum elevation 400 m) (Kitagawa et al., 1995; Nakagawa et al., 2005). The main tributary feeding the five Mikata lakes is the River Hasu (ca. 10 km in length), which enters on the southeast side of Lake Mikata (Figure 4.1b). Water subsequently flows through the Seto Channel into Lake Suigetsu. This channel is particularly shallow (ca. 2 m in depth), meaning coarse sediment is deposited or trapped in Lake Mikata before reaching Lake Suigetsu (Nakagawa et al., 2005). This natural filter, means that sediments entering Lake Suigetsu are predominantly comprise of autochthonous and authigenic material (Schlolaut et al., 2012). These sediment characteristics and the geomorphic protection of the lake mean the sedimentary environment is particularly stable and allows for continuous fine-grain deposition.

4.2.3. Coring campaigns

The Suigetsu lake sediments have been studied for over two decades, with significant interest sparking in 1993, with the 'SG93' campaign, which obtained a 72.4 m piston core from the basal lake sediments (Kitagawa and van der Plicht, 1998a). This revealed that much of the sequence contained varves (*'nenko*' in Japanese) i.e., seasonal laminations, with alternations of diatom-rich (darker coloured) and mineral-rich (lighter coloured) layers (Fukusawa, 1995; Kitagawa et al., 1995; Kitagawa and Van der Plicht, 1998a). The lake was re-

drilled in the summer of 2006 as part of the 'Lake Suigetsu Varved Sediment Project' with the aim of obtaining a complete overlapping 'master' sedimentary sequence by recovering overlapping cores from four parallel boreholes (A, B, C and D, situated ca. 20 m apart; Figure 4.1b) (see Nakagawa et al., 2012). This coring campaign successfully obtained a 73.19 m-long composite core ('SG06'), providing a continuous record of sedimentation spanning the last ca. 150 ka (Nakagawa et al., 2012). The sequence has been extensively radiocarbon (^{14}C) dated and is varved between ca. 10 and 70 ka, which provides a very high-resolution chronology for this palaeoenvironmental record (Staff et al., 2011; Bronk Ramsey et al., 2012; Marshall et al., 2012 and Schlolaut et al., 2012).

A new coring campaign was undertaken during the summer of 2014 to obtain another continuous core sequence to: i) generate thin-sections for a display at a purpose-built Lake Suigetsu museum, and ii) provide more material for scientific analysis. The coring site was located ca. 320 m east of the SG06 boreholes (Figure 4.1b) and was similarly obtained using a hydro-pressure piston sampler, and also a triple sampler for deeper parts. This campaign retrieved a composite overlapping sedimentary sequence again from four boreholes (E, F, G and H) and it spans ca. 98 m, which records ca. 25 m of extra sedimentation compared to SG06, reaching a thick basal gravel. This composite master sequence, named 'Fukui-SG14' ('SG14' in short), was used for this Holocene cryptotephra investigation. The SG14 sequence (correlation model 30 May '17) has been precisely tied to the SG06 composite core (correlation model 08 May '16) using 361 common marker layers (which include visible tephra layers), permitting the high-precision SG06 chronology to be transferred to the SG14 core.

4.2.4. Lake Suigetsu tephrostratigraphy

Hitherto, 31 visible tephra layers from SG06 have been identified and characterised (using major element geochemical analysis), providing a detailed record of East Asian eruption events over the past 150 ka (Smith et al., 2011a; Smith et al., 2013; McLean et al., 2016). These include some of the most widespread tephra layers from southern Japan and South Korea, including the B-Tm, K-Ah, U-Oki, AT, Aso-4, K-Tz, Aso-ABCD and Ata tephra layers.

Four visible layers were identified from the Holocene section of the SG06 sediments. These include the following tephra layers: SG06-1288 that has been correlated to the U-Oki (U-4) eruption; SG06-0967 which has been correlated to the K-Ah tephra; SG06-0588 from an unknown eruption source; and SG06-0226 that is correlated to the B-Tm tephra (Smith et al., 2011a; Smith et al*.,* 2013; McLean et al., 2016). During the 2014 coring campaign, several new visible tephra layers were identified, including two in the Holocene sediments (SG14-1091 and SG14-0781) that are characterised and dated herein.

4.3. Materials and methods

4.3.1. Tephra identification

The master SG14 core (composite sequence) was contiguously sub-sampled at a ca. 5 cm resolution, from the U-Oki tephra to the core top, avoiding the known high-energy event layers (e.g., flood horizons) defined by Yamada et al*.,* (in prep.). If elevated shard concentrations were observed in the ca. 5 cm sample,

the sediment was resampled at a 1 cm resolution to determine the precise stratigraphic positioning of the peak. All samples were wet sieved through a 25 μm mesh, and processed using the heavy liquid floatation method outlined by Turney (1998) and Blockley et al. (2005). These samples were prepared alongside blanks to test for possible laboratory contamination. The extraction residues were mounted on slides using Canada Balsam, and glass shards were counted via microscopic examination to quantify the number of shards per gram of dried sediment (shards/gram). The following characteristics were also recorded for the glass shards (Figure 4.2.):

(i) Colour (e.g., clear, brown or green)

(ii) Size (length of the longest axis of shards in the fraction extracted, i.e., > 25 microns)

(iii) Morphology (e.g., blocky, platy, cuspate or fluted)

(iv) Vesicle size (small/microvesicular or large) and density (rich or poor)

(v) Microlite density (rich or poor)

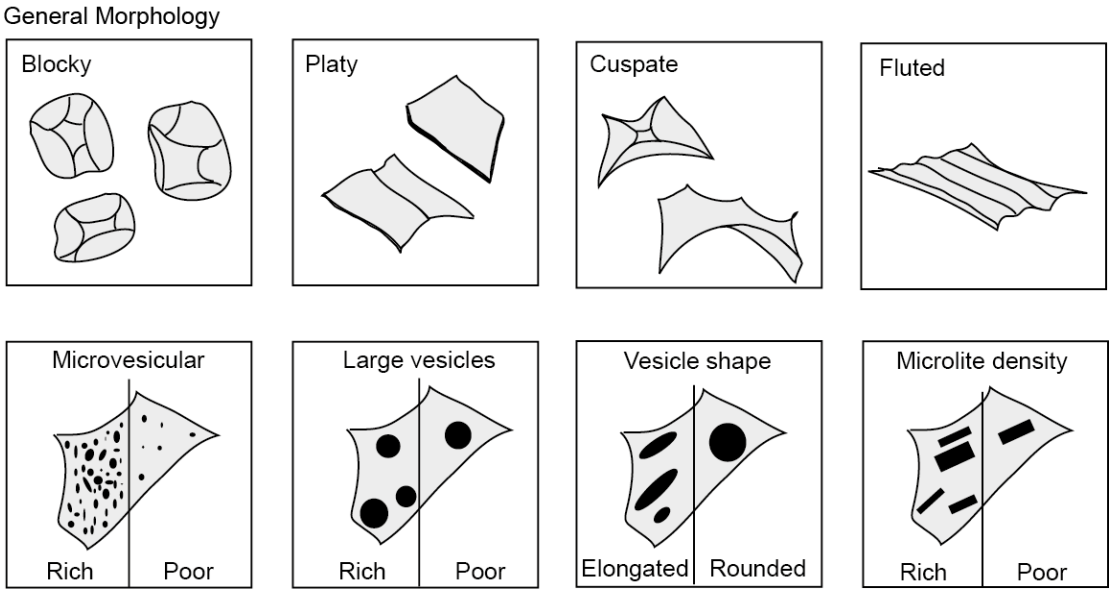


Figure 4.2. Schematic representation of the end member glass morphologies observed in the Lake Suigetsu sequence. Glass shards from an individual layer (i.e., primary isochron) typically possess a uniform shard size and consistent morphology. Glass shards which are both blocky and microvesicular are referred to as pumiceous.

4.3.2. Glass geochemical analysis

Glass shards were extracted from samples chosen for geochemical analysis and hand-picked from a welled-slide using a micromanipulator (see Lane et al., 2014). These shards were mounted in Epoxy resin stubs, which were sectioned and polished to expose a flat surface, and carbon coated for chemical analysis. Major and minor element compositions of individual glass shards were measured using a JEOL-8600 wavelength-dispersive electron microprobe (WDS-EMP) at the Research Laboratory for Archaeology and History of Art (RLAHA), University of Oxford. All analyses used an accelerating voltage of 15 kV, beam current of 6 nA and 10 μm-diameter beam. Peak counting times were 12 s for Na, 50 s for Cl, 60 s for P, and for 30 s for all other elements. The electron microprobe was calibrated using a suite of mineral standards, and the

PAP absorption correction method was applied for quantification. The accuracy and precision of this data were assessed using analyses of the MPI-DING reference glasses (Jochum et al., 2006), which were run as secondary standards during all runs of the Lake Suigetsu tephra samples. Analyses of these secondary standards lie within a standard deviation of the preferred values and are provided in the Supplementary Material (Appendix B). Data were filtered to remove non-glass analyses, and those with analytical totals < 93%. The raw values were normalised (to 100 %) for comparative purposes and to account for variable hydration, and are presented as such in all tables and figures.

Proximal glass data from several eruptive units at Mashu, Towada and Kawagodaira volcanoes were analysed using the same procedure to validate tephra correlations. Details of these sampling localities and glass datasets are provided in the Supplementary Material (Appendix B).

4.3.3. Chronology

As introduced above, the master SG14 sequence was precisely tied to SG06, permitting the high-precision SG06 chronology to be transferred to the SG14 core. SG06 event-free depth(s) (EFD, ver. 29th Jan '11) were used within the age model, which excludes instantaneous deposits > 5 mm in thickness, (i.e., event layers; floods, and tephra deposits; Staff et al., 2011; Scholaut et al., 2012). The software package developed to handle the correlation of parallel core sections, 'LevelFinder' (ver. 7.5.5, http://polsyems.rits-palaeo.com), was

used to linearly extrapolate between the common marker layers and determine any given composite depth (CD) or EFD from the individual SG06 and SG14 cores (see Nakagawa et al., 2012).

The composite Suigetsu sedimentary sequence was modelled on to the IntCal13 timescale (Reimer et al*.,* 2013) implementing three successive cross-referenced Poisson-process (‘*P_Sequence’*) depositional models using OxCal (ver. 4.3; Bronk Ramsey 2008; 2017). These include 775 AMS ^{14}C dates obtained from terrestrial plant macrofossils from the upper 38 m (SG06-CD) of the SG93 and SG06 cores (Kitagawa and van der Plicht, 1998a, 1998b, 2000; Staff et al., 2011, 2013a, 2013b) and varve counting between 12.88 and 31.67 m SG06 CD (Marshall et al*.,* 2012; Schlolaut et al*.,* 2012).

The uppermost Holocene sediments, from the core top down to the SG06-1288 (U-Oki) tephra (12.88 m SG06 CD, ca. 10,200 cal. yrs BP), are not composed of clearly defined and countable varves, and the chronology is instead constrained by 124 ^{14}C dates. Several additional chronological constraints are incorporated within the Holocene section of the age model, including a calendar age for the Urami Canal construction (AD 1664 ± 5 yrs positioned at 87.8 cm SG06-CD; as determined by an influx of marine diatom species into Lake Suigetsu; Saito-Kato et al*.,* 2013), a calendar age for event layer A-01-01c (AD 1976 ± 2 positioned at 32.5 cm SG06-CD; as determined by varve counting of the uppermost sediments; Suzuki et al*.,* 2016) and a constrained age for the core top (which cannot post-date AD 2006). Three precise tephra-based ages are also included following the findings of this study, including a remodelled tree-

ring wiggle-matched ^{14}C age for the KGP tephra (3,151 – 3,126 cal. yrs BP, 95.4% confidence interval; Tani et al., 2013) imported as a '*Prior'* within the model (spanning the cryptotephra sampling interval of 484.0 – 485.0 cm SG06-CD), a historical age for the Iz-Kt eruption (AD 838; spanning the cryptotephra sampling interval 239.1 – 240.1 cm SG06-CD; Tsukui et al., 2006) and a tree-ring wiggle-matched age for the B-Tm tephra (AD 946 ± 1; McLean et al*.,* 2016; Oppenheimer et al., 2017) positioned at 225.5 cm SG06-CD.

Cryptotephra layers are usually inserted into age models using the sub-sampling mid-point instead of the depth range and therefore, the date may not be accurate and the precision is underestimated. In this study, we have included this cryptotephra sample depth uncertainty into our age modelling. Our results indicate that the effect on the chronology in this case is negligible, but this modelling approach should be applied in other such cryptotephra studies to account for the full age uncertainty.

4.4. Tephrostratigraphy Results

4.4.1. Discriminating primary tephra layers

When interpreting the visible and cryptotephra record, it is necessary to consider the possibility of syn- and post- depositional processes which may: i) obscure the original stratigraphic positioning of the eruption event, and ii)

incorporate older or background volcanic glasses that have been reworked and redeposited in the sediments (Davies et al., 2007; Pyne-O'Donnell, 2011).

Some sedimentary sequences, especially those located too close to a volcanic source, may be unsuitable for cryptotephra analysis, as they might be continuously inundated with ash. High concentrations of tephra shards are often observed following a large explosive eruption that has previously blanketed the catchment with ash, and can produce a large and persistent background of volcanic glass in the lake sediments after the event (e.g., Zawalna-Geer et al., 2016; Matsu-ura et al., 2017). As expected, high concentrations of glass shards are observed in the Lake Suigetsu core sediments following the visible ash layers, for example, after the ca. 3 cm thick K-Ah tephra (SG06-0967) distinctive platy shards were continuously observed, in excess of 5,000 shards/gram, for several metres. However, these concentrations did not obscure the stratigraphic positioning of all primary ash layers deposited during this period, due to contrasting shard morphologies (e.g., peaks in cuspate or vesicular glass shard populations) or colour of subsequent primary ash layers.

Other peaks in shard concentrations may not always represent in-situ or primary ash input, as shards from older eruptions may be reworked from the catchment or local geology during high-energy events (e.g., MacLeod and Davies, 2016). Such high-energy events may be caused by heavy rains or earthquakes, which can erode sediments and thus remobilise older volcanic material from the catchment. These events can usually be visually identified within the core, since they deposit a distinct detrital layer that is typically clay-

rich, which contrasts to the authigenically-produced, organic-rich sediments that are commonly deposited (Katsuta et al., 2007; Bussmann and Anselmetti, 2010; Swierczynski et al., 2012; Corella et al., 2014).

Several lines of evidence can also be used to distinguish between primary and secondary ash layers that are not accompanied by an obvious high-energy event deposit within the sediment core (Gudmundsdóttir et al., 2011; Abbott et al., 2016). A high-energy or reworking event will typically incorporate volcanic glasses from several older eruptions, meaning the shards will often possess a mixed morphology, size and geochemical affinity. In the Lake Suigetsu sequence peaks in shard concentrations were ultimately evaluated using a set of criteria outlined in Figure 4.3. Glasses from flood horizons, and other positions where shard concentrations were largely constant, were geochemically analysed to establish the background compositional range. Peaks in volcanic glass concentrations were considered to be primary tephra if the shards possessed a consistent morphology, size and geochemical affinity that was different from the known background compositions.

4.4.2. Overview of Lake Suigetsu Holocene tephrostratigraphy

In total, twenty primary ash layers (six visible and fourteen cryptotephra layers) were identified within the Lake Suigetsu SG14 core (Figure 4.4; Figure 4.5; Table 4.1.). Newly identified ash layers are herein labelled using their SG14 composite depth in cm (SG14-CD, correlation model 30 May '17) that is rounded to the nearest integer. For continuity, SG06 codes are used for the

visible tephra layers that were previously identified in the Holocene sections of the SG06 core; SG06-1288 (U-Oki ash), SG06-0967 (K-Ah ash) SG06-0588 and SG06-0226 (B-Tm ash) (Table 4.1; Smith et al., 2011a; Smith et al., 2013; McLean et al., 2016).

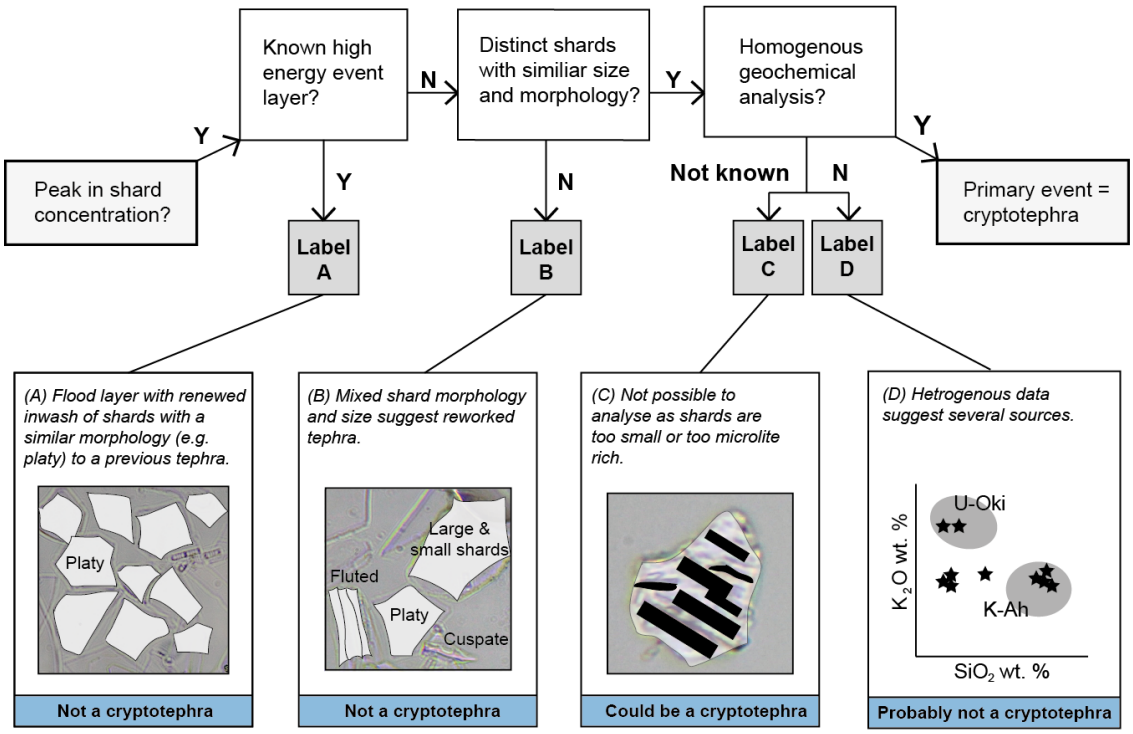


Figure 4.3. Criteria used to decipher primary ash fall events within the Lake Suigetsu sedimentary sequence (Y=yes, N=no). Peaks in glass concentration that fail these criteria and unlikely to reflect a primary event are marked by A, B, C or D on Figure 4.4.

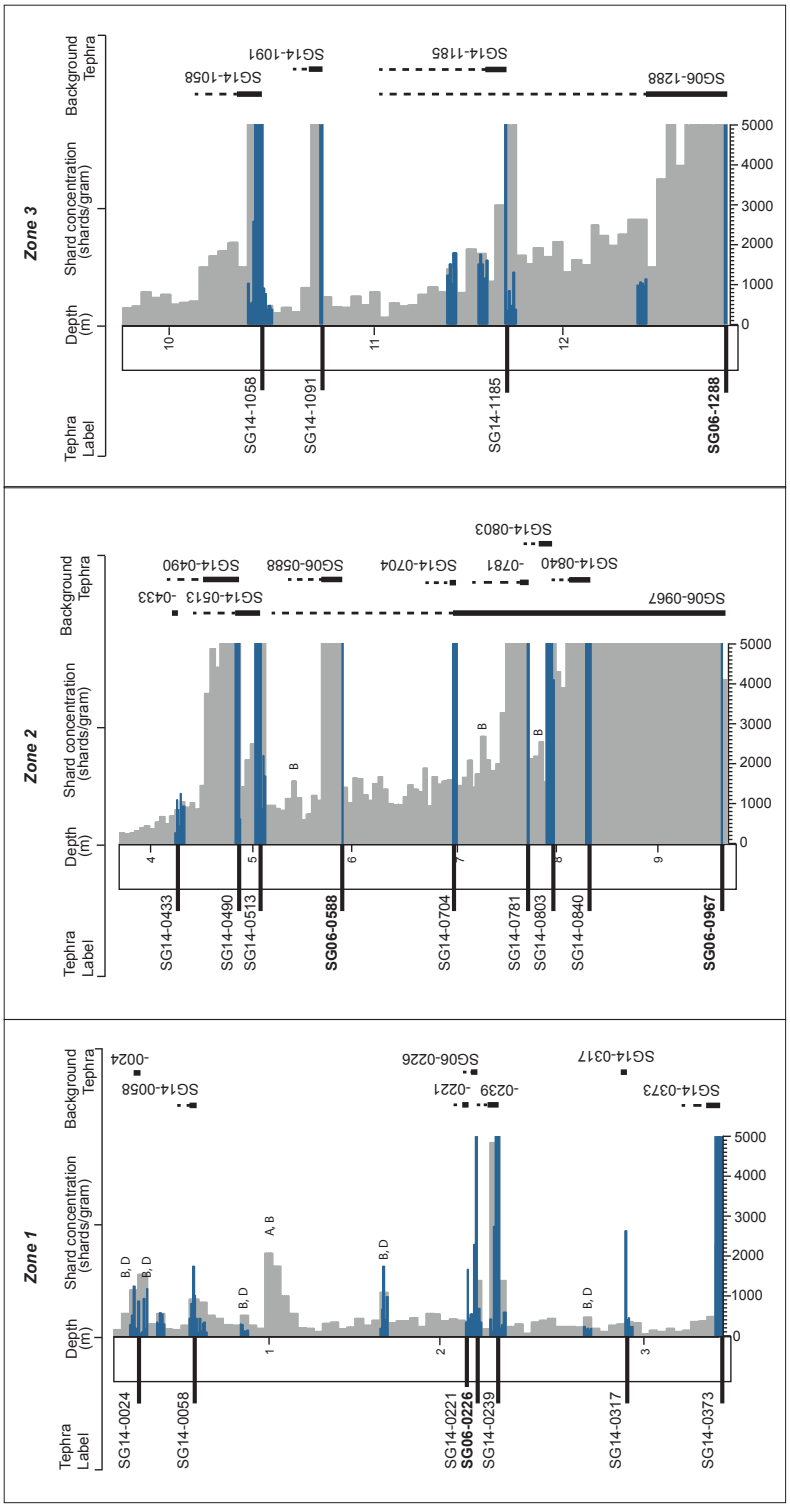


Figure 4.4. Glass shard concentrations (shards per gram of dry sediment; capped at 5,000) in the Holocene sediments of the Lake Suigetsu SG14 core. The tephrostratigraphy is divided into three Zones (1 to 3) for ease of description in Section 4. Concentration of low-resolution (5 cm) samples are shown in grey and high-resolution samples (1 cm) are overlain in blue. Tephra isochrons are labelled using their SG06/SG14 composite depth. Vertical bars indicate the relative concentration of dominant (solid line) and minor (dotted line) background glasses in the section, based on the typical morphology of the glass shards.

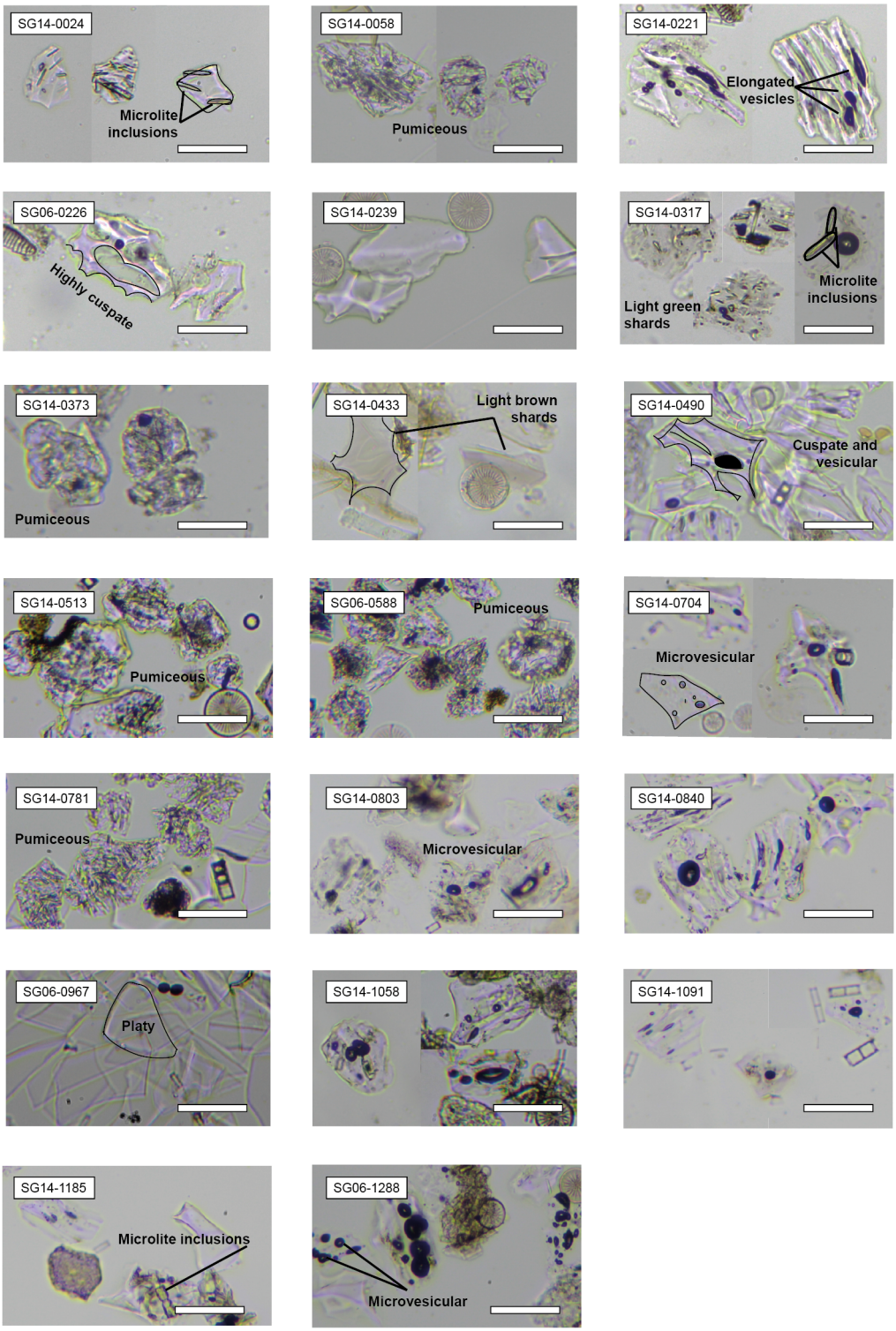


Figure 4.5: Photographs of typical glass shards preserved in the SG14 Holocene tephra layers, scale bar = 50 µm. Morphologies vary from platy (e.g., SG06-0967), highly cuspate (e.g., SG06-0226) to pumiceous (e.g., SG14-0781). Some shard morphologies are densely vesicular (e.g., SG06-1288) and/or contain microlite inclusions (e.g., SG14-0024).

Table 4.1. Summary table of the Holocene tephras within the Lake Suigetsu SG06 and SG14 sediment cores

Label	V/C	SG14 Master core and position *	SG14 Composite Sampling Depth (cm) *	SG06 Composite Sampling Depth (cm) *	Glass shard morphology	Shard length (μm)**	Glass compositions of dominant population (wt %)				^{14}C date (AD / cal. yrs BP) 95.4 % uncertainty	Correlation based on glass geochemistry (tephra, volcano)***	Distance of source volcano from Lake Suigetsu (km)	Magnitude of eruption (VEI)
							SiO_2	K_2O	CaO	*n*				
SG14-0024	C	E-01 (15.1 - 16.0 cm)	23.3 - 24.2	39.1 - 40.0	MI	30	68.50 - 69.90	2.48 - 2.62	3.12 - 3.68	6	AD 1963 - 1920	-	-	-
SG14-0058	C	E-01 (48.9 - 49.9 cm)	57.1 - 58.1	70.6 - 71.4	PU, MV, MI	70	-	-	-	-	AD 1746 - 1902	-	-	-
SG14-0221	C	F-02 (81.0 - 82.0 cm)	219.7 - 220.7	220.5 - 221.6	C, F, V, MV	50	71.92 - 73.79	0.72 - 0.88	0.57 - 0.69	14	AD 960 - 992	Ma-b, Mashu	1160 NE	5
SG06-0226[1]	V	**F-02 (85.7)**	**224.4**	**225.5**	C, V	80	65.14 - 75.49	6.15 - 4.21	0.18 - 1.42	30	AD 946[4]	B-Tm, Changbaishan[1]	980 NW	7
SG14-0239	C	E-03 (15.0 - 15.9 cm)	237.8 - 238.7	239.1 - 240.1	C	100	77.49 - 78.37	3.20 - 4.08	0.32 - 0.93	20	AD 767 - 839	Iz-Kt, Kozushima	340 SE	4
SG14-0317	C	F-03 (60.0 - 61.0 cm)	315.5 - 316.5	317.0 - 317.9	V, MI	40	-	-	-		1815 - 1735	-	-	-
SG14-0373	C	E-04 (68.1 - 69.1 cm)	372.1 - 373.1	371.3 - 372.3	PU, MV, MI	40 - 100	-	-	-	-	2192 - 2117	-		-
SG14-0433	C	F-04 (57.8 - 58.8 cm)	431.9 - 432.9	429.0 - 430.0	PL, C	60 - 80	61.53 - 62.00	4.48 - 4.75	2.47 - 2.72	8	2737 - 2620	U-1, Ulleungdo ?	980 NW	-
SG14-0490	C	G-02 (50.2 - 51.2 cm)	489.4 - 490.4	484.0 - 485.0	C, F, V	30 - 100	76.49 - 77.56	2.65 - 2.94	1.43 - 1.83	19	3227 - 3129	KGP, Kawagodaira	290 E	4
SG14-0513	C	G-02 (73.2 - 74.2 cm)	512.4 - 513.4	506.3 - 507.3	PU, MI	50	-	-	-	-	3428 - 3312	-	-	-
SG06-0588[2]	V	**F-06-04**	**593.7**	**587.8**	PU, MV, MI	30 - 70	74.40 - 77.97	2.25 - 3.99	1.45 - 2.37	11	4066 - 3986	-	-	-
SG14-0704	C	E-08 (36.0 - 37.0 cm)	703.2 - 704.2	699.1 - 700.0	C, F, V, MV	50	70.39 - 72.97	2.49 - 2.91	2.41 - 3.64	10	4894 - 4827	Unknown, Kikai ?	750 SW	-
SG14-0781	V	**F-08-06**	**780.5**	**775.4**	PU, MI	30 - 100	74.41 - 78.00	1.98 - 3.79	1.25 - 2.48	26	5519 - 5480	-	-	-
SG14-0803	C	E-09 (43.7 - 44.7 cm)	802.1 - 803.1	797.9 - 798.9	MV	30 - 50	59.43 - 61.76	6.26 - 7.02	1.23 - 2.49	19	5681 - 5619	U-2, Ulleungdo	500 NW	-
SG14-0840	C	E-09 (80.7 - 81.7 cm)	839.1 - 840.1	835.9 - 836.9	C, MV	40	73.43 - 74.41	1.09 - 1.31	2.60 - 3.13	25	5986 - 5899	To-Cu, Towada	700 NE	5
SG06-0967[2]	V	**F-10-04**	**977.1**	**967.2**	PL	50 - 100	72.60 - 74.60	2.77 - 3.03	1.82 - 2.34	14	7307 - 7196	K-Ah , Kikai[2]	750 SW	7
SG14-1058	C	F-11 (28.6 - 29.4 cm)	1057.1 - 1057.9	1050.8 - 1051.6	C, F, V	50	74.54 - 75.30	4.39 - 4.60	0.17 - 0.26	25	8166 - 8099	Unknown, Changbaishan	980 NW	-
SG14-1091	V	**E-12-03b**	**1090.5**	**1085.2**	MV	40	59.62 - 60.81	6.66 - 7.37	1.08 - 1.82	24	8455 - 8367	U-3, Ulleungdo	500 NW	-
SG14-1185	C	F-12 (62.0 - 63.0 cm)	1184.0 - 1185.0	1180.2 - 1181.2	MV, MI	40 - 50	67.55 - 77.92	3.03 - 4.38	0.67 - 4.13	18	9372 - 9301	-	-	-
SG06-1288[3]	V	**G-03-02**	**1301.3**	**1287.9**	MV	60	60.49 - 62.00	6.57 - 7.48	1.42 - 2.03	12	10230 - 10171	U-4, Ulleungdo[3]	500 NW	6

References 1) McLean et al. (2016); 2) Smith et al. (2013); 3) Smith et al. (2011b); 4) Oppenheimer et al. (2017)
V / C = Visible / Cryptotephra layer
PU = Pumiceous, PL = Platy, C = Cuspate, F= Fluted, V= Vesicular, MV = Microvesicular, MI = Microlite Inclusions (see Figure 2)
n= number of analyses
* Sampling range for cryptotephra layers and base of visible ash layers
** General shard length in the fraction extracted, i.e. in the population >25 μm
*** Tephra marked with a dash have not been able to be robustly correlated to a particular eruption or volcano

The Holocene tephrostratigraphy is described in three zones for simplicity (Figure 4.4.), and are demarcated by the variable concentrations of background glasses through the core. Due to these background glasses, the identified cryptotephra isochrons possess different shard concentrations within these zones, with > 5,000 shards/gram in Zone 3 and Zone 2, but < 2,000 shards/gram in Zone 1.

4.4.3. Zone 3

Zone 3 covers the Early Holocene sedimentation at Lake Suigetsu, spanning from the visible (ca. 2 cm thick) U-Oki tephra (SG06-1288; 13.0 m SG14-CD) to the visible (ca. 3 cm thick) K-Ah tephra (SG06-0967; 9.7 m SG14-CD) (Figure 4.4). The age-model for the Lake Suigetsu sediments constrains the age of these tephra layers and sediments between ca. 10.2 and 7.3 cal. yrs BP. Within Zone 3, two visible and two cryptotephra primary ash layers are identified and labelled by their SG06/SG14-CD: SG06-1288 (visible layer that was correlated to the U-Oki tephra by Smith et al., 2011a), SG14-1185, SG14-1091 (visible) and SG14-1058. These are dated to 10,230 – 10,171 cal. yrs BP, 9,372 – 9,301 cal. yrs BP, 8,455 – 8,367 cal. yrs BP, and 8,166 – 8,099 cal. yrs BP (95.4% confidence interval), respectively (Table 4.1.).

Glass shards in SG06-1288 (U-Oki tephra) are generally ca. 60 μm in length and are clear to medium brown in colour (Figure 4.5.). The U-Oki shards have a characteristic pumiceous, microvesicular morphology, which are seen in high concentrations for ca. 2 m (ca. 2 ka) after the primary deposition of the visible

layer. SG14-1058 is positioned above a known event layer, but is deemed a primary tephra isochron since all observed shards possessed a consistent morphology (highly cuspate, with very large elongated vesicles), size and a homogeneous geochemical composition which is distinct from the underlying visible tephras layers. Furthermore, these shard characteristics were not observed in the subsequent 2 meters of older sediments.

Within Zone 3, background platy shards were observed between ca. 10.0 - 10.5 m SG14-CD, and some clear cuspate glasses were also observed between ca. 11 – 13 m SG14-CD. There is no clear peak in these glass compositions, suggesting either: i) the primary input is obscured within the background glass concentrations, or ii) the isochron is positioned below the U-Oki tephra layer.

4.4.4. Zone 2

Zone 2 contains the highest concentrations of background glasses, and extends from the visible K-Ah tephra (SG06-0967) at 9.7 m to 3.7 m SG14-CD; ca. 7.3 to 2.2 ka yrs BP (Figure 4.4.). Within Zone 2, three visible and six cryptotephra layers are recognised: visible layer SG06-0967 (previously correlated to the K-Ah tephra by Smith et al., 2013), SG14-0840, SG14-0803, visible layer SG14-0781, SG14-0704, visible layer SG06-0588 (previously characterised by Smith et al., 2013), SG14-0513, SG14-0490 and SG14-0433. These are dated to 7,307 – 7,196 cal. yrs BP, 5,986 – 5,899 cal. yrs BP, 5,681 – 5,619 cal. yrs BP, 4,894 – 4,827 cal. yrs BP, 4,066 – 3,986 cal. yrs BP, 3,428 – 3,312 cal. yrs BP,

3,227 – 3,129 cal. yrs BP, and 2,737 – 2,620 cal. yrs BP (95.4 % confidence interval), respectively (Table 4.1.).

Glass shards in SG06-0967 (K-Ah tephra) range in size from 50 – 100 μm, and are clear or brown (minor population) with platy morphologies (Figure 4.5.). These shards are seen in high concentrations (> 5,000 shards/gram) for ca. 1 m of sedimentation following the deposition of the K-Ah visible layer. Since these background glasses are very distinctive, other primary tephra layers with distinctive shard morphologies, such as SG14-0840 (highly cuspate and fluted in shape), were easily identified (Figure 4.5.).

4.4.5. Zone 1

Late Holocene sedimentation in Zone 1 extends from ca. 3.7 m SG14-CD (2.2 ka) to the core top (Figure 4.4.), and considerably lower background glasses were observed than in Zone 2. One visible and six cryptotephra layers are found within Zone 1. The visible layer is the previously identified B-Tm tephra associated with the 'Millennium' eruption from Changbaishan volcano in China/North Korea (SG06-0226; McLean et al*.,* 2016). Newly identified cryptotephras, labelled using their SG14 composite depths, are: SG14-0373, SG14-0317, SG14-0239, SG14-0221, SG14-0058 and SG14-0024, and are dated to 2,192 – 2,117 cal. yrs BP, 1,815 – 1,735 cal. yrs BP, 1,183 – 1,111 cal. yrs BP, 990 – 959 cal. yrs BP, 204 – 48 cal. yrs BP, 30 – -13 cal. yrs BP (95.4 % confidence interval), respectively (Table 4.1.).

The lower levels of background glasses observed during this period are probably because the majority of the K-Ah tephra has worked its way through the catchment. Since there are lower concentrations of background glasses, small peaks (< 2,000 shards/gram) in shard concentrations could be more easily identified. Several further peaks in shard concentrations had shards with variable sizes, morphologies and heterogeneous glass compositions (spanning both typical Kikai and Aira glass chemistries). These peaks (labelled B and C on Figure 4.4.) are not deemed primary tephra layers and likely represent flood or secondary reworking events.

4.5. Glass geochemistry results

Major element glass compositions of the SG14 Holocene tephra layers are presented in Table 4.2. and selected bi-plots in Figure 4.6. SG14-0513, SG14-0373, SG14-0317 and SG14-0058 glass shards could not be analysed as they were too small or had too many microlite inclusions (Figure 4.5.). Geochemical analyses of background shards were excluded from the presented datasets but are included in the Supplementary Material.

The most abundant oxides, SiO_2, K_2O, CaO, Al_2O_3 and FeO^T (all Fe as FeO) are predominantly used to characterise and discriminate the tephra layers since they can be precisely measured by the electron microprobe. The glass compositions of the Holocene tephra layers in the Lake Suigetsu record range from phono-trachytic to rhyolitic, with the exception of the dacitic SG14-1185 and SG14-0024 tephra layers (Figure 4.6.).

Table 4.2. Glass compositions (normalised) of the SG14 Holocene tephra layers identified in this study (FeO^T = all Fe reported as FeO). Raw dataset and secondary standards are included in the Supplementary Material (Appendix B).

	SG14-0024		SG14-0221		SG14-0239		SG14-0433		SG14-0490		SG14-0704	
wt. (%)	Avg.	± 1 σ	Avg.	± 1 σ	Avg.	± 1 σ	Avg.	± 1 σ	Avg.	± 1 σ	Avg.	± 1 σ
SiO_2	69.33	0.52	73.43	0.44	77.87	0.21	61.76	0.16	77.14	0.23	72.19	0.75
TiO_2	0.81	0.03	0.63	0.04	0.08	0.03	0.79	0.05	0.25	0.04	0.56	0.04
Al_2O_3	14.32	0.25	13.15	0.44	12.76	0.16	16.66	0.05	12.57	0.10	13.78	0.66
FeO^T	4.15	0.21	3.12	0.12	0.54	0.10	5.65	0.17	1.20	0.11	3.18	0.45
MnO	0.13	0.03	0.17	0.04	0.07	0.04	0.23	0.05	0.05	0.04	0.10	0.06
MgO	0.97	0.13	0.77	0.05	0.06	0.04	1.09	0.06	0.29	0.04	0.58	0.13
CaO	3.35	0.20	3.24	0.13	0.39	0.14	2.57	0.08	1.61	0.09	2.63	0.37
Na_2O	4.01	0.31	4.47	0.15	4.15	0.23	6.07	0.18	3.92	0.09	3.93	0.16
K_2O	2.56	0.06	0.77	0.04	3.90	0.20	4.59	0.10	2.79	0.09	2.82	0.12
P_2O_5	0.23	0.02	0.13	0.04	0.03	0.02	0.36	0.04	0.05	0.02	0.12	0.02
Cl	0.14	0.03	0.14	0.04	0.15	0.04	0.23	0.03	0.12	0.02	0.12	0.02
n	*6*		*14*		*20*		*8*		*19*		*10*	

	SG14-0781		SG14-0803		SG14-0840		SG14-1058		SG14-1091		SG14-1185	
wt. (%)	Avg.	± 1 σ	Avg.	± 1 σ	Avg.	± 1 σ	Avg.	± 1 σ	Avg.	± 1 σ	Avg.	± 1 σ
SiO_2	76.18	0.95	60.54	0.63	74.15	0.23	75.01	0.18	60.52	0.24	72.29	2.78
TiO_2	0.16	0.03	0.62	0.07	0.47	0.03	0.20	0.03	0.51	0.08	0.56	0.12
Al_2O_3	13.90	0.57	19.48	0.30	13.50	0.23	10.28	0.11	19.87	0.22	13.75	0.91
FeO^T	0.90	0.23	3.16	0.42	2.33	0.11	3.89	0.10	2.77	0.24	2.80	0.80
MnO	0.06	0.04	0.14	0.10	0.11	0.05	0.07	0.03	0.15	0.03	0.07	0.04
MgO	0.28	0.14	0.48	0.12	0.61	0.06	0.01	0.01	0.23	0.03	0.63	0.28
CaO	1.87	0.30	1.99	0.33	2.81	0.11	0.20	0.02	1.48	0.14	2.45	0.94
Na_2O	3.92	0.30	6.60	0.60	4.57	0.15	5.30	0.16	6.95	0.40	3.46	0.28
K_2O	2.55	0.40	6.61	0.21	1.22	0.05	4.50	0.06	7.03	0.19	3.73	3.73
P_2O_5	0.05	0.03	0.17	0.05	0.08	0.02	0.01	0.01	0.05	0.04	0.10	0.04
Cl	0.14	0.05	0.21	0.04	0.11	0.02	0.52	0.02	0.40	0.08	0.12	0.04
n	*27*		*19*		*25*		*25*		*24*		*18*	

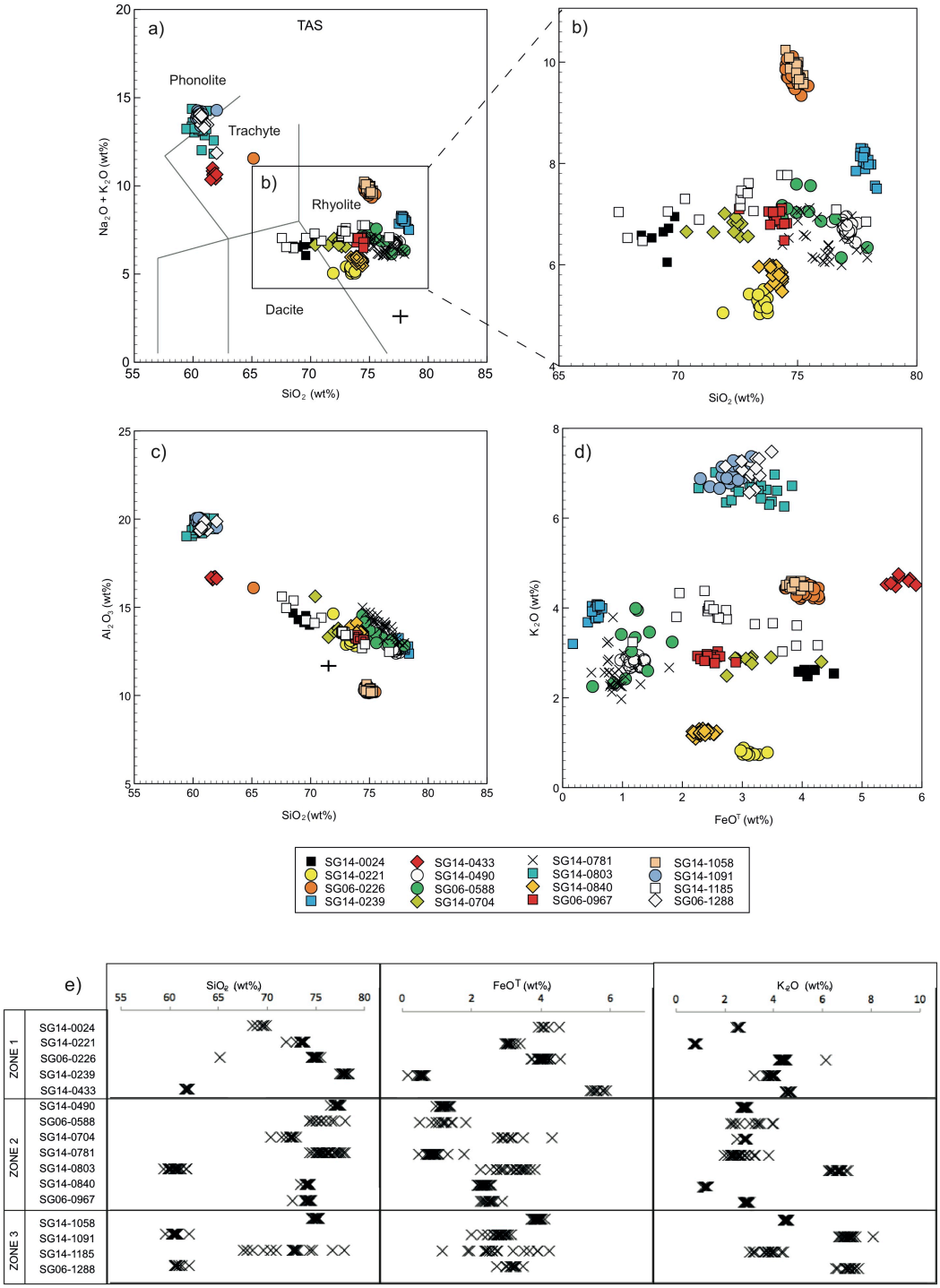


Figure 4.6. Major element compositions of the tephra layers within the Holocene sediments of the Lake Suigetsu SG14 core. These tephras are labelled using their SG06/SG14 composite depths. (a) Total alkalis versus silica plot (TAS; with whole-rock classifications based on Le Bas et al., 1986), (b, c, d) Bivariate plots for SiO_2, FeO^T, K_2O and Al_2O_3 compositions (error bars represent 2 x standard deviation of repeat analyses of the StHs6/80-G MPI-DING standard glass), (e) SiO_2, FeO^T, K_2O compositions of Holocene tephras that have been analysed from Lake Suigetsu (SG06 and SG14) versus stratigraphic position (including data from Smith et al., 2011a; Smith et al., 2013; McLean et al., 2016).

As illustrated in the major element bi-plots and Figure 4.6e, the glass compositions of the tephra layers are generally homogenous with narrow compositional ranges, with the exception of those from SG14-1185, SG14-0781 and SG06-0588. Some of these tephras have very similar or indistinguishable major element glass compositions, for example, SG06-1288, SG14-1091 and SG14-0803.

The glasses range from Low-K (tholeiitic) through to High-K (calc-alkaline and shoshonitic) compositions (Figure 4.7; Peccerillo and Taylor, 1976), which can be used to discriminate between the different volcanic regions in East Asia. Back-arc volcanoes in South Korea (Ulleungdo) and North Korea/China (Changbaishan) erupt K_2O-rich (> 3 wt. %) glasses, which contrast with eruption deposits from Hokkaido and northern Honshu that typically have < 1 wt. % K_2O (Machida and Arai, 2003; Smith et al., 2013). Tephra layers with different ages that possess similar or identical geochemical compositions are likely to represent eruptions from the same or closely located volcano (e.g., Shane, 2000; Smith et al., 2005; Albert et al., 2012, 2017).

The glass morphology, relative stratigraphy, geochemical compositions and precise chronology of the tephra layers, were used to correlate the SG14 Holocene isochrons to their volcanic sources and specific eruptions. The glass compositions of the SG14 tephra layers were compared to new and published compositions obtained from proximal outcrops with known eruption deposits.

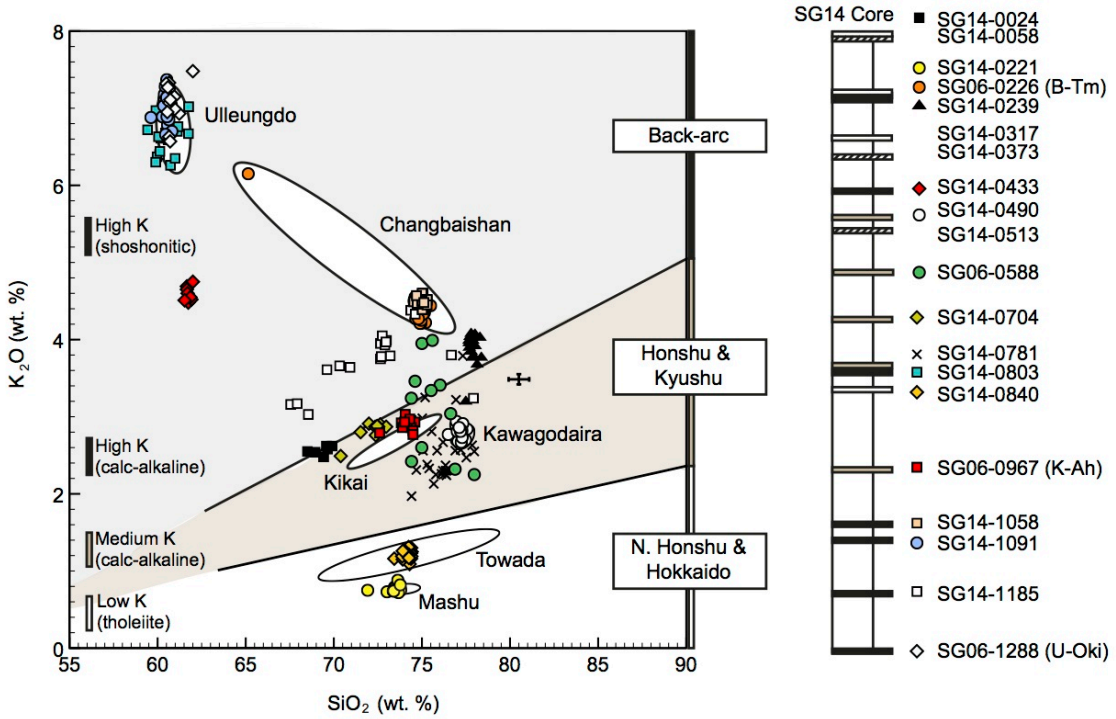


Figure 4.7. SiO_2 and K_2O glass compositions of the SG14 tephra layers (labelled using their SG06/SG14 composite depths) compared to proximal glasses originating from the back-arc volcanism from South Korea (Ulleungdo = U-Oki; Smith et al., 2011a), North Korea/China (Changbaishan = B-Tm; Chen et al., 2016; McLean et al., 2016), and the Japanese arc (Aira = AT, Kikai = K-Ah from Smith et al., 2013; and Kawagodaira = KGP, Towada = To-Cu and Mashu = Ma-b from this study). Glass analyses are plotted on the whole-rock K-classification scheme of Peccerillo and Taylor (1976). The back-arc and intraplate volcanism produces High-K (shoshonitic) compositions, which contrast to the eruptive products from northern Honshu and Hokkaido, which have Low-K (tholeiite) compositions. Geochemical analyses of SG14-0058, SG14-0373 and SG14-0513 could not be obtained due to their small shard sizes and/or abundance of microlite inclusions. Error bars represent 2 x standard deviation of repeat analyses of the StHs6/80-G MPI-DING standard glass.

These compositions indicate that the SG14 tephra layers are from the following volcanoes or regions:

1. North Korea/China: Changbaishan- SG14-1058 and SG06-0226.
2. South Korea: Ulleungdo - SG06-1288, SG14-1091, SG14-0803 and SG14-0433.
3. Northern Japan: Towada - SG14-0840, and Mashu - SG14-0221.

4. Southwest Japan: Kawagodaira - SG14-0490, and Kozushima - SG14-0239.
5. Southern Japan: Kikai - SG06-0967 and SG14-0704.

These correlations and geochemical compositions are discussed below along with the other tephra that have not yet been correlated to known eruptions or volcanoes.

4.6. Source of the tephra layers

4.6.1. Changbaishan tephra layers (SG14-1058 and SG06-0226)

Changbaishan (also referred to as Baitoushan, Baekdusan, Paektu or Hakutosan) volcano is situated on the border of North Korea and China (128°03'E, 41°00'N), and almost 1000 km NW of Lake Suigetsu (Figure 4.1.). Despite evidence of numerous highly explosive episodes during the Quaternary (Machida et al., 1990; Lim et al., 2013), and recent seismic activity (Xu et al., 2012), the eruptive history of Changbaishan volcano has not been established (Wei et al., 2003; Ramos et al., 2016; Pan et al., 2017). This is largely due to the difficulties in accessing the proximal outcrops, and that successive eruption deposits are geochemically indistinguishable (Lim et al., 2013). Several eruption deposits, potentially of Holocene age have been identified proximally, however this stratigraphy and chronology varies considerably across studies (see Pan et al., 2017). Consequently, distal archives are essential to establish the number of eruptions and date past explosive activity from Changbaishan.

The B-Tm tephra (AD 946; Oppenheimer et al., 2017; Hakozak et al., 2017) is the only confirmed distal layer from Changbaishan Holocene activity. This was dispersed during the highly explosive 'Millennium' eruption, which was one of the most violent in the past 2000 years (see Sun et al*.,* 2014b). The B-Tm tephra has been identified in numerous marine, lacustrine and archaeological sequences across central Japan, northeast China and coastal regions of Russia (see McLean et al*.,* 2016). Furthermore, B-Tm glass shards have also been identified in the Greenland ice cores (Sun et al., 2014a). Tephra layer SG06-0226 has previously been correlated to the B-Tm tephra (McLean et al., 2016) and currently presents the most southerly occurrence of this isochron. The precise age (AD 946; Oppenheimer et al., 2017; Hakozak et al., 2017) is incorporated within the Lake Suigetsu age model to constrain the chronology of the upper portion of the core.

The Changbaishan compositions can easily be distinguished from the lower alkali glasses produced from the Japanese arc, and the phonolitic glasses from Ulleungdo, South Korea (Figure 4.7.). The SG14 core contains an additional isochron (SG14-1058) that has glass compositions that are consistent with those erupted at Changbaishan (Figure 4.8.). SG14-1058 glass compositions overlap on all major elements with the rhyolitic member of SG06-0226 (B-Tm ash), and glasses from the B-Tm distal type-site (Tomakomai Port; McLean et al., 2016), with SiO_2 ranging from 74.5 – 75.3 wt. %, K_2O from 4.4 – 4.6 wt.% and CaO ca. 0.2 wt. % (Figure 4.8b; Figure 4.8c).

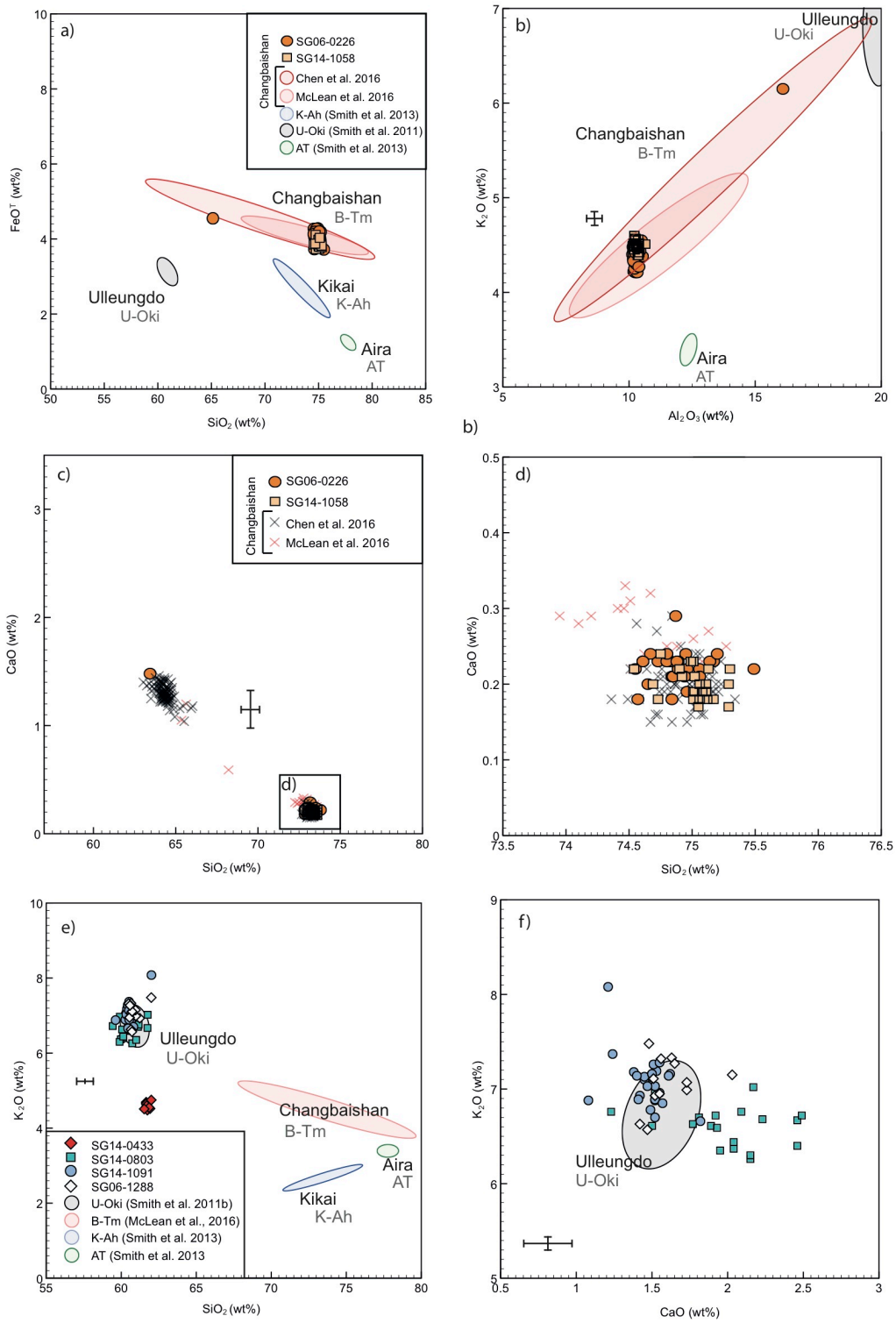


Figure 4.8. Glass shard major element compositions of: (a, b, c, d) tephra layers SG14-1058 and SG06-0226 compared to Changbaishan (B-Tm) glasses (Chen et al., 2016; McLean et al., 2016), and (e, f) tephra layers SG14-0803, SG14-1091 and SG06-1288 (U-Oki ash) compared to Ulleungdo (U-Oki) glasses (Smith et al., 2011a). Proximal compositional fields are labelled by volcano (black) and tephra (grey). Error bars represent 2 x standard deviation of repeat analyses of the StHs6/80-G MPI-DING standard glass.

This geochemical affinity is consistent with the identical compositions of older eruptions from Changbaishan, observed as thick deposits in the Sea of Japan (Lim et al., 2013). The Lake Suigetsu tephrostratigraphy therefore provides the first evidence for an additional Holocene eruption from Changbaishan at 8,166 – 8,099 cal. yrs BP (95.4% confidence interval) (Table 4.1.).

4.6.2. Ulleungdo tephra layers (SG06-1288, SG14-1091, SG14-0803 and SG14-0433)

Ulleungdo volcano is an island located in the southwest Japan Sea (37°30'N 130°52'E), ca. 110 km from the Korean Peninsula and ca. 500 km NW of Lake Suigetsu (Figure 4.1.). Ulleungdo is known to have erupted four times during the Holocene, as determined by proximal deposits identified on the island (Machida et al., 1984; Shiihara et al., 2011). These are proximally named (oldest to youngest): U-4, U-3, U-2 and U-1, with the K-Ah tephra positioned between the U-3 and U-2 deposits. The largest known Plinian eruption from Ulleungdo generated the Ulleung-Oki (U-Oki) tephra layer (Machida and Arai, 1983; Okuno et al., 2010; Lim et al., 2014), which equates to the proximal U-4 of Shiihara et al. (2011). The U-4 eruption is dated using the Lake Suigetsu chronology to have occurred between 10,230 – 10,171 cal. yrs BP (95.4 % confidence interval; Smith et al., 2011a; Staff et al., 2011) (Table 4.1.). The U-3 eruption has been dated (^{14}C of charcoal preserved within the proximal eruption deposits) to 8,440 – 8,360 cal. yrs BP (95.4% confidence interval; Im et al., 2012; Kim et al., 2014) and the U-2 has been dated to 5,749 – 5,604 cal. yrs BP

(Okuno et al., 2010). The youngest U-1 eruption is considered to be from a small strombolian eruption and has not been dated (Kim et al., 2014).

The U-Oki (U-4) tephra is a key widespread marker bed found in most sedimentary sequences east of Ulleungdo, in the Sea of Japan and central Honshu (Figure 4.1.). Distal equivalents of the U-3 eruption have also been reported in the Sea of Japan (TRG1 sediment core; Domitsu et al., 2002), Lake Biwa (Nagahashi et al., 2004) and close to Hakusan volcano, central Honshu (Higashino et al., 2005). U-2 and U-1 have only been found on the flanks of the volcano (Kim et al., 2014).

Glass compositions from Ulleungdo are distinctively alkali-rich, containing ca. 6.5 wt. % higher K_2O, and ca. 15 wt. % lower SiO_2 (ca. 60 wt. %) compared to eruptive products from the Japanese arc (Smith et al., 2011a; Smith et al., 2013). Ulleungdo glasses are also typically higher in K_2O content than the trachytic (lower SiO_2) end-member of Changbaishan eruptive products (Figure 4.7.). Proximal compositions from the Holocene eruptions of Ulleungdo (U-4, U-3 and U-2) straddle the phonolite-trachyte boundary and appear to be indistinguishable on major and trace element compositions (Shiihara et al., 2011). No glass compositions have been published for the U-1 eruption.

Three tephra layers in the Lake Suigetsu cores (SG06-1288, SG14-1091 and SG14-0803) contain alkali-rich glasses from Ulleungdo (Figure 4.8e, Figure 4.8f; Smith et al., 2011a), and represent the distal equivalents of proximal deposits of U-4, U-3 and U-2, respectively. The geochemical compositions

obtained from the U-4 (SG06-1288) and U-3 (SG14-1091) glasses preserved in Lake Suigetsu are indistinguishable using major and minor element compositions. However, we find the younger SG14-0803/U-2 glasses are more elevated in CaO (by ca. 0.5 wt. %) compared to the early Holocene eruptions, SG06-1288/U-4 and SG14-1091/U-3 (Figure 4.8f). Furthermore, SG14-0803/U-2 glass shards contain a greater portion of brown, highly vesicular, pumiceous shards (Figure 4.5), which may also help to distinguish this layer from the older Ulleungdo deposits elsewhere. The modelled ages of SG14-1091 (8,455 – 8,367 cal. yrs BP) and SG14-0803 (5,681 – 5,619 cal. yrs BP) (95.4% confidence interval) are in agreement with the published chronological information and further constrain the dates for U-3 and U-2.

SG14-0433 glass compositions also contain ca. 60 wt. % SiO_2, but have ca. 2.5 wt. % lower K_2O, and ca. 2 wt. % higher CaO compared to the typical compositions erupted during large explosive eruptions from Ulleungdo (Figure 4.8e; Table 4.2.). Since no other volcanoes in this region, especially those along the Japanese arc, produce such evolved compositions; it suggests that SG14-0433 is a distal occurrence of U-1. The age of this tephra (2,737 – 2,620 cal. yrs BP) is consistent with a repose interval of < 3 ka throughout the Holocene.

4.6.3. Towada (SG14-0840) and Mashu (SG14-0221) tephra layers

Towada is a large caldera, situated in northern Honshu (40°28'N 140°52'E), ca. 700 km NE of Lake Suigetsu (Figure 4.1.). Towada has erupted repeatedly

throughout the Holocene, the largest of which dispersed the Towada-Chuseri (To-Cu) ash across northern Honshu and the coastal regions of the Pacific (Machida and Arai, 2003; Figure 4.1.). In proximal localities, three eruptive units are recognised in the To-Cu sequence, an opening Plinian fall (named Chuseri), which is overlain by the Kanagasawa pumice fall and topped by the Utarube ash, a dilute pyroclastic density current (PDC), deposit (Hayakawa, 1985). All three units of To-Cu are predominantly recorded to the east of the volcano (Hayakawa, 1985; Figure 4.1.).

The To-Cu eruption is proximally dated to 6,293 – 6,029 cal. yrs BP based upon a ^{14}C age of charcoal fragments preserved in the dilute PDC deposits (Hayakawa, 1983). Furthermore, the soil beneath the To-Cu is dated to 6,313 – 6,180 cal. yrs BP (Inoue et al., 2011), providing a maximum age constraint for the eruption. As observed for other volcanoes situated in northern Honshu and Hokkaido, the tholeiitic glasses from Towada contain low K_2O (< 1.5 wt. %) and between 5 – 6 wt. % total alkalis (Figure 4.9.). Glass analyses of the three proximal units from To-Cu (Supplementary Material) show that the Plinian Chuseri pumice fall deposits are more homogenous than the overlying Kanegasawa and Utarube eruptive units (Figure 4.9d).

The SG14-0840 glasses are geochemically indistinguishable from the proximal compositions of the To-Cu ash (Figure 4.9); in particular the glass compositions at Lake Suigetsu sit within the tight geochemical range of the Chuseri Plinian pumice fall (Figure 4.9d). This suggests that only ash from the initial Plinian phase of the eruption reached Lake Suigetsu/central Honshu. The Lake

Suigetsu age model provides an eruption age of To-Cu of 5,986 – 5,899 cal. yrs BP (95.4% confidence interval; Table 4.1.), which is marginally younger than proposed by Hayakawa (1983).

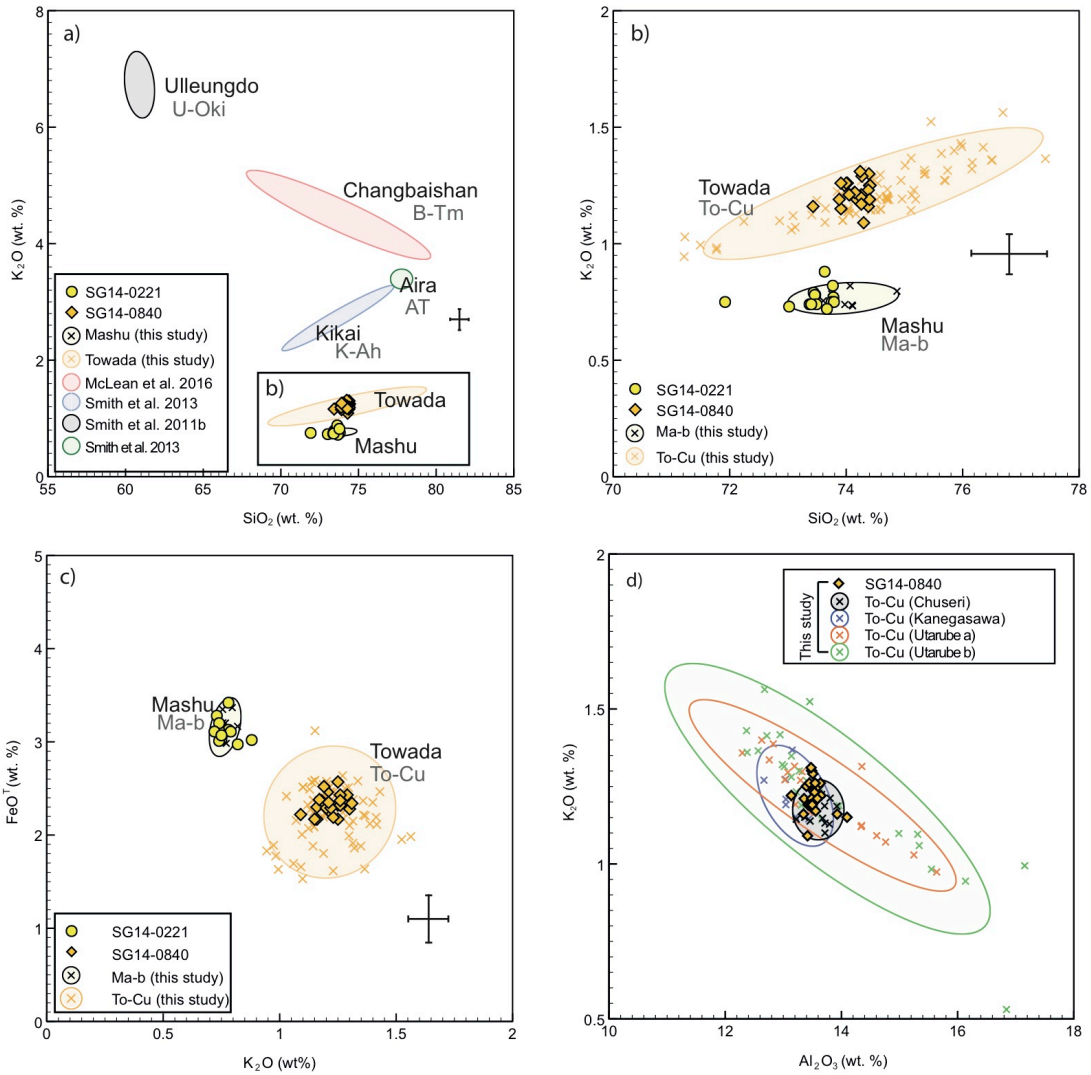


Figure 4.9. Glass shard major element compositions of tephra layers SG14-0221 and SG14-0840 compared to proximal glass compositions from Towada (To-Cu, this study) and Mashu volcano (Ma-b, this study). Glass compositions for other large explosive eruptions from Ulleungdo (U-Oki; Smith et al., 2011a), Kikai (K-Ah, Smith et al., 2013), Aira (AT, Smith et al., 2013) and Changbaishan (McLean et al., 2013) volcanoes are also shown for comparison. Glasses from northern Honshu and Hokkaido have low-K compositions (tholeiite). Volcano (black) and tephra (grey) labels indicate the glasses used to generate the compositional fields. Error bars represent 2 x standard deviation of repeat analyses of the StHs6/80-G MPI-DING standard glass.

Mashu volcano (43°35'N 144°31'E) is situated on the eastern side of Kutcharo caldera in eastern Hokkaido (Figure 4.1.) and is 1160 km NE of Lake Suigetsu. The most recent phase of activity (during the cone building) at Mashu volcano produced three widespread distal ash layers: Ma-c2, Ma-c1 and Ma-b, the youngest (Ma-b) was a large eruption with a Volcanic Explosivity Index (VEI; Newhall and Self, 1982) of 5, which ejected 4.6 km^3 DRE (dense rock equivalent) of magma (Kishimoto et al., 2009). This Ma-b eruption dispersed ash directly southwards (Machida and Arai, 2003), and forms an isochronous marker in several palaeoenvironmental and archaeological sequences in eastern Hokkaido (Wada et al., 2001; Nakagawa et al., 2002; Nakamura et al., 2009). The Ma-b eruption is dated to have occurred between 976 and 774 cal. yrs BP (AD 974 – 1176; Shoji and Masui, 1974).

Glasses erupted during the Holocene activity of Mashu are very low in K_2O (< 1 wt. %) (Nakamura, 2016) and ca. 0.5 wt. % lower than glass compositions from Towada volcano (Figure 4.9; Supplementary Material B). The proximal deposits of the Ma-b eruption have homogenous glass compositions (ca. 73 wt. % SiO_2, ca. 13 wt. % Al_2O_3 and ca. 3 wt. % CaO). Geochemically, the tholeiitic glasses of SG14-0221 are indistinguishable from those of the Ma-b tephra, confirming Mashu (Ma-b) is the source of this ash fall event in Lake Suigetsu. The Lake Suigetsu age model provides the most precise age for the Ma-b eruption (due to the chronological constraint imposed on this portion of the Lake Suigetsu record by the B-Tm ash, dated to AD 946; Oppenheimer, 2017; Hakozak et al., 2017), of 990 – 958 cal. yrs BP (AD 960 – 992; 95.4 % confidence interval).

4.6.4. Kawagodaira (SG14-0490) and Kozushima (SG14-0239) tephra layers

Kawagodaira (34°51'N 138°58'E) is situated on the northwest slope of Amagi volcano, and forms part of the Izu-Tobu cluster of cones on the Izu Peninsula, 290 km E of Lake Suigetsu (Figure 4.1.). The Kawagodaira pumice (KGP) was dispersed during a mid-Holocene eruption from this volcano, and forms a marker layer in sedimentary archives across the central and western parts of Honshu (Hamuro, 1977; Ikeya et al., 1990; Shimada, 2000; Takemura et al., 2010; Figure 4.1.). The KGP tephra layer is very precisely dated by radiocarbon wiggle-matching of a Japanese cedar timber, which was found charred within pyroclastic density deposits of the eruption (Tani et al., 2013), to 3,151 – 3,126 cal. yrs BP (95.4% confidence interval).

Glasses preserved in proximal deposits of the KGP ash span a broad compositional range, with SiO_2 from 77.1 to 77.8 wt. %, CaO from 1.5 to 1.6 wt. %, and K_2O from 2.6 to 2.8 wt. % (Figure 4.10a; Figure 4.10b; Appendix B). The SG14-0490 glasses share the same composition, providing a confident correlation to the KGP. The existing Lake Suigetsu age model provides an age of 3,227 – 3,129 cal. yrs BP (95.4% confidence interval) for the distal KGP tephra (SG14-0490), which overlaps with the wiggle-matched age of the cedar wood from the PDC deposits (Tani et al., 2013). This wiggle-matched age is very precise and therefore, was incorporated into the updated Lake Suigetsu age model presented herein to further constrain the chronology of this portion of the core stratigraphy.

Kozushima (34°12'N 139°09'E), a volcanic island on the Izu arc, 340 km E of Lake Suigetsu (Figure 4.1.), has erupted 18 rhyolitic lava domes that have also been accompanied by explosive phases. The youngest dome, Tenjo-san, was last active during AD 838, which dispersed the distal ash Izu-Kōzushima-Tenjosan (Iz-Kt) tephra westwards (Machida and Arai, 2003). The age of this eruption is recorded in several historical documents including the *Shoku Nihon Koki,* an officially commissioned Japanese historical text (Tsukui et al., 2006). Distally, the Iz-Kt is difficult to stratigraphically and geochemically distinguish from the Niijima-Mukai-yama (Iz-Nm) tephra (Sugiuchi and Fukuoka, 2005; Kobayashi et al., 2007; Suzuki et al., 2017; Tsuchiya et al., 2017), which was dispersed during an eruption from Niijima volcanic island (20 km north of Kozushima) and believed to have occurred in AD 886 (Tsukui et al., 2006).

SG14-0239 glasses overlap the average glass compositions known for both Iz-Kt and Iz-Nm ash layers (Figure 4.10a; Figure 4.10b; Suzuki et al., 2017; Sugiuchi and Fukuoka, 2005). The existing Lake Suigetsu age model provides an age of AD 839 – 767 (95.4 % confidence interval) for the SG14-0239 tephra, which overlaps with the Iz-Kt historical age, and suggests SG14-0239 is too young to correlate to the Iz-Nm tephra. This precise historical age of AD 838 is now incorporated into the Lake Suigetsu age model herein at the position of the SG14-0239/Iz-Kt tephra to further constrain the chronology of this portion of the core.

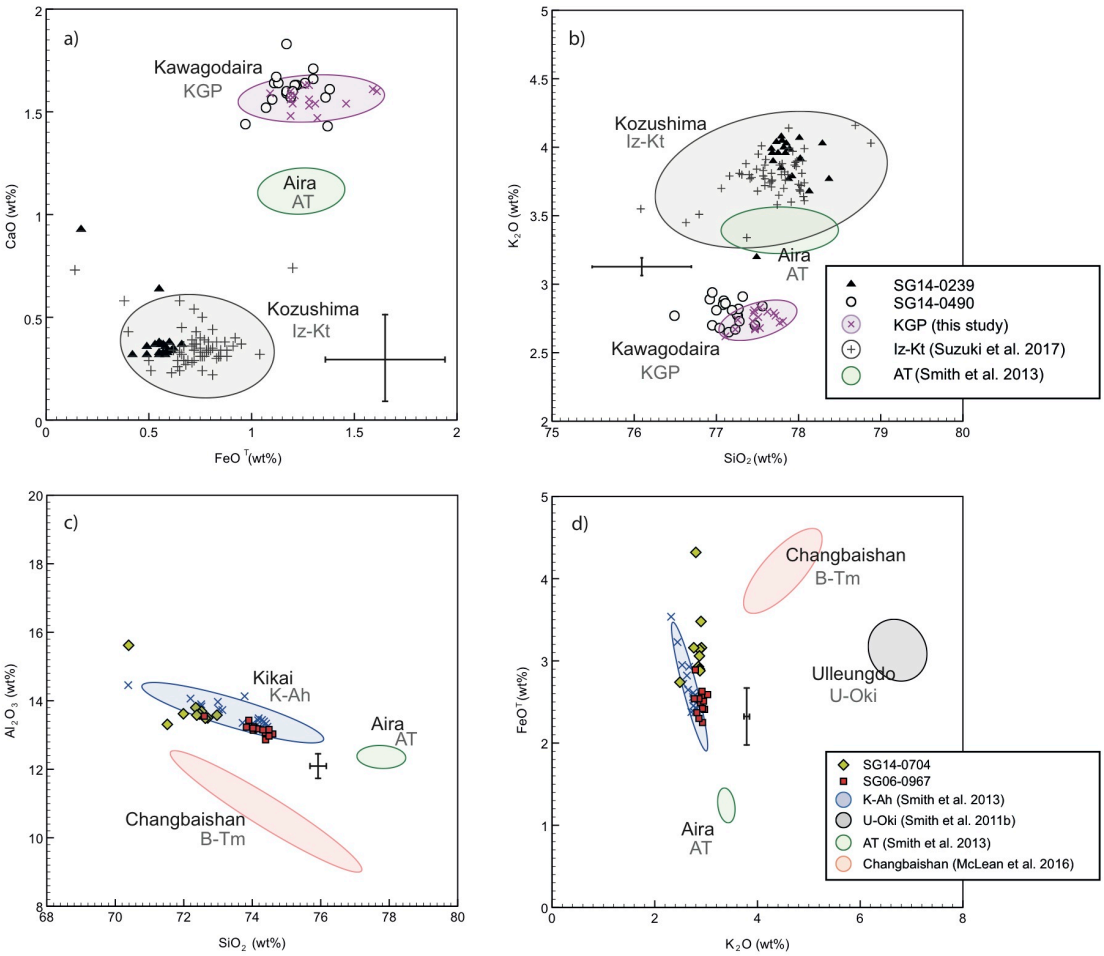


Figure 4.10. Glass shard major element compositions of: (a, b) tephra layers SG14-0239 and SG14-0490 compared to proximal glass compositions from Kawagodaira (KGP; this study) and Kozushima (Iz-Kt; Suzuki et al., 2017) volcanoes, and (c, d) tephra layers SG14-0704 and SG06-0967 (K-Ah ash) compared to other large explosive eruptions from Ulleungdo (U-Oki; Smith et al., 2011a), Aira (AT; Smith et al., 2013) and Changbaishan (B-Tm; McLean et al., 2013). Error bars represent 2 x standard deviation of repeat analyses of the StHs6/80-G MPI-DING standard glass.

4.6.5. Kikai tephra layers (SG06-0967 and SG14-0704)

Kikai caldera (30°47'N 130°18'E) is an active volcano situated 50 km south of Kyushu (Figure 4.1.) and was responsible for the most recent VEI 7 Japanese eruption, which dispersed the Kikai-Akahoya (K-Ah) ash over much of Japan, the Sea of Japan, the Pacific Ocean and the East China Sea (Machida and Arai, 1983). This was one of the largest eruptions during the Holocene,

alongside the Changbaishan ‘Millennium’, Mazama (Crater Lake; Bacon and Lanphere, 2006) and Minoan (Santorini; Watkins et al., 1978) eruptions. The SG06-0967 layer at Lake Suigetsu is correlated to the K-Ah ash (Figure 4.10c; Figure 4.10d; Smith et al., 2013) and was deposited between 7,307 – 7,196 cal. yrs BP (95.4 % confidence interval).

The Lake Suigetsu K-Ah glass compositions are geochemically homogenous, with SiO_2 ranging from 72.6 – 74.6 wt. %, K_2O from 2.8 – 3.0 wt. % and CaO from 1.8 – 2.3 wt. % (Figure 4.10c; Figure 4.10d; Smith et al., 2013). However, glass chemistries obtained by Smith et al., (2013) from medial ash deposits suggests that the K-Ah eruption was more heterogeneous, with SiO_2 ranging from 70.4 – 77.8 wt. %. Interestingly, the younger SG14-0704 glass compositions overlap with the less evolved end-member of the K-Ah medial tephra (Smith et al., 2013; Figure 4.10c), which suggests that the SG14-0704 tephra could correlate to another eruption from Kikai caldera. SG14-0704 is dated to 4,894 – 4,827 cal. yrs BP (95.4 % confidence interval) via the Lake Suigetsu chronology, which does not correlate to any known eruption events from Kikai (Moriwaki et al., 2016). Many of the Holocene eruptions from in and around Kyushu Island are poorly dated and lack detailed geochemical data, which means it is problematic to robustly correlate these events. Additional geochemical datasets are required from proximal deposits in the south of Japan to strengthen this potential correlation.

4.6.6. Tephra layers pending further analysis for correlation

The rhyolitic glasses from visible tephra layers SG14-0781 (5,519 – 5,480 cal. yrs BP) and SG06-0588 (4,066 – 3,986 cal. yrs BP) are compositionally heterogeneous, spanning broad SiO_2, FeOt, CaO and Al_2O_3 ranges that are typical of central Japan arc volcanism (Table 4.1; Figure 4.7.). Visible tephra layers with similar compositions are also observed in the older SG06 sediments (Smith et al., 2013), suggesting that they are older eruptions from the same volcanic source/s or region. Both SG14-0781 and SG06-0588 contain shards with similar morphologies (i.e., pumiceous and densely vesicular), which are also observed in SG14-0513, SG14-0373 and SG14-0058 cryptotephra layers. Chronologically, SG14-0781 and SG06-0588 are consistent with ages of known Holocene eruptions at Sambe volcano (Figure 4.1.), the Shigaku S2 and Taiheisan tephra layers (Fukuoka and Matsui, 2002), but there are no proximal datasets for these units**.** The geochemical assessments of these layers and other pre-Holocene activity at Sambe are further explored by Albert et al*.,* (2018).

SG14-1185 glass compositions are not consistent with those known from Japan or from Changbaishan or Ulleungdo (Figure 4.7.), and therefore may originate from a more distal volcanic source. The compositional range is similar to glasses from Kamchatka (Ponomareva et al., 2017), however slight differences in FeO^T, Na_2O and CaO place SG14-1185 on a different evolutionary trend and a preclude a correlation at this time. The source of this tephra layer is currently unknown, and it could represent a very far-travelled ash layer.

4.7. Discussion

4.7.1. An integrated tephrostratigraphic framework

The Lake Suigetsu record provides the most comprehensive Holocene tephrostratigraphy for the East Asian/Pacific region, with twenty isochrons from at least nine different volcanic centres (Figure 4.11). This new framework precisely dates and integrates ash layers from across Japan, South Korea (Ulleungdo volcano) and North Korea/China (Changbaishan volcano), and therefore is a key tephrostratotype for correlating and dating records in this region (Figure 4.12). These results clearly demonstrate the potential of cryptotephra analysis, even in a productive arc setting, to identify new isochrons from distal sources and provide new insights into the dispersal characteristics and age of these eruptions.

The cryptotephra study from Lake Suigetsu has significantly extended the known ash dispersal of numerous key Holocene marker layers, including the Ma-b, Iz-Kt, To-Cu, U-2 and U-3 tephra layers, and has also identified tephra from eruptions with primary plume dispersals in the opposite direction (e.g., To-Cu; Figure 4.1.). Previously, the Ma-b ash had only been found in SE Hokkaido, but is now confirmed over 1100 km from its source as a cryptotephra marker in the Lake Suigetsu SG14 core. This establishes the Ma-b tephra as one of the most widely dispersed Japanese Holocene isochrons, and suggests that it may be preserved in more terrestrial and marine sedimentary sequences across East Asia.

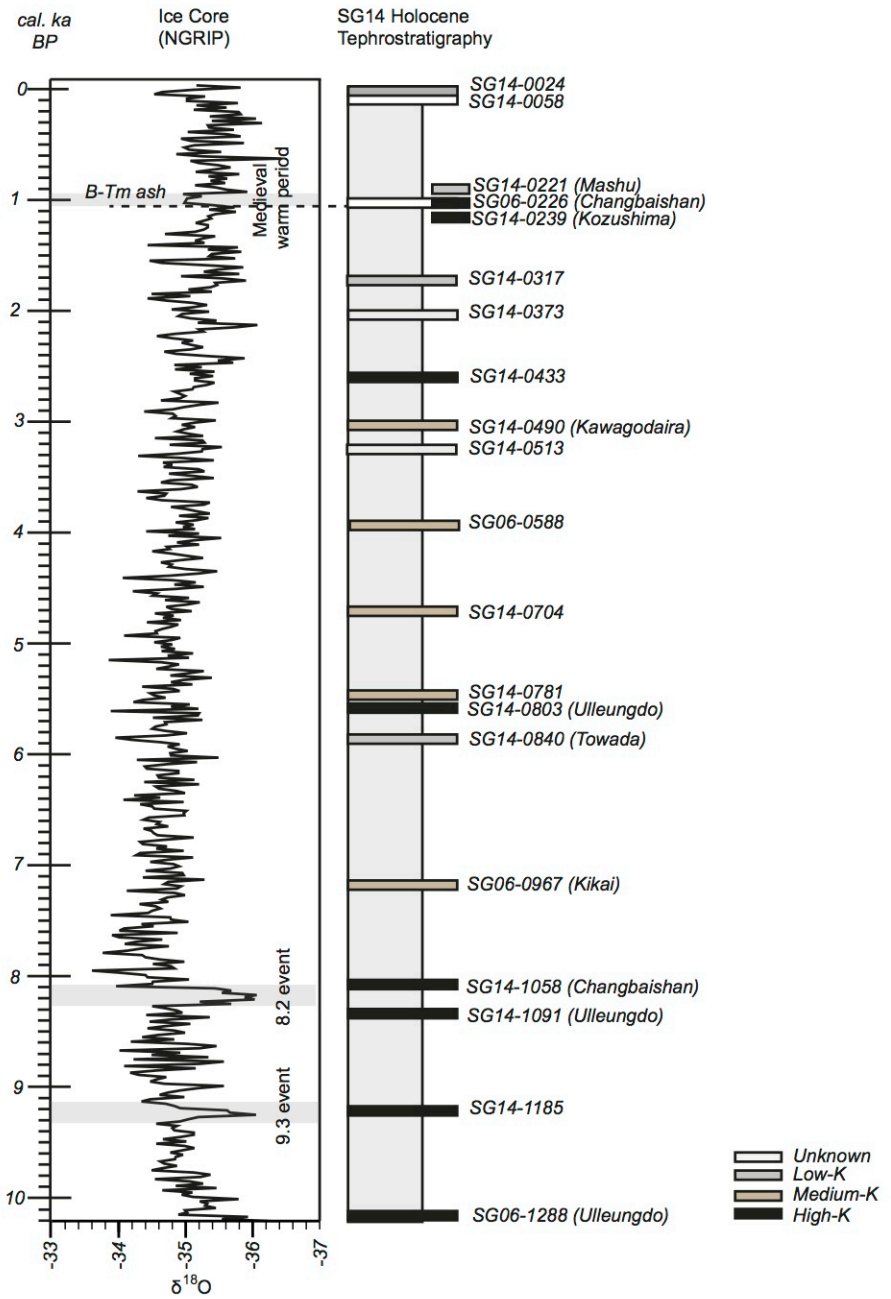


Figure 4.11. Summary of the Lake Suigetsu Holocene tephrostratigraphy, and the positioning of isochrons against the Greenland ice core (NGRIP) $\delta^{18}O$ record (NGRIP members, 2004). The B-Tm ash (AD 946; Oppenheimer et al., 2017) is identified in both high-resolution archives, and occurs close to the onset of the Medieval Warm Period climate anomaly. The K-content of the glasses in these isochrons is shown. A few distinctive tephra are recorded in Lake Suigetsu during the early Holocene, which occur close to several rapid climatic anomalies, such as the 8.2 ka event that is observed in Greenland. These marker layers could be used to establish whether these events are synchronous with anomalies recorded in Japan.

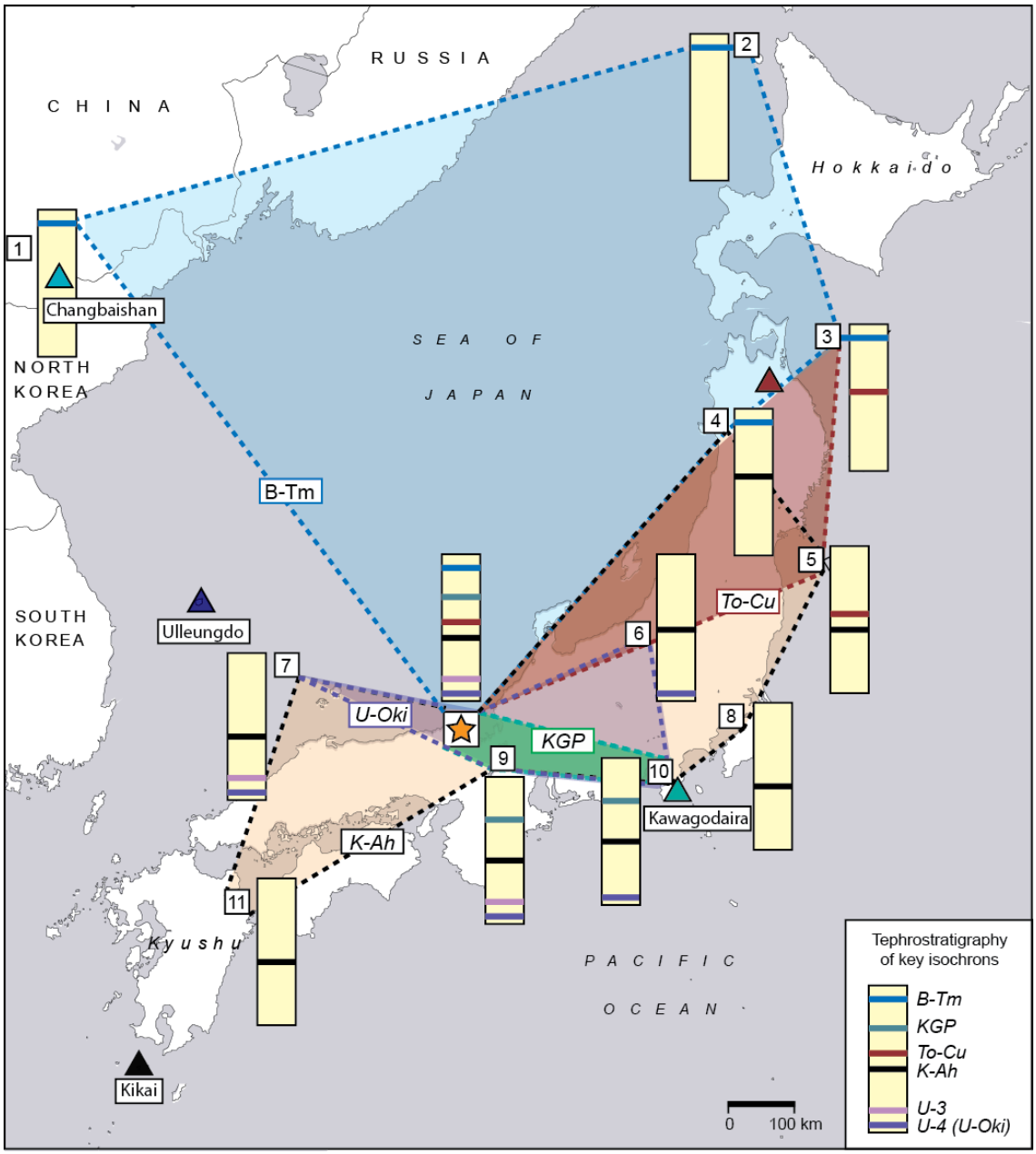


Figure 4.12. Holocene sections of sedimentary archives (numbered squares) situated in eastern China and Japan that can be integrated using the widespread B-Tm, KGP, To-Cu, K-Ah, U-3 and U-4 (U-Oki) tephra layers. [1] Longgang volcanic field (Sun et al., 2015); [2] Lake Kushu (Chen et al., 2016); [3] Sanriku Coast (Ishimura et al., 2014); [4] Lake Ichi-no-Megata, (Okuno et al., 2011); [5] SK-2 core (Sagawa et al., 2014); [6] Lake Nojiri (Kumon et al., 2003); [7] KT96-17 P-2 (Domitsu et al., 2002); [8] Lake Aoki (Adhikari et al., 2002); [9] Lake Biwa (Nagahashi et al., 2004); [10] Ukishima-ka-hara (Fujiwara et al., 2007); [11] Beppu Bay (Yamada et al., 2017). Tephra layers identified in the Lake Suigetsu sequence originate from several different volcanic sources in the East Asian/Pacific region and thus can be used to precisely integrate terrestrial and marine records spanning these dispersal axes.

In this study, we have discovered several new previously unreported ash layers, which have now been incorporated within the master tephrostratigraphic framework for this region. One previously unknown eruption from Changbaishan is now confirmed (dated to 8,166 – 8,099 cal. yrs BP; 95.4% confidence interval), which provides significant development in resolving the poorly constrained explosive history of this volcano. These previously unreported distal ash layers are either from eruptions that are not preserved in the proximal eruption sequences, or the reported ages from the proximal deposits are incorrect.

4.7.2. Resolving the tempo of East Asian volcanism

The exceptional chronology of the Lake Suigetsu sediments enables us to provide precise and constrained eruption ages for the tephra layers (Table 4.1.). This chronology has significantly improved the eruption ages for many significant explosive events, like the large (VEI 5) Holocene eruption of Mashu (Ma-b tephra), which now has a reduced uncertainty of ca. 170 years (95.4 % confidence interval). The improved eruption ages for many of these key widespread ash layers can now be incorporated into other site-specific age models containing these markers, meaning it may be of significant benefit to specifically search for such isochrons in these records. Furthermore, since many of these marker layers were dispersed across the Pacific and/or the Sea of Japan, like those originating from Ulleungdo, our terrestrially-based ages can be used to circumvent reservoir offsets that result in inaccurate radiocarbon-based marine chronologies (e.g., Ikehara et al., 2011).

The detailed Lake Suigetsu tephrostratigraphy has significant importance for hazard assessment studies in the East Asian/Pacific region. For example, Suigetsu is the first distal record to unequivocally contain, characterise and date three successive Holocene eruptions from Ulleungdo (U-4, U-3, and U-2 tephra layers) and most likely contains the first distal evidence of the U-1 event. The uncertainty of the U-2 eruption has now been significantly reduced (by ca. 25 years), which indicates that there was a repose interval of ca. 2.8 ka following the U-3 eruption. If SG14-0433 is confirmed as a tephra isochron of the U-1 eruption, a very similar repose interval of ca. 3 ka is also calculated. It is likely that the older sediments of Lake Suigetsu may also preserve a detailed record of Quaternary volcanism from Ulleungdo, which can permit a further understanding of the tempo and frequency of this volcanic centre.

In general, the Lake Suigetsu tephrostratigraphy suggests that an ash fall reached the central Honshu region at least once every 500 years throughout the Holocene. We suggest that these must have been at least VEI 4 events to be recorded as cryptotephra layers in Lake Suigetsu. It is clear that cryptotephra analysis in high-resolution distal archives can be used to provide additional information on these smaller eruption events that currently appear to be missing from the geological record (Kiyosugi et al., 2015). These findings are of significant importance for risk assessments in East Asia. For instance, the ‘International Atomic Energy Agency’ require a detailed catalogue of past Holocene ash fall events to be compiled (e.g., eruption frequency, tephra

thickness and direction of dispersal) before power plant construction is considered (Aspinall et al., 2016).

4.7.3 Layers for synchronising palaeoenvironmental records

The most valuable tephra layers for palaeoenvironmental research are those which are i) regionally widespread, ii) possess a unique geochemical signature, iii) are precisely dated, and iv) occur at, or bracket a climate/cultural change. A key example from East Asia is the B-Tm ash, since it is identified across the Northern hemisphere (reaching Greenland; Sun et al., 2014b), is precisely dated to AD 946 (Oppenheimer et al., 2017; Hakozak et al., 2017) is easily distinguished by its heterogeneous high-K composition, and occurs stratigraphically close to the onset of the Medieval Warm Period. The updated Holocene tephrostratigraphy from Lake Suigetsu indicates that there are several other widespread, geochemically unique, and now precisely dated isochrons that could be used to test and assess a range of questions relating to palaeoenvironmental change and drivers of the climate. For example, an abrupt cooling transition is known to have occurred ca. 8.2 ka yrs BP (widely known as the '8.2 event') via proxy records in Greenland (Figure 4.11.) and across the North Atlantic region (see Alley et al., 1997). The global synchronicity and duration of this event remains widely debated, however a similar abrupt cold event is dated to have occurred at 8.21 ± 0.05 kyr BP in China (Cheng et al., 2009). The newly identified Changbaishan ash layer, dated to 8,166 – 8,099 cal. yrs BP (Figure 4.12.), could therefore offer an important isochron to improve the chronology of palaeoclimate records in Japan, and assess any synchronous

environmental changes during this time. It is therefore of significant importance to continue to search for ash layers in other palaeoenvironmental sites in the East Asian/Pacific region, which can permit a new perspective on such long-standing climate questions.

4.8. Conclusions

This study provides the first detailed Holocene cryptotephra study for the East Asian/Pacific region, and highlights the ability to identify distal ash layers in a productive arc setting. Primary ash layers can be resolved even in lacustrine sediments that contain high concentrations of background glasses, if they contain distinctive shard morphologies and/or unique geochemical compositions. The Lake Suigetsu Holocene tephrostratigraphy provides the most comprehensive record to date of volcanism from East Asia, and is able to integrate twenty ash layers from a range of eruption magnitudes. As a result, these findings have now significantly extended the known ash dispersal of numerous key Holocene marker layers, including the Ma-b ash (Mashu), which is now identified over 1,100 km from its source, and thus forms one of the most widely dispersed Japanese isochrons.

The Lake Suigetsu chronology is able to provide constrained eruption ages for all twenty ash layers, which offer a new insight into the frequency of explosive events from many of the volcanoes, including more precise repose intervals. These isochrons can now be robustly used to date and synchronise sedimentary records across Japan. Several of these stratigraphically constrain

the onset and occurrence of rapid climate anomalies that occurred during the Holocene, and could provide a better understanding of climate drivers in this region. More work is required to robustly constrain the dispersal boundaries of these isochrons, with additional proximal glass geochemical datasets essential to testing future regional and hemispheric scale tephra correlations.

Acknowledgements

DM is funded by NERC (grant: NE/L002612/1) and part of the Environmental Research Doctoral Training Program at the University of Oxford. PGA and RAS are supported by Early Career Fellowships from the Leverhulme Trust (grant: ECF-2014-438 and ECF-2015-396). The Fukui-SG14 sediment coring campaign was funded by the Fukui Prefectural government, and the coring was conducted by the team of Seibushisui Co. Ltd. Japan, led by A. Kitamura. KAKENHI grant by MEXT, Japan (15H021443) was used to purchase laboratory equipment and consumables during the project. The authors would also like to thank M. Yamada for his assistance during the proximal sampling field campaign and two anonymous reviewers for their comments.

See Appendix B for Supplementary Material

CHAPTER 5: THIRD ARTICLE

AN IMPROVED ERUPTION CHRONOLOGY FOR EXPLOSIVE VOLCANISM IN EAST ASIA (ASO AND AIRA) BETWEEN 50 AND 30 KA: A HIGH-RESOLUTION STUDY FROM LAKE SUIGETSU, JAPAN

DANIELLE MCLEAN[a], PAUL G ALBERT[a], TAKEHIKO SUZUKI[b], TAKESHI NAKAGAWA[c], JUN-ICHI KIMURA[d], QING CHANG[d], ALISON MACLEOD[e,f], SIMON BLOCKLEY[e], RICHARD STAFF[a,c], KEITARO YAMADA[h], IKUKO KITABA[c], TSUYOSHI HARAGUCHI[l], JUNKO KITAGAWA[j], SG14 PROJECT MEMBERS[k] AND VICTORIA C SMITH[a]

[a] *Research Laboratory for Archaeology and the History of Art, University of Oxford, Oxford, OX1 3TG, UK*

[b] *Department of Geography, Tokyo Metropolitan University, Tokyo, 192-0397, Japan*

[c] *Research Centre for Palaeoclimatology, Ritsumeikan University, Kyoto, 603-8577, Japan*

[d] *Department of Solid Earth Geochemistry, Japan Agency for Marine-Earth Science and Technology, Yokosuka, Japan*

[e] *Department of Geography, Royal Holloway University of London, TW20 OEX, UK*

[f] *Department of Geography and Environmental Science, University of Reading, RG66AB, UK*

[g] *Scottish Universities Environmental Research Centre, University of Glasgow, East Kilbride, G75 0QF, UK*

[h] *Institute for Geothermal Sciences, Kyoto University, Kusatsu, 525-8577, Japan*

[i] *Osaka City University, Osaka, 558-8585, Japan*

[j] *Fukui Prefectural Satoyama-Satoumi Research Institute, Wakasa, 919-1331, Japan*

[k] *www.suigetsu.org*

Highlights:

- Cryptotephra layers are four times more frequent than visible markers in the Suigetsu cores spanning 50 - 30 ka
- New insight into ash fall events dispersed to central Japan
- Explosive events are dated using the high-precision Suigetsu chronology
- Insight into eruption tempo and magma evolution at Aso caldera
- Aira eruption history constrained prior to the enormous AT event (VEI 7)

Abstract

Volcanoes in the East Asian/Pacific region have been the source of some of the largest magnitude eruptions during the Quaternary, and accurately evaluating their eruptive histories is essential for hazard assessments. To overcome difficulties in resolving and precisely dating eruption events in the proximal realm, the high-resolution sediments of Lake Suigetsu (central Honshu, Japan) were examined for the presence of non-visible (cryptotephra) layers prior to the AT caldera-forming event of Aira (e.g., 50 to 30 ka). Cryptotephra layers are four times more frequently preserved than visible markers in the Suigetsu sediments, providing a unique and unprecedented record of eruptions that were dispersed towards the densely populated regions of central Honshu. Major and trace element volcanic glass chemistry is used to fingerprint the ash layers and pinpoint their volcanic origin. Tephra are found throughout the investigated sediments, but the highest abundance of ash fall events are recorded between 38 – 30 ka, capturing a period of intense volcanism at calderas on Kyushu Island (Japan). The augmented Suigetsu tephrostratigraphy records seven eruption events from Aso caldera (southern Kyushu) that post-date the

widespread ACP-4 Plinian eruption (ca. 50 ka), and four explosive events from Aira (central Kyushu) that occurred leading up to the enormous caldera-forming AT eruption (VEI 7). Cryptotephra investigations also reveal ash fall from intraplate volcanoes west of Japan, Ulleungdo (ca. 500 km NW from Suigetsu, South Korea) and Changbaishan (ca.1000 km NW, North Korea/China), which have not been reported in proximal eruption stratigraphies.

Keywords: Japanese volcanism; Aso caldera, Aira caldera; Lake Suigetsu; Cryptotephra; Glass geochemistry; Bayesian age-modelling

5.1. Introduction

Volcanoes distributed across the heavily populated East Asian/Pacific region have been the source of some of the largest known caldera-forming events, known to have blanketed Japan and the surrounding seas in ash (Simkin and Siebert, 2000; Machida and Arai, 2003). Accurately reconstructing the tempo and magnitude of pre-historic eruptions at these volcanoes is an essential component of risk and hazard assessments (Kiyosugi et al., 2015). Unfortunately, the burial, destruction and subsequent erosion of eruption deposits in near-source areas contribute to an incomplete geological record, hampering our ability to accurately reconstruct eruption histories. Piecing together fragmentary records from around the volcano, is further complicated by the fact that many centres, including Japanese volcanoes, erupt successive deposits with geochemically overlapping compositions (e.g., Kimura et al., 2015; Albert et al., accepted), consequently deciphering the true number of

events is challenging and results in an under-recording of eruptions (e.g., Albert et al., 2018). Furthermore, precisely evaluating the tempo and reoccurrence intervals of past eruptions using proximal volcanic successions is difficult, and for many volcanoes in Japan this remains a significant obstacle, particularly at Low-K (Tholeiitic) and Medium-K (calc-alkaline) centres where mineral phases are largely unsuitable for the $^{40}Ar/^{39}Ar$ method. Consequently, dating of eruptions in the last 50 ka is heavily reliant on the sporadic discovery of charcoal fragments suitable for ^{14}C dating.

Fortunately, volcanic ash (tephra) deposits are routinely identified in distal sedimentary (palaeoclimate and archaeological) archives in and around Japan (Machida and Arai, 2003), which provide critical insights into the tempo, behaviour and dispersal of highly-explosive volcanism in East Asia (e.g., Furuta et al., 1986; Kimura et al., 2015; Mahony et al., 2016; Kutterolf et al. 2017; Albert et al., 2018; McLean et al., 2018). The Lake Suigetsu sedimentary archive provides a key tephrostratotype of explosive events, and the unique high-precision chronology (Bronk Ramsey et al., 2012) means that tephra layers identified in the radiocarbon timeframe can be robustly dated (Smith et al., 2011a, 2013; McLean et al., 2016, 2018; Albert et al., 2018, accepted). The Suigetsu sediments also preserve numerous non-visible (cryptotephra) layers throughout the sequence (McLean et al., 2018), which are derived from more distal and/or lower magnitude events.

This paper explores the cryptotephra record preserved in the fourteen meters of varved Lake Suigetsu sediments (SG14 core), dated between 50 and 30 ka, to

provide new insight into the frequency, magnitude and dispersal of large eruptions prior to the AT event (VEI 7; Aira volcano). Large calderas downwind of Suigetsu (i.e., on the Ryukyu-Kyushu arc; Figure 5.1), and Aira and Aso in particular, are thought to have been very active between this period, based on the record preserved in the proximal stratigraphies (Nagakoa et al., 2001; Miyabuchi, 2009; 2011), yet almost no distal ash equivalents are widely identified. Most eruption ages established through this period are poorly constrained, and are either broadly extrapolated with their association to the AT ash, or radiocarbon dated via palaeosols developed during periods of quiescence. A more precise eruption chronology can aid our understanding of the magmatic behaviour of these centres prior-to (e.g., Aira) or following (e.g., Aso) large caldera-forming events.

5.2. Study site

5.2.1. Lake Suigetsu

Lake Suigetsu is the largest of the 'Mikata Five Lakes', located in a small tectonic basin on the western side of the Mikata fault line, Honshu Island, central Japan (Figure 5.1; 35°35'0''N, 135°53'0''E, 0 m above present sea level). Suigetsu covers an area of ca. 4.3 km^2 and has an average water depth of ca. 34 m (Kitagawa and van der Plicht, 1998a). The main tributary is the River Hasu, which enters on the southeast side of Lake Mikata and flows through a narrow channel into Lake Suigetsu. This hydrological setting means coarse sediments are preferentially deposited in Lake Mikata, and only fine-grain sedimentation accumulates in Lake Suigetsu (Schlolaut et al., 2012).

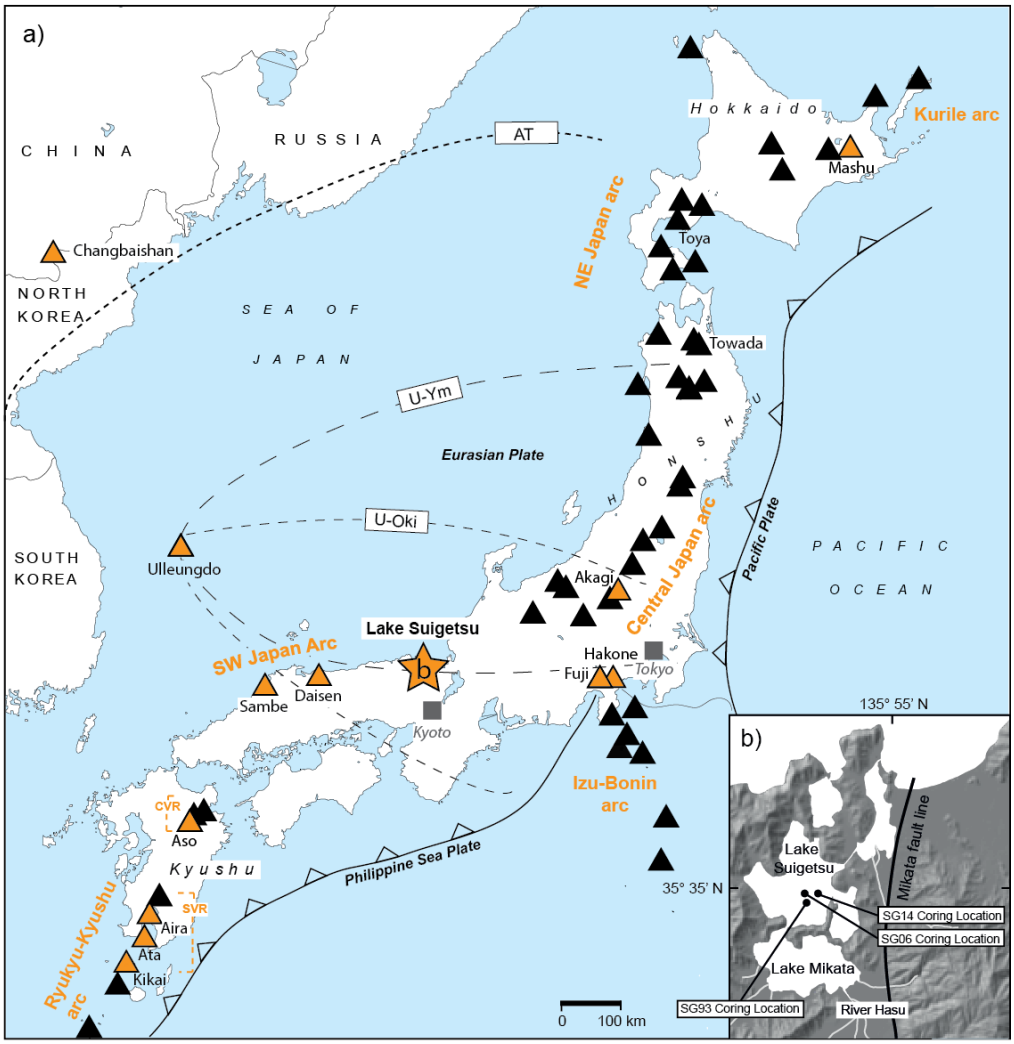


Figure 5.1. (a) Volcanoes in Japan, North Korea/China (Changbaishan) and South Korea (Ulleungdo) (black and orange triangles) known to have been active during the Quaternary (data from Machida and Arai, 2003). Large caldera volcanoes are concentrated on the Kyushu Central and Southern Volcanic Region (CVR/SVR; south) and the NE Japan arc in Hokkaido (north), associated with areas of largest magma production (Kimura et al., 2015). In contrast, only two Quaternary volcanoes (Sambe and Daisen) are found on the SW Japan arc. Volcanoes mentioned within the text are coloured orange, and a star denotes the location of Lake Suigetsu. The visible ash dispersal for the AT (Aira volcano; 30 ka) tephra and two Ulleungdo eruptions (U-Oki; 10 ka and U-Ym; 39.8 ka) are marked by dashed lines (AT and U-Oki as defined by Machida and Arai, 2003 and in Chapter 6). (b) Location of the five Mikata lakes, which are situated west of the active Mikata fault line, adjacent to Wakasa Bay. The positions of coring campaigns SG93, SG06 and SG14 are marked on Lake Suigetsu (modified after Nakagawa et al., 2005).

The Suigetsu lake sediments have been cored on multiple occasions, with the first complete piston core (named 'SG93') recovering 72.4 m of sedimentation

from the centre of the lake (35°34'51''N, 135°53'75''E; Kitagawa and van der Plicht, 1998a). In addition, the 'SG06' core (ca. 250 m north of SG93; 35°35'08''N, 135°52'57''E) was obtained as part of the 'Lake Suigetsu Varved Sediment Project' in 2006, which retrieved 73.2 m of continuous sedimentation, from four overlapping boreholes (A, B, C and D, situated ca. 20 m apart; Nakagawa et al., 2012). The SG06 core has been extensively radiocarbon (^{14}C) dated and is varved between ca. 10 and 70 ka (Staff et al., 2011; Bronk Ramsey et al., 2013; Marshall et al., 2012; Schlolaut et al., 2012), which provides a very high-resolution chronology for this key palaeoenvironmental record.

More recently, the lake was re-cored to recover another complete master sequence, named 'Fukui-SG14' ('SG14' in short), to provide additional material for scientific analysis and to prepare sediments for display at the *Suigetsu Varve Museum*, located in Fukui Prefecture. The sediments were obtained from new boreholes E, F, G and H, which were located ca. 320 m further east of those from SG06.

5.2.2. Sources of tephra dispersed to Lake Suigetsu

Thirty-one visible ash layers (named using their SG06 Composite Depths (CD)) were originally identified in the SG06 core (Smith et al., 2011a, 2013; McLean et al., 2016), most of which originate from arc volcanoes south of Suigetsu and were dispersed via the prevailing westerly winds. The thickest tephra beds preserved in the sediments are correlated to well-known caldera forming

eruptions (VEI 6 – 8) from four active or buried volcanoes situated on the Kyushu Central and Southern Volcanic region (Kikai, Aira, Aso and Ata; Figure 5.1.), that also form key tephrostratigraphic markers in terrestrial and basin records of the Japanese islands, and hemipelagic sediments in the northwest Pacific (see Machida and Arai, 2003). These include the K-Ah and K-Tz (7.2 ka and ca. 95 ka, respectively; Kikai caldera), AT (30 ka; Aria caldera), Aso-4, Aso-A (86.4 ± 1.1 ka and ca. 98 ka respectively; Aso caldera) and Ata (ca. 100 ka; Ata) tephra markers (Smith et al., 2013; Albert et al., accepted). Glass erupted from caldera volcanoes located in and around the Kyushu Islands are typically Medium-K (calc-alkaline) or High-K (ca-alkaline) in composition (Machida and Arai, 2003; Kimura et al., 2015; Albert et al., accepted).

Many of the thinnest visible ash layers preserved in the core possess overlapping rhyolitic glass chemistries which span heterogeneous major element compositions, and are correlated using trace element analysis to activity from Daisen and Sambe volcanoes on the SW Japan arc (Albert et al., 2018). Furthermore, three visible tephra layers (SG06-0226, SG14-1091 and SG06-1288) were erupted from intraplate volcanoes, Ulleungdo (South Korea) and Changbaishan (North Korea/China) (Figure 5.1.), which have dispersed ash over Japan several times during the Quaternary and are easily discriminated by their alkaline compositions (Machida and Arai, 2003; Smith et al., 2011a; McLean et al., 2016, 2018)

The visible tephrostratigraphic sequence investigated here (50 to 30 ka), is composed of four key markers, which include the Central Pumice Cone 4

(ACP4) eruption from Aso (ca. 50 ka; correlated to Suigetsu tephra SG06-3912), Ikeda (SI) tephra erupted from Sambe (ca. 46 ka; SG06-3668), an eruption from Ko-Fuji (ca. 44 ka; SG06-3485) and the AT tephra (ca. 30 ka; SG06-2650) erupted from Aira (Smith et al., 2013; Albert et al., 2018; accepted). As previously outlined, detailed cryptotephra analysis is able to integrate eruption stratigraphies from more distal sources (e.g., ash erupted form along the Izu-Bonin and NE Japan arc; McLean et al., 2018), and therefore is it possible that cryptotephra layers identified within these sediments may also originate from other more distal sources across East Asia.

5.3. Materials and Methods

5.3.1. Cryptotephra extraction techniques

The master SG14 core (composite sequence) was contiguously sub-sampled at a ca. 5 cm resolution, from the ACP4 tephra (39.1 m CD) to the base of the AT tephra (26.5 m CD), avoiding the known high-energy event layers (e.g., flood horizons). If elevated shard concentrations were observed in the ca. 5 cm sample, the sediment was resampled at a 1 cm resolution to determine the precise stratigraphic positioning of the peak. All samples were wet sieved through a 25 μm mesh, and processed using the heavy liquid floatation method outlined by Turney (1998) and Blockley et al. (2005). These samples were prepared alongside blanks to test for possible laboratory contamination. The extraction residues were mounted on slides using Canada Balsam, and glass

shards were counted via microscopic examination to quantify the number of shards per gram of dried sediment (s/g). Glass shards were extracted from samples chosen for geochemical analysis and hand-picked from a welled-slide using a micromanipulator (see Lane et al., 2012). These shards were mounted in Epoxy resin stubs, which were sectioned and polished to expose a flat surface, and carbon coated for electron microprobe analysis.

5.3.2. Major element glass compositions

Major and minor element compositions of individual glass shards were measured using a JEOL-8600 wavelength-dispersive electron microprobe (WDS-EMP) at the Research Laboratory for Archaeology and History of Art (RLAHA), University of Oxford. All analyses used an accelerating voltage of 15 kV, beam current of 6 nA and 10 µm-diameter beam. Peak counting times were 12 s for Na, 50 s for Cl, 60 s for P, and for 30 s for all other elements. The electron microprobe was calibrated using a suite of mineral standards, and the PAP absorption correction method was applied for quantification. The accuracy and precision of this data were assessed using analyses of the MPI-DING reference glasses (ATHO-G-1, StHS6180-G and GOR132-G) from the Max Plank Institute (Jochum et al., 2006), which were run as secondary standards. Analyses of these secondary standards lie within the standard deviation of the preferred values and are presented in the Supplementary Material (Appendix C). Data were filtered to remove non-glass analyses, and those with analytical totals < 93%. The raw values were normalised (to 100 %) for comparative

purposes and to account for variable hydration, and are presented as such in all tables and figures.

5.3.3. Trace element analysis of the glass shards

Trace element compositions were measured by laser ablation inductively coupled plasma mass spectrometry (LA-ICP-MS) at the Department of Solid Earth Geochemistry, Japan Agency for Marine-Earth Science and Technology (JAMSTEC). The analytical equipment used include the deep-ultraviolet (200 nm) femtosecond laser ablation system (DUV-FsLA) of OK-Fs2000K (OK Laboratory, Tokyo, Japan) connected to the modified high-sensitivity sector field ICP-MS of Element XR (Thermo Scientific, Bremen, Germany). All analyses used a 25 μm crater diameter and depth, and conditions followed that reported by Kimura and Chang (2012). Ten major elements including P_2O_5 and 33 trace elements were analysed for each sample, and were also run alongside several MPI-DING references glasses (Jochum et al., 2006), and the BHVO-2G standard provided by the Geological Survey of Japan. Accuracies of the BHVO-2G glass analyses are typically < 3 % for most elements, < 5 % for Sc, Ga, Sm, Eu, Gd, U and < 10 % for Ni, Cu, Lu. Full trace element datasets and secondary standard analyses are provided in the Supplementary Material (Appendix C).

5.3.4. Chronology of the Lake Suigetsu sediment cores

The SG06 and SG14 master sequences have been precisely tied using 361 common marker layers (including tephra layers), which permits the high-precision SG06 chronology to be transferred to the SG14 core (correlation model 08 May ’16). The software package developed to handle the correlation of parallel core sections, ‘LevelFinder’ (ver. 7.5.5, http://polsyems.rits-palaeo.com), was used to linearly extrapolate between the common marker layers and determine any given composite depth (CD) or EFD from the individual SG06 and SG14 cores (see Nakagawa et al., 2012). The composite Suigetsu sedimentary sequence was modelled on to the IntCal13 timescale (Reimer et al., 2013) implementing three successive cross-referenced Poisson-process (‘P_Sequence’) depositional models using OxCal (ver. 4.3; Bronk Ramsey, 2008, 2017). These include 775 AMS ^{14}C dates obtained from terrestrial plant macrofossils from the upper 38 m (SG06-CD) of the SG93 and SG06 cores (Kitagawa and Van der Plicht, 1998a; 1998b, 2000; Staff et al., 2011, 2013a, 2013b) and varve counting between 12.88 and 31.67m SG06 CD (Marshall et al., 2012; Schlolaut et al., 2012). SG06 event-free depth(s) (EFD, ver. 29th Jan '11) were used within the age model, which excludes instantaneous deposits > 5 mm in thickness, (i.e., event layers) (Staff et al., 2011; Scholaut et al., 2012).

5.4. Results

5.4.1. Tephrostratigraphy

Twenty-five ash layers (five visible and twenty cryptotephra layers) are identified in the SG14 varved sediments between 50 and 30 ka (39.1 m CD to 26.5 m CD) (Figure 5.2; Table 5.1.). These ash layers are herein labelled using their SG14 composite depth in cm (SG14-CD correlation model 30 May ’17) that is rounded to the nearest integer (Table 5.1.). For continuity, SG06 labels are used for the visible tephra layers that were previously identified and geochemically characterised in the SG06 cores, SG06-3912 (ACP4, Aso), SG06-3668 (SI, Sambe), SG06-3485 (Ko-Fuji), SG06-2650 (AT, Aira) (Smith et al., 2013; Albert et al., 2018; accepted) (Figure 5.2.). An additional visible ash layer < 1 mm thick (named SG14-3216) was identified in this study of the SG14 cores.

Cryptotephra layers are clearly identified within the sediments as they are characterised by significant peaks in glass shard concentrations, which range from 1,400 s/g to > 20,000 s/g. Glass shard characteristics (e.g., shard size, morphology and colour) vary considerably between isochrons (Table 5.1.), but remain relatively uniform in each layer. This provides a first order discrimination between primary and secondary ash layers, since ash is well-sorted during dispersal, but reworking processes tend to mix glass from several sources (as observed in event layers; McLean et al., 2018).

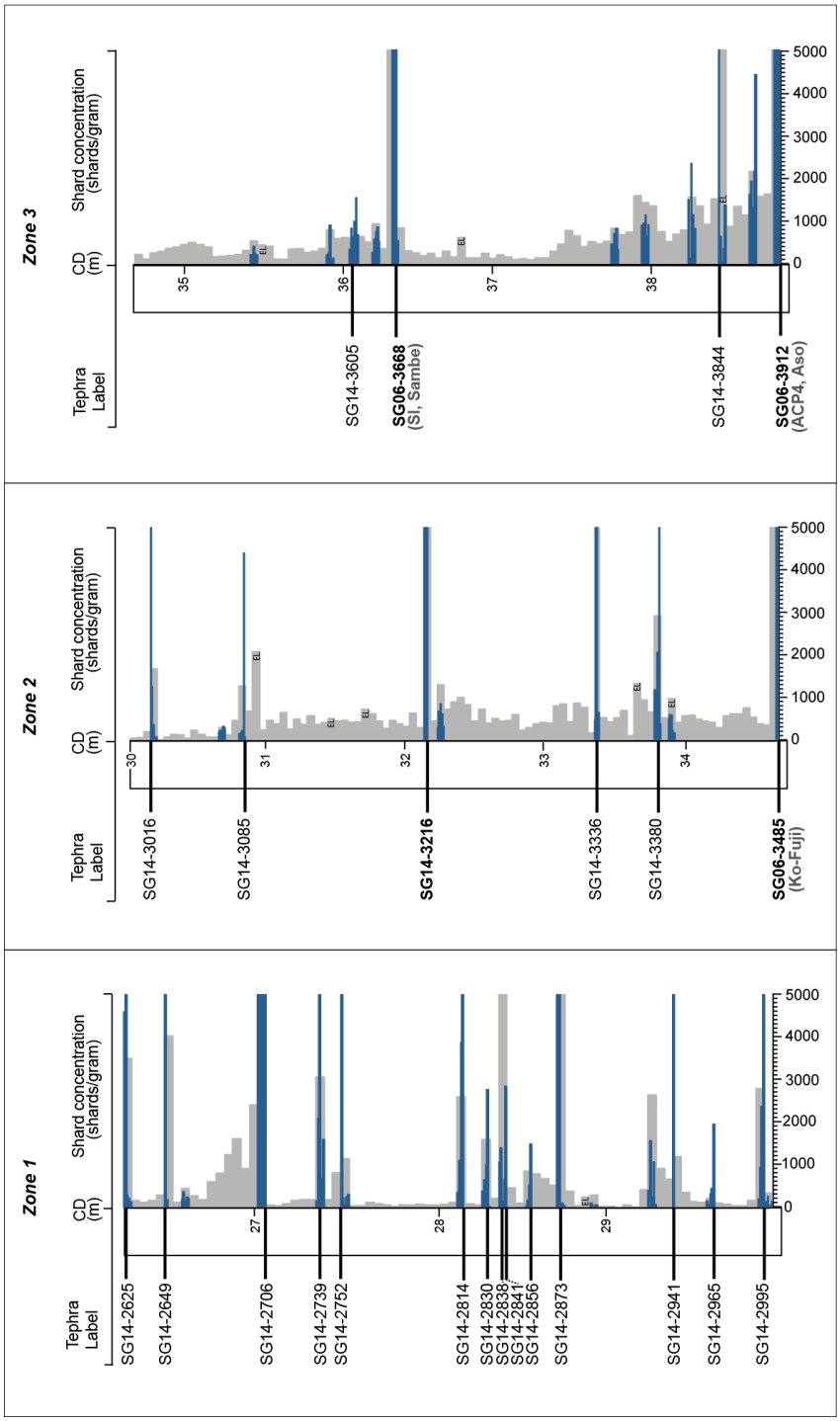


Figure 5.2. Glass shard concentrations (shards per gram of dry sediment; capped at 5,000) in the laminated sediments (50 to 30 ka) of the Lake Suigetsu SG14 core. The tephrostratigraphy is divided into three Zones (1 - 3) for illustrative purposes. Concentration of low-resolution (5 cm) samples are shown in grey and high-resolution samples (1 cm) are overlain in blue. Tephra isochrons are labeled using their SG06/SG14 composite depth and visible layers are bold. Peaks in shard concentrations that coincide with visible event layers (EL) are not considered primary.

Table 5.1. Summary of the tephra layers identified the sediments of the Lake Suigetsu (SG14 core) between 50 and 30 ka.

Suigetsu Tephra Label	V / C	SG14 master core and position	SG14 Composite Sampling Depth (cm)	Shards per gram	Glass shard morphology	Major element glass compositions (wt. %)				Trace element analyses	Suigetsu age (cal. yrs BP; 95.4 %)	Compositional Group	Source
						SiO_2	K_2O	CaO	*n*	*n*			
SG06-2650	**V**	**G-6-base**	**2614.9**	**> 20,000**	**PL**	**77.02 - 78.41**	**3.24 - 3.55**	**1.03 - 1.20**	**35** [1]	**19** [2]	**30,009 ± 189**	**3**	**AT, Aira** [1]
SG14-2625	C	E-23 (6.0 - 7.0 cm)	2624.2 - 2625.2	9,838	MI, C, V	60.51 - 65.12	2.61 - 3.88	3.57 - 5.48	21	-	30,114 ± 188	2	Aso
SG14-2649	C	E-23 (30.0 - 31.0 cm)	2648.2 - 2649.2	23,117	MI, PL	74.14 - 77.75	3.69 - 4.63	1.00 - 1.70	15	-	30,449 ± 202	2	Aso
SG14-2706	C	F-28 (29.8 - 30.8 cm)	2705.4 - 2706.4	> 20,000	F, V	78.54 - 79.35	3.54 - 4.20	0.93 - 1.10	49	-	31,411 ± 208	3	Ryukyu-Kyushu arc
SG14-2739	C	F-28 (62.8 - 63.8 cm)	2738.4 - 2739.4	8,367	PL, MI	63.70 - 65.18	3.58 - 3.92	3.39 - 4.20	16	-	32,090 ± 206	2	Aso
SG14-2752	C	F-28 (75.8 - 76.8 cm)	2751.4 - 2752.4	10,067	F, C, MV	68.84 - 70.11	3.95 - 4.50	1.66 - 2.02	17	9	33,102 ± 208	2	Aso
SG14-2814	C	F-29 (35.0 - 36.0 cm)	2813.3 - 2814.3	7,125	F	77.23 - 78.09	3.72 - 4.08	0.79 - 1.01	33	9	33,610 ± 208	3	Aira
SG14-2830	C	E-30 (14.0 - 15.0 cm)	2828.6 - 2829.6	2,767	PL	73..91 - 75.80	2.70 - 2.94	1.43 - 2.49	16	8	33,949 ± 210	3	Ryukyu-Kyushu arc
SG14-2838	C	E-30 (22.0 - 23.0 cm)	2836.6 - 2837.6	1,400	PU, MI	-	-	-	5	-	34,120 ± 208	-	-
SG14-2841	C	E-30 (25.0 - 26.0 cm)	2839.6 - 2840.6	2,850	PL, MI	61.23 - 70.12	2.97 - 5.723	1.74 - 5.13	28	8	34,183 ± 208	2	Aso
SG14-2856	C	E-30 (40.0 - 41.0 cm)	2854.6 - 2855.6	1,482	C, V	77.56 - 78.86	3.50 - 3.95	0.81 - 1.30	15	-	34,495 ± 204	3	Aira
SG14-2873	C	E-30 (57.0 - 58.0 cm)	2871.6 - 2872.6	12,575	F, V	75.46 76.76	2.85 - 3.73	0.95 - 1.64	22	9	34,840 ± 190	3	Aira
SG14-2941	C	E-31 (16.0 - 17.0 cm)	2939.6 - 2940.6	-	MI, P	-	-	-	-	-	35,978 ± 170	-	-
SG14-2965	C	E-31 (40.0 - 41.0 cm)	2963.6 - 2964.6	1,950	V, MV, MI	74.14 - 74.65	0.74 - 0.81	2.56 - 2.80	4	-	36,384 ± 176	4	Kurile arc
SG14-2995	C	E-31 (70.0 - 71.0 cm)	2993.6 - 2994.6	>20,000	V	76.55 - 78.42	3.09 - 3.42	1.04 - 1.58	20	-	36,871 ± 174	3	Ryukyu-Kyushu arc
SG14-3016	C	F-31 (24.0 - 25.0 cm)	3014.6 - 3015.6	6,567	PL, F	75.15 - 76.15	2.76 - 3.68	1.44 - 1.67	10	-	37,201 ± 172	3	Ryukyu-Kyushu arc
SG14-3085	C	G-08 (52.0 - 53.0 cm)	3083.5 - 3084.5	4,400	PU	57.89 - 68.16	1.88 - 4.55	2.56 - 6.95	28	12	38,213 ± 168	2	Aso
SG14-3216	**V**	**G-09-06**	**3216.2**	**> 20,000**	**MV**	**59.46 - 62.92**	**5.79 - 7.23**	**1.14 - 1.55**	**37**	**9**	**39,832 ± 196**	**1**	**U-Ym, Ulleungdo**
SG14-3336	C	F-34 (29.0 - 30.0 cm)	3335.1 - 3336.1	5,750	PU, MI	70.63 - 80.17	1.45 - 2.97	0.90 - 3.16	19	-	41,657 ± 160	4	-
SG14-3380	C	E-35 (39.5 - 40.5 cm)	3378.9 - 3379.9	18,383	MV, F	65.45 - 67.95	5.31 - 5.67	0.85 - 1.56	16	10	41,827 ± 162	1	Changbaishan
SG06-3485	**V**	**E-36-04**	**3468.7**	**> 20,000**	**F, V, PL**	**53.11 - 55.43**	**0.33 - 0.67**	**8.50 - 10.58**	**13** [1]	**13** [2]	**43,710 ± 156**	**-**	**Fuji**
SG14-3605	C	E-37 (58.3 - 59.3 cm)	3603.6 - 3604.6	2,200	MI, G	62.27 - 70.28	2.62 - 4.47	0.38 - 5.53	11	10	45,864 ± 188	2	Aso
SG06-3668	**V**	**E-37-13**	**3638.6**	**> 20,000**	**PU, MV, F**	**70.62 - 78.69**	**2.22 - 5.19**	**0.50 - 2.90**	**36** [1,4]	**15** [3]	**46,372 ± 202**	**-**	**SI, Sambe** [2]
SG14-3844	C	F-39 (25.0 - 26.0 cm)	3842.9 - 3843.9	16,013	F, V, MI	77.69 - 78.12	3.54 - 4.03	0.84 - 1.06	9	6	49,523 ± 318	3	Aira
SG06-3912	**V**	**F-39-07**	**3683.5**	**>20,000**	**F, C**	**69.64 - 73.63**	**4.46 - 4.90**	**1.05 - 2.33**	**20** [1,4]	**16** [2]	**49,893 ± 334**	**2**	**ACP4, Aso** [2]

References 1) Smith et al. (2013); 2) Albert et al., accepted 3) Albert et al., 2018; 4) This study

V / C = **Visible** / Cryptotephra layer

PU = Pumiceous, PL = Platy, C = Cuspate, F = Fluted, V = Vesicular, MV = Microvesicular, MI = Microlite inclusions, G = Green

n = number of analyses

[a] Sampling range for cryptotephra layers and base of visible ash layer.

[b] General shard length in the fraction extracted, i.e. in the population > 25 um.

[c] Tephra marked with a dash have not been able to be robustly correlated to a particular eruption or volcano

On average, one ash layer per metre is observed between 39 – 30 m CD (Zones 3 and 2; Figure 5.2.), whereas fifteen ash layers are identified in the 4 m prior to the AT ash (30 – 26 m CD; Zone 1). Several of the cryptotephras identified in Zone 1 are closely located, such as SG14-2841 and SG14-2838 that are only separated by 3 cm of sediment (equivalent to ca. 50 years).

Despite the relatively high glass concentrations in primary isochrons, very low levels of background glasses (i.e., those identified consistently through the sediments) are observed, which indicates very little reworking of material in the lake catchment at the time of deposition. As expected, background glass concentrations are lowest in regions furthest from visible ash horizons, for example throughout Zone 1 that remain below 100 s/g (Figure 5.2.). Following the 1 mm thick visible layer SG06-3912, similar shard characteristics and glass compositions are observed for ca. 1 m of sedimentation. Higher background concentrations are observed during the Holocene sediments (typically between 500 – 5,000 s/g), due to the presence of several much thicker visible ash layers (e.g., U-Oki and K-Ah tephra), which are more easily reworked and in-washed continuously from the catchment.

5.4.2. Geochemical Composition

Major and minor element glass compositions of the ash layers identified between 50 and 30 ka are presented in Table 5.2. and in Figure 5.3.

Table 5.2. Major and trace element glass compositions (normalised) of the newly identified ash layers preserved in the SG14 core between 50 and 30 ka (FeO^T = all Fe reported as FeO). Raw datasets and secondary standards are included in the Supplementary Material (Appendix C).

	SG14-2625		SG14-2649		SG14-2706		SG14-2739		SG14-2752		SG14-2814		SG14-2830		SG14-2841a	
wt. (%)	Avg.	± 1 σ	Avg.	± 1 σ	Avg.	± 1 σ	Avg.	± 1 σ	Avg.	± 1 σ	Avg.	± 1 σ	Avg.	± 1 σ	Avg.	± 1 σ
SiO_2	61.78	1.05	74.51	0.26	78.97	0.16	64.41	0.36	69.54	0.32	77.76	0.19	75.38	0.29	68.14	1.36
TiO_2	1.21	0.11	0.42	0.07	0.12	0.03	0.97	0.04	0.74	0.05	0.11	0.03	0.60	0.04	0.84	0.06
Al_2O_3	15.56	0.30	13.25	0.30	12.40	0.10	15.45	0.13	15.24	0.22	12.49	0.09	12.40	0.13	15.05	0.54
FeO^T	6.95	0.57	1.77	0.15	1.14	0.08	5.34	0.21	2.67	0.12	1.04	0.07	2.29	0.10	3.60	0.41
MnO	0.15	0.07	0.04	0.03	0.05	0.04	0.09	0.05	0.12	0.04	0.04	0.02	0.06	0.03	0.12	0.04
MgO	2.11	0.22	0.37	0.04	0.12	0.02	1.56	0.08	0.62	0.06	0.10	0.03	0.45	0.05	0.89	0.23
CaO	4.90	0.42	1.63	0.06	1.03	0.04	3.70	0.19	1.85	0.10	0.90	0.06	1.78	0.13	2.45	0.53
Na_2O	3.91	0.16	3.42	0.11	3.62	0.11	4.34	0.13	4.64	0.16	3.54	0.13	4.03	0.11	4.17	0.20
K_2O	3.04	0.27	4.48	0.08	3.68	0.07	3.73	0.10	4.29	0.14	3.89	0.08	2.82	0.08	4.51	0.41
P_2O_5	0.41	0.02	0.05	0.01	0.02	0.02	0.41	0.04	0.13	0.02	0.02	0.02	0.09	0.02	0.19	0.06
Cl	-	-	-	-	-	-	-	-	0.14	0.03	0.12	0.01	0.11	0.02	0.11	0.01
total	99.00	0.81	95.74	1.31	95.01	0.62	98.66	0.69	94.68	2.13	95.90	1.03	95.93	1.45	98.11	1.02
n	*21*		*14*		*48*		*16*		*17*		*33*		*14*		*25*	
ppm																
Rb	-	-	-	-	-	-	-	-	131.84	6.28	153.31	10.16	82.56	2.97	133.45	28.86
Sr	-	-	-	-	-	-	-	-	175.86	17.17	54.79	6.53	101.52	2.55	225.17	106.11
Y	-	-	-	-	-	-	-	-	34.69	2.40	23.75	2.21	37.16	1.26	37.04	3.62
Zr	-	-	-	-	-	-	-	-	260.52	12.63	92.34	7.03	205.41	7.77	272.92	43.04
Nb	-	-	-	-	-	-	-	-	15.89	0.87	7.48	0.92	6.49	0.68	17.01	2.80
Ba	-	-	-	-	-	-	-	-	623.29	23.55	568.58	56.15	387.48	14.19	648.38	57.94
La	-	-	-	-	-	-	-	-	27.57	1.69	25.46	2.54	17.33	0.96	29.83	4.00
Ce	-	-	-	-	-	-	-	-	62.48	3.19	51.23	5.00	39.18	2.18	67.14	8.71
Pr	-	-	-	-	-	-	-	-	7.36	0.52	5.18	0.64	4.71	0.37	7.98	1.08
Nd	-	-	-	-	-	-	-	-	29.94	2.30	18.61	2.58	19.96	0.69	32.04	5.39
Sm	-	-	-	-	-	-	-	-	6.85	0.79	3.96	1.56	4.44	0.45	6.71	2.13
Eu	-	-	-	-	-	-	-	-	1.30	0.16	0.55	0.29	1.11	0.29	1.24	0.27
Gd	-	-	-	-	-	-	-	-	5.60	1.62	2.54	2.75	4.20	1.42	7.54	2.06
Dy	-	-	-	-	-	-	-	-	5.51	0.83	3.62	0.73	5.54	0.87	5.54	1.50
Er	-	-	-	-	-	-	-	-	3.29	0.66	2.07	0.63	3.49	0.48	3.83	0.87
Yb	-	-	-	-	-	-	-	-	3.69	0.41	2.79	0.93	3.67	0.80	4.33	0.90
Hf	-	-	-	-	-	-	-	-	6.56	0.68	3.34	0.61	5.70	0.49	7.25	1.47
Ta	-	-	-	-	-	-	-	-	1.04	0.21	0.77	0.13	0.53	0.09	1.17	0.31
Th	-	-	-	-	-	-	-	-	12.30	0.68	15.15	1.44	7.76	0.65	13.47	2.47
U	-	-	-	-	-	-	-	-	3.27	0.15	3.26	0.36	1.83	0.16	3.47	0.82
Y/Th	-	-	-	-	-	-	-	-	2.82	0.20	1.58	0.17	4.81	0.35	2.79	0.30
Zr/Th	-	-	-	-	-	-	-	-	21.20	0.85	6.12	0.48	26.57	1.83	20.36	1.24
n									*9*		*9*		*8*		*7*	

Table 5.2. (continued)

	SG14-2841b		SG14-2856		SG14-2873		SG14-2965		SG14-2995		SG14-3016		SG14-3085a		SG14-3085b	
wt. (%)	Avg.	± 1 σ	Avg.	± 1 σ	Avg.	± 1 σ	Avg.	± 1 σ	Avg.	± 1 σ	Avg.	± 1 σ	Avg.	± 1 σ	Avg.	± 1 σ
SiO_2	61.95	0.40	77.97	0.18	78.00	0.13	74.32	0.20	77.36	0.61	75.95	0.15	67.68	0.68	59.14	0.58
TiO_2	1.11	0.03	0.11	0.02	0.14	0.03	0.23	0.03	0.35	0.04	0.59	0.02	0.88	0.30	1.05	0.07
Al_2O_3	16.20	0.01	12.33	0.16	12.53	0.12	13.34	0.10	12.14	0.24	12.21	0.06	14.44	0.31	16.06	0.67
FeO^T	6.20	0.53	1.07	0.11	1.06	0.07	3.31	0.21	1.47	0.16	2.18	0.14	4.39	0.29	7.93	0.38
MnO	0.15	0.01	0.05	0.04	0.03	0.03	0.16	0.06	0.05	0.03	0.10	0.04	0.10	0.04	0.17	0.03
MgO	2.15	0.10	0.12	0.02	0.12	0.02	0.25	0.03	0.27	0.05	0.42	0.03	1.00	0.07	2.78	0.36
CaO	5.06	0.01	1.05	0.09	1.03	0.05	2.69	0.09	1.34	0.15	1.63	0.05	2.89	0.40	6.37	0.40
Na_2O	3.70	0.22	3.61	0.10	3.35	0.12	4.61	0.14	3.70	0.15	3.93	0.17	3.88	0.19	3.61	0.29
K_2O	3.03	0.01	3.68	0.13	3.60	0.07	0.78	0.03	3.31	0.07	2.91	0.09	4.39	0.12	2.54	0.26
P_2O_5	0.36	0.04	0.02	0.02	0.02	0.02	0.06	0.01	0.02	0.01	0.07	0.02	0.26	0.03	0.29	0.03
Cl	0.08	0.01	-	-	0.12	0.02	0.25	0.04	-	-	-	-	0.09	0.01	0.07	0.02
total	98.18	0.32	95.58	0.75	95.03	1.10	95.18	2.23	95.53	0.89	93.69	1.64	97.89	1.05	97.31	1.55
n	*2*		*14*		*18*		*5*		*20*		*5*		*5*		*20*	
ppm																
Rb	85.47	-	-	-	144.54	7.06	-	-	-	-	-	-	142.34	4.71	74.48	8.48
Sr	325.70	-	-	-	62.68	4.05	-	-	-	-	-	-	211.75	21.88	409.30	70.34
Y	31.15	-	-	-	21.77	1.56	-	-	-	-	-	-	40.21	3.03	30.52	3.18
Zr	195.62	-	-	-	96.33	3.54	-	-	-	-	-	-	297.08	8.27	167.36	18.16
Nb	11.36	-	-	-	7.48	0.83	-	-	-	-	-	-	17.54	1.58	10.08	0.89
Ba	480.77	-	-	-	523.60	22.10	-	-	-	-	-	-	663.24	35.11	464.95	23.96
La	23.04	-	-	-	24.04	1.45	-	-	-	-	-	-	33.09	2.34	20.80	2.65
Ce	52.20	-	-	-	48.17	2.30	-	-	-	-	-	-	71.68	2.18	48.11	4.20
Pr	6.21	-	-	-	4.81	0.40	-	-	-	-	-	-	8.99	0.22	6.14	0.83
Nd	25.04	-	-	-	17.70	3.68	-	-	-	-	-	-	39.35	2.52	26.13	3.30
Sm	7.29	-	-	-	3.78	1.24	-	-	-	-	-	-	8.55	0.60	6.13	1.12
Eu	1.99	-	-	-	0.37	0.27	-	-	-	-	-	-	1.75	0.20	1.38	0.36
Gd	5.46	-	-	-	2.64	2.01	-	-	-	-	-	-	6.97	0.61	5.31	1.96
Dy	3.97	-	-	-	2.95	0.60	-	-	-	-	-	-	6.21	1.99	5.39	1.18
Er	2.46	-	-	-	2.03	0.45	-	-	-	-	-	-	4.38	0.32	3.07	0.69
Yb	2.94	-	-	-	2.40	0.78	-	-	-	-	-	-	3.96	0.38	2.75	0.77
Hf	4.14	-	-	-	3.40	0.66	-	-	-	-	-	-	8.36	0.74	4.16	0.54
Ta	0.86	-	-	-	0.67	0.17	-	-	-	-	-	-	1.40	0.29	0.59	0.20
Th	8.88	-	-	-	14.28	0.61	-	-	-	-	-	-	15.00	1.78	7.21	0.71
U	2.16	-	-	-	2.94	0.48	-	-	-	-	-	-	3.70	0.12	1.82	0.29
Y/Th	3.51	-	-	-	1.53	0.13	-	-	-	-	-	-	2.69	0.15	4.24	0.31
Zr/Th	22.02	-	-	-	6.76	0.38	-	-	-	-	-	-	19.96	1.94	23.25	1.70
n	*1*				*9*								*3*		*9*	

Table 5.2. (Continued)

	SG14-3216		SG14-3336		SG14-3380		SG14-3605a		SG14-3605b		SG14-3844	
wt. (%)	Avg.	± 1 σ	Avg.	± 1 σ	Avg.	± 1 σ	Avg.	± 1 σ	Avg.	± 1 σ	Avg.	± 1 σ
SiO_2	60.75	0.67	76.89	3.01	66.26	0.70	70.18	0.15	64.51	1.86	77.90	0.16
TiO_2	0.39	0.07	0.21	0.06	0.60	0.09	0.82	0.03	1.16	0.12	0.10	0.03
Al_2O_3	19.85	0.28	12.77	0.91	14.97	0.28	13.86	0.09	15.58	0.77	12.27	0.11
FeO^T	3.12	0.16	1.46	0.77	5.12	0.14	3.68	0.17	5.21	0.57	0.85	0.09
MnO	0.18	0.05	0.10	0.04	0.15	0.04	0.10	0.01	0.11	0.04	0.04	0.03
MgO	0.17	0.07	0.85	0.95	0.25	0.06	0.96	0.02	1.54	0.33	0.10	0.02
CaO	1.34	0.12	1.69	0.78	1.24	0.17	2.44	0.08	4.23	0.77	0.91	0.08
Na_2O	7.28	0.96	3.34	0.52	5.67	0.66	3.23	0.17	3.88	0.19	3.83	0.09
K_2O	6.50	0.33	2.50	0.39	5.49	0.09	4.47	0.01	3.35	0.41	3.87	0.19
P_2O_5	0.05	0.03	0.09	0.03	0.09	0.03	0.31	0.07	0.31	0.07	0.02	0.02
Cl	0.37	0.10	0.11	0.02	0.16	0.02	0.13	0.03	0.13	0.03	0.10	0.01
total	97.03	1.62	95.78	0.88	95.90	1.54	97.02	0.80	96.97	2.72	93.89	0.88
n	*37*		*11*		*14*		*2*		*9*		*9*	
ppm												
Rb	195.42	19.06	-	-	143.55	8.91	123.00	25.59	88.93	3.68	146.33	11.47
Sr	14.31	10.20	-	-	25.01	24.41	273.84	99.60	351.22	31.88	52.25	7.96
Y	26.04	2.94	-	-	51.11	3.94	30.10	5.46	32.64	2.49	18.19	2.52
Zr	709.63	104.31	-	-	741.36	45.81	267.43	78.60	268.35	14.59	74.00	14.87
Nb	175.17	21.16	-	-	96.98	5.52	13.67	1.58	12.65	0.82	7.11	0.54
Ba	16.29	13.34	-	-	77.31	57.26	695.85	75.80	649.66	20.93	508.70	28.90
La	98.17	9.04	-	-	76.42	4.75	34.25	2.72	32.95	0.47	21.73	1.19
Ce	161.66	15.70	-	-	154.34	9.55	71.11	6.93	68.96	5.34	43.75	2.77
Pr	14.46	1.24	-	-	17.05	1.14	8.14	0.94	8.23	0.35	4.56	0.52
Nd	43.92	4.69	-	-	65.57	6.37	33.59	5.09	33.51	3.63	15.62	1.57
Sm	6.41	0.70	-	-	12.91	1.91	5.91	2.74	6.96	0.43	3.22	0.88
Eu	0.59	0.24	-	-	0.61	0.20	1.58	0.36	1.81	0.18	0.41	0.11
Gd	5.45	1.93	-	-	10.69	1.42	7.36	1.12	6.97	2.07	3.01	1.89
Dy	4.44	0.61	-	-	9.26	0.89	5.83	1.28	5.54	1.28	2.88	0.31
Er	2.77	0.62	-	-	5.08	0.73	2.61	0.75	3.41	1.10	2.23	0.25
Yb	3.09	0.70	-	-	4.30	0.59	3.11	0.83	3.71	0.54	1.78	0.23
Hf	13.39	2.09	-	-	16.92	1.24	6.80	1.97	6.40	0.74	2.45	0.58
Ta	9.72	1.09	-	-	5.56	0.46	0.79	0.16	0.64	0.31	0.77	0.22
Th	25.23	3.23	-	-	14.14	1.05	12.17	2.75	9.49	0.88	13.63	1.07
U	5.29	0.86	-	-	2.79	0.34	2.21	0.46	1.64	0.16	2.86	0.21
Y/Th	1.04	0.07	-	-	3.62	0.23	2.59	0.69	3.45	0.26	1.35	0.26
Zr/Th	28.14	2.30	-	-	52.56	3.32	23.48	8.80	28.39	1.67	5.50	1.41
n	*8*				*10*		*5*		*5*		*6*	

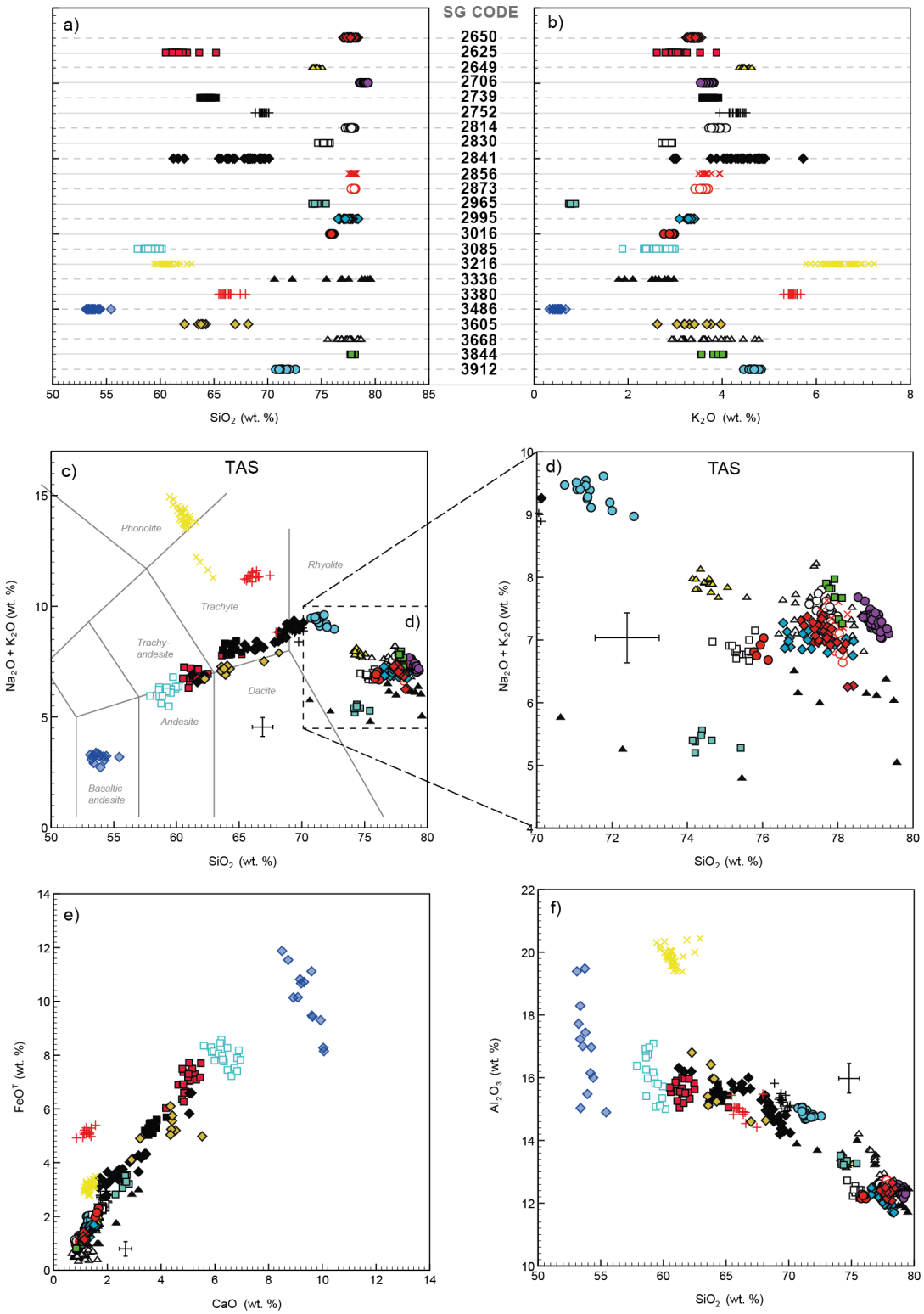


Figure 5.3. Major element compositions of the tephra layers preserved within the laminated sediments of Lake Suigetsu (SG14 core) between 50 to 30 ka. These are labelled using their SG06/SG14 composite depths. (a, b) SiO_2 and K_2O compositions of tephra layers versus their stratigraphic position. (c, d) Total alkalis versus silica plot (TAS; with whole-rock classification based on Le Bas et al., 1986). (e, f) Bivariate plots for FeO^T, CaO, SiO_2 and Al_2O_3 (error bars represent 2 x standard deviation of repeat analyses of the StHs6/80-G MPI-DING standard glass).

The major element compositions of SG14-2941 and SG14-2838 could not be analysed due to the high abundance of microlite inclusions within the glass. Trace element compositions were obtained for several cryptotephra layers with suitable shard sizes to further characterise and assist correlations (Table 5.2; Figure 5.4.). Geochemical outliers have been excluded from subsequent datasets but are presented in the Supplementary Material (Appendix C).

The geochemical glass compositions range from Low-K (Tholeiitic) to High-K (calc-alkaline and shoshonitic) (Peccerillo and Taylor, 1976), and are basaltic through to rhyolitic and phonolitic in composition (TAS; Le Bas et al., 1986; Figure 5.3.). Some tephra layers span a wide compositional range (e.g., SG14-3605), whereas other tephras are relatively homogenous (e.g., SG14-2752). The cryptotephras can be categorised using their glass affinities into four compositional groups, described below and outlined in Table 5.1.

Compositional Group 1 comprises of two alkali-rich ($Na_2O + K_2O$ = > 10 wt. %) tephra layers named SG14-3216 and SG14-3380, which are classified as phonolites and trachytes, respectively (Figure 5.3c). When normalised to the primitive mantle (Sun and McDonough, 1989), both tephras show significant depletions in Ba, Sr and Eu, typical of K-feldspar fractionation (Figure 5.4.). SG14-3216 has a Y/Th ratio of 1.04 ± 0.7, whereas SG14-3380 is 3.62 ± 0.23 (Table 5.2.). The paucity of a depletion in Nb and Ta of these volcanic glasses is inconsistent with a subduction related volcanism (Figure. 5.4.).

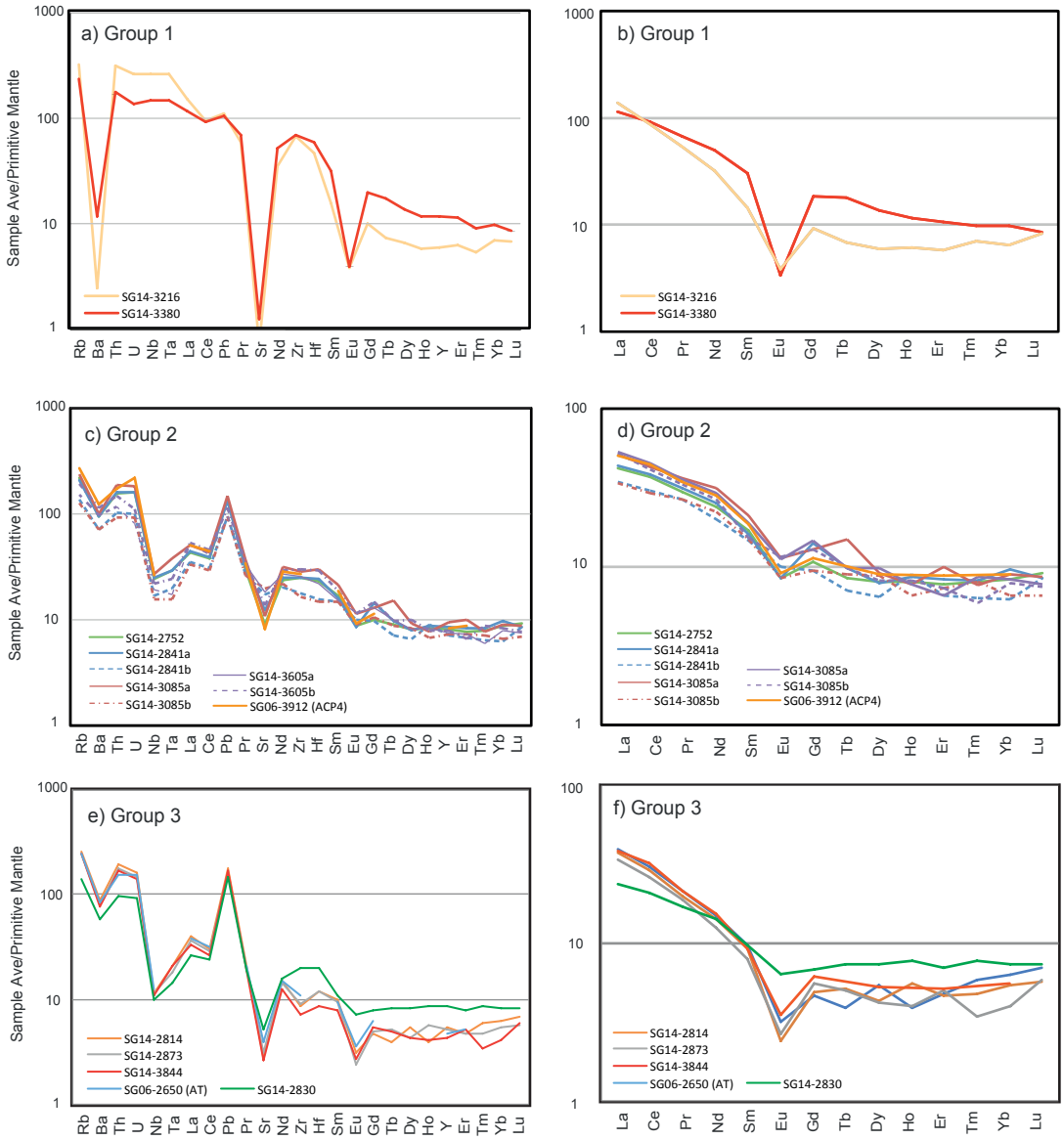


Figure 5.4. Average Primitive Mantle normalised glass compositions (of Sun and McDonough 1989) of the tephra layers preserved within the laminated sediments of Lake Suigetsu (SG14 core) between 50 to 30 ka. Trace element data for SG06-3912 (ACP4) and SG06-2650 (AT) are from Albert et al. (accepted).

Compositional Group 2 span a wide SiO_2 (58 – 72 wt. %) and K_2O (2 – 5 wt. %) range, and include seven cryptotephra and one visible (SG06-3912) tephra layer (Table 5.1.). Four of these tephra layers have homogeneous compositions (SG14-2625; SG14-2649; SG14-2739; SG14-2752), and three are heterogeneous (SG14-2841, SG14-3085 and SG14-3605) with both silicic

(population a) and a less evolved (population b) end-members (Figure 5.4c; 5.4d). When normalised to the primitive mantle, the lower SiO_2 population are more depleted in Large Ion Lithophile Elements (LILE; e.g., Rb, Ba, K) and High Field Strength Elements (HFSEs), compared to the silicic population, but possess very similar Rare Earth Element (REE) profiles, which show light REE enrichment relative to the heavy REE. Compositional Group 2 show strong depletions in Nb and Ta consistent with a subduction related genesis (Fig. 5.4).

Compositional Group 3 are characterised by highly silicic glass compositions (> 75 wt. % SiO_2) which all have > 2.7 wt. % K_2O (Figure 5.3.). Four of these tephra layers contain glasses that are very homogenous and compositionally similar (SG14-3814, SG14-2856, SG14-2873, SG14-3844), which are also distinguished by their low CaO (0.79 – 1.64 wt. %) content. Furthermore, SG14-2814, SG14-2873 and SG14-3844 all have identical mantle normalised profiles, which can be easily distinguished from compositional Group 2 by a deeper Eu trough and steeper REE profiles (La/Yb; Table 5.2; Figure 5.4.). This sub-group are also more negative in HFSE elements, in particular Nb (Figure 5.4c – d). In comparison, silicic glasses from SG14-2830 have similar mantle normalised profiles, but lower in light REE, and therefore exhibit a flatter REE profile (La/Yb ratios).

Compositional Group 4 consist of tephra layers SG14-3336 and SG14-2965, which contain Medium and Low-K glasses, respectively. SG14-3336 glass compositions are particularly heterogeneous, with SiO_2 from 70.5 to 80.0 wt. %, K_2O from 1.45 to 2.97 and CaO from 0.90 to 3.16 wt. % (Figure 5.4.). The four geochemical analyses for SG14-2952 (and several other low-total results; Supplementary Material) show that these are very distinctive from the other SG14 glasses presented here, with SiO_2 from 74.14 to 74.65 wt. %, K_2O from 0.74 – 0.81 wt. % and CaO from 2.56 to 2.80 wt. %. Unfortunately, SG14-3336 and SG14-2965 could not be characterised to a trace element level due to the glass characteristics (size and shape).

5.5. Provenance for Suigetsu cryptotephras between 50 and 30 ka

Geochemical glass datasets for key widespread ash layers in East Asia are well established (e.g., Machida and Arai, 2003; Kimura et al., 2015, Albert et al., accepted, and references therein), and their characteristics can be used to help provenance the other tephra layers preserved in the Lake Suigetsu sequence. Only intraplate volcanoes Ulleungdo (South Korea) and Changbaishan (North Korea/China) are known to have dispersed alkaline tephras across Japan during the Quaternary (Machida and Arai, 2003; Lim et al., 2013; Sun et al., 2014b). Volcanic glasses from these centres can be easily discriminated from those originating from Japan and other nearby arc region settings (e.g., Kamchatka) owing to their more abundant alkali content, and importantly the absence of Nb and Ta depletions in their trace element profiles (Figure 5.4;

Figure 5.5).

It is also relatively straightforward to distinguish tephra erupted from different arc sources distributed along length of Japan, which can often be discriminated by their SiO_2 to K_2O ratios (Figure 5.5a – b). For instance, Late Quaternary glasses erupted from the CVR and SVR typically contain Medium to High-K compositions, and are different for most major elements to those on the SW and NE Japan arc (see Kimura et al., 2015; Albert et al., accepted; Figure 5.5.). Vitreous tephra erupted from Aso has the highest known K_2O for Japan (> 3 wt. % at 66 wt. SiO_2, and the most evolved glasses extend to 6 wt. % in K_2O), and are therefore some of the most compositionally distinct. However, some centres (e.g., Kikai, Ata and Aira) erupt very compositionally similar tephra over tens to hundreds of thousands of years, with only slight major element variances. Therefore, trace element compositions, that reflect more subtle magmatic processes (e.g., Allan et al., 2008; Tomlinson et al., 2010), can be used to fingerprint these sources.

Vitreous tephra derived from all sources in Japan are enriched in LILE (e.g., Rb, Ba, K), relative to REE (e.g., LA to Yb) (Kimura et al., 2015; Albert et al., accepted) as expected due to their subduction genesis. Since, LILE concentrations are linked to K_2O, these elements are also very useful discriminators between different arc sources (Figure 5.5d - f). Furthermore, Y and Th can clearly separate glass erupted from fore-arc Kyushu calderas (e.g., Kikai, Ata and Aira) (Albert et al., accepted; Figure 5.5d).

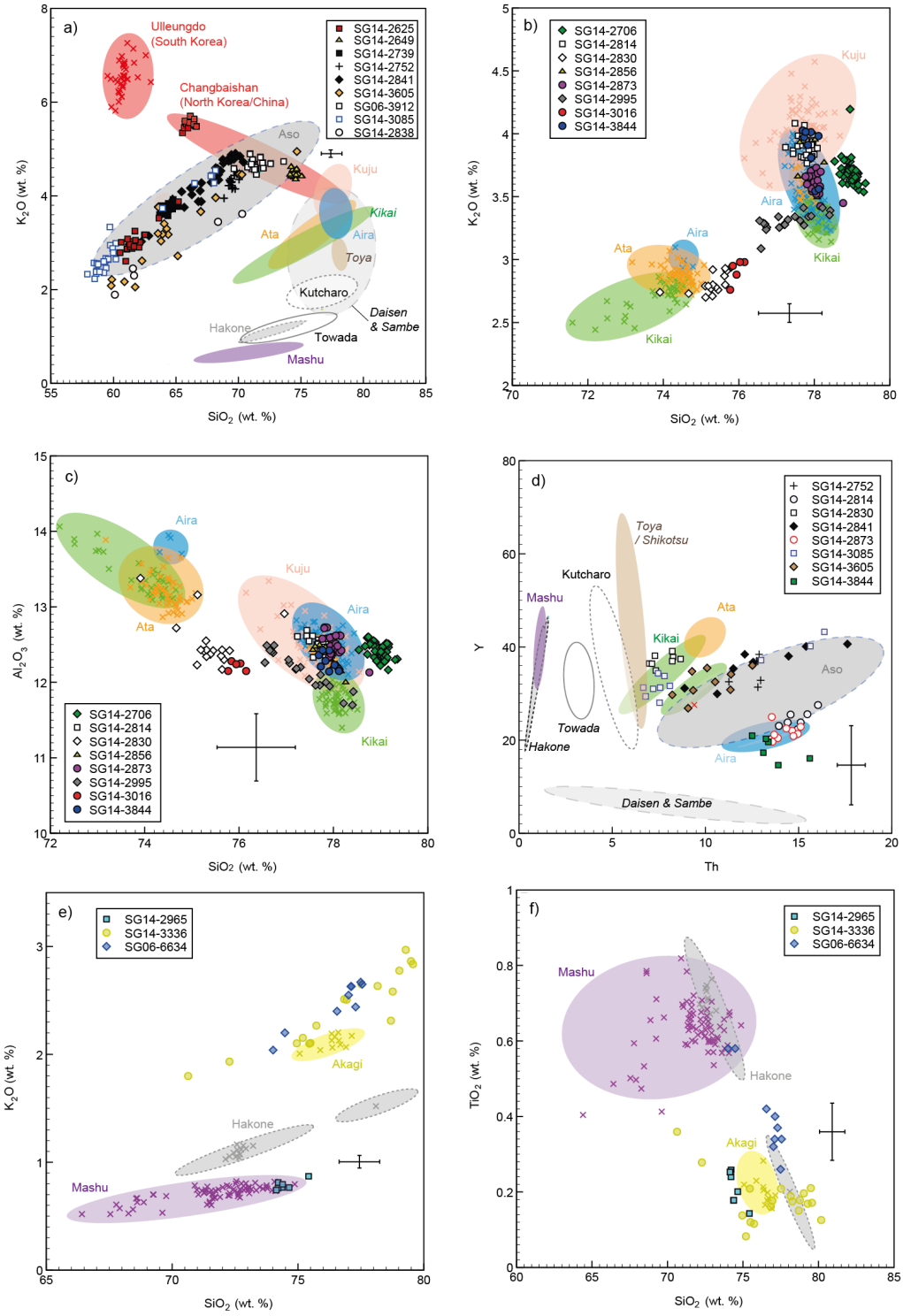


Figure 5.5. Major and trace element compositions of the SG14 cryptotephra layers (50 to 30 ka) in comparison to those established for major eruptive centres in Japan. Proximal geochemical fields are shown for Japanese volcanoes (data from Albert et al., accepted), Changbaishan volcano (North Korea/China; McLean et al., 2016; Chen et al., 2016) and Ulleungdo volcano (South Korea; Smith et al., 2011a; McLean et al., 2018). Error bars represent 2 x standard deviation of repeat analyses of the StHs6/80-G MPI-DING standard glass.

The SG14 cryptotephra layers are provenanced following comparisons to near-source reference glass datasets (e.g., Kimura et al., 2015; Albert et al., 2018; accepted), supported by careful examination of their physical characteristics (e.g., shape, vesicularity and vesicle size), relative stratigraphic positions and chronological constraints. These parameters indicate that the SG14 cryptotephra layers are derived from the following source regions or volcanoes:

Group 1: Ulleungdo (South Korea) and Changbaishan (North Korea/China), (*n = 2 layers preserved in Lake Suigetsu*)

Group 2*:* Kyushu Central Volcanic Region (CVR), Japan: Aso caldera, (*n* = *8*)

Group 3: Kyushu Southern Volcanic Region (SVR), Japan: Aira, and other southern Kyushu sources (*n* = *3*)

Group 4: Central and northern Honshu/Kurile arc tephras, (*n* = *2*)

The correlations and geochemical compositions of the Japanese tephra layers (Group 2 and 3) are discussed in detail below, as well as other tephra that have not yet been correlated to known eruptions or volcanoes (Group 4). Group 1 tephras that are derived from intraplate volcanic sources west of the Japanese arc (e.g., SG14-3216 and SG14-3380) are briefly summarised, but are comprehensively reviewed in Chapter 6, in order to establish a more complete eruptive record for Changbaishan and Ulleungdo.

5.5.1. Group 1: Ulleungdo and Changbaishan

5.5.1.1. Ulleungdo, East Japan Sea (South Korea)

Ulleungdo volcano is an island located in the southwest Japan Sea (37°30′N, 130°52′E), 110 km from the Korean Peninsula and 500 km NW of Lake Suigetsu (Figure 5.1.). Ulleungdo is known to have produced numerous large eruptions throughout the late Quaternary (Machida et al., 1984; Kim et al., 1999; Okuno et al., 2010; Shiihara et al., 2011; Lim et al., 2013; McLean et al., 2018), including the largest (VEI 6) of which dispersed the U-Oki (Ulleung-Oki; 10 ka) tephra eastward (correlated to the 3 cm thick layer SG06-1288 in Suigetsu; Smith et al., 2011a). Pre-Holocene Ulleungdo eruptions have been recognised in several marine cores northeast of the island (e.g., Lim et al., 2013), which include the Ulleung-Yamato (U-Ym) ash, which is identified stratigraphically below the AT tephra and dated to have occurred ca. 40 ka. (Arai et al., 1982; Chen et al., 2007; Lim et al., 2013).

The alkaline glasses of SG14-3216 (SiO_2 59.5 – 62.5 wt. %, and $Na_2O + K_2O$ = 11.6 – 14.9 wt. %) overlap with Holocene compositions derived from Ulleungdo in Lake Suigetsu (SG06-1288 and SG14-1091), as well as other distal occurrences of the U-Oki tephra (Machida and Arai, 2003). Furthermore, trace element compositions of SG14-3216 are consistent with proximal glass chemistries, which also show significant depletions in Ba, Sr and Eu consistent with K-feldspar fractionation (Brenna et al., 2014). Due to this geochemical and chronological consistency SG14-3216 is correlated to the U-Ym ash, as

identified in the Sea of Japan basin (e.g., Chen et al., 2007; Lim et al., 2013). The Suigetsu eruption age of 39,832 ± 196 cal. yrs BP (95.4 % confidence interval) provides the most constrained eruption age to date, which can be imported into other site-specific age models that contain this marker.

5.5.1.2. Changbaishan, North Korea/China

Changbaishan (also referred to as Baitoushan) is a stratovolcano situated on the border of North Korea/China (41°00'N, 128°03'E; Figure 5.1.), and is known for its explosive AD 946 'Millennium' eruption (ME) (Hakozaki et al., 2017; Oppenheimer et al., 2017) that dispersed the Baegdusan-Tomakomai (B-Tm) tephra over northern Japan, northeast China and coastal areas of Russia (Machida and Arai, 2003; Sun et al., 2014b), and is also identified as a thin visible layer in the Lake Suigetsu record (correlated to SG06-0226; McLean et al., 2016). Several pre-Holocene Changbaishan eruptions have been identified within the Sea of Japan marine cores, including the Baegdusan-Japan (B-J) ash, which is stratigraphically identified below the AT and U-Ym tephra (Ikehara et al., 2004; Lim et al., 2013). The B-J tephra has an estimated eruption age of ca. 50 ka, based on radiocarbon ages and the thinly-laminated marine chronology (Tada, 1999; Ikehara et al., 2014; Lim et al., 2013).

SG14-3380 glass compositions (65.4 – 67.9 wt. % SiO_2, 14.4 – 15.5 wt. % Al_2O_3, and $Na_2O + K_2O$ = 8.7 – 11.7 wt. %) geochemically overlap with the known composition of the late phase of the ME (i.e., the trachytic B-Tm end member) (Figure 5.5a), and is dated to 41,827 ± 162 cal. yrs BP via the Suigetsu chronology (95.4 % confidence interval). Although also

stratigraphically positioned between the AT and U-Ym tephra in the Suigetsu core, other distal occurrences of the B-J tephra report a homogenous silicic composition (71.2 wt. % SiO_2, ca.12.0 wt. % Al_2O_3, and $Na_2O + K_2O$ = 11.1 wt. %; Ikehara et al., 2004; Lim et al., 2013). These compositional and chronological differences preclude a correlation of SG14-3380 to the B-J tephra, as identified in the Sea of Japan basin (e.g., Ikehara et al., 2004; Lim et al., 2013), and are therefore considered as separate eruption events.

5.5.2. Group 2: Aso, Kyushu CVR

Aso caldera (32°53'04''N, 131°06'14''E) is situated 530 km SW from Lake Suigetsu on the Kyushu CVR arc (Figure 5.1.). Aso is one of the largest active volcanoes in the world, and the caldera was formed by a series of at least four VEI 6 - 7 eruptions (oldest to youngest): Aso-1 (ca. 270 ka), Aso-2 (ca. 140 ka), Aso-3 (ca. 112-134 ka) and Aso-4 (ca. 89 ka; correlated to SG06-5181 in Lake Suigetsu) (Ono and Watanabe, 1985; Matsumoto et al., 1991). Post-caldera cones that formed after the Aso-4 eruption cycle, are thought to have produced small, frequent explosive episodes, that have generated deposits over 100 m thick on the eastern side of the caldera (Miyabuchi, 2009). The largest of these post-Aso-4 caldera events is proximally named Aso Central Cone Pumice 4 (ACP4; VEI 4; Takada, 1986), which is correlated to tephra SG06-3912 and dated to 49,974 ± 337 cal. yrs. BP via the SG06 chronology (95.4 % confidence interval; Albert et al., accepted). This layer is located at the base of the cryptotephra analysis presented here.

Miyabuchi (2009; 2011) provides details of proximal evidence of other post-caldera forming events between the ACP4 (ca. 50 ka; SG06-3912) and AT ash (ca. 30 ka) (Figure 5.6a). Following the ACP4 event, a dacitic sub-Plinian pumice fall named ACP3 is identified, which has an estimated bulk volume of 0.07 km^3. Two other eruptive units named Nakakubo 2 (NbT2) and 1 (NbT1), are estimated to have occurred ca. 50 and 40 ka with a bulk volume of 0.37 and 0.49 km^3, respectively. The NbT2 and NbT1 units comprise of alternating beds of scoria and ash fall deposits in proximal locations that represent phases of activity at the volcano, and are separated by a minor rhyodacititic fine ash (0.54 km^3), named Mizunomoto pumice 2 (MzP2).

It is considered that activity from Aso was relatively low between ca. 32 and 31 ka, due to the presence of a thick, black humic soil and evidence of a dwarf bamboo grassland (Watanabe and Takada, 1990*)*. Interbedded in this soil is the Mizunomoto Pumice 1 (MzP1), which includes a thin scoria and several ash fall units (Miyabuchi, 2011). A series of intense silicic activity is estimated to have occurred between 31 and 30 ka, directly after the soil and prior to the catastrophic AT eruption. This includes the Kusasenrigahama pumice (Kpfa; Watanabe et al., 1982) which is found 1 m below the AT ash, and is the most voluminous of the fall units erupted from Kusasenrigahama crater, with a bulk volume of 2.21 km^3 (Miyabuchi, 2011).

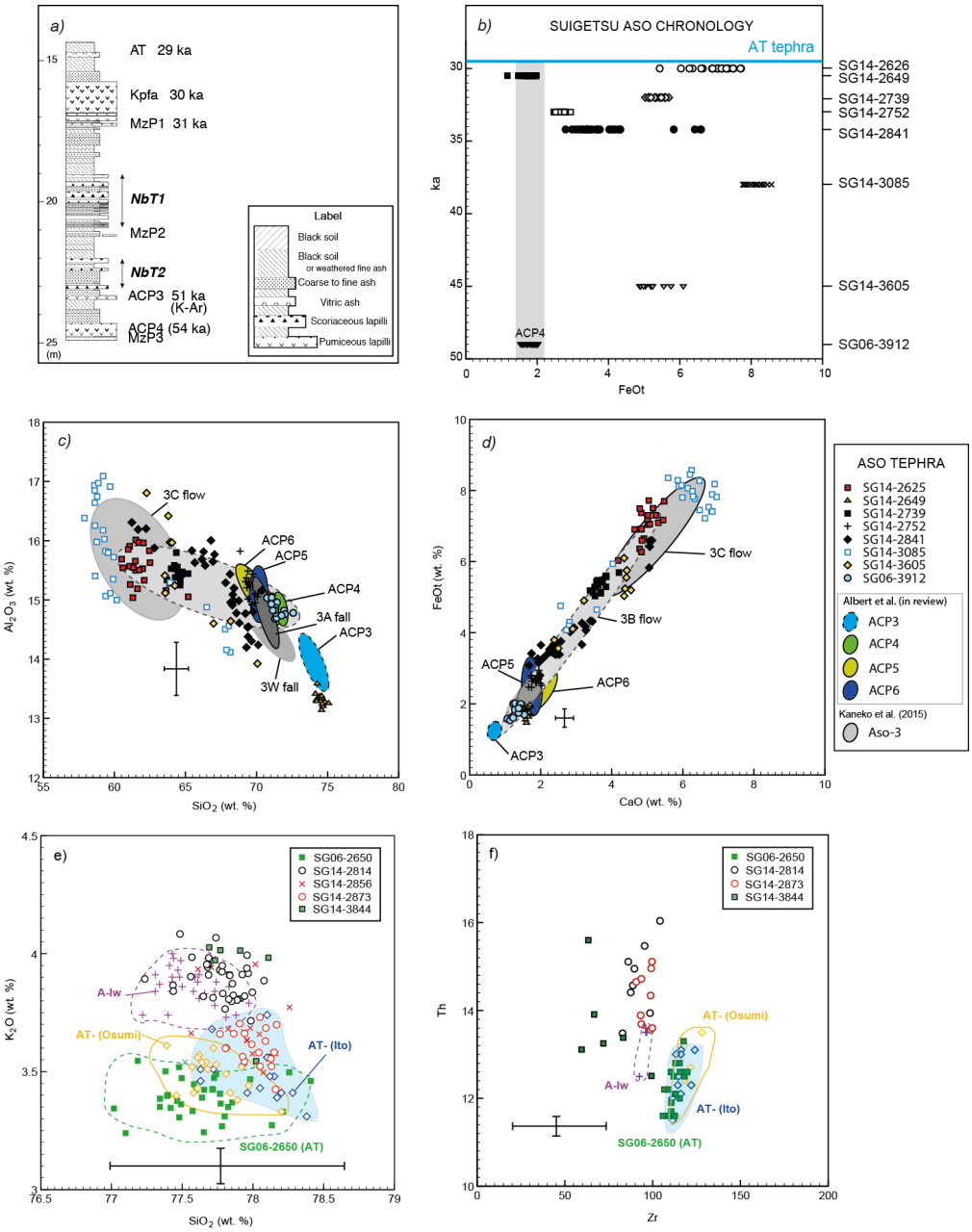


Figure 5.6. (a) Proximal volcanic stratigraphy compiled at outcrops at Aso caldera (Miyabuchi, 2011), (b) FeO^T content verses Suigetsu age for Aso derived tephra layers, (c – d) Major element glass compositions of compositional Group 2 (Aso derived tephra layers) in comparison to other proximal deposits derived from Aso outcrops (Albert et al., submitted), (e – f) Major and trace element compositions for Aira derived tephras (Compositional Group 3) in relation to Aira proximal glass chemistries (Smith et al., 2013; Albert et al., accepted).

As previously outlined, glass compositions from Aso are easily discriminated from other centres across Japan and importantly those situated further south in the Kyushu SVR (e.g., Aira, Kikai, Ata) (Figure 5.5a), with their clear HKCA affinity. Glass erupted from Aso have a wide compositional range, from basalt to rhyolite (Figure 5.6c - d), which have been sequentially erupted during caldera forming events (e.g., Aso-3 eruption; Kaneko et al., 2015). Whole rock data of the proximal units identified in Miyabuchi (2009; 2011) between 67 to 30 ka, suggest that explosive mafic (basaltic to basaltic andesite; SiO_2 = 48 – 56 wt. %) eruptions were dominant, with infrequent silicic pumice and ash-fall units (SiO_2 = 65 – 72 wt. %) events (Ono, 1989; Miyabuchi, 2009).

Seven cryptotephra layers (SG14-2625, SG14-2649, SG14-2739, SG14-2752, SG14-2841, SG14-2997, SG14-3085) have glass compositions that are characteristic of those derived from Aso (Figure 5.6b – d). These glasses are mafic (e.g., SG14-2625), intermediate (e.g., SG14-2841) and silicic (e.g., SG14-2649, SG14-2649) in composition, or with the case of SG14-3085 and SG14-3605, contain glasses that span the entire compositional range. These lie within the known geochemical rage of the Aso-3 eruption (Kaneko et al., 2015). Trace elements signatures of SG14-2752, SG14-2841, SG14-3085 and SG14-3605 are enriched in the LILE (Rb) and HFSE (Th, U, Zr), typical of Aso glasses (Figure 5.4c; Kaneko et al., 2015; Albert et al., accepted).

Although detailed glass datasets of proximal units erupted from Aso have not yet been generated, the geochemical distinctiveness of the deposits, based on published data of 12 different units (Albert et al., accepted), means they can be

confidently correlated to this centre. These cryptotephra layers likely represent the fine ash components of some of the units that are recorded in the proximal locations and described by Miyabuchi (2009; 2011). The Suigetsu eruption record for Aso broadly corresponds with the proximal stratigraphy, indicating a significant period of explosive activity occurred prior to the AT eruption (Miyabuchi, 2011). However, the Suigetsu chronology suggests that this period commenced at ca. 34.2 ka, with a minimum of five explosive events over ca. 4 ka. This might suggest that the thick soil bed in the Aso volcanic stratigraphy (reflecting a period of quiescence) developed prior to the eruption that deposited the 34.2 ka (SG14-2841) tephra layer in Lake Suigetsu. Only two eruption events (SG14-2605 and SG14-3085) from Aso are verified in the Lake Suigetsu sequence following the ACP4 and prior to this period of quiescence, and may be distal equivalents of NbT2 and NbT1. These correlations must be confirmed by future geochemical characterisation of the near source deposits.

5.5.3. Group 3: Aira and other sources south of Suigetsu

5.5.3.1. Aira, southern Kyushu

Aira caldera is situated at the northern end of Kagoshima Bay in southern Kyushu (31°40'N 130°40'E; Figure 5.1.). The collapsed caldera was formed by the enormous VEI 7 eruption that dispersed the AT ash across the majority of Japan (Aramaki, 1984; Machida and Arai, 1976; 2003; Figure 5.1.). The AT eruption ejected approximately 463 km^3 of bulk tephra, and is preserved as a > 30 cm thick sand-sized tephra (SG06-2650) in Lake Suigetsu (Fukushima and Kobayashi, 2000; Machida and Arai, 2003; Smith et al., 2013). This eruption is

most precisely dated using the Lake Suigetsu chronology to 30,009 ± 189 cal. yrs BP (95.4 % confidence interval) and forms the upper boundary of the cryptotephra record presented here (Albert et al., accepted). The caldera-forming event began with the Plinian eruption (Osumi pumice fall), which was followed by the Tsumaya and Ito pyroclastic flows (Aramaki, 1984).

Sedimentary outcrops around Aira indicate that the centre erupted explosively numerous times between 60 and 30 ka. These include the Aira-Iwato tephra formation, (A-Iw, ca. 60 ka; VEI 6), Shimuzu rhyolitic lava (A-Sm; 39 – 33 ka), Otsuka pumice fall deposit (A-Ot; ca. 33 ka, VEI 4), Fukaminato tephra formation (A-Fm; 31 ka, VEI 5) and the Kenashino tephra formation (A-Kn; 30 ka) (Machida and Arai, 2003). Nagakoa et al. (2001) constrained the age of several of these eruptions using ^{14}C ages of palaeosols that developed between the A-Ot, A-Fm and A-Kn units. Here, we incorporate these radiocarbon dates within an OxCal Bayesian phase model (ver. 4.3.2; Bronk Ramsey, 2018), to generate calibrated age estimates for these eruptions. This model is further constrained by inserting the Suigetsu-derived AT eruption age, which must post-date these deposits (shown in the Supplementary Material: Appendix C). Using this phase model, the A-Ot eruption is dated to 33,216 – 30,730 cal. yrs BP, A-Fm to 30,933 – 29,865 cal. yrs BP, and A-Kn to 30,437 – 29,545 cal. yrs BP (95.4 % confidence interval).

Volcanic glass erupted from Aira is relatively homogenous, with AT glass compositions spanning SiO_2 77.0 – 78.4 wt. %, 12.0 – 12.2 wt. % Al_2O_3, and $Na_2O + K_2O$ = ca. 7 wt. % (Smith et al., 2013). Glass compositions of the A-Iw

eruption (ca. 60 ka; Albert et al., accepted), are slightly elevated (ca. 0.3 wt. %) in K_2O, but can be discriminated using their trace element concentrations of HFSE (e.g., Zr; Figure 5.6f). Volcanic glass from Aira can be distinguished from other Kyushu SVR Kyushu arc sources by their lower Y/HREE and higher Th content (Figure 5.5d; Albert et al., accepted), which means that although detailed glass datasets are not yet available for all proximal eruption deposits, distal tephra from Aira can still be robustly correlated.

Four cryptotephra layers, SG14-3844, SG14-2873, SG14-2856 and SG14-2814, with the distinct Aira glass compositions are identified in the Suigetsu sediments, and are dated to ca. 49.5 ka, 34.8 ka, 34.5 ka and 33.6 ka, respectively. Trace element compositions are subtly depleted in Zr and more enriched in Th, compared to the AT (Oshumi and Ito) tephra, which is more consistent to the older A-Iw eruption (Figure 5.6f). The Suigetsu-derived eruption ages do not lie with the two sigma uncertainty range for the A-Ot, A-Fm or A-Kn eruptions modelled here, and reported by Nagakoa et al. (2001), so it is not yet possible to correlate these cryptotephra layers to specific proximal counterparts.

5.5.3.2. Uncorrelated tephra from Kyushu

Tephra layers SG14-2830 (ca. 34.0 ka), SG14-2995 (ca. 36.9 ka) and SG14-3016 (ca. 37.2 ka) are also attributed to explosive volcanism on the Kyushu arc, due to their similarity in major and trace element compositions (Figure 5.5b – c). Considering the compositional overlap, and equivalent shard textures (platy,

bubble-walled shards), SG14-2830 and SG14-3016 at least are highly likely to originate from the same source. Trace element compositions obtained for SG14-2830 are less depleted in Nb, Sr and Eu compared to glass erupted from Aira, and therefore more consistent with deposits from Ata and Kikai that are elevated in HFSE (Figure 5.4e – f; Albert et al., accepted). Ata is known to be active between 50 and 30 ka (Machida and Arai, 2003; Nagaoka et al., 2001) but further proximal samples are required to build geochemical datasets for these regions and secure a correlation for these events.

5.5.4. Group 4: Uncorrelated tephra from central and northern Japan

5.5.4.1. Uncorrelated tephra from central Honshu

SG14-3336 (ca. 41.7 ka) is compositionally similar to the older visible tephra layer SG06-6634 in the Suigetsu core, although it has FeO^T glass compositions that are ca. 0.5 wt. % lower (Albert et al., accepted). Heterogeneous and Medium-K series eruptions are known from stratovolcanoes in central Honshu, including Akagi and Haruna (Figure 5.5e – f). SG14-3336 may potentially be the distal equivalent of the Haruna Hassaki (Hr-Hs) eruption (0.62 km^3; Suzuki, 1996), which is dated to ca. 45 ka, via two ^{14}C dates obtained from the Shirakawa pyroclastic flow (Geshu and Oishi, 2011). Alternatively, it is also possible that SG14-3336 could be the distal equivalent of the Akagi-Kanuma (Ag-KP) eruption (erupted to ca. 44 ka; 25.9 km^3; Suzuki, 1996). Proximal samples from these deposits will be obtained in the future to investigate this possibility.

5.5.4.2. Uncorrelated from Hokkaido and the Kurile arc

SG14-2965 (ca. 36.4 ka) glass shards are very distinctive and contain < 1 wt. % K_2O. The only known Low-K source to have dispersed ash to central Honshu is Mashu (Ma-b tephra), situated in eastern Hokkaido (McLean et al., 2018). However, SG14-2965 glass compositions can be distinguished from Mashu tephra (e.g., Ma-b and older deposits), by CaO (ca. 0.5 wt. % lower) and other minor elements including TiO_2 (Figure 5.5e – f). Mashu is situated on the ESE caldera rim of Kutcharo, which is known for many widespread eruptions dated between 50 and 30 ka (Machida and Arai, 2003), however glass erupted from Kutcharo contain between 1.5 to 2 wt. % K_2O (Figure 5a – b; Albert et al., accepted). Derkachev et al. (2016) report a Low-K tephra (named T; 65.7 – 77.1 SiO_2, 0.5 – 1.1 K_2O) in the Okhotsk Sea (north of the Kurile Islands; Figure 5.1.), which is dated to have occurred between 30,320 – 34,690 cal. yrs BP (Hasegawa et al., 2009; 2012; Yamamoto et al., 2010). However, glass compositions can be distinguished via offsets in several major elements, including SiO_2, Al_2O_3 and NaO_2, which preclude a correlation for SG14-2965 at this time.

5.6. Discussion

5.6.1. Tempo and origin of ash fall events reaching central Honshu

The augmented Lake Suigetsu tephrostratigraphic record (50 to 30 ka) indicates that on average an ash fall event reached central Honshu at least

once every 1,300 years (Figure 5.7.). However, between 38 and 30 ka the average return interval was significantly higher, with at least one eruption recorded ca. 500 years, which is in close agreement to that observed during the Holocene (McLean et al., 2018). The record is dominated by ash fall events erupted from sources south of Suigetsu on the SVR and CVR (n = 18; Figure 5.7.), and most of which (n = 8) are derived from explosive activity from Aso (CVR).

Four eruption events are identified from different arc regions in Japan (e.g., central Honshu) and other nearby volcanic settings (Changbaishan and Ulleungdo), which highlights that other sources also have the potential to disperse ash more widely than previously anticipated. Interestingly, these eruption events are clustered between 45 and 38 ka, when no other ash layers are recorded from productive centres southwest of Suigetsu. However, it is not possible to attribute the cause of this change, due to the number of controlling parameters and preservation biases that affect the presence of cryptotephra. For example, this may represent a change in eruption styles and mechanisms (e.g., explosivity; efficient fragmentation of magma; Cassidy et al., 2018) or external differences during eruptions (e.g., wind direction and strength; Carey and Sparks, 1986).

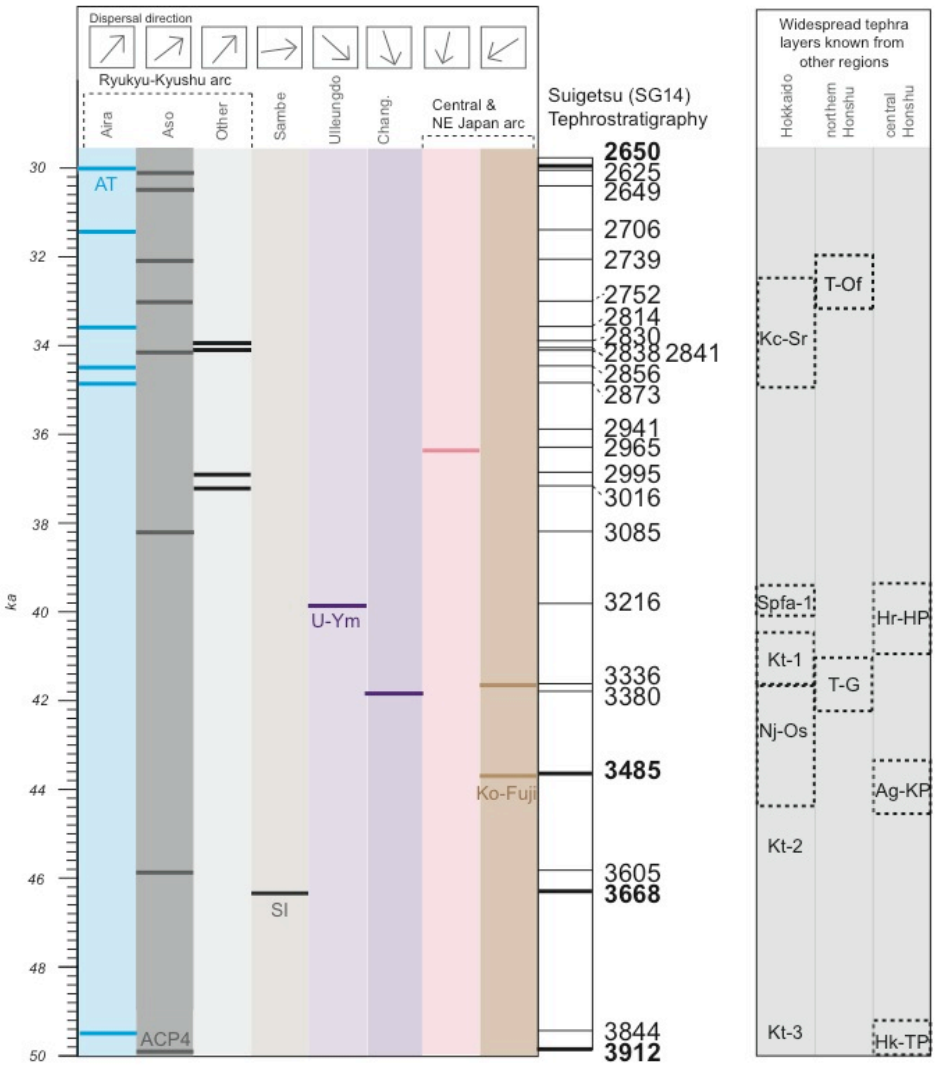


Figure 5.7. (a) Summary of the augmented Lake Suigetsu (SG14) tephrostratigraphy (visible and cryptotephra layers) spanning 50 to 30 ka. The distal tephra layers are correlated to their volcanic sources, and where possible specific eruptions, using the compositions of the volcanic glass. The Suigetsu sediments preserve evidence of a significant period of activity from centres on the Ryukyu-Kyushu arc (e.g., Aira and Aso) prior to the AT caldera-forming eruption dated to ca. 30 ka. (b) The timing of other key widespread and large magnitude (VEI 7 – 5) eruptions known from other regions north of Lake Suigetsu, which were not identified in the sediments (data from Machida and Arai, 2003). Approximate eruption ages are shown by dashed boxes, as reported by Suzuki (1996); Machida and Arai (2003); Yamamoto et al. (2010); Geshu and Oishi (2011); Uesawa et al. (2016); Matsu'ura et al., (2017).

Several volcanoes in northern Honshu and Hokkaido are known to have been very active between 50 to 30 ka (e.g., Towada, Shikotsu), yet distal ash deposits from these large magnitude events (VEI 7 – 5) have not identified in

this study of the Suigetsu sediments (Figure 5.7). It is possible that they are preserved as lower concentrated peaks of glass shards in the sediments, or are hidden in the reworking 'tails' that follow visible tephra layers. Identifying these markers would be of significant value for tephrochronology, and help to constrain their eruption histories. The identification of other primary cryptotephra peaks in the sediments may be achieved through detailed studies of shard morphologies, supplemented by further geochemical analysis. This was shown to be possible in the Holocene sedimentation, where the distinctive vesicular To-Cu (Towada) shards were clear within the platy K-Ah remobilised glass (McLean et al., 2018).

Additional distal occurrences of these eruption deposits between Suigetsu and their sources are required to better constrain the magnitude of these events. However, it is clear that they must have been at least a VEI 4, in order to be dispersed and preserved as a cryptotephra layer in Lake Suigetsu (located 300 km from the nearest potential source). Cryptotephra ash fall events are likely to be thin and perhaps of limited consequence so far from source, but such fine ash (typically < 80 μm), may have implications for air traffic, air and water quality and critical infrastructure (e.g., Horwell et al., 2006).

5.6.2. Further insights into pre- (Aira) and post- (Aso) caldera activity

The Suigetsu tephrostratigraphy provides detailed insight into the behaviour of two of the most active calderas in Japan, which are central to hazard assessments for Japan and even possible candidates for the next VEI 7

eruption (Newhall et al., 2018). Here, we confirm both centres were very active between 50 and 30 ka (as educated by their proximal stratigraphies), producing moderate to large explosive events within short temporal scales (ca. 300 years for both Aso and Aira). Almost all of these eruptions have yet to be the subject of detailed petrological investigations, so the glass compositions, and constrained eruption ages allow a new insight and comparisons into the magma generation and storage pre- (Aira) and post- (Aso) caldera-forming events.

Prior-to the AT eruption (VEI 7; Machida and Arai, 2003) of Aira, the Suigetsu record indicates that at least four large eruption events occurred and are dated to ca. 33.6 ka, 34.5 ka, 34.8 ka and 39.5 ka (Table 5.1; Figure 5.7.). The Suigetsu chronology also indicates that pre-caldera forming events occurred as little as 3,600 years before the AT event. These erupted compositionally similar and highly silicic glass compositions (75.5 – 78.9 wt. % SiO_2) that are characteristic of this centre (Machida and Arai, 2003; Albert et al., accepted), but we show they can be geochemically distinguished from the AT ash using their trace element compositions (e.g., Zr, Y, Th).

The Suigetsu sediments indicate that Aso erupted compositionally different magmas through time (rhyolitic to andesitic in composition), producing at least eight widespread events over 20 ka (Table 5.1). Furthermore, Aso was also very active prior to the AT eruption at ca. 30 ka, with at least one eruption every 750 years between ca. 33.1 – 30.1 ka. The bulk volumes estimated for the Aso eruption events (Miyabuchi, 2009; 2011), in some cases are small, yet they are preserved over 600 km from the vent. This could imply that perhaps the

eruption volumes are underestimated, that the transport mechanism is highly efficient or the eruption mechanism produced very fine ash suitable for widespread ash dispersal.

5.7. Conclusions

New insights into the frequency and tempo of East Asian volcanism between 50 to 30 ka are elucidated through the identification of non-visible (cryptotephra) layers preserved in the laminated (varved) sediments of Lake Suigetsu (Japan). Four times more microscopic ash layers are preserved over visible layers, meaning that this tephrostratigraphy provides an unprecedented record of ash fall events that have been dispersed over central Honshu. Major and trace element compositions of the glass shards allow most of these distal tephras to be correlated to source, however additional datasets are pivotal from proximal outcrops to integrate these records and learn more about these individual eruption events.

Of the twenty-five ash layers presented in the augmented tephrostratigraphy, nineteen of these were dispersed from eruptive centres southwest of Suigetsu, which is unsurprising considering the prevailing westerly wind direction across Japan. However, the record indicates that other sources have the potential to reach central Honshu, including Ulleungdo (500 km NW of Suigetsu) and Changbaishan (980 km NW). Explosive activity from Aso and Aira are most frequently recorded in the record, and indicate that these calderas were very active between 35 to 30 ka. Aso erupted compositionally different magmas

through time, producing eight widespread events over 20 ka. Here we show that Aira erupted explosively 1.3 ka before the enormous VEI 7 caldera-forming eruption that blanketed Japan in the AT ash.

Acknowledgements

DM is funded by NERC (grant: NE/L002612/1) and part of the Environmental Research Doctoral Training Program at the University of Oxford. PGA and RAS are supported by Early Career Fellowships from the Leverhulme Trust (grant: ECF-2014-438 and ECF-2015-396). The Fukui-SG14 sediment coring campaign was funded by the Fukui Prefectural government, and the coring was conducted by the team of Seibushisui Co. Ltd. Japan, led by A. Kitamura. KAKENHI grant by MEXT, Japan (15H021443) was used to purchase laboratory equipment and consumables during the project. Trace element analysis was funded by the JSPS Summer Award. Geochemical bi-plots were generated using the RESET plot function (https://c14.arch.ox.ac.uk).

See Appendix C for Supplementary Material

CHAPTER 6: FOURTH ARTICLE

REFINING THE ERUPTIVE HISTORY OF ULLEUNGDO AND CHANGBAISHAN VOLCANOES (EAST ASIA) OVER THE LAST 86 KA USING DISTAL RECORDS

DANIELLE MCLEAN[a], PAUL G ALBERT[a], TAKEHIKO SUZUKI[b], TAKESHI NAKAGAWA[c], JUN-ICHI KIMURA[d], QING CHANG[d], ALISON MACLEOD[e,f], SIMON BLOCKLEY[e], RICHARD STAFF[a,c], KEITARO YAMADA[h], IKUKO KITABA[c], TSUYOSHI HARAGUCHI[I], JUNKO KITAGAWA[j], SG14 PROJECT MEMBERS[k] AND VICTORIA C SMITH[a]

[a] *Research Laboratory for Archaeology and the History of Art, University of Oxford, Oxford, OX1 3TG, UK*

[b] *Department of Geography, Tokyo Metropolitan University, Tokyo, 192-0397, Japan*

[c] *Research Centre for Palaeoclimatology, Ritsumeikan University, Kyoto, 603-8577, Japan*

[d] *Department of Solid Earth Geochemistry, Japan Agency for Marine-Earth Science and Technology, Yokosuka, Japan*

[e] *Department of Geography, Royal Holloway University of London, TW20 OEX, UK*

[f] *Department of Geography and Environmental Science, University of Reading, RG66AB, UK*

[g] *Scottish Universities Environmental Research Centre, University of Glasgow, East Kilbride, G75 0QF, UK*

[h] *Institute for Geothermal Sciences, Kyoto University, Kusatsu, 525-8577, Japan*

[i] *Osaka City University, Osaka, 558-8585, Japan*

[j] *Fukui Prefectural Satoyama-Satoumi Research Institute, Wakasa, 919-1331 Japan*

[k] *www.suigetsu.org*

Highlights:

- Review of distal ash occurrences indicate eruptions are more frequent and widespread than previously considered
- At least seven Changbaishan eruptions produced significant ash dispersals over the last 86 ka
- Newly recognised eruption of Changbaishan at ca. 41.8 ka (B-Sg-42 ash)
- Four Ulleungdo eruptions are precisely dated using the Lake Suigetsu chronology
- U-Ym tephra is identified in Japan and dated to 40,230 – 39,636 cal. yrs BP

Abstract

The eruptive histories of Ulleungdo (South Korea) and Changbaishan (North Korea/China border) volcanoes are not well constrained since their proximal stratigraphies are poorly exposed or largely inaccessible. However, determining the past behaviour of these volcanoes is critical since future eruptions are likely to disperse ash over some of the world's largest metropolitan regions. Alkaline tephra erupted from both centres are routinely identified in marine cores extracted from the Sea of Japan, as well as high-resolution lacustrine records east of the volcanoes. Here, we provide a review of the distal ash occurrences derived from Ulleungdo and Changbaishan to provide a more complete and constrained eruption framework. The intensely-dated Lake Suigetsu archive (central Honshu, Japan) provides one of the most comprehensive distal eruption records for both centres, despite being located 600 km E of Ulleungdo and 1000 km SSE of Changbaishan, and can be utilised to precisely date and geochemically fingerprint (using major and trace glass compositions) ash fall events that reached central Honshu. A non-visible (cryptotephra) layer identified

in the Suigetsu sediments reveals a previously unreported explosive event from Changbaishan, dated to 41,989 – 41,665 cal. yrs BP (95.4 % confidence interval), which is chronologically and geochemically distinct to the B-J (Baegdusan-Japan Basin) tephra previously reported in the Sea of Japan. Furthermore, the widespread U-Ym tephra erupted from Ulleungdo is identified and precisely dated to 40,028 – 39,636 cal. yrs BP (95.4 % confidence interval), and this terrestrial ^{14}C age can be used to constrain the chronology of marine records containing the same isochron. This integrated framework highlights the pivotal role that distal sedimentary records can play in evaluating the eruptive histories and hazard potential of Ulleungdo and Changbaishan.

Keywords: Ulleungdo, Changbaishan; Tephra; Eruption history; Sedimentary archives; East Asia/Pacific; Glass geochemistry

6.1. Introduction

Intraplate volcanoes Ulleungdo (South Korea) and Changbaishan (North Korea/China border) are responsible for two of the largest Holocene eruptions (≥ Volcanic Explosivity Index (VEI) 6; Newhall and Self, 1982) in East Asia, blanketing large parts of Japan and the surrounding seas in ash (Figure 6.1; Machida and Arai, 2003). Fine ash from the AD 946 'Millennium Eruption' (ME) (Hakozaki et al., 2017; Oppenheimer et al., 2017) of Changbaishan has also been identified ca. 9,000 km from its source in northern Greenland (Sun et al., 2014a), which demonstrates the enormous potential of the volcano to cause major disruption to airspace across the East Asian and Pacific region. Yet, the complete eruptive histories of Ulleungdo and Changbaishan are poorly

understood since proximal eruption deposits are poorly exposed and are largely inaccessible.

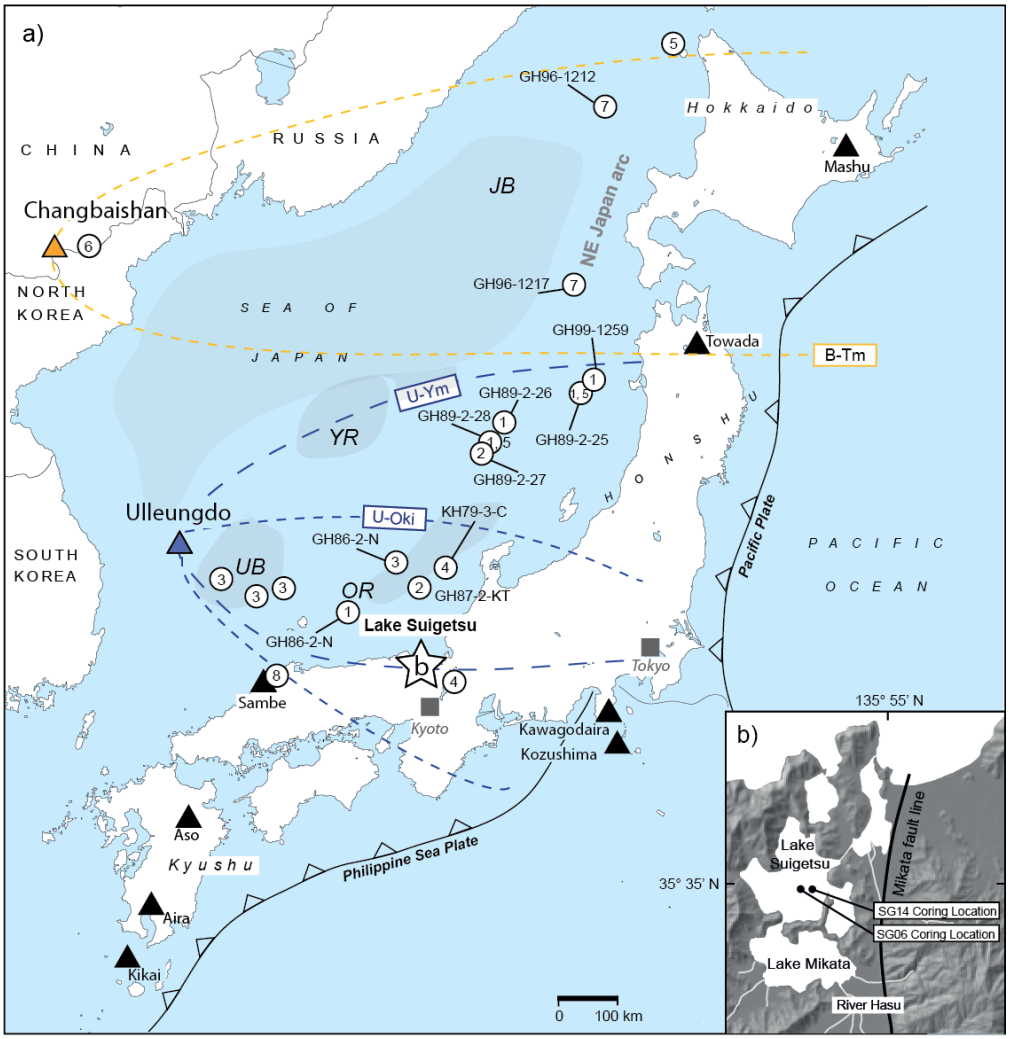


Figure 6.1. (a) Location of Ulleungdo (South Korea; blue triangle) and Changbaishan (North Korea/China; orange triangle) and other sources of Japanese tephra outlined in the text (black triangles). Distal sites mentioned in the text are marked by white circles; 1 = Marine cores; Lim et al. (2013); 2 = Marine cores; Arai et al. (1981); Chun et al. (2007); 3 = Marine cores = Chun et al. (2007); 4 = Lake Biwa; Nagahashi et al (2004); 5 = Lake Kushu (Chen et al., 2016); 6 = Yuanchi Lake; Sun et al. (2018); 7 = Marine cores; Ikehera (2003); 8 = Lake Hane; (Higashino et al., 2005). A star notates the location of Lake Suigetsu, and ocean basins are marked in dark blue (JB= Japan Basin; YR= Yamato Rise; OR= Oki Ridge; UB = Ulleungdo Basin). Dispersal boundaries of the B-Tm (AD 946; Oppenheimer et al., 2017), U-Oki (ca. 10 ka) and U-Ym (ca. 39.8 ka) are marked by dashed lines (B-Tm and U-Oki as defined by Machida and Arai, 2003). (b) Location of Lake Suigetsu, which is the largest of the five Mikata lakes, adjacent to Wakasa Bay. The positions of coring campaigns SG06 and SG14 are marked on Lake Suigetsu (modified after Nakagawa et al., 2005).

It is likely that evidence of older eruptions, especially those of low- to mid-intensity, have been destroyed, or are now completely buried, following more recent large magnitude Holocene events. At Changbaishan clear depositional breaks and soils are not well documented within proximal eruption successions (e.g., Chen et al., 2016; Sun et al., 2017), making it unclear how many eruption deposits are preserved.

Distal sedimentary records (e.g., marine and lacustrine sequences) have proved very important archives of past explosive eruptions, and can be used to help constrain the frequency and dispersal of tephra-forming events (e.g., Wulf et al., 2004; Albert et al., 2013; Smith et al., 2013; Tomlinson et al., 2014; Ponomareva et al., 2018). Ulleungdo and Changbaishan are the only sources known to have dispersed alkaline tephra across Japan (Machida and Arai, 2003; Kimura et al., 2015; Albert et al., accepted), and their distal deposits can be easily discriminated from other intraplate sources in the back-arc (e.g., Doki and Jeju volcanoes; Brenna et al., 2014). Tephra layers preserved in marine cores extracted from the Sea of Japan (Oki ridge, Yamato and Japan basins; Figure 6.1.), indicate both Ulleungdo and Changbaishan have been very active during the Late Quaternary, however the number and precise timing of these events remains uncertain. This is partly since successive eruption deposits are difficult to geochemically distinguish, and that marine cores in some localities are susceptible to reworking processes (e.g., turbidites; Albert et al., 2012; Cassidy et al., 2014), and often cannot be directly dated (i.e., due to the likelihood of the reservoir effect; Ikehara et al., 2013).

In order to provide new insight into the eruptive histories of Ulleungdo and Changbaishan, this study provides a review of the distal occurrences of alkaline ash deposited in sedimentary records (marine and lacustrine cores) that span the last 86 ka (i.e., post-dating the deposition of the widespread Aso-4 tephra that is $^{40}Ar/^{39}Ar$ dated to 86.4 ± 1.1 ka (2σ); Albert et al., accepted). The intensely-dated Lake Suigetsu archive (central Honshu, Japan) has significant potential to develop a comprehensive eruption record for both centres, despite being located 600 km E of Ulleungdo and 1000 km SSE of Changbaishan. Indeed, recent studies (McLean et al., 2016, 2018) of the Suigetsu sediments have identified thinner (sub-millimetre in thickness) and non-visible (cryptotephra) ash layers preserved in the sequence, which potentially represent previously unreported eruptions/ash fall events from both volcanoes. Constructing an integrated distal eruption framework for Ulleungdo and Changbaishan will permit new insight into the hazard potential of these active centres.

6.2. Regional setting

6.2.1. Ulleungdo Island, South Korea

Ulleungdo Island (12 km x 10 km) is the sub-aerial portion of a Quaternary stratovolcano located in the mid-western part of the Sea of Japan (37°30′N, 130°52′E), 130 km east of the Korean Peninsula (Figure 6.1; Kim, 1985). Ulleungdo is the youngest volcano in the back-arc basin, and is known to have erupted intermittently from the Pliocene until the mid-Holocene (Kim et al.,

1999; Okuno et al., 2011; Im et al., 2012). Nari caldera is located at the center of the island (2.8 km in diameter) and is the source of the most recent phase of activity (< 19 ka; Kim et al., 2014), erupting rocks that range from alkali basalt to trachyandesite in composition (Kim, 1985; Brenna et al., 2014; Chen et al., 2018).

The most recent activity of Ulleungdo is exposed at several outcrops near or within Nari caldera. Machida et al. (1984) defined seven pyroclastic units at extra-caldera outcrops in the north (named in ascending order, U-7 to U-1), which are comprised of trachytic or phonolitic ash and pumice that were emplaced as fall and/or by pyroclastic flows (Figure 6.2.). The Holocene stratigraphy (U-4 to U-2) was further subdivided by Okuno et al. (2011) and Shiihara et al. (2011) at exposures in the southeast, where the units have also been geochemically analysed and radiocarbon dated (Figure 6.2.). Two widespread Japanese tephra marker layers erupted from volcanoes of southern Kyushu Island are found within the soils that formed between these pumice falls, and are named the Aira-Tanzawa (AT ash; ca. 30.0 ka) and Kikai-Akahoya (K-Ah; ca. 7.3 ka) ash. The U-7 to U-5 eruption units are stratigraphically identified below the AT tephra, and the K-Ah ash is positioned between the U-3 and U-2 eruptions (Shiihara et al., 2011). Radiocarbon dates obtained from buried soils (ca. 2 cm thick) between units, and charred tree material preserved in the Holocene deposits suggest the U-3 eruption occurred ca. 8.3 or 9 cal. ka BP, and the U-2 eruption at ca. 5.6 cal. ka BP.

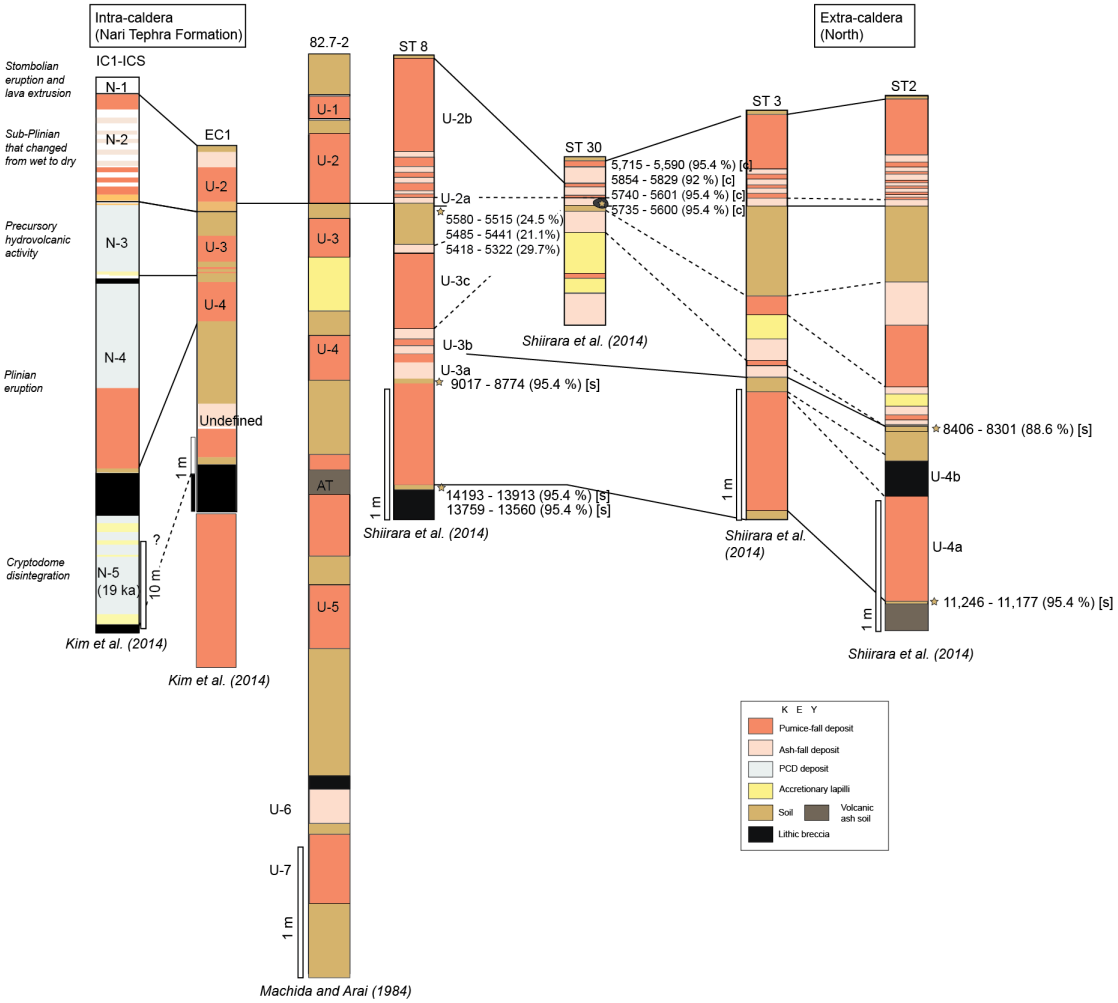


Figure 6.2. Sedimentological and stratigraphic characteristics of the intra- and extra-caldera outcrops on Ulleungdo Island (Machida and Aria, 1984; Okuno et al., 2010; Shiihara et al., 2011; Kim et al., 2014). The radiocarbon ages (s = soil; c = charcoal) reported by Okuno et al. (2010) have been recalibrated using IntCal13 (cal. yrs BP). Two Japanese tephra layers erupted from volcanoes in Kyushu are identified within the soils of the extra-caldera sequences, which include the AT (30 ka; Smith et al., 2013) and K-Ah (7.3 ka) ash.

Major element glass compositions for Holocene eruptions U-4 to U-2 are known to be geochemically similar (Machida et al., 1984; Martin Jones, 2012; Shiihara et al., 2014). Slight geochemical differences between some subunits are reported by Shiihara et al. (2014), who show U-4a and U-3c contain glass with lower Al_2O_3 and higher CaO and FeO^T. Furthermore, subunits U-3a and U-2a

are characterised by slightly lower CaO, TiO_2 and FeO^T contents compared to the other units.

Intra-caldera outcrops at Nari are ca. 70 m thick, and are composed of un-welded pyroclastic and epiclastic deposits spanning ca. 19 ka (Figure 6.2; Im et al., 2012; Kim et al., 2014). This sequence is named the Nari Tephra Formation, and consists of five eruptive units (in ascending order, N-5 to N-1), some of which exhibit signs of weathering and soil formation (Figure 6.2.). Several radiocarbon ages have been obtained from this formation by Im et al. (2012), which have been used to correlate the intra- and extra-caldera Holocene deposits (U-4 to U-2, and N-4 to N-2) as shown in Figure 6.2. Kim et al. (2014) have proposed a detailed succession of eruption styles for the last 19 ka, and suggest that only a few of the events generated sustained eruption columns or pyroclastic density current (PDC) deposits large enough to overtop the caldera wall, and therefore extra-caldera sequences may underestimate the eruption frequency.

6.2.2. Changbaishan, North Korea/ China border

Changbaishan (also referred to as Baitoushan or Paektu) is an intraplate stratovolcano situated on the border of North Korea and China (41°00'N, 128°03'E; Figure 6.1.), located on a Neogene trachybasalt lava shield (the Gaema Plateau). Activity at Changbaishan began in the Middle Pleistocene, has been divided into three main episodes: early shield building, middle cone construction and a late explosive stage (Wei et al., 2007; 2013). The most recent of which (< 20 ka) culminated with the caldera-forming ME (VEI 7) which

ejected ca. 100 km^3 of tephra (Dense Rock Equivalent ca. 25 km^3), blanketing the northernmost regions of Japan in ash (Horn and Schmincke, 2000; Zou et al., 2010; Wei et al., 2013; Sun et al., 2014b; McLean et al., 2016) and injecting 45 Tg of S to the atmosphere (Iacovino et al., 2016). This eruption produced a ca. 4.5 km wide caldera, which today contains Lake Tianchi, (meaning "Heavenly Lake"; Machida et al., 1990). The age of the ME has been precisely dated to AD 946, by combining dendrochronology and the presence of a Miyake event (radiocarbon peak) preserved in charred tree deposits (Hakozaki et al., 2017; Oppenheimer et al., 2017). The hazard potential of Changbaishan is considerable and is concerning as there has been recent seismic unrest at the crater (Stone, 2010; Xu et al., 2012; Wei et al., 2013).

The most comprehensively studied proximal outcrop at Changbaishan is at Twianwenfeng peak, which is on the northern Chinese flank of the summit (e.g., Chen et al., 2016; Pan et al., 2017; Sun et al., 2017; 2018). There are many inconsistent interpretations of these Late Quaternary eruption deposits, even amongst those assigned to the ME (see Pan et al., 2017). Sun et al. (2017) identify and geochemically characterise five sequential deposits (oldest to youngest, named NS-1 to NS-5) at Twianwenfeng peak, and suggest that the three uppermost units (NS-3 to NS-5) are associated with the ME, due to the geochemical (major element glass chemistry) overlap with distal ash deposits, and that no depositional break is evident between units NS-4 and NS-5. This is in contrast to other studies that suggest the youngest unit (NS-5) may correlate to post-ME events in AD 1668 or AD 1702, as suggested by historical records (Cui et al., 1995; Liu et al., 1998).

The ME eruption had two explosive phases, with the initial main phase (ca. 95% by volume) associated with a ca. 25 km-high Plinian column, producing a widespread rhyolitic pumice fall unit (e.g., NS-3 of Sun et al. (2017)) (Machida et al., 1990; Horn and Schmincke, 2000). This fall unit is overlain by partially-welded PDC deposits attributed to the partial collapse of the Plinian column. Trachytic magma was erupted in a late phase of the eruption (e.g., NS-4 and NS-5), forming moderately welded PDC units that overlie the rhyolitic fall and PDC deposits (Horn and Schmincke, 2000). Chen et al. (2016) report trace element compositions for the ME at Twianwenfeng peak (therein named units C-3 to C-1), and show the rhyolitic fall deposits (i.e., C-3 to C-2) had higher contents of incompatible trace elements (e.g., Th, Ta, Nd, Y) and lower contents of compatible elements (e.g., Ba, Sr) relative to the upper trachyte units (C-1).

Sun et al. (2017) identify two pre-ME pyroclastic fall deposits at Twianwenfeng peak, NS-1 (grey fall unit) and NS-2 (yellow fall unit), which are compositionally distinct from the ME deposits. These units are estimated to have been erupted between 4 – 5 ka based on $^{40}Ar/^{39}Ar$, uranium series disequilibrium, ^{14}C and optically stimulated luminescence (OSL) methods (Liu et al., 1998; Wan and Zheng, 2000; Wang et al., 2001; Yang et al., 2014).

A large “lava flow” landform, named the Qixiangzhan Comendite (5 km in length, 400 – 800 m in width), is observed on the northern summit of Changbaishan (Yang et al., 2014; Sun et al., 2017). This is widely considered as another pre-Me event, although $^{40}Ar/^{39}Ar$ ages generated from this deposit span several thousand years (Singer et al., 2014; Yang et al., 2014) and its

stratigraphic relationship to the units preserved at Twianwenfeng peak is unclear (Sun et al., 2017). Major element glass compositions of the Qixiangzhan comendite overlap with those of the rhyolitic phase of the ME (Sun et al., 2018).

6.2.3. Marine and lacustrine tephra archives

The Sea of Japan (East Sea) is a semi-enclosed marginal sea located between the Japanese islands and the Asian continent, and is the product of the rear-arc extension (Figure 6.1.). Due to the prevailing westerly winds, tephra erupted from Ulleungdo and Changbaishan is typically dispersed east and deposited in the surrounding marine basins (Arai et al., 1981; Chun et al., 1997, 2007; Ikehara, 2003; Machida and Arai, 2003; Ikehara et al., 2004; Lim et al., 2013; Chen et al., 2017). Furthermore, several Japanese tephra layers erupted from Kyushu Island have been dispersed to the Sea of Japan, including the K-Ah, AT and Aso-4 eruption deposits (Machida and Arai, 2003). The marine sediments across the Sea of Japan are characterised by alternations of light and dark coloured sediments, which have been correlated with short-term (millennial-scale) palaeoenvironmental changes relating to the fluctuation of the East Asian summer monsoon (Tada, 1999; Ikehara, 2003; 2014). These dark-layers are commonly used to date tephra layers that are preserved in the marine sediments (Tada et al., 1999). It has proved very difficult to correlate between the proximal eruption successions exposed at Ulleungdo and Changbaishan with those in distal archives. Typically, only the largest Holocene eruptions that

reached the Japanese islands have been correlated to specific eruption units within proximal stratigraphies at the volcanoes.

The most widespread tephra layer from Changbaishan is associated with the AD 946 ME, and is distally named the Baegdusan-Tomakomai (B-Tm tephra). The B-Tm tephra was named and characterised (using glass refractive indices and major element compositions) at a distal type-locality in Tomakomai Port, Hokkaido, where it was identified above the Tarumai-c (ca. 50 BC) and below the Tarumai-b (AD 1667) tephra layers (from the nearby Tarumae volcano) (Machida and Arai, 1983). The B-Tm tephra has since been identified in numerous marine, lacustrine and archaeological sequences across northern Japan, northeast China and coastal regions of Russia (see Sun et al., 2014b; McLean et al., 2016) and B-Tm glass shards have been identified in the Greenland ice cores (Sun et al., 2014a).

The most widespread tephra erupted from Ulleungdo is the Ulleung-Oki (U-Oki), which is correlated to the proximal U-4 deposits on the island (Machida et al., 1984; Okuno et al., 2010; Shiihara et al., 2011; Smith et al., 2011; Kim et al., 2014). The U-Oki tephra has been identified in several marine cores in the Sea of Japan, and in archives on the islands of Japan, including Lake Biwa, Lake Suigetsu and Lake Hane (Chun et al., 1997; Domitsu et al., 2002; Nagahashi et al., 2004; Smith et al., 2011; Figure 6.1.). As outlined further below, several of these archives contain a younger phonolitic/trachytic ash that post-dates the U-Oki tephra, and thought to be distal correlatives of the U-3 eruption of Ulleungdo.

One of the most comprehensive records of East Asian eruptions is the Lake Suigetsu sedimentary archive, which is located ca. 500 km E of Ulleungdo and ca. 900 km SSE of Changbaishan (35°35'0''N, 135°53'0''E, 0 m above present sea level; Figure 6.1.). The sequence spans approximately 150 ka, and contains a detailed record of visible and non-visible (cryptotephra) layers derived from Ulleungdo and Changbaishan, as well as over thirty tephra layers erupted from sources that span the length of Japan (Smith et al., 2013; McLean et al., 2016, 2018; Albert et al., 2018, accepted). Despite the difficulties of identifying non-visible layers in a productive arc setting, cryptotephra layers are precisely preserved and identified in Lake Suigetsu, due to its unique hydrological setting. Suigetsu is a tectonic lake, adequately situated away from the large calderas in Hokkaido and Kyushu, so is not inundated with locally sourced volcanic products (i.e., background glasses) that could obscure the cryptotephra record. Furthermore, no rivers flow directly into Lake Suigetsu, which mean that the basal sediments are rarely disturbed by inflows from the immediate lake surroundings (Figure 6.1b). The fine-grain sedimentation is often interrupted by deposits of coarse volcanic ash, which fall through the water column.

Since the Lake Suigetsu sediments have been extensively radiocarbon (^{14}C) dated, and contains seasonal laminae (varves) between ca. 10 and 50 ka (Staff et al., 2011; Bronk Ramsey et al., 2013; Marshall et al., 2012; Schlolaut et al., 2012), eruptions can be precisely dated when tephra layers are identified within the radiocarbon timeframe. The Lake Suigetsu tephrostratigraphic record is

utilised in this study to integrate and precisely date ash fall events of Ulleungdo and Changbaishan that reached central Honshu.

6.3. Tephra identification and analytical methods

6.3.1. Tephra identification in Lake Suigetsu

In order to provide constraints on the timing of widespread ash fall events in the East Asian/Pacific region, the high-resolution and intensely dated sediments of Lake Suigetsu (SG06/SG14 core) were investigated for the presence of thin (e.g., sub millimetre in thickness) and cryptotephra layers. Cryptotephra extraction procedures (see Turney, 1998; Blockley et al., 2005) were undertaken through the 14 m of annually laminated (varved) sediments dated between 50 and 30 ka, as well as 12 m of the Holocene sediments (≤ 10 ka; McLean et al., 2016, 2018). These sections were chosen for analysis as they were expected to contain low-background levels of volcanic glass, which would not obscure primary peaks of volcanic glass (see McLean et al., 2018). On average, cryptotephra layers are four times more frequently preserved than visible ash layers (McLean et al., 2018; Chapter 5).

The Suigetsu Bayesian age model (Staff et al., 2011; Bronk Ramsey et al., 2013; Marshall et al., 2012; Schlolaut et al., 2012) was used to determine the age for ash layers preserved in the sediments. The composite Suigetsu sedimentary sequence was modelled on to the IntCal13 timescale (Reimer et al., 2013) implementing three successive cross-referenced Poisson-process

('P_Sequence') depositional models using OxCal (ver. 4.3; Bronk Ramsey, 2008, 2017). These include 775 AMS ^{14}C dates obtained from terrestrial plant macrofossils from the upper 38 m (SG06-CD) of the SG93 and SG06 cores (Kitagawa and Van der Plicht, 1998a; 1998b, 2000; Staff et al., 2011, 2013a, 2013b) and varve counting between 12.88 and 31.67m SG06 CD (Marshall et al., 2012; Schlolaut et al., 2012). SG06 event-free depth(s) (EFD, ver. 29th Jan '11) were used within the age model, which excludes instantaneous deposits > 5 mm in thickness, (e.g., floods, and tephra deposits; Staff et al., 2011; Scholaut et al., 2012).

6.3.2. Major and trace element analysis of the glass shards

Major and minor element compositions of individual glass shards extracted from the Suigetsu visible and cryptotephra layers were measured using a JEOL-8600 wavelength-dispersive electron microprobe (WDS-EMP) at the Research Laboratory for Archaeology and History of Art (RLAHA), University of Oxford. All analyses used an accelerating voltage of 15 kV, beam current of 6 nA and 10 μm-diameter beam. Peak counting times were 12 s for Na, 50 s for Cl, 60 s for P, and for 30 s for all other elements. The electron microprobe was calibrated using a suite of mineral standards, and the PAP absorption correction method was applied for quantification. The accuracy and precision of this data were assessed using analyses of the MPI-DING reference glasses from the Max Plank Institute (Jochum et al., 2006), which were run as secondary standards. Analyses of these secondary standards lie within the standard deviation of the preferred values and are presented in the Supplementary Material (Appendix

D). Data were filtered to remove non-glass analyses, and those with analytical totals < 93%. The raw values were normalised (to 100 %) for comparative purposes and to account for variable hydration, and are presented as such in all tables and figures.

Trace element compositions of the glass shards large enough for analysis were measured by laser ablation inductively-coupled plasma mass spectrometry (LA-ICP-MS) at the Department of Solid Earth Geochemistry, Japan Agency for Marine-Earth Science and Technology (JAMSTEC). The analytical equipment used include the deep-ultraviolet (200 nm) femtosecond laser ablation system (DUV-FsLA) of OK-Fs2000K (OK Laboratory, Tokyo, Japan) connected to the modified high-sensitivity sector field ICP-MS of Element XR (Thermo Scientific, Bremen, Germany). All analyses used a 25 μm crater diameter and depth, and conditions followed that reported by Kimura and Chang (2012). Ten major elements including P_2O_5 and 33 trace elements were analysed for each sample, and were also run alongside several MPI-DING references glasses (Jochum et al., 2006), and the BHVO-2G standard provided by the Geological Survey of Japan. Accuracies of the BHVO-2G glass analyses are typically < 3 % for most elements, < 5 % for Sc, Ga, Sm, Eu, Gd, U and < 10 % for Ni, Cu, Lu. Full trace element datasets and secondary standard analyses are provided in the Supplementary Material (Appendix D).

6.4. Results

6.4.1. Suigetsu tephrostratigraphy

Thirty-three visible tephra layers (Smith et al., 2011, 2013; Albert et al., 2018; McLean et al., 2016, 2018) and thirty-four cryptotephra layers (between 50 to 30 ka, and > 10 ka; McLean et al., 2018; in prep) have been identified and geochemically fingerprinted in the Lake Suigetsu sediments to date. These are named, and are referred to using their SG06 or SG14 core composite depth. The distinctively high alkali content of glass shards (Na_2O + K_2O = >9 wt. %; Figure 6.3.) in some tephra layers indicates that they are not from the Japanese arc volcanoes (Machida and Arai, 2003; Kimura et al., 2015; Albert et al., accepted), and are correlated here and in McLean et al. (2016, 2018) to eruptions from Ulleungdo and Changbaishan.

Ash layers SG14-3380 and SG14-3216 are identified between the SI (46.4 ka; Albert et al., accepted) and AT (30.0 ka; Smith et al, 2013; Albert et al., accepted) tephra layers in the Suigetsu sediments (Figure 6.3; Table 6.1.). SG14-3380 is a discrete cryptotephra horizon erupted from Changbaishan, and contains over 18,000 shards per gram of dried sediment (Figure 6.4a.). This eruption is dated to between 41,989 – 41,665 cal. yrs BP (95.4 % confidence interval) using the Suigetsu age model. SG14-3216 is a thin (ca. 1 mm) white ash layer (Figure 6.4b), which is ca. 1.6 m above SG14-3380, and represents a Ulleungdo eruption between 40,028 – 39,636 cal. yrs. BP (95.4 % confidence interval).

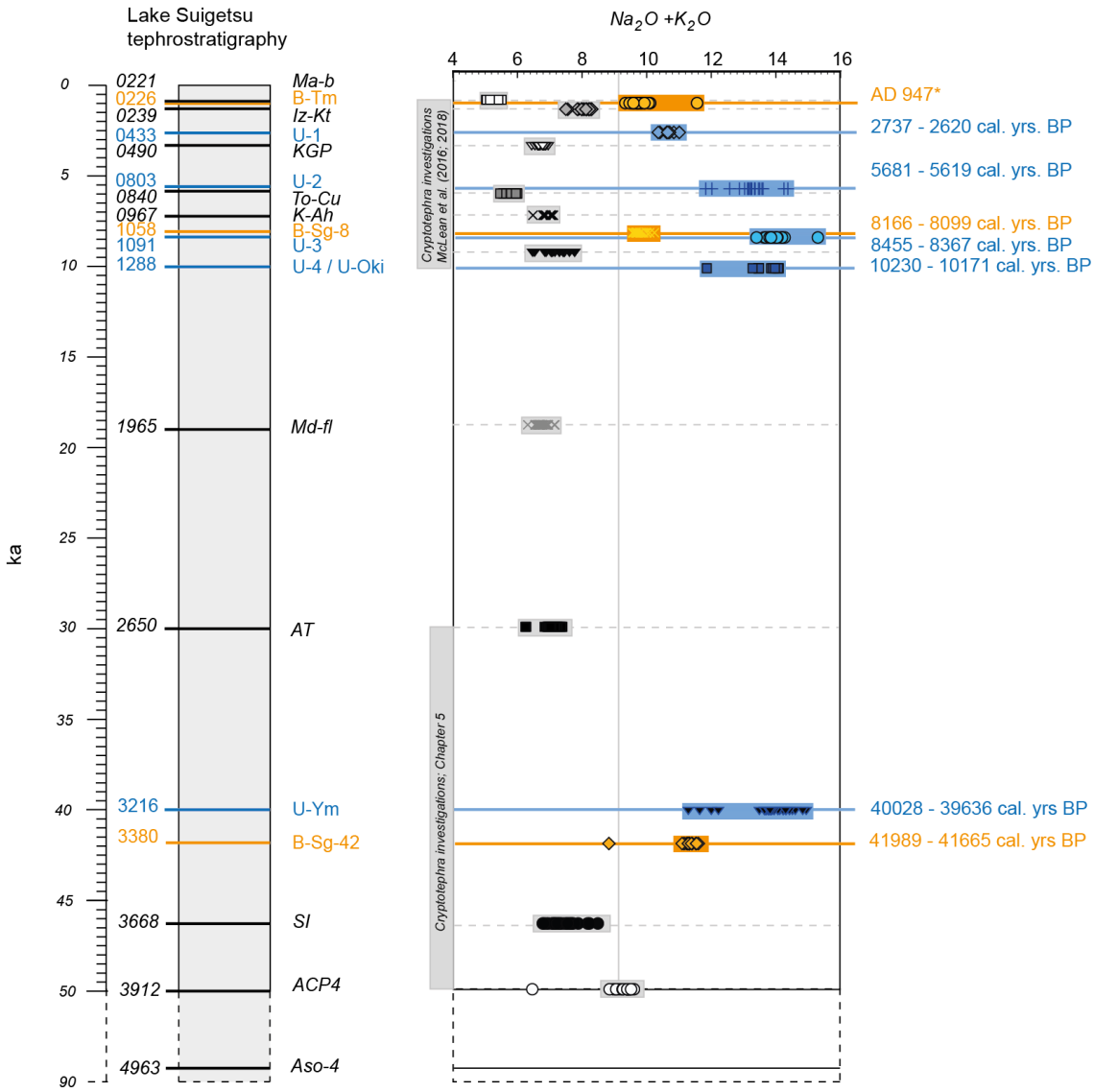


Figure 6.3. The composite Lake Suigetsu core and the positioning of Ulleungdo (blue lines), Changbaishan (orange) and other key Japanese (black/grey) tephra layers preserved through the sequence (Smith et al., 2013; McLean et al., 2016, 2018). The glass shard alkali content ($Na_2O + K_2O$) of these layers are also shown, with Ulleungdo and Changbaishan tephras containing > 9 wt. %.

Table 6.1. Summary of the Ulleungdo and Changbaishan tephra layers identified in the Lake Suigetsu (SG06 & SG14) sequence (in bold and shaded grey) and the stratigraphic positioning of other key Japanese isochrons. Tephra correlations for SG06 tephra layers are discussed in Smith et al. (2013), McLean et al. (2016) and Albert et al., (2018, accepted).

SG Label	Tephra code	Tephra name	Source volcano	Source location	^{14}C date (AD / cal. yrs BP)
SG14-0221	Ma-b	Mashu-b	Mashu	Kurile arc, Japan	AD 960 - 992[1]
SG14-0226	**B-Tm**	**Baegdusan-Tomakomai**	**Changbaishan**	**North Korea / China**	**AD 946[2]**
SG14-0239	Iz-Kt	Izu-Kozushima-Tenjosan	Kozushima	Izu arc, Japan	AD 838[3]
SG14-0433	**U-1**	**Ulleung-1**	**Ulleungdo**	**South Korea**	**2,737 - 2,620**
SG14-0490	KGP	Kawagodaira Pumice	Kawagodaira	Izu arc, Japan	3,227 - 3,129
SG14-0803	**U-2**	**Ulleung-2**	**Ulleungdo**	**South Korea**	**5,681 - 5,619**
SG14-0840	To-Cu	Towada-Chuseri	Towada	northern Honshu, Japan	5,986 - 5,899
SG06-0967	K-Ah	Kikai-Akohoya	Kikai	**southern Kyushu, Japan**	**7,307 - 7,196**
SG14-1058	**B-Sg-8**	**Baegdusan-Suigetsu-42**	**Changbaishan**	**North Korea / China**	**8,166 - 8,099**
SG14-1091	**U-3**	**Ulleung-3**	**Ulleungdo**	**South Korea**	**8,455 - 8,367**
SG14-1185	1185	-	unknown	-	**9,372 - 9,301**
SG06-1288	**U-Oki / U-4**	**Ulleung-1 / Ulleung-Oki**	**Ulleungdo**	**South Korea**	**10,230 - 10,171**
SG06-1965	Md-fl	Sambe-Midorigaoka fl	Sambe	**SW Japan**	19,631 - 19,471[4]
SG06-2650	AT	Aira-Tanzawa	Aira	**southern Kyushu, Japan**	30,174 - 30,078[4]
SG14-3216	**U-Ym**	**Ulleung-Yamato**	**Ulleungdo**	**South Korea**	**40,028 - 39,636**
SG14-3380	**B-Sg-42**	**Baegdusan-Suigetsu-42**	**Changbaishan**	**North Korea / China**	**41,989 - 41,665**
SG06-3668	SI	Sambe-Ikeda	Sambe	**SW Japan**	46,566 - 46,162[4]
SG06-3912	ACP4	Aso-Central Pumice 4	Aso	**central Kyushu, Japan**	50,311 - 49,637[4]
SG06-4963	Aso-4	Aso-4	Aso	**central Kyushu, Japan**	86.4 ± 1.1 ^{40}Ar/^{39}Ar[4]

1) McLean et al. (2018); 2) Oppenhemier et al. (2017); 3) Tsukui et al. (2006); 3) Smith et al. (2013); Albert et al. (accepted)

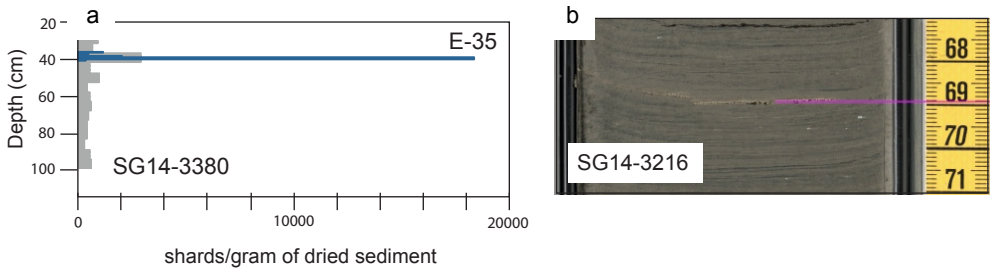


Figure 6.4. (a) Glass shard concentrations (shards per gram of dry sediment) preserved in SG14 core E-35 and the positioning of cryptotephra SG14-3380. Concentration of low-resolution (5 cm) samples are shown in grey and high-resolution samples (1 cm) are overlain in blue. (b) Photograph of visible tephra layer SG14-3216 in Lake Suigetsu Core G-09.

As previously reported in McLean et al. (2018), the Lake Suigetsu Holocene tephrostratigraphy contains three eruptions from Ulleungdo, named SG06-1288, SG14-1091 and SG14-0803, which are dated to 10,230 – 10,171 cal. yrs BP, 8,455 – 8,367 cal. yrs BP, 5,681 – 5,619 cal. yrs BP (95.4 % confidence interval), respectively (Table 6.1; Figure 6.3; Smith et al., 2011; McLean et al.,

2018). A younger ash layer, potentially also erupted from Ulleungdo (SG14-0433), is dated to between 2,737 – 2,620 cal. yrs BP (Table 6.1; Figure 6.3.).

Two Holocene Changbaishan eruptions are preserved in the sediments, named SG14-1058 dated to 8,166 – 8,099 cal. yrs BP (McLean et al., 2018), and SG06-0226, which has been correlated to the AD 946 B-Tm tephra (McLean et al., 2016; Hakozaki et al., 2017; Oppenheimer et al., 2017). Several other widespread markers have been identified in the Holocene sediments, which are able to stratigraphically separate eruption events from Ulleungdo and Changbaishan (Figure 6.3; Table 6.1.). SG14-1185 stratigraphically separates Ulleungdo layers SG06-1288 and SG14-1091, and the K-Ah (7.3 ka; Kikai volcano) and To-Cu (5.9 ka; Towada) tephras separate SG14-1091 and SG14-0830 (McLean et al., 2018; Table 6.1; Figure 6.3).

6.4.2. Glass geochemistry

Glass compositions of the four Ulleungdo derived tephra layers preserved in the Suigetsu tephrostratigraphy (e.g., SG14-3216, SG06-1288, SG14-1091 and SG14-0803), straddle the phonolitic/trachytic boundary on the basis of the Total Alkalis versus Silica (TAS) classification (Le Bas et al., 1986) and contain 60 – 63 wt. % SiO_2, ca. 7 wt. % K_2O and 19 – 20 wt. % Al_2O_3 (Table 6.2; Figure 6.5). These glasses are characterised by < 2.5 wt. % CaO and contain between 2.5 and 3.5 wt. % FeO^T.

Table 6.2. Average glass compositions (major element data normalised) of the Ulleungdo and Changbaishan tephra layers in the Suigetsu sequence (FeO^T = all Fe reported as FeO). Raw dataset and secondary standards are included in the Supplementary Material (Appendix D).

	SG14-0433		SG14-0803		SG14-1091		SG06-1288		SG14-3216	
wt. (%)	Avg.	± 1 σ	Avg.	± 1 σ	Avg.	± 1 σ	Avg.	± 1 σ	Avg.	± 1 σ
SiO_2	61.76	0.16	60.54	0.63	60.52	0.24	60.85	0.42	60.75	0.67
TiO_2	0.79	0.05	0.62	0.07	0.51	0.08	0.50	0.07	0.39	0.07
Al_2O_3	16.66	0.05	19.48	0.30	19.87	0.22	19.55	0.17	19.85	0.28
FeO^T	5.65	0.17	3.16	0.42	2.77	0.24	3.16	0.19	3.12	0.16
MnO	0.23	0.05	0.14	0.10	0.15	0.03	0.14	0.05	0.18	0.05
MgO	1.09	0.06	0.48	0.12	0.23	0.03	0.30	0.06	0.17	0.07
CaO	6.07	0.18	6.60	0.60	6.95	0.40	1.61	0.17	1.34	0.12
Na_2O	2.57	0.08	1.99	0.33	1.48	0.14	6.51	0.79	7.28	0.96
K_2O	4.59	0.10	6.61	0.21	7.03	0.19	7.07	0.28	6.50	0.33
P_2O_5	0.36	0.04	0.17	0.05	0.05	0.04	0.10	0.03	0.05	0.03
Cl	0.23	0.03	0.21	0.04	0.40	0.08	0.24	0.03	0.37	0.10
total	96.85	1.72	96.84	1.49	97.81	1.89	99.72	0.67	97.03	1.62
n	*8*		*19*		*24*		*12*		*37*	

	SG06-0226		SG14-1058		SG14-3380	
wt. (%)	Avg.	± 1 σ	Avg.	± 1 σ	Avg.	± 1 σ
SiO_2	74.89	0.21	75.01	0.18	66.26	0.70
TiO_2	0.22	0.04	0.20	0.03	0.60	0.09
Al_2O_3	10.27	0.10	10.28	0.11	14.97	0.28
FeO^T	4.05	0.14	3.89	0.10	5.12	0.14
MnO	0.08	0.05	0.07	0.03	0.15	0.04
MgO	0.02	0.03	0.01	0.01	0.25	0.06
CaO	0.22	0.02	5.30	0.16	1.24	0.17
Na_2O	5.36	0.15	0.20	0.02	5.67	0.66
K_2O	4.38	0.09	4.50	0.06	5.49	0.09
P_2O_5	-	-	0.01	0.01	0.09	0.03
Cl	0.50	0.03	0.52	0.02	0.16	0.02
total	96.19	1.35	95.54	1.34	95.90	1.54
n	*29*		*24*		*14*	

	SG06-0226		SG14-1058		SG14-1091		SG14-3216		SG14-3380	
ppm	**Avg.**	± 1 σ	**Avg.**	± 1 σ	**Avg.**	± 1 σ	**Avg.**	± 1 σ	**Avg.**	± 1 σ
Rb	396.38	9.83	383.89	23.90	188.65	10.10	195.42	19.06	143.55	8.91
Sr	2.17	0.64	4.42	0.91	59.52	36.19	14.31	10.20	25.01	24.41
Y	143.29	3.92	149.84	11.42	23.52	1.97	26.04	2.94	51.11	3.94
Zr	2415.22	79.96	2302.53	189.84	626.03	50.94	709.63	104.31	741.36	45.81
Nb	286.08	8.89	261.14	21.13	169.82	11.52	175.17	21.16	96.98	5.52
Ba	6.40	0.90	6.58	2.51	99.07	83.54	16.29	13.34	77.31	57.26
La	138.88	4.54	125.25	14.62	86.45	4.26	98.17	9.04	76.42	4.75
Ce	286.94	13.46	243.19	12.33	144.75	6.85	161.66	15.70	154.34	9.55
Pr	31.88	1.24	28.30	1.78	12.84	0.88	14.46	1.24	17.05	1.14
Nd	115.80	4.83	102.32	6.94	39.33	3.47	43.92	4.69	65.57	6.37
Sm	27.58	1.22	26.06	4.55	5.64	0.95	6.41	0.70	12.91	1.91
Eu	0.32	0.10	0.32	0.32	1.45	0.34	0.59	0.24	0.61	0.20
Gd	26.73	1.47	28.05	3.26	4.97	1.38	5.45	1.93	10.69	1.42
Dy	25.32	1.80	25.50	2.18	3.75	0.62	4.44	0.61	9.26	0.89
Er	14.04	0.57	14.02	1.59	2.52	0.48	2.77	0.62	5.08	0.73
Yb	11.45	0.46	11.19	2.03	2.58	0.44	3.09	0.70	4.30	0.59
Hf	55.60	2.34	55.59	5.39	11.97	1.07	13.39	2.09	16.92	1.24
Ta	17.02	1.08	16.38	1.91	9.84	0.67	9.72	1.09	5.56	0.46
Th	49.89	3.05	49.55	5.00	23.54	1.85	25.23	3.23	14.14	1.05
U	10.81	0.68	9.69	0.94	4.84	0.51	5.29	0.86	2.79	0.34
Y/Th	2.88	0.16	3.02	0.12	1.00	1.1	1.04	0.07	3.62	0.23
Zr/Th	48.52	2.54	46.47	1.98	26.59	27.49	28.14	2.30	52.56	3.32
La/Yb	12.14	0.42	11.33	1.38	34.44	6.51	32.72	4.93	18.03	2.37
n	*8*		5		*13*		*8*		*10*	

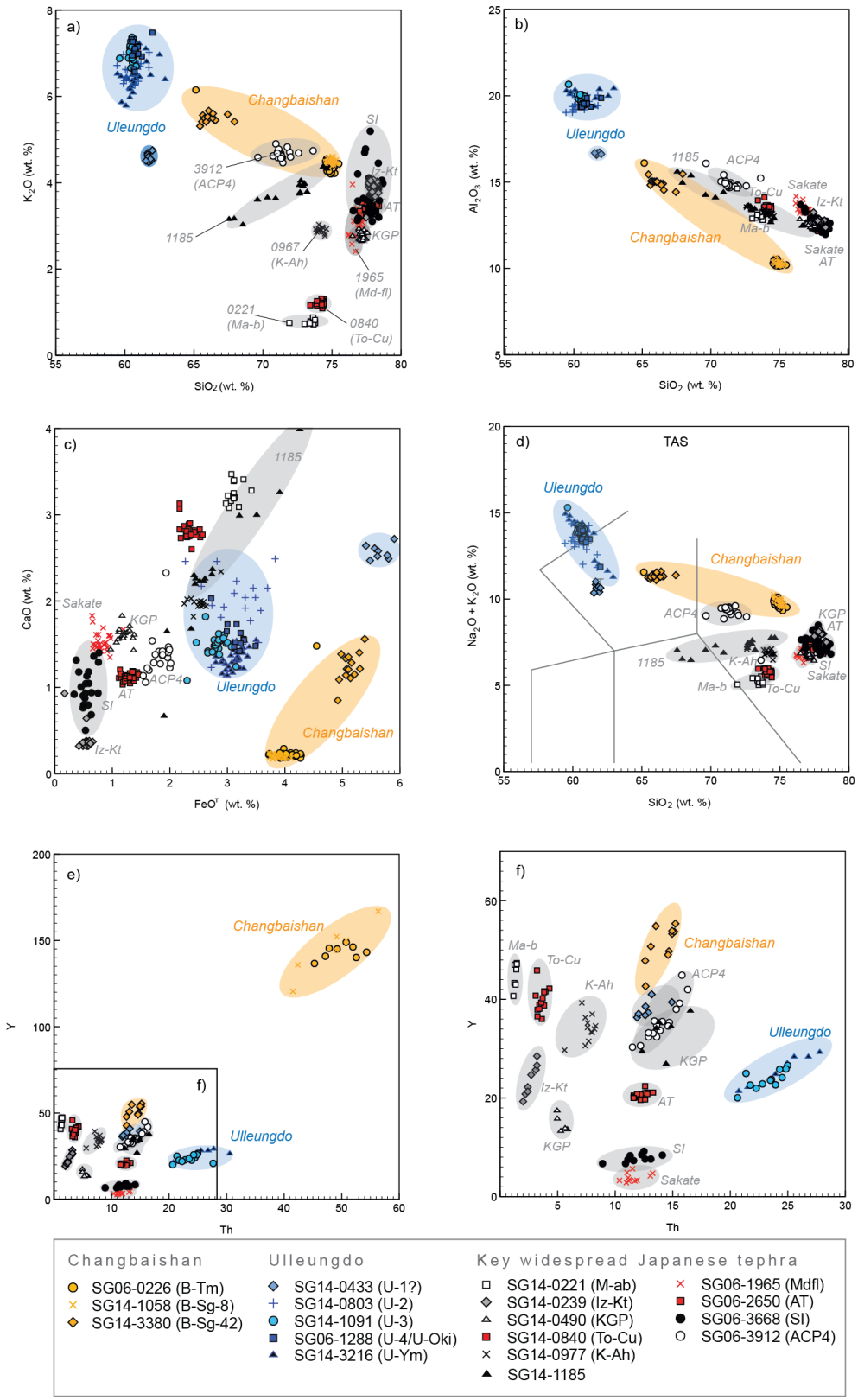


Figure 6.5. Glass shard major and trace element compositions of Ulleungdo (South Korea; shown in blue), Changbaishan (North Korea/China; shown in orange), and key Japanese tephra layers that are preserved in the Lake Suigetsu sediments (shown in grey and black) (Smith et al., 2013; McLean et al., 2016; 2018; Albert et al., 2018; accepted).

When normalised to the primitive mantle (Sun and McDonough, 1989), SG14-3216 and SG14-1091 show Light Rare Earth Element (LREE) enrichment relative to Heavy Rare Earth Element (HREE) (La/Yb = 30 – 35 ppm) and significant depletions in Ba, Sr and Eu typical of K-feldspar fractionation (Figure 6.6.). The paucity of a depletion in Nb and Ta content within these volcanic glasses, when normalised to the primitive mantle, is inconsistent with a subduction related volcanism (Figure 6.6).

The four tephra layers with Ulleungdo compositions are difficult to distinguish using their major element glass compositions, but we find the younger glasses of SG14-0803 are more elevated in CaO (by ca. 0.5 wt. %), compared to the early Holocene and SG14-3216 glass (Figure 6.5c). In addition, the alkaline glasses of SG14-3216 (SiO_2 59.5 – 62.5 wt. %, and $Na_2O + K_2O$ = 11.6 – 14.9 wt. %) can be discriminated from SG14-1091 by larger feldspar-related depletions in Sr, Ba and Eu, that are normalised to primitive mantle compositions (Figure 6.6.). The alkaline glass shards of SG14-0433 ($Na_2O + K_2O$ = 10.4 – 11.0) are also likely to derive from Ulleungdo, but contain ca. 2.5 wt. % lower K_2O, and ca. 2 wt. % higher CaO compared to the older eruption events outlined here (Figure 6.5a; 6.5c).

The three Changbaishan derived tephra layers (e.g., SG14-3380, SG14-1058 and SG06-0226) contain both rhyolitic and trachytic glass compositions ($Na_2O + K_2O$ = > 9.5 wt. %; Le Bas et al., 1986), with SiO_2 ranging from 65.5 to 75.5 wt. % (Table 6.2; Figure 6.5d). They contain < 1.6 wt. % CaO, and between 3.7 and 5.4 wt. % FeO^T (Figure 6.5c). Normalised to primitive mantle compositions, all

glasses are enriched in LREE relative to HREE, with La/Yb ratios higher in those of SG14-3880, relative to SG14-1058 and SG06-0226 (Table 6.2.) and show pronounced negative feldspar-related anomalies in Ba, Sr and Eu (Figure 6.6.).

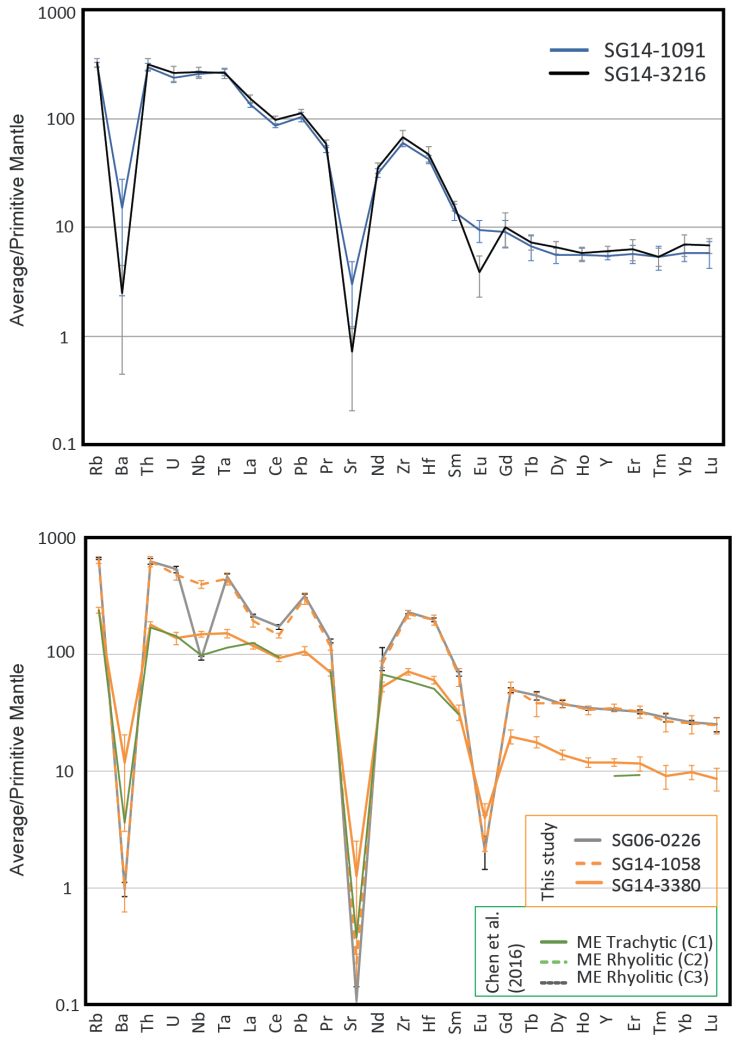


Figure 6.6. Primitive mantle normalised trace element compositions of glasses of: (a) Ulleungdo tephra layers (SG14-1091 and SG14-3216) in the Lake Suigetsu sequence; (b) Changbaishan tephra layers (SG06-0225, SG1401058 and SG14-3380) in comparison to proximal ME rhyolitic (C1 – C2) and trachytic (C1) proximal deposits (Chen et al., 2016). Primitive mantle values are from Sun and McDonough (1989).

The SG14-3380 glasses are exclusively trachytic (SiO_2 65.4 – 67.9 wt. %, 14.4 – 15.5 wt. % Al_2O_3, and $Na_2O + K_2O$ = 8.7 – 11.7 wt. %) and are compositionally similar to the single trachytic analysis from SG06-0226. Trace element compositions for SG14-3380 are homogenous, with 14.1 ± 1.1 ppm Th, 144 ± 9.0 ppm Rb; and 51 ± 4 ppm Y (Table 6.2.). Unfortunately, no trace elements were obtained for the trachytic end-member of SG06-0226 for further comparison with SG14-3380.

The rhyolitic SG06-0226 glass compositions overlap with SG14-1058 for all major elements (Table 6.2; Figure 6.5.). Both tephras contain glass compositions that are geochemically homogenous, with ca. 75 wt. % SiO_2, 10.3 wt. % Al_2O_3 and ca. 4.4 wt. % K_2O, and are characterised by very low CaO concentrations (< 0.3 wt. %). Trace element compositions of SG14-0226 and SG06-1058 show significant overlap, and are more enriched in incompatible elements (e.g., Th, Ta and Y), whilst depleted in compatible elements (e.g., Sr, Ba, and Eu) relative to the trachytic glass of SG14-3380 (Table 6.2; Figure 6.6b). SG06-0226 and SG14-1058 have similar mantle normalised profiles and levels of incompatible trace element enrichment (Figure 6.6). Glasses of both tephra layers have greater feldspar-related depletions in Ba, Sr and Eu relative to SG14-3380. SG06-0226 glasses show a significant depletion in Nb, which is not observed in SG14-1058 and SG14-3380, given the intraplate setting of the volcano it may relate to late stage, high-level fractionation processes.

6.5. Review of eruption framework

Here, the distal ash deposits erupted from Ulleungdo and Changbaishan are outlined and reviewed using the relative stratigraphy, geochemical glass compositions and eruption chronology. Published occurrences are centred on the Lake Suigetsu tephrostratigraphy to provide an integrated framework that is constrained by widespread ash layers erupted from Japanese volcanoes (Figure 6.7.). There are no pre-50 ka visible ash layers in Lake Suigetsu with Ulleungdo or Changbaishan compositions, but thus far cryptotephra extraction techniques have not yet been carried out on these older sediments, so it is possible other cryptotephra layers are preserved during these periods.

6.5.1. Post 86 ka (Aso-4) Ulleungdo eruptions

Distal ash layers erupted from Ulleungdo were identified below the AT tephra (30 ka) in marine sediments obtained from the Oki ridge (Arai et al., 1981) and Yamato Basin (Ikehara et al., 2004). These pre-AT Ulleungdo tephra were originally considered to be from a single eruption, but the age was controversial. However, Chun et al. (2007) identified two separate alkaline ash deposits in marine core MD01-2407 (Figure 6.1.), which they named SKPI and SKPII, and were dated to 40 – 41 ka and 60 – 61 ka, respectively, based on correlations with the regional-scale thinly-laminated marine stratigraphy (Tada, 1999; Chun et al., 2007).

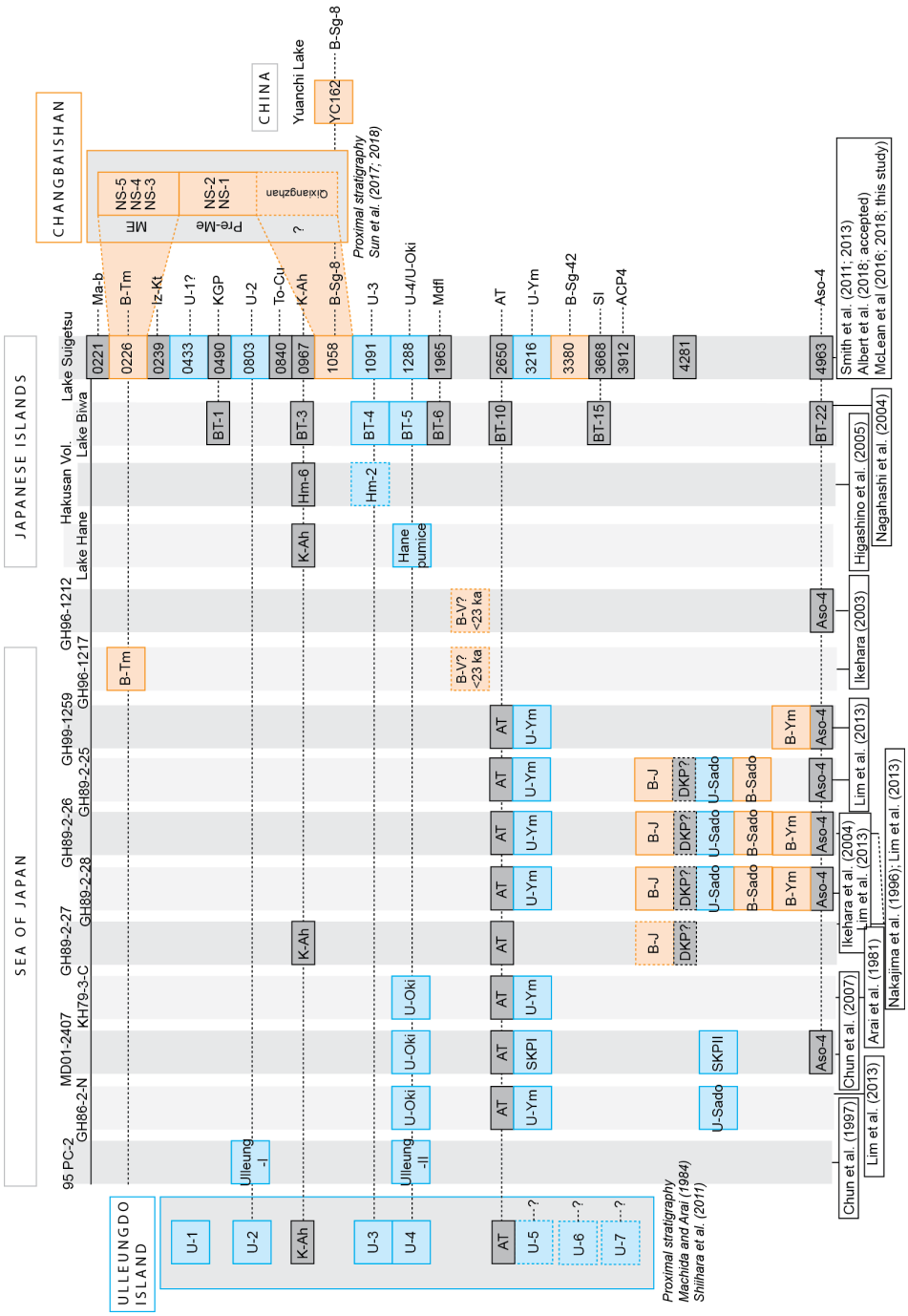


Figure 6.7. Summary tephrostratigraphy of proximal and distal archives that contain ash erupted from Ulleungdo (blue boxes) and Changbaishan (orange boxes) (see Figure 6.1. for archive location). Widespread Japanese tephra layers, which provide valuable chronostratigraphic markers, are also shown in grey boxes. Alkali-rich ashes erupted from Ulleungdo and Changbaishan are routinely identified in marine cores extracted from the Sea of Japan (East Sea). Several high-resolution archives in Japan also preserve distal tephra layers from these centres (references are in boxes at the base), including Lake Biwa (Nagahashi et al., 2014), and Lake Suigetsu (Smith et al., 2011; McLean et al., 2016; 2018), which provide precise eruption chronologies for widespread ash-fall events. Due to the paucity of glass data from pre-Holocene eruptions of Ulleungdo and Changbaishan, these units cannot be correlated to distal ash deposits elsewhere.

Lim et al. (2013) also identified two equivalent cryptotephra layers in several other marine cores northeast of Ulleungdo (e.g., GH86-2-N, GH89-2-25, GH89-2-26 and GH89-2-28), which were stratigraphically positioned between the rhyolitic Aso-4 (86.4 ± 1.1 ka; Albert et al., accepted) and AT tephra. These distal tephra layers were therein named the Ulleung-Yamato (U-Ym) and Ulleung-Sado-Oki (U-Sado), and are considered to be equivalent to SKP-I and SKP-II, respectively (Figure 6.7.).

The Lake Suigetsu sediments verify that an ash fall event from Ulleungdo occurred at 39,832 ± 196 cal. yrs BP (95.4 % confidence interval), which reached the Japanese island of Honshu. This 1 mm thick ash layer (SG14-3216; Figure 6.4.) contains volcanic glass that compositionally overlap with the other Ulleungdo-derived tephra deposits preserved in the Suigetsu sequence (e.g. SG06-1288, SG14-1091), and other distal and proximal occurrences of the U-Oki tephra (Figure 6.5; Figure 6.8; Furuta et al., 1986; Nagahashi et al., 2004; Chun et al., 2007; Park et al., 2007).

Although grain-specific glass compositional datasets for the U-Ym tephra preserved in the Sea of Japan have not been published for comparison, the broad geochemical and chrono-stratigraphic consistency with SG14-3216, means this ash must also correlate to the same eruption of Ulleungdo. The Suigetsu-derived deposit age of 39,832 ± 196 cal. yrs BP (95.4 % confidence interval), provides the most constrained eruption age, and this date can now be imported into other site-specific age models that contain this marker.

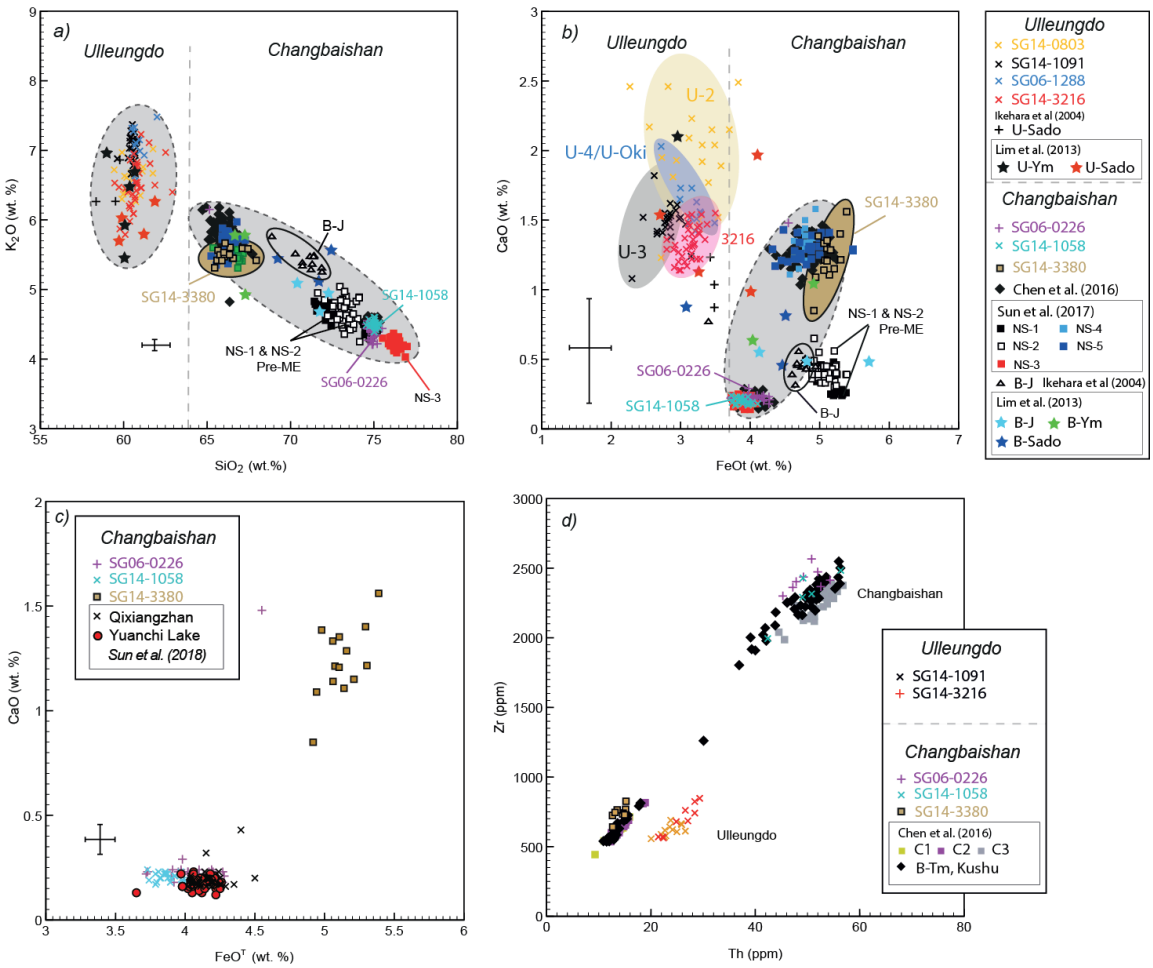


Figure 6.8. Glass shard major and trace element compositions of Ulleungdo (SG14-0803; SG14-1091; SG06-1288; SG14-3216) and Changbaishan (SG06-0226; SG14-1058; SG14-3380) tephra layers preserved in the Lake Suigetsu archive, compared to other proximal (Chen et al., 2016; Sun et al., 2017, 2018) and distal occurrences (Ikehara et al., 2004; Lim et al., 2013). Error bars represent 2 x standard deviations of repeat analysis of the StHs6/80-G MPI-DING reference glass analyses, error bars for (d) are smaller than the data symbols.

No other distal ash occurrences have been reported that are chronologically or geochemically consistent to the ca. 19 ka eruption (proximal unit N-5; Kim et al., 2014), suggesting that this eruption was probably not widespread.

6.5.2. Post 86 ka (Aso-4) Changbaishan eruptions

Three tephra layers originating from Changbaishan have been recognised in marine cores stratigraphically positioned between the Aso-4 and AT tephra layers. The two oldest of which are named the Baegdusan-Yamato Basin (B-Ym; ca. 85.8 ka) and Baegdusan-Sado-Oki (B-Sado; ca. 67.6 ka) tephra, and have been identified as cryptotephra isochrons in both GH89-2-26 and GH89-2-28 marine cores (Figure 6.7; Lim et al., 2013). Lim et al. (2013) report that the B-Ym and B-Sado distal glass are trachytic in composition (Figure 6.8.). Furthermore, the Baegdusan-Japan (B-J) tephra is found between Ulleungdo U-Ym and U-Sado tephra layers (Figure 6.7.), which is estimated to have been erupted ca. 50 ka based on correlations with the regional-scale thinly laminated layer stratigraphy (Shirai et al., 2003; Ikehara et al., 2004; Lim et al., 2013). Ikehara et al. (2004) and Lim et al. (2013) report a homogenous rhyolitic composition for the B-J tephra (ca. 71.2 wt. % SiO_2, ca. 12.0 wt. % Al_2O_3, and $Na_2O + K_2O$ = 11.1 wt. %; Figure 6.8.) that contrasts with the exclusively trachytic glass compositions of the ca. 67.6 ka B-Sado tephra (Lim et al., 2013).

The Lake Suigetsu sediments provide evidence of another explosive eruption of Changbaishan. There is a cryptotephra layer (SG14-3380) discovered ca. 1.6 m below the U-Ym tephra (SG14-3216) and dated to 41,989 – 41,665 cal. yrs BP (95.4 % confidence interval). The glass compositions of SG14-3380 are exclusively trachytic and geochemically overlap with proximal units assigned to the late phase of the ME (e.g., NS-4 and NS-5 proximal deposits; Sun et al., 2017) (Figure 6.8.), and other distal occurrences of the trachytic end member of

the B-Tm ash (e.g., Okuno et al., 2011; Hughes et al., 2013; Sun et al., 2015; Chen et al., 2016). The trace element compositions of the trachytic unit of the ME (referred to as C1 and C2; Chen et al., 2016) also show considerable overlap with SG14-3380, although slight differences in High Field Strength Elements (HFSE) (e.g., Nb and Ta) are observed (Figure 6.6.). SG14-3380 glass compositions are therefore clearly distinguishable from the proximal pre-ME deposits reported by Sun et al. (2017) (i.e., NS-1 and NS-2; Figure 6.8a – b). The compositional and chronological differences of SG14-3380 (ca. 41.8 ka) and the B-J (ca. 51.5 ka) tephra indicate that they must represent separate eruptions of Changbaishan. Here, we name the distal ash of this Changbaishan eruption (ca. 42 ka) as the Baegdusan-Suigetsu-42 (B-Sg-42) tephra, following the convention of naming proximally undefined distal deposits using the type-locality.

No other distal ash deposits erupted from Changbaishan have been identified between the AT and Aso-4 tephra layers, although a distal tephra named the Baegdusan-Vladivostok (B-V) ash was found in the Primorye regions of Russia, and in the north-eastern part of the Japan Sea (Figure 6.1.). The eruption age is estimated to be younger than 24.5 ka (Machida and Arai, 2003; Ikehara, 2003), and the geochemical fingerprint of this tephra has not yet been established.

6.5.3. Holocene Ulleungdo eruptions

As previously outlined, the largest known Plinian eruption from Ulleungdo generated the U-Oki tephra layer that is dated to 10,230 – 10,171 cal. yrs BP

(95.4 % confidence interval; Smith et al., 2011, 2013). The U-Oki ash is found in several high-resolution palaeoenvironmental archives in Japan, including Lake Biwa (BT-4; Nagahashi et al., 2004) and Lake Suigetsu (SG06-1288; Smith et al., 2011) (Figure 6.7.). This U-Oki tephra is the only distal tephra that has been correlated to proximal deposits on Ulleungdo, and equates to the proximal U-4 unit of Shiihara et al. (2010).

Lake Suigetsu tephra layers SG14-1091 (ca. 8.4 ka) and SG14-0803 (ca. 5.7 ka) overlay the U-Oki tephra and are considered distal equivalents of proximal deposits U-3 and U-2, respectively, due to their close agreement to the proximal radiocarbon dates of soils between fall units (Okuno et al., 2010). Furthermore, K-Ah tephra is stratigraphically positioned between the U-3 (SG14-1091) and U-2 (SG14-0803) deposits (Shiihara et al., 2010). Distal equivalents of the U-3 eruption have been reported in the Sea of Japan (TRG1 sediment core; Domitsu et al., 2002), Lake Biwa (Nagahashi et al., 2004) and close to Hakusan volcano, central Honshu (Higashino et al., 2005). In comparison, SG14-0803 is the only known distal equivalent of the U-2 tephra, indicating that it was perhaps a lower magnitude event, or the eruption had a different dispersal direction.

The proximal deposits of the youngest U-1 eruption of Ulleungdo suggest it was a small strombolian-type eruption with a lava dome extrusion (Kim et al., 2014). Whole rock trace element data reported for this youngest event have a distinct tephriphonolite composition (Brenna et al., 2014). Similarly, the distal SG14-0433 glass compositions are compositionally distinct from the other Ulleungdo derived tephras in Suigetsu and contain ca. 60 wt. % SiO_2, but have lower ca.

2.5 wt. % lower K_2O, and ca. 2 wt. % higher CaO content (Figure 6.5.). This suggests that SG14-0433 is very likely to provide the first distal occurrence and eruption age of the U-1 event (2,737 – 2,620 cal. yrs BP; 95.4 % confidence interval), but additional U-1 glass data is required to confirm this proximal-distal correlation.

6.5.4. Holocene Changbaishan eruptions

An eruption from Changbaishan was identified in Lake Suigetsu (SG14-1058) that is dated to 8,166 – 8,099 cal. yrs. BP (95.4 % confidence interval; McLean et al., 2018) and is the first known report of a large early Holocene eruption from the volcano. As outlined, the compositions are exclusively rhyolitic and are identical at a major element level to the rhyolitic end-member of the ME deposits. A visible patchy grey peralkaline tephra has since been identified in Lake Yuanchi, located ca. 30 km east of Changbaishan in China, which is dated to 8,831 – 8,100 cal. yrs BP (95.4 % confidence interval; Sun et al., 2018). The major element glass compositions of this tephra broadly overlap with those of SG14-1058 (Figure 5.8c), although some offsets are observed that are close to instrumental/analytical uncertainty. Sun et al. (2018) also correlate Suigetsu tephra SG14-1058 and Yuanchi tephra as distal deposits dispersed during the eruption that produced the Qixiangzhan comendite. However, further work is required to secure this correlation as $^{40}Ar/^{39}Ar$ ages generated for the Qixiangzhan comendite span several thousand years (e.g., Singer et al., 2014; Yang et al., 2014), and the stratigraphic relationship between the Qixiangzhan comendite and other pre-ME fall deposits is not known. When normalised to

mantle concentrations, we find that SG14-1058 only shows a minor depletion in Nb, unlike SG06-0226 (B-Tm ash) and C-3 unit (Chen et al., 2016), which may be useful to confirm the proximal deposit. We suggest that the distal ash erupted from Changbaishan at ca. 8.1 ka (e.g., SG14-1508) is named Baegdusan-Suigetsu-8 (B-Sg-8).

No distal ash deposits have been identified that geochemically or chronologically overlap with the pre-ME proximal deposits of NS-4 and NS-5 that are dated to ca. 4 – 5 ka (Sun et al., 2017). Similarly, even in the high-resolution archives in northern Japan (e.g., Lake Kushu; Chen et al., submitted), no distal occurrences of post-ME eruptions from Changbaishan have been identified.

6.6. Conclusions

Distal records can provide useful information on past eruption activity from volcanoes, whose deposits are inaccessible due to various reasons (e.g., burial or deposition into dynamic ocean environments). A review of the distal occurrences of alkali-rich ashes preserved in marine and lacustrine cores (spanning ca. 86 ka) in the East Asian/Pacific region has provided an improved eruption framework for intraplate volcanoes Ulleungdo and Changbaishan. This framework shows that there are numerous explosive magnitude eruptions responsible for distal ash fall events that are only cryptically recorded in the geological record.

Ulleungdo has erupted explosively at least five times over the past 86 ka (since the deposition of the Aso-4 tephra), and these are dated to 60 – 61 ka (U-Sado tephra; Lim et al., 2013), ca. 39.8 (U-Ym tephra; this study); ca. 10 ka (U-Oki/U-4; Smith et al., 2011; 2013); ca. 8.4 ka (U-3; McLean et al., 2018) ca. 5.7 (U-2; McLean et al., 2018). Furthermore, it is likely that a younger eruption from Ulleungdo occurred ca. 2.7 ka, but further work is required to characterise proximal deposits on the island that potentially correlate. This age would be consistent with a repose interval of <3 ka throughout the Holocene.

The new Changbaishan-derived tephra layers identified in the Suigetsu sediments, mean that at least seven explosive eruptions have produced significant ash dispersals over the past 86 ka, which are dated to ca. 85.8 ka (B-Ym; Lim et al., 2013), ca. 67.6 ka (B-Sado; Lim et al., 2013), ca. 50.5 (B-J tephra; Ikehara et al., 2014; Lim et al., 2013), ca. 41.8 (B-Sg-42; this study), ca. 25 ka (B-V; Machida and Arai, 2003), 8.1 ka (B-Sg-8; McLean et al., 2018) and AD 946 (B-Tm; Hakozaki et al., 2017; Oppenheimer et al., 2007). It is possible that additional widely dispersed ash fall events will be discovered in other distal records the future, since there are compositionally distinct proximal outcrops at Changbaishan (e.g., NS-4 and NS-5; Sun et al., 2017) that have yet to be correlated to any distal markers.

Even though Lake Suigetsu is located 600 km E of Ulleungdo, and 1000 km SSE of Changbaishan (i.e., not downwind of the current prevailing winds), tephra from these volcanoes are clearly preserved in the sediments. The

eruptions responsible for the B-Sg-42 and B-Sg-8 distal tephra must have been large eruption events (i.e., greater than VEI 5), considering the shard concentration preserved in Suigetsu (> 18,000 shards per gram of dried sediment). Unfortunately, it is not possible to get better constraints on volume and magnitude of these events given that they have not been found visibly in multiple locations. The ages provided in this paper may help researchers to look for these deposits in other archives, which would also help understand more about the dispersal of the events. For instance, dispersal modelling suggests that ash from Changbaishan could be dispersed directly south, if controlled by the summer monsoon prevailing winds (e.g., Lee et al., 2018; Yun, 2018), which could offer an explanation as to why they have not been identified in sedimentary records further north, or in marine sediments in the Sea of Japan. Critically, these tephra occurrences demonstrate that both Ulleungdo and Changbaishan have been more active than previously thought, and indicate that the ash plumes were widespread.

Acknowledgements

The Fukui-SG14 sediment coring campaign was funded by the Fukui Prefectural government, and the coring was conducted by the team of Seibushisui Co. Ltd. Japan, led by A. Kitamura. KAKENHI grant by MEXT, Japan (15H021443) was used to purchase laboratory equipment and consumables during the project. Trace element analysis was funded by the JSPS Summer Award. DM is funded by NERC (grant: NE/L002612/1) and part of the Environmental Research Doctoral Training Program at the University of

Oxford. PGA and RAS are supported by Early Career Fellowships from the Leverhulme Trust (grant: ECF-2014-438 and ECF-2015-396). Geochemical bi-plots were generated using the RESET plot function (https://c14.arch.ox.ac.uk).

See Appendix D for Supplementary Material

CHAPTER 7: GENERAL DISCUSSION

Overview

This chapter brings together a discussion of the overarching aim of this research project and the insights that can be established from building very detailed dossiers of eruption events. Firstly, a comprehensive tephrostratigraphic framework for Japan is presented, which has been constructed using 24 key tephra archives distributed across East Asia and the western Pacific region. This demonstrates Lake Suigetsu's position as a key node in the tephrostratigraphic framework, and the importance of detailed systematic studies of distal archives to expand and integrate local eruption records. In order to help focus future research efforts, a table of 22 key isochrons are presented, and their suitability to help answer palaeoenvironmental questions is explored. The presented table summarises published geochemical information, chronological data, and known dispersal limits for these key marker layers.

This chapter also provides an example of the synchronisation potential of widespread ash deposits that form valuable isochrons across East Asia. The AT tephra layer is used to compare regional climate records reconstructed from the sediments of Lake Biwa (central Honshu, Japan), Lake Sihailongwan (eastern China) and a marine core from the northwest coast of Honshu (MD179-3312). This chapter closes with a review of the augmented Lake Suigetsu (SG06/SG14) tephrostratigraphy. This is an important resource for

volcanological research as it provides better constraints on the frequency, magnitude and dispersal of eruption events, which is valuable for assessing hazards and the risk to the densely populated regions of central Honshu.

7.1. Establishing a detailed tephrochronological framework

7.1.1. Context and rationale

The overarching aim of this research project is to help establish a detailed tephrostratigraphic framework for Japan that can be used to synchronise palaeoclimate records across the Asian/Pacific region. This framework (sometimes referred to as a lattice) can be constructed using the sequence of ash layers preserved in the geological record to create a network of sites that are connected by co-located markers (e.g., Davies et al., 2012; Blockley et al., 2014; Lowe et al., 2015; Mackay et al., 2016; Abbott et al., 2018b). This framework is necessary to grasp a comprehensive understanding of the number and frequency of eruption events, and to generate constrained eruption chronologies.

Tephra erupted from the East Asian/Pacific region has already been identified ca. 9,000 km from source in northern Greenland (Sun et al., 2014a; Bourne et al., 2016) and therefore able to synchronise palaeoclimate records across hemispheric scales. At present there is no detailed framework that integrates key tephra archives across East Asia, pulling together the wealth of recent chronological and geochemical datasets. Constructing this tephrostratigraphic

framework would permit an improved understanding of the dispersal extent of these isochrons and likelihood of other useful markers in newly obtained records. This would facilitate the application of tephrochronology and provide a useful dataset for the emerging cryptotephra studies in this region.

7.1.2. A tephrostratigraphic framework for Japan

A tephrostratigraphic framework for Japan, spanning the last 100 ka is presented here (Figure 7.1.), which has been constructed using sedimentary records (e.g., lacustrine, marine and peat cores) distributed across the East Asian and the western Pacific region (Figure 7.2.). This framework is comprised of 24 tephra archives, and shows all ash layers currently reported for each record, including those that have not yet been correlated to source. The tephrostratigraphic network contains over 50 different isochrons, that erupted from more than 15 different volcanic sources, across three geographical regions (Japan, North Korea/China and South Korea). This schematic framework uses median eruption ages reported for these layers, to illustrate the synchronisation potential. In reality, the age of some tephra layers (particularly those outside the radiocarbon timeframe, > 50 ka) are not yet precisely constrained, and are further discussed in Section 7.1.3. For the vast majority of instances, these ash layers have been robustly correlated using their glass chemistry.

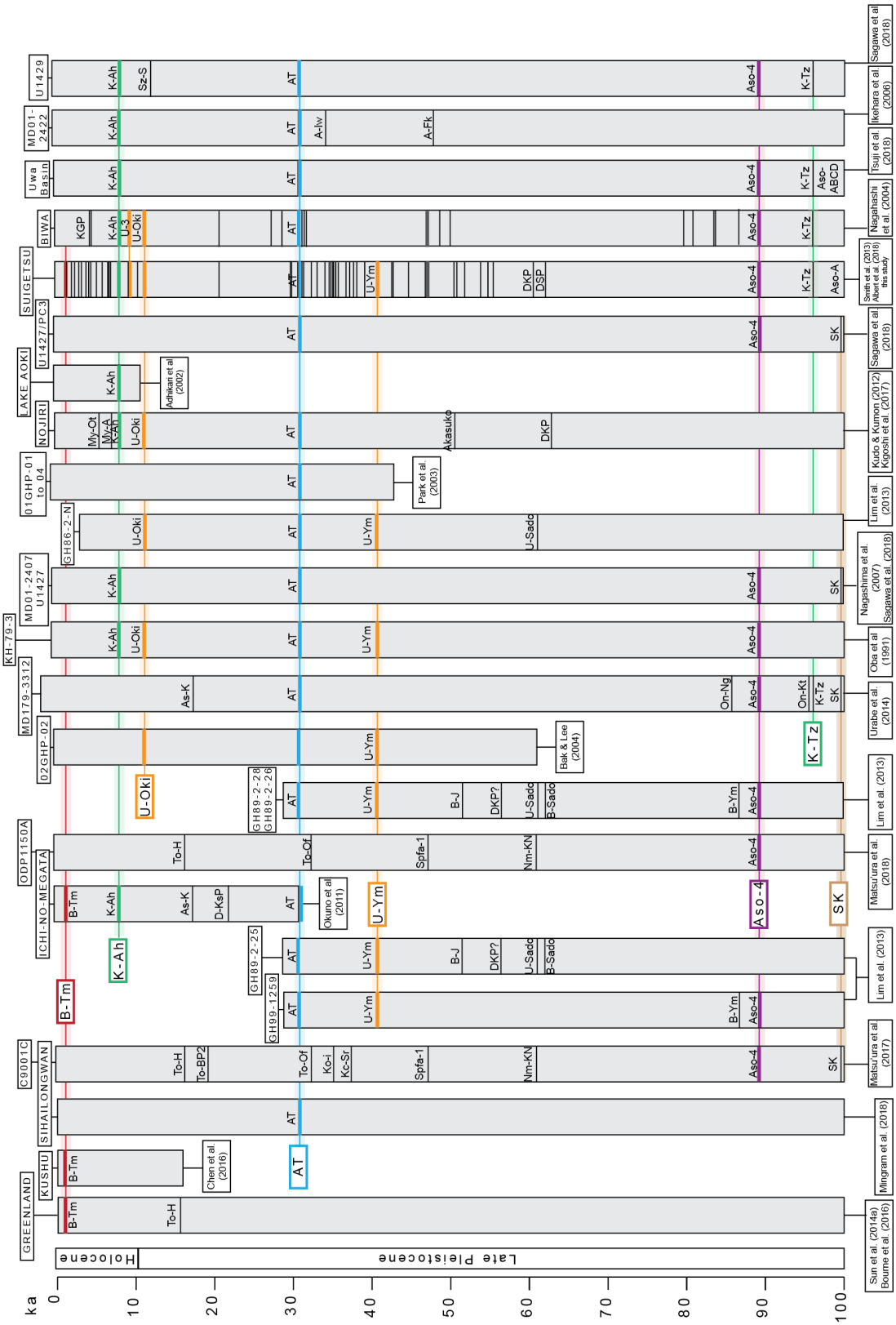


Figure 7.1. Tephrostratigraphic framework for Japan constructed for the past 100 ka (i.e., Late Pleistocene and Holocene). The framework is assembled using 24 sedimentary records (plotted here from north to south; see Figure 7.2.), with tephra markers shown by a black (uncorrelated or regional marker) or coloured (key widespread marker layer) dash. Site names and references are shown in the white boxes, and tephra codes/correlations are outlined in Figure 7.2. and Table 7.1. Marker layers are plotted using approximate eruption ages to illustrate their synchronisation potential.

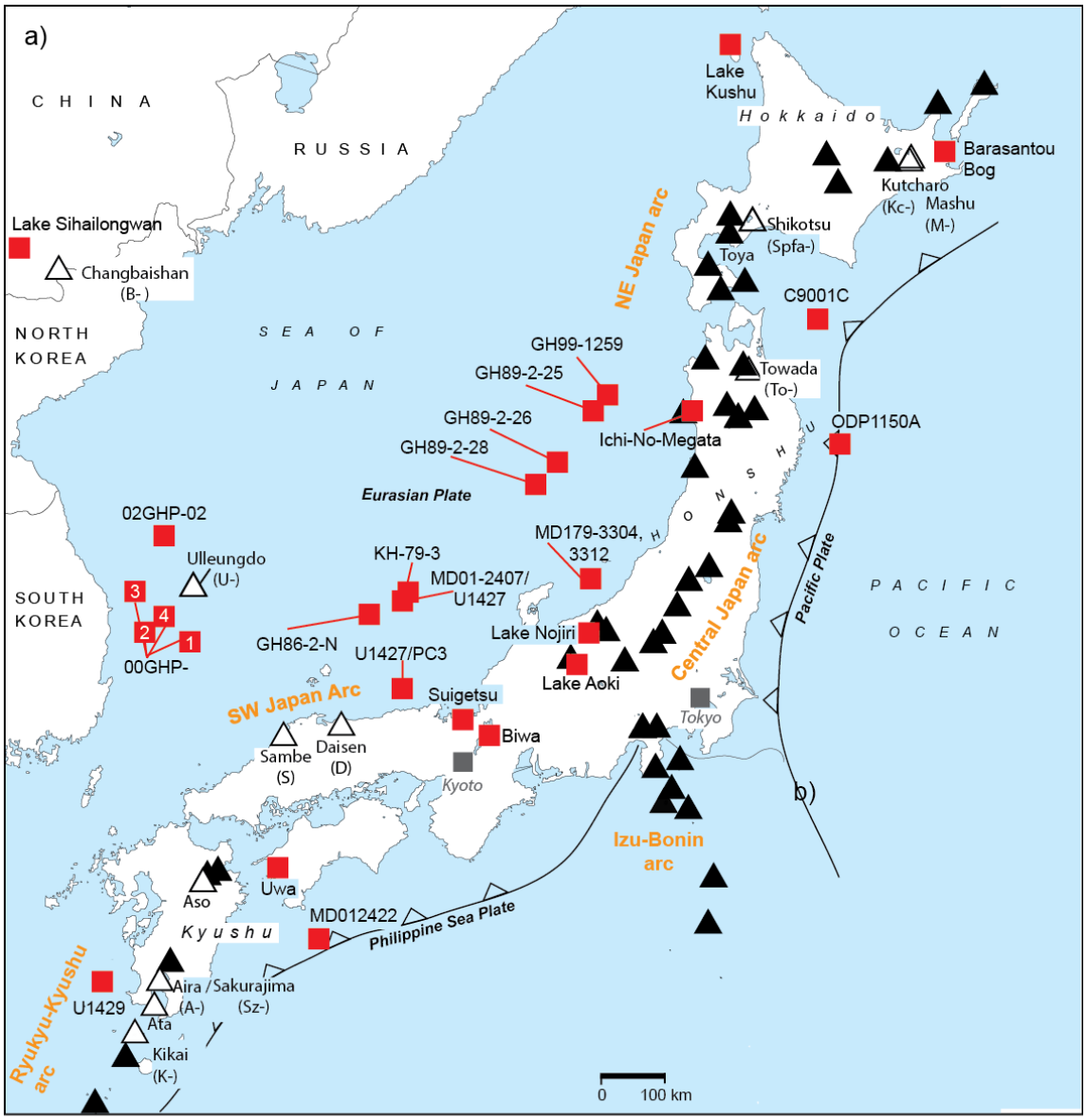


Figure 7.2. Key sedimentary records (marine, lacustrine and peat cores; red squares) used to construct the tephrostratigraphic framework for Japan (see Figure 7.1. for tephra sequence and site reference). Source volcanoes of key widespread tephra markers are shown as white triangles, and black triangles depict other centres known to have been active during the late Quaternary (data from Machida and Arai, 2003). Codes used to name distal tephra layers are shown in brackets in the labels.

Due to the number and complexity of proximal stratigraphic sequences, these outcrops have not been integrated within the tephrostratigraphic framework presented here, but available glass datasets from these units are highlighted in Section 7.1.3. and documented in Machida and Arai (2003).

As recognised at the onset of this project, the tephrostratigraphic framework is underpinned by a number of significant widespread markers (e.g., B-Tm, U-Oki, AT, Aso-4, K-Tz, Ata), which are predominantly found as thick visible ash layers in sedimentary records across central Japan, and principally lie within the dispersal isopachs mapped by Machida and Arai (2003). With the exception of the alkaline glass derived from Ulleungdo and Changbaishan, these widespread eruptions are rhyolitic with medium to high-K compositions (Machida and Arai, 2003; Kimura et al., 2015; Albert et al., accepted).

The AT tephra erupted from Aira (30 ka; Smith et al., 2013) is the most commonly identified and widespread time-stratigraphic marker and can synchronise records over 1,200 km apart in East Asia, from marine cores on the south coast of Kyushu (Japan) (Sagawa et al., 2018) to high-resolution lacustrine records in eastern China (Mingram et al., 2018), and also provides a key stratigraphic marker on the volcanic island of Ulleungdo in South Korea (Kim et al., 2014). The B-Tm tephra (erupted from Changbaishan at AD 946; Oppenheimer et al., 2017) synchronises the late Holocene Greenland ice core stratigraphy (Sun et al., 2014b) providing a significant step towards comparing records on a hemispheric scale.

It has not yet been possible to extensively interlink this regional record to other neighbouring frameworks, such as the comprehensive Kamchatka eruption tephrostratigraphy (e.g., Kyle et al., 2011; Ponomareva et al., 2015a), although sediment cores in the Sea of Okhotsk (located between the Kurile arc and Kamchatka) are known to contain ash from several Hokkaido eruptions (e.g.,

Derkachev et al., 2016), but these have not yet been tied to specific eruption events. Isochrons derived from northern Honshu and Hokkaido will be key to extending the northernmost limits of this framework, due to the prevailing westerlies. In the future it may be possible to trace the very large magnitude events from Kamchatka in northern parts of Japan, such as the Kurile Lake eruption (KO tephra; ca. 7.5 ka), since visible deposits from this eruption have been found in the sediment cores of the Sea of Okhotsk (Gorbarenko et al., 2002, 2014).

Notably, the tephra-based framework is underpinned by eruption events from volcanic sources west of Japan (e.g., Ulleungdo and Changbaishan), which have routinely deposited ash over Honshu and the surrounding seas. Systematic investigations through the sediments of Lake Suigetsu (this study) and the Sea of Japan (e.g., Lim et al., 2013) reveal that these occurrences have been more frequent and more widespread than previously anticipated. These isochrons are of considerable value since their distinctive alkaline geochemistry can be easily distinguished from the arc sources distributed along the length of Japan, and these ash layers provide important time-stratigraphic markers to precisely link marine and terrestrial sequences. However, further work is required to constrain all eruptive events from these centres and investigate the dispersal limits of eruptions prior to the B-Tm eruption of Changbaishan (see Chapter 6).

There are several archives that form key nodes in the tephrostratigraphic framework for Japan, which include Lake Biwa, Lake Suigetsu and Lake Nojiri

(Nagahashi et al., 2004; Smith et al., 2013; Kigoshi et al., 2017; this study) and well as coastal marine cores (e.g., C9001C; Matsu'ura et al., 2017). This is partly because these are some of the most high-resolution sedimentary archives, but also because these records have been systematically examined to catalogue, and fingerprint all ash layers preserved in the sediments. In many cases, although ash layers are frequently identified within sedimentary records, only stratigraphic or chronological information is published for key markers that can be confidently correlated to source, or are used to constrain site-specific age-models. This currently limits the integration of local eruption events and possibility of more distal links, that could be established by examining the sediments for thinner, or finer ash units. For instance, systematic investigations through marine core C9001C revealed a detailed eruption record of Towada volcano, that is interbedded with key widespread markers erupted from Hokkaido, and thus their stratigraphic and chronological relationships could be determined (Matsu'ura et al., 2017).

Cryptotephra investigations are in their infancy in Japan, and realistically are not possible in all sedimentary archives, particularly those located close to very active volcanic sources. However, where this technique can be applied successfully, the wealth of markers revealed, as well as their distal origins, indicate that there is substantial potential to precisely synchronise records throughout the Late Quaternary. Several lacustrine records, including Lake Kushu (Chen et al., 2016), Lake Suigetsu (this study), and marine cores, e.g., C9001C (Matsu'ura et al., 2017) and GH982-25 to 28 (Lim et al., 2013), have been targeted for detailed cryptotephra investigations, which have enabled a

significant extension of the number and the possibility of very distal links. Furthermore, this has also permitted the identification of Japanese ash in eastern China for the first time (Mingram et al., 2018).

Cryptotephra investigations show that non-visible ash layers can be derived from eruptions that lie outside of their previously known fall footprints. Arguably the most remarkable of which is the presence of a late Holocene tephra erupted from Mashu (Ma-b tephra), which has been identified almost 1,000 km from source (McLean et al., 2018), and against the predominant dispersal mapped for the eruption (Machida and Arai, 2003). This eruption event is established as potentially one of the most widespread Late Quaternary isochrons, but to date has been very infrequently identified, with only visible occurrences reported on the eastern regions of Hokkaido (Nakamura, 2016). This may be a function of having erupted ca. 50 years following the large magnitude Changbaishan eruption that dispersed the B-Tm tephra (AD 946; Oppenheimer et al., 2017), which is frequently found as a thick ash unit in northern Japan, and it may not be possible to stratigraphically separate the Ma-b ash in other lower-resolution distal sediments. This highlights the importance of undertaking detailed glass geochemistry to ensure robust correlations and to consider the possibility of very frequent eruption events.

The development of cryptotephra studies in this region will present both challenges and new opportunities due to the significant number of eruption events, and that the isopachs of the majority of these markers remain poorly constrained. Very detailed and systematic studies will be needed to robustly

extend this framework, and to utilise the many possible local and regional tie-points and chronological markers. This will also rely on detailed glass geochemical fingerprinting for these isochrons, since most centres have erupted compositionally similar tephra over thousands of years (e.g., Machida and Arai, 2003; Kimura et al., 2015; Albert et al., accepted). Trace element analysis will be key to strengthening these correlations, however this may not be possible in some ultra-distal locations where shard sizes are very small. Nevertheless, this exercise shows that despite the geochemical overlap of tephra erupted from sources on the same tectonic arc, the number of distinct and widespread isochrons separating these events suggest it is possible to use almost all these as time-stratigraphic markers where some chronological certainty is known.

7.1.3. Key isochrons for palaeoclimate investigations

Although there are numerous high-resolution palaeoenvironmental records distributed across East Asia, tephra layers are infrequently reported and have not been used to investigate the spatio-temporal variability of past climate change. Some tephra layers are used to provide age-constraints within depositional models, but commonly sedimentary archives are also tuned to global climate stratotypes (e.g., the LR05 marine isotope stack; Lisiecki and Raymo, 2005). In order to highlight the significant potential of East Asian tephra markers for palaeoclimate research and focus future research efforts, a list of 22 key marker layers are presented in Table 7.1.

Table 7.1. Key isochrons for palaeoenvironmental investigations (see text for further details).

Marine Isotope Stage	Tephra Label	Tephra Name	Source	Age	Age Reference	Distribution area	Key Glass Composition References
1	Ma-b	Mashu-b	Mashu, Hokkido Island, Japan	AD 960 - 992 (SG)	McLean et al. (2018)	Unconstrained. Identified in northeastern Hokkaido and as a cryptotephra layer in Lake Suigetsu (McLean et al., 2018).	Nakamura, 2016; McLean et al. (2018)*
	B-Tm	Baegdusan-Tomakomai	Changbaishan, China/North Korea	AD 946 (D)	Oppenheimer et al. (2017)	Widespread distribution across the Sea of Japan, northern Honshu and Hokkaido. Furthest southern occurrence is a 1 mm thick ash layer identified in Lake Suigetsu. B-Tm cryptotephra layer is also identified in the Greenland ice cores (Sun et al., 2014a).	Furuta et al. (1986); Machida and Arai (2003); Chen et al. (2016)*; McLean et al. (2016)*; Sun et al. (2017)
					Hakozaki et al. (2017)		
	To-Cu	Towada-Chuseri	Towada, Honshu Island, Japan	5,986 - 5,899 cal. yrs BP (SG)	McLean et al. (2018)	Widespread across northern Honshu and the coastal regions of the Pacific. Identified as a cryptotephra layer in the Suigetsu cores.	McLean et al. (2018)*
	K-Ah	Kikai-Akahoya	Kikai, Kyushu Island, Japan	7,307 - 7,196 cal. yrs BP (SG)	Smith et al. (2013); McLean et al. (2018)	Found widespread across the Sea of Japan, and southern and central Japan.	Machida and Arai (2003); Smith et al. (2013)*; Tsuji et al. (2018)*; Albert et al. (accepted)
	B-Sg-8	Baegdusan-Suigetsu-8	Changbaishan, China/North Korea	8,166 - 8,099 cal. yrs BP (SG)	McLean et al. (2018)	Unconstrained. Two cryptotephra occurrences to date: Lake Suigetsu (central Honshu) Lake Yushu (eastern China).	McLean et al. (2018); Sun et al. (2018)
	U-Oki	Ulleung-Oki	Ulleungdo, South Korea	10,230 - 10,171 cal. yrs (SG)	Smith et al. (2011a); McLean et al. (2018)	Found in marine cores from the southern part of the Japan Sea and terrestrial western Japan.	Furuta et al. (1986); Smith et al. (2011)*
2	Sz-S	Sakurajima-Satsuma	Sakurajima, Kyushu Island, Japan	ca. 12.8 cal. ka BP (14C)	Okuno (2002)	Widely dispersed over southern Kyushu and East China Sea, forming a circular distribution pattern.	Moriwaki et al. (2011); Albert et al. (accepted)*
				13.8 ± 1.3 ka (TL)	Shitaoka et al. (2016)		
				13.4 ± 2 ka (TL)	Shitaoka et al. (2016)		
	As-K	Asama-Kusatsu	Asama, Honshu Island, Japan	ca. 17 ka (14C)	Okuno et al. (2011)	Dispersed across central and northern Honshu. Identified in Ichi-no-Megata (Okuno et al. (2011), cores off the Joetsu City (Japan Sea) (Urabe et al., 2014), Pacific coast.	Okuno et al. (2011); Urabe et al. (2014)
				ca. 16 - 17 cal. ka BP (14C)	Nakamura et al. (1997)		
	To-H	Towada-Hachinohe	Towada, Honshu Island, Japan	14.9 - 15.3 ka (OI)	Aoki and Aria (2000)	Unconstrained. Eastward dispersal, found as a cryptotephra in the Greenland ice cores (Bourne et al., 2016).	Machida and Arai, 2003; Bourne et al. (2016); Albert et al. (accepted)*
				15,364 - 15,679 cal. yrs BP (14C)	Horiuchi et al. (2007)		
				15,707 ± 226 yrs BP (NGRIP GICC05) (IC)	Bourne et al. (2016)		
3	AT	Aira-Tanzawa	Aira, Kyushu Island, Japan	30,174 - 30,078 cal. yrs BP (SG)	Smith et al. (2013); Albert et al. (accepted)	Found widespread across the Sea of Japan, and southern and central Japan.	Furuta et al. (1986); Machida and Aria (2003); Smith et al. (2013)*; Schindlbeck et al. (2018); Tsuji et al. (2018)*
	U-Ym	Ulleung-Yamato	Ulleungdo, South Korea	41,989 - 41,665 cal. yrs BP (SG)	McLean et al. (forthcoming); Chapter 6	Sea of Japan cores and onshore at Lake Suigetsu (central Honshu).	Park et al. (2003); Ikehara et al., 2004; Lim et al. (2013); McLean et al. (forthcoming)

Table 7.1. (continued)

Marine Isotope Stage	Tephra Label	Tephra Name	Source	Age	Age Reference	Distribution area	Key Glass Composition References
3	Kc-Sr	Kutcharo-Shoro	Kutcharo, Hokkaido Island, Japan	40.03 - 40.23 cal. kyrs	Yamamoto et al. (2010)	E dispersal found across eastern parts of Hokkaido.	Machida and Arai, 2003; Matsu'ura et al. (2018); Albert et al. (accepted)*
				ca. 30 - 32 cal. kyr (ST)	Okumuro, 1991; Aira et al. (1986); Machida and Arai, 2003)		
	Spfa-1	Shikotsu-1	Shikotsu, Hokkaido Island, Japan	45,105 - 46,560 cal. yrs BP (14C)	Uesawa et al. (2016)	SE dispersal found widespread across central and eastern parts of Hokkaido.	Machida and Arai, 2003; Kimura et al., 2015; Matsu'ura et al. (2018); Albert et al. (accepted)*
				39.43 - 40.12 cal. yrs BP (14C)	Katoh et al. (1995)		
				39.5 - 40.1 cal. kyr BP	Aoki and Aria (2000); Hunt and Najman (2003)		
				ca. 42 - 43 (cal. kyrs) (14C)	Sakamoto et al. (2006)		
4	SAN1	SAN1	Kuju, Kyushu Island, Japan	54.4 ± 1.6 (SG)	Albert et al. (2018)	Widespread across the Sea of Japan (Ikehara et al., 2014) and a visible layer in Lake Suigetsu (Albert et al., 2018).	Ikehara et al. (2004); Albert et al. (2018)
	DKP	Daisen-Kurayoshi Pumice	Daisen, Honshu Island, Japan	59.6 ± 5.5 (SG)	Smith et al. (2013); Albert et al. (accepted)	NE dispersal, found widespread across central and northern Honshu.	Machida and Arai, 2003; Albert et al. (2018)*
5a	On-Kt	Ontake-Katamachi	Ontake, central Honshu, Japan	ca. 85.1	Nagahashi et al. (2007)	NE dispersal, found across central Honshu.	Machida and Arai, 2003*; Albert et al., accepted*
5b	Aso-4	Aso-4	Aso, Kyushu Island, Japan	86.8-87.3 ka (ST)	Aoki, 2008	Very widespread, in marine cores from south and to northern Honshu core (C9001). Also in	Furuta et al. (1986); Schindlbeck et al. (2018);
				86.4 ± 1.1 ka (Ar/Ar)	Albert et al. (accepted)		
5c	On-Pm1	Ontake-Pm1	Ontake, Honshu Island, Japan	ca. 95 (ST)	Machida and Arai (2003)	SE dispersal over central Honshu.	Albert et al. (accepted)*
	K-Tz	Kikai-Tozurahara	Kikai, Kyushu Island, Japan	ca. 95 ka (ST)	Machida and Arai (2003)	NE dispersal (radial), found widespread in southern Japan and in the Lake Suigetsu record in central Honshu.	Furuta et al. (1986); Tsuji et al. (2018)*
				95.2 (ST)	Nagahashi et al. (2007)		
	Aso-A	Aso-A	Aso, Kyushu Island, Japan	ca. 95 (SG)	Smith et al. (2013); Albert et al., (accepted)	NE dispersal, found in Uwa basin, Lake Suigetsu and Lake Biwa as visible deposits.	Smith et al. (2013); Albert et al. (accepted)*; Tsuji et al. (2018)
	SK	Sambe-Kisuki	Sambe, Honshu Island, Japan	106 ka (ST)	Matsu'ura et al. (2014)	NE dispersal extending to northern most parts of Honshu island. Not identified in Lake	Machida and Arai (2003); Matsu'ura et al. (2018)
				98 ± 96 ka (FT)	Danhara (1995)		
	Ata	Ata	Ata, Kyushu Island, Japan	~100 ka (SG)	Smith et al. (2013)	Radial dispersal in southern and central Honshu. Found in marine core RN89-PC-3, south of Kyushu island.	Machida and Arai (2003); Albert et al. (accepted)

SG = Lake Suigetsu age model, 14C = radiocarbon dating method, IC = Ice core chronology D= Dendrochronology, FT= fission track, K-Ar = Potassium-Argon dating, Ar-Ar = Argon-Argon dating,
OI = Oxygen isotope ratio cycles; ST = stratigraphy
* indicates and/or proximal glass compositions

The criteria for determining valuable isochronous markers follow that outlined by the INTIMATE community (see Davies et al., 2012), and are those which are i) regionally widespread, ii) possess a unique geochemical signature, iii) are precisely dated, and iv) occur at, or bracket a climatic/cultural change. As with the European INTIMATE tephra-based framework (Davies et al., 2012), many key isochrons do not currently meet all selection criteria, and some valuable markers (i.e., those stratigraphically close to rapid climate events) are not yet found geographically widespread. However, this exercise highlights several key areas for future research efforts, as briefly outlined below.

The stratigraphic positioning of the Ma-b (ca. AD 960 – 992; McLean et al., 2018) and B-Tm tephra (AD 946; Oppenheimer et al., 2017) offer significant potential to help constrain late Holocene climate variations, such as the onset of the Medieval Warm Period (MWP; ca. AD 900 – 1300; Lamb, 1965). Although this warming episode has been identified in numerous global palaeoclimate proxy records, its spatio-temporal variability and regional magnitude is still debated (Broecker, 2001; Hunt, 2006). Furthermore, proxy data and climate models indicate that during the MWP, a centennial episode of weaker East Asian Summer Monsoon occurred between AD 980 – 1100 (Figure 7.3; Jin et al., 2018). Precisely dating and correlating late Holocene palaeoclimate archives using these markers would provide new insight into the complex spatial structures of the monsoon system on an interannual to decadal timescale.

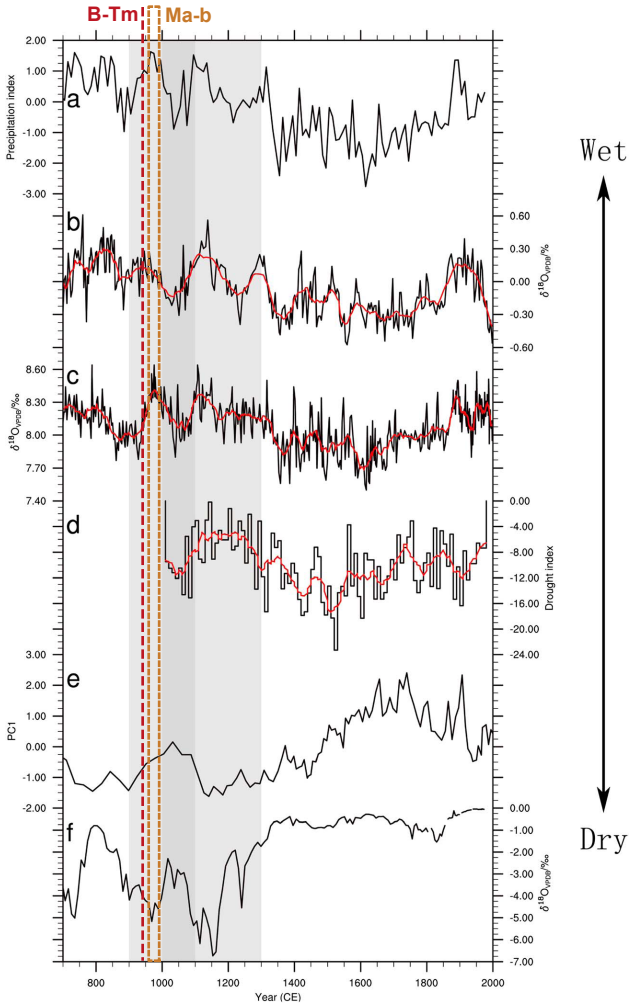


Figure 7.3. Late Holocene proxy data from East Asia (figure modified from Jin et al., 2018). (a) Precipitation index for north central China (Tan et al., 2011); (b) $\delta^{18}O$ record from Huangye Cave, eastern Qinghai-Tibet (Tan et al., 2011); (c) $\delta^{18}O$ record from Wanxiang Cave, Gansu Provience (Zhang et al., 2008); (d) drought index from the northeastern Asian monsoon region, Korea (Kim and Choi, 1987); (e) record of PC1 of a principal components analysis of diatom assemblages from Tsuifong Lake, Taiwan (Wang et al., 2013); and (f) carbonate record from Huguangyan maar Lake, Guangdong Province (Chu et al., 2002). The grey bars are used to emphasize the periods over the AD 900 – 1300 and AD 1000 – 1100, which are considered to represent the Medieval Warm Period. The chronological age of the B-Tm (AD 946; Oppenheimer et al., 2017) and the Ma-b tephra (McLean et al., 2018) are also shown by the dotted line.

Furthermore, the early Holocene B-Sg-8 tephra (Changbaishan) is identified in the Lake Suigetsu and Lake Yuanchi (eastern China) sediment cores and is dated to 8,166 – 8,099 cal. yrs BP (95.4% uncertainty; McLean et al., 2018; Sun

et al., 2018). The eruption age of this marker is positioned at the onset of the abrupt cooling transition (Figure 7.4.) that occurred at around 8.2 kyr BP (i.e., the north hemispheric “8.2 ka event”, the duration of which is about 300 years; Alley et al., 1997). This B-Sg-8 tephra would therefore provide an excellent marker for understanding more about the causes, timing and regional mechanisms of this climate oscillation.

Several tephra layers are stratigraphically positioned to investigate the timing and amplitude of Late-Glacial climate oscillations, including the To-H tephra (Towada volcano) that was erupted ca. 15.5 ka and close to the transition of Marine Isotope Stage (MIS) 2 and 1. Furthermore, glass compositions for Greenland ice core layer NEEM 1503.60 m (correlated to NGRIP 1628.25 m), overlap with those known for the To-H event from Towada caldera (northern Honshu), and suggest an eruption age of 15.7 ± 0.2 ka b2k (Bourne et al., 2016) (Table 7.1.). Further work is required to constrain the dispersal route of this event and determine other high-resolution archives that can be synchronised using this isochron.

MIS 3 is a very distinctive climatic period characterised by abrupt oscillations of cold and warm events, recognised in marine sediments as Dansgaard-Oescher (D-O) events (Johnsen et al., 1992; Dansgaard et al., 1993; Bond et al., 2001). Chapter 5 showed that there are numerous widespread isochrons that have been dispersed from Aso and Aria during this period (e.g., 50 to 30 ka), however the majority of these are currently only identified in a single site (Lake Suigetsu). Obtaining high-resolution proxy data from Lake Suigetsu is

necessary to investigate their positioning in relation to these climate oscillations, as well as research efforts to find other distal deposits of these eruptions.

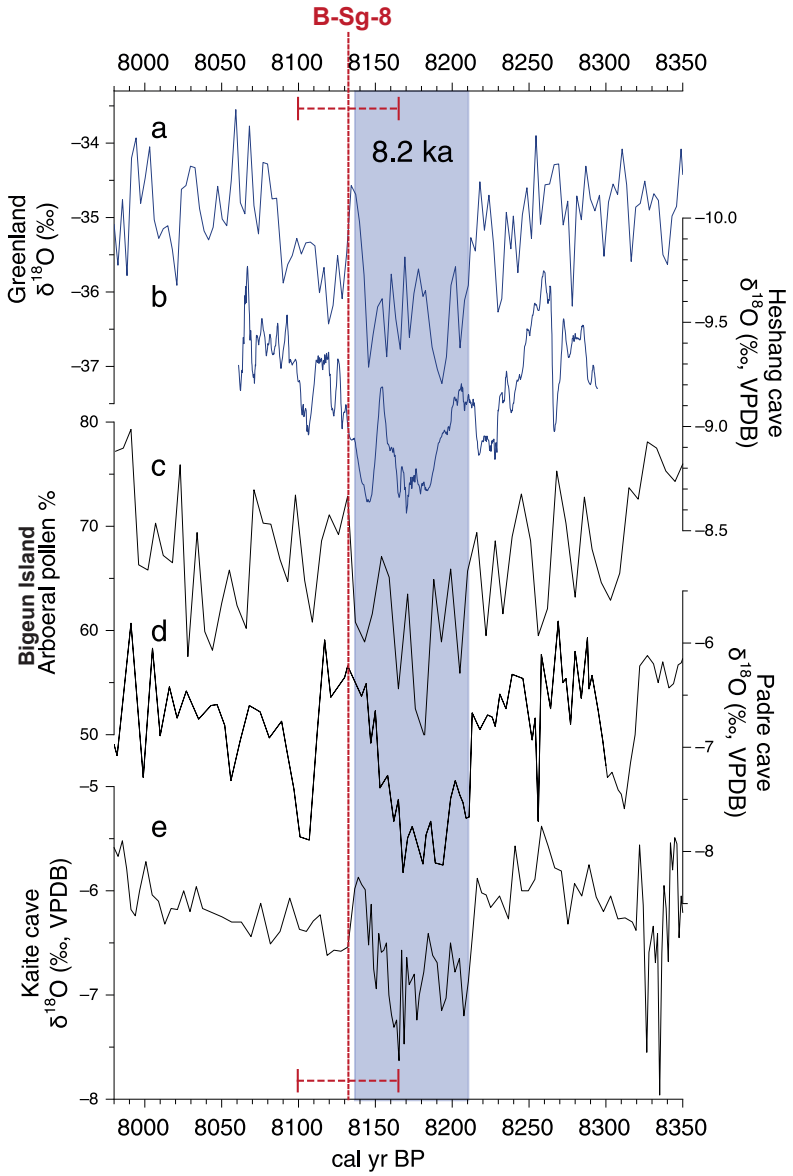


Figure 7.4. (a) Comparison of the Greenland ice core $\delta^{18}O$ record (Thomas et al., 2007); and (b) stalagmite $\delta^{18}O$ record from Heshang cave, central China, (Cheng et al., 2009); (c) the percentage content of total arboreal pollen from Bigeum Island (Park et al., 2018); (d) stalagmite $\delta^{18}O$ record from Padre cave, eastern Brazil (Cheng et al., 2009); (e) and stalagmite $\delta^{18}O$ record from Kaite Cave, Spain (Domínguez-Villar, et al., 2009). The 8.2 ka cooling event is indicated by the transparent blue bar, and the chronological age of the B-Sg-8 tephra is shown (with a two sigma uncertainty) by a dotted line. Figure modified from Park et al. (2018).

The U-Ym tephra (ca. 39 ka; Ulleungdo) is an important marine and terrestrial marker that occurs at the time of the Laschamp magnetic excursion (ca. 41 ka; Guillou et al., 2004; Singer et al., 2009). This excursion is also identified in deep-sea sediments and ice cores, as an abrupt change in the rate of cosmogenic nuclide flux, lasting around ca. 440 years (Nowaczyk et al., 2012). The timing and cause of this event remains poorly understood (Guillou et al., 2004), and therefore the position of the U-Ym tephra could be used to help constrain the age and duration of this event in other onshore and marine archives. Chapter 5 and 6 showed for the first time that ash from the U-Ym eruption reached at least the western coast of Honshu, and could be identified in other high-resolution records in Japan.

The SK tephra is a widespread marker layer erupted from Sambe volcano on the SW Japan Arc, and is dated to ca. 100 ka (MIS 5). Despite providing a key isochronous tie-point for several key lacustrine records (Figure 7.1.), the age of this eruption remains poorly constrained (Table 7.1.). Although ash was predominantly dispersed NE, this marker is not preserved as a visible deposit in the Suigetsu cores (Machida and Arai, 2003; Smith et al., 2013; Albert et al., 2018). It is however likely that this eruption is preserved as a cryptotephra deposit within the sediments, which would determine its stratigraphic relationship and age to the Aso-ABCD eruption event.

In order to truly investigate palaeoclimate variability on a global scale it is essential to identify more widely dispersed tephra layers preserved in high-resolution archives outside the East Asian/Pacific region. Bourne et al. (2016)

report additional tephra layers preserved in the NGRIP ice cores that are likely to derive from Japan (e.g., NGRIP 2441.28 and 2033.75), but there are currently no known widespread eruptions at those times. In order to robustly identify these sources, detailed proximal geochemical datasets and new comprehensive distal studies are required to help constrain the complete eruptive histories of centres active during this period.

7.1.4. Synchronising records using the AT tephra

To provide an example of the synchronisation potential of widespread ash deposits across East Asia, here the AT tephra layer is used to compare regional climate records from Lake Biwa (central Honshu, Japan; Hayashida et al., 2007), Lake Sihailongwan (eastern China; Mingram et al., 2018) and a marine core from the northeast coast of Honshu (MD179-3312; Urabe et al., 2014) (Figure 7.5.). The AT tephra from Aira volcano, Kyushu Island was deposited shortly before the Last Glacial Maximum (dated to 30,078 ± 98 cal. yrs BP via the Lake Suigetsu chronology; Albert et al., accepted), just prior to the MIS 3 and 2 transition.

The palaeoenvironmental records outlined above are underpinned by three separate age-models that have been constructed using different chronological dating methods. The Lake Sihailongwan age-model is constrained using a detailed varve chronology and 50 AMS ^{14}C dates (see Mingram et al., 2018). The AT tephra is independently dated using this age-depth model to 28,577 – 29,831 cal. yrs BP (95.4% uncertainty), overlapping with the Lake Suigetsu

derived age and providing an independent test of this chronology. The Lake Biwa (BIW95-4) age-model is constrained using several tephra ages reported in Takemura et al. (2000), and 10 AMS radiocarbon dates, that are modelled using a cubic spline interpolation. An age of 28.78 ka was inserted for the AT at 11.76 m composite depth (Hayashida et al., 2007). In contrast, the age model for marine core MD179-3312 was constructed using 8 tephra ages (as reported in Nakamura et al., 2013; using an AT eruption age of 30.0 ka), 3 radiocarbon dates (Matsumoto et al., 2011), and 6 event markers which are based on the correlation of the $\delta^{18}O$ curve of planktonic foraminifera (Ishihama et al., 2014) to the LR04 curve (Lisiecki and Raymo, 2005). These age-models and their chronological uncertainties mean that the timing of palaeoenvironmental oscillations could not be compared without the AT isochron (Figure 7.5.).

Different environmental proxies preserved in the Biwa, Sihailongwan and marine sediment cores are used to show biological and vegetation responses to regional climate change, and the AT isochron can be used to precisely compare their different response times and climatic sensitivity. Total organic carbon (TOC) concentrations provide an indication of the biological productivity in the lake and ocean water environments (Kumon et al., 2005), with an increase observed during warmer interstadial periods. For Lake Biwa, the pollen abundance of *Cryptomeria japonica* is shown to respond quickly to rapid climate oscillations, and shows four significant fluctuations that follow Dansgaard-Oeschger (D-O) cycles D-05 to 8, prior to the deposition of the AT tephra (Figure 7.5; Hayashi et al., 2010).

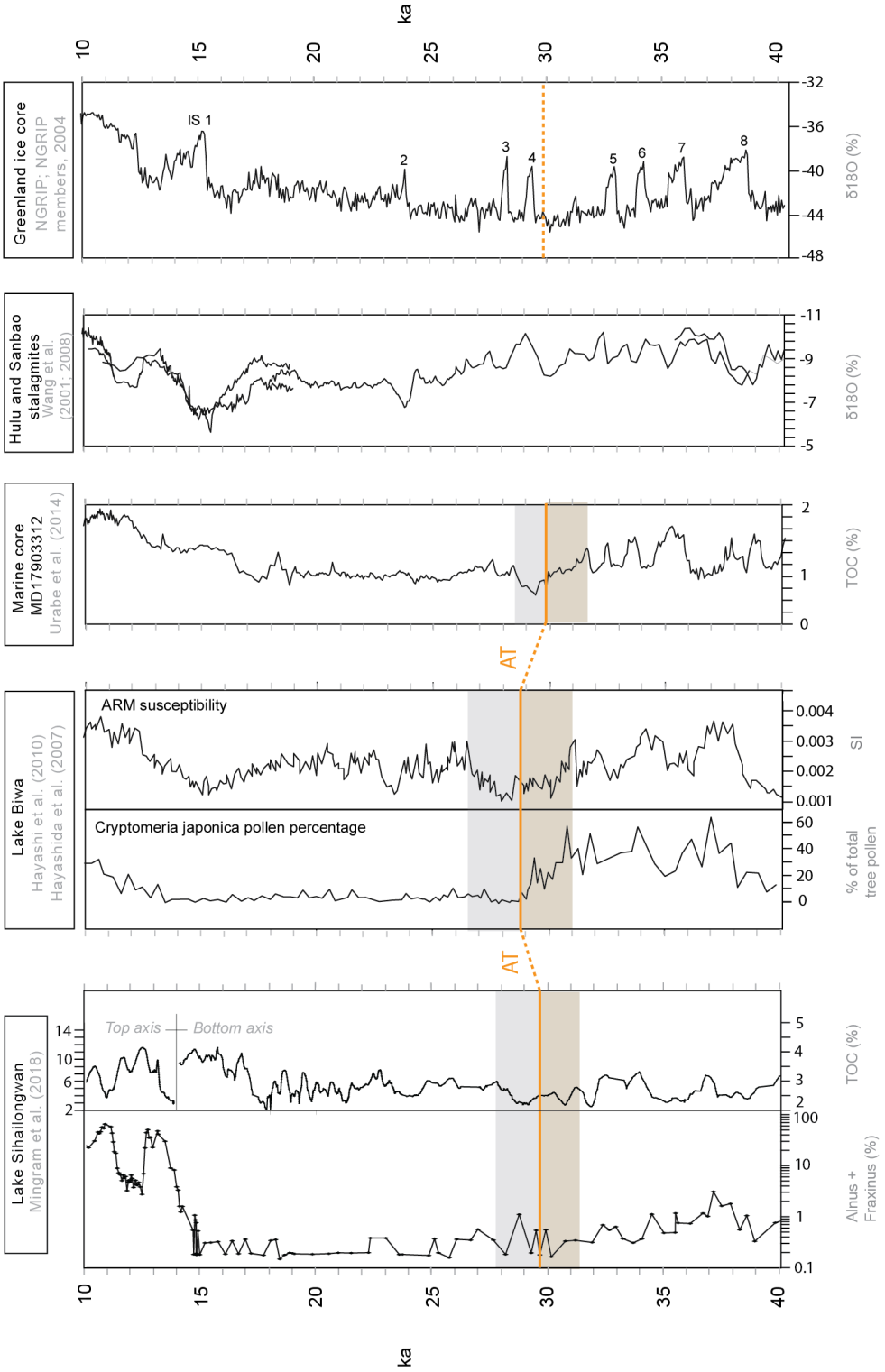


Figure 7.5. Synchronisation of Lake Sihailongwan (Mingram et al., 2018), Lake Biwa (Hayashida et al., 2007; Hayashi et al., 2010); MD179-3312 (Urabe et al., 2014) proxy records using the AT (Aira volcano; orange line) tephra. The Hulu stalagmite (Wang et al., 2001) and Greenland ice core isotope record (NGRIP members, 2004) are plotted alongside using their independent chronologies, and a dashed line is shown to depict the Suigetsu derived AT eruption age (Smith et al., 2013; Albert et al., 2018). Grey and brown shading is shown to highlight the proxy signal above and below the tephra layer, respectively.

These changes are also reflected in the Biwa palaoemagnetic signal (ARM; anhysterestic remanent magnetization), as published by Hayashida et al. (2007), which is also considered as a proxy for precipitation, since higher rainfall rates will in-wash greater concentrations of magnetic particles from the lake catchment.

The most widely-accepted AT age places this eruption event just prior to D-O event 4 as observed in the Greenland $\delta^{18}O$ record (NGRIP members, 2004) and the Hulu stalagmite record (Wang et al., 2001) (Figure 7.5.). For the Biwa and marine record, the AT ash is positioned within a sawtooth-like cooling trend in their palaeonvironmental proxy data, which continues for several hundred years following the isochron. This is followed by a significant warming peak in both records, possibly representing D-O event 4. The Biwa *C. japonica* assemblage disappears at the boundary of the AT, which may be caused by the effect of the thick ash fall on the vegetation in this region, and the subsequent climate transition prevents its reestablishment. No clear climate offsets can be observed here between the Biwa and marine record using the AT tephra. The sawtooth-like cooling pattern is not defined in the Sihailongwan climate proxies, which is most likely due to its lower resolution, rather representing a true regional climatic difference.

7.1.6. Summary

Detailed and systematic studies through the sediments of high-resolution archives in Japan reveal that there are numerous isochronous markers that can

be used for local or regional correlations. As shown by the construction of a detailed tephrostratigraphic framework for Japan (Section 7.1.2.), there are very widespread markers that can be traced across broad regions of Japan (i.e., over the migratory paths of the East Asian Monsoon). Widely dispersed ash layers (like the AT tephra) are able to precisely synchronise varied and distance sedimentary archives (e.g., marine and lacustrine sequences), and overcome the significant problems in dating uncertainties. It is clear that very high-resolution multi-proxy regional climate records are required to investigate the rapid oscillations observed in global stratotypes like the Greenland ice cores.

7.2. Building eruption records for hazard assessments

7.2.1. Context and rationale

Distal tephra studies can provide a significant resource for volcanology, offering further constraints on the frequency, magnitude and dispersal of past explosive events, as well as providing information on the societal risks of volcanic eruptions. Honshu Island hosts the most densely populated regions of Japan (e.g., Tokyo, Yokohama, Osaka and Nagoya) (Figure 7.6.), and the Asian-Pacific region dominates the world's top ten busiest airspace routes, with four of these involving paths from Tokyo-Haneda (OAG report, 2018). The tephra archive from Lake Suigetsu can therefore be used to understand more about the long-distance ash-fall events that have reached these regions, and their societal and economic significance.

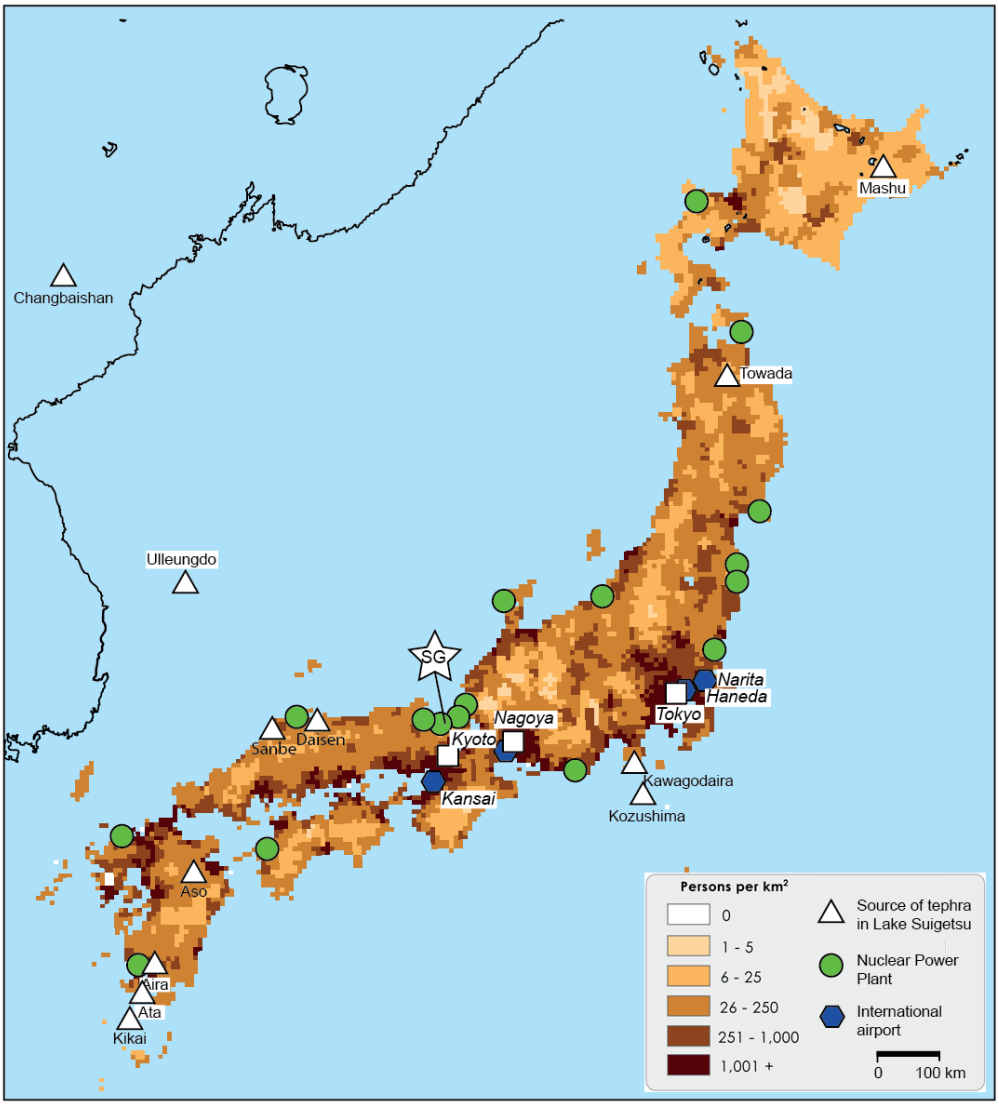


Figure 7.6. Population density map of Japan (Global Rural-Urban Mapping Project; 2009), showing the sources of tephra to Lake Suigetsu (white triangles); position of nuclear power plants (green circles); and key international airports (blue hexagons). The position of Lake Suigetsu is shown by a white star. Several nuclear power stations operate in Fukui Prefecture (central Honshu) and in close proximity to Aira caldera (southern Kyushu).

7.1.2. Frequency of ash fall events to central Honshu

The visible Lake Suigetsu tephrostratigraphy indicates that a large ash fall event reached central Honshu, on average once every 5 ka. However, this return interval is not particularly representative, since the majority of large

magnitude events are clustered in time, most notably between 20 – 30 ka and 46 – 60 ka (Figure 7.7; Smith et al., 2013; Albert et al., accepted). Distinct time periods that do not preserve any thick ash fall events are also evident, significantly between 10 – 20 ka in the Suigetsu sediments. These patterns are also observed for other long and comprehensive eruption records in Japan, including Lake Biwa (Nagahashi et al., 2004), Uwa basin (Tsuji et al., 2018), and the deep-sea drilling cores off the eastern coast of Japan (e.g., Mahony et al., 2016; Schindlbeck et al., 2018) (Figure 7.2.).

The Suigetsu tephrostratigraphy has been extended using density separation techniques to identify non-visible ash layers preserved within the sediments (Chapters 4 – 6), and is able to provide new insight into the lower magnitude and more distal eruption events. The archive now contains 66 isochronous markers, 32 of which are preserved in the core as visible ash deposits and 34 of which are non-visible cryptotephra layers (Figure 7.7.). In the investigated sediments (50 – 30 ka and ≤ 10 ka), at least one significant cryptotephra marker is detected in each meter of sediment (an event approximately every 500 years), although there are periods with high-concentrations of background glass which could mask some other events. On average, events that form cryptotephra layers in the Lake Suigetsu sediments occur between four to five times more frequently than the very large magnitude events (VEI 6 – 7), and typically occur more regularly.

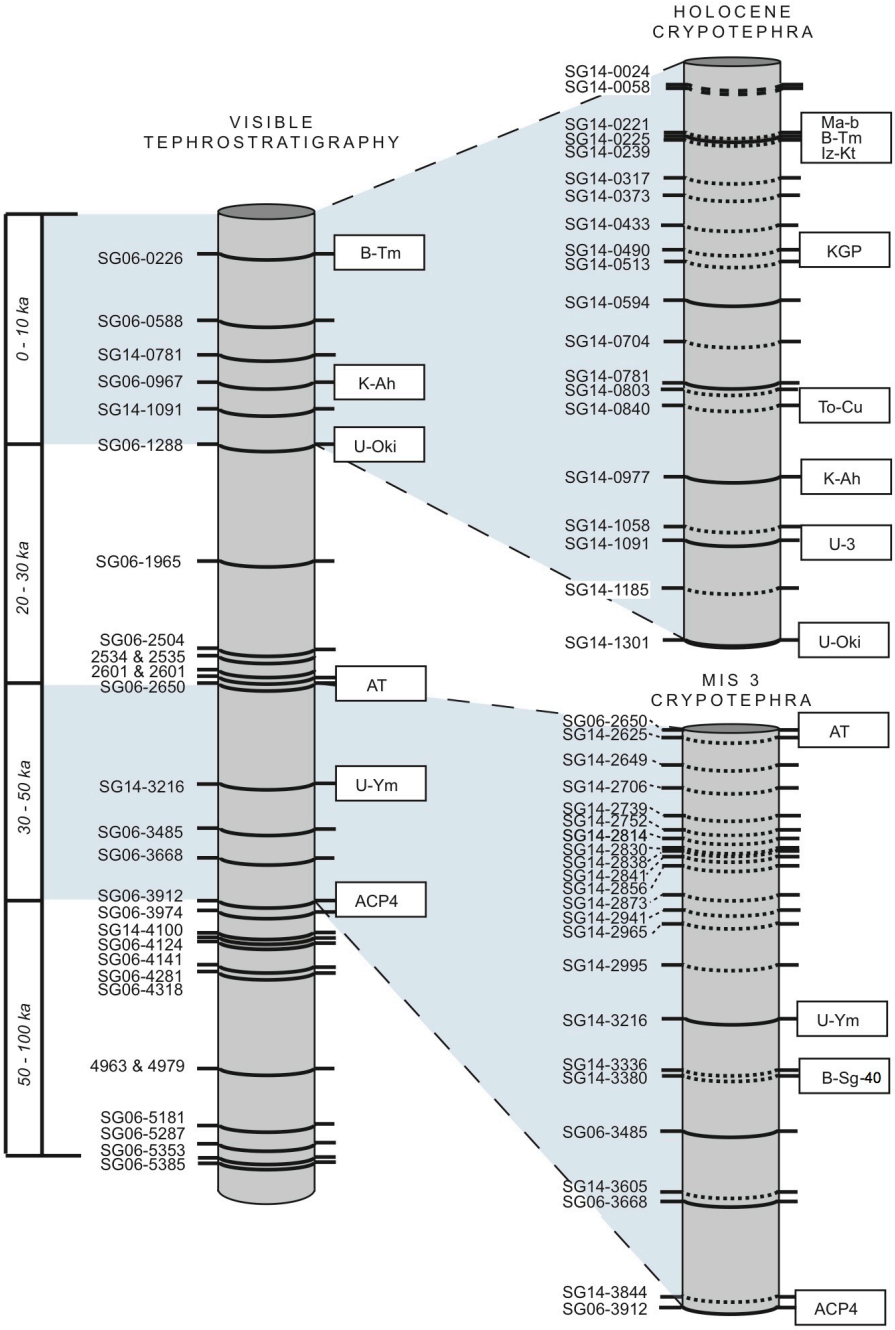


Figure 7.7. Summary of the Lake Suigetsu tephrostratigraphy and tephra research presented in this thesis (Smith et al., 2013; Albert et al., accepted; this study*)*. Non-visible (cryptotephra) layers are shown by a dashed line. Fifteen isochrons were identified in the Holocene sediments of Lake Suigetsu (Chapters 3 – 4; McLean et al., 2016; 2018), and twenty isochrons were identified in the sediments dated between 50 and 30 ka (Chapters 5 – 6).

Cryptotephra studies based on the sediments of Lake Suigetsu have provided new insight into the following topics:

1. The majority of sources that produced thick ash fall events in the Suigetsu sediments remain very active between these periods (e.g., Aso, Aira and Kikai), producing eruption events that are large enough to preserve cryptotephra layers in the Suigetsu sediments. Since Suigetsu is situated over 400 km downwind of the nearest volcanoes (Daisen and Sambe; SW Japan arc), cryptotephra-forming events are likely to have been at least VEI 4 – 5 (i.e., had eruptive phases that were at least sub-Plinian). Unfortunately, since the majority of the tephra layers have only been identified within a single distal site, these occurrences cannot yet help constrain the magnitude of these events. However, the glass chemistry can be used to identify their proximal deposit counterparts, where they may be mapped more precisely.

2. Cryptotephra identifications show that many eruptions dispersed ash considerably more widely than previously anticipated. It is not yet clear whether this is caused by an underestimation of the eruption magnitude, the prevailing westerly winds providing a highly effective transport mechanism, or whether Lake Suigetsu is a unique high-resolution record able to capture, and accumulate very low shard concentrations in a particularly low energy environment.

3. The vast majority of ash fall events preserved as cryptotephra markers in the sediments are derived from centres south of Lake Suigetsu, which

are in-line with current hazard assessments which assume ash fall is dispersed by the prevailing westerly winds (e.g., Prata, 2009; Jenkins et al., 2012). Large magnitude events erupted from Hokkaido and northern Honshu (e.g., Komagatake and Shikotsu) are not known to have reached central Honshu, however, the Lake Suigetsu record records some moderate magnitude eruptions from volcanoes that are not typically downwind of Suigetsu (e.g., Towada, Mashu, Kozushima). It is not yet clear what eruption and climatic conditions are required for these events.

4. Eruptions from Changbaishan and Ulleungdo have the potential to disperse ash to the populated regions of Honshu, and the risk of ash fall events is not given enough consideration. This is largely since little has been known about their eruption histories.

These outcomes show that even in very comprehensively studied region, we do not have a very detailed understanding of the tempo of medium (and in some cases large) explosive events that have occurred over the Late Quaternary. This is agreement with other studies, such as Kiyosugi et al. (2015) who show a significant under-recording of VEI 4 – 5 (Newhall and Self, 1982) Japanese eruptions in the LaMEVE (Large Magnitude Explosive Volcanic Eruptions; Crosweller et al., 2012) database. They suggest that ca. 89 % of VEI 4 events have yet to be reported at 100 ka. Bourne et al. (2016) also postulate that the Pacific arc tephra layers identified in the Greenland ice core records are derived from medium magnitude events that are currently undocumented in the geological record. Cryptotephra investigations in medial and distal archives are

key to understand more about the dispersal potential of moderate sized eruptions, which may have been underestimated in terms of their eruptive volume and dispersal potential.

Finally, it is not yet clear how cryptotephra records can be used to constrain calculations of tephra volumes and eruption magnitudes. When the distal thickness and data density is not known, classic tephra volume calculations cannot be applied (e.g., Fierstein and Nathenson, 1992; Pyle, 1995; Bonadonna and Houghton, 2005), and isopach shapes can only be estimated (Schindlebeck et al., 2018). Cryptotephra layers may represent an event that was originally deposited a visible unit across the regional area, and therefore a maximum thickness (e.g., 1 mm), could be used to account for variability across the catchment. Further work is required to investigate these possibilities and techniques to derive first order estimates of eruptive volumes.

CHAPTER 8: CONCLUSIONS

This thesis has explored the potential of establishing a detailed tephrostratigraphic framework for Japan, to enable the synchronisation of palaeoenvironmental records in the East Asian/Pacific region. This research aim was achieved by undertaking detailed cryptotephra investigations through the high-resolution and intensely dated sediments of Lake Suigetsu (central Japan), between 50 and 30 ka and over the last 10 ka, which revealed an unprecedented record of eruptions that dispersed ash to the populated regions of central Honshu. The augmented Suigetsu tephrostratigraphy to date contains thirty-two visible and thirty-four non-visible ash layers, which provides new constraints on the chronology and reoccurrence intervals of these eruption events. Lake Suigetsu is now established as a key tephrostratotype for correlating and dating palaeoenvironmental records in this region, and the archive forms a key connecting-node within the tephrostratigraphic framework for Japan.

The identification of the B-Tm ash deposit in the Lake Suigetsu sediments (dispersed during the AD 946 ‘Millennium’ eruption of Changbaishan on the border of China and North Korea; Oppenheimer et al., 2017) demonstrates that it is possible for widely dispersed ash layers from this region to synchronise archives over hemispheric scales (see Chapter 3). The B-Tm ash is the first direct tephra tie-point between a high-resolution mid-latitude palaeoenvironmental archive (Lake Suigetsu) and the Greenland ice cores,

which demonstrates that other tephra may also be as widely dispersed. Such links between high-resolution archives are crucial for research into the propagation and drivers of past palaeoenvironmental change. The stratigraphic positioning of the B-Tm ash holds significant potential to help constrain late Holocene climate variations, such as the onset of the Medieval Warm Period (ca. AD 900 – 1300). This discovery may also help encourage other researchers to look for the B-Tm tephra in palaeoenvironmental records in and around southern Japan.

High-resolution cryptotephra investigations through the Holocene sediments of Lake Suigetsu confirmed that it is possible to identify non-visible layers in productive arc settings (see Chapter 4). Primary and secondary ash layers can be distinguished using the variations of contrasting shard textures (e.g., size, shape and vesicularity) in conjunction with the geochemical compositions of the volcanic glass. The Lake Suigetsu Holocene tephrostratigraphy was extended from four to twenty tephra layers, which for the first time integrates ash derived from North Korea/China, South Korea and the Japanese arcs. These findings significantly extend the known ash dispersal of numerous key regional marker layers, including the Ma-b ash (Mashu) that is now identified over 1,100 km from its source, and thus one of the most widely dispersed isochrons in Japan. Furthermore, the Holocene sediments contained several previously unreported ash fall events, confirming a new eruption from Changbaishan dated to 8,166 – 8,099 cal. yrs BP (95.4 % confidence interval). This marker has since been identified in Lake Yuanchi, ~30 km east of Changbaishan (Sun et al., 2018),

suggesting it may be suitable to precisely synchronise palaeoenvironmental records at the onset of the 8.2 climate event.

In order to augment our understanding of the tempo and dispersal of eruptions prior to the AT caldera-forming event, the Suigetsu sediments between 50 to 30 ka were targeted for detailed cryptotephra analysis (see Chapter 5). This revealed that there are four times more cryptotephra layers preserved than visible layers in these sediments, providing an unprecedented record of eruption events that were dispersed to the currently densely populated regions of central Honshu. Major and trace element glass chemistry was used to fingerprint the ash layers and pinpoint their volcanic origin. Explosive activity from Aso and Aira caldera (Kyushu Island), were most frequently recorded in the sediments, which indicates these centres were very active between 35 to 30 ka. Aso erupted compositionally different magmas through time, producing eight widespread events over 20 ka. Furthermore, four eruptions from Aira are recorded leading up to the enormous caldera-forming AT event (VEI 7). Additional occurrences of these deposits are required to help constrain the magnitude of these events, and learn more about the hazard potential of these very active centres.

Ash derived from back-arc volcanoes west of Japan (Changbaishan and Ulleungdo) underpin the tephrostratigraphic framework for the East Asian/Pacific region, yet their complete eruptive histories are poorly constrained. This is partly since their proximal eruption deposits are not well exposed and are largely inaccessible. A review of all distal occurrences of the

alkaline ash deposits derived from Changbaishan and Ulleungdo has constructed a more complete eruption framework for these centres. This record was supplemented using the chronological and geochemical datasets generated using the Lake Suigetsu record, which was able to integrate other previously unreported tephra-forming events, herein named Baegdusan-Suigetsu-8 (B-Sg-8; 8.1 ka) and Baegdusan-Suigetsu-42 (B-Sg-42; 41.8 ka). These occurrences highlight the pivotal role that distal records have in constraining magnitude and reoccurrence intervals of these centres.

This thesis closes with a discussion of the current East Asian tephrostratigraphic framework, which is constructed using 24 key tephra archives that are distributed across Japan, North Korea/China and South Korea (see Chapter 7). There are numerous valuable tephra markers that can be used to investigate palaeoclimate questions and overcome chronological uncertainties, which prohibit precise comparisons of key palaeoenvironmental records. For example, the AT tephra can synchronise marine and lacustrine archives spanning the length of Japan, and as far as eastern China, permitting an assessment of the climate sensitivity of different environmental proxies. A final review of the Lake Suigetsu tephrostratigraphy highlighted that distal tephra studies can provide a significant resource for volcanology, offering further constraints on the frequency, magnitude and dispersal of past explosive events, as well as providing information on the societal risks of volcanic eruptions. It is clear that detailed cryptotephra investigations are able to facilitate exciting new insights within both palaeoclimate and hazard research in the East Asian/Pacific region.

Consolidated List of References

Abbott, P. M. and Davies, S. M. 2012. Volcanism and the Greenland ice-cores: the tephra record. *Earth-Science Reviews*, 115: 173-191

Abbott, P. M., Bourne, C. S., Purcell, C. S., Davies, S. M., Scourse, J. D. and Pearce, N. J. G. 2016. Last glacial period cryptotephra deposits in an eastern North Atlantic marine sequence: exploring linkages to the Greenland ice-cores. *Quaternary Geochronology,* 31: 62-76

Abbott, P. M., Griggs, A. J., Bourne, A. J. and Davies, S. M. 2018a. Tracing marine cryptotephras in the North Atlantic during the last glacial period: Protocols for identification, characterisation and evaluating depositional controls. *Marine Geology*, 401: 81-97

Abbott, P. M., Griggs, A. J., Bourne, A. J., Chapman, M. R. and Davies, S. M. 2018b. Tracing marine cryptotephras in the North Atlantic during the last glacial period: Improving the North Atlantic marine tephrostratigraphic framework. *Quaternary Science Reviews*, 189: 169-186.

Adhikari, D. P., Kumon, F. and Kawajiri, K. 2002. Holocene climate variability as deduced from the organic carbon and diatom records in the sediments of Lake Aoki, central Japan. *Jour. Geol. Soc. Japan.* 108: 249-265

Ahn, Y. S., Mizugaki, S., Nakamura, F. and Nakamura, Y. 2006. Historical change in lake sedimentation in Lake Takkobu, Kushiro Mire, northern Japan over the last 300 years. *Geomorphology*, 78: 321-334

Albert, P. G., Tomlinson, E. L., Smith, V. C., Di Roberto, A., Todman, A., Rosi, M., Marani, M., Muller, W. and Menzies, M. A. 2012. Marine-continental tephra correlations: volcanic glass geochemistry from the Marsili Basin and the Aeolian Islands, Southern Tyrrhenian Sea, Italy. *Journal of Volcanology and Geothermal Research*, 229: 74-94

Albert, P. G., Tomlinson, E. L., Lane, C. S., Wulf, S., Smith, V. C., Coltelli, M., Keller, J., Castro, D. L., Manning, C. J., Müller, W. and Menzies, M. A. 2013. Late glacial explosive activity on Mount Etna: Implications for proximal–distal tephra correlations and the synchronisation of Mediterranean archives. *Journal of Volcanology and Geothermal Research*, 265: 9-26

Albert, P. G., Hardiman, M., Keller, J., Tomlinson, E. L., Smith, V. C., Bourne, A. J., Wulf, S., Zanchetta, G., Sulpizio, R., Müller, U. C., Pross, J., Ottolini, L., Matthews, I.P., Blockley, S. P. E., Menzies, M. A. 2015. Revisiting the Y-3 tephrostratigraphic marker:

a new diagnostic glass geochemistry, age estimate, and details on its climatostratigraphical context. *Quaternary Science Reviews,* 118: 105-121

Albert, P. G., Tomlinson, E. L., Smith, V. C., Di Traglia, F., Pistolesi, M., Morris, A., Donato, P., De Rosa, R., Sulpizio, R., Keller, J. and Rosi, M. 2017. Glass geochemistry of pyroclastic deposits from the Aeolian Islands in the last 50 ka: A proximal database for tephrochronology. *Journal of Volcanology and Geothermal Research*, 336: 81-107

Albert, P. G., Smith, V. C., Suzuki, T., Tomlinson, E., Nakagawa, T., Yamada, K., McLean, D., Staff, R. A., Schlolaut, G., Takemura, K., Nagahashi, Y., Kimura, I-P, SG06 Project Members. (submitted) Constraints on the frequency and dispersal of explosive eruptions at Sambe and Daisen volcanoes (South-West Japan Arc) from the distal Lake Suigetsu record (SG06 core). *Earth-Science Reviews,* 185: 1004-1028

Albert, P. G., Smith, V. C., Suzuki, T., McLean, D., Tomlinson, E. L., Miyabuchi, Y., Kitaba, I., Mark, D. F., Moriwaki, H., SG06 Project Members, Nakagawa, T. *accepted.* Geochemical characterisation of the widespread Japanese tephrostratigraphic markers and correlations to the Lake Suigetsu sedimentary archive (SG06 core). *Quaternary Geochronology*

Allan, A. S., Baker, J. A., Carter, L. and Wysoczanksi, R. J. 2008. Reconstructing the Quaternary evolution of the world's most active silicic volcanic system: insights from an～ 1.65 Ma deep ocean tephra record sourced from Taupo Volcanic Zone, New Zealand. *Quaternary Science Reviews*, 27: 341-2360

Alley, R. B., Meese, D. A., Shuman, C. A., Gow, A. J., Taylor, K. C., Grootes, P. M., White, J. W. C., Ram, M., Waddington, E. D., Mayewski, P. A. and Zielinski, G. A. 1993. Abrupt increase in Greenland snow accumulation at the end of the Younger Dryas event. *Nature*, 362: 527

Alley, R. B., Mayewski, P. A., Sowers, T., Stuiver, M., Taylor, K. C. and Clark, P. U. 1997. Holocene climatic instability: A prominent, widespread event 8200 yr ago. *Geology*, 25: 483-486

Alloway, B. V., Andreastuti, S., Setiawan, R., Miksic, J. and Hua, Q. 2017. Archaeological implications of a widespread 13th Century tephra marker across the central Indonesian Archipelago. *Quaternary Science Reviews*, 155: 86-99

Andersen, K. K., Azuma, N., Barnola, J. M., Bigler, M., Biscaye, P., Caillon, N., Chappellaz, J., Clausen, H. B., Dahl-Jensen, D., Fischer, H. and Flückiger, J. 2004. High-resolution record of Northern Hemisphere climate extending into the last interglacial period. *Nature*, 431: 147

Aoki, K. and Arai, F. 2000. Late Quaternary tephrostratigraphy of marine core KH94-3, LM-8 off Sanriku, Japan. *The Quaternary Research (Daiyonki-kenkyu)*, 39: 107-120 (in Japanese with English abstract)

Aoki, K. and Machida, H., 2006. Major element composition of volcanic glass shards in

the late Quaternary widespread tephras in Japan-Distinction of tephras using K2O-TiO2 diagrams. *Bulletin of the Geological Survey of Japan*, 57: 239-258

Aoki, K., Irino, T., Oba, T. 2008. Late Pleistocene tephrostratigraphy of the sediment core MD01-2421 collected off the Kashima coast, Japan. The Quat Res (Daiyonki-kenkyu), 47:391–407 (In Japanese with English abstract)

Arai, F. 1972. Identification of particular tephras by means of refractive indices of orthopyroxenes or hornblendes e a fundamental study of tephrochronology. Quaternary Research, Japan 11, 254-270 (In Japanese with English abstract)

Arai, F., Oba, T., Kitazato, H., Horibe, Y., Machida, H. 1981. Late Quaternary tephrochronology and paleo-oceanography of the sediments of the Japan Sea. Quat. Res. (Daiyonki-kenkyu) 20: 209–230 (in Japanese, with English Abstract)

Aramaki, S. 1984. Formation of the Aira caldera, southern Kyushu, ~ 22,000 years ago. *Journal of Geophysical Research: Solid Earth*, 89: 8485-8501

Aspinall, W. P., Charbonnier, S., Connor, C. B., Connor, L. J. C., Costa, A., Courtland, L. M., Delgado Granados, H., Godoy, A., Hibino, K., Hill, B. E. and Komorowski, J. C. 2016. *Volcanic Hazard Assessments for Nuclear Installations Methods and Examples in Site Evaluation* (No. 1795). International Atomic Energy Agency

Bacon, C. R. and Lanphere, M. A. 2006. Eruptive history and geochronology of Mount Mazama and the Crater Lake region, Oregon. *Geological Society of America Bulletin*, 118: 1331-1359

Barton, R. N. E., Lane, C. S., Albert, P. G., White, D., Collcutt, S. N., Bouzouggar, A., Ditchfield, P., Farr, L., Oh, A., Ottolini, L., Smith, V. C., Van Peer, P. and Kindermann, K. 2015. The role of cryptotephra in refining the chronology of Late Pleistocene human evolution and cultural change in North Africa. *Quaternary Science Reviews*, 118: 151-169

Bergman, J., Wastegård, S., Hammarlund, D., Wohlfarth, B and Roberts, S. J. 2004. Holocene tephra horizons at Klocka Bog, west-central Sweden: aspects of reproducibility in subarctic peat deposits. *Journal of Quaternary Science*, 19: 241-249

van der Bilt, W.G., Lane, C.S. and Bakke, J. 2017. Ultra-distal Kamchatkan ash on Arctic Svalbard: towards hemispheric cryptotephra correlation. *Quaternary Science Reviews*, 164: 230-235

Björck, S., Walker, M. J., Cwynar, L. C., Johnsen, S., Knudsen, K. L., Lowe, J. J. and Wohlfarth, B. 1998. An event stratigraphy for the Last Termination in the North Atlantic region based on the Greenland ice-core record: a proposal by the INTIMATE group. *Journal of Quaternary Science: Published for the Quaternary Research Association*, 13: 283-292

Blaauw, M. 2012. Out of tune: the dangers of aligning proxy archives. *Quaternary Science Reviews*, 36: 38-49

Blockley, S. P., Lowe, J. J., Walker, M. J., Asioli, A., Trincardi, F., Coope, G. R. and Donahue, R. E. 2004. Bayesian analysis of radiocarbon chronologies: examples from the European Late-glacial. *Journal of Quaternary Science*, 19: 159-175

Blockley, S. P. E., Pyne-O'Donnell, S. D. F., Lowe, J. J., Matthews, I. P., Stone, A., Pollard, A. M., Turney, C. S. M. and Molyneux, E. G. 2005. A new and less destructive laboratory procedure for the physical separation of distal glass tephra shards from sediments. *Quaternary Science Reviews*, 24: 1952-1960

Blockley, S. P., Lane, C. S., Hardiman, M., Rasmussen, S. O., Seierstad, I. K., Steffensen, J. P., Svensson, A., Lotter, A. F., Turney, C. S., Ramsey, C. B. and Intimate Members. 2012. Synchronisation of palaeoenvironmental records over the last 60,000 years, and an extended INTIMATE1 event stratigraphy to 48,000 b2k. *Quaternary Science Reviews*, 36: 2-10

Blockley, S. P. E., Bourne, A. J., Brauer, A., Davies, S. M., Hardiman, M., Harding, P. R., Lane, C. S., MacLeod, A., Matthews, I. P., Pyne-O-Donnell, S. D. F., Rasmussen, S. O., Wulf, S., Zanchetta, G. 2014. Tephrochronology and the extended INTIMATE (integration of ice-Core, marine and terrestrial records) event stratigraphy 8- 128 ka b2k. *Quaternary Science Reviews,* 106: 88-100

Bonadonna, C. and Houghton, B.F. 2005. Total grain-size distribution and volume of tephra-fall deposits. *Bulletin of Volcanology*, 67: 441-456

Bond, G., Kromer, B., Beer, J., Muscheler, R., Evans, M. N., Showers, W., Hoffmann, S., Lotti-Bond, R., Hajdas, I. and Bonani, G. 2001. Persistent solar influence on North Atlantic climate during the Holocene. *Science*, 294: 2130-2136

Bourne, A. J., Davies, S. M., Abbott, P. M., Rasmussen, S. O., Steffensen, J. P. and Svensson, A. 2013. Revisiting the Faroe Marine Ash Zone III in two Greenland ice cores: implications for marine-ice correlations. *Journal of Quaternary Science*, 28: 641-646

Bourne, A. J., Cook, E., Abbott, P. M., Seierstad, I. K., Steffensen, J. P., Svensson, A., Fischer, H., Schüpbach, S. and Davies, S. M. 2015. A tephra lattice for Greenland and a reconstruction of volcanic events spanning 25–45 ka b2k. *Quaternary Science Reviews*, 118: 122-141

Bourne, A., Abbott, P., Albert, P., Cook, E., Pearce, N., Ponomareva, V., Svensson , A. and Davies, S. 2016. Underestimated risks of recurrent long-range ash dispersal from northern Pacific Arc volcanoes, *Scientific Reports,* 6*:* 29837

Brauer, A., Hajdas, I., Blockley, S. P., Ramsey, C. B., Christl, M., Ivy-Ochs, S., Moseley, G. E., Nowaczyk, N. N., Rasmussen, S. O., Roberts, H. M. and Spötl, C. 2014. The importance of independent chronology in integrating records of past climate

change for the 60–8 ka INTIMATE time interval. *Quaternary Science Reviews*, 106: 47-66

Brenna, M., Price, R., Cronin, S. J., Smith, I. E., Sohn, Y. K., Kim, G. B. and Maas, R. 2014. Final magma storage depth modulation of explosivity and trachyte–phonolite genesis at an intraplate volcano: a case study from Ulleung Island, South Korea. *Journal of Petrology*, 55: 709-747

Broecker, W.S. 2001. Was the medieval Warm period global? *Science*. 291: 1497-1499

Bronk Ramsey, C. 2008. Deposition models for chronological records. *Quaternary Science Reviews*, *27*: 42-60

Bronk Ramsey, C. 2016. OxCal Project, Version 4.2. Retrieved April 2016. https://c14.arch.ox.ac.uk/oxcal/OxCal.html.

Bronk Ramsey, C. 2017 OxCal Project, Version 4.3. Retrieved December 2017. https://c14.arch.ox.ac.uk/oxcal/OxCal.html Retrieved June 2017

Bronk Ramsey, C. 2017 OxCal Project, Version 4.3.2 Retrieved December 2018. https://c14.arch.ox.ac.uk/oxcal/OxCal.html Retrieved June 2017

Bronk Ramsey, C., Staff, R. A., Bryant, C. L., Brock, F., Kitagawa, H., Van Der Plicht, J., Schlolaut, G., Marshall, M. H., Brauer, A., Lamb, H. F., Payne, R. L., Tarasov, P. E. Haraguchi, T., Gotanda, K., Yonenobu, H., Yokoyama, Y., Tada, R. and Nakagawa, T. 2012. A complete terrestrial radiocarbon record for 11.2 to 52.8 kyr BP. *Science*, 338: 370-374

Bussmann, F. and Anselmetti, F. S. 2010. Rossberg landslide history and flood chronology as recorded in Lake Lauerz sediments (Central Switzerland). *Swiss Journal of Geosciences*, 103: 43-59

Carey, S. and Sparks, R. S. J. 1986. Quantitative models of the fallout and dispersal of tephra from volcanic eruption columns. *Bulletin of volcanology*, 48: 109-125

Charman, D. J., Barber, K. E., Blaauw, M., Langdon, P. G., Mauquoy, D., Daley, T. J., Hughes, P. D. and Karofeld, E. 2009. Climate drivers for peatland palaeoclimate records. *Quaternary Science Reviews*, 28: 1811-1819

Cassidy, M., Watt, S. F., Palmer, M. R., Trofimovs, J., Symons, W., Maclachlan, S. E. and Stinton, A. J. 2014. Construction of volcanic records from marine sediment cores: A review and case study (Montserrat, West Indies). *Earth-Science Reviews*, 138: 137-155

Cassidy, M., Manga, M., Cashman, K. and Bachmann, O. 2018. Controls on explosive-effusive volcanic eruption styles. *Nature Communications*, 9: 2839

Chen, S. S., Lee, S. G., Lee, T. J., Lee, Y. S. and Liu, J. Q. 2018. Multi-stage magmatic plumbing system of the volcano: A case study from Ulleung Island, South Korea. *Lithos*. 314: 201-215

Chen, X. Y., Blockley, S. P., Tarasov, P. E., Xu, Y. G., McLean, D., Tomlinson, E. L., Albert, P. G., Liu, J. Q., Müller, S., Wagner, M. and Menzies, M. A., 2016. Clarifying the distal to proximal tephrochronology of the Millennium (B–Tm) eruption, Changbaishan Volcano, northeast China. *Quaternary Geochronology*, 33: 61-75

Chen X. Y., McLean, D., Blockley, S., Tarasov, P., Xu. Y. G. and Menzies, M. *submitted.* Developing a Holocene tephrostratigraphy for northern Japan using the sedimentary record from Lake Kushu, Rebun Island, *Quaternary Science Reviews*

Cheng, H., Fleitmann, D., Edwards, R. L., Wang, X., Cruz, F. W., Auler, A. S., Mangini, A., Wang, Y., Kong, X., Burns, S. J. and Matter, A. 2009. Timing and structure of the 8.2 kyr BP event inferred from δ18O records of stalagmites from China, Oman, and Brazil. *Geology*, 37: 1007-1010

Chu, G., Liu, J., Sun, Q., Lu, H., Gu, Z., Wang, W. and Liu, T. 2002. The 'Mediaeval Warm Period' drought recorded in Lake Huguangyan, tropical South China. *The Holocene*, 12: 511-516

Chun, J. H., Han, S. J. and Cheong, D. K., 1997. Tephrostratigraphy in the Ulleung Basin, East Sea: Late Pleistocene to Holocene. *Geosciences Journal*, 1: 154-166

Chun, J. H., Cheong, D., Ikehara, K. and Han, S. J. 2007. Age of the SKP-I and SKP-II tephras from the southern East Sea/Japan Sea: implications for interstadial events recorded in sediment from marine isotope stages 3 and 4. *Palaeogeography, Palaeoclimatology, Palaeoecology*, 247: 100-114

Cook, E. R., Anchukaitis, K. J., Buckley, B. M., D'Arrigo, R. D., Jacoby, G. C., Wright, W.E. 2010. Asian monsoon failure and megadrought during the last Millennium. *Science,* 328: 486-489

Cook, E., Davies, S. M., Guðmundsdóttir, E. R., Abbott, P. M. and Pearce, N. J. 2018. First identification and characterization of Borrobol-type tephra in the Greenland ice cores: new deposits and improved age estimates. *Journal of Quaternary Science*, 33: 212-224

Corella, J. P., Benito, G., Rodriguez-Lloveras, X., Brauer, A. and Valero-Garcés, B. L. 2014. Annually-resolved lake record of extreme hydro-meteorological events since AD 1347 in NE Iberian Peninsula. *Quaternary Science Reviews*, 93: 77-90

Costa, A., Smith, V.C., Macedonio, G., Matthews, N.E. 2014. The magnitude and impact of the Youngest Toba Tuff super-eruption. *Frontiers in Earth Science*, 2: 16

Coulter, S. E., Pilcher, J. R., Plunkett, G., Baillie, M., Hall, V. A., Steffensen, J. P., Vinther, M. B., Clausen, H. B., Johnsen, S. J. 2012. Holocene tephras highlight

complexity of volcanic signals in Greenland ice cores. *Journal of Geophysical Research: Atmospheres,* 117

Crosweller, H. S., Arora, B., Brown, S. K., Cottrell, E., Deligne, N. I., Guerrero, N. O., Hobbs, L., Kiyosugi, K., Loughlin, S. C., Lowndes, J. and Nayembil, M. 2012. Global database on large magnitude explosive volcanic eruptions (LaMEVE). *Journal of Applied Volcanology*, 1: 4

Cui, Z. X., Wei, H. Q., Liu, R. X. 1995. Historical documentation research of eruptions of the tianchi volcano, changbaishan. In: Liu, R.X. (Ed.), Volcanism and Human Environment. Seismol. Press, Beijing, pp. 36-39 (In Chinese).

Curzio, P., Folco, L., Laurenzi, M. A., Mellini, M. and Zeoli, A. 2008. A tephra chronostratigraphic framework for the Frontier Mountain blue-ice field (northern Victoria Land, Antarctica). *Quaternary Science Reviews*, 27: 602-620

Dansgaard, W., Johnsen, S. J., Clausen, H. B., Dahl-Jensen, D., Gundestrup, N. S., Hammer, C. U., Hvidberg, C. S., Steffensen, J. P., Sveinbjörnsdottir, A. E., Jouzel, J. and Bond, G. 1993. Evidence for general instability of past climate from a 250-kyr ice-core record. *Nature*, 364: 218

Davies, S. M. 2015. Cryptotephras: the revolution in correlation and precision dating. *Journal of Quaternary Science*, 30: 114-130

Davies, S. M., Branch, N. P., Lowe, J. J. and Turney, C. S. 2002. Towards a European tephrochronological framework for Termination 1 and the Early Holocene. *Philosophical Transactions of the Royal Society of London A: Mathematical, Physical and Engineering Sciences*, 360: 767-802

Davies, S. M., Elmquist, M., Bergman, J., Wohlfarth, B. and Hammarlund, D. 2007. Cryptotephra sedimentation processes within two lacustrine sequences from west central Sweden. *The Holocene*, 17: 319-330

Davies, S. M., Abbott, P. M., Pearce, N. J., Wastegård, S. and Blockley, S. P. 2012. Integrating the INTIMATE records using tephrochronology: rising to the challenge. *Quaternary Science Reviews*, 36: 11-27

Davies, S. M., Abbott, P. M., Meara, R. H., Pearce, N. J., Austin, W. E., Chapman, M. R., Svensson, A., Bigler, M., Rasmussen, T. L., Rasmussen, S. O. and Farmer, E. J., 2014. A North Atlantic tephrostratigraphical framework for 130–60 ka b2k: new tephra discoveries, marine-based correlations, and future challenges. *Quaternary Science Reviews*, 106: 101-121

Derkachev, A. N., Nikolaeva, N. A., Gorbarenko, S. A., Portnyagin, M. V., Ponomareva, V. V., Nürnberg, D., Sakamoto, T., Iijima, K., Liu, Y., Shi, X. and Lv, H. 2016. Tephra layers of in the quaternary deposits of the Sea of Okhotsk: Distribution, composition, age and volcanic sources. *Quaternary International*, 425: 248-272

Domínguez-Villar, D., Fairchild, I. J., Baker, A., Wang, X., Edwards, R. L. and Cheng, H. 2009. Oxygen isotope precipitation anomaly in the North Atlantic region during the 8.2 ka event. *Geology*, 37: 1095-1098

Domitsu, H., Shiihara, M., Torii, M., Tsukawaki, S. and Oda, M. 2002. Tephrostratigraphy of the piston cored sediment KT96-17 P-2 in the southern Japan Sea: the eruption age of Daisen-Kusadanihara Pumice (KsP). Journal of the Geological Society of Japan. 108: 545-556 (in Japanese with English abstract)
Dugmore, A. J. and Newton, A. J. 1992. Thin tephra layers in peat revealed by X-radiography. *Journal of Archaeological Science,* 19: 163–170

Fierstein, J. and Nathenson, M. 1992. Another look at the calculation of fallout tephra volumes. *Bulletin of Volcanology*, 54: 156-167

Fontijn, K., Rawson, H., Van Daele, M., Moernaut, J., Abarzúa, A. M., Heirman, K., Bertrand, S., Pyle, D. M., Mather, T. A., De Batist, M. and Naranjo, J. A. 2016. Synchronisation of sedimentary records using tephra: A postglacial tephrochronological model for the Chilean Lake District. *Quaternary Science Reviews*, 137: 234-254

Froggatt, P. C. 1983. Toward a comprehensive Upper Quaternary tephra and ignimbrite stratigraphy in New Zealand using electron microprobe analysis of glass shards. *Quaternary Research*, 19: 188-200

Fujiwara, O., Sawa, Y., Morita, Y., Komatsubara, J. and Abe, K. 2007. Coseismic subsidence recorded in the Holocene sequence in the Ukishima-ka-hara, Shizuoka Prefecture, central Japan. *Annual Report on Active Fault and Paleoearthquake Researches*, 7: 91-118

Fukuoka, T. and Matsui, S. 2002. Stratigraphy of pyroclastic deposits post-dating the AT tephra, Sambe Volcano. *Earth Science* (Chikyu Kagaku), 56: 105-122. (In Japanese with English abstract)

Fukusawa, H. 1995. Non-glacial varved lake sediment as a natural timekeeper and detector on environmental changes. *The Quaternary Research (Daiyonki-kenkyu*), 34: 135-149

Fukusawa, H., Tsukamoto, S., Tsukamoto, H., Ikeda, M., Okamura, M., Matsuoka, M. 1998. Falling age of Baegdusan-Tomakomai tephra (B-Tm) estimated by using non-glacial varves. *Laguna,* 5: 55-62

Fukushima, D. and Kobayashi, T. 2000. Mechanism of generation and emplacement of the Tarumizu pyroclastic flow associated with Osumi plinian eruption from Aira caldera, Japan. *Bulletin of Volcanological Society of Japan*, 45: 225-240

Furukawa, R. and Nanayama, F. 2006. Holocene pyroclastic fall deposits along the Pacific coastal region of eastern Hokkaido. *Bulletin of Volcanological Society of Japan*, 51: 351-371

Furuta, T., Fujioka, K. and Arai, F. 1986. Widespread submarine tephras around Japan—petrographic and chemical properties. *Marine Geology*, 72: 125-142

Geshi, N. and Oishi, M. 2011. The ^{14}C ages of the late Pleistocene – Holocene volcanic products erupted from the Haruna volcano. *Bull. Geol. Surv. Japan,* 62*:* 177 – 183

Global Rural—Urban Mapping Project, alpha version (GRUMP alpha), Centre for International Earth Science Information Network (CIESIN), Columbia University, International Food Policy Research Institute (IFPRI), The World Bank and Centro Internacional de Agricultura Tropical (CIAT). 2009. Japan Population Density, 2000. Socioeconomic Data and Applications Centre (SEDAC), Columbia University, Palisades, NY. Last accessed December 2018.

Gorbarenko, S. A., Nürnberg, D., Derkachev, A. N., Astakhov, A. S., Southon, J. R. and Kaiser, A., 2002. Magnetostratigraphy and tephrochronology of the Upper Quaternary sediments in the Okhotsk Sea: implication of terrigenous, volcanogenic and biogenic matter supply. *Marine Geology*, 183: 107-129

Gorbarenko, S., Chebykin, E. P., Goldberg, E. L., Ol'ga, G. S. and Lu, H. 2014. Chronicle of regional volcanic eruptions recorded in Okhotsk Sea sediments over the last 350 ka. *Quaternary Geochronology*, 20: 29-38

Grant, K. M., Rohling, E. J., Bar-Matthews, M., Ayalon, A., Medina-Elizalde, M., Bronk Ramsey, C., Satow, C., and Roberts, A. P. 2012. Rapid coupling between ice volume and polar temperature over the past 150,000 years. *Nature*, 491: 744-747

Gudmundsdóttir, E. R., Eiríksson, J. and Larsen, G. 2011. Identification and definition of primary and reworked tephra in Late Glacial and Holocene marine shelf sediments off North Iceland. *Journal of Quaternary Science*, 26: 589-602

Guillou, H., Carracedo, J.C., Paris, R. and Torrado, F.J.P. 2004. Implications for the early shield-stage evolution of Tenerife from K/Ar ages and magnetic stratigraphy. *Earth and Planetary Science Letters*, 222: 599-614

Guo, Z., Liu, J., Sui, S., Liu, Q., He, H., Ni, Y. 2002. The mass estimation of volatile emission during 1199/1200 AD eruption of Baitoushan volcano and its significance. *Science in China Series D: Earth Sciences*, 46: 530-539

Ha, K. J., Heo, K. Y., Lee, S. S., Yun, K. S., Jhun, J.G. 2012. Variability in the east asian monsoon: a review. *Meteorological Applications*, 19: 200-215

Hakozaki, M., Miyake, F., Nakamura, T., Kimura, K., Masuda, K. and Okuno, M. 2017. Verification of the Annual Dating of the 10th Century Baitoushan Volcano Eruption Based on an AD 774–775 Radiocarbon Spike. *Radiocarbon*, 1-8

Hall, V. A. and Pilcher, J. R. 2002. Late-Quaternary Icelandic tephras in Ireland and Great Britain: detection, characterization and usefulness. *The Holocene*, 12: 223-230

Hayakawa, Y. 1983. Chuseri tephra formation from Towada volcano, Japan. *Bull. Volcanol. Soc. Japan, Ser*, 2: 263-273

Hayashi, R., Takahara, H., Hayashida, A. and Takemura, K. 2010. Millennial-scale vegetation changes during the last 40,000 yr based on a pollen record from Lake Biwa, Japan. *Quaternary Research*, 74: 91-99

Hayashida, A., Ali, M., Kuniko, Y., Kitagawa, H., Torii, M. and Takemura, K. 2007. Environmental magnetic record and paleosecular variation data for the last 40 kyrs from the Lake Biwa sediments, Central Japan. *Earth, Planets and Space*, 59: 807-814

Hemming, S.R. 2004. Heinrich events: Massive late Pleistocene detritus layers of the North Atlantic and their global climate imprint. *Reviews of Geophysics*, 42: 1

Higashino, T., Tsujimori T. and Itaya T. 2005. An alkaline tephra found at Midagahara, Mt. Hakusan. 32. Ann Report Hakusan Nat Conserv Center, 32: 1 –7

Horiuchi, K., Sonoda, S., Matsuzaki, H. and Ohyama, M. 2007. Radiocarbon analysis of tree rings from a 15.5-cal kyr BP pyroclastically buried forest: a pilot study. *Radiocarbon*, 49: 1123-1132.

Horn, S. and Schmincke, H. U. 2000. Volatile emission during the eruption of Baitoushan Volcano (China/North Korea) ca. 969 AD. *Bulletin of Volcanology,* 61: 537-555

Horwell, C. J. and Baxter, P. J. 2006. The respiratory health hazards of volcanic ash: a review for volcanic risk mitigation. *Bulletin of Volcanology*, 69: 1-24

Hughes, P. D. M., Mallon, G., Brown, A., Essex, H. J., Stanford, J. D., Hotes, S. 2013. The impact of high tephra loading on late-Holocene carbon accumulation and vegetation succession in peatland communities*. Quaternary Science Reviews,* 67: 160-175

Hunt, B. G. 2006. The medieval Warm period, the little ice age and simulated climatic variability. *Climate Dynamics,* 27: 677-694

Hunt, J. B. and Hill, P. G. 1993. Tephra geochemistry: a discussion of some persistent analytical problems. *The Holocene*, 3: 271-278

Hunt, J. B. and Najman, Y. M. R. 2003. Tephrochronological and tephrostratigraphical potential of Pliocene-Pleistocene volcaniclastic deposits in the Japan Forearc, ODP Leg 186. In *Proceedings of the Ocean Drilling Program, Scientific Results*, 186: 1-29

Iacovino, K., Ju-Song, K., Sisson, T., Lowenstern, J., Kuk-Hun, R., Jong-Nam, J., Kun-Ho, S., Song-Hwan, H., Oppenheimer, C., Hammond, J. O. and Donovan, A. 2016. Quantifying gas emissions from the “Millennium Eruption” of Paektu volcano, Democratic People’s Republic of Korea/China. *Science advances*, *2:* 1600913

Ikehara, K., 2003. Late Quaternary seasonal sea-ice history of the northeastern Japan Sea. *Journal of Oceanography*, 59: 585-593

Ikehara, K., Kikkawa, K., Chun, J. H. 2004. Origin and correlation of three tephras that erupted during oxygen isotope stage 3 found in cores from the Yamato Basin, central Japan Sea. The Quaternary Research (Japanese) 43, 201–212 (in Japanese with English abstract)

Ikehara, M., Murayama, M., Tadai, O., Hokanishi, N., Daido, N., Kawahata, H. and Yasuda, H. 2006. Late Quaternary tephrostratigraphy of two IMAGES cores taken from the off Shikoku in the Northwest Pacific. *Fossils (Kaseki)*, 79: 60-76

Ikehara, K., Danhara, T., Yamashita, T., Tanahashi, M., Morita, S. and Ohkushi, K. I. 2011. Paleoceanographic control on a large marine reservoir effect offshore of Tokai, south of Japan, NW Pacific, during the last glacial maximum-deglaciation. *Quaternary International*, 246: 213-221

Ikehara, K., Ohkushi, K., Noda, A., Danhara, T. and Yamashita, T. 2013. A new local marine reservoir correction for the last deglacial period in the Sanriku region, northwestern North Pacific, based on radiocarbon dates from the Towada-Hachinohe (To-H) tephra. *The Quat Res (Daiyonki-kenkyu)*, 52: 127-37

Ikeya, N., Wada, H., Akutsu, H. and Takahashi, M. 1990. Origin and sedimentary history of Hamana-ko Bay, Pacific coast of central Japan. *Memoirs of the Geological Society of Japan: Lakes-Origin, Environment and Geology* 36: 129-150

Im, J. H., Shim, S. H., Choo, C. O., Jang, Y. D. and Lee, J. S. 2012. Volcanological and palaeoenvironmental implication of charcoals of the Nari Formation in Nari Caldera, Ulleung Island, Korea. *Geosci. J,* 16: 105-114

Ishihama, S., Oi, T., Hasegawa, S., Matsumoto, R. 2014. Paleoceanographic changes of surface and deep water based on oxygen and carbon isotope records during the last 130 kyr identified in MD179 cores, off Joetsu, Japan Sea. Journal of Asian Earth Science, 90: 218–227

Ishimura, D., Yamada, K., Miyauchi, T. and Hayase, R. 2014. Characteristics of tephras interbedded with the Holocene sediments in the Sanriku Coast, northeast Japan. *J Geogra*, 123: 671-697

Jenkins, S., McAneney, J., Magill, C. and Blong, R. 2012. Regional ash fall hazard II: Asia-Pacific modelling results and implications. *Bulletin of volcanology*, 74: 1713-1727

Jensen, B. J., Pyne-O'Donnell, S., Plunkett, G., Froese, D. G., Hughes, P. D., Sigl, M., McConnell, J. R., Amesbury, M. J., Blackwell, P. G., van den Bogaard, C. and Buck, C.E. 2014. Transatlantic distribution of the Alaskan white river ash. *Geology*, 42: 875-878

Jin, C., Liu, J., Wang, B., Wang, Z. and Yan, M. 2018. A Centennial Episode of Weak East Asian Summer Monsoon in the Midst of the Medieval Warming. *Paleoceanography and Paleoclimatology*, 33: 1035-1048

Jochum, K. P., Stoll, B., Herwig, K., Willbold, M., Hofmann, A. W., Amini, M. *et al.,* 2006. MPI-DING reference glasses for in situ microanalysis: New reference values for element concentrations and isotope ratios. *Geochemistry, Geophysics, Geosystems*, 7: 2

Johnsen, S. J., Clausen, H. B., Dansgaard, W., Fuhrer, K., Gundestrup, N., Hammer, C. U., Iversen, P., Jouzel, J. and Stauffer, B. 1992. Irregular glacial interstadials recorded in a new Greenland ice core. *Nature*, 359: 311

Kaneko, K., Inoue, K., Koyaguchi, T., Yoshikawa, M., Shibata, T., Takahashi, T. and Furukawa, K., 2015. Magma plumbing system of the Aso-3 large pyroclastic eruption cycle at Aso volcano, Southwest Japan: Petrological constraint on the formation of a compositionally stratified magma chamber. *Journal of Volcanology and Geothermal Research*, 303: 41-58

Karkanas, P., White, D., Lane, C. S., Stringer, C., Davies, W., Cullen, V. L., Smith, V. C., Ntinou, M., Tsartsidou, G. and Kyparissi-Apostolika, N. 2015. Tephra correlations and climatic events between the MIS6/5 transition and the beginning of MIS3 in Theopetra Cave, central Greece. *Quaternary Science Reviews*, 118: 170-181

Katoh, S., Yamagata, K. and Okumura, K. 1995. AMS-14C dates of Late Quaternary tephra layers erupted from the Shikotsu and Kuttara volcanoes. *The Quaternary Research (Daiyonki-Kenkyu)*, 34: 309-313 (in Japanese with English abstract)

Katsuta, N., Takano, M., Kawakami, S. I., Togami, S., Fukusawa, H., Kumazawa, M. and Yasuda, Y. 2007. Advanced micro-XRF method to separate sedimentary rhythms and event layers in sediments: its application to lacustrine sediment from Lake Suigetsu, Japan. *Journal of Paleolimnology*, 37: 259-271

Kigoshi, T., Kumon, F., Kawai, S. and Kanauchi, A. 2017. Quantitative reconstruction of paleoclimate in central Japan for the past 158,000 years based on a modern analogue technique of pollen composition. *Quaternary International*, 455: 126-140

Kim, Y. K. 1985. Petrology of Ulreung volcanic island, Korea—part 1 Geology. J Mineral Petrol Econ Geol 80: 128–135

Kim, G. and Choi, I.S. 1987. A preliminary study on long-term variation of unusual climate phenomena during the past 1000 years in Korea. *The Climate of China and Global Climate*, 30-37

Kim, K. H, Tanaka T, Nagao K, Jang, S. K. 1999. Nd and Sr isotopes and K- Ar ages of the Ulreungdo alkali volcanic rocks in the East Sea, South Korea. Geochem J 33: 317–341

Kim, G. B., Cronin, S. J., Yoon, W. S. and Sohn, Y. K. 2014. Post 19 ka BP eruptive history of Ulleung Island, Korea, inferred from an intra-caldera pyroclastic sequence. *Bulletin of Volcanology*, 76: 802

Kimura, J. I. and Chang, Q. 2012. Origin of the suppressed matrix effect for improved analytical performance in determination of major and trace elements in anhydrous silicate samples using 200 nm femtosecond laser ablation sector-field inductively coupled plasma mass spectrometry, *Journal of Analytical Atomic Spectrometry,* 27: 1549 – 1559

Kimura, J. I., Nagahashi, Y., Satoguchi, Y. and Chang, Q. 2015. Origins of felsic magmas in Japanese subduction zone: Geochemical characterizations of tephra from caldera-forming eruptions< 5 Ma. *Geochemistry, Geophysics, Geosystems*, 16: 2147-2174

Kishimoto, H., Hasegawa, T., Nakagawa, M., Wada, K., 2009. Tephrostratigraphy and Eruption Style of Mashu Volcano, during the last 14,000 years, Eastern Hokkaido, Japan. Bulletin of the Volcanological Society of Japan 54, 15–36 (in Japanese with English abstract)

Kitagawa, H. and van der Plicht, H. 1998a. A 40,000-year varve chronology from Lake Suigetsu, Japan: Extension of the C-14 calibration curve. *Radiocarbon,* 40: 505-515

Kitagawa, H. and van der Plicht, H. 1998b. Atmospheric Radiocarbon Calibration to 45,000 yr B.P.: Late Glacial Fluctuations and Cosmogenic Isotope Production. *Science,* 279: 1187-1190

Kitagawa, H. and van der Plicht, J. 2000. Atmospheric radiocarbon calibration beyond 11,900 cal BP from Lake Suigetsu laminated sediments. *Radiocarbon*, 42: 370-381

Kitagawa, H., Fukuzawa, T. Nakamura, M., Okumura, K., Takemura, A., Hayashida, A. and Yasuda, Y. 1995. AMS ^{14}C dating of varved sediments from Lake Suigetsu, central Japan and atmospheric ^{14}C change during the late Pleistocene, *Radiocarbon,* 37: 371-378

Kiyosugi, K., Connor, C., Sparks, R. S. J., Crosweller, H. S., Brown, S. K., Siebert, L., Wang, T. and Takarada, S. 2015. How many explosive eruptions are missing from the geologic record? Analysis of the quaternary record of large magnitude explosive eruptions in Japan. *Journal of Applied Volcanology*, 4: 1-15

Kobayashi, M., Takada, A. and Nakano, S. 2007. Eruption history of Fuji Volcano from AD 700 to AD 1,000 using stratigraphic correlation of the Kouzushima-Tenjosan Tephra. *Bulletin of the Geological Survey of Japan*, 57: 409-430

Kossler, A., Tarasov, P., Schlolaut, G., Nakagawa, T., Marshall, M., Brauer, A., Staff, R., Ramsey, C. B., Bryant, C., Lamb, H. and Demske, D. 2011. Onset and termination of the late-glacial climate reversal in the high-resolution diatom and sedimentary

records from the annually laminated SG06 core from Lake Suigetsu, Japan. *Palaeogeography, Palaeoclimatology, Palaeoecology*, 306: 103-115

Kudo, Y. and Kumon, F. 2012. Paleolithic cultures of MIS 3 to MIS 1 in relation to climate changes in the central Japanese islands. *Quaternary International*, 248: 22-31

Kumon, F., Kawai, S. and Inouchi, Y. 2003. Climate Changes between 25, 000 and 6, 000 yrs BP Deduced from TOC, TN, and Fossil Pollen Analyses of a Sediment Core from Lake Nojiri, Central Japan. *The Quaternary Research (Daiyonki-Kenkyu)*, *42*: 13-26

Kumon, F., Kanamaru, K., Tawara, T., Kakuta, N., Yamamoto, M. and Hayashi, H., 2005. Relationships among weather factors, biological productivity and TOC content of sediments in Lake Kizaki, central Japan. *Journal-Geological Society of Japan,* 111: 599

Kutterolf, S., Schindlbeck, J.C., Robertson, A. H. F., Avery, A., Baxter, A.T., Petronotis, K. and Wang, K. L. 2018. Tephrostratigraphy and Provenance From IODP Expedition 352, Izu-Bonin Arc: Tracing Tephra Sources and Volumes From the Oligocene to Recent. *Geochemistry, Geophysics, Geosystems*, 19: 150-174

Kylander, M. E., Lind, E. M., Wastegård, S. and Löwemark, L. 2012. Recommendations for using XRF core scanning as a tool in tephrochronology. *The Holocene*, 22: 371-375

Kyle, P. R., Ponomareva, V. V. and Rourke Schluep, R. 2011. Geochemical characterization of marker tephra layers from major Holocene eruptions, Kamchatka Peninsula, Russia. *International Geology Review*, 53: 1059-1097

Lamb, H. H., 1965. The early medieval warm epoch and its sequel. *Palaeogeography, Palaeoclimatology, Palaeoecology*, 1: 13-37

Lane, C. S., Blockley, S. P. E., Lotter, A. F., Finsinger, W., Filippi, M. L. and Matthews, I. P. 2012. A regional tephrostratigraphic framework for central and southern European climate archives during the Last Glacial to Interglacial transition: comparisons north and south of the Alps. *Quaternary Science Reviews*, 36: 50-58

Lane, C. S., Brauer, A., Blockley, S. P. and Dulski, P. 2013. Volcanic ash reveals time-transgressive abrupt climate change during the Younger Dryas. *Geology*, 41: 1251-1254

Lane, C. S., Cullen, V. L., White, D., Bramham-Law, C. W. F. and Smith, V. C. 2014. Cryptotephra as a dating and correlation tool in archaeology. *Journal of Archaeological Science*, 42: 42-50

Lane, C. S., Brauer, A., Martín-Puertas, C., Blockley, S. P., Smith, V. C. and Tomlinson, E. L. 2015. The Late Quaternary tephrostratigraphy of annually laminated sediments from Meerfelder Maar, Germany. *Quaternary Science Reviews*, 122: 192-206

Le Bas, M. J., Le Maitre, R. W., Streckeisen, A. and Zanettin, B. 1986. A chemical classification of volcanic rocks based on the total alkali-silica diagram. *Journal of petrology*, 27: 745-750

Lee, Seung-Yeon, Gil-Yong Suh, Soo-Yeon Park, Yeon-Su Kim, Jong-Hyun Nam, Seung-Hyun Yu, Ji-Hoon Park et al. 2018. Prediction of Dispersal Directions and Ranges of Volcanic Ashes from the Possible Eruption of Mt. Baekdu. Korean Society of Soil Sciences and Fertilizer. 51: 16-27

Lisiecki, L. E. and Raymo, M. E. 2005. A Pliocene-Pleistocene stack of 57 globally distributed benthic δ18O records. *Paleoceanography*, 20: 1

Lim, C., Ikehara, K. and Toyoda, K. 2008. Cryptotephra detection using high-resolution trace-element analysis of Holocene marine sediments, southwest Japan. *Geochimica et Cosmochimica Acta*, 72: 5022-5036

Lim, C., Toyoda, K., Ikehara, K. and Peate, D.W. 2013. Late Quaternary tephrostratigraphy of Baegdusan and Ulleung volcanoes using marine sediments in the Japan Sea/East Sea. *Quaternary Research*, 80: 76-87

Lim, C., Kim, S. and Lee, C. 2014. Geochemical fingerprint of the primary magma composition in the marine tephras originated from the Baegdusan and Ulleung volcanoes. *Journal of Asian Earth Sciences*, 95: *266-273*

Liu, T. and Ding, Z. 1998. Chinese loess and the paleomonsoon. *Annual review of Earth and Planetary Sciences*, 26: 111-145

Liu, T. S., Guo, Z. T., Liu, J. Q., Han, J. M., Ding, Z. L., Gu, Z. Y. and Wu, N. Q. 1995. Variations of eastern Asian monsoon over the last 140,000 years, *Société Géologique de France Bulletin*, 166: 221–229

Liu, R. X., Wei, H. Q., Li, J. T. 1998. The Latest Eruptions from Tianchi Volcano. Changbaishan. Sci. Press, Beijing, p. 159 (In Chinese)

Lowe, J. J., Hoek, W. Z. and I.N.T.I.M.A.T.E. Group. 2001. Inter-regional correlation of palaeoclimatic records for the Last Glacial–Interglacial Transition: a protocol for improved precision recommended by the INTIMATE project group. *Quaternary Science Reviews*, 20: 1175-1187

Lowe, J. J., Rasmussen, S. O., Björck, S., Hoek, W. Z., Steffensen, J. P., Walker, M. J., Yu, Z. C. and Intimate Group. 2008. Synchronisation of palaeoenvironmental events in the North Atlantic region during the Last Termination: a revised protocol recommended by the INTIMATE group. *Quaternary Science Reviews*, 27: 6-17

Lowe, J., Barton, N., Blockley, S., Ramsey, C. B., Cullen, V. L., Davies, W., Gamble, C., Grant, K., Hardiman, M., Housley, R., Lane, C. S., Lee, S., Lewis, M., MacLeod, A., Menzies, M., Müller, W., Pollard, M., Price, C., Roberts, A. P., Rohling, E. J., Satow, C.,

Smith, V. C., Stringer, C. B., Tomlinson, E. L., White, D., Albert, P., Arienzo, I., Barker, G., Borić, D., Carandente, A., Civetta, L., Ferrier, C., Guadelli, J., Karkanas, P., Koumouzelis, M., Müller, U. C., Orsi, G., Pross, J., Rosi, M., Shalamanov-Korobar, L., Sirakov, N. and Tzedakis, P. C. 2012. Volcanic Ash Layers Illuminate the Resilience of Neanderthals and Early Modern Humans to Natural Hazards. *Proceedings of the National Academy of Sciences,* 109: 13532-13537

Lowe, J. J., Ramsey, C. B., Housley, R. A., Lane, C. S., Tomlinson, E. L., R.E.S.E.T. Team, R.E.S.E.T. Associates. 2015. The RESET project: constructing a European tephra lattice for refined synchronization of environmental and archaeological events during the last c. 100 ka. *Quaternary Science Reviews,* 118: 1-17

Machida, H. 1999. Quaternary widespread tephra catalog in and around Japan. *The Quaternary Research (Daiyonki-Kenkyu)*, 38: 194-201

Machida, H. and Arai, F. 1976. The discovery and significance of the very widespread tephras: the Aira-Tn ash. *Kagaku (Science),* 46: 339-347

Machida, H. and Arai, F. 1983. Extensive ash falls in and around the Sea of Japan from large late Quaternary eruptions. *Journal of Volcanology and Geothermal Research*, 18: 151-164

Machida, H. and Arai, F. 2003. *Atlas of tephra in and around Japan*. Revised ed. Tokyo University Press, Tokyo

Machida, H., Arai, F., Lee, B., Moriwaki, H. and Furuta, T. 1984. Late Quaternary tephras in Ulreung-do Island, Korea. Journal of Geography (Chigaku-Zasshi) 93: 1-14 (in Japanese with English abstract)

Machida, H., H. Moriwaki, and D. Zhao. 1990. The recent major eruption of Changbai volcano and its environmental effects, *Geogr. Rep. Tokyo Metrop. Univ.*, 25: 1–20

Mackay, H., Hughes, P. D., Jensen, B. J., Langdon, P. G., Pyne-O'Donnell, S. D., Plunkett, G., Froese, D. G., Coulter, S. and Gardner, J. E. 2016. A mid to late Holocene cryptotephra framework from eastern North America. *Quaternary Science Reviews*, 132: 101-113

MacLeod, A. and Davies, S. M., 2016. Caution in cryptotephra correlation: resolving Lateglacial chemical controversies at Sluggan Bog, Northern Ireland. *Journal of Quaternary Science*, 31: 406-415

Marshall, M., Schlolaut, G., Nakagawa, T., Lamb, H., Brauer, A., Staff, R., Ramsey, C.B., Tarasov, P., Gotanda, K., Haraguchi, T. and Yokoyama, Y. 2012. A novel approach to varve counting using μXRF and X-radiography in combination with thin-section microscopy, applied to the Late Glacial chronology from Lake Suigetsu, Japan. *Quaternary Geochronology*, 13: 70-80

Martin-Jones, C. 2012. *Defining fractionation in LA-ICP-MS analysis of volcanic glass shards and its application to the correlation of tephra deposits from Ulleungdo, Korea* (Doctoral dissertation, MPhil thesis, Aberystwyth University).

Matthews, I. P., Trincardi, F., Lowe, J. J., Bourne, A. J., MacLeod, A., Abbott, P. M., Andersen, N., Asioli, A., Blockley, S. P. E., Lane, C. S. and Oh, Y. A. 2015. Developing a robust tephrochronological framework for Late Quaternary marine records in the Southern Adriatic Sea: new data from core station SA03-11. *Quaternary Science Reviews*, 118: 84-104.

Matsu'ura, T., Kimura, J. I., Chang, Q. and Komatsubara, J. 2017. Using tephrostratigraphy and cryptotephrostratigraphy to re-evaluate and improve the Middle Pleistocene age model for marine sequences in northeast Japan (Chikyu C9001C). *Quaternary Geochronology*, 40: 129-145

Matsu'ura, T., Komatsubara, J. and Ahagon, N. 2018. Using Late and Middle Pleistocene tephrostratigraphy and cryptotephrostratigraphy to refine age models of Holes ODP1150A and ODP1151C, NW Pacific Ocean: A cross-check between tephrostratigraphy and biostratigraphy. *Quaternary Geochronology*, 47: 29-53

McDonald, R. 1974. Nomenclature and petrochemistry of the peralkaline over-saturated extrusive rocks. *Bulletin Volcanologique*, 38: 498-516

Mahony, S. H., Sparks, R. S. J., Wallace, L. M., Engwell, S. L., Scourse, E. M., Barnard, N. H., Kandlbauer, J. and Brown, S. K. 2016. Increased rates of large-magnitude explosive eruptions in Japan in the late Neogene and Quaternary. *Geochemistry, Geophysics, Geosystems*, 17: 2467-2479

Matsumoto, A., Uto, K., Ono, K., Watanabe, K. 1991. K–Ar age determinations for Aso volcanic rocks — concordance with volcanostratigraphy and application to pyroclastic flows. Programme and abstracts of the Volcanological Society of Japan 1991 2:73 (in Japanese).

Matsumoto, R., Kakuwa, Y. and Tanahashi, M. 2011. Occurrence and origin of shallow gas hydrates of the eastern margin of Japan Sea as revealed by Calypso and CASQ corings of R/V Marion Dufresne. In *Proceedings of the 7th International Conference on Gas Hydrates (ICGH 2011).* 459-468. Scotland: Edinburgh.

McCanta, M.C., Hatfield, R.G., Thomson, B.J., Hook, S.J. and Fisher, E. 2015. Identifying cryptotephra units using correlated rapid, nondestructive methods: VSWIR spectroscopy, X-ray fluorescence, and magnetic susceptibility. *Geochemistry, Geophysics, Geosystems*, 16: 4029-4056

McLean, D., Albert, P. G., Nakagawa, T., Staff, R. A., Suzuki, T. and Smith, V.C. 2016. Identification of the Changbaishan 'Millennium' (B-Tm) eruption deposit in the Lake Suigetsu (SG06) sedimentary archive, Japan: Synchronisation of hemispheric-wide palaeoclimate archives. *Quaternary Science Reviews*, 150: 301-307

McLean, D., Albert, P. G., Nakagawa, T., Suzuki, T., Staff, R. A., Yamada, K., Kitaba, I., Haraguchi, T., Kitagawa, J., Members, S.P. and Smith, V. 2018. Integrating the Holocene tephrostratigraphy for East Asia using a high-resolution cryptotephra study from Lake Suigetsu (SG14 core), central Japan. *Quaternary Science Reviews*, 183: 36-58

Mingram, J., Stebich, M., Schettler, G., Hu, Y., Rioual, P., Nowaczyk, N., Dulski, P., You, H., Opitz, S., Liu, Q. and Liu, J. 2018. Millennial-scale East Asian monsoon variability of the last glacial deduced from annually laminated sediments from Lake Sihailongwan, NE China. *Quaternary Science Reviews*, 201: 57-76

Miyabuchi, Y. 2009. A 90,000-year tephrostratigraphic framework of Aso Volcano, Japan. *Sedimentary Geology*, 220: 169 – 189

Miyabuchi, Y. 2011. Post-caldera explosive activity inferred from improved 67 – 30 ka tephrostratigraphy at Aso Volcano, Japan. *Journal of Volcanology and Geothermal Research,* 205: 94 – 113

Moriwaki, H., Suzuki, T., Murata, M., Ikehara, M., Machida, H. and Lowe, D.J. 2011. Sakurajima-Satsuma (Sz-S) and Noike-Yumugi (N-Ym) tephras: new tephrochronological marker beds for the last deglaciation, southern Kyushu, Japan. *Quaternary International*, 246: 203-212

Moriwaki, H., Nakamura, N., Nagasako, T., Lowe, D. J. and Sangawa, T. 2016. The role of tephras in developing a high-precision chronostratigraphy for palaeoenvironmental reconstruction and archaeology in southern Kyushu, Japan, since 30,000 cal. BP: An integration. *Quaternary International*, 397: 79-92

Morrill, C., Overpeck, J.T. and Cole, J.E. 2003. A synthesis of abrupt changes in the Asian summer monsoon since the last deglaciation. *The Holocene*, 13: 465-476

Nagahashi, Y., Yoshikawa, S., Miyakawa, C., Uchiyama, T. and Inouchi, Y. 2004. Stratigraphy and chronology of widespread tephra layers during the past 430 ky in the Kinki District and the Yatsugatake Mountains: major element composition of the glass shards using EDS analysis. The Quaternary Research (Daiyonki-Kenkyu) 43: 15-35 (in Japanese with English abstract)

Nagaoka, S., Okuno, M. and Arai, F. 2001. Tephrostratigraphy and eruptive history of the Aira caldera volcano during 100-30 ka, Kyushu, Japan. *Journal of the Geological Society of Japan*, 107: 432-450

Nagashima, K., Tada, R., Matsui, H., Irino, T., Tani, A. and Toyoda, S. 2007. Orbital- and millennial-scale variations in Asian dust transport path to the Japan Sea. *Palaeogeography, Palaeoclimatology, Palaeoecology*, 247: 144-161

Nakagawa, M., Ishizuka, Y., Kudo, T., Yoshimoto, M., Hirose, W., Ishizaki, Y., Gouchi, N., Katsui, Y., Solovyow, A. W., Steinberg, G. S. and Abdurakhmanov, A. I. 2002.

Tyatya volcano, southwestern Kuril arc: recent eruptive activity inferred from widespread tephra. *Island Arc*, 11: 236-254

Nakagawa, T., Kitagawa, H., Yasuda, Y., Tarasov, P. E., Nishida, K., Gotanda, K., Sawai, Y., Yangtze River and Civilization Program members. 2003. Asynchronous Climate Changes in the North Atlantic and Japan During the Last Termination. *Science*, 299: 688-691

Nakagawa, T., Kitagawa, H., Yasuda, Y., Tarasov, P. E., Gotanda, K. and Sawai, Y. 2005. Pollen/event stratigraphy of the varved sediment of Lake Suigetsu, central Japan from 15,701 to 10,217 SG vyr BP (Suigetsu varve years before present): description, interpretation, and correlation with other regions. *Quaternary Science Reviews* 24: 1691–1701

Nakagawa, T., Gotanda, K., Haraguchi, T., Danhara, T., Yonenobu, H., Brauer, A., Yokoyama, Y., Tada, R., Takemura, K., Staff, R. A., Payne, R., Bronk Ramsey, C., Bryant, C., Brock, F., Schlolaut, G., Marshall, M., Tarasov, P., Lamb, H. and Suigetsu 2006 Project Members. 2012. SG06, a perfectly continuous and varved sediment core from Lake Suigetsu, Japan: stratigraphy and potential for improving the radiocarbon calibration model and understanding of late Quaternary climate changes. *Quaternary Science Reviews,* 36: 164-176

Nakajima, T. 1996. Marine sediments and Late Quaternary stratigraphy in the southeastern part of the Japan Sea-concerning the timing of dark-layer deposition. *J. Geol. Soc. Japan*, 102: 125-138

Nakamura, Y. 2016. Stratigraphy, distribution, and petrographic properties of Holocene tephras in Hokkaido, northern Japan. *Quaternary International*, 397: 52-62

Nakamura, Y., Nishimura, Y., Nakagawa, M., Kaistrenko, V. M., Iliev, A. Ya, 2009. Holocene marker tephras in the coastal lowlands of Kunashiri and Shikotan Islands, southern Kuril Islands. Bulletin of the Volcanological Society of Japan (Kazan) 54: 263-274 (in Japanese, with English abstract)

Nakamura, Y., Sugai, T., Ishihara, T., Freire, A.F. and Matsumoto, R. 2013. Late Pleistocene tephrostratigraphy of sea-bottom sediments in the Eastern Margin of Japan Sea by MD 179–Japan Sea Gas Hydrate Expedition. *Journal of the Japanese Association of Petroleum Technology*, 78: 79-91

Nanayama, F., Satake, K., Furukawa, R., Shimokawa, K., Atwater, B.F., Shigeno, K., Yamaki, S. 2003. Unusually large earthquakes inferred from tsunami deposits along the Kuril trench. Nature. 424: 660-663

Newhall, C. G. and Self, S. 1982. The volcanic explosivity index (VEI) an estimate of explosive magnitude for historical volcanism. *Journal of Geophysical Research: Oceans*, 87: 1231-1238

Newhall, C., Self, S. and Robock, A., 2018. Anticipating future Volcanic Explosivity Index (VEI) 7 eruptions and their chilling impacts. *Geosphere*, 14: 572-603

North Greenland Ice Core Project Members, 2004. High-resolution record of Northern Hemisphere climate extending into the last interglacial period. *Nature*, 431: 147-151

Nowaczyk, N. R., Arz, H. W., Frank, U., Kind, J. and Plessen, B. 2012. Dynamics of the Laschamp geomagnetic excursion from Black Sea sediments. *Earth and Planetary Science Letters*, 351: 54-69

OAG Aviation Worldwide Limited. 2018. OAG Report, Busiest Routes 2018: Official Airline Guide. https://www.oag.com/2018-busiest-routes.html Retrieved November 2018

Oba T, Kato M, Kitazato H, Koizumi I, Omura A, Sakai T, Takayama T. 1991. Paleoenvironmental changes in the Japan Sea during the last 85,000 years. Paleoceanography 6: 499–518

Okuno, M. 2002. chronology of tephra layers in southern Kyushu, SW Japan, for the last 30,000 years. *The Quaternary Research (Daiyonki-Kenkyu)*, 41: 225-236 (in Japanese with English abstract)

Okuno, M., Shiihara, M., Torii, M., Nakamura, T., Kim, K. H., Domitsu, H., Moriwaki, H. and Oda, M. 2010. AMS radiocarbon dating of Holocene tephra layers on Ulleung Island, South Korea. *Radiocarbon*, 52: 1465-1470

Okuno, M., Torii, M., Yamada, K., Shinozuka, Y., Danhara, T., Gotanda, K., Yonenobu, H. and Yasuda, Y. 2011. Widespread tephras in sediments from lake Ichi-no-Megata in northern Japan: Their description, correlation and significance. *Quaternary International*, 246: 270-277

Ono, K. and Watanabe, K., 1985. Geological map of Aso volcano. Geological map of volcanoes. *Geological Survey of Japan*, *4*.

Oppenheimer, C., Wacker, L., Xu, J., Galván, J. D., Stoffel, M., Guillet, S., Corona, C., Sigl, M., Di Cosmo, N., Hajdas, I. and Pan, B. 2017. Multi-proxy dating the 'Millennium Eruption' of Changbaishan to late 946 CE. *Quaternary Science Reviews*, 158: 164-171

Pan, B., de Silva, S.L., Xu, J., Chen, Z., Miggins, D.P. and Wei, H. 2017. The VEI-7 Millennium eruption, Changbaishan-Tianchi volcano, China/DPRK: New field, petrological, and chemical constraints on stratigraphy, volcanology, and magma dynamics. *Journal of Volcanology and Geothermal Research*, 343: 45-59

Park, M. H., Kim, I. S. and Shin, J. B. 2003. Characteristics of the late Quaternary tephra layers in the East/Japan Sea and their new occurrences in western Ulleung Basin sediments. *Marine Geology*, 202: 135-142

Park, J. 2017. Solar and tropical ocean forcing of late-Holocene climate change in coastal East Asia. *Palaeogeography, Palaeoclimatology, Palaeoecology*, 469: 74-83

Park, M. H., Kim, J. H. and Kil, Y. W. 2007. Identification of the Late Quaternary tephra layers in the Ulleung Basin of the East Sea using geochemical and statistical methods. *Marine Geology*, 244: 196-208

Park, J., Park, J., Yi, S., Kim, J.C., Lee, E. and Jin, Q. 2018. The 8.2 ka cooling event in coastal East Asia: High-resolution pollen evidence from southwestern Korea. *Scientific Reports*, 8: 12423

Pearce, N. J., Denton, J. S., Perkins, W. T., Westgate, J. A. and Alloway, B. V. 2007. Correlation and characterisation of individual glass shards from tephra deposits using trace element laser ablation ICP-MS analyses: current status and future potential. *Journal of Quaternary Science*, 22*:* 721-736

Pearce, N. J., Perkins, W. T., Westgate, J. A. and Wade, S. C. 2011. Trace-element microanalysis by LA-ICP-MS: the quest for comprehensive chemical characterisation of single, sub-10 μm volcanic glass shards. *Quaternary International*, 246: 57-81

Peccerillo, A. and Taylor, S. R. 1976. Geochemistry of Eocene calc-alkaline volcanic rocks from the Kastamonu area, northern Turkey. *Contributions to Mineralogy and Petrology*, 58: 63-81

Ponomareva, V., Portnyagin, M., Pevzner, M., Blaauw, M., Kyle, P. and Derkachev, A. 2015a. Tephra from andesitic Shiveluch volcano, Kamchatka, NW Pacific: chronology of explosive eruptions and geochemical fingerprinting of volcanic glass. *International Journal of Earth Sciences*, 104: 1459-1482

Ponomareva, V., Portnyagin, M. and Davies, S. M. 2015b. Tephra without borders: far-reaching clues into past explosive eruptions. *Frontiers in Earth Science*, 3: 83

Ponomareva, V., Polyak, L., Portnyagin, M., Abbott, P. M., Zelenin, E., Vakhrameeva, P. and Garbe-Schönberg, D. 2018. Holocene tephra from the Chukchi-Alaskan margin, Arctic Ocean: Implications for sediment chronostratigraphy and volcanic history. *Quaternary Geochronology*, 45: 85-97

Porter, S. C. and An. Z. S. 1995. Correlation between climate events in the north Atlantic and China during the last glaciation, *Nature,* 375: 305-308

Prata, A. J. 2009. Satellite detection of hazardous volcanic clouds and the risk to global air traffic. *Natural hazards*, 51; 303-324

Pyle, D. M. 1995. Assessment of the minimum volume of tephra fall deposits. Journal of Volcanology and Geothermal Research, 69: 379–382

Pyne-O'Donnell, S. 2011. The taphonomy of Last Glacial–Interglacial Transition (LGIT) distal volcanic ash in small Scottish lakes. *Boreas*, 40: 131-145

Pyne-O'Donnell, S. D., Hughes, P. D., Froese, D. G., Jensen, B. J., Kuehn, S. C., Mallon, G., Amesbury, M.J., Charman, D. J., Daley, T. J., Loader, N. J. and Mauquoy, D. 2012. High-precision ultra-distal Holocene tephrochronology in North America. *Quaternary Science Reviews*, 52: 6-11

Ramos, F. C., Heizler, M. T., Buettner, J. E., Gill, J. B., Wei, H. Q., Dimond, C. A. and Scott, S. R. 2016. U-series and 40Ar/39Ar ages of Holocene volcanic rocks at Changbaishan volcano, China. *Geology*, 44: 511-514

Rasmussen, S. O., Bigler, M., Blockley, S. P., Blunier, T., Buchardt, S. L., Clausen, H. B. Cvijanovic, I., Dahl-Jensen, D., Johnsen, S.J., Fischer, H. and Gkinis, V., 2014. A stratigraphic framework for abrupt climatic changes during the Last Glacial period based on three synchronized Greenland ice-core records: refining and extending the INTIMATE event stratigraphy. *Quaternary Science Reviews*, 106: 14-28.

Reimer, P.J. and Reimer, R.W., 2001. A marine reservoir correction database and on-line interface. *Radiocarbon*, 43: 461-463

Reimer, P. J., Bard, E., Bayliss, A., Beck, J. W., Blackwell, P. G., Ramsey, C. B., Buck, C. E., Cheng, H., Edwards, R. L., Friedrich, M. and Grootes, P.M. 2013. IntCal13 and Marine13 radiocarbon age calibration curves 0–50,000 years cal BP. *Radiocarbon*, 55: 1869-1887

Rohling, E. J., Grant, K., Bolshaw, M., Roberts, A. P., Siddall, M., Hemleben, C. and Kucera, M. 2009. Antarctic temperature and global sea level closely coupled over the past five glacial cycles. *Nature Geoscience*, 2: 500

Sagawa, T., Kuwae, M., Tsuruoka, K., Nakamura, Y., Ikehara, M. and Murayama, M. 2014. Solar forcing of centennial-scale East Asian winter monsoon variability in the mid-to late Holocene. *Earth and Planetary Science Letters*, 395: 124-135

Sagawa, T., Nagahashi, Y., Satoguchi, Y., Holbourn, A., Itaki, T., Gallagher, S.J., Saavedra-Pellitero, M., Ikehara, K., Irino, T. and Tada, R. 2018. Integrated tephrostratigraphy and stable isotope stratigraphy in the Japan Sea and East China Sea using IODP Sites U1426, U1427, and U1429, Expedition 346 Asian Monsoon. *Progress in Earth and Planetary Science*, 5: 18

Saito-Kato, M., Yamada, K., Staff, R. A., Nakagawa, T., Yonenobu, H., Haraguchi, T., Takemura, K. and Bronk Ramsey, C. 2013. An assessment of the magnitude of the AD 1586 Tensho tsunami inferred from Lake Suigetsu sediment cores. *Journal of Geography (Chigaku Zasshi)* 122: 493-501 (in Japanese, with English abstract)

Sakamoto, T., Ikehara, M., Uchida, M., Aoki, K., Shibata, Y., Kanamatsu, T., Harada, N., Iijima, K., Katsuki, K., Asahi, H. and Takahashi, K. 2006. Millennial-scale variations of sea-ice expansion in the southwestern part of the Okhotsk Sea during the past 120 kyr: Age model and ice-rafted debris in IMAGES Core MD01-2412. *Global and Planetary Change*, 53: 58-77

Sarna-Wojcicki, A. M., Morrison, S. D., Meyer, C. E. and Hillhouse, J. W. 1987. Correlation of upper Cenozoic tephra layers between sediments of the western United States and eastern Pacific Ocean and comparison with biostratigraphic and magnetostratigraphic age data. *Geological Society of America Bulletin*, 98: 207-223

Schindlbeck, J.C., Kutterolf, S., Straub, S.M., Andrews, G.D., Wang, K.L. and Mleneck-Vautravers, M.J. 2018. One Million Years tephra record at IODP Sites U1436 and U1437: Insights into explosive volcanism from the Japan and Izu arcs. *Island Arc*, 27: 12244

Schlolaut, G., Marshall, M. H., Brauer, A., Nakagawa, T., Lamb, H. F., Staff, R. A., Bronk Ramsey, C., Bryant, C. L., Brock, F., Kossler, A., Tarasov, P. E., Yokoyama, Y., Tada, R. and Haraguchi, T. 2012. An automated method for varve interpolation and its application to the Late Glacial chronology from Lake Suigetsu, Japan. *Quaternary Geochronology.* 13: 52-69

Schlolaut, G., Brauer, A., Marshall, M. H., Nakagawa, T., Staff, R. A., Ramsey, C. B., Lamb, H. F., Bryant, C.L., Naumann, R., Dulski, P., Brock, F., Yokoyama, Y., Tada, R., Haraguchi, T., Suigetsu 2006 project members. 2014. Event layers in the Japanese Lake Suigetsu 'SG06' sediment core: description, interpretation and climatic implications. *Quaternary Science Reviews.* 83: 157-170

Schlolaut, G., Brauer, A., Nakagawa, T., Lamb, H. F., Tyler, J. J., Staff, R. A., Marshall, M.H., Ramsey, C. B., Bryant, C. L. and Tarasov, P. E. 2017. Evidence for a bi-partition of the Younger Dryas Stadial in East Asia associated with inversed climate characteristics compared to Europe. *Scientific Reports*, 7: 44983.

Shanahan, T. M., McKay, N. P., Hughen, K. A., Overpeck, J. T., Otto-Bliesner, B., Heil, C. W., King, J., Scholz, C. A. and Peck, J. 2015. The time-transgressive termination of the African Humid Period. *Nature Geoscience*, 8: 140

Shane, P. 2000. Tephrochronology: a New Zealand case study. *Earth Science Reviews,* 49*:* 223-259

Shane, P. 2005. Towards a comprehensive distal andesitic tephrostratigraphic framework for New Zealand based on eruptions from Egmont volcano. *Journal of Quaternary Science*, 20: 45-57

Shane, P., Sikes, E. L. and Guilderson, T. P. 2006. Tephra beds in deep-sea cores off northern New Zealand: implications for the history of Taupo Volcanic Zone, Mayor Island and White Island volcanoes. *Journal of Volcanology and Geothermal Research*, 154: 276-290

Shane, P. and Smith, I. 2000. Geochemical fingerprinting of basaltic tephra deposits in the Auckland Volcanic Field. *New Zealand Journal of Geology and Geophysics*, 43: 569-577

Shiihara, M., Torii, M., Okuno, M., Domitsu, H., Nakamura, T., Kim, K., Moriwaki, H. and Oda, M. 2011. Revised stratigraphy of Holocene tephras on Ulleung Island, South Korea, and possible correlatives for the U-Oki tephra. *Quaternary International* 246: 222-232

Shimada, S. 2000. Eruption of the Amagi-Kawagodaira Volcano and paleo-environments in the late and latest Jomon periods around Izu Peninsula. The Quaternary Research (Daiyonki-Kenkyu) 39: 151-164 (in Japanese with English abstract)

Sigl, M., Winstrup, M., McConnell, J. R., Welten, K. C., Plunkett, G., Ludlow, F., Büntgen, U., Caffee, M., Chellman, N., Dahl-Jensen, D., Fischer, H., Kipfstuhl, S., Kostick, C., Maselli, O.J., Mekhaldi, F., Mulvaney, R., Muscheler, R., Pasteris, D.R., Pilcher, J. R., Salzer, M., Schüpbach, S., Steffensen, J. P., Vinther, B. M., Woodruff, T. E. 2015. Timing and climate forcing of volcanic eruptions for the past 2,500 years. *Nature*, 523: 543-549

Simkin, T., and Siebert, L., 2000. Earth's volcanoes and eruptions: An overview, *in* Sigurdsson, H.,et al., eds., Encyclopedia of Volcanoes: San Diego, Academic Press, 249-261

Singer, B. S., Guillou, H., Jicha, B. R., Laj, C., Kissel, C., Beard, B. L. and Johnson, C.M. 2009. 40Ar/39Ar, K–Ar and 230Th–238U dating of the Laschamp excursion: a radioisotopic tie-point for ice core and climate chronologies. *Earth and Planetary Science Letters*, 286: 80-88

Singer, B. S., Jicha, B. R., He, H. and Zhu, R. 2014. Geomagnetic field excursion recorded 17 ka at Tianchi volcano, China: New $^{40}Ar/^{39}Ar$ age and significance. *Geophysical Research Letters*, 41: 2794–2802

Shirai, M., Tada, R., Fujioka, K. 1997. Identification and chronostratigraphy of middle to upper Quaternary marker tephras occurring in the Anden Coast based on com- parison with ODP cores in the Sea of Japan. *Quaternary Research* 36: 183–196 (in Japanese).

Shitaoka, Y., Moriwaki, H., Akai, F., Nakamura, N., Miyoshi, M. and Yamamoto, J. 2016. Eruption age of Sakurajima-Satsuma tephra using thermoluminescence dating. *Bull Geol Environ Sci*, 18: 29-35.

Shoji, S., Masui, J., 1974. ^{14}C age of Kamuinupuri volcanic ash soils in Shibecha, Kawakami country, Hokkaido ^{14}C age of the Quaternary deposits in Japan (97). Earth Science (Chikyu Kagaku) 28: 101 (in Japanese)

Smith, D. G. W. and Westgate, J. A. 1968. Electron probe technique for characterising pyroclastic deposits. *Earth and Planetary Science Letters*, 5: 313-319

Smith, V. C., Shane, P. and Nairn, I. A. 2005. Trends in rhyolite geochemistry, mineralogy, and magma storage during the last 50 kyr at Okataina and Taupo volcanic

centres, Taupo Volcanic Zone, New Zealand. *Journal of Volcanology and Geothermal Research*, 148: 372-406

Smith, V. C., Pearce, N. J., Matthews, N. E., Westgate, J. A., Petraglia, M. D., Haslam, M., Lane, C. S., Korisettar, R. and Pal, J. N., 2011a. Geochemical fingerprinting of the widespread Toba tephra using biotite compositions. *Quaternary International*, 246: 97-104

Smith, V. C., Mark, D. F., Staff, R. A., Blockley, S. P. E., Bronk-Ramsey, C., Bryant, C. L., Nakagawa, T., Han, K. K., Weh, A., Takemura, K., Danhara, T. and Suigetsu 2006 Project Members. 2011b. Toward establishing precise Ar/Ar chronologies for Late Pleistocene palaeoclimate archives: an example from the Lake Suigetsu (Japan) sedimentary record, *Quaternary Science Reviews*, 30: 2845-2850

Smith, V. C., Staff, R. A., Blockley, S. P. E., Bronk Ramsey, C., Nakagawa, T., Mark, D. F., Takemura, K., Danhara, T. 2013. Identification and correlation of visible tephras in the Lake Suigetsu SG06 sedimentary archive, Japan: Chronostratigraphic markers for synchronising of east Asian/west Pacific Pacific palaeoclimatic records for 150ka, *Quaternary Science Reviews*, 61: 121-137

Smith, V. C., Isaia, R., Engwell, S. L. and Albert, P. G., 2016. Tephra dispersal during the Campanian Ignimbrite (Italy) eruption: implications for ultra-distal ash transport during the large caldera-forming eruption. *Bulletin of Volcanology,* 78: 45

Staff, R. A., Bronk Ramsey, C., Bryant, C. L., Brock, F., Payne, R. L., Schlolaut, G., Marshall, M. H., Brauer, A., Lamb, H. F., Tarasov, P., Yokoyama, Y., Haraguchi, T., Gotanda, K., Yonenobu, H., Nakagawa, T. and Suigetsu 2006 project members. 2011. New 14C determinations from Lake Suigetsu, Japan: 12,000 to 0 cal. bp, *Radiocarbon,* 53: 511-528

Staff, R. A., Schlolaut, G., Ramsey, C. B., Brock, F., Bryant, C. L., Kitagawa, H., Van der Plicht, J., Marshall, M. H., Brauer, A., Lamb, H. F. and Payne, R. L. 2013a. Integration of the old and new Lake Suigetsu (Japan) terrestrial radiocarbon calibration data sets. *Radiocarbon*, 55: 2049-2058

Staff, R. A., Nakagawa, T., Schlolaut, G., Marshall, M.H., Brauer, A., Lamb, H. F., Bronk Ramsey, C., Bryant, C. L., Brock, F., Kitagawa, H. and Plicht, J., 2013b. The multiple chronological techniques applied to the Lake Suigetsu SG06 sediment core, central Japan. *Boreas*, 42: 259-266

Steffensen, J. P., Andersen, K. K., Bigler, M., Clausen, H. B., Dahl-Jensen, D., Fischer, H., Goto-Azuma, K., Hansson, M., Johnsen, S. J., Jouzel, J. and Masson-Delmotte, V., 2008. High-resolution Greenland ice core data show abrupt climate change happens in few years. *Science*, 321*:* 680-684

Stone, R. 2010. Is China's riskiest volcano stirring or merely biding its time? *Science*, 329: 498-499

Sun, C., Plunkett, G., Liu, J., Zhao, H., Sigl, M., McConnell, J. R., Pilcher, J. R., Vinther, B., Steffensen, J. P. and Hall, V. 2014a. Ash from Changbaishan Millennium eruption recorded in Greenland ice: Implications for determining the eruptions timing and impact. *Geophysical Research Letters,* 41: 694-701

Sun, C., You, H., Liu, J., Li, X., Gao, J. and Chen, S. 2014b. Distribution, geochemistry and age of the Millennium eruptives of Changbaishan volcano, Northeast China—A review. *Frontiers of Earth Science*, 8*:* 216-230

Sun, C., You, H., He, H., Zhang, L., Gao, J., Guo, W., Chen, S., Mao, Q., Liu, Q., Chu, G. and Liu, J., 2015. New evidence for the presence of Changbaishan Millennium eruption ash in the Longgang volcanic field, Northeast China. *Gondwana Research*, 28: 52-60

Sun, C., Liu, J., You, H. and Nemeth, K. 2017. Tephrostratigraphy of Changbaishan volcano, northeast China, since the mid-Holocene. *Quaternary Science Reviews*, 177: 104-119

Sun, C., Wang, L., Plunkett, G., You, H., Zhu, Z., Zhang, L., Zhang, B., Chu, G. and Liu, J. 2018. Ash from the Changbaishan Qixiangzhan eruption: A new early Holocene marker horizon across East Asia. *Journal of Geophysical Research: Solid Earth*, 123: 6442-6450

Sugimura, A., 1960. Zonal arrangement of some geophysical and petrological features in Japan and its environs. *J. Fac. Sci., Univ. Tokyo, SecII*: 133-153.

Sugiuchi, Y. and Kukuoka, T. 2005. Tephrochronology of recent (~1200 YBP) Mt. Fuji eruption history using rhyolitic tephra derived from outside Mt. Fuji Volcano, *International Field Conference and Workshop on Tephrochronology and Volcanism: "Tephra Rush 2005", INQUA Sub-Commission for Tephrochronology and Volcanism (SCOTAV)*

Suzuki, T. 1996. Discharge rates of fallout tephra and frequency of plinian eruptions during the last 400,000 years in the southern Northeast Japan Arc. *Quaternary International*, 34: 79-87

Suzuki, Y., Tada, R., Yamada, K., Irino, T., Nagashima, K., Nakagawa, T. and Omori, T. 2016. Mass accumulation rate of detrital materials in Lake Suigetsu as a potential proxy for heavy precipitation: a comparison of the observational precipitation and sedimentary record. *Progress in Earth and Planetary Science*, 3: 5

Suzuki, T., Nishizawa, F., Ishimura, D. Ito, M., Maruyama, S., Danhara, T. and Hirata, T. 2017. Re-examination of identification and discrimination of Kozu-Tenjosan and Nijima-Mukaiyama tephras, Izu Islands, Japan. Japan Association for Quaternary Research, Programme and Abstracts, 47: 49 (In Japanese)

Swierczynski, T., Brauer, A., Lauterbach, S., Martín-Puertas, C., Dulski, P., von Grafenstein, U. and Rohr, C. 2012. A 1600 yr seasonally resolved record of decadal-scale flood variability from the Austrian Pre-Alps. *Geology*, 40: 1047-1050

Tada, R., 1999. Late Quaternary paleoceanography of the Japan Sea. *The Quaternary Research (Daiyonki-Kenkyu)*, 38: .216-222.

Tada, R. and Murray, R. W. 2016. Preface for the article collection "Land–Ocean Linkages under the Influence of the Asian Monsoon". *Progress in Earth and Planetary Science*, 3: 24

Tan, L., Cai, Y., An, Z., Yi, L., Zhang, H. and Qin, S. 2011. Climate patterns in north central China during the last 1800 yr and their possible driving force. *Climate of the Past*, 7: 685-692

Tani, S., Kitagawa, H., Hong, W., Park, J. H., Sung, K. and Park, G. 2013. Age determination of the Kawagodaira volcanic eruption in Japan by 14C wiggle-matching. *Radiocarbon*, 55: 748-52

Takada, H., 1989. Preliminary report on tephra from Aso central cones. Journal of the Kumamoto Geoscience Association 90: 8–11 (in Japanese)

Takemura, T., Kitagawa, H., Hayashida, A. and Yasuda, Y. 1994. Sedimentary facies and chronology of core samples from Lake Mikata, Lake Suigetsu and Kurota Lowland, Central Japan- Sedimentary environment in Mikara Lowland since the last interglacial time, *Journal of Geography,* 103: 233-242

Takemura, K., Iwabe, C., Hayashida, A., Danhara, T., Kitagawa, H., Haraguchi, T., Sato, T., Ishikawa, N. 2010. Stratigraphy of marker tephras and sediments during the past 50,000 years from multiple sites in Lake Biwa, Japan. *Quaternary Research* 49: 147–60 (In Japanese with English abstract)

Thomas, E. R., Wolff, E.W., Mulvaney, R., Steffensen, J.P., Johnsen, S. J., Arrowsmith, C., White, J. W., Vaughn, B. and Popp, T. 2007. The 8.2 ka event from Greenland ice cores. *Quaternary Science Reviews*, 26: 70-81

Tomlinson, E. L., Thordarson, T., Müller, W., Thirlwall, M. and Menzies, M. A., 2010. Microanalysis of tephra by LA-ICP-MS—strategies, advantages and limitations assessed using the Thorsmörk Ignimbrite (Southern Iceland). *Chemical Geology*, 279: 73-89

Tomlinson, E. L., Albert, P. G., Wulf, S., Brown, R. J., Smith, V. C., Keller, J., Orsi, G., Bourne, A. J. and Menzies, M. A. 2014. Age and geochemistry of tephra layers from Ischia, Italy: constraints from proximal-distal correlations with Lago Grande di Monticchio. *Journal of Volcanology and Geothermal Research*, 287: 22-39

Tomlinson, E. L., Smith, V. C., Albert, P. G., Aydar, E., Civetta, L., Cioni, R., Çubukçu, E., Gertisser, R., Isaia, R., Menzies, M. A. and Orsi, G. 2015. The major and trace

element glass compositions of the productive Mediterranean volcanic sources: tools for correlating distal tephra layers in and around Europe. *Quaternary Science Reviews*, 118: 48-66

Thorarinsson, S. 1944. Tefrokronologiska studier på Island: Þjórsárdalur och dess förödelse. *Geografiska annaler*, 26: 1-217

Turney, C.S., 1998. Extraction of rhyolitic component of Vedde microtephra from minerogenic lake sediments. *Journal of Paleolimnology*, 19: 199-206

Tsuchiya, M., Mannen, K., Kobayashi, M. and Fukuoka, T. 2017. Two types of glass shards within the Owakidani tephra group deposit, Hakone Volcano: Constraints on their sources and ages, 62: 23-30 (in Japanese with English abstract)

Tsuji, T., Ikeda, M., Furusawa, A., Nakamura, C., Ichikawa, K., Yanagida, M., Nishizaka, N., Ohnishi, K. and Ohno, Y. 2018. High resolution record of Quaternary explosive volcanism recorded in fluvio-lacustrine sediments of the Uwa basin, southwest Japan. *Quaternary International*, 471: 278-297

Tsukui, M., Saito, K. and Hayashi, K. 2006. Frequent and intensive eruptions in the 9th century, Izu Islands, Japan: Revision of volcano-stratigraphy based on tephras and historical document. *Bulletin of Volcanological Society of Japan*, 1: 327-338

Turney, C. S. M., Den Burg, K. V., Wastegård, S., Davies, S. M., Whitehouse, N. J., Pilcher, J. R. and Callaghan, C. 2006. North European last glacial–interglacial transition (LGIT; 15–9 ka) tephrochronology: extended limits and new events. *Journal of Quaternary Science: Published for the Quaternary Research Association*, 21: 335-345

Tyler, J., Kashiyama, Y., Ohkouchi, N., Ogawa, N., Yokoyama, Y., Chikaraishi, Y., Staff, R. A., Ikehara, M., Bronk Ramsey, C., Bryant, C. and Brock, F., 2010. Tracking aquatic change using chlorin-specific carbon and nitrogen isotopes: The last glacial-interglacial transition at Lake Suigetsu. *Geochemistry, Geophysics, Geosystems*, 11: 9

Uesawa, S., Nakagawa, M. and Umetsu, A. 2016. Explosive eruptive activity and temporal magmatic changes at Yotei Volcano during the last 50,000 years, southwest Hokkaido, Japan. *Journal of Volcanology and Geothermal Research*, 325: 27-44

Urabe, T., Kuriyama, M., Matsumoto, R. and Kumon, F. 2014 Late Quaternary climates of East Asia deduced from the total organic carbon contents of cored sediments (MD179-3304, 3312) off Joetsu City, Japan Sea. *Journal of Asian Earth Sciences*, 90: 209-217

Wada, K., Nakamura, M. and Okuno, M. 2001. Identification of source volcano from the chemical Ccompositions of glasses from the widespread ashes in the surface layers of Asahidake volcano, Central Hokkaido, Japan. *Reports of the Taisetsuzan Institute of Science*, 35: 9-18

Walker, M. J .C., Björck, S., Lowe, J. J., Cwynar, L. C., Johnsen, S., Knudsen, K. L., Wohlfarth, B. and Intimate Group. 1999. Isotopic 'events' in the GRIP ice core: a stratotype for the Late Pleistocene. *Quaternary Science Reviews*, 18: 1143-1150

Walker, M., Johnsen, S., Rasmussen, S. O., Popp, T., Steffensen, J. P., Gibbard, P., Hoek, W., Lowe, J., Andrews, J., Björck, S. and Cwynar, L. C. 2009. Formal definition and dating of the GSSP (Global Stratotype Section and Point) for the base of the Holocene using the Greenland NGRIP ice core, and selected auxiliary records. *Journal of Quaternary Science*, 24: 3-17

Wan, J. and Zheng, D. 2000. Several notable problems on dating of young volcanic rocks by FT method-illustrated by dating of Changbaishan volcanic rocks. Seismol. Geol. 22: 19-24 (In Chinese with English abstract)

Wang, Y. J., Cheng, H., Edwards, R. L., An, Z. S., Wu, J. Y., Shen, C. C. and Dorale, J. A. 2001. A high-resolution absolute-dated late Pleistocene monsoon record from Hulu Cave, China. *Science*, 294: 2345-2348

Wang, Y., Cheng, H., Edwards, R. L., He, Y., Kong, X., An, Z., Wu, J., Kelly, M. J., Dykoski, C.A. and Li, X. 2005. The Holocene Asian monsoon: links to solar changes and North Atlantic climate. *Science*, 308: 854-857

Wang, Y., Cheng, H., Edwards, R.L., Kong, X., Shao, X., Chen, S., Wu, J., Jiang, X., Wang, X. and An, Z. 2008. Millennial-and orbital-scale changes in the East Asian monsoon over the past 224,000 years. *Nature*, 451: 1090

Wanner, H., Beer, J., Bütikofer, J., Crowley, T.J., Cubasch, U., Flückiger, J., Goosse, H., Grosjean, M., Joos, F., Kaplan, J.O. and Küttel, M. 2008. Mid-to Late Holocene climate change: an overview. *Quaternary Science Reviews*, 27: 1791-1828

Watanabe, K. and Takada, H. 1990. Nonparallel relation between volcanic ash beds and "Kuro-boku" soil around the Aso caldera, Japan. Memoirs of the Faculty of Education, Kumamoto University, Natural Science 39, 21–27 (in Japanese with English abstract)

Wastegård, S., 2002. Early to middle Holocene silicic tephra horizons from the Katla volcanic system, Iceland: new results from the Faroe Islands. *Journal of Quaternary Science*, 17: 723-730

Wastegård, S., Rasmussen, T. L., Kuijpers, A., Nielsen, T. and van Weering, T. C. 2006. Composition and origin of ash zones from Marine Isotope Stages 3 and 2 in the North Atlantic. *Quaternary Science Reviews*, 25: 2409-2419

Watkins, N. D., Sparks, R. S. J., Sigurdsson, H., Huang, T. C., Federman, A., Carey, S. and Ninkovich, D. 1978. Volume and extent of the Minoan tephra from Santorini Volcano: new evidence from deep-sea sediment cores. *Nature,* 271: 122-6

Wei, H., Sparks, R. S. J., Liu, R., Fan, Q., Wang, Y., Hong, H., Zhang, H., Chen, H., Jiang, C., Dong, J. and Zheng, Y. 2003. Three active volcanoes in China and their hazards. *Journal of Asian Earth Sciences*, 21: 515-526

Wei, H., Wang, Y., Jin, J., Gao, L., Yun, S.H. and Jin, B. 2007. Timescale and evolution of the intracontinental Tianchi volcanic shield and ignimbrite-forming eruption, Changbaishan, Northeast China. *Lithos*, 96: 315-324

Wei, H., Liu, G. and Gill, J. 2013. Review of eruptive activity at Tianchi volcano, Changbaishan, northeast China: implications for possible future eruptions. *Bulletin of volcanology*, 75: 706

Wulf, S., Kraml, M., Brauer, A., Keller, J. and Negendank, J.F., 2004. Tephrochronology of the 100 ka lacustrine sediment record of Lago Grande di Monticchio (southern Italy). *Quaternary International*, 122: 7-30

Xu, J., Liu, G., Wu, J., Ming, Y., Wang, Q., Cui, D., Shangguan, Z., Pan, B., Lin, X. and Liu, J. 2012. Recent unrest of Changbaishan volcano, northeast China: A precursor of a future eruption? *Geophysical Research Letters*, 39: 16

Yang, L., Wang, F., Feng, H., Wu, L. and Shi, W. 2014. $^{40}Ar/^{39}Ar$ geochronology of Holocene volcanic activity at Changbaishan, Northeast China. *Quaternary Geochronology,* 21*:* 106 – 114

Yamada, K., Takemura, K., Kuwae, M., Ikehara, K. and Yamamoto, M. 2016. Basin filling related to the Philippine Sea Plate motion in Beppu Bay, southwest Japan. *Journal of Asian Earth Sciences*, 117: 13-22

Yamada, K., Nakagawa, T., Staff, R., Kitaba, I., Kitagawa, J., McLean, D., Smith, V., Haraguchi, Albert, P., Suzuki, Y., Gotanda, K., Hyodo, M. and Takemura, K. *in prep.* Stratigraphy and sedimentation rate changes of the Lake Suigetsu (SG14) core, Fukui Prefecture, central Japan

Yamamoto, T., Itho, J., Nakagawa, M., Hasegawa, T. and Kishimoto, H. 2010. 14C ages for the ejecta from Kutcharo and Mashu caldera, eastern Hokkaido, Japan, *Bull. Geol. Surv. Japan,* 61: 161- 170 (in Japanese with English abstract)

Yasuda, Y., Yamaguchi, T., Nakagawa, T., Fukusawa, K., Kitagawa, J. and Okamura, M. 2004. Environmental variability and human adaptation during the Lateglacial/Holocene transition in Japan with reference to pollen analysis of the SG4 core from Lake Suigetsu, 123: 11-19

Yun, S. 2018. Volcanological interpretation of historic record of ash cloud movement from Mt. Baegdu volcano on October 21, 1654. *Journal Petrol. Soc. Korea.* 27*:* 17 – 24

Zawalna-Geer, A., Lindsay, J.M., Davies, S., Augustinus, P. and Davies, S. 2016. Extracting a primary Holocene crytoptephra record from Pupuke maar sediments, Auckland, New Zealand. *Journal of Quaternary Science*, 31: 442-457

Zhang, P., Cheng, H., Edwards, R. L., Chen, F., Wang, Y., Yang, X., Liu, J., Tan, M., Wang, X., Liu, J. and An, C. 2008. A test of climate, sun, and culture relationships from an 1810-year Chinese cave record. *Science*, 322: 940-942

Zou, H., Fan, Q., Zhang, H. 2010. Rapid development of the great millennium eruption of Changbaishan (Tianchi) volcano, China/North Korea: evidence from U-Th zircon dating. *Lithos,* 119: 289-296

SUPPLEMENTARY MATERIAL: TABLE OF CONTENTS

Appendix A: Supplementary Material for Chapter 3 (Article 1)

A1: Major element glass analyses of SG06-0225 (B-Tm tephra). 255

A2: Major element glass analyses of the B-Tm type-site. 257

A3: Major element glass analyses of the MPI-DING reference glass. 258

Appendix B: Supplementary Material for Chapter 4 (Article 2)

B1: Major element glass analyses of the Holocene cryptotephra layers identified in the Lake Suigetsu sediments. 263

B2: Major element glass analyses of the MPI-DING reference glass. 275

B3: Average major element glass analyses of proximal samples Ma-b (Mashu), Iz-Kt (Kozushima), KGP (Kawagodaira), To-C (Towada). 290

Appendix C: Supplementary Material for Chapter 5 (Article 3)

C1: Major element glass analyses of the cryptotephra layers preserved in the Lake Suigetsu sediments between 50 to 30 ka. 291

C2: Major element glass analyses of the MPI-DING reference glass. 305

C3: Trace element glass compositions of cryptotephra layers preserved in the Lake Suigetsu sediments between 50 to 30 ka. 317

C4: Trace element glass compositions of BHVO-2G, LIP3 and the MPI-DING reference glasses (StHs6/80-G and ATHO-G). 321

C5: OxCal phase model used to generate constrained eruption ages of the A-Ot, A-Fm and A-Kn (Aira volcano) deposits. 327

Appendix D: Supplementary Material for Chapter 6 (Article 4)

D1: Major element glass analyses of SG14-3216 (U-Ym; Ulleungdo) and SG14-3380 (B-Sg-42; Changbaishan). 328

D2: Major element glass analyses of the MPI-DING reference glass. 331

D3: Trace element glass compositions of Changbaishan (SG14-0226, SG14-1058, SG14-3380) and Ulleungdo (SG14-1091 and SG14-3216) tephra layers. 338

D4: Trace element glass compositions of BHVO-2G, LIP3 and the MPI-DING reference glasses (StHs6/80-G and ATHO-G). 340

Appendix A: Supplementary Material for Article 1.

Table A1. Major element glass analyses of SG06-0226 (B-Tm tephra)

SG Label	Tephra	Run Date	SiO_2	TiO_2	Al_2O_3	FeOt	MnO	MgO	CaO	Na_2O	K_2O	P_2O_5	Cl	Analytical total
SG06-0226	B-Tm	14/09/15	72.86	0.20	9.95	3.81	-	-	0.17	5.56	4.29	-	0.44	97.35
SG06-0226	B-Tm	14/09/15	72.90	0.23	9.87	3.83	-	-	0.22	5.04	4.30	-	0.46	96.97
SG06-0226	B-Tm	14/09/15	73.35	0.25	10.10	4.12	-	-	0.23	5.19	4.33	-	0.47	98.03
SG06-0226	B-Tm	14/09/15	71.81	0.19	9.71	3.54	-	-	0.21	4.85	4.22	-	0.45	95.12
SG06-0226	B-Tm	14/09/15	73.45	0.17	10.02	3.91	-	-	0.21	5.23	4.37	-	0.50	97.99
SG06-0226	B-Tm	14/09/15	73.37	0.26	9.92	3.89	-	-	0.23	5.32	4.31	-	0.50	97.90
SG06-0226	B-Tm	14/09/15	72.30	0.28	10.03	3.84	-	-	0.28	5.02	4.20	-	0.49	96.56
SG06-0226	B-Tm	14/09/15	73.12	0.19	9.89	3.91	-	-	0.22	5.20	4.23	-	0.45	97.31
SG06-0226	B-Tm	14/09/15	69.67	0.18	9.47	3.89	-	-	0.22	4.98	4.18	-	0.48	93.22
SG06-0226	B-Tm	14/09/15	72.32	0.22	9.80	4.03	-	-	0.23	4.93	4.06	-	0.47	96.17
SG06-0226	B-Tm	14/09/15	71.95	0.16	9.77	4.03	-	-	0.20	4.99	4.23	-	0.44	95.89
SG06-0226	B-Tm	14/09/15	70.18	0.22	9.87	3.81	-	-	0.22	4.85	4.28	-	0.51	94.05
SG06-0226	B-Tm	14/09/15	71.48	0.24	9.77	4.08	-	-	0.20	5.02	4.01	-	0.50	95.38
SG06-0226	B-Tm	23/07/15	72.22	0.22	9.97	3.97	-	-	0.24	5.31	4.28	-	0.47	96.72
SG06-0226	B-Tm	23/07/15	72.92	0.23	10.05	3.87	-	-	0.22	5.37	4.10	-	0.47	97.36
SG06-0226	B-Tm	23/07/15	72.77	0.18	10.04	4.17	-	-	0.18	5.38	4.34	-	0.49	97.59
SG06-0226	B-Tm	23/07/15	72.13	0.23	9.93	4.12	-	-	0.22	5.14	4.12	-	0.49	96.42
SG06-0226	B-Tm	23/07/15	70.97	0.19	9.68	3.83	-	-	0.18	4.98	4.21	-	0.41	94.53
SG06-0226	B-Tm	23/07/15	72.32	0.28	9.96	4.06	0.17	-	0.19	5.25	4.14	-	0.50	96.88
SG06-0226	B-Tm	23/07/15	72.54	0.19	9.91	3.93	-	-	0.20	5.36	4.18	-	0.49	96.91

SG Label	Tephra	Run Date	SiO_2	TiO_2	Al_2O_3	FeOt	MnO	MgO	CaO	Na_2O	K_2O	P_2O_5	Cl	Analytical total
SG06-0226	B-Tm	23/07/15	72.72	0.18	10.23	3.79	-	-	0.20	5.18	4.25	-	0.46	97.15
SG06-0226	B-Tm	23/07/15	63.11	0.56	15.60	4.41	-	0.28	1.43	5.24	5.95	-	0.09	96.87
SG06-0226	B-Tm	23/07/15	72.22	0.18	9.85	3.85	-	-	0.18	5.28	4.10	-	0.48	96.33
SG06-0226	B-Tm	23/07/15	72.18	0.23	9.91	3.91	-	-	0.21	5.22	4.15	-	0.46	96.39
SG06-0226	B-Tm	23/07/15	73.09	0.17	9.92	3.92	-	-	0.22	5.31	4.21	-	0.49	97.38
SG06-0226	B-Tm	23/07/15	70.81	0.25	9.78	3.92	-	-	0.21	5.09	4.28	-	0.48	94.98
SG06-0226	B-Tm	23/07/15	70.82	0.26	9.90	3.54	-	-	0.22	5.34	4.21	-	0.53	94.93
SG06-0226	B-Tm	23/07/15	71.68	0.22	9.96	3.75	-	-	0.23	5.24	4.09	-	0.50	95.83
SG06-0226	B-Tm	23/07/15	69.99	0.17	9.56	3.75	-	-	0.21	5.09	4.19	-	0.48	93.48
SG06-0226	B-Tm	23/07/15	70.97	0.19	9.69	3.97	-	-	0.20	4.89	4.18	-	0.45	94.55
SG06-0226 (outlier)	-	23/07/15	72.85	0.17	11.86	1.15	-	-	1.05	3.53	3.07	-	0.11	94.00
SG06-0226 (outlier)	-	14/09/15	72.59	0.48	12.75	2.41	-	0.49	1.92	3.03	4.28	-	0.14	98.28

Table A2. Major element glass analyses of the B-Tm type-site (Tomakomai Port)

Reference Site	Tephra	Run Date	SiO_2	TiO_2	Al_2O_3	FeOt	MnO	MgO	CaO	Na_2O	K_2O	P_2O_5	Cl	Analytical total
Tomakomai Port	B-Tm	07/03/14	69.93	0.17	9.78	3.72	-	-	0.23	5.01	4.03	-	0.55	93.49
Tomakomai Port	B-Tm	07/03/14	72.95	0.21	10.32	3.80	-	-	0.25	4.65	4.17	-	0.50	96.91
Tomakomai Port	B-Tm	07/03/14	72.94	0.23	10.43	3.99	-	-	0.30	5.18	4.27	-	0.46	97.88
Tomakomai Port	B-Tm	07/03/14	74.68	0.18	10.45	4.06	-	-	0.27	4.95	4.23	-	0.47	99.41
Tomakomai Port	B-Tm	07/03/14	66.51	0.43	14.82	4.59	-	-	1.18	5.83	4.91	-	0.19	98.78
Tomakomai Port	B-Tm	07/03/14	73.31	0.20	10.29	3.79	-	-	0.24	5.17	4.28	-	0.49	97.90
Tomakomai Port	B-Tm	07/03/14	73.27	0.23	10.34	3.89	-	-	0.23	5.13	4.09	-	0.47	97.73
Tomakomai Port	B-Tm	07/03/14	72.78	0.25	10.62	3.76	-	-	0.29	4.96	4.52	-	0.51	97.82
Tomakomai Port	B-Tm	07/03/14	73.38	0.23	10.92	3.85	-	-	0.32	5.02	4.24	-	0.50	98.54
Tomakomai Port	B-Tm	07/03/14	72.34	0.19	10.20	3.83	-	-	0.22	4.92	4.06	-	0.53	96.35
Tomakomai Port	B-Tm	07/03/14	71.11	0.16	9.85	4.05	-	-	0.30	5.04	4.09	-	0.56	95.24
Tomakomai Port	B-Tm	07/03/14	73.33	0.28	10.78	4.10	-	-	0.28	5.28	4.40	-	0.47	98.96
Tomakomai Port	B-Tm	22/07/15	72.45	0.25	10.42	3.88	-	-	0.21	5.06	4.37	-	0.47	97.22
Tomakomai Port	B-Tm	22/07/15	69.77	0.23	9.87	3.85	-	-	0.28	4.97	4.13	-	0.52	93.69
Tomakomai Port	B-Tm	22/07/15	66.11	0.36	14.81	4.55	0.17	-	1.04	5.96	5.36	-	0.17	98.60
Tomakomai Port	B-Tm	22/07/15	66.10	0.29	12.91	4.03	-	-	0.56	5.49	4.84	-	0.29	94.54
Tomakomai Port	B-Tm	22/07/15	71.99	0.18	10.40	3.98	-	-	0.28	5.67	4.25	-	0.50	97.36
Tomakomai Port	B-Tm	22/07/15	72.54	0.18	10.05	3.92	-	-	0.25	4.91	4.27	-	0.47	96.71
Tomakomai Port	B-Tm	22/07/15	72.89	0.20	10.17	4.01	-	-	0.24	5.14	4.41	-	0.45	97.60
Tomakomai Port	B-Tm	22/07/15	72.31	0.19	10.03	3.83	-	-	0.23	5.34	4.36	-	0.50	96.90
Tomakomai Port	B-Tm	22/07/15	72.56	0.24	10.47	4.03	-	-	0.29	5.32	4.39	-	0.46	97.79

Table A3. Major element glass analyses of the MPI-DING reference glass (StHs6/80-G, GOR132-G and ATHO-G)

Reference Glass (Jochum et al., 2006)	Run Date	SiO_2	TiO_2	Al_2O_3	FeOt	MnO	MgO	CaO	Na_2O	K_2O	P_2O_5	Cl	Analytical total
StHs6/80-G_1	07/03/14	63.75	0.57	17.40	4.41	0.09	2.01	5.35	4.44	1.31	0.14	0.00	99.46
StHs6/80-G_2	07/03/14	63.62	0.74	17.62	4.39	0.05	1.95	5.37	4.39	1.29	0.13	0.00	99.54
StHs6/80-G_3	07/03/14	64.07	0.74	17.60	4.62	0.03	1.95	5.17	4.24	1.29	0.16	0.00	99.88
StHs6/80-G_4	07/03/14	63.68	0.65	17.60	4.16	0.05	1.91	5.45	4.24	1.26	0.15	0.00	99.15
StHs6/80-G_5	07/03/14	63.65	0.73	17.58	4.33	0.11	2.00	5.23	4.32	1.20	0.16	0.00	99.30
StHs6/80-G_6	07/03/14	63.93	0.70	17.52	4.26	0.07	1.92	5.32	4.52	1.27	0.15	0.03	99.68
StHs6/80-G_7	07/03/14	63.57	0.66	17.08	4.40	0.06	1.94	5.20	4.22	1.29	0.15	0.03	98.60
StHs6/80-G_8	07/03/14	62.60	0.66	17.13	4.29	0.14	2.01	5.28	4.58	1.25	0.16	0.02	98.11
StHs6/80-G_9	07/03/14	63.52	0.69	17.29	4.32	0.06	1.98	5.40	4.59	1.25	0.17	0.01	99.27
StHs6/80-G_1	22/07/15	63.80	0.77	17.69	4.27	0.03	1.99	5.37	4.39	1.37	0.14	0.01	99.83
StHs6/80-G_2	22/07/15	63.59	0.72	17.58	4.14	0.11	1.93	5.08	4.47	1.36	0.11	0.01	99.10
StHs6/80-G_3	22/07/15	63.62	0.65	17.52	4.31	0.09	1.95	5.18	4.56	1.29	0.15	0.00	99.32
StHs6/80-G_4	22/07/15	63.84	0.74	17.70	4.24	0.14	1.93	5.31	4.68	1.36	0.16	0.00	100.10
StHs6/80-G_5	22/07/15	63.37	0.66	17.76	4.65	0.06	1.87	5.22	4.76	1.37	0.16	0.00	99.88
StHs6/80-G_6	22/07/15	63.43	0.73	17.79	4.57	0.04	1.95	5.29	4.05	1.30	0.23	0.00	99.38
StHs6/80-G_7	22/07/15	63.45	0.72	17.37	4.57	0.05	1.97	5.23	4.62	1.31	0.17	0.01	99.47
StHs6/80-G_1	22/07/15	63.39	0.69	17.04	4.31	0.09	1.97	5.27	4.53	1.32	0.11	0.00	98.73
StHs6/80-G_3	22/07/15	63.42	0.72	17.64	4.43	0.04	1.92	5.27	4.49	1.32	0.10	0.00	99.36
StHs6/80-G_8	22/07/15	63.27	0.68	17.74	4.36	0.03	1.98	5.25	4.80	1.36	0.14	0.01	99.62
StHs6/80-G_4	22/07/15	63.79	0.69	17.70	4.34	0.10	1.90	5.33	4.69	1.32	0.14	0.01	100.00
StHs6/80-G_5	22/07/15	63.24	0.66	17.50	4.45	0.06	1.92	5.24	4.69	1.39	0.13	0.00	99.28
StHs6/80-G_7	22/07/15	63.53	0.67	17.69	4.62	0.18	1.91	5.21	4.70	1.26	0.14	0.00	99.89
StHs6/80-G_6	23/07/15	63.85	0.66	17.58	4.47	0.10	1.86	5.34	4.60	1.24	0.15	0.00	99.85

Reference Glass (Jochum et al., 2006)	Run Date	SiO_2	TiO_2	Al_2O_3	FeOt	MnO	MgO	CaO	Na_2O	K_2O	P_2O_5	Cl	Analytical total
StHS6/80-G_1	14/09/15	64.01	0.69	17.65	4.50	0.04	1.98	5.31	4.36	1.28	0.14	0.00	99.97
StHS6/80-G_2	14/09/15	63.94	0.72	17.47	4.17	0.10	1.96	5.28	4.23	1.35	0.11	0.01	99.32
StHS6/80-G_3	14/09/15	64.46	0.65	17.48	4.44	0.09	1.94	5.13	4.32	1.32	0.13	0.01	99.97
StHS6/80-G_4	14/09/15	63.47	0.71	17.44	4.43	0.08	1.94	5.12	4.43	1.35	0.12	0.00	99.10
StHS6/80-G_5	14/09/15	63.75	0.74	17.44	4.54	0.06	1.89	5.17	4.55	1.33	0.14	0.00	99.61
StHS6/80-G_6	14/09/15	63.87	0.77	17.63	4.36	0.09	1.99	5.20	4.29	1.30	0.13	0.01	99.65
StHS6/80-G_7	14/09/15	64.33	0.70	17.75	4.64	0.08	1.94	5.15	4.56	1.29	0.11	0.03	100.58
StHS6/80-G_8	14/09/15	63.31	0.71	17.32	4.51	0.10	2.00	5.18	4.14	1.29	0.13	0.01	98.71
StHS6/80-G_9	14/09/15	64.01	0.66	17.60	4.48	0.02	1.93	5.24	4.75	1.34	0.11	0.01	100.15
StHS6/80-G_10	14/09/15	63.32	0.66	17.32	4.36	0.11	1.88	5.01	4.20	1.33	0.14	0.00	98.34
StHS6/80-G_11	14/09/15	64.49	0.66	17.62	4.56	0.11	1.98	5.34	4.57	1.30	0.12	0.01	100.77
ATHO-G_1	07/03/14	75.59	0.20	12.25	3.19	0.07	0.08	1.70	3.91	2.72	0.04	0.04	99.78
ATHO-G_2	07/03/14	75.17	0.23	12.20	3.04	0.17	0.09	1.65	3.73	2.63	0.04	0.05	99.00
ATHO-G_3	07/03/14	75.45	0.26	12.16	3.20	0.12	0.08	1.75	4.12	2.63	0.01	0.03	99.80
ATHO-G_4	07/03/14	75.19	0.22	12.01	3.15	0.05	0.10	1.74	4.15	2.64	0.03	0.05	99.34
ATHO-G_5	07/03/14	75.54	0.27	12.01	3.22	0.15	0.09	1.64	4.09	2.67	0.00	0.04	99.71
ATHO-G_6	07/03/14	74.84	0.29	12.00	3.23	0.01	0.10	1.72	4.12	2.62	0.04	0.03	99.01
ATHO-G_7	07/03/14	75.08	0.26	11.81	3.12	0.07	0.10	1.64	4.00	2.65	0.04	0.04	98.82
ATHO-G_8	07/03/14	75.58	0.29	12.10	3.24	0.11	0.10	1.66	3.92	2.77	0.05	0.07	99.90
ATHO-G_9	07/03/14	75.74	0.26	12.20	3.35	0.04	0.09	1.69	4.11	2.66	0.05	0.04	100.23
ATH01-G_1	22/07/15	74.87	0.26	12.17	3.51	0.03	0.10	1.72	3.90	2.78	0.00	0.01	99.35
ATH01-G_2	22/07/15	74.94	0.32	12.16	3.31	0.12	0.08	1.73	4.22	2.75	0.04	0.02	99.69
ATH01-G_3	22/07/15	75.24	0.25	12.22	3.25	0.06	0.05	1.71	4.41	2.86	0.04	0.04	100.13

Reference Glass (Jochum et al., 2006)	Run Date	SiO_2	TiO_2	Al_2O_3	FeOt	MnO	MgO	CaO	Na_2O	K_2O	P_2O_5	Cl	Analytical total
ATH01-G_4	22/07/15	74.65	0.26	12.15	3.35	0.15	0.06	1.64	4.17	2.79	0.02	0.03	99.26
ATH01-G_5	22/07/15	75.30	0.26	12.10	3.36	0.01	0.12	1.66	4.13	2.66	0.03	0.04	99.68
ATH01-G_6	22/07/15	75.16	0.24	12.05	3.45	0.11	0.08	1.66	4.48	2.72	0.00	0.05	99.99
ATH01-G_1	22/07/15	74.16	0.24	12.17	3.32	0.11	0.09	1.72	4.09	2.75	0.03	0.03	98.71
ATH01-G_7	22/07/15	74.59	0.23	12.33	3.21	0.11	0.07	1.64	4.05	2.70	0.00	0.04	98.96
ATH01-G_2	22/07/15	74.83	0.21	12.25	3.30	0.16	0.09	1.78	4.04	2.71	0.00	0.05	99.42
ATH01-G_4	22/07/15	74.82	0.30	12.13	3.09	0.12	0.04	1.66	4.32	2.76	0.00	0.04	99.27
ATH01-G_5	22/07/15	75.06	0.24	12.19	3.26	0.15	0.08	1.66	4.15	2.73	0.00	0.04	99.56
ATH01-G_6	22/07/15	75.20	0.20	12.11	3.24	0.07	0.10	1.69	4.01	2.72	0.08	0.02	99.43
ATHO-G_2	14/09/15	74.71	0.25	12.06	3.22	0.04	0.09	1.66	4.31	2.70	0.04	0.04	99.13
ATHO-G_3	14/09/15	75.08	0.26	12.06	3.18	0.12	0.11	1.62	4.19	2.77	0.02	0.03	99.45
ATHO-G_4	14/09/15	75.44	0.22	12.14	3.21	0.08	0.11	1.66	4.24	2.65	0.07	0.02	99.83
ATHO-G_5	14/09/15	74.90	0.23	12.07	3.25	0.12	0.14	1.70	3.94	2.76	0.03	0.04	99.17
ATHO-G_7	14/09/15	74.88	0.23	12.20	3.35	0.11	0.12	1.62	3.94	2.75	0.06	0.05	99.30
ATHO-G_8	14/09/15	74.79	0.23	12.21	3.33	0.15	0.10	1.65	3.92	2.81	0.02	0.04	99.26
ATHO-G_10	14/09/15	75.17	0.19	12.14	3.28	0.11	0.12	1.62	4.11	2.83	0.02	0.05	99.63
ATHO-G_12	14/09/15	74.57	0.26	12.26	3.25	0.05	0.05	1.61	4.21	2.72	0.03	0.04	99.06
GOR132-G_1	07/03/14	45.77	0.28	10.79	9.87	0.17	22.11	8.71	0.80	0.04	0.01	0.00	98.54
GOR132-G_2	07/03/14	45.36	0.29	10.83	10.19	0.10	22.23	8.42	0.70	0.06	0.02	0.00	98.20
GOR132-G_3	07/03/14	46.13	0.31	10.92	10.45	0.18	22.22	8.44	0.70	0.03	0.02	0.00	99.38
GOR132-G_4	07/03/14	46.10	0.30	11.20	9.98	0.13	22.40	8.59	0.76	0.03	0.09	0.01	99.59
GOR132-G_5	07/03/14	45.52	0.29	10.80	10.27	0.15	22.15	8.51	0.72	0.02	0.01	0.00	98.43
GOR132-G_6	07/03/14	45.95	0.29	11.02	10.09	0.10	22.55	8.74	0.79	0.02	0.05	0.00	99.59

Reference Glass (Jochum et al., 2006)	Run Date	SiO_2	TiO_2	Al_2O_3	FeOt	MnO	MgO	CaO	Na_2O	K_2O	P_2O_5	Cl	Analytical total
GOR132-G_7	07/03/14	45.68	0.31	10.76	10.27	0.23	22.38	8.39	0.78	0.02	0.03	0.00	98.86
GOR132-G_8	07/03/14	45.59	0.28	10.89	10.22	0.18	22.37	8.55	0.89	0.05	0.04	0.03	99.08
GOR132-G_9	07/03/14	45.15	0.27	10.60	9.56	0.18	22.11	8.45	0.70	0.02	0.04	0.00	97.09
GOR132-G_1	22/07/15	45.95	0.33	10.70	10.70	0.14	22.27	8.50	0.79	0.03	0.08	0.01	99.51
GOR132-G_2	22/07/15	45.69	0.34	10.98	10.27	0.11	22.07	8.47	0.70	0.02	0.02	0.01	98.67
GOR132-G_3	22/07/15	45.55	0.28	10.75	10.20	0.12	22.13	8.71	0.80	0.03	0.08	0.02	98.67
GOR132-G_4	22/07/15	45.37	0.30	10.83	10.09	0.18	22.21	8.73	0.86	0.05	0.04	0.01	98.67
GOR132-G_5	22/07/15	45.53	0.31	10.95	10.62	0.16	22.09	8.47	0.91	0.04	0.13	0.00	99.21
GOR132-G_6	22/07/15	45.49	0.34	10.81	10.49	0.17	21.83	8.57	0.92	0.07	0.04	0.00	98.73
GOR132-G_7	22/07/15	45.55	0.33	10.78	10.19	0.17	21.75	8.64	0.92	0.04	0.03	0.01	98.41
GOR132-G_1	23/07/15	45.57	0.36	10.92	10.51	0.10	22.23	8.54	0.75	0.02	0.07	0.01	99.06
GOR132-G_3	23/07/15	45.38	0.32	10.68	10.47	0.23	22.10	8.65	0.62	0.02	0.07	0.00	98.54
GOR132-G_2	23/07/15	45.76	0.32	10.68	10.22	0.15	22.04	8.60	0.87	0.02	0.00	0.00	98.66
GOR132-G_4	23/07/15	45.37	0.30	10.93	10.43	0.07	22.31	8.68	0.82	0.03	0.01	0.00	98.96
GOR132-G_5	23/07/15	45.43	0.32	10.85	10.07	0.12	22.31	8.38	0.87	0.04	0.06	0.01	98.45
GOR132-G_6	23/07/15	45.25	0.32	10.84	10.01	0.20	22.35	8.51	0.84	0.05	0.00	0.00	98.37
GOR132-G_1	14/09/15	45.57	0.31	10.82	10.48	0.17	22.30	8.36	0.72	0.04	0.05	0.00	98.80
GOR132-G_2	14/09/15	46.09	0.30	10.97	10.50	0.20	22.59	8.24	0.71	0.07	0.05	0.00	99.71
GOR132-G_3	14/09/15	45.44	0.30	10.83	10.57	0.09	21.99	8.31	0.70	0.03	0.03	0.01	98.28
GOR132-G_4	14/09/15	45.88	0.29	10.97	10.60	0.16	22.01	8.30	0.69	0.05	0.07	0.01	99.02
GOR132-G_5	14/09/15	45.63	0.33	10.85	10.65	0.15	22.42	8.11	0.86	0.03	0.08	0.01	99.12
GOR132-G_6	14/09/15	45.89	0.34	11.01	10.35	0.14	22.17	8.23	0.87	0.05	0.06	0.01	99.13
GOR132-G_7	14/09/15	45.31	0.28	10.78	10.45	0.06	21.91	8.31	0.78	0.03	0.02	0.00	97.92
GOR132-G_8	14/09/15	45.33	0.29	10.89	10.48	0.16	22.07	8.41	0.89	0.03	0.02	0.01	98.57

Reference Glass (Jochum et al., 2006)	Run Date	SiO_2	TiO_2	Al_2O_3	FeOt	MnO	MgO	CaO	Na_2O	K_2O	P_2O_5	Cl	Analytical total
GOR132-G_9	14/09/15	45.73	0.26	10.92	10.27	0.11	21.90	8.26	0.80	0.00	0.06	0.00	98.30
GOR132-G_10	14/09/15	45.84	0.29	10.99	10.42	0.15	22.33	8.38	0.82	0.02	0.01	0.00	99.26
GOR132-G_11	14/09/15	46.13	0.36	11.05	10.12	0.19	22.27	8.31	0.89	0.02	0.04	0.00	99.36
GOR132-G_12	14/09/15	45.46	0.28	10.86	10.13	0.15	22.01	8.36	0.83	0.02	0.07	0.02	98.18

Appendix B: Supplementary Material for Article 2.

Table B1. Major element glass analyses of the Holocene cryptotephra layers identified in the Lake Suigetsu sediments

SG Label	Tephra	Run Date	SiO_2	TiO_2	Al_2O_3	FeOt	MnO	MgO	CaO	Na_2O	K_2O	P_2O_5	Cl	Analytical total
SG14-0024	-	28/04/2017	66.45	0.75	13.78	4.37	0.12	0.98	3.28	3.84	2.44	0.23	0.14	96.40
SG14-0024	-	28/04/2017	63.77	0.79	13.66	3.81	0.11	1.06	3.42	3.75	2.37	0.18	0.17	93.09
SG14-0024	-	28/04/2017	67.29	0.80	13.70	3.97	0.17	0.96	3.25	4.05	2.40	0.24	0.11	96.94
SG14-0024	-	28/04/2017	67.76	0.75	14.15	4.10	0.13	0.98	3.29	3.34	2.56	0.24	0.08	97.38
SG14-0024	-	28/04/2017	68.28	0.80	13.66	3.94	0.08	0.73	3.05	4.23	2.56	0.23	0.12	97.68
SG14-0024	-	28/04/2017	65.21	0.75	13.40	3.69	0.12	0.84	2.97	3.87	2.41	0.22	0.15	93.64
N.B high number of outliers due to surrounding background														
SG14-0024 Outlier	-	11/08/2016	75.41	0.15	12.07	1.17	0.10	0.13	1.09	3.64	2.99	0.00	0.12	96.87
SG14-0024 Outlier	-	11/08/2016	74.73	0.11	12.16	1.16	0.06	0.13	1.08	3.54	3.14	0.05	0.14	96.30
SG14-0024 Outlier	-	11/08/2016	74.62	0.14	11.92	1.14	0.09	0.13	1.06	3.27	3.08	0.00	0.13	95.58
SG14-0024 Outlier	-	11/08/2016	75.28	0.17	12.16	1.12	0.07	0.13	1.09	3.78	3.08	0.03	0.14	97.05
SG14-0024 Outlier	-	11/08/2016	75.44	0.16	12.15	1.21	0.07	0.11	1.07	3.67	3.22	0.00	0.12	97.23
SG14-0024 Outlier	-	11/08/2016	75.73	0.13	12.26	1.14	0.02	0.11	1.06	3.60	3.10	0.02	0.09	97.26
SG14-0024 Outlier	-	11/08/2016	73.67	0.54	13.06	2.66	0.10	0.42	1.93	3.84	2.65	0.06	0.15	99.08
SG14-0024 Outlier	-	11/08/2016	76.10	0.13	12.23	1.11	0.07	0.13	1.15	3.74	3.38	0.04	0.13	98.22
SG14-0024 Outlier	-	11/08/2016	72.34	0.13	11.45	1.04	0.09	0.16	1.07	3.51	3.00	0.05	0.18	93.02
SG14-0024 Outlier	-	11/08/2016	75.27	0.15	12.01	1.22	0.00	0.13	1.11	3.37	3.36	0.04	0.13	96.78
SG14-0024 Outlier	-	11/08/2016	74.62	0.18	12.06	1.10	0.04	0.11	1.02	3.52	3.37	0.02	0.08	96.14
SG14-0024 Outlier	-	11/08/2016	74.69	0.15	11.94	1.16	0.01	0.12	0.99	3.39	3.23	0.02	0.12	95.82
SG14-0024 Outlier	-	11/08/2016	72.17	0.17	11.52	1.14	0.04	0.12	1.04	3.24	3.23	0.05	0.18	92.89

SG Label	Tephra	Run Date	SiO_2	TiO_2	Al_2O_3	FeOt	MnO	MgO	CaO	Na_2O	K_2O	P_2O_5	Cl	Analytical total
SG14-0024 Outlier	-	11/08/2016	74.16	0.08	11.71	1.04	0.01	0.14	1.05	3.68	3.03	0.00	0.10	95.01
SG14-0024 Outlier	-	11/08/2016	75.49	0.11	11.96	1.05	0.02	0.13	1.09	2.74	3.19	0.01	0.13	95.91
SG14-0024 Outlier	-	11/08/2016	73.11	0.55	12.81	2.63	0.12	0.40	1.97	3.50	2.81	0.06	0.13	98.10
SG14-0024 Outlier	-	11/08/2016	75.31	0.12	12.12	1.21	0.07	0.15	1.03	3.56	3.34	0.03	0.12	97.07
SG14-0024 Outlier	-	11/08/2016	74.84	0.14	11.86	1.19	0.04	0.12	1.07	3.62	3.16	0.02	0.09	96.16
SG14-0024 Outlier	-	11/08/2016	74.07	0.48	13.19	2.29	0.02	0.49	2.00	4.03	2.80	0.07	0.13	99.58
SG14-0024 Outlier	-	11/08/2016	74.13	0.11	11.78	1.17	0.02	0.11	1.07	3.66	3.34	0.00	0.13	95.52
SG14-0024 Outlier	-	11/08/2016	73.48	0.60	12.99	2.24	0.05	0.40	1.89	4.07	2.71	0.08	0.15	98.67
SG14-0024 Outlier	-	28/04/2017	72.40	0.15	11.49	1.18	0.09	0.14	1.15	3.49	3.04	0.02	0.11	93.25
SG14-0024 Outlier	-	28/04/2017	73.16	0.08	11.63	1.10	0.07	0.13	1.06	3.46	3.28	0.00	0.11	94.09
SG14-0024 Outlier	-	28/04/2017	72.28	0.07	11.57	0.87	0.03	0.12	1.01	3.26	3.26	0.00	0.14	92.60
SG14-0024 Outlier	-	28/04/2017	72.22	0.26	13.92	1.00	0.06	0.36	1.15	3.41	4.44	0.02	0.17	97.01
SG14-0024 Outlier	-	28/04/2017	72.02	0.53	12.59	2.22	0.06	0.47	1.90	1.83	2.75	0.10	0.18	94.64
SG14-0221	Ma-b	04/02/2016	71.07	0.57	12.34	2.99	0.13	0.72	3.13	4.40	0.75	0.11	0.12	96.32
SG14-0221	Ma-b	04/02/2016	70.69	0.66	12.48	3.18	0.14	0.85	3.30	4.54	0.71	0.14	0.13	96.81
SG14-0221	Ma-b	04/02/2016	71.71	0.63	12.74	3.05	0.21	0.76	3.12	4.36	0.76	0.15	0.11	97.61
SG14-0221	Ma-b	04/02/2016	70.42	0.66	12.42	2.98	0.17	0.79	3.25	4.23	0.76	0.08	0.12	95.88
SG14-0221	Ma-b	04/02/2016	71.01	0.61	12.52	3.30	0.16	0.79	3.17	4.11	0.76	0.07	0.15	96.66
SG14-0221	Ma-b	04/02/2016	68.42	0.61	12.06	2.91	0.19	0.68	3.17	4.25	0.69	0.06	0.21	93.25
SG14-0221	Ma-b	04/02/2016	69.75	0.57	12.35	2.86	0.10	0.68	2.95	4.38	0.84	0.11	0.15	94.74
SG14-0221	Ma-b	12/08/2016	68.71	0.53	12.20	2.85	0.15	0.70	2.94	4.10	0.70	0.10	0.19	93.17
SG14-0221	Ma-b	12/08/2016	71.73	0.60	12.80	2.95	0.17	0.74	2.99	4.18	0.73	0.17	0.15	97.21
SG14-0221	Ma-b	12/08/2016	72.89	0.65	13.01	3.17	0.23	0.80	3.06	4.40	0.74	0.12	0.11	99.18

SG Label	Tephra	Run Date	SiO_2	TiO_2	Al_2O_3	FeOt	MnO	MgO	CaO	Na_2O	K_2O	P_2O_5	Cl	Analytical total
SG14-0221	Ma-b	12/08/2016	73.47	0.65	12.98	3.10	0.15	0.72	3.18	4.54	0.72	0.16	0.07	99.74
SG14-0221	Ma-b	12/08/2016	72.89	0.60	13.00	2.99	0.23	0.76	3.20	4.64	0.73	0.13	0.13	99.30
SG14-0221	Ma-b	12/08/2016	69.82	0.59	14.21	2.98	0.15	0.75	3.37	4.17	0.73	0.17	0.13	97.08
SG14-0221	Ma-b	28/04/2017	72.64	0.58	13.06	2.93	0.15	0.73	3.09	4.26	0.80	0.14	0.10	98.46
SG14-0221 Outlier	-	12/08/2016	73.01	0.62	13.00	3.36	0.10	0.72	3.12	1.71	0.83	0.09	0.10	96.66
SG14-0221 Outlier	-	04/02/2016	72.30	0.11	11.48	1.24	0.07	0.13	1.04	3.55	3.19	0.00	0.11	93.22
SG14-0221 Outlier	-	04/02/2016	72.60	0.11	11.48	1.12	0.08	0.13	0.95	3.73	3.09	0.06	0.15	93.50
SG14-0221 Outlier	-	04/02/2016	70.35	0.24	9.43	3.81	0.09	0.01	0.18	5.32	4.26	0.02	0.52	94.22
SG14-0221 Outlier	-	12/08/2016	75.51	0.40	12.41	2.01	0.18	0.50	2.41	4.49	0.88	0.07	0.11	98.98
SG14-0239	-	08/06/2015	75.57	0.09	12.50	0.53	0.07	0.05	0.37	4.00	3.66	0.06	0.13	97.02
SG14-0239	-	08/06/2015	77.37	0.12	13.23	0.17	0.01	0.09	0.92	4.64	3.19	0.05	0.05	99.85
SG14-0239	-	08/06/2015	76.50	0.09	12.50	0.57	0.01	0.05	0.31	4.14	3.92	0.00	0.11	98.22
SG14-0239	-	08/06/2015	74.91	0.08	12.20	0.55	0.01	0.08	0.36	4.10	3.82	0.00	0.13	96.24
SG14-0239	-	08/06/2015	75.32	0.05	12.43	0.47	0.15	0.02	0.31	4.09	3.92	0.00	0.15	96.91
SG14-0239	-	08/06/2015	76.45	0.12	12.45	0.41	0.08	0.06	0.31	4.21	3.60	0.01	0.16	97.85
SG14-0239	-	08/06/2015	75.34	0.04	12.42	0.51	0.10	0.09	0.36	4.06	3.73	0.04	0.17	96.85
SG14-0239	-	08/06/2015	75.35	0.01	12.36	0.56	0.03	0.00	0.32	4.08	3.95	0.06	0.15	96.87
SG14-0239	-	08/06/2015	75.91	0.07	12.46	0.58	0.10	0.00	0.33	4.03	3.90	0.02	0.14	97.55
SG14-0239	-	08/06/2015	75.80	0.06	12.37	0.54	0.10	0.10	0.36	3.41	3.90	0.03	0.14	96.82
SG14-0239	-	08/06/2015	75.43	0.10	12.31	0.59	0.00	0.08	0.33	4.27	3.79	0.01	0.19	97.09
SG14-0239	-	08/06/2015	74.36	0.09	12.28	0.53	0.10	0.00	0.32	4.01	3.79	0.00	0.16	95.65
SG14-0239	-	08/06/2015	74.69	0.10	11.79	0.52	0.09	0.12	0.61	3.55	3.59	0.04	0.19	95.31
SG14-0239	-	08/06/2015	76.09	0.06	12.53	0.58	0.09	0.01	0.37	4.11	3.70	0.01	0.12	97.66

SG Label	Tephra	Run Date	SiO_2	TiO_2	Al_2O_3	FeOt	MnO	MgO	CaO	Na_2O	K_2O	P_2O_5	Cl	Analytical total
SG14-0239	-	08/06/2015	76.05	0.07	12.56	0.54	0.07	0.09	0.32	4.16	3.88	0.03	0.13	97.90
SG14-0239	-	08/06/2015	73.67	0.10	12.09	0.62	0.06	0.01	0.35	3.93	3.78	0.00	0.22	94.84
SG14-0239	-	08/06/2015	76.29	0.07	12.31	0.57	0.10	0.07	0.32	3.91	3.98	0.04	0.13	97.80
SG14-0239	-	08/06/2015	75.10	0.10	12.22	0.47	0.11	0.03	0.35	3.91	3.78	0.04	0.15	96.25
SG14-0239	-	08/06/2015	76.35	0.02	12.42	0.57	0.08	0.07	0.35	4.11	3.95	0.03	0.13	98.08
SG14-0239	-	08/06/2015	74.18	0.06	12.17	0.59	0.05	0.05	0.33	3.89	3.86	0.04	0.13	95.35
SG14-0433	U-1?	11/08/2016	61.31	0.81	16.58	5.52	0.21	1.11	2.59	6.15	4.45	0.32	0.25	99.30
SG14-0433	U-1?	11/08/2016	59.07	0.76	15.95	5.38	0.27	0.96	2.47	5.89	4.49	0.33	0.23	95.81
SG14-0433	U-1?	11/08/2016	59.36	0.69	15.96	5.59	0.15	0.99	2.39	6.12	4.48	0.30	0.24	96.27
SG14-0433	U-1?	11/08/2016	61.11	0.86	16.44	5.72	0.18	1.12	2.51	5.96	4.56	0.37	0.21	99.05
SG14-0433	U-1?	11/08/2016	58.24	0.75	15.71	5.09	0.26	1.07	2.48	5.54	4.25	0.42	0.27	94.05
SG14-0433	U-1?	11/08/2016	60.04	0.73	16.23	5.32	0.28	1.06	2.40	5.98	4.42	0.37	0.22	97.05
SG14-0433	U-1?	11/08/2016	59.75	0.80	16.21	5.73	0.22	1.13	2.64	5.68	4.38	0.36	0.20	97.10
SG14-0433	U-1?	11/08/2016	59.63	0.75	15.98	5.40	0.22	1.00	2.42	5.67	4.57	0.33	0.21	96.17
SG14-0433 Outlier	-	11/08/2016	73.86	0.53	13.03	2.39	0.03	0.43	1.95	4.20	2.99	0.07	0.13	99.61
SG14-0490	KGP	20/05/2016	72.55	0.19	11.81	1.15	0.00	0.29	1.53	3.62	2.60	0.04	0.12	93.90
SG14-0490	KGP	20/05/2016	73.17	0.21	11.90	1.06	0.02	0.26	1.55	3.86	2.73	0.04	0.11	94.92
SG14-0490	KGP	20/05/2016	73.83	0.19	11.84	0.93	0.08	0.25	1.37	3.79	2.70	0.06	0.15	95.20
SG14-0490	KGP	20/05/2016	73.38	0.21	12.09	1.24	0.02	0.25	1.63	3.82	2.57	0.02	0.13	95.36
SG14-0490	KGP	20/05/2016	73.42	0.25	12.07	1.12	0.05	0.31	1.52	3.80	2.76	0.02	0.15	95.46
SG14-0490	KGP	20/05/2016	73.77	0.26	11.99	1.15	0.00	0.26	1.56	3.71	2.65	0.02	0.11	95.50

SG Label	Tephra	Run Date	SiO_2	TiO_2	Al_2O_3	FeOt	MnO	MgO	CaO	Na_2O	K_2O	P_2O_5	Cl	Analytical total
SG14-0490	KGP	20/05/2016	74.01	0.22	12.02	1.12	0.03	0.24	1.53	3.58	2.58	0.08	0.12	95.53
SG14-0490	KGP	20/05/2016	73.89	0.25	11.98	1.32	0.10	0.26	1.54	3.72	2.54	0.04	0.13	95.78
SG14-0490	KGP	20/05/2016	73.73	0.27	12.02	1.20	0.09	0.23	1.57	3.72	2.81	0.06	0.11	95.82
SG14-0490	KGP	20/05/2016	73.96	0.28	12.06	1.25	0.02	0.30	1.59	3.80	2.57	0.03	0.15	96.00
SG14-0490	KGP	20/05/2016	74.23	0.26	12.07	1.09	0.00	0.30	1.58	3.84	2.57	0.07	0.11	96.13
SG14-0490	KGP	20/05/2016	74.42	0.19	12.11	1.03	0.08	0.28	1.46	3.74	2.80	0.04	0.09	96.25
SG14-0490	KGP	20/05/2016	73.74	0.27	12.38	1.13	0.04	0.33	1.77	3.93	2.68	0.04	0.11	96.41
SG14-0490	KGP	20/05/2016	74.34	0.30	12.07	1.31	0.03	0.38	1.52	3.64	2.75	0.03	0.08	96.45
SG14-0490	KGP	20/05/2016	74.69	0.25	11.98	1.32	0.10	0.32	1.39	3.71	2.73	0.06	0.11	96.66
SG14-0490	KGP	20/05/2016	74.71	0.20	12.23	1.06	0.10	0.28	1.51	3.82	2.64	0.06	0.07	96.68
SG14-0490	KGP	20/05/2016	74.51	0.29	12.20	1.08	0.10	0.27	1.62	3.84	2.72	0.05	0.09	96.76
SG14-0490	KGP	20/05/2016	74.94	0.29	12.24	1.17	0.00	0.27	1.55	3.73	2.73	0.07	0.09	97.08
SG14-0490	KGP	20/05/2016	74.99	0.23	12.16	1.16	0.08	0.31	1.53	3.82	2.79	0.07	0.14	97.25
SG14-0490 Outlier	-	20/05/2016	69.39	0.18	15.47	0.75	0.04	0.14	4.21	4.00	1.76	0.01	0.08	96.02
SG14-0704	-	20/05/2016	66.87	0.55	12.44	4.04	0.16	0.57	2.42	3.59	2.62	0.13	0.11	93.50
SG14-0704	-	20/05/2016	68.65	0.56	12.75	2.77	0.12	0.61	2.30	3.74	2.69	0.11	0.13	94.42
SG14-0704	-	20/05/2016	68.37	0.59	12.93	3.01	0.07	0.63	2.52	3.90	2.76	0.10	0.11	94.97
SG14-0704	-	20/05/2016	69.32	0.52	12.88	3.32	0.10	0.51	2.35	3.50	2.77	0.09	0.09	95.45
SG14-0704	-	20/05/2016	69.67	0.51	12.97	2.77	0.07	0.61	2.34	3.52	2.75	0.13	0.15	95.48
SG14-0704	-	20/05/2016	67.33	0.45	14.94	2.62	0.03	0.22	3.49	3.98	2.39	0.11	0.10	95.66
SG14-0704	-	20/05/2016	70.27	0.49	13.40	3.05	0.12	0.56	2.34	3.86	2.79	0.14	0.09	97.12
SG14-0704	-	20/05/2016	70.57	0.55	13.32	2.98	0.00	0.58	2.43	3.85	2.80	0.11	0.12	97.31
SG14-0704	-	20/05/2016	70.65	0.56	13.27	2.81	0.10	0.59	2.47	3.96	2.81	0.17	0.12	97.51

SG Label	Tephra	Run Date	SiO_2	TiO_2	Al_2O_3	FeOt	MnO	MgO	CaO	Na_2O	K_2O	P_2O_5	Cl	Analytical total
SG14-0704	-	20/05/2016	70.58	0.54	13.25	3.08	0.18	0.65	2.56	3.79	2.69	0.10	0.10	97.51
SG14-0704 Outlier	-	20/05/2016	71.23	0.46	12.89	2.48	0.02	0.63	2.62	4.34	1.21	0.07	0.12	96.07
SG14-0781	-	11/06/2015	73.24	0.18	13.31	0.75	0.12	0.28	1.80	4.23	2.47	0.01	0.16	96.56
SG14-0781	-	11/06/2015	75.29	0.16	13.77	0.90	0.01	0.16	1.93	3.90	2.27	0.00	0.14	98.54
SG14-0781	-	11/06/2015	74.91	0.08	13.90	0.77	0.08	0.19	1.96	3.85	2.22	0.07	0.13	98.16
SG14-0781	-	11/06/2015	72.58	0.15	13.12	0.45	0.07	0.30	1.96	3.23	2.42	0.07	0.05	94.39
SG14-0781	-	11/06/2015	73.50	0.17	13.56	0.92	0.02	0.35	1.95	3.68	2.18	0.07	0.16	96.56
SG14-0781	-	11/06/2015	76.02	0.16	13.21	0.73	0.08	0.21	1.47	3.57	3.19	0.03	0.15	98.82
SG14-0781	-	11/06/2015	74.24	0.22	13.87	0.97	0.09	0.30	2.06	3.79	2.21	0.07	0.15	97.96
SG14-0781	-	11/06/2015	73.90	0.16	13.24	1.26	0.09	0.60	1.75	3.64	2.23	0.00	0.14	97.00
SG14-0781	-	11/06/2015	73.35	0.14	13.35	0.80	0.06	0.23	2.03	3.67	2.15	0.11	0.12	96.02
SG14-0781	-	11/06/2015	74.07	0.16	14.25	0.80	0.00	0.22	2.12	3.93	2.09	0.09	0.15	97.89
SG14-0781	-	11/06/2015	70.84	0.14	13.00	0.75	0.01	0.14	1.71	3.79	2.13	0.03	0.25	92.80
SG14-0781	-	11/06/2015	73.76	0.13	14.07	1.00	0.06	0.33	1.79	4.01	2.93	0.09	0.15	98.32
SG14-0781	-	11/06/2015	73.87	0.15	13.94	0.92	0.07	0.36	2.16	4.13	2.34	0.03	0.13	98.11
SG14-0781	-	11/08/2016	70.00	0.16	13.79	0.86	0.12	0.34	2.19	3.96	2.16	0.05	0.12	93.74
SG14-0781	-	11/08/2016	73.09	0.16	14.32	0.68	0.08	0.17	2.04	4.20	2.49	0.05	0.10	97.38
SG14-0781	-	11/08/2016	73.39	0.15	12.30	0.99	0.03	0.25	1.42	3.62	2.34	0.03	0.16	94.68
SG14-0781	-	11/08/2016	74.83	0.11	13.57	0.90	0.05	0.29	1.90	3.92	2.32	0.05	0.07	98.02
SG14-0781	-	11/08/2016	75.13	0.15	12.96	0.76	0.00	0.17	1.62	3.83	2.50	0.05	0.15	97.32
SG14-0781	-	11/08/2016	75.81	0.19	12.92	0.83	0.06	0.13	1.23	3.11	3.72	0.04	0.01	98.05
SG14-0781	-	11/08/2016	76.26	0.23	13.14	1.78	0.01	0.74	1.53	3.56	2.67	0.03	0.12	100.08
SG14-0781	-	11/08/2016	74.54	0.15	12.30	0.90	0.01	0.22	1.37	3.52	2.52	0.05	0.17	95.74

SG Label	Tephra	Run Date	SiO_2	TiO_2	Al_2O_3	FeOt	MnO	MgO	CaO	Na_2O	K_2O	P_2O_5	Cl	Analytical total
SG14-0781	-	11/08/2016	70.59	0.10	14.22	0.93	0.10	0.32	2.36	4.19	1.87	0.07	0.12	94.87
SG14-0781	-	11/08/2016	71.51	0.15	13.42	0.71	0.06	0.25	1.61	4.08	2.66	0.05	0.17	94.66
SG14-0781	-	11/08/2016	71.44	0.08	13.77	0.73	0.06	0.22	1.81	3.64	3.09	0.08	0.09	95.02
SG14-0781	-	11/08/2016	75.58	0.17	13.36	0.75	0.03	0.19	1.57	3.64	2.80	0.01	0.08	98.17
SG14-0781	-	11/06/2015	75.77	0.16	12.62	0.84	0.10	0.09	1.45	3.49	2.47	0.07	0.11	97.19
SG14-0781 Outlier	-	11/06/2015	73.49	0.51	13.05	2.53	0.12	0.54	2.03	2.15	2.69	0.10	0.22	97.42
SG14-0781 Outlier	-	11/06/2015	68.06	0.13	18.68	0.57	0.00	0.08	4.66	4.27	1.69	0.11	0.12	98.37
SG14-0781 Outlier	-	11/08/2016	78.67	0.15	11.34	0.67	0.04	0.15	1.69	3.55	1.68	0.09	0.07	98.10
SG14-0781 Outlier	-	11/06/2015	75.71	0.16	11.46	0.91	0.09	0.38	1.07	3.29	2.82	0.00	0.15	96.03
SG14-0781 Outlier	-	11/06/2015	79.36	0.11	11.40	0.70	0.06	0.23	1.47	3.47	1.86	0.06	0.09	98.80
SG14-0781 Outlier	-	11/08/2016	72.42	0.22	16.32	0.59	0.05	0.29	2.59	4.94	2.64	0.08	0.02	100.16
SG14-0781 Outlier	-	11/06/2015	73.12	0.56	12.92	2.37	0.12	0.47	2.00	4.19	2.74	0.05	0.19	98.73
SG14-0781 Outlier	-	11/08/2016	74.40	0.53	13.30	2.33	0.11	0.46	1.87	4.25	2.82	0.09	0.20	100.35
SG14-0803	U-2	20/05/2016	56.55	0.62	18.07	3.45	0.41	0.54	2.00	5.36	5.83	0.18	0.12	93.13
SG14-0803	U-2	20/05/2016	57.98	0.60	18.24	2.39	0.09	0.40	2.04	5.21	6.59	0.17	0.17	93.87
SG14-0803	U-2	20/05/2016	58.35	0.53	18.93	2.14	0.09	0.58	2.33	4.87	6.30	0.24	0.13	94.50
SG14-0803	U-2	20/05/2016	58.35	0.55	19.18	2.62	0.10	0.32	1.87	6.23	6.07	0.12	0.25	95.67
SG14-0803	U-2	20/05/2016	58.66	0.68	18.53	3.01	0.18	0.36	2.02	6.17	6.53	0.16	0.24	96.54
SG14-0803	U-2	20/05/2016	58.23	0.63	18.59	3.46	0.16	0.59	1.83	6.52	6.40	0.15	0.20	96.76
SG14-0803	U-2	20/05/2016	59.43	0.54	19.12	2.81	0.02	0.36	1.76	6.34	6.52	0.16	0.17	97.24
SG14-0803	U-2	20/05/2016	58.48	0.53	19.44	2.75	0.13	0.44	2.39	6.45	6.23	0.27	0.19	97.30
SG14-0803	U-2	20/05/2016	58.97	0.52	19.09	2.87	0.10	0.35	1.88	6.72	6.41	0.16	0.23	97.31
SG14-0803	U-2	20/05/2016	58.44	0.61	18.92	3.31	0.25	0.49	1.72	6.76	6.45	0.18	0.19	97.32

SG Label	Tephra	Run Date	SiO_2	TiO_2	Al_2O_3	FeOt	MnO	MgO	CaO	Na_2O	K_2O	P_2O_5	Cl	Analytical total
SG14-0803	U-2	20/05/2016	59.17	0.57	18.84	3.22	0.09	0.38	1.87	6.23	6.54	0.17	0.23	97.32
SG14-0803	U-2	20/05/2016	58.40	0.68	18.56	3.45	0.10	0.51	1.48	7.21	6.79	0.12	0.19	97.49
SG14-0803	U-2	20/05/2016	59.02	0.56	19.02	3.08	0.10	0.37	2.18	6.34	6.52	0.21	0.25	97.66
SG14-0803	U-2	20/05/2016	59.13	0.62	19.15	3.20	0.21	0.40	1.46	6.70	6.46	0.15	0.22	97.69
SG14-0803	U-2	20/05/2016	58.70	0.70	18.79	3.41	0.03	0.57	2.00	7.08	6.23	0.18	0.20	97.89
SG14-0803	U-2	20/05/2016	58.63	0.66	18.96	3.37	0.14	0.56	2.10	6.91	6.17	0.16	0.24	97.89
SG14-0803	U-2	20/05/2016	58.25	0.70	18.65	3.76	0.08	0.78	2.44	6.38	6.59	0.21	0.18	98.01
SG14-0803	U-2	20/05/2016	60.01	0.47	19.08	2.67	0.15	0.30	1.21	7.35	6.63	0.04	0.20	98.12
SG14-0803	U-2	20/05/2016	59.11	0.62	19.19	3.25	0.22	0.47	2.01	6.70	6.33	0.19	0.22	98.30
SG14-0803 outlier	U-2	20/05/2016	71.63	0.54	12.50	2.44	0.13	0.43	1.99	4.02	2.75	0.08	0.15	96.66
SG14-0840	To-Cu	20/05/2016	69.32	0.41	12.77	2.15	0.14	0.53	2.57	4.25	1.14	0.10	0.11	93.50
SG14-0840	To-Cu	20/05/2016	70.31	0.48	13.35	2.08	0.17	0.49	2.99	4.60	1.11	0.09	0.10	95.76
SG14-0840	To-Cu	20/05/2016	71.11	0.46	12.95	2.28	0.06	0.60	2.71	4.28	1.13	0.09	0.15	95.82
SG14-0840	To-Cu	20/05/2016	71.46	0.47	12.97	2.19	0.11	0.57	2.66	4.19	1.25	0.06	0.11	96.06
SG14-0840	To-Cu	20/05/2016	71.42	0.45	13.00	2.34	0.00	0.56	2.71	4.26	1.24	0.07	0.10	96.16
SG14-0840	To-Cu	20/05/2016	71.67	0.42	12.95	2.14	0.08	0.62	2.73	4.57	1.05	0.08	0.13	96.46
SG14-0840	To-Cu	20/05/2016	71.74	0.44	12.89	2.22	0.13	0.55	2.65	4.52	1.12	0.08	0.13	96.46
SG14-0840	To-Cu	20/05/2016	71.57	0.44	12.96	2.44	0.13	0.64	2.64	4.34	1.14	0.05	0.12	96.47
SG14-0840	To-Cu	20/05/2016	71.39	0.42	13.63	2.09	0.02	0.50	2.96	4.28	1.11	0.10	0.09	96.59
SG14-0840	To-Cu	20/05/2016	71.55	0.48	12.92	2.17	0.13	0.72	2.77	4.53	1.17	0.06	0.11	96.62
SG14-0840	To-Cu	20/05/2016	71.90	0.45	13.16	2.10	0.05	0.54	2.73	4.36	1.20	0.07	0.09	96.64
SG14-0840	To-Cu	20/05/2016	71.94	0.48	13.00	2.23	0.07	0.58	2.69	4.32	1.21	0.07	0.09	96.68
SG14-0840	To-Cu	20/05/2016	71.93	0.45	13.11	2.12	0.09	0.60	2.64	4.38	1.19	0.12	0.09	96.70

SG Label	Tephra	Run Date	SiO_2	TiO_2	Al_2O_3	FeOt	MnO	MgO	CaO	Na_2O	K_2O	P_2O_5	Cl	Analytical total
SG14-0840	To-Cu	20/05/2016	71.79	0.51	13.05	2.26	0.10	0.57	2.66	4.33	1.27	0.07	0.10	96.71
SG14-0840	To-Cu	20/05/2016	71.82	0.44	13.06	2.38	0.19	0.61	2.67	4.21	1.17	0.05	0.12	96.72
SG14-0840	To-Cu	20/05/2016	72.00	0.51	13.04	2.26	0.13	0.59	2.80	4.14	1.15	0.07	0.09	96.77
SG14-0840	To-Cu	20/05/2016	71.59	0.46	12.98	2.49	0.14	0.57	2.68	4.49	1.21	0.08	0.10	96.78
SG14-0840	To-Cu	20/05/2016	71.93	0.45	13.13	2.22	0.10	0.50	2.66	4.52	1.16	0.09	0.11	96.87
SG14-0840	To-Cu	20/05/2016	72.01	0.52	13.10	2.26	0.11	0.59	2.76	4.59	1.23	0.02	0.11	97.29
SG14-0840	To-Cu	20/05/2016	72.18	0.46	12.80	2.23	0.20	0.75	2.73	4.63	1.18	0.09	0.08	97.35
SG14-0840	To-Cu	20/05/2016	72.17	0.47	13.26	2.29	0.15	0.62	2.83	4.33	1.18	0.05	0.12	97.47
SG14-0840	To-Cu	20/05/2016	72.12	0.45	13.18	2.46	0.02	0.57	2.77	4.70	1.16	0.08	0.10	97.62
SG14-0840	To-Cu	20/05/2016	72.35	0.44	13.35	2.38	0.10	0.60	2.74	4.43	1.23	0.07	0.09	97.77
SG14-0840	To-Cu	20/05/2016	72.72	0.48	13.29	2.33	0.08	0.60	2.54	4.53	1.15	0.09	0.10	97.93
SG14-0840	To-Cu	20/05/2016	72.39	0.40	13.28	2.32	0.15	0.62	2.71	4.59	1.24	0.12	0.12	97.94
SG14-0840 Outlier	-	20/05/2016	73.69	0.43	13.21	2.13	0.13	0.61	2.63	1.98	1.23	0.09	0.11	96.25
SG14-0840 Outlier	-	20/05/2016	72.22	0.55	12.60	2.38	0.09	0.42	1.97	4.21	2.72	0.04	0.15	97.36
SG14-0840 Outlier	-	20/05/2016	72.08	0.53	12.75	2.35	0.09	0.46	2.04	4.21	2.72	0.09	0.19	97.51
SG14-1058	-	28/04/2017	72.76	0.17	9.94	3.66	0.02	0.00	0.17	5.05	4.36	0.00	0.51	96.64
SG14-1058	-	28/04/2017	72.50	0.24	9.84	3.74	0.04	0.02	0.22	5.06	4.29	0.03	0.51	96.50
SG14-1058	-	28/04/2017	71.85	0.23	9.98	3.71	0.03	0.00	0.21	5.54	4.33	0.01	0.49	96.39
SG14-1058	-	28/04/2017	71.42	0.18	9.80	3.82	0.07	0.02	0.17	4.97	4.28	0.00	0.48	95.22
SG14-1058	-	28/04/2017	72.96	0.17	9.92	3.63	0.06	0.01	0.19	5.35	4.36	0.00	0.50	97.18
SG14-1058	-	28/04/2017	69.39	0.14	9.88	3.46	0.06	0.01	0.22	5.00	4.19	0.02	0.48	92.84
SG14-1058	-	28/04/2017	71.00	0.19	9.79	3.72	0.06	0.01	0.20	5.01	4.15	0.00	0.51	94.65
SG14-1058	-	28/04/2017	71.29	0.15	9.87	3.70	0.11	0.02	0.19	4.88	4.20	0.00	0.50	94.90

SG Label	Tephra	Run Date	SiO_2	TiO_2	Al_2O_3	FeOt	MnO	MgO	CaO	Na_2O	K_2O	P_2O_5	Cl	Analytical total
SG14-1058	-	28/04/2017	72.11	0.20	9.83	3.72	0.09	0.00	0.22	5.24	4.38	0.00	0.49	96.27
SG14-1058	-	28/04/2017	72.83	0.25	9.96	3.85	0.06	0.01	0.17	5.00	4.42	0.00	0.49	97.04
SG14-1058	-	28/04/2017	71.54	0.22	9.68	3.75	0.07	0.01	0.20	5.25	4.27	0.00	0.50	95.48
SG14-1058	-	28/04/2017	71.89	0.18	9.78	3.66	0.07	0.00	0.20	5.10	4.41	0.00	0.49	95.77
SG14-1058	-	28/04/2017	73.46	0.19	10.16	3.81	0.04	0.01	0.18	5.05	4.42	0.00	0.47	97.79
SG14-1058	-	28/04/2017	70.89	0.18	9.79	3.90	0.07	0.00	0.17	5.12	4.24	0.00	0.51	94.86
SG14-1058	-	28/04/2017	72.27	0.16	9.99	3.83	0.08	0.01	0.18	5.08	4.23	0.00	0.50	96.34
SG14-1058	-	28/04/2017	68.74	0.13	9.49	3.49	0.07	0.02	0.21	4.79	4.18	0.02	0.50	91.64
SG14-1058	-	28/04/2017	71.42	0.23	9.65	3.78	0.09	0.00	0.17	4.92	4.27	0.00	0.48	95.01
SG14-1058	-	28/04/2017	71.53	0.15	9.89	3.62	0.10	0.00	0.17	5.11	4.25	0.03	0.47	95.30
SG14-1058	-	28/04/2017	73.01	0.23	9.94	3.87	0.07	0.00	0.19	5.05	4.48	0.00	0.50	97.34
SG14-1058	-	28/04/2017	71.87	0.24	9.72	3.61	0.09	0.03	0.21	4.84	4.31	0.02	0.50	95.45
SG14-1058	-	28/04/2017	71.56	0.19	9.71	3.68	0.05	0.00	0.22	5.18	4.32	0.01	0.49	95.40
SG14-1058	-	28/04/2017	71.14	0.17	9.75	3.76	0.04	0.02	0.21	5.02	4.27	0.01	0.46	94.86
SG14-1058	-	28/04/2017	71.76	0.22	9.74	3.65	0.09	0.01	0.19	4.88	4.24	0.01	0.52	95.31
SG14-1058	-	28/04/2017	71.04	0.21	9.76	3.69	0.11	0.00	0.19	5.25	4.35	0.04	0.48	95.11
SG14-1058	-	12/08/2016	71.42	0.18	9.69	3.83	0.09	0.00	0.18	4.92	4.26	0.00	0.51	95.09
SG14-1058 Outlier	-	12/08/2016	72.30	0.19	9.78	3.93	0.10	0.04	0.19	2.07	4.14	0.03	0.55	93.31
SG14-1058 Outlier	-	28/04/2017	72.71	0.17	9.81	3.92	0.10	0.00	0.18	1.42	4.19	0.01	0.49	93.00
SG14-1058 Outlier	-	28/04/2017	74.88	0.12	12.18	1.23	0.02	0.15	1.14	3.59	3.39	0.02	0.12	96.86
SG14-1091	U-3	11/06/2015	59.76	0.50	19.47	2.72	0.15	0.21	1.45	6.73	6.92	0.00	0.42	98.33
SG14-1091	U-3	11/06/2015	59.14	0.53	19.35	2.80	0.17	0.27	1.49	6.64	7.03	0.06	0.34	97.83
SG14-1091	U-3	11/06/2015	57.33	0.50	18.75	2.69	0.12	0.24	1.37	6.31	6.71	0.01	0.46	94.49

SG Label	Tephra	Run Date	SiO_2	TiO_2	Al_2O_3	FeOt	MnO	MgO	CaO	Na_2O	K_2O	P_2O_5	Cl	Analytical total
SG14-1091	U-3	11/06/2015	59.81	0.53	19.77	2.75	0.12	0.16	1.43	6.97	7.07	0.07	0.39	99.07
SG14-1091	U-3	11/06/2015	59.67	0.50	19.44	2.78	0.14	0.33	1.47	6.34	7.02	0.11	0.32	98.13
SG14-1091	U-3	11/06/2015	59.60	0.45	19.76	2.74	0.16	0.17	1.47	6.98	6.67	0.01	0.40	98.41
SG14-1091	U-3	11/06/2015	60.52	0.45	19.75	2.65	0.15	0.23	1.41	7.27	6.92	0.02	0.36	99.72
SG14-1091	U-3	11/06/2015	59.67	0.61	19.49	2.75	0.19	0.28	1.49	6.88	6.78	0.02	0.39	98.57
SG14-1091	U-3	11/06/2015	59.72	0.47	19.53	2.72	0.18	0.23	1.52	6.65	6.85	0.10	0.46	98.42
SG14-1091	U-3	11/06/2015	59.12	0.57	19.11	2.91	0.17	0.22	1.47	6.39	7.08	0.09	0.34	97.46
SG14-1091	U-3	11/06/2015	59.62	0.55	19.58	2.79	0.18	0.25	1.50	6.74	6.93	0.09	0.34	98.58
SG14-1091	U-3	11/06/2015	59.95	0.45	19.68	2.84	0.18	0.25	1.37	7.04	7.13	0.05	0.36	99.29
SG14-1091	U-3	11/06/2015	57.96	0.60	18.76	2.72	0.16	0.31	1.55	6.24	6.85	0.07	0.45	95.66
SG14-1091	U-3	11/06/2015	59.68	0.59	19.12	2.90	0.14	0.33	1.58	6.54	7.02	0.03	0.29	98.23
SG14-1091	U-3	11/06/2015	58.99	0.52	19.32	2.78	0.08	0.20	1.51	6.70	7.10	0.05	0.36	97.62
SG14-1091	U-3	11/06/2015	55.71	0.46	18.54	2.78	0.16	0.21	1.41	6.43	6.37	0.00	0.37	92.45
SG14-1091	U-3	11/06/2015	60.01	0.61	19.66	2.90	0.20	0.34	1.55	6.48	6.78	0.11	0.32	98.95
SG14-1091	U-3	11/06/2015	59.65	0.50	19.59	3.03	0.16	0.23	1.45	6.86	6.95	0.07	0.36	98.86
SG14-1091	U-3	11/06/2015	59.66	0.50	19.61	2.62	0.13	0.25	1.38	6.95	7.04	0.06	0.38	98.59
SG14-1091	U-3	11/06/2015	59.61	0.44	19.70	2.70	0.14	0.22	1.39	7.02	6.79	0.04	0.42	98.48
SG14-1091	U-3	11/06/2015	60.15	0.48	19.75	2.44	0.11	0.15	1.50	7.27	6.62	0.03	0.42	98.93
SG14-1091	U-3	11/06/2015	56.50	0.46	18.34	2.94	0.19	0.20	1.16	6.21	6.88	0.08	0.38	93.36
SG14-1091	U-3	11/06/2015	60.02	0.50	19.92	2.60	0.14	0.19	1.81	7.14	6.61	0.01	0.37	99.29
SG14-1091	U-3	11/06/2015	58.79	0.21	20.37	2.27	0.09	0.01	1.07	8.31	6.79	0.00	0.71	98.61
SG14-1185	-	12/08/2016	69.75	0.64	14.18	3.15	0.08	0.67	2.94	3.19	3.58	0.06	0.10	98.35
SG14-1185	-	12/08/2016	74.58	0.15	11.89	1.12	0.07	0.09	1.10	3.45	3.10	0.04	0.11	95.71

SG Label	Tephra	Run Date	SiO_2	TiO_2	Al_2O_3	FeOt	MnO	MgO	CaO	Na_2O	K_2O	P_2O_5	Cl	Analytical total
SG14-1185	-	12/08/2016	72.24	0.54	13.52	2.73	0.09	0.59	2.36	3.39	3.73	0.14	0.12	99.44
SG14-1185	-	12/08/2016	71.37	0.58	13.37	2.68	0.04	0.53	2.27	3.29	3.88	0.08	0.14	98.24
SG14-1185	-	12/08/2016	70.92	0.52	13.04	2.51	0.09	0.55	2.16	3.16	3.68	0.08	0.18	96.88
SG14-1185	-	12/08/2016	72.37	0.55	13.49	2.40	0.02	0.56	2.28	3.49	3.90	0.09	0.11	99.27
SG14-1185	-	12/08/2016	70.07	0.49	12.84	2.34	0.05	0.53	2.12	3.48	3.83	0.11	0.16	96.01
SG14-1185	-	12/08/2016	69.33	0.68	14.21	3.90	0.06	0.95	3.24	3.42	3.59	0.11	0.09	99.59
SG14-1185	-	12/08/2016	69.56	0.57	13.04	2.34	0.05	0.55	2.16	3.22	3.87	0.10	0.15	95.60
SG14-1185	-	12/08/2016	74.35	0.56	12.09	1.84	0.12	0.29	0.65	3.19	3.68	0.15	0.05	96.98
SG14-1185	-	12/08/2016	74.16	0.55	12.65	2.37	0.03	0.36	1.67	3.38	4.37	0.06	0.13	99.72
SG14-1185	-	12/08/2016	71.81	0.57	13.45	2.58	0.05	0.53	2.23	3.64	3.73	0.11	0.09	98.79
SG14-1185	-	12/08/2016	67.75	0.66	15.66	3.91	0.05	0.89	4.06	3.90	3.17	0.17	0.08	100.30
SG14-1185	-	12/08/2016	71.82	0.56	13.22	2.48	0.07	0.57	2.19	3.38	3.90	0.12	0.11	98.43
SG14-1185	-	12/08/2016	66.91	0.62	15.01	3.58	0.03	0.89	4.03	3.36	2.96	0.11	0.10	97.61
SG14-1185	-	12/08/2016	65.56	0.57	13.15	3.27	0.08	0.80	2.80	3.39	3.42	0.07	0.11	93.21
SG14-1185	-	12/08/2016	71.97	0.40	12.45	1.88	0.09	0.37	1.60	3.31	4.18	0.04	0.17	96.45
SG14-1185	-	12/08/2016	67.31	0.65	14.82	4.22	0.17	1.31	3.96	3.33	3.14	0.12	0.07	99.10
SG14-1185 Outlier	-	12/08/2016	71.39	0.48	12.57	1.90	0.05	0.33	1.68	3.20	3.99	0.06	0.11	95.78

Table B2. Major element glass analyses of the MPI-DING reference glass (StHs6/80-G, GOR132-G and ATHO-G)

Reference Glass (Jochum et al., 2006)	Run Date	SiO_2	TiO_2	Al_2O_3	FeOt	MnO	MgO	CaO	Na_2O	K_2O	P_2O_5	Cl	Analytical total
StHs6/80-G_5	08/06/2015	63.05	0.72	17.56	4.24	0.09	1.87	5.28	4.59	1.33	0.17	0.01	98.92
StHs6/80-G_2	08/06/2015	63.66	0.76	17.48	4.25	0.14	1.95	5.24	4.47	1.29	0.18	0.03	99.44
StHs6/80-G_4	08/06/2015	63.39	0.65	17.41	4.45	0.08	1.90	5.21	4.51	1.35	0.15	0.02	99.12
StHs6/80-G_1	08/06/2015	63.65	0.73	17.50	4.34	0.08	1.87	5.28	4.24	1.34	0.18	0.03	99.24
StHs6/80-G_3	08/06/2015	63.28	0.67	17.34	4.45	0.10	1.84	5.22	4.70	1.36	0.13	0.00	99.10
StHs6/80-G_3	09/06/2015	63.23	0.72	17.75	4.22	0.06	1.92	5.23	4.31	1.31	0.19	0.00	98.92
StHs6/80-G_5	09/06/2015	63.76	0.69	17.71	4.41	0.00	1.87	5.39	4.38	1.31	0.15	0.00	99.66
StHs6/80-G_2	09/06/2015	63.69	0.68	17.54	4.40	0.11	1.99	5.17	4.58	1.31	0.18	0.02	99.67
StHs6/80-G_1	09/06/2015	63.23	0.72	17.55	4.31	0.03	1.98	5.30	4.02	1.30	0.19	0.02	98.64
StHs6/80-G_1	10/06/2015	63.57	0.70	17.78	4.47	0.09	1.92	5.47	4.58	1.28	0.16	0.01	100.03
StHs6/80-G_6	10/06/2015	63.55	0.77	17.75	4.40	0.06	1.95	5.24	4.81	1.31	0.24	0.00	100.08
StHs6/80-G_2	10/06/2015	63.48	0.69	17.64	4.64	0.06	1.92	5.36	4.59	1.37	0.15	0.01	99.92
StHs6/80-G_3	10/06/2015	63.71	0.69	17.75	4.40	0.11	1.98	5.22	4.47	1.27	0.22	0.01	99.83
StHs6/80-G_4	10/06/2015	63.24	0.70	17.67	4.51	0.01	1.93	5.35	4.48	1.29	0.21	0.02	99.42
StHs6/80-G_5	10/06/2015	63.53	0.70	17.61	4.20	0.14	1.92	5.34	4.45	1.28	0.14	0.03	99.34
StHs6/80-G_7	10/06/2015	63.72	0.70	17.83	4.45	0.11	1.98	5.17	4.44	1.31	0.16	0.04	99.92
StHs6/80-G_22	11/06/2015	63.68	0.75	17.51	4.45	0.13	1.95	5.21	4.52	1.35	0.10	0.00	99.65
StHs6/80-G_1	11/06/2015	63.41	0.80	17.67	4.30	0.12	1.85	5.41	4.55	1.30	0.11	0.02	99.53
StHs6/80-G_2	11/06/2015	63.65	0.69	17.53	4.27	0.09	2.02	5.22	4.43	1.27	0.02	0.00	99.18
StHs6/80-G_3	11/06/2015	63.47	0.69	17.61	4.34	0.03	2.02	5.31	4.62	1.35	0.08	0.01	99.53
StHs6/80-G_4	11/06/2015	63.60	0.67	17.57	4.36	0.15	2.02	5.17	4.71	1.29	0.05	0.00	99.57

Reference Glass (Jochum et al., 2006)	Run Date	SiO_2	TiO_2	Al_2O_3	FeOt	MnO	MgO	CaO	Na_2O	K_2O	P_2O_5	Cl	Analytical total
StHs6/80-G_5	11/06/2015	63.86	0.75	17.67	4.21	0.07	1.89	5.27	4.61	1.30	0.10	0.01	99.73
StHs6/80-G_6	11/06/2015	63.85	0.74	17.62	4.29	0.09	2.02	5.26	4.33	1.36	0.12	0.02	99.68
StHs6/80-G_7	11/06/2015	63.73	0.67	17.74	4.35	0.07	1.86	5.27	4.74	1.32	0.13	0.00	99.89
StHs6/80-G_8	11/06/2015	63.98	0.73	17.63	4.40	0.06	1.95	5.25	4.17	1.28	0.10	0.00	99.56
StHs6/80-G_9	11/06/2015	63.89	0.75	17.93	4.24	0.04	1.90	5.28	4.78	1.41	0.11	0.01	100.32
StHs6/80-G_10	11/06/2015	63.07	0.73	17.59	4.29	0.04	1.91	5.22	4.25	1.28	0.13	0.00	98.52
StHs6/80-G_11	11/06/2015	63.02	0.65	17.84	4.12	0.00	2.01	5.23	4.52	1.36	0.15	0.05	98.94
StHs6/80-G_12	11/06/2015	63.30	0.66	17.78	4.50	0.07	1.98	5.15	4.75	1.28	0.21	0.02	99.72
StHs6/80-G_13	11/06/2015	63.30	0.64	17.75	4.24	0.06	1.97	5.18	4.61	1.27	0.18	0.01	99.21
StHs6/80-G_14	11/06/2015	62.86	0.73	17.60	4.29	0.06	1.94	5.19	4.60	1.32	0.11	0.00	98.69
StHs6/80-G_15	11/06/2015	63.18	0.75	17.68	4.25	0.11	1.99	5.24	4.60	1.26	0.18	0.01	99.25
StHs6/80-G_16	11/06/2015	62.97	0.74	17.88	4.75	0.05	1.84	5.18	4.44	1.32	0.23	0.02	99.42
StHs6/80-G_18	11/06/2015	63.58	0.64	17.61	4.59	0.08	2.05	5.25	4.36	1.33	0.17	0.01	99.66
StHs6/80-G_19	11/06/2015	63.59	0.77	17.77	4.53	0.08	1.98	5.30	4.67	1.29	0.19	0.01	100.19
StHs6/80-G_20	11/06/2015	63.59	0.72	17.73	4.52	0.06	1.95	5.32	4.40	1.28	0.18	0.03	99.77
StHs6/80-G_21	11/06/2015	63.17	0.73	17.68	4.31	0.00	1.97	5.14	4.43	1.36	0.13	0.01	98.93
StHs6/80-G_1	23/06/2015	63.18	0.70	17.70	4.54	0.08	1.99	5.24	4.61	1.37	0.18	0.01	99.59
StHs6/80-G_2	23/06/2015	63.53	0.72	17.76	4.47	0.08	2.05	5.36	4.83	1.29	0.18	0.02	100.29
StHs6/80-G_3	23/06/2015	63.40	0.72	17.84	4.51	0.03	1.98	5.23	4.75	1.23	0.15	0.00	99.85
StHs6/80-G_4	23/06/2015	63.61	0.66	18.04	4.26	0.09	1.97	5.24	4.85	1.32	0.21	0.00	100.26
StHs6/80-G_5	23/06/2015	63.47	0.72	17.66	4.29	0.14	2.02	5.24	4.52	1.30	0.24	0.02	99.62
StHs6/80-G_6	23/06/2015	63.69	0.71	17.89	4.46	0.02	1.93	5.17	4.61	1.36	0.13	0.02	99.99
StHs6/80-G_7	23/06/2015	63.69	0.80	17.70	4.62	0.05	1.92	5.24	4.66	1.30	0.13	0.00	100.10

Reference Glass (Jochum et al., 2006)	Run Date	SiO_2	TiO_2	Al_2O_3	FeOt	MnO	MgO	CaO	Na_2O	K_2O	P_2O_5	Cl	Analytical total
StHs6/80-G_1	23/07/2015	63.39	0.69	17.04	4.31	0.09	1.97	5.27	4.53	1.32	0.11	0.00	98.73
StHs6/80-G_3	23/07/2015	63.42	0.72	17.64	4.43	0.04	1.92	5.27	4.49	1.32	0.10	0.00	99.36
StHs6/80-G_8	23/07/2015	63.27	0.68	17.74	4.36	0.03	1.98	5.25	4.80	1.36	0.14	0.01	99.62
StHs6/80-G_4	23/07/2015	63.79	0.69	17.70	4.34	0.10	1.90	5.33	4.69	1.32	0.14	0.01	100.00
StHs6/80-G_5	23/07/2015	63.24	0.66	17.50	4.45	0.06	1.92	5.24	4.69	1.39	0.13	0.00	99.28
StHs6/80-G_7	23/07/2015	63.53	0.67	17.69	4.62	0.18	1.91	5.21	4.70	1.26	0.14	0.00	99.89
StHs6/80-G_6	23/07/2015	63.85	0.66	17.58	4.47	0.10	1.86	5.34	4.60	1.24	0.15	0.00	99.85
StHs6/80-G_1	24/07/2015	63.43	0.72	17.64	4.43	0.10	1.94	5.24	4.55	1.30	0.18	0.00	99.54
StHs6/80-G_10	24/07/2015	63.23	0.83	17.58	4.41	0.11	2.04	5.33	4.77	1.38	0.19	0.00	99.86
StHs6/80-G_2	24/07/2015	63.69	0.76	17.57	4.54	0.05	2.02	5.26	4.41	1.26	0.12	0.00	99.69
StHs6/80-G_3	24/07/2015	63.69	0.66	17.38	4.67	0.09	1.94	5.30	4.61	1.28	0.13	0.01	99.76
StHs6/80-G_5	24/07/2015	63.66	0.77	17.66	4.43	0.07	1.99	5.02	4.45	1.24	0.09	0.00	99.39
StHs6/80-G_6	24/07/2015	63.96	0.68	17.60	4.40	0.09	2.01	5.48	4.30	1.30	0.12	0.01	99.95
StHs6/80-G_7	24/07/2015	63.47	0.73	17.65	4.53	0.05	1.82	5.27	4.37	1.28	0.14	0.02	99.34
StHs6/80-G_4	24/07/2015	63.45	0.67	17.65	4.30	0.05	1.98	5.30	4.57	1.33	0.11	0.01	99.43
StHs6/80-G_8	24/07/2015	63.59	0.71	17.69	4.41	0.04	1.93	5.23	5.08	1.32	0.12	0.01	100.13
StHs6/80-G_9	24/07/2015	63.62	0.78	17.36	4.30	0.04	1.98	5.41	4.62	1.26	0.14	0.00	99.52
StHs6/80-G_1	14/09/2015	64.01	0.69	17.65	4.50	0.04	1.98	5.31	4.36	1.28	0.14	0.00	99.97
StHs6/80-G_2	14/09/2015	63.94	0.72	17.47	4.17	0.10	1.96	5.28	4.23	1.35	0.11	0.01	99.32
StHs6/80-G_3	14/09/2015	64.46	0.65	17.48	4.44	0.09	1.94	5.13	4.32	1.32	0.13	0.01	99.97
StHs6/80-G_4	14/09/2015	63.47	0.71	17.44	4.43	0.08	1.94	5.12	4.43	1.35	0.12	0.00	99.10
StHs6/80-G_5	14/09/2015	63.75	0.74	17.44	4.54	0.06	1.89	5.17	4.55	1.33	0.14	0.00	99.61
StHs6/80-G_6	14/09/2015	63.87	0.77	17.63	4.36	0.09	1.99	5.20	4.29	1.30	0.13	0.01	99.65

Reference Glass (Jochum et al., 2006)	Run Date	SiO_2	TiO_2	Al_2O_3	FeOt	MnO	MgO	CaO	Na_2O	K_2O	P_2O_5	Cl	Analytical total
StHs6/80-G_7	14/09/2015	64.33	0.70	17.75	4.64	0.08	1.94	5.15	4.56	1.29	0.11	0.03	100.58
StHs6/80-G_8	14/09/2015	63.31	0.71	17.32	4.51	0.10	2.00	5.18	4.14	1.29	0.13	0.01	98.71
StHs6/80-G_9	14/09/2015	64.01	0.66	17.60	4.48	0.02	1.93	5.24	4.75	1.34	0.11	0.01	100.15
StHs6/80-G_10	14/09/2015	63.32	0.66	17.32	4.36	0.11	1.88	5.01	4.20	1.33	0.14	0.00	98.34
StHs6/80-G_11	14/09/2015	64.49	0.66	17.62	4.56	0.11	1.98	5.34	4.57	1.30	0.12	0.01	100.77
StHs6/80-G_1	18/05/2016	63.90	0.74	17.80	4.30	0.09	1.99	5.25	4.56	1.33	0.20	0.01	100.16
StHs6/80-G_10	18/05/2016	63.34	0.76	17.67	4.34	0.06	1.95	5.40	4.86	1.25	0.16	0.00	99.80
StHs6/80-G_11	18/05/2016	63.13	0.76	17.41	4.47	0.10	1.93	5.24	4.56	1.32	0.23	0.00	99.15
StHs6/80-G_12	18/05/2016	63.21	0.63	17.51	4.46	0.01	1.94	5.35	4.73	1.37	0.16	0.00	99.37
StHs6/80-G_13	18/05/2016	63.48	0.75	17.50	4.40	0.12	1.93	5.49	4.59	1.37	0.17	0.00	99.81
StHs6/80-G_2	18/05/2016	63.78	0.70	18.04	4.42	0.15	2.02	5.33	4.51	1.31	0.17	0.03	100.44
StHs6/80-G_3	18/05/2016	63.55	0.74	17.63	4.38	0.17	1.97	5.49	4.69	1.27	0.18	0.00	100.07
StHs6/80-G_4	18/05/2016	63.84	0.69	17.91	4.38	0.04	1.99	5.19	4.67	1.19	0.20	0.01	100.12
StHs6/80-G_5	18/05/2016	63.67	0.69	17.58	4.22	0.03	1.88	5.17	4.31	1.27	0.19	0.01	99.03
StHs6/80-G_6	18/05/2016	63.46	0.69	17.80	4.40	0.09	2.02	5.39	4.84	1.30	0.13	0.03	100.14
StHs6/80-G_7	18/05/2016	63.84	0.67	17.68	4.33	0.11	1.94	5.29	4.60	1.29	0.11	0.01	99.86
StHs6/80-G_8	18/05/2016	63.38	0.73	17.57	4.26	0.06	1.93	5.27	4.77	1.18	0.19	0.01	99.34
StHs6/80-G_9	18/05/2016	63.34	0.75	17.61	4.40	0.10	1.97	5.30	4.69	1.34	0.15	0.02	99.66
StHs6/80-G_1	20/05/2016	64.13	0.68	17.85	4.62	0.05	1.94	5.23	4.67	1.27	0.17	0.02	100.63
StHs6/80-G_10	20/05/2016	63.94	0.64	17.63	4.36	0.08	1.92	5.17	4.50	1.31	0.17	0.00	99.71
StHs6/80-G_2	20/05/2016	63.81	0.67	17.61	4.39	0.09	1.99	5.54	4.70	1.29	0.11	0.00	100.20
StHs6/80-G_3	20/05/2016	64.33	0.67	17.81	4.11	0.11	1.92	5.44	4.57	1.28	0.11	0.02	100.37
StHs6/80-G_4	20/05/2016	63.84	0.69	17.68	4.30	0.09	1.91	5.13	4.67	1.22	0.13	0.02	99.69

Reference Glass (Jochum et al., 2006)	Run Date	SiO_2	TiO_2	Al_2O_3	FeOt	MnO	MgO	CaO	Na_2O	K_2O	P_2O_5	Cl	Analytical total
StHs6/80-G_5	20/05/2016	63.57	0.69	17.56	4.40	0.00	1.95	5.31	4.73	1.30	0.18	0.01	99.70
StHs6/80-G_6	20/05/2016	63.21	0.69	17.60	4.62	0.09	1.93	5.37	4.57	1.30	0.14	0.00	99.51
StHs6/80-G_7	20/05/2016	63.27	0.71	17.51	4.04	0.06	1.94	5.29	4.56	1.24	0.18	0.00	98.80
StHs6/80-G_8	20/05/2016	63.54	0.73	17.67	4.21	0.03	1.92	5.20	4.60	1.33	0.18	0.02	99.43
StHs6/80-G_9	20/05/2016	63.50	0.74	17.59	4.40	0.02	1.92	5.27	4.70	1.33	0.14	0.02	99.64
StHs6/80-G_1	11/08/2016	64.50	0.70	18.19	4.25	0.10	1.92	5.29	4.45	1.32	0.18	0.00	100.92
StHs6/80-G_1	12/08/2016	63.41	0.68	17.69	4.53	0.17	1.90	5.30	4.78	1.27	0.15	0.00	99.90
StHs6/80-G_3	12/08/2016	63.45	0.74	18.03	4.48	0.06	1.96	5.19	4.64	1.33	0.12	0.02	100.01
StHs6/80-G_2	12/08/2016	63.51	0.70	17.81	4.61	0.05	1.87	5.17	4.74	1.31	0.14	0.02	99.92
StHs6/80-G_4	12/08/2016	63.51	0.69	17.79	4.36	0.14	1.89	5.14	4.52	1.33	0.14	0.02	99.54
StHs6/80-G_5	12/08/2016	63.40	0.69	17.93	4.49	0.11	1.86	5.28	4.74	1.26	0.16	0.04	99.95
StHs6/80-G_6	12/08/2016	63.32	0.70	17.73	4.18	0.05	1.83	5.41	4.48	1.32	0.16	0.01	99.19
StHs6/80-G_7	12/08/2016	63.67	0.76	17.78	4.55	0.10	1.78	5.34	4.69	1.21	0.17	0.01	100.03
StHs6/80-G_8	12/08/2016	63.74	0.68	17.83	4.49	0.07	1.88	5.26	4.30	1.39	0.20	0.02	99.87
StHs6/80-G_1	01/05/2017	62.79	0.70	17.57	4.43	0.08	1.91	5.25	4.63	1.36	0.04	0.00	98.76
StHs6/80-G_2	01/05/2017	62.73	0.75	17.64	4.19	0.06	1.96	5.40	4.45	1.33	0.10	0.01	98.63
StHs6/80-G_3	01/05/2017	63.47	0.69	17.46	4.33	0.07	1.94	5.20	4.44	1.34	0.09	0.00	99.04
StHs6/80-G_4	01/05/2017	63.53	0.67	17.46	4.26	0.09	1.99	5.32	4.77	1.25	0.12	0.00	99.47
StHs6/80-G_5	01/05/2017	64.04	0.74	17.70	4.33	0.05	2.01	5.36	4.51	1.26	0.16	0.01	100.16
StHs6/80-G_6	01/05/2017	63.54	0.74	17.73	4.37	0.09	2.01	5.29	4.66	1.27	0.17	0.02	99.88
GOR132-G_3	08/06/2015	45.66	0.30	10.76	10.06	0.21	22.12	8.59	0.88	0.05	0.07	0.00	98.72
GOR132-G_9	08/06/2015	45.44	0.30	10.86	10.24	0.13	22.00	8.47	0.82	0.01	0.04	0.00	98.33

Reference Glass (Jochum et al., 2006)	Run Date	SiO_2	TiO_2	Al_2O_3	FeOt	MnO	MgO	CaO	Na_2O	K_2O	P_2O_5	Cl	Analytical total
GOR132-G_2	08/06/2015	45.51	0.30	10.79	10.11	0.13	22.21	8.59	0.76	0.03	0.05	0.01	98.50
GOR132-G_4	08/06/2015	45.59	0.28	10.82	10.13	0.17	21.86	8.56	0.76	0.05	0.07	0.01	98.31
GOR132-G_1	08/06/2015	45.55	0.33	10.77	10.36	0.13	22.07	8.53	0.80	0.03	0.08	0.00	98.67
GOR132-G_5	08/06/2015	45.66	0.30	10.94	10.10	0.14	22.34	8.54	0.80	0.03	0.04	0.00	98.88
GOR132-G_3	09/06/2015	45.60	0.26	10.76	10.22	0.16	22.06	8.83	0.82	0.02	0.10	0.02	98.86
GOR132-G_4	09/06/2015	45.68	0.31	10.84	10.05	0.09	22.33	8.38	0.67	0.04	0.05	0.00	98.44
GOR132-G_2	09/06/2015	45.62	0.31	10.74	10.32	0.13	22.13	8.49	0.68	0.02	0.05	0.00	98.49
GOR132-G_1	09/06/2015	45.22	0.29	10.74	10.33	0.24	21.83	8.47	0.83	0.05	0.10	0.01	98.09
GOR132-G_1	10/06/2015	45.27	0.31	11.13	10.14	0.12	22.22	8.48	0.95	0.06	0.04	0.01	98.72
GOR132-G_6	10/06/2015	45.17	0.31	10.88	10.49	0.15	22.11	8.56	0.76	0.02	0.06	0.00	98.52
GOR132-G_2	10/06/2015	45.45	0.28	10.94	10.34	0.10	22.22	8.39	0.66	0.05	0.03	0.01	98.48
GOR132-G_3	10/06/2015	45.72	0.29	11.12	10.09	0.20	22.02	8.45	0.91	0.02	0.04	0.02	98.88
GOR132-G_4	10/06/2015	45.59	0.25	11.08	10.45	0.10	22.34	8.48	0.79	0.02	0.07	0.02	99.18
GOR132-G_5	10/06/2015	45.85	0.21	11.03	10.34	0.18	22.40	8.46	0.80	0.03	0.01	0.01	99.31
GOR132-G_7	10/06/2015	45.73	0.34	11.07	10.09	0.11	22.19	8.51	0.86	0.04	0.03	0.00	98.96
GOR132-G_22	11/06/2015	45.87	0.30	10.87	10.23	0.22	22.27	8.56	0.81	0.03	0.04	0.00	99.19
GOR132-G_1	11/06/2015	45.37	0.22	10.98	10.01	0.12	22.15	8.45	0.75	0.06	0.05	0.01	98.17
GOR132-G_2	11/06/2015	45.64	0.31	10.80	10.22	0.20	22.46	8.64	0.84	0.02	0.07	0.01	99.23
GOR132-G_3	11/06/2015	45.77	0.25	11.07	10.22	0.17	22.13	8.37	0.72	0.04	0.03	0.00	98.79
GOR132-G_4	11/06/2015	45.66	0.31	10.77	10.33	0.14	22.39	8.40	0.82	0.03	0.00	0.00	98.85
GOR132-G_5	11/06/2015	45.43	0.25	10.95	10.13	0.18	22.12	8.31	0.75	0.02	0.01	0.02	98.18
GOR132-G_6	11/06/2015	45.59	0.28	10.84	9.98	0.11	22.04	8.35	0.88	0.01	0.06	0.02	98.15
GOR132-G_7	11/06/2015	45.69	0.33	11.00	10.18	0.15	22.09	8.58	0.69	0.01	0.05	0.02	98.80

Reference Glass (Jochum et al., 2006)	Run Date	SiO_2	TiO_2	Al_2O_3	FeOt	MnO	MgO	CaO	Na_2O	K_2O	P_2O_5	Cl	Analytical total
GOR132-G_8	11/06/2015	45.19	0.28	10.97	10.45	0.12	21.96	8.50	0.84	0.04	0.00	0.00	98.34
GOR132-G_9	11/06/2015	45.42	0.35	11.00	10.23	0.07	22.12	8.50	0.94	0.04	0.01	0.00	98.67
GOR132-G_10	11/06/2015	45.40	0.35	10.81	10.63	0.14	22.27	8.49	0.70	0.04	0.01	0.00	98.84
GOR132-G_11	11/06/2015	45.20	0.27	10.93	10.32	0.15	21.97	8.57	0.90	0.03	0.02	0.00	98.37
GOR132-G_12	11/06/2015	45.62	0.31	10.97	10.29	0.19	22.49	8.36	0.87	0.07	0.13	0.00	99.29
GOR132-G_13	11/06/2015	45.19	0.31	10.88	10.27	0.19	22.16	8.42	0.77	0.04	0.04	0.00	98.27
GOR132-G_14	11/06/2015	45.52	0.33	10.99	10.26	0.15	22.05	8.43	0.78	0.03	0.05	0.00	98.58
GOR132-G_15	11/06/2015	45.22	0.34	10.96	9.99	0.14	21.97	8.36	0.92	0.02	0.11	0.02	98.03
GOR132-G_16	11/06/2015	45.68	0.30	10.95	10.23	0.19	21.88	8.61	0.96	0.02	0.10	0.00	98.93
GOR132-G_18	11/06/2015	45.76	0.29	10.88	10.35	0.20	21.96	8.48	0.89	0.01	0.05	0.00	98.88
GOR132-G_19	11/06/2015	45.67	0.29	10.82	10.33	0.15	22.26	8.58	0.83	0.04	0.05	0.01	99.05
GOR132-G_20	11/06/2015	45.39	0.33	10.89	10.35	0.21	22.25	8.55	0.74	0.05	0.02	0.00	98.78
GOR132-G_21	11/06/2015	45.77	0.28	10.91	10.24	0.12	22.07	8.43	0.89	0.02	0.04	0.00	98.76
GOR132-G_1	23/07/2015	45.57	0.36	10.92	10.51	0.10	22.23	8.54	0.75	0.02	0.07	0.01	99.06
GOR132-G_3	24/07/2015	45.38	0.32	10.68	10.47	0.23	22.10	8.65	0.62	0.02	0.07	0.00	98.54
GOR132-G_2	25/07/2015	45.76	0.32	10.68	10.22	0.15	22.04	8.60	0.87	0.02	0.00	0.00	98.66
GOR132-G_4	26/07/2015	45.37	0.30	10.93	10.43	0.07	22.31	8.68	0.82	0.03	0.01	0.00	98.96
GOR132-G_5	27/07/2015	45.43	0.32	10.85	10.07	0.12	22.31	8.38	0.87	0.04	0.06	0.01	98.45
GOR132-G_6	28/07/2015	45.25	0.32	10.84	10.01	0.20	22.35	8.51	0.84	0.05	0.00	0.00	98.37
GOR132-G_1	24/07/2015	45.24	0.35	11.01	10.74	0.18	22.32	8.49	0.86	0.02	0.08	0.00	99.30
GOR132-G_10	24/07/2015	45.17	0.28	10.87	10.50	0.16	22.11	8.43	0.68	0.03	0.02	0.00	98.24
GOR132-G_2	24/07/2015	45.33	0.32	10.94	10.12	0.22	22.10	8.50	0.83	0.03	0.03	0.00	98.42
GOR132-G_3	24/07/2015	45.28	0.27	10.74	10.06	0.09	22.08	8.49	0.84	0.04	0.00	0.01	97.90

Reference Glass (Jochum et al., 2006)	Run Date	SiO_2	TiO_2	Al_2O_3	FeOt	MnO	MgO	CaO	Na_2O	K_2O	P_2O_5	Cl	Analytical total
GOR132-G_5	24/07/2015	45.33	0.33	11.05	9.82	0.07	21.91	8.45	0.79	0.02	0.05	0.01	97.83
GOR132-G_6	24/07/2015	45.65	0.31	11.12	10.17	0.18	22.02	8.60	0.90	0.04	0.06	0.01	99.07
GOR132-G_7	24/07/2015	45.75	0.32	10.87	10.56	0.15	22.31	8.49	0.77	0.04	0.02	0.00	99.28
GOR132-G_4	24/07/2015	45.37	0.28	10.93	10.32	0.16	21.91	8.45	0.79	0.04	0.10	0.00	98.34
GOR132-G_8	24/07/2015	45.04	0.40	10.92	10.17	0.16	22.07	8.52	0.83	0.01	0.01	0.00	98.13
GOR132-G_9	24/07/2015	45.45	0.26	10.82	10.46	0.21	22.46	8.63	0.71	0.04	0.02	0.00	99.05
GOR132-G_1	11/08/2016	45.77	0.26	11.05	10.20	0.13	21.96	8.39	0.81	0.00	0.03	0.00	98.60
GOR132-G_2	11/08/2016	45.92	0.28	11.10	10.39	0.15	22.14	8.29	0.76	0.01	0.03	0.01	99.06
GOR132-G_3	11/08/2016	45.45	0.29	10.90	9.65	0.13	22.02	8.37	0.79	0.03	0.02	0.01	97.65
GOR132-G_4	11/08/2016	45.10	0.30	10.78	10.02	0.09	21.99	8.41	0.76	0.07	0.00	0.00	97.52
GOR132-G_5	11/08/2016	45.15	0.26	10.68	10.39	0.18	22.17	8.36	0.80	0.05	0.02	0.01	98.07
GOR132-G_6	11/08/2016	44.79	0.20	10.51	9.96	0.21	21.85	8.46	0.85	0.04	0.00	0.01	96.89
GOR132-G_7	11/08/2016	44.20	0.29	10.61	9.69	0.23	22.08	8.39	0.83	0.03	0.01	0.00	96.36
GOR132-G_1	12/08/2016	45.25	0.34	10.98	10.72	0.12	21.74	8.41	0.78	0.05	0.06	0.01	98.46
GOR132-G_3	12/08/2016	45.16	0.32	10.98	10.32	0.21	21.78	8.55	0.89	0.02	0.10	0.00	98.33
GOR132-G_2	12/08/2016	45.93	0.30	10.87	10.39	0.10	21.74	8.52	0.79	0.06	0.01	0.00	98.70
GOR132-G_4	12/08/2016	45.70	0.29	10.88	10.50	0.09	21.83	8.58	0.90	0.02	0.04	0.01	98.85
GOR132-G_5	12/08/2016	45.70	0.28	10.74	10.06	0.18	21.90	8.57	0.79	0.05	0.08	0.02	98.35
GOR132-G_6	12/08/2016	45.60	0.33	10.84	10.04	0.13	21.81	8.43	0.78	0.02	0.00	0.00	97.98
GOR132-G_8	12/08/2016	45.64	0.32	11.02	10.73	0.14	21.81	8.64	0.79	0.04	0.04	0.02	99.20
GOR132-G_7	12/08/2016	45.73	0.33	11.10	10.79	0.16	21.96	8.30	0.85	0.06	0.04	0.03	99.34
GOR132-G_1	14/09/2015	45.57	0.31	10.82	10.48	0.17	22.30	8.36	0.72	0.04	0.05	0.00	98.80
GOR132-G_2	14/09/2015	46.09	0.30	10.97	10.50	0.20	22.59	8.24	0.71	0.07	0.05	0.00	99.71

Reference Glass (Jochum et al., 2006)	Run Date	SiO_2	TiO_2	Al_2O_3	FeOt	MnO	MgO	CaO	Na_2O	K_2O	P_2O_5	Cl	Analytical total
GOR132-G_3	14/09/2015	45.44	0.30	10.83	10.57	0.09	21.99	8.31	0.70	0.03	0.03	0.01	98.28
GOR132-G_4	14/09/2015	45.88	0.29	10.97	10.60	0.16	22.01	8.30	0.69	0.05	0.07	0.01	99.02
GOR132-G_5	14/09/2015	45.63	0.33	10.85	10.65	0.15	22.42	8.11	0.86	0.03	0.08	0.01	99.12
GOR132-G_6	14/09/2015	45.89	0.34	11.01	10.35	0.14	22.17	8.23	0.87	0.05	0.06	0.01	99.13
GOR132-G_7	14/09/2015	45.31	0.28	10.78	10.45	0.06	21.91	8.31	0.78	0.03	0.02	0.00	97.92
GOR132-G_8	14/09/2015	45.33	0.29	10.89	10.48	0.16	22.07	8.41	0.89	0.03	0.02	0.01	98.57
GOR132-G_9	14/09/2015	45.73	0.26	10.92	10.27	0.11	21.90	8.26	0.80	0.00	0.06	0.00	98.30
GOR132-G_10	14/09/2015	45.84	0.29	10.99	10.42	0.15	22.33	8.38	0.82	0.02	0.01	0.00	99.26
GOR132-G_11	14/09/2015	46.13	0.36	11.05	10.12	0.19	22.27	8.31	0.89	0.02	0.04	0.00	99.36
GOR132-G_12	14/09/2015	45.46	0.28	10.86	10.13	0.15	22.01	8.36	0.83	0.02	0.07	0.02	98.18
GOR132-G_1	20/05/2016	45.81	0.24	11.13	10.16	0.17	21.92	8.50	0.85	0.03	0.06	0.01	98.86
GOR132-G_10	20/05/2016	45.97	0.27	11.11	10.43	0.14	22.15	8.51	0.81	0.05	0.05	0.02	99.52
GOR132-G_2	20/05/2016	45.86	0.24	11.02	9.89	0.15	21.67	8.57	0.86	0.05	0.04	0.00	98.34
GOR132-G_3	20/05/2016	45.45	0.37	10.86	9.96	0.18	22.19	8.41	0.81	0.05	0.05	0.00	98.31
GOR132-G_4	20/05/2016	45.52	0.29	10.84	10.24	0.19	22.21	8.52	0.72	0.03	0.04	0.00	98.59
GOR132-G_5	20/05/2016	45.33	0.32	10.94	10.89	0.09	22.21	8.65	0.83	0.02	0.06	0.00	99.34
GOR132-G_6	20/05/2016	45.43	0.35	11.00	10.47	0.17	22.11	8.58	0.80	0.05	0.05	0.03	99.03
GOR132-G_7	20/05/2016	45.53	0.30	10.95	10.31	0.15	22.15	8.46	0.77	0.02	0.08	0.00	98.72
GOR132-G_8	20/05/2016	45.54	0.27	10.89	10.11	0.19	22.09	8.66	0.84	0.03	0.00	0.01	98.64
GOR132-G_9	20/05/2016	45.21	0.27	10.89	10.25	0.22	22.19	8.47	0.76	0.04	0.01	0.00	98.30
GOR132-G_1	23/06/2015	45.34	0.35	10.91	10.27	0.17	22.58	8.62	0.86	0.02	0.02	0.00	99.15
GOR132-G_2	23/06/2015	45.43	0.32	10.84	10.10	0.17	22.18	8.64	0.83	0.01	0.08	0.02	98.62
GOR132-G_3	23/06/2015	45.34	0.28	11.04	10.41	0.14	22.16	8.53	0.84	0.03	0.06	0.00	98.83

Reference Glass (Jochum et al., 2006)	Run Date	SiO_2	TiO_2	Al_2O_3	FeOt	MnO	MgO	CaO	Na_2O	K_2O	P_2O_5	Cl	Analytical total
GOR132-G_4	23/06/2015	45.83	0.25	11.06	10.07	0.09	21.97	8.49	0.79	0.02	0.04	0.01	98.63
GOR132-G_5	23/06/2015	45.82	0.30	11.12	10.14	0.17	21.98	8.65	0.71	0.04	0.05	0.01	98.99
GOR132-G_6	23/06/2015	45.51	0.33	10.98	10.31	0.19	22.21	8.50	0.84	0.02	0.05	0.03	98.97
GOR132-G_7	23/06/2015	45.50	0.33	10.97	10.00	0.14	22.28	8.59	0.96	0.04	0.04	0.00	98.85
GOR132-G_1	01/05/2017	45.06	0.24	10.90	10.35	0.11	22.07	8.58	0.75	0.05	0.05	0.01	98.17
GOR132-G_2	01/05/2017	45.27	0.30	11.11	9.95	0.13	22.42	8.55	0.87	0.03	0.05	0.00	98.68
GOR132-G_3	01/05/2017	45.52	0.27	10.84	9.73	0.13	22.21	8.75	0.89	0.03	0.04	0.02	98.42
GOR132-G_4	01/05/2017	45.64	0.33	10.90	9.74	0.19	22.43	8.47	0.82	0.03	0.03	0.00	98.59
GOR132-G_5	01/05/2017	45.56	0.28	10.97	9.93	0.12	22.18	8.57	0.92	0.03	0.06	0.00	98.62
GOR132-G_6	01/05/2017	45.34	0.33	11.07	10.28	0.17	22.17	8.48	0.67	0.04	0.02	0.01	98.58
ATHO-G_5	08/06/2015	75.13	0.20	12.31	3.08	0.14	0.05	1.65	4.22	2.74	0.02	0.05	99.60
ATHO-G_7	08/06/2015	74.89	0.27	11.97	3.30	0.11	0.02	1.74	4.15	2.81	0.01	0.04	99.31
ATHO-G_2	08/06/2015	75.00	0.27	12.12	3.17	0.15	0.08	1.62	4.03	2.76	0.05	0.01	99.26
ATHO-G_3	08/06/2015	75.13	0.24	12.11	3.18	0.01	0.10	1.68	4.18	2.77	0.03	0.06	99.50
ATHO-G_1	08/06/2015	75.30	0.22	12.04	3.22	0.02	0.11	1.68	4.13	2.74	0.03	0.04	99.53
ATHO-G_4	08/06/2015	75.08	0.23	12.04	3.20	0.11	0.08	1.67	4.09	2.73	0.02	0.05	99.29
ATHO-G_1	09/06/2015	75.22	0.25	12.12	3.08	0.13	0.04	1.80	4.06	2.72	0.01	0.06	99.50
ATHO-G_4	09/06/2015	74.46	0.26	12.18	3.14	0.10	0.13	1.64	4.12	2.79	0.00	0.02	98.84
ATHO-G_2	09/06/2015	74.90	0.24	12.19	3.16	0.05	0.09	1.67	4.18	2.71	0.03	0.03	99.28
ATHO-G_3	09/06/2015	75.09	0.24	12.37	3.02	0.07	0.11	1.66	4.06	2.77	0.00	0.05	99.45
ATHO-G_1	10/06/2015	75.44	0.26	12.36	3.09	0.16	0.08	1.70	4.02	2.85	0.00	0.03	99.98
ATHO-G_6	10/06/2015	74.88	0.24	12.45	3.09	0.10	0.11	1.74	4.23	2.71	0.09	0.03	99.67

Reference Glass (Jochum et al., 2006)	Run Date	SiO_2	TiO_2	Al_2O_3	FeOt	MnO	MgO	CaO	Na_2O	K_2O	P_2O_5	Cl	Analytical total
ATHO-G_2	10/06/2015	75.42	0.21	12.34	3.25	0.12	0.04	1.69	4.18	2.71	0.00	0.05	100.00
ATHO-G_3	10/06/2015	75.62	0.23	12.32	3.19	0.11	0.10	1.68	4.18	2.70	0.01	0.03	100.19
ATHO-G_4	10/06/2015	75.01	0.19	12.27	3.18	0.11	0.13	1.74	4.33	2.64	0.04	0.05	99.67
ATHO-G_5	10/06/2015	75.33	0.26	12.37	3.40	0.13	0.06	1.77	4.01	2.67	0.06	0.08	100.13
ATHO-G_7	10/06/2015	75.53	0.28	12.25	3.52	0.10	0.07	1.70	4.03	2.80	0.00	0.07	100.34
ATHO-G_1	10/06/2015	74.17	0.23	12.35	3.06	0.07	0.04	1.77	3.97	2.77	0.00	0.04	98.47
ATHO-G_2	10/06/2015	74.86	0.25	12.24	3.04	0.08	0.04	1.67	4.21	2.78	0.00	0.05	99.22
ATHO-G_3	10/06/2015	74.61	0.31	12.42	3.35	0.11	0.12	1.74	4.32	2.74	0.01	0.07	99.80
ATHO-G_4	10/06/2015	74.84	0.21	12.28	3.19	0.12	0.06	1.68	4.14	2.75	0.02	0.04	99.34
ATHO-G_5	10/06/2015	74.77	0.20	12.25	3.40	0.04	0.05	1.63	4.00	2.78	0.00	0.04	99.16
ATHO-G_6	10/06/2015	75.07	0.28	12.32	3.23	0.08	0.10	1.71	4.29	2.72	0.02	0.05	99.85
ATHO-G_7	10/06/2015	74.90	0.27	12.13	3.15	0.04	0.05	1.69	4.18	2.77	0.02	0.03	99.23
ATHO-G_8	10/06/2015	74.89	0.23	12.38	3.15	0.12	0.12	1.62	4.28	2.71	0.04	0.06	99.59
ATHO-G_9	10/06/2015	74.99	0.24	12.28	3.21	0.06	0.09	1.70	4.22	2.69	0.00	0.07	99.56
ATHO-G_10	10/06/2015	75.02	0.26	12.27	3.29	0.05	0.09	1.75	3.93	2.71	0.05	0.05	99.48
ATHO-G_11	10/06/2015	75.37	0.17	12.26	3.31	0.13	0.18	1.73	3.96	2.80	0.07	0.03	100.02
ATHO-G_12	10/06/2015	75.13	0.23	12.29	3.18	0.14	0.08	1.65	3.99	2.70	0.01	0.05	99.47
ATHO-G_13	10/06/2015	75.30	0.18	12.19	3.12	0.12	0.07	1.68	4.26	2.74	0.04	0.04	99.75
ATHO-G_14	10/06/2015	75.43	0.26	12.15	3.27	0.07	0.07	1.70	4.12	2.80	0.04	0.04	99.95
ATHO-G_15	10/06/2015	75.49	0.26	12.24	3.07	0.09	0.08	1.69	3.87	2.81	0.02	0.03	99.66
ATHO-G_16	10/06/2015	75.22	0.26	12.32	3.30	0.07	0.12	1.68	4.15	2.84	0.03	0.03	100.02
ATHO-G_18	10/06/2015	75.13	0.23	12.21	3.29	0.06	0.09	1.67	4.09	2.74	0.09	0.06	99.65
ATHO-G_19	10/06/2015	75.14	0.25	12.24	3.33	0.12	0.16	1.61	4.04	2.73	0.01	0.05	99.68

Reference Glass (Jochum et al., 2006)	Run Date	SiO_2	TiO_2	Al_2O_3	FeOt	MnO	MgO	CaO	Na_2O	K_2O	P_2O_5	Cl	Analytical total
ATHO-G_20	10/06/2015	74.86	0.29	12.14	3.11	0.03	0.12	1.65	3.98	2.79	0.00	0.08	99.06
ATHO-G_21	10/06/2015	75.49	0.29	12.28	3.38	0.12	0.08	1.70	4.09	2.78	0.02	0.05	100.26
ATHO-G_1	18/05/2016	12.36	1.74	0.09	0.12	0.24	3.98	2.71	0	0.02	75.89	0.01	97.17
ATHO-G_10	18/05/2016	12.18	1.59	0.09	0.08	0.22	4.12	2.79	0	0.03	75.37	0.00	96.48
ATHO-G_11	18/05/2016	12.17	1.66	0.09	0.10	0.28	4.12	2.81	0	0.05	75.28	0.05	96.61
ATHO-G_12	18/05/2016	12.19	1.65	0.11	0.00	0.19	4.18	2.72	0	0.02	75.13	0.04	96.22
ATHO-G_13	18/05/2016	11.98	1.64	0.11	0.07	0.29	3.76	2.72	0	0.07	75.00	0.02	95.66
ATHO-G_2	18/05/2016	12.59	1.70	0.10	0.09	0.23	4.18	2.72	0	0.04	75.83	0.00	97.48
ATHO-G_1	18/05/2016	12.05	1.70	0.10	0.11	0.26	4.37	2.78	0	0.07	74.62	0.03	96.08
ATHO-G_4	18/05/2016	12.25	1.65	0.11	0.11	0.24	4.24	2.68	0	0.04	75.64	0.02	96.97
ATHO-G_5	18/05/2016	12.35	1.73	0.09	0.16	0.25	4.25	2.71	0	0.06	75.12	0.01	96.73
ATHO-G_6	18/05/2016	12.37	1.71	0.09	0.14	0.20	4.17	2.74	0	0.04	75.51	0.00	96.96
ATHO-G_7	18/05/2016	12.40	1.68	0.11	0.10	0.22	4.18	2.71	0	0.04	75.73	0.03	97.20
ATHO-G_8	18/05/2016	12.33	1.73	0.12	0.02	0.28	4.20	2.76	0	0.05	75.61	0.07	97.16
ATHO-G_9	18/05/2016	12.35	1.72	0.09	0.07	0.26	3.70	2.54	0	0.04	75.69	0.04	96.51
ATHO-G_1	23/07/2015	74.16	0.24	12.17	3.32	0.11	0.09	1.72	4.09	2.75	0.03	0.03	98.71
ATHO-G_7	23/07/2015	74.59	0.23	12.33	3.21	0.11	0.07	1.64	4.05	2.70	0.00	0.04	98.96
ATHO-G_2	23/07/2015	74.83	0.21	12.25	3.30	0.16	0.09	1.78	4.04	2.71	0.00	0.05	99.42
ATHO-G_4	23/07/2015	74.82	0.30	12.13	3.09	0.12	0.04	1.66	4.32	2.76	0.00	0.04	99.27
ATHO-G_5	23/07/2015	75.06	0.24	12.19	3.26	0.15	0.08	1.66	4.15	2.73	0.00	0.04	99.56
ATHO-G_6	23/07/2015	75.20	0.20	12.11	3.24	0.07	0.10	1.69	4.01	2.72	0.08	0.02	99.43
ATHO-G_1	24/07/2015	74.53	0.25	12.07	3.21	0.12	0.05	1.64	4.19	2.86	0.02	0.02	98.96
ATHO-G_10	24/07/2015	75.02	0.27	12.09	3.25	0.08	0.05	1.75	4.21	2.75	0.03	0.04	99.54

Reference Glass (Jochum et al., 2006)	Run Date	SiO_2	TiO_2	Al_2O_3	FeOt	MnO	MgO	CaO	Na_2O	K_2O	P_2O_5	Cl	Analytical total
ATHO-G_2	24/07/2015	74.47	0.26	12.20	3.26	0.17	0.07	1.74	3.99	2.70	0.08	0.03	98.98
ATHO-G_3	24/07/2015	75.34	0.26	12.12	3.21	0.11	0.09	1.64	4.17	2.72	0.01	0.04	99.72
ATHO-G_5	24/07/2015	74.72	0.21	12.33	3.36	0.13	0.10	1.58	4.26	2.84	0.00	0.04	99.57
ATHO-G_6	24/07/2015	75.42	0.25	12.12	3.46	0.19	0.10	1.73	3.51	2.81	0.02	0.02	99.63
ATHO-G_7	24/07/2015	74.91	0.22	12.32	3.31	0.01	0.09	1.71	4.14	2.65	0.00	0.05	99.40
ATHO-G_4	24/07/2015	74.97	0.26	12.34	3.17	0.03	0.12	1.67	4.39	2.70	0.01	0.04	99.69
ATHO-G_8	24/07/2015	75.00	0.22	12.34	3.14	0.08	0.11	1.71	4.07	2.72	0.00	0.06	99.44
ATHO-G_9	24/07/2015	75.34	0.26	12.30	2.98	0.11	0.06	1.65	4.26	2.76	0.00	0.01	99.73
ATHO-G_1	11/08/2016	75.23	0.27	12.16	3.25	0.15	0.06	1.73	4.17	2.87	0.05	0.02	99.97
ATHO-G_2	11/08/2016	75.16	0.21	12.28	2.99	0.13	0.10	1.60	4.08	2.73	0.03	0.04	99.35
ATHO-G_3	11/08/2016	74.58	0.27	11.94	3.29	0.09	0.10	1.59	4.29	2.79	0.02	0.02	99.00
ATHO-G_4	11/08/2016	74.93	0.26	11.97	3.46	0.07	0.10	1.70	4.25	2.74	0.02	0.01	99.51
ATHO-G_5	11/08/2016	74.89	0.25	12.06	3.43	0.13	0.09	1.68	4.18	2.93	0.03	0.03	99.70
ATHO-G_6	11/08/2016	74.89	0.31	12.05	3.30	0.15	0.13	1.59	4.13	2.91	0.03	0.02	99.52
ATHO-G_7	11/08/2016	74.98	0.28	11.87	3.37	0.09	0.10	1.75	4.15	2.85	0.00	0.02	99.46
ATHO-G_8	11/08/2016	74.85	0.29	12.20	3.45	0.13	0.10	1.65	4.04	2.85	0.02	0.03	99.61
ATHO-G_1	11/08/2016	75.39	0.22	12.29	3.13	0.08	0.10	1.73	4.28	2.73	0.03	0.02	100.00
ATHO-G_3	11/08/2016	75.36	0.27	12.24	3.20	0.08	0.10	1.71	4.06	2.82	0.00	0.05	99.89
ATHO-G_2	11/08/2016	74.97	0.23	12.21	2.99	0.08	0.06	1.68	4.41	2.68	0.03	0.05	99.37
ATHO-G_4	11/08/2016	75.14	0.19	12.34	3.19	0.10	0.11	1.69	4.23	2.67	0.03	0.03	99.74
ATHO-G_5	11/08/2016	74.52	0.24	12.31	3.30	0.03	0.06	1.80	4.06	2.92	0.04	0.02	99.30
ATHO-G_6	11/08/2016	74.86	0.24	12.42	3.30	0.10	0.13	1.69	4.15	2.71	0.00	0.03	99.63
ATHO-G_7	11/08/2016	74.67	0.18	12.35	3.49	0.14	0.07	1.66	4.06	2.74	0.03	0.02	99.41

Reference Glass (Jochum et al., 2006)	Run Date	SiO_2	TiO_2	Al_2O_3	FeOt	MnO	MgO	CaO	Na_2O	K_2O	P_2O_5	Cl	Analytical total
ATHO-G_8	11/08/2016	74.46	0.24	12.32	3.35	0.05	0.10	1.65	4.19	2.60	0.03	0.02	99.01
ATHO-G_2	14/09/2015	74.71	0.25	12.06	3.22	0.04	0.09	1.66	4.31	2.70	0.04	0.04	99.13
ATHO-G_3	14/09/2015	75.08	0.26	12.06	3.18	0.12	0.11	1.62	4.19	2.77	0.02	0.03	99.45
ATHO-G_4	14/09/2015	75.44	0.22	12.14	3.21	0.08	0.11	1.66	4.24	2.65	0.07	0.02	99.83
ATHO-G_5	14/09/2015	74.90	0.23	12.07	3.25	0.12	0.14	1.70	3.94	2.76	0.03	0.04	99.17
ATHO-G_7	14/09/2015	74.88	0.23	12.20	3.35	0.11	0.12	1.62	3.94	2.75	0.06	0.05	99.30
ATHO-G_8	14/09/2015	74.79	0.23	12.21	3.33	0.15	0.10	1.65	3.92	2.81	0.02	0.04	99.26
ATHO-G_10	14/09/2015	75.17	0.19	12.14	3.28	0.11	0.12	1.62	4.11	2.83	0.02	0.05	99.63
ATHO-G_12	14/09/2015	74.57	0.26	12.26	3.25	0.05	0.05	1.61	4.21	2.72	0.03	0.04	99.06
ATHO-G_1	20/05/2016	75.63	0.28	12.55	3.21	0.11	0.08	1.77	4.13	2.73	0.00	0.03	100.51
ATHO-G_10	20/05/2016	75.60	0.24	12.31	3.25	0.19	0.08	1.75	4.16	2.61	0.04	0.05	100.27
ATHO-G_2	20/05/2016	75.65	0.21	12.62	3.25	0.04	0.09	1.65	4.30	2.62	0.08	0.01	100.51
ATHO-G_3	20/05/2016	75.70	0.25	12.31	3.35	0.12	0.12	1.79	4.37	2.71	0.01	0.04	100.77
ATHO-G_4	20/05/2016	75.49	0.23	12.44	3.28	0.10	0.11	1.82	4.27	2.69	0.03	0.03	100.49
ATHO-G_5	20/05/2016	75.56	0.23	12.22	3.28	0.14	0.09	1.68	3.87	2.63	0.01	0.04	99.75
ATHO-G_6	20/05/2016	75.16	0.29	12.24	3.12	0.05	0.09	1.69	4.18	2.69	0.00	0.03	99.55
ATHO-G_7	20/05/2016	75.44	0.27	12.23	3.30	0.13	0.10	1.75	4.17	2.82	0.05	0.03	100.28
ATHO-G_8	20/05/2016	75.04	0.23	12.24	2.88	0.12	0.11	1.77	4.18	2.76	0.04	0.03	99.40
ATHO-G_9	20/05/2016	75.36	0.21	12.31	3.02	0.18	0.06	1.70	4.01	2.76	0.03	0.04	99.70
ATHO-G_1	23/06/2015	75.42	0.25	12.17	3.16	0.10	0.03	1.74	3.98	2.77	0.00	0.03	99.66
ATHO-G_3	23/06/2015	74.67	0.23	12.11	3.10	0.09	0.10	1.67	3.97	2.82	0.03	0.04	98.84
ATHO-G_4	23/06/2015	75.33	0.18	12.23	3.13	0.06	0.05	1.62	3.77	2.71	0.00	0.05	99.13
ATHO-G_5	23/06/2015	75.23	0.28	12.33	3.20	0.09	0.05	1.67	4.28	2.58	0.02	0.05	99.78

Reference Glass (Jochum et al., 2006)	Run Date	SiO_2	TiO_2	Al_2O_3	FeOt	MnO	MgO	CaO	Na_2O	K_2O	P_2O_5	Cl	Analytical total
ATHO-G_6	23/06/2015	74.77	0.26	12.41	3.16	0.07	0.14	1.59	4.12	2.72	0.01	0.05	99.30
ATHO-G_1	01/05/2017	74.23	0.23	12.23	3.18	0.12	0.10	1.70	4.03	2.78	0.00	0.04	98.64
ATHO-G_2	01/05/2017	74.58	0.28	12.26	3.07	0.09	0.10	1.70	4.39	2.71	0.03	0.03	99.22
ATHO-G_3	01/05/2017	74.94	0.30	12.33	3.22	0.12	0.11	1.62	4.25	2.80	0.01	0.05	99.75
ATHO-G_4	01/05/2017	74.60	0.28	12.34	3.34	0.11	0.06	1.65	3.97	2.70	0.05	0.03	99.13
ATHO-G_5	01/05/2017	75.10	0.24	12.30	3.24	0.13	0.08	1.73	4.31	2.84	0.00	0.02	100.00
ATHO-G_6	01/05/2017	75.60	0.28	12.40	3.37	0.13	0.12	1.68	4.24	2.70	0.05	0.02	100.58

Table B3. Average glass analyses of proximal samples Ma-b (Mashu), Iz-Kt (Kozushima), KGP (Kawagodaira), To-C (Towada)

Tephra	Ma-b (Mashu)		Iz-Kt[1] (Kozushima)		KGP (Kawagodaira)		To-C (Chuseri)		To-C (Kanegasawa)		To-C (Utarube-a)		To-C (Utarube-b)	
Grid Ref.	43°33'54.94"N, 144°38'45.42"E		34°11'52.9"N, 139°7'31.4"E		35° 7′52″N, 139° 0′48″E		40°23'14", 140°58'19''E		40°23'14", 140°58'19''E		40°23'14", 140°58'19''E		40°23'14", 140°58'19''E	
wt. (%)	Avg.	± 1 σ	Avg.	± 1 σ	Avg.	± 1 σ	Avg.	± 1 σ	Avg.	± 1 σ	Avg.	± 1 σ	Avg.	± 1 σ
SiO_2	73.95	0.39	77.71	0.67	77.30	0.84	74.15	0.32	74.80	0.68	74.32	1.35	74.17	2.92
TiO_2	0.62	0.04	0.11	0.08	0.24	0.03	0.49	0.04	0.46	0.03	0.46	0.05	0.46	0.15
Al_2O_3	13.03	0.11	12.90	0.39	12.39	0.35	13.60	0.18	13.20	0.27	13.68	0.94	13.76	1.14
FeO^T	3.16	0.13	0.74	0.15	1.42	0.57	2.41	0.14	2.41	0.28	2.25	0.26	2.32	1.23
MnO	0.13	0.05	0.14	0.08	0.06	0.06	0.09	0.04	0.10	0.03	0.10	0.05	0.09	0.04
MgO	0.72	0.04	0.14	0.04	0.46	0.73	0.59	0.05	0.60	0.09	0.57	0.16	0.54	0.31
CaO	3.18	0.08	0.36	0.10	1.56	0.05	2.72	0.09	2.60	0.14	2.76	0.57	2.83	0.97
Na_2O	4.19	0.48	4.15	0.26	3.68	0.18	4.58	0.15	4.43	0.23	4.49	0.16	4.44	0.38
K_2O	0.77	0.03	3.74	0.27	2.72	0.08	1.17	0.04	1.22	0.07	1.22	0.13	1.21	0.18
P_2O_5	0.13	0.03	-	-	0.03	0.02	0.08	0.04	0.07	0.03	0.08	0.04	0.09	0.04
Cl	0.12	0.03	-	-	0.12	0.03	0.12	0.02	0.10	0.02	0.09	0.02	0.10	0.02
n	*10*		*60*		*17*		*16*		*10*		*19*		*38*	

1) Suzuki, T., Nishizawa, F., Ishimura, D. Ito, M., Maruyama, S., Danhara, T. and Hirata, T. 2017. Re-examination of identification and discrimination of Kozu-Tenjosan and Nijima-Mukaiyama tephras, Izu Islands, Japan. Japan Association for Quaternary Research, Programme and Abstracts, 47: 49 (In Japanese)

Appendix C: Supplementary Material for Article 3.

Table C1. Major element glass analyses of the cryptotephra layers identified in the Lake Suigetsu sediments between 50 to 30 ka

SG Label	Run Date	SiO_2	TiO_2	Al_2O_3	FeOt	MnO	MgO	CaO	Na_2O	K_2O	P_2O_5	Cl	Analytical total
SG14-2625	24/04/2010	60.29	1.07	15.28	6.14	0.11	1.93	4.62	3.65	3.06	0.39	-	96.53
SG14-2625	24/04/2010	60.82	1.25	15.51	7.28	0.33	2.23	5.23	3.74	2.85	0.39	-	99.61
SG14-2625	24/04/2010	60.78	1.20	15.32	7.28	0.12	2.13	4.78	3.80	2.99	0.44	-	98.84
SG14-2625	24/04/2010	61.42	1.23	15.39	6.59	0.27	2.06	4.86	3.88	2.99	0.40	-	99.08
SG14-2625	24/04/2010	61.76	1.14	15.44	6.19	0.19	2.06	4.78	3.72	3.14	0.39	-	98.81
SG14-2625	24/04/2010	60.60	1.21	15.78	7.04	0.09	2.14	5.27	3.84	2.85	0.39	-	99.23
SG14-2625	24/04/2010	60.50	1.20	15.52	7.49	0.09	2.27	5.15	4.24	3.01	0.38	-	99.84
SG14-2625	24/04/2010	60.97	1.32	15.53	6.98	0.16	2.00	4.98	3.97	2.85	0.42	-	99.18
SG14-2625	24/04/2010	64.60	0.93	14.92	5.39	0.16	1.40	3.54	3.92	3.85	0.40	-	99.09
SG14-2625	24/04/2010	61.31	1.14	15.96	7.03	0.08	2.04	5.05	3.78	2.90	0.38	-	99.68
SG14-2625	24/04/2010	60.41	1.39	15.31	7.09	0.18	2.15	4.93	3.80	2.87	0.38	-	98.50
SG14-2625	24/04/2010	62.91	1.00	14.99	5.96	0.14	1.71	4.13	4.20	3.49	0.35	-	98.87
SG14-2625	24/04/2010	60.79	1.10	15.74	6.80	0.12	1.91	4.58	3.86	3.20	0.42	-	98.53
SG14-2625	24/04/2010	61.82	1.30	15.91	6.57	0.04	2.12	4.83	3.75	2.89	0.41	-	99.65
SG14-2625	24/04/2010	60.47	1.27	14.84	7.61	0.07	2.26	4.97	3.84	2.93	0.40	-	98.66
SG14-2625	24/04/2010	60.45	1.24	15.72	7.11	0.18	2.42	5.40	3.67	2.58	0.38	-	99.16
SG14-2625	24/04/2010	60.37	1.21	15.65	7.68	0.08	2.20	5.46	3.94	2.78	0.39	-	99.77
SG14-2625	24/04/2010	61.39	1.27	15.13	7.47	0.22	2.22	4.77	3.82	2.91	0.43	-	99.63
SG14-2625	24/04/2010	60.43	1.23	14.92	6.72	0.18	2.20	4.67	3.64	2.93	0.40	-	97.32
SG14-2625	24/04/2010	60.69	1.25	15.16	7.26	0.13	2.23	4.98	4.09	3.06	0.46	-	99.32
SG14-2625	24/04/2010	61.55	1.18	15.46	6.90	0.13	2.11	4.82	4.07	3.05	0.43	-	99.69

SG Label	Run Date	SiO_2	TiO_2	Al_2O_3	FeOt	MnO	MgO	CaO	Na_2O	K_2O	P_2O_5	Cl	Analytical total
SG14-2649	16/04/2010	71.44	0.38	12.68	1.74	0.00	0.31	1.56	3.07	4.27	0.04	-	95.49
SG14-2649	16/04/2010	72.74	0.41	13.04	1.86	0.03	0.34	1.49	3.43	4.30	0.05	-	97.69
SG14-2649	16/04/2010	71.75	0.42	12.87	1.66	0.04	0.38	1.51	3.45	4.40	0.03	-	96.51
SG14-2649	16/04/2010	70.80	0.38	12.95	1.63	0.00	0.41	1.62	3.23	4.21	0.07	-	95.31
SG14-2649	16/04/2010	73.15	0.39	12.92	1.43	0.01	0.32	1.56	3.33	4.31	0.02	-	97.43
SG14-2649	16/04/2010	71.97	0.45	12.88	1.67	0.06	0.29	1.53	3.40	4.21	0.03	-	96.48
SG14-2649	16/04/2010	71.28	0.43	12.81	1.66	0.03	0.36	1.55	3.29	4.29	0.04	-	95.74
SG14-2649	16/04/2010	71.46	0.42	12.59	1.80	0.00	0.32	1.56	3.25	4.36	0.04	-	95.81
SG14-2649	16/04/2010	69.20	0.39	12.41	1.45	0.05	0.37	1.46	3.29	4.12	0.04	-	92.78
SG14-2649	16/04/2010	71.24	0.40	12.60	1.57	0.07	0.37	1.58	3.16	4.37	0.05	-	95.40
SG14-2649	16/04/2010	71.88	0.41	12.76	1.69	0.06	0.35	1.61	3.19	4.29	0.07	-	96.32
SG14-2649	16/04/2010	71.36	0.40	12.81	1.87	0.09	0.41	1.64	3.25	4.26	0.05	-	96.14
SG14-2649	16/04/2010	70.96	0.42	12.84	1.84	0.02	0.37	1.59	3.36	4.27	0.03	-	95.71
SG14-2649	16/04/2010	69.41	0.37	12.43	1.85	0.03	0.34	1.59	3.12	4.33	0.05	-	93.51
SG14-2649 (outlier)	16/04/2010	74.73	0.17	11.77	1.12	0.07	0.11	0.96	3.64	3.53	0.02	-	96.12
SG14-2706	16/04/2010	74.02	0.10	11.70	1.10	0.06	0.09	0.97	3.35	3.51	0.00	-	94.90
SG14-2706	16/04/2010	74.79	0.18	11.88	1.05	0.02	0.09	0.97	3.41	3.41	0.05	-	95.85
SG14-2706	16/04/2010	75.03	0.11	11.65	1.15	0.03	0.11	1.04	3.45	3.50	0.02	-	96.10
SG14-2706	16/04/2010	75.50	0.14	11.91	1.14	0.11	0.13	0.92	3.39	3.56	0.01	-	96.81
SG14-2706	16/04/2010	76.04	0.11	11.97	1.10	0.05	0.16	0.95	3.22	3.54	0.02	-	97.14
SG14-2706	16/04/2010	74.68	0.09	11.82	1.01	0.01	0.09	0.94	3.33	3.43	0.02	-	95.41
SG14-2706	16/04/2010	75.24	0.10	12.03	1.05	0.02	0.10	1.02	3.51	3.52	0.03	-	96.64
SG14-2706	16/04/2010	74.48	0.15	11.77	1.03	0.02	0.09	1.00	3.36	3.43	0.06	-	95.38

SG Label	Run Date	SiO_2	TiO_2	Al_2O_3	FeOt	MnO	MgO	CaO	Na_2O	K_2O	P_2O_5	Cl	Analytical total
SG14-2706	16/04/2010	74.53	0.13	11.71	1.15	0.01	0.09	0.97	3.69	3.53	0.01	-	95.83
SG14-2706	16/04/2010	75.14	0.15	11.92	1.02	0.08	0.12	0.94	3.51	3.52	0.02	-	96.43
SG14-2706	16/04/2010	72.86	0.09	11.66	0.98	0.03	0.13	0.95	3.31	3.54	0.00	-	93.54
SG14-2706	16/04/2010	74.92	0.10	11.63	1.10	0.00	0.12	1.02	3.51	3.47	0.05	-	95.91
SG14-2706	16/04/2010	74.80	0.11	11.71	1.18	0.03	0.07	0.96	3.47	3.58	0.00	-	95.92
SG14-2706	16/04/2010	75.46	0.12	11.81	1.10	0.05	0.12	0.96	3.53	3.54	0.00	-	96.69
SG14-2706	16/04/2010	75.35	0.14	11.90	1.01	0.00	0.10	0.89	3.38	3.38	0.02	-	96.18
SG14-2706	16/04/2010	74.96	0.12	11.62	1.15	0.07	0.10	0.96	3.55	3.44	0.03	-	96.00
SG14-2706	16/04/2010	75.45	0.10	11.71	1.16	0.02	0.09	0.97	3.64	3.42	0.01	-	96.56
SG14-2706	16/04/2010	74.86	0.10	11.73	0.87	0.05	0.14	0.99	3.46	3.50	0.01	-	95.73
SG14-2706	16/04/2010	74.59	0.09	11.87	1.14	0.06	0.11	0.98	3.38	3.49	0.01	-	95.73
SG14-2706	16/04/2010	75.38	0.11	11.80	1.23	0.07	0.12	0.89	3.46	3.55	0.00	-	96.60
SG14-2706	16/04/2010	75.04	0.09	11.73	1.12	0.02	0.11	1.02	3.53	3.60	0.00	-	96.27
SG14-2706	16/04/2010	74.97	0.12	11.83	1.06	0.03	0.10	0.95	3.44	3.43	0.04	-	95.97
SG14-2706	16/04/2010	75.18	0.10	11.90	1.07	0.00	0.10	0.97	3.44	3.61	0.02	-	96.40
SG14-2706	16/04/2010	75.49	0.14	11.99	1.12	0.03	0.12	0.98	3.40	3.63	0.02	-	96.93
SG14-2706	16/04/2010	75.15	0.13	11.79	1.09	0.00	0.11	1.02	3.37	3.48	0.00	-	96.13
SG14-2706	16/04/2010	75.63	0.17	11.85	1.09	0.08	0.12	1.00	3.26	3.65	0.00	-	96.84
SG14-2706	16/04/2010	75.74	0.14	11.78	1.15	0.09	0.13	0.99	3.56	3.53	0.00	-	97.12
SG14-2706	16/04/2010	75.38	0.13	11.69	1.16	0.00	0.11	0.92	3.32	3.43	0.01	-	96.15
SG14-2706	16/04/2010	75.12	0.13	11.78	1.00	0.06	0.10	0.95	3.46	3.42	0.03	-	96.06
SG14-2706	16/04/2010	74.91	0.14	11.85	0.95	0.00	0.10	0.98	3.17	3.49	0.02	-	95.60
SG14-2706	16/04/2010	75.42	0.09	11.97	1.12	0.05	0.14	1.05	3.52	3.51	0.01	-	96.87
SG14-2706	16/04/2010	74.66	0.11	11.95	0.94	0.08	0.09	0.92	3.56	3.42	0.02	-	95.75
SG14-2706	16/04/2010	74.93	0.16	11.82	1.05	0.05	0.11	0.93	3.34	3.44	0.01	-	95.86

SG Label	Run Date	SiO_2	TiO_2	Al_2O_3	FeOt	MnO	MgO	CaO	Na_2O	K_2O	P_2O_5	Cl	Analytical total
SG14-2706	16/04/2010	74.92	0.09	11.78	1.21	0.12	0.13	0.96	3.40	3.47	0.02	-	96.10
SG14-2706	16/04/2010	74.54	0.12	11.70	1.01	0.06	0.14	0.93	3.39	3.45	0.00	-	95.34
SG14-2706	16/04/2010	74.50	0.09	11.68	1.06	0.00	0.12	0.98	3.30	3.48	0.00	-	95.20
SG14-2706	16/04/2010	74.86	0.13	11.68	1.02	0.02	0.12	0.97	3.40	3.48	0.01	-	95.70
SG14-2706	16/04/2010	74.87	0.09	11.85	1.13	0.06	0.12	0.98	3.72	3.60	0.03	-	96.46
SG14-2706	16/04/2010	75.44	0.14	11.97	0.96	0.18	0.13	0.96	3.53	3.53	0.02	-	96.85
SG14-2706	16/04/2010	74.82	0.11	11.78	1.10	0.10	0.11	1.03	3.40	3.49	0.02	-	95.95
SG14-2706	16/04/2010	75.01	0.12	11.78	1.13	0.01	0.11	1.02	3.43	3.45	0.02	-	96.07
SG14-2706	16/04/2010	75.59	0.17	11.77	1.14	0.03	0.14	1.03	3.46	3.55	0.06	-	96.93
SG14-2706	16/04/2010	74.95	0.13	11.60	1.09	0.02	0.14	0.98	3.52	3.53	0.02	-	95.96
SG14-2706	16/04/2010	75.12	0.15	11.73	1.09	0.00	0.09	1.02	3.33	3.52	0.00	-	96.05
SG14-2706	16/04/2010	75.70	0.10	11.79	1.02	0.08	0.13	1.02	3.32	3.50	0.01	-	96.67
SG14-2706	16/04/2010	74.87	0.11	11.62	1.15	0.06	0.14	0.95	3.44	3.46	0.02	-	95.83
SG14-2706	16/04/2010	75.33	0.12	11.58	1.02	0.09	0.10	0.97	3.52	3.42	0.03	-	96.17
SG14-2706	16/04/2010	75.11	0.05	11.65	1.06	0.00	0.09	1.01	3.45	3.35	0.00	-	95.77
SG14-2739	16/04/2010	63.08	0.97	14.95	4.96	0.04	1.43	3.36	4.01	3.65	0.33	-	96.78
SG14-2739	16/04/2010	63.69	0.96	15.36	5.06	0.03	1.56	3.64	4.41	3.80	0.41	-	98.92
SG14-2739	16/04/2010	64.10	0.88	15.28	5.24	0.10	1.53	3.48	4.26	3.69	0.48	-	99.02
SG14-2739	16/04/2010	63.26	0.93	15.11	4.91	0.02	1.36	3.45	4.43	3.83	0.37	-	97.68
SG14-2739	16/04/2010	62.83	0.88	15.03	5.47	0.13	1.60	3.78	4.45	3.73	0.44	-	98.35
SG14-2739	16/04/2010	63.96	1.01	15.09	5.09	0.15	1.50	3.64	4.38	3.76	0.37	-	98.97
SG14-2739	16/04/2010	63.95	0.92	15.24	5.37	0.07	1.46	3.71	4.28	3.71	0.37	-	99.07
SG14-2739	16/04/2010	63.20	0.96	15.12	5.23	0.10	1.58	3.55	4.22	3.67	0.40	-	98.03
SG14-2739	16/04/2010	63.66	0.99	15.35	5.23	0.11	1.59	3.79	4.21	3.54	0.43	-	98.91

SG Label	Run Date	SiO_2	TiO_2	Al_2O_3	FeOt	MnO	MgO	CaO	Na_2O	K_2O	P_2O_5	Cl	Analytical total
SG14-2739	16/04/2010	63.65	0.96	15.37	5.05	0.08	1.63	3.65	4.33	3.67	0.42	-	98.80
SG14-2739	16/04/2010	62.75	0.93	15.11	5.61	0.11	1.58	4.14	4.35	3.55	0.39	-	98.51
SG14-2739	16/04/2010	64.34	1.03	15.28	5.16	0.18	1.50	3.37	4.47	3.80	0.40	-	99.54
SG14-2739	16/04/2010	63.60	0.99	15.44	5.57	0.15	1.59	3.82	4.20	3.59	0.47	-	99.40
SG14-2739	16/04/2010	63.38	1.00	15.38	5.42	0.08	1.60	3.69	4.13	3.58	0.45	-	98.70
SG14-2739	16/04/2010	63.75	0.95	15.25	5.56	0.06	1.62	3.80	4.11	3.68	0.40	-	99.18
SG14-2739	16/04/2010	63.49	0.93	15.58	5.41	0.07	1.45	3.55	4.24	3.54	0.40	-	98.65
SG14-2752	25/04/2018	69.39	0.71	14.99	2.63	0.10	0.59	1.74	4.46	4.44	0.14	0.09	99.27
SG14-2752	25/04/2018	65.48	0.65	14.40	2.45	0.07	0.65	1.77	4.50	4.05	0.12	0.12	94.27
SG14-2752	25/04/2018	65.20	0.67	14.32	2.51	0.17	0.63	1.74	4.44	3.90	0.10	0.15	93.83
SG14-2752	25/04/2018	65.01	0.79	14.06	2.62	0.14	0.58	1.63	4.48	4.10	0.10	0.16	93.67
SG14-2752	25/04/2018	67.33	0.71	14.47	2.37	0.06	0.59	1.68	4.49	4.19	0.14	0.09	96.11
SG14-2752	25/04/2018	65.53	0.71	15.06	2.80	0.13	0.41	1.85	4.67	3.76	0.14	0.12	95.18
SG14-2752	25/04/2018	65.74	0.75	14.17	2.32	0.06	0.56	1.56	4.19	4.14	0.14	0.14	93.76
SG14-2752	25/04/2018	68.43	0.79	15.07	2.62	0.09	0.66	1.86	4.57	4.24	0.10	0.10	98.53
SG14-2752	25/04/2018	64.82	0.71	14.35	2.49	0.14	0.55	1.81	3.95	3.86	0.13	0.14	92.93
SG14-2752	25/04/2018	65.46	0.74	14.48	2.65	0.09	0.62	1.80	4.44	3.99	0.13	0.17	94.57
SG14-2752	25/04/2018	64.29	0.67	13.75	2.50	0.11	0.53	1.61	4.10	4.14	0.11	0.18	91.99
SG14-2752	25/04/2018	65.08	0.74	13.94	2.59	0.08	0.56	1.62	4.38	4.14	0.14	0.13	93.40
SG14-2752	25/04/2018	64.31	0.63	14.36	2.38	0.14	0.60	1.85	4.17	3.98	0.13	0.14	92.68
SG14-2752	25/04/2018	66.19	0.68	14.69	2.60	0.14	0.64	1.85	4.41	4.15	0.09	0.10	95.54
SG14-2752	25/04/2018	63.66	0.67	13.93	2.39	0.14	0.61	1.70	4.34	3.83	0.09	0.18	91.53
SG14-2752	25/04/2018	66.43	0.67	14.62	2.64	0.14	0.59	1.83	4.42	4.04	0.14	0.14	95.67
SG14-2752	25/04/2018	66.98	0.66	14.69	2.43	0.15	0.68	1.95	4.65	4.17	0.13	0.12	96.62

SG Label	Run Date	SiO_2	TiO_2	Al_2O_3	FeOt	MnO	MgO	CaO	Na_2O	K_2O	P_2O_5	Cl	Analytical total
SG14-2830	03/05/2018	71.55	0.56	12.19	2.22	0.06	0.49	1.86	4.06	2.61	0.10	0.13	95.83
SG14-2830	03/05/2018	73.57	0.62	11.96	2.10	0.11	0.40	1.65	3.79	2.83	0.08	0.10	97.21
SG14-2830	03/05/2018	72.18	0.53	11.82	1.96	0.08	0.30	1.36	4.01	2.80	0.08	0.11	95.22
SG14-2830	03/05/2018	73.15	0.56	12.04	2.25	0.07	0.43	1.75	3.89	2.68	0.03	0.11	96.95
SG14-2830	03/05/2018	71.01	0.62	11.65	2.10	0.05	0.46	1.72	3.75	2.62	0.09	0.11	94.19
SG14-2830	03/05/2018	69.50	0.60	11.32	2.29	0.04	0.42	1.79	3.81	2.58	0.07	0.13	92.53
SG14-2830	03/05/2018	72.47	0.59	11.95	2.27	0.02	0.44	1.78	3.89	2.67	0.10	0.12	96.30
SG14-2830	03/05/2018	73.11	0.54	11.98	2.32	0.08	0.44	1.76	3.91	2.72	0.10	0.11	97.08
SG14-2830	03/05/2018	72.11	0.52	11.78	2.16	0.02	0.44	1.70	3.77	2.74	0.05	0.07	95.37
SG14-2830	03/05/2018	73.68	0.63	12.28	2.27	0.03	0.42	1.80	3.90	2.65	0.09	0.09	97.85
SG14-2830	03/05/2018	71.58	0.54	11.52	2.16	0.01	0.42	1.60	3.85	2.77	0.08	0.10	94.63
SG14-2830	03/05/2018	73.71	0.59	12.12	2.16	0.04	0.49	1.67	3.77	2.73	0.09	0.10	97.46
SG14-2830	03/05/2018	72.35	0.58	11.94	2.25	0.11	0.39	1.70	3.79	2.80	0.08	0.07	96.07
SG14-2830	03/05/2018	72.47	0.56	11.98	2.19	0.06	0.45	1.76	3.97	2.69	0.13	0.11	96.38
SG14-2841a	17/04/2010	69.08	0.78	14.03	3.03	0.08	0.58	1.65	4.34	4.78	0.17	-	98.52
SG14-2841a	17/04/2010	67.81	0.89	14.61	3.41	0.15	0.80	2.29	4.25	4.48	0.17	-	98.88
SG14-2841a	17/04/2010	66.58	0.83	14.14	3.26	0.08	0.73	2.08	4.35	4.55	0.18	-	96.79
SG14-2841a	17/04/2010	67.85	0.76	14.48	3.10	0.16	0.67	1.90	4.29	4.65	0.15	-	98.02
SG14-2841a	17/04/2010	65.28	0.78	15.64	3.58	0.11	1.07	3.09	4.21	3.79	0.16	-	97.73
SG14-2841a	17/04/2010	66.46	0.83	14.68	3.30	0.18	0.82	2.34	4.07	4.46	0.13	-	97.26
SG14-2841a	17/04/2010	65.11	0.90	15.28	4.06	0.19	1.15	2.88	4.13	4.12	0.25	-	98.07
SG14-2841a	17/04/2010	67.24	0.85	14.94	3.33	0.15	0.85	2.41	4.12	4.27	0.12	-	98.28
SG14-2841a	17/04/2010	66.29	0.72	13.89	3.26	0.08	0.57	1.66	3.47	5.47	0.13	-	95.56

SG Label	Run Date	SiO_2	TiO_2	Al_2O_3	FeOt	MnO	MgO	CaO	Na_2O	K_2O	P_2O_5	Cl	Analytical total
SG14-2841a	17/04/2010	67.56	0.79	13.84	3.56	0.11	0.74	1.96	4.07	4.69	0.18	-	97.50
SG14-2841a	17/04/2010	68.32	0.76	14.03	3.18	0.13	0.65	1.90	4.27	4.70	0.15	-	98.09
SG14-2841a	17/04/2010	67.94	0.79	14.08	3.22	0.09	0.71	2.03	4.23	4.66	0.16	-	97.91
SG14-2841a	17/04/2010	66.55	0.75	14.12	2.67	0.17	0.61	1.89	3.86	4.68	0.10	-	95.39
SG14-2841a	17/04/2010	64.54	0.99	15.61	4.27	0.13	1.32	3.35	4.11	4.04	0.25	-	98.60
SG14-2841a	17/04/2010	67.10	0.83	14.65	3.66	0.05	0.91	2.39	4.12	4.37	0.17	-	98.25
SG14-2841a	17/04/2010	67.59	0.85	14.81	3.46	0.07	0.90	2.36	4.21	4.41	0.16	-	98.81
SG14-2841a	17/04/2010	67.05	0.83	14.71	3.61	0.13	0.86	2.32	4.16	4.52	0.16	-	98.34
SG14-2841a	24/04/2018	68.01	0.82	14.25	3.34	0.10	0.57	1.71	4.12	4.78	0.15	-	97.85
SG14-2841a	24/04/2018	68.36	0.81	14.90	3.51	0.03	0.79	2.23	3.79	4.75	0.15	-	99.32
SG14-2841a	24/04/2018	66.80	0.79	15.06	3.70	0.08	0.95	2.53	4.02	4.23	0.24	-	98.40
SG14-2841a	24/04/2018	67.58	0.76	15.31	3.36	0.08	0.91	2.51	3.99	4.36	0.19	-	99.05
SG14-2841a	24/04/2018	64.82	0.88	15.43	4.26	0.12	1.37	3.41	4.29	3.71	0.32	-	98.61
SG14-2841a	24/04/2018	65.26	0.96	15.47	4.21	0.12	1.16	3.12	3.85	4.11	0.25	-	98.51
SG14-2841a	24/04/2018	65.34	0.88	15.59	4.12	0.09	1.08	3.21	3.92	3.97	0.30	-	98.50
SG14-2841a	24/04/2018	66.73	0.82	15.60	4.01	0.14	1.09	2.82	4.02	4.10	0.27	-	99.60
SG14-2841b	24/04/2018	60.95	1.07	15.87	5.71	0.14	2.04	4.95	3.78	2.97	0.38	-	97.86
SG14-2841b	24/04/2018	60.68	1.11	15.93	6.47	0.16	2.19	4.98	3.49	2.97	0.33	-	98.31
SG14-2856	17/04/2010	74.14	0.10	11.57	1.07	0.01	0.13	1.02	3.44	3.40	0.01	-	94.88
SG14-2856	17/04/2010	74.37	0.07	11.95	0.81	0.02	0.08	0.78	3.49	3.77	0.00	-	95.33
SG14-2856	17/04/2010	74.71	0.12	12.02	0.86	0.07	0.09	0.92	3.55	3.79	0.02	-	96.14
SG14-2856	17/04/2010	74.15	0.09	11.52	1.07	0.00	0.12	1.04	3.48	3.39	0.00	-	94.86
SG14-2856	17/04/2010	75.02	0.09	12.03	1.10	0.11	0.13	1.02	3.68	3.54	0.00	-	96.72
SG14-2856	17/04/2010	74.85	0.10	12.00	1.07	0.07	0.10	0.99	3.36	3.49	0.00	-	96.02

SG Label	Run Date	SiO_2	TiO_2	Al_2O_3	FeOt	MnO	MgO	CaO	Na_2O	K_2O	P_2O_5	Cl	Analytical total
SG14-2856	17/04/2010	75.14	0.11	11.78	1.14	0.01	0.12	1.07	3.50	3.37	0.02	-	96.25
SG14-2856	17/04/2010	74.77	0.13	11.86	0.91	0.05	0.13	1.01	3.45	3.53	0.03	-	95.89
SG14-2856	17/04/2010	74.94	0.09	12.01	0.99	0.02	0.11	1.06	3.53	3.54	0.02	-	96.29
SG14-2856	17/04/2010	73.36	0.09	11.73	0.99	0.08	0.11	1.09	3.22	3.42	0.01	-	94.11
SG14-2856	17/04/2010	74.81	0.15	11.47	0.97	0.00	0.11	0.96	3.48	3.61	0.02	-	95.59
SG14-2856	17/04/2010	73.90	0.09	11.58	1.12	0.03	0.16	1.08	3.26	3.46	0.00	-	94.69
SG14-2856	17/04/2010	74.89	0.09	11.83	1.05	0.11	0.14	0.98	3.42	3.52	0.06	-	96.09
SG14-2856	17/04/2010	74.31	0.10	11.64	1.12	0.11	0.09	1.00	3.45	3.41	0.04	-	95.27
SG14-2873	23/04/2018	74.46	0.11	11.79	1.02	0.04	0.13	1.01	3.34	3.54	0.03	0.11	95.58
SG14-2873	23/04/2018	74.56	0.12	11.94	0.99	0.02	0.14	0.98	3.41	3.39	0.03	0.09	95.66
SG14-2873	23/04/2018	74.15	0.17	11.78	1.10	0.00	0.12	1.02	3.25	3.48	0.00	0.08	95.14
SG14-2873	23/04/2018	75.12	0.13	12.29	1.04	0.04	0.12	0.95	3.23	3.48	0.04	0.11	96.54
SG14-2873	23/04/2018	74.55	0.16	11.85	1.15	0.00	0.10	0.97	3.19	3.27	0.01	0.13	95.38
SG14-2873	23/04/2018	74.59	0.13	12.02	1.02	0.05	0.12	0.91	3.24	3.46	0.01	0.11	95.64
SG14-2873	23/04/2018	75.12	0.10	11.99	1.03	0.00	0.11	0.97	3.39	3.45	0.00	0.11	96.26
SG14-2873	23/04/2018	71.95	0.14	11.45	0.88	0.05	0.12	0.98	3.03	3.39	0.00	0.15	92.14
SG14-2873	23/04/2018	74.95	0.12	11.89	0.98	0.07	0.14	0.93	3.31	3.41	0.02	0.11	95.94
SG14-2873	23/04/2018	73.11	0.08	11.81	1.06	0.04	0.10	0.99	2.92	3.30	0.05	0.11	93.58
SG14-2873	23/04/2018	73.73	0.09	12.05	0.92	0.00	0.10	1.05	3.18	3.47	0.00	0.10	94.69
SG14-2873	23/04/2018	74.61	0.15	12.05	1.07	0.00	0.14	1.04	3.12	3.41	0.03	0.11	95.75
SG14-2873	23/04/2018	73.97	0.11	11.76	0.98	0.07	0.12	0.91	3.08	3.50	0.04	0.10	94.63
SG14-2873	23/04/2018	74.78	0.19	11.95	0.98	0.05	0.11	0.96	3.13	3.48	0.04	0.10	95.76
SG14-2873	23/04/2018	73.35	0.11	11.99	1.04	0.07	0.10	1.00	3.08	3.39	0.03	0.11	94.27
SG14-2873	23/04/2018	74.26	0.13	12.01	0.95	0.02	0.13	1.03	3.30	3.49	0.02	0.15	95.49

SG Label	Run Date	SiO_2	TiO_2	Al_2O_3	FeOt	MnO	MgO	CaO	Na_2O	K_2O	P_2O_5	Cl	Analytical total
SG14-2873	23/04/2018	73.33	0.16	11.84	0.97	0.00	0.09	0.96	2.99	3.36	0.03	0.11	93.83
SG14-2873	23/04/2018	73.60	0.15	11.90	0.89	0.09	0.12	1.01	3.07	3.32	0.00	0.14	94.30
SG14-2873 (outlier)	23/04/2018	70.41	0.29	12.82	1.48	0.04	0.27	1.53	3.55	2.66	0.07	0.18	93.31
SG14-2965	23/04/2018	71.06	0.23	12.77	3.36	0.12	0.23	2.55	4.42	0.73	0.06	0.22	95.76
SG14-2965	23/04/2018	71.52	0.17	12.76	3.11	0.18	0.22	2.59	4.58	0.76	0.06	0.20	96.15
SG14-2965	23/04/2018	72.15	0.25	13.15	3.13	0.10	0.26	2.73	4.53	0.72	0.05	0.24	97.31
SG14-2965	23/04/2018	71.10	0.19	12.71	2.91	0.25	0.21	2.44	4.41	0.73	0.06	0.24	95.26
SG14-2965 (low total)	23/04/2018	67.85	0.24	12.12	3.24	0.13	0.27	2.49	4.02	0.74	0.05	0.29	91.43
SG14-2965 (low total)	23/04/2018	66.00	0.13	11.61	2.47	0.18	0.16	2.02	3.86	0.76	0.00	0.32	87.51
SG14-2965 (low total)	23/04/2018	65.20	0.16	11.59	2.88	0.23	0.20	2.37	4.13	0.67	0.04	0.21	87.67
SG14-2995	17/04/2010	73.78	0.36	11.73	1.43	0.01	0.24	1.34	3.69	3.12	0.03	-	95.72
SG14-2995	17/04/2010	73.86	0.32	11.66	1.58	0.06	0.27	1.26	3.38	3.17	0.00	-	95.55
SG14-2995	17/04/2010	73.72	0.35	12.00	1.53	0.02	0.29	1.51	3.48	3.13	0.04	-	96.06
SG14-2995	17/04/2010	74.93	0.23	11.35	1.12	0.07	0.15	0.99	3.43	3.24	0.03	-	95.55
SG14-2995	17/04/2010	71.71	0.34	11.45	1.50	0.06	0.28	1.35	3.27	3.11	0.00	-	93.07
SG14-2995	17/04/2010	72.75	0.38	11.75	1.60	0.05	0.29	1.31	3.59	3.07	0.03	-	94.82
SG14-2995	17/04/2010	73.55	0.33	11.90	1.56	0.10	0.28	1.45	3.55	3.15	0.03	-	95.90
SG14-2995	17/04/2010	73.82	0.38	11.97	1.49	0.06	0.32	1.41	3.70	3.17	0.00	-	96.31
SG14-2995	17/04/2010	73.91	0.33	12.05	1.60	0.10	0.34	1.52	3.65	2.98	0.02	-	96.51
SG14-2995	17/04/2010	71.43	0.36	11.44	1.57	0.03	0.28	1.40	3.69	3.09	0.02	-	93.31
SG14-2995	17/04/2010	74.69	0.25	11.19	1.28	0.09	0.20	1.06	3.44	3.26	0.03	-	95.49
SG14-2995	17/04/2010	73.71	0.37	11.62	1.38	0.09	0.25	1.33	3.56	3.13	0.04	-	95.47
SG14-2995	17/04/2010	74.83	0.33	11.54	1.18	0.03	0.22	1.24	3.52	3.21	0.04	-	96.13

SG Label	Run Date	SiO_2	TiO_2	Al_2O_3	FeOt	MnO	MgO	CaO	Na_2O	K_2O	P_2O_5	Cl	Analytical total
SG14-2995	17/04/2010	74.83	0.30	11.16	1.35	0.03	0.19	1.10	3.24	3.20	0.03	-	95.44
SG14-2995	17/04/2010	74.67	0.31	11.45	1.18	0.02	0.26	1.29	3.42	3.21	0.01	-	95.83
SG14-2995	17/04/2010	74.55	0.35	11.61	1.33	0.00	0.27	1.26	3.38	3.14	0.03	-	95.92
SG14-2995	17/04/2010	74.12	0.32	11.41	1.28	0.00	0.25	1.19	3.55	3.25	0.00	-	95.38
SG14-2995	17/04/2010	74.26	0.32	11.44	1.29	0.05	0.30	1.18	3.65	3.17	0.02	-	95.67
SG14-2995	17/04/2010	74.64	0.34	11.60	1.33	0.08	0.19	1.20	3.72	3.22	0.01	-	96.33
SG14-2995	17/04/2010	74.21	0.35	11.71	1.40	0.02	0.27	1.25	3.72	3.15	0.03	-	96.11
SG14-3016	16/04/2010	71.27	0.56	11.43	2.18	0.15	0.44	1.57	3.81	2.60	0.05	-	94.07
SG14-3016	16/04/2010	70.65	0.57	11.27	2.01	0.10	0.40	1.53	3.43	2.76	0.05	-	92.77
SG14-3016	16/04/2010	69.45	0.51	11.19	1.81	0.05	0.40	1.42	3.70	2.72	0.10	-	91.34
SG14-3016	16/04/2010	72.00	0.55	11.66	2.19	0.10	0.38	1.59	3.61	2.80	0.07	-	94.93
SG14-3016	16/04/2010	72.38	0.57	11.67	2.05	0.09	0.36	1.53	3.85	2.75	0.07	-	95.32
SG14-3016 (outlier)	16/04/2010	59.62	1.23	15.85	6.52	0.10	2.52	5.48	3.79	2.72	0.29	-	98.13
SG14-3016 (outlier)	16/04/2010	59.54	1.19	15.69	6.70	0.14	2.47	5.40	3.59	2.70	0.28	-	97.69
SG14-3016 (outlier)	16/04/2010	58.23	1.16	15.15	6.87	0.19	2.43	5.26	3.30	2.60	0.31	-	95.50
SG14-3085a	09/05/2018	65.96	0.88	13.66	4.16	0.13	0.97	2.72	3.56	4.40	0.26	0.07	96.77
SG14-3085a	09/05/2018	65.83	0.83	13.73	4.61	0.03	0.93	2.48	3.84	4.31	0.28	0.10	96.96
SG14-3085a	09/05/2018	66.95	0.84	14.32	4.14	0.09	0.92	2.77	4.00	4.37	0.24	0.10	98.75
SG14-3085a	09/05/2018	67.46	0.84	14.44	4.04	0.12	0.99	2.70	4.00	4.24	0.21	0.09	99.13
SG14-3085a	09/05/2018	65.05	0.88	14.56	4.55	0.09	1.09	3.50	3.58	4.18	0.29	0.08	97.83
SG14-3085b	09/05/2018	56.80	1.06	14.41	8.20	0.18	3.39	5.97	2.89	2.35	0.29	0.09	95.64
SG14-3085b	09/05/2018	58.86	1.24	14.68	8.17	0.20	2.56	5.47	3.32	2.92	0.34	0.07	97.84
SG14-3085b	09/05/2018	58.22	1.06	14.74	8.08	0.17	2.52	5.71	3.75	2.88	0.30	0.07	97.50

SG Label	Run Date	SiO_2	TiO_2	Al_2O_3	FeOt	MnO	MgO	CaO	Na_2O	K_2O	P_2O_5	Cl	Analytical total
SG14-3085b	09/05/2018	57.57	1.02	14.75	7.80	0.21	2.67	5.66	3.26	2.77	0.29	0.09	96.09
SG14-3085b	09/05/2018	54.87	0.92	14.83	7.19	0.18	2.53	5.87	3.37	2.39	0.31	0.08	92.53
SG14-3085b	09/05/2018	57.49	1.02	15.10	8.29	0.21	3.30	6.08	3.63	2.51	0.34	0.08	98.04
SG14-3085b	09/05/2018	59.04	1.11	15.48	7.68	0.14	2.51	5.90	3.52	2.74	0.29	0.06	98.46
SG14-3085b	09/05/2018	56.95	0.99	15.49	7.93	0.15	2.57	6.68	3.39	2.47	0.25	0.07	96.93
SG14-3085b	09/05/2018	58.65	1.04	15.56	8.02	0.19	2.66	5.87	3.55	2.60	0.24	0.07	98.46
SG14-3085b	09/05/2018	58.39	1.02	15.56	7.93	0.16	2.87	6.04	3.42	2.63	0.26	0.07	98.35
SG14-3085b	09/05/2018	58.72	1.06	15.58	7.87	0.14	2.70	6.18	3.39	2.61	0.29	0.06	98.60
SG14-3085b	09/05/2018	58.03	1.03	15.86	7.30	0.12	2.79	6.34	3.65	2.55	0.27	0.07	98.03
SG14-3085b	09/05/2018	57.35	1.06	15.90	7.72	0.23	2.76	6.68	3.44	2.34	0.26	0.08	97.82
SG14-3085b	09/05/2018	57.00	0.89	16.13	8.14	0.15	3.58	6.37	3.56	2.29	0.27	0.09	98.46
SG14-3085b	09/05/2018	56.67	1.00	16.14	7.54	0.17	2.44	6.70	3.12	2.30	0.25	0.07	96.41
SG14-3085b	09/05/2018	56.52	0.95	16.25	7.15	0.14	2.49	6.57	3.79	2.26	0.25	0.08	96.45
SG14-3085b	09/05/2018	57.30	1.01	16.26	7.66	0.15	2.77	6.15	4.36	1.83	0.24	0.01	97.74
SG14-3085b	09/05/2018	56.45	0.94	16.29	6.88	0.12	2.13	6.31	3.61	2.25	0.27	0.09	95.35
SG14-3085b	09/05/2018	57.73	0.96	16.68	7.42	0.21	2.40	6.63	3.81	2.35	0.27	0.08	98.52
SG14-3085b	09/05/2018	58.27	1.01	16.80	7.33	0.16	2.39	6.76	3.54	2.36	0.30	0.06	98.98
SG14-3216	11/06/2015	59.18	0.39	19.45	2.86	0.18	0.16	1.29	7.83	6.10	0.04	0.42	97.90
SG14-3216	11/06/2015	58.36	0.32	18.85	3.01	0.18	0.10	1.26	7.05	6.51	0.07	0.44	96.13
SG14-3216	11/06/2015	56.48	0.31	18.57	2.96	0.23	0.06	1.14	7.72	5.59	0.00	0.52	93.57
SG14-3216	11/06/2015	58.25	0.32	19.10	2.86	0.16	0.16	1.22	7.43	6.25	0.07	0.40	96.23
SG14-3216	11/06/2015	58.67	0.48	18.95	3.20	0.13	0.22	1.49	6.52	6.73	0.09	0.34	96.82
SG14-3216	11/06/2015	59.03	0.27	19.26	2.72	0.17	0.08	1.25	7.91	6.12	0.05	0.44	97.30
SG14-3216	11/06/2015	59.15	0.46	19.24	3.11	0.13	0.20	1.29	7.10	6.25	0.04	0.40	97.37

SG Label	Run Date	SiO_2	TiO_2	Al_2O_3	FeOt	MnO	MgO	CaO	Na_2O	K_2O	P_2O_5	Cl	Analytical total
SG14-3216	11/06/2015	58.84	0.33	19.57	2.99	0.18	0.12	1.18	7.89	6.31	0.01	0.46	97.88
SG14-3216	11/06/2015	59.41	0.37	19.59	3.31	0.20	0.22	1.34	7.43	6.31	0.02	0.40	98.58
SG14-3216	11/06/2015	59.53	0.38	19.19	3.20	0.12	0.15	1.43	6.99	6.57	0.02	0.34	97.94
SG14-3216	11/06/2015	58.46	0.36	19.09	2.86	0.23	0.11	1.15	7.24	6.30	0.04	0.42	96.27
SG14-3216	11/06/2015	58.89	0.37	19.41	3.02	0.17	0.18	1.25	5.24	6.19	0.02	0.45	95.19
SG14-3216	11/06/2015	60.31	0.27	19.59	3.02	0.12	0.05	1.21	4.69	6.14	0.00	0.45	95.84
SG14-3216	11/06/2015	58.44	0.33	19.66	3.01	0.20	0.16	1.26	7.95	6.33	0.02	0.49	97.85
SG14-3216	11/06/2015	57.07	0.26	19.48	2.86	0.22	0.01	1.10	8.07	6.27	0.05	0.59	95.97
SG14-3216	11/06/2015	59.75	0.27	19.71	2.97	0.27	0.20	1.13	8.14	6.14	0.09	0.38	99.04
SG14-3216	11/06/2015	59.38	0.47	19.16	3.38	0.12	0.24	1.49	5.22	6.57	0.07	0.33	96.44
SG14-3216	11/06/2015	57.35	0.38	19.00	3.06	0.15	0.16	1.16	7.00	6.03	0.00	0.43	94.73
SG14-3216	11/06/2015	58.88	0.53	18.97	3.00	0.10	0.24	1.48	6.61	6.62	0.08	0.32	96.83
SG14-3216	11/06/2015	59.91	0.46	19.12	3.05	0.07	0.26	1.46	6.35	7.09	0.09	0.28	98.14
SG14-3216	11/06/2015	59.67	0.43	19.09	2.99	0.19	0.21	1.40	4.46	6.66	0.09	0.28	95.46
SG14-3216	11/06/2015	59.49	0.35	19.08	2.83	0.22	0.20	1.26	7.42	6.29	0.09	0.25	97.48
SG14-3216	11/06/2015	59.82	0.44	19.00	3.05	0.16	0.17	1.40	7.34	6.33	0.05	0.22	97.98
SG14-3216	11/06/2015	59.89	0.45	19.11	3.19	0.23	0.22	1.42	7.20	6.44	0.08	0.23	98.47
SG14-3216	07/07/2010	58.57	0.27	19.81	3.02	0.12	0.06	1.15	8.78	5.75	0.05	0.41	98.00
SG14-3216	07/07/2010	56.93	0.49	18.35	3.16	0.20	0.26	1.38	6.32	6.33	0.06	0.28	93.76
SG14-3216	07/07/2010	60.41	0.41	19.68	3.14	0.15	0.21	1.53	7.10	6.46	0.02	0.28	99.37
SG14-3216	07/07/2010	55.80	0.41	18.43	2.82	0.14	0.15	1.27	7.06	5.61	0.03	0.38	92.10
SG14-3216	07/07/2010	58.99	0.40	19.47	3.09	0.15	0.16	1.33	7.49	5.93	0.02	0.33	97.36
SG14-3216	07/07/2010	58.98	0.28	19.97	2.86	0.32	0.06	1.14	8.38	5.68	0.02	0.47	98.15
SG14-3216	07/07/2010	59.67	0.43	19.31	3.20	0.12	0.26	1.38	6.73	6.66	0.09	0.26	98.12
SG14-3216	07/07/2010	60.00	0.42	19.41	3.15	0.13	0.23	1.31	7.01	6.57	0.00	0.24	98.48

SG Label	Run Date	SiO_2	TiO_2	Al_2O_3	FeOt	MnO	MgO	CaO	Na_2O	K_2O	P_2O_5	Cl	Analytical total
SG14-3216	07/07/2010	59.59	0.34	19.72	2.98	0.24	0.13	1.22	8.02	6.09	0.02	0.34	98.69
SG14-3216	07/07/2010	59.40	0.39	19.33	3.09	0.15	0.20	1.36	7.14	6.39	0.12	0.24	97.82
SG14-3216	07/07/2010	59.57	0.48	19.50	3.23	0.24	0.22	1.38	6.92	6.76	0.06	0.28	98.64
SG14-3216	07/07/2010	59.03	0.36	19.50	3.19	0.14	0.19	1.19	7.25	6.16	0.00	0.29	97.30
SG14-3216	07/07/2010	59.50	0.41	18.75	2.71	0.15	0.22	1.31	6.49	6.88	0.09	0.21	96.72
SG14-3336	25/10/2017	74.18	0.17	13.06	0.95	0.12	0.29	1.55	3.52	2.42	0.06	0.09	96.42
SG14-3336	25/10/2017	73.44	0.15	12.65	0.94	0.12	0.24	1.62	3.82	2.40	0.10	0.09	95.58
SG14-3336	25/10/2017	75.75	0.19	11.46	0.98	0.07	0.28	1.05	3.20	2.66	0.10	0.11	95.85
SG14-3336	25/10/2017	74.58	0.17	11.30	0.90	0.07	0.37	1.23	3.38	2.45	0.13	0.11	94.68
SG14-3336	25/10/2017	73.12	0.20	11.47	1.43	0.15	0.71	1.32	3.16	2.50	0.10	0.16	94.31
SG14-3336	25/10/2017	76.46	0.16	11.43	0.85	0.10	0.16	0.87	3.29	2.86	0.11	0.14	96.44
SG14-3336	25/10/2017	75.60	0.16	11.84	1.03	0.03	0.29	1.12	2.10	2.70	0.04	0.10	95.02
SG14-3336	25/10/2017	75.88	0.20	11.19	0.95	0.07	0.31	0.92	3.03	2.73	0.05	0.12	95.45
SG14-3336	25/10/2017	72.38	0.20	13.44	1.69	0.06	1.15	2.23	2.59	2.01	0.08	0.09	95.93
SG14-3336	25/10/2017	68.59	0.35	13.50	2.91	0.14	2.80	3.07	3.85	1.75	0.05	0.10	97.11
SG14-3336	25/10/2017	69.94	0.27	13.25	2.73	0.11	2.39	2.81	3.22	1.87	0.08	0.09	96.77
SG14-3605a	23/04/2018	67.79	0.77	13.30	3.66	0.11	0.94	2.30	2.99	4.30	0.18	0.11	96.45
SG14-3605a	23/04/2018	68.38	0.82	13.59	3.47	0.10	0.92	2.43	3.27	4.36	0.13	0.11	97.59
SG14-3605b	23/04/2018	63.24	1.24	15.00	5.46	0.12	1.52	4.34	3.82	3.25	0.32	0.11	98.42
SG14-3605b	23/04/2018	65.42	0.90	14.05	3.94	0.05	0.96	2.78	3.77	3.80	0.15	0.11	95.95
SG14-3605b	23/04/2018	59.71	1.15	14.92	4.85	0.10	1.57	4.24	3.47	2.98	0.29	0.13	93.43
SG14-3605b	23/04/2018	59.08	1.05	14.73	4.83	0.04	1.29	4.04	3.59	3.14	0.25	0.19	92.24
SG14-3605b	23/04/2018	62.63	1.30	14.89	5.66	0.13	1.83	4.36	3.45	3.71	0.39	0.14	98.49

SG Label	Run Date	SiO_2	TiO_2	Al_2O_3	FeOt	MnO	MgO	CaO	Na_2O	K_2O	P_2O_5	Cl	Analytical total
SG14-3605b	23/04/2018	66.14	1.05	14.42	4.84	0.12	1.16	3.18	3.79	3.62	0.30	0.12	98.75
SG14-3605b	23/04/2018	61.07	1.21	14.81	5.86	0.10	1.65	4.18	3.73	3.08	0.30	0.10	96.10
SG14-3605b	23/04/2018	63.87	1.16	16.44	5.04	0.15	1.44	4.36	4.14	3.04	0.37	0.11	100.12
SG14-3605b	23/04/2018	61.78	1.07	16.67	4.94	0.13	2.05	5.48	4.07	2.60	0.31	0.12	99.22
SG14-3844	09/05/2018	73.13	0.05	11.66	0.75	0.05	0.09	0.79	3.63	3.58	0.02	0.12	93.86
SG14-3844	09/05/2018	73.64	0.11	11.48	0.73	0.05	0.08	0.84	3.48	3.75	0.04	0.08	94.28
SG14-3844	09/05/2018	73.20	0.08	11.50	0.80	0.09	0.11	0.90	3.67	3.74	0.00	0.08	94.17
SG14-3844	09/05/2018	73.29	0.11	11.66	0.73	0.02	0.09	0.84	3.65	3.80	0.04	0.09	94.33
SG14-3844	09/05/2018	74.02	0.12	11.60	0.90	0.05	0.12	0.97	3.59	3.36	0.02	0.10	94.87
SG14-3844	09/05/2018	71.66	0.07	11.17	0.73	0.02	0.09	0.78	3.64	3.69	0.04	0.10	91.98
SG14-3844	09/05/2018	73.79	0.12	11.48	0.98	0.02	0.13	1.00	3.49	3.36	0.00	0.09	94.46
SG14-3844	09/05/2018	72.39	0.10	11.43	0.79	0.07	0.09	0.80	3.63	3.64	0.00	0.07	93.01
SG14-3844	09/05/2018	73.14	0.12	11.69	0.76	0.00	0.09	0.79	3.58	3.78	0.03	0.08	94.04

Table C2. Major element glass analyses of the MPI-DING reference glass (StHs6/80-G, GOR132-G and ATHO-G)

Reference Glass (Jochum et al., 2006)	Run Date	SiO_2	TiO_2	Al_2O_3	FeOt	MnO	MgO	CaO	Na_2O	K_2O	P_2O_5	Cl	Analytical total
StHs6/80-G_1	16/04/2010	63.47	0.76	17.31	4.43	0.06	1.96	5.22	4.60	1.34	0.20	-	99.35
StHs6/80-G_2	16/04/2010	63.42	0.70	17.49	4.53	0.08	1.98	5.21	4.72	1.37	0.16	-	99.67
StHs6/80-G_3	16/04/2010	63.40	0.71	17.53	4.42	0.09	2.03	5.17	4.38	1.29	0.14	-	99.17
StHs6/80-G_4	16/04/2010	63.84	0.77	17.70	4.34	0.04	1.94	5.22	4.74	1.33	0.18	-	100.11
StHs6/80-G_5	16/04/2010	63.19	0.65	17.51	4.49	0.01	1.89	5.18	4.75	1.30	0.17	-	99.13
StHs6/80-G_6	16/04/2010	62.77	0.69	17.74	4.50	0.12	1.93	5.31	4.59	1.33	0.15	-	99.13
StHs6/80-G_7	16/04/2010	63.71	0.70	17.57	4.51	0.08	2.08	5.14	4.29	1.28	0.12	-	99.48
StHs6/80-G_1	17/04/2010	63.00	0.75	17.34	4.18	0.06	1.98	5.17	4.51	1.33	0.12	-	98.45
StHs6/80-G_2	17/04/2010	63.04	0.71	17.50	4.53	0.12	1.97	5.29	4.52	1.28	0.15	-	99.11
StHs6/80-G_3	17/04/2010	63.27	0.74	17.42	4.61	0.10	2.02	5.24	4.80	1.31	0.13	-	99.63
StHs6/80-G_4	17/04/2010	63.67	0.74	17.57	4.35	0.07	1.97	5.37	4.49	1.28	0.13	-	99.64
StHs6/80-G_5	17/04/2010	62.96	0.75	17.26	4.28	0.04	1.88	5.32	4.89	1.40	0.15	-	98.93
StHs6/80-G_6	17/04/2010	63.56	0.70	17.51	4.58	0.01	1.97	5.19	4.40	1.32	0.13	-	99.37
StHs6/80-G_1	07/07/2010	63.19	0.62	17.94	4.55	0.12	1.90	5.16	4.64	1.29	0.18	0.00	99.59
StHs6/80-G_2	07/07/2010	63.48	0.69	17.67	4.40	0.12	1.92	5.73	4.51	1.29	0.17	0.00	99.97
StHs6/80-G_3	07/07/2010	63.55	0.69	18.03	4.63	0.00	1.97	5.24	4.55	1.24	0.13	0.01	100.06
StHs6/80-G_4	07/07/2010	63.43	0.66	17.87	4.40	0.13	1.96	5.72	4.55	1.26	0.17	0.01	100.17
StHs6/80-G_5	07/07/2010	63.73	0.71	17.94	4.59	0.07	1.95	5.06	4.39	1.26	0.13	0.03	99.85
StHs6/80-G_6	07/07/2010	61.82	0.69	17.48	4.66	0.05	1.94	5.51	4.55	1.24	0.17	0.01	98.11
StHs6/80-G_7	07/07/2010	63.19	0.66	17.86	4.29	0.03	1.92	5.02	4.68	1.32	0.23	0.01	99.20
StHs6/80-G_8	07/07/2010	63.70	0.72	18.06	4.29	0.00	1.95	5.62	4.48	1.26	0.22	0.00	100.29

Reference Glass (Jochum et al., 2006)	Run Date	SiO_2	TiO_2	Al_2O_3	FeOt	MnO	MgO	CaO	Na_2O	K_2O	P_2O_5	Cl	Analytical total
StHs6/80-G_1	11/06/2015	63.41	0.80	17.67	4.30	0.12	1.85	5.41	4.55	1.30	0.11	0.02	99.54
StHs6/80-G_2	11/06/2015	63.65	0.69	17.53	4.27	0.09	2.02	5.22	4.43	1.27	0.02	0.00	99.19
StHs6/80-G_3	11/06/2015	63.47	0.69	17.61	4.34	0.03	2.02	5.31	4.62	1.35	0.08	0.01	99.53
StHs6/80-G_4	11/06/2015	63.60	0.67	17.57	4.36	0.15	2.02	5.17	4.71	1.29	0.05	0.00	99.59
StHs6/80-G_5	11/06/2015	63.86	0.75	17.67	4.21	0.07	1.89	5.27	4.61	1.30	0.10	0.01	99.74
StHs6/80-G_6	11/06/2015	63.85	0.74	17.62	4.29	0.09	2.02	5.26	4.33	1.36	0.12	0.02	99.70
StHs6/80-G_7	11/06/2015	63.73	0.67	17.74	4.35	0.07	1.86	5.27	4.74	1.32	0.13	0.00	99.88
StHs6/80-G_8	11/06/2015	63.98	0.73	17.63	4.40	0.06	1.95	5.25	4.17	1.28	0.10	0.00	99.55
StHs6/80-G_9	11/06/2015	63.89	0.75	17.93	4.24	0.04	1.90	5.28	4.78	1.41	0.11	0.01	100.34
StHs6/80-G_10	11/06/2015	63.07	0.73	17.59	4.29	0.04	1.91	5.22	4.25	1.28	0.13	0.00	98.51
StHs6/80-G_11	11/06/2015	63.02	0.65	17.84	4.12	0.00	2.01	5.23	4.52	1.36	0.15	0.05	98.95
StHs6/80-G_12	11/06/2015	63.30	0.66	17.78	4.50	0.07	1.98	5.15	4.75	1.28	0.21	0.02	99.70
StHs6/80-G_13	11/06/2015	63.30	0.64	17.75	4.24	0.06	1.97	5.18	4.61	1.27	0.18	0.01	99.21
StHs6/80-G_14	11/06/2015	62.86	0.73	17.60	4.29	0.06	1.94	5.19	4.60	1.32	0.11	0.00	98.70
StHs6/80-G_15	11/06/2015	63.18	0.75	17.68	4.25	0.11	1.99	5.24	4.60	1.26	0.18	0.01	99.25
StHs6/80-G_16	11/06/2015	62.97	0.74	17.88	4.75	0.05	1.84	5.18	4.44	1.32	0.23	0.02	99.42
StHs6/80-G_17	11/06/2015	63.58	0.64	17.61	4.59	0.08	2.05	5.25	4.36	1.33	0.17	0.01	99.67
StHs6/80-G_18	11/06/2015	63.59	0.77	17.77	4.53	0.08	1.98	5.30	4.67	1.29	0.19	0.01	100.18
StHs6/80-G_19	11/06/2015	63.59	0.72	17.73	4.52	0.06	1.95	5.32	4.40	1.28	0.18	0.03	99.78
StHs6/80-G_20	11/06/2015	63.17	0.73	17.68	4.31	0.00	1.97	5.14	4.43	1.36	0.13	0.01	98.93
StHs6/80-G_22	11/06/2015	63.68	0.75	17.51	4.45	0.13	1.95	5.21	4.52	1.35	0.10	0.00	99.65
StHs6/80-G_1	25/10/2017	63.56	0.76	17.94	4.41	0.06	1.90	5.13	4.54	1.27	0.13	0.00	99.70
StHs6/80-G_2	25/10/2017	63.54	0.66	17.84	4.20	0.08	1.88	5.11	4.50	1.36	0.13	0.00	99.30
StHs6/80-G_3	25/10/2017	63.56	0.70	17.62	4.05	0.11	1.88	5.22	4.45	1.27	0.11	0.00	98.96

Reference Glass (Jochum et al., 2006)	Run Date	SiO_2	TiO_2	Al_2O_3	FeOt	MnO	MgO	CaO	Na_2O	K_2O	P_2O_5	Cl	Analytical total
StHs6/80-G_4	25/10/2017	63.36	0.71	17.72	4.41	0.01	1.91	5.40	4.74	1.32	0.15	0.01	99.76
StHs6/80-G_5	25/10/2017	63.94	0.73	17.79	4.53	0.07	1.92	5.21	4.40	1.32	0.11	0.01	100.04
StHs6/80-G_6	25/10/2017	63.61	0.69	17.86	4.56	0.04	1.92	5.27	4.63	1.34	0.07	0.00	100.00
StHs6/80-G_7	25/10/2017	63.74	0.65	17.39	4.37	0.12	1.90	5.30	4.48	1.27	0.09	0.01	99.31
StHs6/80-G_13	23/04/2018	63.45	0.70	17.79	4.40	0.08	1.91	5.22	4.56	1.36	0.09	0.01	99.56
StHs6/80-G_1	23/04/2018	64.21	0.68	17.65	4.32	0.10	1.88	5.19	4.51	1.36	0.04	0.00	99.95
StHs6/80-G_3	23/04/2018	63.71	0.70	17.38	4.38	0.07	1.92	5.13	4.67	1.27	0.08	0.01	99.32
StHs6/80-G_4	23/04/2018	63.92	0.72	17.42	4.38	0.06	1.88	5.17	4.55	1.24	0.10	0.01	99.45
StHs6/80-G_5	23/04/2018	63.36	0.69	17.43	4.38	0.13	1.97	5.16	4.64	1.30	0.04	0.00	99.10
StHs6/80-G_6	23/04/2018	64.03	0.76	17.85	4.15	0.06	1.86	5.10	4.37	1.33	0.09	0.01	99.60
StHs6/80-G_1	24/04/2018	63.67	0.70	17.81	4.20	0.18	1.90	5.25	4.68	1.36	0.12	0.00	99.88
StHs6/80-G_2	24/04/2018	63.44	0.75	17.80	4.29	0.05	1.95	5.20	4.47	1.29	0.08	0.02	99.33
StHs6/80-G_3	24/04/2018	63.30	0.68	17.87	4.27	0.01	1.88	5.28	4.67	1.30	0.12	0.01	99.38
StHs6/80-G_4	24/04/2018	63.25	0.71	17.75	4.31	0.03	1.91	5.28	4.51	1.36	0.15	0.01	99.27
StHs6/80-G_5	24/04/2018	63.30	0.61	17.94	4.65	0.07	1.94	5.28	4.55	1.25	0.19	0.01	99.78
StHs6/80-G_6	24/04/2018	63.88	0.68	17.95	4.21	0.08	1.85	5.20	4.70	1.29	0.16	0.01	99.99
StHs6/80-G_7	24/04/2018	63.66	0.74	18.10	4.32	0.00	1.99	5.36	4.20	1.28	0.17	0.00	99.82
StHs6/80-G_8	24/04/2018	63.51	0.68	18.06	4.52	0.10	1.98	5.32	4.57	1.36	0.16	0.02	100.26
StHs6/80-G_1	25/04/2018	63.59	0.68	17.75	4.42	0.06	1.82	5.43	4.35	1.36	0.19	0.04	99.68
StHs6/80-G_2	25/04/2018	64.84	0.71	18.24	4.34	0.08	1.94	5.19	4.65	1.31	0.10	0.00	101.39
StHs6/80-G_3	25/04/2018	64.43	0.67	17.89	4.35	0.03	1.85	5.15	4.58	1.29	0.13	0.00	100.37
StHs6/80-G_4	25/04/2018	64.96	0.70	17.99	4.28	0.07	2.01	5.19	3.90	1.31	0.13	0.00	100.53
StHs6/80-G_5	25/04/2018	63.79	0.77	17.52	4.22	0.10	1.91	5.14	4.44	1.29	0.11	0.01	99.30
StHs6/80-G_6	25/04/2018	63.50	0.66	17.67	4.31	0.12	1.92	5.26	4.49	1.32	0.05	0.01	99.30

Reference Glass (Jochum et al., 2006)	Run Date	SiO_2	TiO_2	Al_2O_3	FeOt	MnO	MgO	CaO	Na_2O	K_2O	P_2O_5	Cl	Analytical total
StHs6/80-G_7	25/04/2018	63.63	0.75	17.34	4.46	0.02	1.92	5.31	4.66	1.32	0.08	0.00	99.48
StHs6/80-G_8	25/04/2018	63.46	0.72	17.23	4.36	0.16	1.95	5.28	4.69	1.32	0.10	0.01	99.28
StHs6/80-G_1	03/05/2018	63.28	0.66	18.23	4.22	0.09	1.99	5.20	4.62	1.28	0.19	0.02	99.77
StHs6/80-G_2	03/05/2018	63.41	0.72	18.09	4.48	0.07	2.00	5.33	4.63	1.27	0.17	0.01	100.18
StHs6/80-G_3	03/05/2018	63.45	0.68	17.70	4.52	0.09	1.98	5.22	4.84	1.29	0.13	0.01	99.92
StHs6/80-G_4	03/05/2018	63.55	0.68	17.71	4.28	0.08	1.96	5.18	4.48	1.33	0.18	0.01	99.45
StHs6/80-G_5	03/05/2018	63.80	0.66	17.63	4.18	0.03	1.98	5.27	4.64	1.34	0.17	0.00	99.70
StHs6/80-G_6	03/05/2018	63.63	0.69	17.98	4.25	0.10	1.90	5.27	4.53	1.30	0.15	0.00	99.79
StHs6/80-G_1	08/05/2018	63.36	0.70	17.94	4.27	0.06	1.98	5.23	4.68	1.41	0.16	0.02	99.81
StHs6/80-G_2	08/05/2018	63.55	0.67	17.93	4.35	0.00	1.97	5.15	4.39	1.30	0.18	0.01	99.50
StHs6/80-G_3	08/05/2018	63.52	0.66	17.63	4.35	0.06	1.97	5.31	4.44	1.27	0.14	0.02	99.38
StHs6/80-G_4	08/05/2018	63.76	0.72	18.10	4.32	0.09	1.95	5.32	4.34	1.25	0.17	0.01	100.03
StHs6/80-G_5	08/05/2018	63.73	0.73	17.90	4.29	0.06	1.89	5.31	4.74	1.33	0.17	0.00	100.15
StHs6/80-G_6	08/05/2018	63.91	0.74	18.03	4.16	0.11	1.96	5.15	4.85	1.37	0.16	0.00	100.44
StHs6/80-G_2	09/05/2018	63.71	0.67	17.54	4.39	0.10	1.93	5.24	4.70	1.27	0.19	0.02	99.76
StHs6/80-G_3	09/05/2018	63.35	0.70	17.72	4.40	0.04	2.04	5.13	4.79	1.33	0.18	0.00	99.67
StHs6/80-G_4	09/05/2018	63.64	0.71	17.65	4.30	0.06	1.94	5.35	4.36	1.29	0.16	0.01	99.49
StHs6/80-G_5	09/05/2018	63.98	0.73	17.78	4.27	0.11	1.95	5.19	4.59	1.28	0.18	0.03	100.10
StHs6/80-G_6	09/05/2018	63.68	0.68	17.62	4.33	0.04	1.96	5.21	4.75	1.26	0.19	0.01	99.73
StHs6/80-G_7	09/05/2018	63.47	0.70	17.69	4.41	0.01	1.96	5.20	4.63	1.31	0.14	0.01	99.54
StHs6/80-G_8	09/05/2018	64.31	0.76	17.75	4.26	0.18	1.95	5.18	4.65	1.38	0.15	0.00	100.56
StHs6/80-G_9	09/05/2018	63.72	0.72	17.44	4.46	0.10	1.98	5.29	4.63	1.29	0.17	0.03	99.84
StHs6/80-G_10	09/05/2018	63.64	0.71	17.51	4.29	0.10	1.98	5.30	4.69	1.31	0.16	0.03	99.71
StHs6/80-G_11	09/05/2018	62.48	0.72	17.22	4.41	0.10	2.01	5.27	4.77	1.32	0.19	0.01	98.50

Reference Glass (Jochum et al., 2006)	Run Date	SiO_2	TiO_2	Al_2O_3	FeOt	MnO	MgO	CaO	Na_2O	K_2O	P_2O_5	Cl	Analytical total
ATHO-G_1	16/04/2010	75.29	0.27	12.13	3.22	0.10	0.10	1.74	3.89	2.81	0.00	-	99.55
ATHO-G_2	16/04/2010	75.06	0.21	12.29	3.38	0.05	0.11	1.66	4.03	2.80	0.04	-	99.62
ATHO-G_3	16/04/2010	74.88	0.24	12.01	3.05	0.11	0.12	1.69	4.15	2.76	0.02	-	99.03
ATHO-G_4	16/04/2010	74.49	0.21	12.27	3.31	0.11	0.10	1.62	3.95	2.76	0.02	-	98.85
ATHO-G_5	16/04/2010	75.43	0.21	12.32	3.23	0.14	0.11	1.70	4.01	2.72	0.03	-	99.91
ATHO-G_1	17/04/2010	75.12	0.24	12.23	3.35	0.14	0.11	1.69	4.21	2.71	0.01	-	99.80
ATHO-G_2	17/04/2010	75.04	0.24	12.10	3.16	0.21	0.09	1.69	4.23	2.74	0.06	-	99.55
ATHO-G_3	17/04/2010	74.85	0.28	12.49	3.00	0.09	0.09	1.77	3.99	2.75	0.00	-	99.32
ATHO-G_4	17/04/2010	75.20	0.24	12.17	3.24	0.09	0.11	1.65	4.13	2.81	0.02	-	99.67
ATHO-G_1	24/04/2010	75.61	0.21	12.09	3.05	0.07	0.06	1.65	3.98	2.68	0.03	0.05	99.43
ATHO-G_2	24/04/2010	75.48	0.23	12.20	3.25	0.10	0.09	1.76	3.89	2.72	0.00	0.05	99.73
ATHO-G_3	24/04/2010	75.92	0.27	12.22	3.06	0.09	0.10	1.71	4.18	2.63	0.04	0.06	100.22
ATHO-G_4	24/04/2010	75.74	0.24	12.24	3.26	0.16	0.08	1.70	3.97	2.70	0.00	0.04	100.09
ATHO-G_1	07/07/2010	75.38	0.25	12.53	3.31	0.12	0.08	1.68	3.97	2.76	0.07	0.05	100.20
ATHO-G_2	07/07/2010	75.58	0.23	12.45	3.32	0.03	0.09	1.82	4.11	2.61	0.02	0.03	100.28
ATHO-G_3	07/07/2010	76.02	0.25	12.33	3.52	0.12	0.08	1.82	4.21	2.66	0.03	0.03	101.06
ATHO-G_4	07/07/2010	75.58	0.28	12.34	3.19	0.14	0.10	1.64	4.08	2.76	0.04	0.02	100.19
ATHO-G_1	25/10/2017	75.16	0.24	12.54	3.24	0.08	0.11	1.72	4.44	2.68	0.00	0.03	100.24
ATHO-G_1	11/06/2015	74.17	0.23	12.35	3.06	0.07	0.04	1.77	3.97	2.77	0.00	0.04	98.47
ATHO-G_2	11/06/2015	74.86	0.25	12.24	3.04	0.08	0.04	1.67	4.21	2.78	0.00	0.05	99.22
ATHO-G_3	11/06/2015	74.61	0.31	12.42	3.35	0.11	0.12	1.74	4.32	2.74	0.01	0.07	99.80
ATHO-G_4	11/06/2015	74.84	0.21	12.28	3.19	0.12	0.06	1.68	4.14	2.75	0.02	0.04	99.33
ATHO-G_5	11/06/2015	74.77	0.20	12.25	3.40	0.04	0.05	1.63	4.00	2.78	0.00	0.04	99.16
ATHO-G_6	11/06/2015	75.07	0.28	12.32	3.23	0.08	0.10	1.71	4.29	2.72	0.02	0.05	99.87

Reference Glass (Jochum et al., 2006)	Run Date	SiO_2	TiO_2	Al_2O_3	FeOt	MnO	MgO	CaO	Na_2O	K_2O	P_2O_5	Cl	Analytical total
ATHO-G_7	11/06/2015	74.90	0.27	12.13	3.15	0.04	0.05	1.69	4.18	2.77	0.02	0.03	99.23
ATHO-G_8	11/06/2015	74.89	0.23	12.38	3.15	0.12	0.12	1.62	4.28	2.71	0.04	0.06	99.60
ATHO-G_9	11/06/2015	74.99	0.24	12.28	3.21	0.06	0.09	1.70	4.22	2.69	0.00	0.07	99.55
ATHO-G_10	11/06/2015	75.02	0.26	12.27	3.29	0.05	0.09	1.75	3.93	2.71	0.05	0.05	99.47
ATHO-G_11	11/06/2015	75.37	0.17	12.26	3.31	0.13	0.18	1.73	3.96	2.80	0.07	0.03	100.01
ATHO-G_12	11/06/2015	75.13	0.23	12.29	3.18	0.14	0.08	1.65	3.99	2.70	0.01	0.05	99.45
ATHO-G_13	11/06/2015	75.30	0.18	12.19	3.12	0.12	0.07	1.68	4.26	2.74	0.04	0.04	99.74
ATHO-G_14	11/06/2015	75.43	0.26	12.15	3.27	0.07	0.07	1.70	4.12	2.80	0.04	0.04	99.95
ATHO-G_15	11/06/2015	75.49	0.26	12.24	3.07	0.09	0.08	1.69	3.87	2.81	0.02	0.03	99.65
ATHO-G_16	11/06/2015	75.22	0.26	12.32	3.30	0.07	0.12	1.68	4.15	2.84	0.03	0.03	100.02
ATHO-G_18	11/06/2015	75.13	0.23	12.21	3.29	0.06	0.09	1.67	4.09	2.74	0.09	0.06	99.66
ATHO-G_19	11/06/2015	75.14	0.25	12.24	3.33	0.12	0.16	1.61	4.04	2.73	0.01	0.05	99.68
ATHO-G_20	11/06/2015	74.86	0.29	12.14	3.11	0.03	0.12	1.65	3.98	2.79	0.00	0.08	99.05
ATHO-G_21	11/06/2015	75.49	0.29	12.28	3.38	0.12	0.08	1.70	4.09	2.78	0.02	0.05	100.28
ATHO-G_2	25/10/2017	74.91	0.23	12.50	3.17	0.00	0.11	1.66	3.92	2.76	0.06	0.04	99.36
ATHO-G_3	25/10/2017	75.14	0.25	12.22	3.41	0.02	0.09	1.71	4.08	2.79	0.06	0.04	99.80
ATHO-G_4	25/10/2017	75.16	0.26	12.31	3.36	0.05	0.07	1.64	4.19	2.69	0.05	0.02	99.81
ATHO-G_5	25/10/2017	75.51	0.32	12.21	3.26	0.07	0.09	1.66	3.88	2.77	0.00	0.03	99.81
ATHO-G_6	25/10/2017	75.24	0.27	12.39	3.42	0.14	0.12	1.69	4.18	2.63	0.07	0.02	100.18
ATHO-G_7	25/10/2017	75.02	0.24	12.45	3.39	0.16	0.12	1.77	4.20	2.71	0.02	0.02	100.09
ATHO-G_1	23/04/2018	75.03	0.25	12.22	3.17	0.12	0.10	1.69	4.38	2.71	0.00	0.02	99.70
ATHO-G_2	23/04/2018	75.25	0.24	12.43	3.18	0.10	0.14	1.76	4.21	2.74	0.01	0.04	100.10
ATHO-G_3	23/04/2018	75.17	0.22	12.44	3.60	0.23	0.11	1.61	4.14	2.70	0.08	0.01	100.32
ATHO-G_4	23/04/2018	75.29	0.18	12.33	3.43	0.13	0.09	1.66	4.18	2.72	0.00	0.02	100.03

Reference Glass (Jochum et al., 2006)	Run Date	SiO_2	TiO_2	Al_2O_3	FeOt	MnO	MgO	CaO	Na_2O	K_2O	P_2O_5	Cl	Analytical total
ATHO-G_5	23/04/2018	75.03	0.16	12.47	3.20	0.14	0.09	1.60	4.08	2.82	0.01	0.05	99.65
ATHO-G_6	23/04/2018	75.25	0.22	12.33	2.95	0.11	0.10	1.72	4.22	2.78	0.00	0.04	99.71
ATHO-G_1	24/04/2018	75.03	0.22	12.27	3.32	0.11	0.07	1.71	4.25	2.75	0.04	0.04	99.83
ATHO-G_2	24/04/2018	75.32	0.23	12.28	3.04	0.10	0.10	1.73	4.11	2.71	0.02	0.04	99.68
ATHO-G_3	24/04/2018	74.78	0.26	12.20	3.43	0.05	0.06	1.67	4.26	2.74	0.01	0.05	99.50
ATHO-G_4	24/04/2018	75.04	0.25	12.14	3.24	0.16	0.12	1.67	4.25	2.72	0.00	0.02	99.62
ATHO-G_5	24/04/2018	75.14	0.23	12.41	3.24	0.03	0.08	1.68	4.08	2.70	0.01	0.06	99.64
ATHO-G_6	24/04/2018	75.27	0.25	12.39	3.26	0.07	0.11	1.67	4.02	2.80	0.04	0.03	99.90
ATHO-G_7	24/04/2018	75.12	0.28	12.34	3.17	0.09	0.06	1.63	3.95	2.69	0.05	0.04	99.43
ATHO-G_8	24/04/2018	74.50	0.28	12.31	3.29	0.06	0.08	1.71	4.30	2.65	0.00	0.04	99.21
ATHO-G_1	25/04/2018	74.98	0.22	12.29	3.33	0.07	0.06	1.67	4.18	2.74	0.01	0.02	99.58
ATHO-G_2	25/04/2018	74.82	0.22	12.15	3.23	0.14	0.10	1.68	4.04	2.68	0.01	0.03	99.08
ATHO-G_3	25/04/2018	74.42	0.24	12.15	3.26	0.10	0.10	1.64	4.17	2.64	0.04	0.04	98.80
ATHO-G_4	25/04/2018	74.53	0.25	12.13	3.31	0.09	0.06	1.67	4.35	2.72	0.01	0.04	99.15
ATHO-G_5	25/04/2018	75.17	0.28	12.29	3.42	0.07	0.11	1.63	4.20	2.71	0.04	0.03	99.95
ATHO-G_6	25/04/2018	75.23	0.24	12.08	3.23	0.08	0.10	1.68	4.13	2.69	0.00	0.04	99.50
ATHO-G_7	25/04/2018	74.55	0.28	12.02	3.29	0.05	0.10	1.66	4.29	2.67	0.02	0.03	98.97
ATHO-G_8	25/04/2018	74.85	0.26	12.15	3.49	0.15	0.11	1.72	4.16	2.78	0.00	0.02	99.68
ATHO-G_1	03/05/2018	74.98	0.26	12.60	3.28	0.11	0.12	1.63	4.06	2.74	0.03	0.03	99.86
ATHO-G_2	03/05/2018	75.08	0.24	12.49	3.10	0.08	0.05	1.67	4.12	2.75	0.04	0.05	99.66
ATHO-G_3	03/05/2018	74.85	0.20	12.44	3.03	0.13	0.10	1.70	3.99	2.72	0.02	0.01	99.20
ATHO-G_4	03/05/2018	75.40	0.24	12.33	3.08	0.13	0.09	1.68	4.07	2.67	0.00	0.03	99.72
ATHO-G_5	03/05/2018	75.14	0.27	12.30	3.23	0.12	0.08	1.66	4.07	2.65	0.01	0.03	99.55
ATHO-G_6	03/05/2018	74.93	0.27	12.10	3.05	0.17	0.10	1.63	4.16	2.72	0.02	0.05	99.18

Reference Glass (Jochum et al., 2006)	Run Date	SiO_2	TiO_2	Al_2O_3	FeOt	MnO	MgO	CaO	Na_2O	K_2O	P_2O_5	Cl	Analytical total
ATHO-G_1	08/05/2018	76.07	0.25	12.40	3.27	0.13	0.11	1.64	4.34	2.72	0.04	0.05	101.02
ATHO-G_2	08/05/2018	75.05	0.29	12.50	3.24	0.06	0.11	1.70	4.18	2.70	0.02	0.05	99.90
ATHO-G_3	08/05/2018	74.61	0.27	12.07	3.22	0.09	0.08	1.66	4.07	2.67	0.07	0.02	98.83
ATHO-G_4	08/05/2018	74.89	0.27	12.38	3.34	0.07	0.08	1.72	4.13	2.64	0.00	0.04	99.57
ATHO-G_5	08/05/2018	74.79	0.22	11.99	3.37	0.11	0.08	1.67	4.37	2.68	0.03	0.03	99.34
ATHO-G_6	08/05/2018	75.01	0.25	12.07	3.14	0.18	0.14	1.62	4.37	2.68	0.02	0.03	99.51
ATHO-G_2	09/05/2018	75.19	0.26	12.04	3.21	0.08	0.12	1.71	4.15	2.66	0.04	0.02	99.49
ATHO-G_3	09/05/2018	74.57	0.24	12.18	3.26	0.11	0.08	1.67	4.16	2.70	0.04	0.05	99.05
ATHO-G_4	09/05/2018	75.42	0.27	12.30	3.24	0.09	0.07	1.63	4.10	2.72	0.00	0.03	99.87
ATHO-G_5	09/05/2018	75.17	0.20	12.22	2.98	0.05	0.08	1.68	4.39	2.80	0.02	0.04	99.63
ATHO-G_6	09/05/2018	75.09	0.26	12.37	3.19	0.11	0.09	1.61	4.31	2.73	0.02	0.04	99.83
ATHO-G_7	09/05/2018	75.14	0.26	12.33	3.14	0.12	0.10	1.64	4.52	2.61	0.02	0.03	99.90
ATHO-G_8	09/05/2018	75.32	0.23	12.19	3.03	0.08	0.09	1.60	4.23	2.65	0.00	0.05	99.47
ATHO-G_9	09/05/2018	75.79	0.20	12.23	3.08	0.13	0.09	1.66	4.08	2.69	0.04	0.03	100.03
ATHO-G_10	09/05/2018	75.75	0.26	12.29	3.10	0.10	0.06	1.72	4.31	2.77	0.04	0.03	100.43
ATHO-G_11	09/05/2018	75.19	0.21	12.25	3.25	0.13	0.12	1.71	4.22	2.68	0.05	0.03	99.84
GOR132-G_1	16/04/2010	46.06	0.27	11.12	10.22	0.21	22.40	8.38	0.75	0.03	0.03	-	99.47
GOR132-G_2	16/04/2010	45.89	0.28	10.74	10.48	0.18	22.21	8.47	0.74	0.03	0.05	-	99.07
GOR132-G_3	16/04/2010	45.92	0.27	10.81	10.21	0.12	22.64	8.41	0.84	0.03	0.06	-	99.32
GOR132-G_4	16/04/2010	45.64	0.32	10.87	10.31	0.21	22.56	8.35	0.81	0.01	0.03	-	99.12
GOR132-G_5	16/04/2010	45.86	0.31	10.91	9.94	0.13	22.49	8.39	0.87	0.04	0.06	-	99.01
GOR132-G_6	16/04/2010	45.82	0.31	10.98	10.09	0.17	22.36	8.38	0.76	0.02	0.02	-	98.91
GOR132-G_7	16/04/2010	46.16	0.28	10.77	10.09	0.16	22.45	8.42	0.74	0.05	0.05	-	99.18
GOR132-G_1	16/04/2010	45.44	0.28	10.89	9.96	0.13	22.30	8.38	0.78	0.02	0.00	-	98.19

Reference Glass (Jochum et al., 2006)	Run Date	SiO_2	TiO_2	Al_2O_3	FeOt	MnO	MgO	CaO	Na_2O	K_2O	P_2O_5	Cl	Analytical total
GOR132-G_2	16/04/2010	45.63	0.26	10.79	10.09	0.11	22.57	8.25	0.83	0.03	0.01	-	98.57
GOR132-G_3	16/04/2010	45.65	0.32	10.74	10.33	0.19	22.24	8.35	0.90	0.01	0.03	-	98.77
GOR132-G_4	16/04/2010	45.60	0.31	10.73	10.27	0.21	22.41	8.46	0.78	0.06	0.03	-	98.85
GOR132-G_5	16/04/2010	45.54	0.32	10.75	10.29	0.19	22.47	8.37	0.84	0.04	0.03	-	98.85
GOR132-G_6	16/04/2010	45.62	0.34	10.96	9.91	0.20	22.81	8.54	0.77	0.02	0.04	-	99.22
GOR132-G_1	16/04/2010	45.87	0.26	11.08	10.09	0.16	21.86	8.40	0.85	0.01	0.01	0.01	98.61
GOR132-G_2	16/04/2010	45.97	0.29	10.89	10.08	0.23	22.04	8.35	0.78	0.03	0.04	0.00	98.71
GOR132-G_3	16/04/2010	45.80	0.29	10.86	10.04	0.14	22.01	8.38	0.69	0.05	0.06	0.00	98.32
GOR132-G_4	16/04/2010	45.91	0.32	10.78	10.52	0.21	22.18	8.43	0.75	0.05	0.00	0.01	99.16
GOR132-G_1	07/07/2010	45.77	0.32	11.14	9.86	0.17	22.50	8.14	0.76	0.00	0.07	0.02	98.75
GOR132-G_2	07/07/2010	45.88	0.31	11.21	10.37	0.21	22.08	8.88	0.60	0.04	0.07	0.01	99.65
GOR132-G_3	07/07/2010	45.79	0.26	11.10	10.25	0.10	22.25	7.93	0.83	0.03	0.07	0.02	98.65
GOR132-G_4	07/07/2010	45.93	0.28	11.02	10.55	0.14	22.24	8.96	0.83	0.04	0.00	0.00	99.99
GOR132-G_5	07/07/2010	45.88	0.27	10.95	10.61	0.28	22.39	8.94	0.92	0.04	0.04	0.00	100.33
GOR132-G_6	07/07/2010	45.72	0.33	11.13	10.24	0.15	22.06	9.01	0.76	0.03	0.07	0.02	99.52
GOR132-G_7	11/06/2015	45.69	0.33	11.00	10.18	0.15	22.09	8.58	0.69	0.01	0.05	0.02	98.79
GOR132-G_8	11/06/2015	45.19	0.28	10.97	10.45	0.12	21.96	8.50	0.84	0.04	0.00	0.00	98.35
GOR132-G_9	11/06/2015	45.42	0.35	11.00	10.23	0.07	22.12	8.50	0.94	0.04	0.01	0.00	98.68
GOR132-G_10	11/06/2015	45.40	0.35	10.81	10.63	0.14	22.27	8.49	0.70	0.04	0.01	0.00	98.84
GOR132-G_11	11/06/2015	45.20	0.27	10.93	10.32	0.15	21.97	8.57	0.90	0.03	0.02	0.00	98.36
GOR132-G_12	11/06/2015	45.62	0.31	10.97	10.29	0.19	22.49	8.36	0.87	0.07	0.13	0.00	99.30
GOR132-G_13	11/06/2015	45.19	0.31	10.88	10.27	0.19	22.16	8.42	0.77	0.04	0.04	0.00	98.27
GOR132-G_14	11/06/2015	45.52	0.33	10.99	10.26	0.15	22.05	8.43	0.78	0.03	0.05	0.00	98.59
GOR132-G_15	11/06/2015	45.22	0.34	10.96	9.99	0.14	21.97	8.36	0.92	0.02	0.11	0.02	98.05

Reference Glass (Jochum et al., 2006)	Run Date	SiO_2	TiO_2	Al_2O_3	FeOt	MnO	MgO	CaO	Na_2O	K_2O	P_2O_5	Cl	Analytical total
GOR132-G_16	11/06/2015	45.68	0.30	10.95	10.23	0.19	21.88	8.61	0.96	0.02	0.10	0.00	98.92
GOR132-G_18	11/06/2015	45.76	0.29	10.88	10.35	0.20	21.96	8.48	0.89	0.01	0.05	0.00	98.87
GOR132-G_19	11/06/2015	45.67	0.29	10.82	10.33	0.15	22.26	8.58	0.83	0.04	0.05	0.01	99.03
GOR132-G_20	11/06/2015	45.39	0.33	10.89	10.35	0.21	22.25	8.55	0.74	0.05	0.02	0.00	98.78
GOR132-G_21	11/06/2015	45.77	0.28	10.91	10.24	0.12	22.07	8.43	0.89	0.02	0.04	0.00	98.77
GOR132-G_22	11/06/2015	45.87	0.30	10.87	10.23	0.22	22.27	8.56	0.81	0.03	0.04	0.00	99.20
GOR132-G_1	25/10/2017	45.31	0.26	11.08	10.06	0.15	22.16	8.63	0.79	0.03	0.01	0.00	98.46
GOR132-G_2	25/10/2017	45.59	0.30	11.05	10.07	0.11	21.76	8.38	0.92	0.04	0.01	0.01	98.23
GOR132-G_3	25/10/2017	45.43	0.32	11.29	10.52	0.17	21.75	8.50	0.85	0.04	0.05	0.02	98.94
GOR132-G_4	25/10/2017	45.86	0.29	10.96	9.96	0.11	22.03	8.41	0.77	0.03	0.08	0.01	98.51
GOR132-G_5	25/10/2017	45.34	0.32	10.95	10.24	0.19	22.05	8.26	0.65	0.05	0.09	0.01	98.14
GOR132-G_6	25/10/2017	45.61	0.28	10.86	10.40	0.23	21.97	8.29	0.78	0.01	0.05	0.00	98.49
GOR132-G_7	25/10/2017	45.48	0.30	11.00	10.24	0.09	22.00	8.37	0.74	0.03	0.02	0.00	98.28
GOR132-G_12	23/04/2018	45.62	0.26	11.00	10.30	0.23	21.97	8.28	0.77	0.04	0.05	0.00	98.52
GOR132-G_2	23/04/2018	45.68	0.25	11.08	10.39	0.14	22.16	8.36	0.78	0.00	0.02	0.00	98.86
GOR132-G_3	23/04/2018	45.68	0.36	11.02	9.89	0.12	21.87	8.38	0.78	0.04	0.05	0.00	98.21
GOR132-G_4	23/04/2018	44.89	0.29	10.94	10.09	0.15	22.10	8.56	0.81	0.04	0.00	0.02	97.88
GOR132-G_5	23/04/2018	45.47	0.30	10.99	10.29	0.07	22.28	8.41	0.82	0.02	0.10	0.00	98.76
GOR132-G_6	23/04/2018	45.22	0.21	11.13	10.17	0.15	22.10	8.44	0.75	0.03	0.03	0.00	98.23
GOR132-G_1	24/04/2018	45.40	0.25	11.17	10.10	0.08	21.90	8.38	0.76	0.03	0.02	0.02	98.10
GOR132-G_2	24/04/2018	45.40	0.35	10.96	10.11	0.18	22.02	8.61	0.67	0.01	0.04	0.01	98.37
GOR132-G_3	24/04/2018	45.20	0.33	10.88	10.31	0.14	22.31	8.48	0.83	0.05	0.05	0.00	98.59
GOR132-G_4	24/04/2018	45.33	0.27	11.01	10.12	0.21	22.24	8.40	0.83	0.03	0.02	0.00	98.47
GOR132-G_5	24/04/2018	45.51	0.31	11.03	10.00	0.11	22.06	8.45	0.81	0.02	0.05	0.00	98.36

Reference Glass (Jochum et al., 2006)	Run Date	SiO_2	TiO_2	Al_2O_3	FeOt	MnO	MgO	CaO	Na_2O	K_2O	P_2O_5	Cl	Analytical total
GOR132-G_6	24/04/2018	45.45	0.28	10.78	10.08	0.18	21.87	8.50	0.79	0.03	0.03	0.01	98.01
GOR132-G_7	24/04/2018	45.03	0.32	11.04	10.22	0.15	21.73	8.45	0.90	0.03	0.07	0.01	97.95
GOR132-G_8	24/04/2018	45.20	0.26	11.02	10.34	0.13	21.99	8.44	0.75	0.01	0.03	0.00	98.15
GOR132-G_1	25/04/2018	45.64	0.28	11.16	10.37	0.15	22.42	8.44	0.87	0.04	0.02	0.00	99.39
GOR132-G_2	25/04/2018	45.50	0.31	11.16	10.23	0.18	22.42	8.34	0.77	0.03	0.05	0.01	99.00
GOR132-G_3	25/04/2018	45.42	0.32	10.99	9.86	0.23	22.43	8.46	0.87	0.03	0.05	0.00	98.66
GOR132-G_4	25/04/2018	45.79	0.31	11.12	10.26	0.15	22.57	8.48	0.82	0.02	0.00	0.02	99.53
GOR132-G_5	25/04/2018	45.74	0.27	10.90	10.31	0.15	22.32	8.54	0.82	0.03	0.02	0.00	99.11
GOR132-G_6	25/04/2018	45.26	0.32	10.91	10.20	0.10	22.50	8.47	0.83	0.04	0.04	0.00	98.67
GOR132-G_7	25/04/2018	45.33	0.28	11.10	10.08	0.17	22.56	8.33	0.77	0.02	0.03	0.00	98.68
GOR132-G_8	25/04/2018	45.59	0.36	10.95	10.43	0.19	22.38	8.55	0.79	0.03	0.06	0.00	99.33
GOR132-G_1	03/05/2018	45.54	0.31	11.16	10.19	0.17	22.28	8.27	0.91	0.05	0.00	0.00	98.88
GOR132-G_2	03/05/2018	45.43	0.32	11.08	10.10	0.18	22.27	8.53	0.74	0.02	0.07	0.02	98.74
GOR132-G_3	03/05/2018	44.80	0.31	10.75	10.61	0.16	22.02	8.39	0.82	0.04	0.04	0.01	97.96
GOR132-G_4	03/05/2018	45.26	0.29	11.00	9.99	0.11	22.42	8.34	0.84	0.04	0.04	0.02	98.36
GOR132-G_5	03/05/2018	44.88	0.25	10.95	10.40	0.12	21.99	8.37	0.76	0.04	0.08	0.00	97.84
GOR132-G_6	03/05/2018	44.87	0.29	10.82	10.21	0.18	22.24	8.30	0.75	0.03	0.05	0.01	97.73
GOR132-G_1	08/05/2018	45.51	0.30	11.21	9.98	0.18	22.44	8.42	0.85	0.04	0.10	0.00	99.02
GOR132-G_2	08/05/2018	45.37	0.30	11.03	10.32	0.13	22.11	8.32	0.88	0.04	0.04	0.00	98.54
GOR132-G_3	08/05/2018	45.32	0.30	10.84	10.18	0.07	22.24	8.37	0.84	0.03	0.04	0.01	98.23
GOR132-G_4	08/05/2018	45.74	0.30	10.94	9.95	0.11	22.33	8.52	0.83	0.03	0.01	0.00	98.75
GOR132-G_5	08/05/2018	45.76	0.37	10.95	9.82	0.12	22.06	8.31	0.80	0.04	0.05	0.00	98.29
GOR132-G_6	08/05/2018	45.41	0.28	11.00	10.26	0.16	22.31	8.32	0.92	0.04	0.01	0.01	98.73
GOR132-G_1	09/05/2018	46.05	0.29	10.98	10.29	0.17	22.20	8.40	0.79	0.03	0.04	0.00	99.23

Reference Glass (Jochum et al., 2006)	Run Date	SiO_2	TiO_2	Al_2O_3	FeOt	MnO	MgO	CaO	Na_2O	K_2O	P_2O_5	Cl	Analytical total
GOR132-G_2	09/05/2018	46.02	0.28	11.13	10.08	0.17	22.11	8.46	0.86	0.01	0.05	0.02	99.19
GOR132-G_3	09/05/2018	45.27	0.30	10.88	9.98	0.15	22.09	8.54	0.73	0.05	0.01	0.01	98.01
GOR132-G_4	09/05/2018	45.26	0.27	11.10	9.90	0.19	22.02	8.41	0.88	0.06	0.02	0.00	98.10
GOR132-G_5	09/05/2018	45.20	0.32	10.80	10.03	0.15	22.36	8.44	0.89	0.02	0.02	0.00	98.23
GOR132-G_6	09/05/2018	45.39	0.33	10.82	10.00	0.14	22.26	8.25	0.88	0.03	0.02	0.00	98.12
GOR132-G_7	09/05/2018	45.92	0.31	10.97	9.91	0.19	22.36	8.37	0.86	0.03	0.07	0.01	99.01
GOR132-G_8	09/05/2018	45.57	0.30	10.90	10.36	0.11	22.35	8.43	0.89	0.03	0.04	0.00	98.99
GOR132-G_9	09/05/2018	45.79	0.37	10.91	9.75	0.18	22.05	8.46	0.88	0.05	0.06	0.00	98.50
GOR132-G_10	09/05/2018	45.76	0.24	11.01	10.39	0.17	22.26	8.43	0.74	0.03	0.03	0.00	99.06
GOR132-G_11	09/05/2018	44.63	0.29	10.58	10.32	0.24	22.37	8.37	0.77	0.08	0.02	0.00	97.67

Table C3. Trace element glass compositions of cryptotephra layers preserved in the Lake Suigetsu sediments between 50 to 30 ka using LA-ICP-MS

SG Label (SG14-)	Run Date (2018)	Rb	Sr	Y	Zr	Nb	Ba	La	Ce	Pr	Nd	Sm	Eu	Gd	Dy	Er	Yb	Hf	Ta	Th	U
2752	11/07	136.2	153.9	32.8	263.6	16.3	641.4	28.1	63.2	7.6	27.5	6.5	1.5	6.0	5.4	3.4	4.1	6.8	1.1	13.0	3.3
2752	11/07	122.6	178.8	32.5	247.0	14.9	605.2	25.4	59.3	6.4	25.4	6.7	1.0	6.1	5.1	2.5	3.6	6.1	1.0	11.3	3.4
2752	11/07	138.7	154.8	36.9	268.2	15.9	633.4	28.3	65.1	7.7	30.7	8.8	1.3	7.4	5.1	4.6	4.1	7.5	1.3	12.8	3.1
2752	11/07	122.5	185.1	34.0	245.1	14.2	577.9	27.4	58.0	6.9	29.6	6.8	1.3	2.3	5.0	3.0	3.5	5.5	0.6	11.4	3.1
2752	11/07	139.3	201.2	38.4	280.8	16.3	662.1	30.3	67.0	8.1	33.0	6.9	1.5	7.1	5.6	4.0	4.0	7.2	1.0	12.9	3.5
2752	11/07	131.3	186.4	31.4	249.2	15.5	614.0	27.0	62.1	7.5	29.4	6.8	1.4	5.1	4.0	3.3	3.3	5.9	1.1	12.8	3.3
2752	11/07	133.1	189.6	37.1	274.7	16.3	621.9	28.5	66.3	7.7	30.8	6.1	1.3	5.7	6.4	3.2	3.9	7.1	1.2	12.7	3.3
2752	11/07	128.4	177.0	33.5	253.6	16.7	626.2	24.7	59.6	7.0	31.8	6.8	1.1	6.7	6.6	3.0	2.9	6.6	0.8	12.0	3.4
2752	11/07	134.5	155.9	35.5	262.4	16.8	627.3	28.2	61.6	7.4	31.3	6.2	1.3	4.0	6.3	2.6	3.8	6.3	1.2	11.9	3.1
2814	12/07	130.7	45.7	20.2	82.8	5.6	442.2	21.0	43.8	4.0	13.1	2.5	0.3	5.0	2.0	1.5	2.4	3.9	0.7	13.5	2.8
2814	12/07	162.4	48.9	22.3	89.6	8.2	550.8	25.7	51.2	5.5	17.1	4.2	0.3	0.7	4.4	2.8	1.8	4.1	0.8	15.0	3.5
2814	12/07	146.8	66.7	23.1	98.5	7.7	559.4	23.3	48.6	5.2	17.4	4.3	0.4	0.3	4.1	1.6	2.2	3.5	0.7	13.9	3.5
2814	12/07	155.0	53.2	23.8	86.1	7.9	555.0	24.6	51.8	5.0	19.4	1.4	0.8	5.3	4.0	2.5	2.3	2.9	0.5	15.1	3.2
2814	12/07	160.0	56.1	27.5	104.2	7.7	626.5	28.7	57.0	5.3	21.3	6.4	0.6	3.2	3.2	0.8	3.5	3.5	1.0	16.0	3.1
2814	12/07	163.5	60.0	22.0	98.2	8.3	633.9	28.7	60.6	6.4	20.6	3.9	1.0	4.4	3.6	2.6	2.5	4.1	0.8	18.4	3.7
2814	12/07	150.3	56.0	23.8	87.5	6.6	591.2	25.0	50.8	4.9	20.6	5.4	<LOD	<LOD	3.1	2.3	4.0	2.6	0.7	14.4	3.0
2814	12/07	158.7	57.9	25.6	95.4	8.4	591.2	27.6	49.5	5.4	17.9	2.6	0.2	3.5	4.0	2.4	1.8	2.7	0.7	15.5	3.8
2814	12/07	152.4	48.5	25.5	88.7	6.9	567.1	24.6	47.8	4.8	20.0	4.9	0.8	3.7	4.0	2.2	4.3	2.8	0.9	14.6	2.8
2830	12/07	78.3	104.6	37.8	202.9	7.5	384.9	16.7	39.2	4.9	20.5	4.2	1.2	5.4	6.5	3.3	3.2	5.2	0.4	8.3	1.8
2830	12/07	83.8	105.6	37.4	213.1	7.0	407.3	18.0	40.9	4.9	19.4	5.3	1.3	4.6	5.4	4.0	3.5	6.2	0.6	8.7	2.1
2830	12/07	86.2	102.4	36.5	209.4	6.6	398.8	17.7	39.2	4.8	20.6	3.9	0.8	5.8	5.6	3.7	3.1	6.1	0.5	7.0	1.5

SG Label (SG14-)	Run Date (2018)	Rb	Sr	Y	Zr	Nb	Ba	La	Ce	Pr	Nd	Sm	Eu	Gd	Dy	Er	Yb	Hf	Ta	Th	U
2830	12/07	81.8	100.1	39.1	215.7	6.4	389.0	17.9	43.5	4.7	20.1	4.0	1.0	5.6	6.1	3.6	5.3	6.0	0.5	8.2	1.9
2830	12/07	86.9	99.1	37.0	210.1	7.2	398.4	18.8	38.4	5.0	20.5	4.3	0.9	3.9	6.7	3.4	2.7	6.0	0.6	8.2	1.9
2830	12/07	81.2	101.9	38.1	194.1	5.9	385.4	16.8	38.6	4.3	19.7	4.7	1.6	4.0	4.3	2.5	3.7	5.1	0.7	7.3	1.7
2830	12/07	82.7	99.7	35.0	197.5	5.7	369.1	16.9	36.7	5.1	20.3	4.8	1.1	2.0	4.6	3.3	3.9	5.9	0.4	7.3	1.8
2830	12/07	79.8	98.8	36.4	200.4	5.7	367.0	15.8	37.0	4.1	18.6	4.3	0.8	2.4	5.1	3.9	4.0	5.0	0.5	7.1	1.9
2841	12/07	136.5	217.8	38.4	259.0	17.1	653.1	29.7	69.4	7.8	38.1	5.5	1.1	8.3	5.5	3.5	4.0	5.7	1.1	12.1	3.4
2841	12/07	179.2	106.8	40.6	336.8	21.4	740.1	37.8	80.4	9.6	35.7	8.1	0.8	6.2	6.9	5.0	4.9	9.8	1.8	17.6	4.9
2841	12/07	103.1	260.7	35.4	222.2	14.3	559.0	26.6	61.1	7.2	30.6	6.7	1.3	11.3	6.4	4.4	5.4	6.0	1.1	11.5	2.4
2841	12/07	156.8	126.7	40.1	319.6	19.1	671.0	30.4	69.7	8.8	35.0	8.0	1.5	6.6	7.4	4.7	3.7	8.3	1.2	15.4	3.9
2841	12/07	141.9	183.5	38.0	287.7	18.4	656.8	30.3	72.8	8.2	30.5	9.7	1.1	8.7	4.9	2.9	3.1	7.7	1.2	14.5	3.8
2841	12/07	115.4	255.9	36.7	246.1	15.1	594.6	28.6	62.9	8.0	32.9	5.8	1.3	6.3	4.7	3.6	5.4	6.2	0.8	12.6	3.1
2841	12/07	101.4	424.8	29.9	239.0	13.8	664.1	25.4	53.7	6.3	21.5	3.2	1.6	5.3	3.0	2.8	3.8	6.9	1.0	10.6	2.8
2841	12/07	85.5	325.7	31.2	195.6	11.4	480.8	23.0	52.2	6.2	25.0	7.3	2.0	5.5	4.0	2.5	2.9	4.1	0.9	8.9	2.2
2873	12/07	140.1	54.5	25.0	98.8	7.0	506.5	25.8	44.1	4.5	12.6	5.7	<LOD	<LOD	3.0	1.4	3.7	4.1	0.4	13.6	2.2
2873	12/07	151.6	64.8	19.7	99.7	7.3	549.7	25.1	49.4	4.7	15.3	4.2	<LOD	4.2	3.5	2.2	2.0	4.0	0.6	13.6	3.0
2873	12/07	155.9	68.4	22.9	99.6	9.5	541.5	25.4	48.3	5.5	17.8	2.6	0.8	2.5	3.6	2.3	3.2	3.9	0.6	15.1	2.8
2873	12/07	138.2	63.0	22.0	90.6	8.0	500.7	21.1	46.4	4.5	13.8	2.3	0.4	3.4	2.1	2.6	2.4	4.2	0.8	14.6	2.9
2873	12/07	151.4	64.8	22.5	98.8	7.5	559.1	24.6	51.6	4.7	17.4	2.9	0.5	5.2	3.4	2.6	2.5	3.3	0.5	14.3	3.7
2873	12/07	136.2	59.0	20.5	93.2	6.7	498.7	23.3	46.4	4.5	18.7	2.9	0.4	3.4	2.8	2.0	1.4	2.6	0.5	13.9	3.1
2873	12/07	146.6	65.5	21.4	99.1	7.0	510.8	24.3	48.7	4.7	20.0	5.5	0.3	2.0	3.5	1.5	2.9	2.5	0.9	15.0	2.4
2873	12/07	141.7	62.1	20.9	93.6	7.2	527.2	22.9	47.9	4.7	25.0	4.4	0.5	4.0	2.5	1.6	1.5	2.8	0.8	14.7	3.4
2873	12/07	139.0	62.1	21.2	93.6	7.1	518.1	24.0	50.6	5.5	18.7	3.7	0.4	0.3	2.1	2.0	1.9	3.2	0.8	13.7	2.9
3085a	11/07	70.8	461.3	29.4	163.5	10.3	470.8	22.0	46.2	6.4	25.1	7.5	1.5	3.3	4.0	2.8	2.3	3.7	0.7	6.8	1.6

SG Label (SG14-)	Run Date (2018)	Rb	Sr	Y	Zr	Nb	Ba	La	Ce	Pr	Nd	Sm	Eu	Gd	Dy	Er	Yb	Hf	Ta	Th	U
3085a	11/07	81.5	343.6	33.8	181.4	9.7	469.7	21.2	50.3	6.4	28.3	4.4	1.6	3.0	6.8	3.7	4.1	4.0	0.7	7.8	2.0
3085a	11/07	79.1	319.1	34.4	186.4	12.0	483.8	25.2	52.9	6.6	29.9	6.4	1.3	4.6	6.9	2.5	2.9	4.0	0.6	7.5	2.4
3085a	11/07	73.4	446.3	31.3	159.6	9.6	457.1	19.8	44.8	7.1	29.9	4.9	0.8	7.8	5.8	2.8	3.3	4.5	0.5	7.6	2.0
3085a	11/07	80.9	409.9	31.0	181.4	10.5	467.3	20.3	48.2	5.9	26.8	6.1	1.3	6.0	5.9	3.0	2.2	4.0	0.7	7.2	1.7
3085a	11/07	75.1	351.6	31.7	171.6	9.4	474.8	22.3	50.9	6.7	25.6	7.3	1.4	6.2	6.2	4.6	2.6	4.9	0.2	8.1	1.7
3085a	11/07	54.2	548.5	23.8	125.2	9.7	404.5	15.1	39.5	4.2	19.0	6.7	1.5	2.8	4.1	2.6	1.7	4.3	0.7	5.8	1.4
3085a	11/07	74.7	390.7	28.1	169.9	9.0	479.9	20.5	48.1	6.3	25.0	4.9	2.1	7.8	4.1	2.4	2.2	4.8	0.8	7.5	1.9
3085a	11/07	80.4	412.5	31.3	167.5	10.4	476.8	20.7	52.2	5.8	25.5	6.9	1.0	6.1	4.7	3.3	3.5	3.2	0.4	6.7	1.7
3085b	11/07	147.1	191.7	37.2	287.9	16.0	629.2	30.5	70.6	8.7	37.6	8.0	1.7	7.5	4.2	4.7	4.0	7.6	1.2	13.0	3.6
3085b	11/07	142.3	235.1	43.2	304.0	17.5	661.2	33.7	70.3	9.1	42.2	9.2	1.6	7.1	8.2	4.3	4.3	8.5	1.7	16.4	3.7
3085b	11/07	137.6	208.5	40.2	299.3	19.1	699.3	35.1	74.2	9.1	38.2	8.5	2.0	6.3	6.2	4.1	3.5	9.0	1.2	15.6	3.8
3216	10/07	200.2	31.9	28.4	823.9	193.9	44.3	99.0	172.4	14.3	48.1	5.2	0.4	3.4	4.7	2.8	2.7	15.9	10.7	25.5	5.8
3216	10/07	198.4	11.0	24.9	679.4	170.3	10.8	95.8	157.7	14.8	42.9	7.2	0.8	6.3	4.1	1.5	3.1	10.9	8.7	23.9	4.9
3216	10/07	219.3	27.6	29.3	847.1	200.0	25.3	106.2	177.5	16.1	48.7	7.2	0.3	5.0	4.6	2.5	4.5	15.2	10.9	27.8	6.3
3216	10/07	199.8	7.2	28.4	741.2	185.0	6.3	107.3	173.3	16.0	50.1	6.2	0.5	9.7	5.3	3.2	2.9	13.6	10.0	26.8	4.9
3216	10/07	193.8	7.7	27.1	684.8	170.5	8.4	99.8	159.0	14.0	43.8	6.7	0.4	5.6	5.0	2.7	3.6	14.1	9.4	24.9	5.2
3216	10/07	170.0	13.8	21.4	570.2	147.8	19.0	86.3	142.8	12.9	39.6	6.8	1.0	5.2	3.8	3.2	2.4	11.1	8.6	20.7	4.1
3216	10/07	215.8	2.8	26.6	760.8	190.8	3.2	107.0	174.9	14.9	41.1	5.9	0.5	4.0	4.5	3.5	3.1	15.2	11.0	30.6	6.6
3216	10/07	166.1	12.4	22.2	569.6	143.1	13.1	84.2	135.8	12.8	37.0	6.1	0.9	4.4	3.5	2.7	2.3	11.1	8.4	21.5	4.6
3380	10/07	138.3	11.0	47.8	723.8	95.9	53.2	72.7	152.2	16.4	65.0	11.9	0.6	11.3	9.4	4.8	4.3	17.4	5.6	12.6	2.6
3380	10/07	141.0	39.0	53.3	742.0	95.9	123.0	76.2	158.9	16.5	65.8	11.6	0.4	8.3	10.4	4.4	4.7	17.8	5.6	14.9	2.5
3380	10/07	148.6	8.9	53.7	767.8	105.3	37.9	78.5	159.6	17.4	59.4	15.0	0.6	10.2	10.4	4.6	4.8	16.7	5.8	15.1	2.9
3380	10/07	136.5	74.6	42.7	641.9	84.9	183.8	65.4	130.2	14.4	54.7	10.5	0.6	9.4	7.7	4.1	3.2	14.7	4.9	12.7	2.6
3380	10/07	145.9	4.5	49.7	740.3	99.3	23.9	76.1	156.2	18.1	66.8	12.6	0.5	10.4	9.2	5.2	4.0	16.4	5.7	14.7	3.0

SG Label (SG14-)	Run Date (2018)	Rb	Sr	Y	Zr	Nb	Ba	La	Ce	Pr	Nd	Sm	Eu	Gd	Dy	Er	Yb	Hf	Ta	Th	U
3380	10/07	134.1	15.2	49.0	734.1	98.0	51.5	77.1	154.8	16.9	66.6	13.1	0.5	10.9	8.5	5.1	4.7	18.0	5.7	14.6	3.2
3380	10/07	155.1	14.6	54.9	763.4	98.2	50.2	80.9	156.2	18.2	73.0	12.6	0.6	12.5	8.3	6.3	4.7	15.0	5.4	13.5	2.3
3380	10/07	131.1	58.5	50.7	745.3	92.6	161.2	75.7	157.5	16.9	59.2	11.0	0.6	12.2	9.3	6.3	4.4	17.1	4.8	13.1	2.5
3380	10/07	158.2	2.9	55.4	826.6	102.4	29.1	82.1	166.8	18.1	74.8	16.7	0.7	12.4	10.0	5.0	4.8	18.1	6.3	15.2	3.2
3380	10/07	146.6	20.9	53.9	728.5	97.2	59.2	79.4	150.9	17.6	70.4	14.0	1.1	9.3	9.4	4.8	3.3	18.0	5.7	14.9	3.2
3605	11/07	95.4	384.8	32.5	285.5	13.1	651.3	33.6	73.5	8.2	36.0	6.5	1.6	5.3	5.9	2.8	3.5	6.7	0.9	10.5	1.8
3605	11/07	87.4	346.4	34.8	273.1	13.4	620.9	32.9	73.4	8.5	35.3	7.0	1.8	6.4	6.1	2.8	3.6	6.7	0.7	9.3	1.5
3605	11/07	87.3	302.2	29.7	246.3	11.4	654.7	32.4	60.6	7.6	27.5	7.3	1.7	5.5	3.8	3.2	3.8	5.1	0.4	8.2	1.5
3605	11/07	86.4	348.9	30.7	273.3	13.2	678.8	33.2	70.0	8.3	36.0	6.6	2.0	10.4	4.8	5.4	3.1	6.7	0.9	9.3	1.6
3605	11/07	88.2	373.8	35.5	263.4	12.2	642.7	32.6	67.4	8.5	32.8	7.5	2.0	7.3	7.1	2.9	4.6	6.8	0.2	10.1	1.8
3605	11/07	103.0	415.5	26.9	271.5	13.3	627.0	37.1	67.7	8.1	34.1	2.3	1.7	7.2	5.2	2.2	2.3	5.0	0.6	9.1	1.6
3605	11/07	167.4	134.5	22.6	131.9	11.6	608.3	30.2	60.9	6.6	24.8	4.3	1.0	5.5	4.1	2.3	2.3	4.4	0.7	16.5	2.8
3605	11/07	114.6	261.9	30.8	304.6	13.7	765.6	33.3	73.2	8.5	36.5	7.5	1.7	8.0	7.5	2.6	3.6	7.7	0.8	11.3	2.4
3605	11/07	109.9	279.9	34.2	298.8	13.8	707.8	34.3	75.5	8.6	34.9	6.1	2.0	8.5	6.2	2.1	3.2	7.8	0.9	11.4	1.9
3605	11/07	120.1	277.4	36.1	330.3	16.0	770.5	36.3	78.3	9.0	37.7	9.4	1.5	7.5	6.1	3.9	4.2	9.0	1.0	12.5	2.4

Table C4.
Trace element glass compositions of BHVO-2G, LIP3 and the MPI-DING reference glass (StHs6/80-G, GOR132-G and ATHO-G)

	BHVO-2G_1	BHVO-2G_2	BHVO-2G_3	BHVO-2G_4	BHVO-2G_5	BHVO-2G_6	BHVO-2G_7	BHVO-2G_8	BHVO-2G_9	BHVO-2G_10	BHVO-2G_1	BHVO-2G_2	BHVO-2G_3	BHVO-2G_4
(%)	10/07/2018	10/07/2018	10/07/2018	10/07/2018	10/07/2018	10/07/2018	10/07/2018	10/07/2018	10/07/2018	10/07/2018	11/07/2018	11/07/2018	11/07/2018	11/07/2018
SiO_2	48.75	49.15	48.51	48.09	47.76	49.06	49.19	49.25	49.46	49.95	49.62	48.67	49.21	48.97
TiO_2	2.83	2.88	2.89	2.93	2.93	2.96	2.88	2.76	2.90	2.85	2.80	3.04	2.91	3.00
Al_2O_3	13.98	13.76	13.75	14.13	13.95	14.32	13.92	13.68	13.84	13.87	14.45	14.05	14.28	14.09
FeO	11.10	11.19	11.20	11.12	11.40	11.04	11.42	11.16	10.73	10.93	10.75	11.52	11.26	11.51
MnO	0.17	0.17	0.17	0.17	0.17	0.18	0.18	0.17	0.17	0.18	0.18	0.18	0.17	0.18
MgO	7.76	7.67	7.73	7.77	7.80	7.38	7.40	7.45	7.58	7.49	7.65	7.70	7.44	7.60
CaO	12.00	11.77	12.34	12.38	12.52	12.19	12.10	12.60	12.44	11.82	11.48	11.79	11.69	11.56
Na_2O	2.44	2.45	2.44	2.44	2.48	2.29	2.32	2.34	2.30	2.34	2.44	2.40	2.40	2.44
K_2O	0.43	0.42	0.44	0.45	0.43	0.43	0.44	0.44	0.44	0.43	0.44	0.45	0.46	0.44
P_2O_5	0.54	0.52	0.52	0.52	0.55	0.16	0.16	0.14	0.15	0.14	0.19	0.19	0.18	0.20
Total	100.00	100.00	100.00	100.00	100.00	100.00	100.00	100.00	100.00	100.00	100.00	100.00	100.00	100.00
CF	**1.27**	**1.29**	**1.30**	**1.33**	**1.36**	**1.58**	**1.56**	**1.55**	**1.54**	**1.51**	**1.51**	**1.56**	**1.58**	**1.62**
(ppm)														
Sc	32.54	34.03	35.43	34.15	35.99	32.18	34.43	33.34	33.78	33.51	32.52	37.65	35.16	36.72
V	308.22	316.75	312.17	312.12	311.86	304.92	302.98	296.53	307.48	305.57	301.62	321.93	300.10	320.01
Cr	276.71	266.06	288.94	295.67	289.80	275.24	266.79	286.28	288.51	285.58	277.70	296.47	270.33	304.62
Co	44.72	44.12	44.57	44.47	43.69	45.66	43.93	44.12	45.25	41.07	42.53	44.06	43.22	44.70
Ni	105.58	108.11	104.87	110.17	113.45	106.99	98.30	113.47	94.27	100.47	100.58	93.75	99.59	120.95
Cu	113.87	112.84	107.19	116.32	116.26	118.77	113.73	111.81	112.02	113.12	112.98	105.46	112.35	118.30
Zn	105.76	105.30	96.65	98.76	103.16	103.93	100.90	102.74	101.86	102.15	104.07	98.24	98.31	101.32
Ga	20.08	20.63	20.49	21.61	21.37	21.90	20.17	18.27	18.25	18.94	20.45	19.62	20.48	22.49
Rb	8.62	9.12	8.27	10.25	9.90	8.26	8.80	8.59	8.60	8.45	8.55	8.55	8.67	8.83
Sr	355.00	369.34	362.38	390.18	402.63	375.81	367.81	350.28	372.39	350.79	373.66	380.43	386.45	373.41
Y	23.41	24.35	23.04	25.32	27.64	26.68	23.59	23.69	27.77	26.13	25.25	24.52	26.13	26.81
Zr	160.04	169.28	158.80	177.13	177.42	174.70	167.71	160.80	168.08	164.90	163.35	167.43	168.67	168.85
Nb	17.11	18.11	19.23	19.46	18.78	18.40	18.55	18.53	18.57	17.46	17.68	17.96	17.80	18.74
Ba	129.26	129.06	130.05	129.74	141.02	129.16	131.47	121.97	122.90	125.41	126.12	129.69	129.03	136.43
La	14.47	14.34	15.11	15.37	14.72	14.97	14.03	13.59	14.87	14.10	14.44	15.44	15.74	14.82
Ce	36.34	35.68	38.07	38.79	39.08	36.83	35.73	34.76	36.16	34.87	35.06	35.48	38.33	39.25
Pr	4.60	5.16	5.33	5.55	4.98	5.87	4.70	5.03	5.03	4.45	5.33	5.24	5.40	5.20
Nd	24.72	24.85	23.20	26.96	25.88	25.28	23.03	21.72	22.65	22.54	23.61	23.95	25.15	24.80
Sm	6.66	7.13	6.47	6.91	6.25	6.94	7.24	5.90	7.68	6.06	6.98	5.51	6.64	6.81
Eu	2.17	2.07	2.27	2.25	2.28	2.16	1.86	1.71	2.11	1.83	2.30	2.04	2.14	2.26
Gd	7.62	6.04	6.42	7.56	5.69	3.23	6.20	7.04	4.32	5.59	6.15	5.60	4.59	6.15
Tb	0.97	0.91	0.86	0.78	1.07	0.93	0.65	0.84	1.07	0.95	0.86	0.82	1.08	0.94
Dy	5.31	6.20	4.79	6.07	4.97	5.76	4.50	5.24	4.47	4.71	5.13	5.22	4.56	5.49
Ho	1.15	0.76	1.06	1.12	1.15	0.99	0.93	0.80	0.99	1.06	0.80	0.92	1.09	1.05
Er	2.81	2.69	2.61	2.74	2.43	3.15	2.39	1.95	2.09	2.94	2.42	2.35	2.02	2.29
Tm	0.42	0.32	0.33	0.41	0.40	0.39	0.31	0.34	0.30	0.31	0.40	0.29	0.43	0.41
Yb	1.90	2.15	1.62	1.80	2.04	2.05	1.51	1.53	2.34	1.53	1.82	2.15	1.84	1.73
Lu	0.29	0.26	0.21	0.24	0.47	0.36	0.13	0.25	0.25	0.30	0.23	0.29	0.33	0.25
Hf	4.50	4.06	4.60	4.53	4.43	5.08	4.52	4.14	3.61	5.24	4.96	4.13	4.66	3.89
Ta	1.10	1.43	1.25	1.21	1.19	0.91	0.95	1.29	0.85	1.02	1.00	0.92	1.21	1.10
Pb	1.99	1.98	1.52	1.79	1.40	1.99	1.34	1.37	1.77	1.74	1.67	1.72	1.39	1.11
Th	1.15	1.04	1.27	0.98	1.39	1.08	0.97	1.13	1.55	1.30	1.27	1.19	1.09	1.22
U	0.42	0.36	0.44	0.35	0.57	0.35	0.31	0.39	0.26	0.34	0.41	0.38	0.35	0.43

	BHVO-2G_5	BHVO-2G_6	BHVO-2G_7	BHVO-2G_8	BHVO-2G_9	BHVO-2G_10	BHVO-2G_1	BHVO-2G_2	BHVO-2G_3	BHVO-2G_4	BHVO-2G_5	BHVO-2G_6	BHVO-2G_7	BHVO-2G_8
(%)	11/07/2018	11/07/2018	11/07/2018	11/07/2018	11/07/2018	11/07/2018	12/07/2018	12/07/2018	12/07/2018	12/07/2018	12/07/2018	12/07/2018	12/07/2018	12/07/2018
SiO_2	48.41	49.39	49.41	48.83	48.41	49.87	48.75	49.15	48.51	48.09	47.76	49.06	49.19	49.25
TiO_2	2.93	2.88	2.87	2.90	2.84	2.80	2.83	2.88	2.89	2.93	2.93	2.96	2.88	2.76
Al_2O_3	14.33	14.02	14.04	13.87	14.20	13.58	13.98	13.76	13.75	14.13	13.95	14.32	13.92	13.68
FeO	11.78	11.17	11.19	11.44	11.78	11.14	11.10	11.19	11.20	11.12	11.40	11.04	11.42	11.16
MnO	0.18	0.17	0.18	0.18	0.18	0.17	0.17	0.17	0.17	0.17	0.17	0.18	0.18	0.17
MgO	7.52	7.39	7.45	7.43	7.60	7.25	7.76	7.67	7.73	7.77	7.80	7.38	7.40	7.45
CaO	11.84	11.96	11.86	12.29	11.95	12.14	12.00	11.77	12.34	12.38	12.52	12.19	12.10	12.60
Na_2O	2.36	2.34	2.32	2.38	2.39	2.38	2.44	2.45	2.44	2.44	2.48	2.29	2.32	2.34
K_2O	0.47	0.44	0.46	0.44	0.44	0.44	0.43	0.42	0.44	0.45	0.43	0.43	0.44	0.44
P_2O_5	0.19	0.24	0.22	0.23	0.22	0.22	0.54	0.52	0.52	0.52	0.55	0.16	0.16	0.14
Total	100.00	100.00	100.00	100.00	100.00	100.00	100.00	100.00	100.00	100.00	100.00	100.00	100.00	100.00
CF	**1.61**	**1.55**	**1.53**	**1.49**	**1.54**	**1.51**	**1.27**	**1.29**	**1.30**	**1.33**	**1.36**	**1.58**	**1.56**	**1.55**
(ppm)														
Sc	35.05	35.60	35.85	33.95	35.34	35.45	32.54	34.03	35.43	34.15	35.99	32.18	34.43	33.34
V	311.18	296.31	308.46	310.71	298.15	299.93	308.22	316.75	312.17	312.12	311.86	304.92	302.98	296.53
Cr	299.46	287.67	295.74	285.84	283.87	289.46	276.71	266.06	288.94	295.67	289.80	275.24	266.79	286.28
Co	46.13	45.42	44.69	45.11	45.50	43.86	44.72	44.12	44.57	44.47	43.69	45.66	43.93	44.12
Ni	95.86	107.52	95.40	103.45	107.01	99.64	105.58	108.11	104.87	110.17	113.45	106.99	98.30	113.47
Cu	111.97	105.70	113.15	110.70	108.16	108.19	113.87	112.84	107.19	116.32	116.26	118.77	113.73	111.81
Zn	108.52	97.90	106.04	103.51	98.39	94.24	105.76	105.30	96.65	98.76	103.16	103.93	100.90	102.74
Ga	21.11	20.78	20.15	20.80	21.59	19.61	20.08	20.63	20.49	21.61	21.37	21.90	20.17	18.27
Rb	10.31	8.84	9.70	8.83	8.39	8.52	8.62	9.12	8.27	10.25	9.90	8.26	8.80	8.59
Sr	386.67	364.00	387.29	379.42	375.73	360.39	355.00	369.34	362.38	390.18	402.63	375.81	367.81	350.28
Y	25.09	24.95	26.38	25.32	24.97	24.31	23.41	24.35	23.04	25.32	27.64	26.68	23.59	23.69
Zr	177.28	163.43	171.10	167.26	168.29	162.81	160.04	169.28	158.80	177.13	177.42	174.70	167.71	160.80
Nb	19.16	17.29	17.32	17.97	17.87	18.80	17.11	18.11	19.23	19.46	18.78	18.40	18.55	18.53
Ba	127.83	124.56	125.82	123.80	127.08	123.45	129.26	129.06	130.05	129.74	141.02	129.16	131.47	121.97
La	15.84	14.52	15.24	14.27	14.47	14.33	14.47	14.34	15.11	15.37	14.72	14.97	14.03	13.59
Ce	38.19	35.37	37.13	36.92	34.73	36.04	36.34	35.68	38.07	38.79	39.08	36.83	35.73	34.76
Pr	5.26	5.35	5.15	4.74	4.93	4.69	4.60	5.16	5.33	5.55	4.98	5.87	4.70	5.03
Nd	24.54	22.93	24.58	23.08	23.01	23.96	24.72	24.85	23.20	26.96	25.88	25.28	23.03	21.72
Sm	4.91	6.05	6.32	5.65	6.83	5.58	6.66	7.13	6.47	6.91	6.25	6.94	7.24	5.90
Eu	1.95	2.18	2.07	1.87	2.26	1.65	2.17	2.07	2.27	2.25	2.28	2.16	1.86	1.71
Gd	5.51	5.98	4.27	7.03	5.77	6.85	7.62	6.04	6.42	7.56	5.69	3.23	6.20	7.04
Tb	1.09	0.73	0.83	0.72	0.91	1.00	0.97	0.91	0.86	0.78	1.07	0.93	0.65	0.84
Dy	5.09	4.79	4.17	4.96	5.64	4.21	5.31	6.20	4.79	6.07	4.97	5.76	4.50	5.24
Ho	1.00	0.91	0.95	1.00	1.03	1.16	1.15	0.76	1.06	1.12	1.15	0.99	0.93	0.80
Er	2.99	2.06	2.37	2.04	2.67	2.39	2.81	2.69	2.61	2.74	2.43	3.15	2.39	1.95
Tm	0.33	0.19	0.28	0.31	0.26	0.30	0.42	0.32	0.33	0.41	0.40	0.39	0.31	0.34
Yb	2.55	1.46	2.01	2.60	1.83	2.28	1.90	2.15	1.62	1.80	2.04	2.05	1.51	1.53
Lu	0.29	0.37	0.33	0.21	0.30	0.19	0.29	0.26	0.21	0.24	0.47	0.36	0.13	0.25
Hf	4.40	3.71	4.75	4.78	4.78	3.64	4.50	4.06	4.60	4.53	4.43	5.08	4.52	4.14
Ta	1.21	1.34	1.17	0.92	1.07	1.06	1.10	1.43	1.25	1.21	1.19	0.91	0.95	1.29
Pb	1.53	1.56	1.81	2.57	1.86	1.86	1.99	1.98	1.52	1.79	1.40	1.99	1.34	1.37
Th	1.19	1.51	1.31	1.21	1.30	1.22	1.15	1.04	1.27	0.98	1.39	1.08	0.97	1.13
U	0.38	0.46	0.52	0.46	0.39	0.36	0.42	0.36	0.44	0.35	0.57	0.35	0.31	0.39

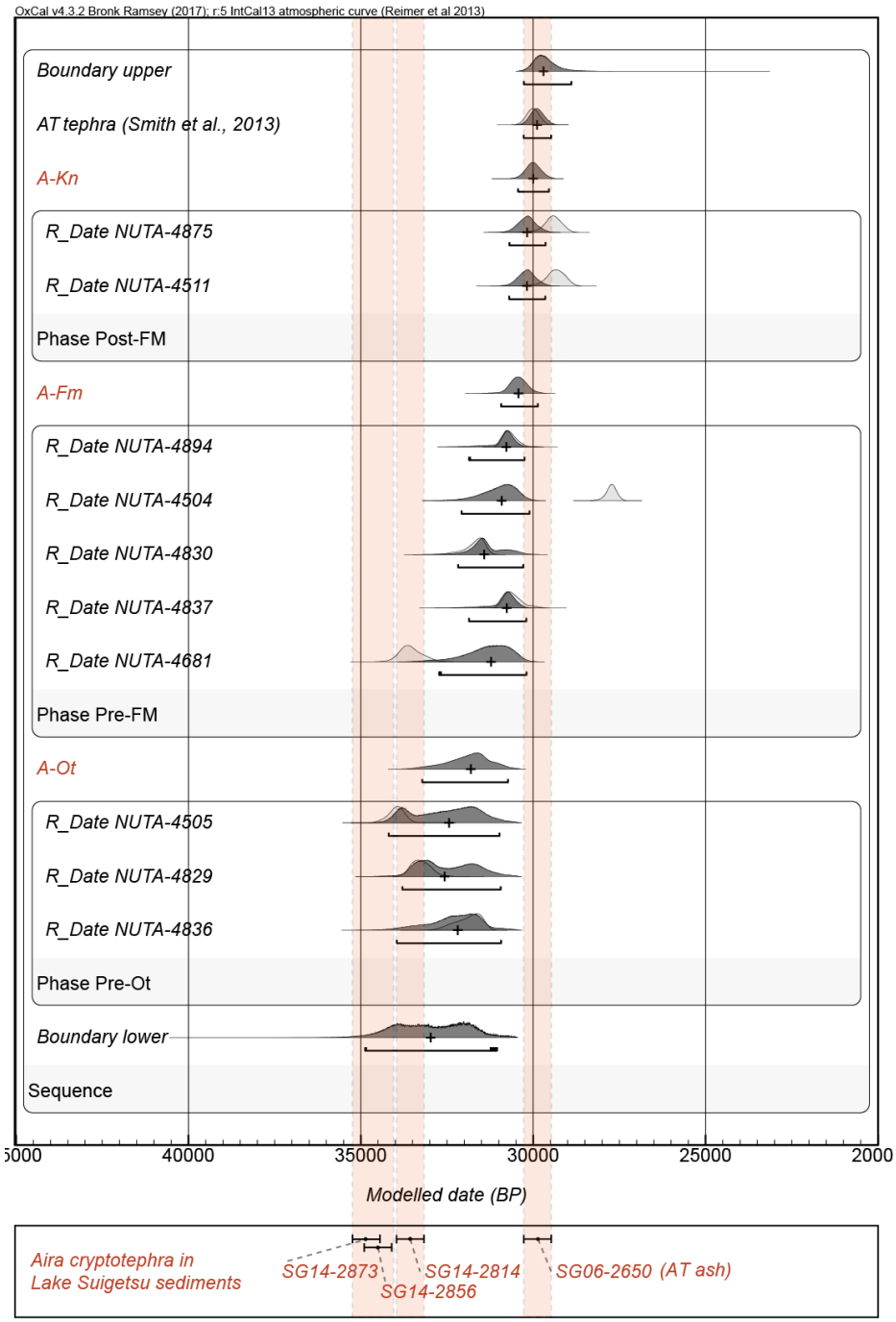
	BHVO-2G_9	BHVO-2G_10	**BHVO-2G**		LIP3_1	LIP3_2	LIP3_3	LIP3_4	LIP3_5	LIP3_1	LIP3_2	LIP3_3	LIP3_4	LIP3_5
(%)	12/07/2018	12/07/2018	**Average**	**SD**	10/07/2018	10/07/2018	10/07/2018	10/07/2018	10/07/2018	11/07/2018	11/07/2018	11/07/2018	11/07/2018	11/07/2018
SiO_2	49.46	49.95	**48.97**	**0.59**	74.00	74.38	74.03	74.02	74.10	74.48	74.53	74.97	74.54	74.15
TiO_2	2.90	2.85	**2.89**	**0.06**	0.08	0.09	0.08	0.09	0.08	0.08	0.08	0.08	0.08	0.08
Al_2O_3	13.84	13.87	**13.98**	**0.22**	13.86	13.42	13.85	13.90	13.72	13.44	13.21	13.52	13.63	13.60
FeO	10.73	10.93	**11.20**	**0.26**	1.60	1.55	1.54	1.57	1.70	1.57	1.67	1.51	1.53	1.54
MnO	0.17	0.18	**0.17**	**0.00**	0.06	0.07	0.06	0.06	0.07	0.07	0.07	0.06	0.06	0.06
MgO	7.58	7.49	**7.57**	**0.16**	0.04	0.04	0.04	0.04	0.04	0.04	0.04	0.04	0.04	0.04
CaO	12.44	11.82	**12.10**	**0.32**	0.76	0.96	0.68	0.69	0.74	0.80	0.89	0.35	0.80	0.85
Na_2O	2.30	2.34	**2.38**	**0.06**	4.15	4.13	4.45	4.29	4.25	4.32	4.23	4.14	4.19	4.29
K_2O	0.44	0.43	**0.44**	**0.01**	5.38	5.27	5.24	5.32	5.24	5.19	5.27	5.32	5.12	5.37
P_2O_5	0.15	0.14	**0.30**	**0.17**	0.07	0.10	0.02	0.02	0.06	0.02	0.01	0.01	0.01	0.01
Total	100.00	100.00			100.00	100.00	100.00	100.00	100.00	100.00	100.00	100.00	100.00	100.00
CF	**1.54**	**1.51**			**1.47**	**1.59**	**1.66**	**1.60**	**1.60**	**1.46**	**1.45**	**1.48**	**1.43**	**1.44**
(ppm)														
Sc	33.78	33.51	**34.40**	**1.38**	4.61	2.05	1.16	2.88	2.14	-0.03	1.35	1.75	1.23	1.34
V	307.48	305.57	**307.52**	**6.82**	1.38	1.26	0.40	0.01	0.05	0.22	0.47	-0.23	0.69	0.66
Cr	288.51	285.58	**284.34**	**10.45**	4.77	5.42	-18.97	-21.77	-4.88	12.47	15.46	-11.89	-10.91	7.45
Co	45.25	41.07	**44.28**	**1.17**	0.85	0.56	-1.06	1.57	0.82	0.11	-0.01	-0.03	-0.53	-0.48
Ni	94.27	100.47	**104.50**	**6.87**	-5.43	-24.23	-9.09	-11.00	1.06	6.52	-6.86	1.98	-2.86	-8.03
Cu	112.02	113.12	**112.63**	**3.58**	6.27	4.80	4.83	5.81	4.74	5.22	4.87	3.80	7.07	4.92
Zn	101.86	102.15	**101.77**	**3.34**	51.32	52.71	58.61	52.54	55.68	53.37	53.52	49.13	51.42	51.32
Ga	18.25	18.94	**20.35**	**1.17**	20.74	21.43	22.40	20.45	21.33	21.27	20.92	21.51	19.69	21.34
Rb	8.60	8.45	**8.90**	**0.63**	327.71	322.59	334.65	332.37	325.65	309.61	317.27	316.36	305.72	316.15
Sr	372.39	350.79	**372.02**	**14.65**	13.70	16.05	13.81	14.12	15.27	13.68	13.42	13.89	12.92	13.53
Y	27.77	26.13	**25.23**	**1.49**	42.11	46.03	43.24	43.43	46.70	43.35	43.80	42.13	40.21	45.07
Zr	168.08	164.90	**167.87**	**5.94**	188.75	194.42	200.26	187.95	203.33	184.90	192.26	186.62	181.89	190.45
Nb	18.57	17.46	**18.30**	**0.69**	38.35	41.45	42.06	38.04	40.78	38.04	39.95	37.83	39.14	38.64
Ba	122.90	125.41	**128.46**	**4.74**	18.35	19.00	17.22	15.78	18.92	16.42	16.90	15.74	15.84	15.67
La	14.87	14.10	**14.67**	**0.58**	63.40	65.20	68.64	64.93	62.59	59.79	62.97	62.54	60.11	59.74
Ce	36.16	34.87	**36.64**	**1.49**	125.90	127.96	131.78	124.28	128.10	120.21	122.42	121.26	120.65	120.70
Pr	5.03	4.45	**5.09**	**0.37**	13.20	13.13	14.40	12.27	13.00	12.54	11.72	12.66	11.80	12.30
Nd	22.65	22.54	**24.04**	**1.41**	39.68	44.09	45.41	46.05	44.37	42.01	42.25	41.82	41.67	39.85
Sm	7.68	6.06	**6.53**	**0.66**	7.97	8.54	8.98	9.03	7.88	6.98	8.79	7.54	8.10	9.45
Eu	2.11	1.83	**2.07**	**0.20**	0.28	0.08	0.22	0.26	0.12	-0.03	0.10	0.21	0.26	0.02
Gd	4.32	5.59	**5.91**	**1.19**	9.07	7.70	7.23	8.57	6.06	6.70	5.71	6.62	6.79	7.13
Tb	1.07	0.95	**0.90**	**0.12**	1.15	1.12	1.29	0.99	1.22	1.05	0.88	1.04	1.12	0.91
Dy	4.47	4.71	**5.11**	**0.58**	6.16	6.97	7.14	6.96	7.79	6.39	6.43	6.66	6.23	7.20
Ho	0.99	1.06	**1.00**	**0.12**	1.47	1.44	1.60	1.45	1.35	1.50	1.64	1.25	1.25	1.46
Er	2.09	2.94	**2.51**	**0.35**	3.59	4.17	5.89	3.84	4.77	3.54	4.06	3.77	4.08	3.88
Tm	0.30	0.31	**0.34**	**0.06**	0.92	0.67	0.61	0.79	0.89	0.68	0.75	0.78	0.67	0.67
Yb	2.34	1.53	**1.91**	**0.32**	4.38	4.68	4.57	5.75	5.28	4.61	4.94	4.66	4.36	4.87
Lu	0.25	0.30	**0.28**	**0.08**	0.70	0.66	0.91	0.66	0.63	0.75	0.84	0.73	0.65	0.83
Hf	3.61	5.24	**4.44**	**0.46**	6.65	6.34	7.59	5.83	7.34	5.82	7.16	6.61	7.13	6.83
Ta	0.85	1.02	**1.11**	**0.17**	2.51	2.66	3.40	2.99	3.05	2.67	2.67	2.69	2.58	2.75
Pb	1.77	1.74	**1.69**	**0.30**	34.63	34.14	37.88	35.27	35.61	33.13	33.06	32.27	30.73	31.88
Th	1.55	1.30	**1.21**	**0.16**	55.16	52.62	55.48	52.25	51.66	52.71	52.87	52.85	51.15	52.80
U	0.26	0.34	**0.39**	**0.08**	16.00	16.31	16.81	16.21	16.11	15.15	15.76	15.64	15.56	16.34

	LIP3_1	LIP3_2	LIP3_3	LIP3_4	LIP3_5	**LIP3**		ATHO_G_1	ATHO_G_2	ATHO_G_3	ATHO_G_4	ATHO_G_5	ATHO_G_1	ATHO_G_2
(%)	12/07/2018	12/07/2018	12/07/2018	12/07/2018	12/07/2018	**Average**	**SD**	10/07/2018	10/07/2018	10/07/2018	10/07/2018	10/07/2018	11/07/2018	11/07/2018
SiO_2	74.00	74.38	74.03	74.02	74.10	**74.25**	**0.29**	74.02	74.34	75.24	74.92	75.11	74.15	74.17
TiO_2	0.08	0.09	0.08	0.09	0.08	**0.08**	**0.00**	0.28	0.27	0.26	0.26	0.26	0.27	0.25
Al_2O_3	13.86	13.42	13.85	13.90	13.72	**13.66**	**0.22**	12.78	12.49	11.82	12.14	12.06	12.56	12.80
FeO	1.60	1.55	1.54	1.57	1.70	**1.58**	**0.06**	3.54	3.43	3.33	3.19	3.23	3.34	3.47
MnO	0.06	0.07	0.06	0.06	0.07	**0.06**	**0.00**	0.11	0.11	0.10	0.10	0.10	0.11	0.10
MgO	0.04	0.04	0.04	0.04	0.04	**0.04**	**0.00**	0.10	0.10	0.10	0.10	0.10	0.10	0.10
CaO	0.76	0.96	0.68	0.69	0.74	**0.76**	**0.15**	1.66	1.67	1.75	1.73	1.59	1.85	1.61
Na_2O	4.15	4.13	4.45	4.29	4.25	**4.24**	**0.11**	4.76	4.87	4.71	4.81	4.81	4.93	4.75
K_2O	5.38	5.27	5.24	5.32	5.24	**5.28**	**0.07**	2.74	2.70	2.66	2.70	2.69	2.67	2.71
P_2O_5	0.07	0.10	0.02	0.02	0.06	**0.04**	**0.03**	0.02	0.02	0.02	0.05	0.05	0.02	0.04
Total	100.00	100.00	100.00	100.00	100.00	**100.00**	**0.00**	100.00	100.00	100.00	100.00	100.00	100.00	100.00
CF	**1.47**	**1.59**	**1.66**	**1.60**	**1.60**	**1.54**	**0.08**	**2.19**	**1.98**	**1.99**	**1.98**	**2.03**	**2.11**	**2.13**
(ppm)														
Sc	4.61	2.05	1.16	2.88	2.14	**2.09**	**1.26**	6.07	6.44	10.25	6.39	5.69	8.86	6.44
V	1.38	1.26	0.40	0.01	0.05	**0.53**	**0.55**	3.88	5.65	4.81	3.11	4.32	2.87	4.84
Cr	4.77	5.42	-18.97	-21.77	-4.88	**-3.89**	**12.83**	23.45	1.47	24.37	-21.92	-16.44	-0.84	-1.37
Co	0.85	0.56	-1.06	1.57	0.82	**0.30**	**0.83**	-0.25	0.92	2.01	0.74	1.42	0.42	2.90
Ni	-5.43	-24.23	-9.09	-11.00	1.06	**-7.11**	**8.66**	1.66	26.17	14.72	-6.58	7.46	-8.26	-13.06
Cu	6.27	4.80	4.83	5.81	4.74	**5.25**	**0.83**	21.96	19.17	19.94	17.51	18.10	17.82	19.63
Zn	51.32	52.71	58.61	52.54	55.68	**53.36**	**2.70**	125.69	126.34	118.22	124.99	113.04	117.93	114.80
Ga	20.74	21.43	22.40	20.45	21.33	**21.16**	**0.71**	27.07	25.27	25.75	24.13	24.29	26.27	26.68
Rb	327.71	322.59	334.65	332.37	325.65	**323.40**	**8.89**	69.42	72.72	67.01	65.25	69.03	65.37	69.08
Sr	13.70	16.05	13.81	14.12	15.27	**14.22**	**0.96**	89.30	93.81	93.57	84.22	93.29	88.91	94.15
Y	42.11	46.03	43.24	43.43	46.70	**43.84**	**1.90**	104.72	107.02	103.63	96.00	106.13	99.34	105.93
Zr	188.75	194.42	200.26	187.95	203.33	**192.37**	**6.77**	528.23	554.34	518.20	514.93	523.62	530.12	534.86
Nb	38.35	41.45	42.06	38.04	40.78	**39.66**	**1.61**	63.48	65.74	61.68	57.93	57.27	63.94	61.37
Ba	18.35	19.00	17.22	15.78	18.92	**17.27**	**1.36**	537.39	563.43	521.81	506.65	522.25	551.11	541.09
La	63.40	65.20	68.64	64.93	62.59	**63.65**	**2.74**	54.80	55.65	53.24	52.05	52.61	53.58	53.23
Ce	125.90	127.96	131.78	124.28	128.10	**125.42**	**3.87**	125.78	127.88	123.79	112.14	120.80	125.85	121.44
Pr	13.20	13.13	14.40	12.27	13.00	**12.87**	**0.79**	14.26	14.83	13.60	14.21	14.66	14.32	15.20
Nd	39.68	44.09	45.41	46.05	44.37	**43.12**	**2.28**	58.90	63.52	54.20	56.29	59.97	60.03	56.05
Sm	7.97	8.54	8.98	9.03	7.88	**8.38**	**0.68**	14.78	15.66	16.20	14.75	12.18	15.60	11.99
Eu	0.28	0.08	0.22	0.26	0.12	**0.17**	**0.10**	2.79	2.68	2.26	2.45	2.62	2.17	2.27
Gd	9.07	7.70	7.23	8.57	6.06	**7.35**	**1.08**	17.17	16.85	13.05	17.66	17.24	16.65	13.54
Tb	1.15	1.12	1.29	0.99	1.22	**1.10**	**0.13**	3.12	2.49	3.03	2.45	2.48	2.62	2.45
Dy	6.16	6.97	7.14	6.96	7.79	**6.86**	**0.53**	16.86	17.18	16.24	15.71	14.89	16.55	15.06
Ho	1.47	1.44	1.60	1.45	1.35	**1.45**	**0.11**	4.09	3.86	3.52	2.96	3.11	3.68	3.30
Er	3.59	4.17	5.89	3.84	4.77	**4.26**	**0.76**	11.88	12.60	11.35	10.24	11.03	11.00	10.53
Tm	0.92	0.67	0.61	0.79	0.89	**0.75**	**0.11**	1.57	1.66	1.48	1.51	1.22	2.05	1.40
Yb	4.38	4.68	4.57	5.75	5.28	**4.85**	**0.46**	11.57	9.89	9.69	9.68	10.56	10.24	10.78
Lu	0.70	0.66	0.91	0.66	0.63	**0.73**	**0.10**	1.70	1.56	1.59	1.41	1.72	1.63	1.67
Hf	6.65	6.34	7.59	5.83	7.34	**6.74**	**0.62**	13.86	14.21	14.20	14.39	14.40	13.72	13.19
Ta	2.51	2.66	3.40	2.99	3.05	**2.84**	**0.29**	4.34	4.26	3.63	3.64	3.62	3.60	4.29
Pb	34.63	34.14	37.88	35.27	35.61	**34.41**	**2.01**	5.34	5.07	4.77	4.76	3.99	4.38	5.03
Th	55.16	52.62	55.48	52.25	51.66	**53.11**	**1.46**	7.91	8.21	6.13	6.84	6.88	7.51	7.46
U	16.00	16.31	16.81	16.21	16.11	**16.09**	**0.44**	2.62	2.49	1.90	1.74	2.28	2.62	2.56

	ATHO_G_3	ATHO_G_4	ATHO_G_5	ATHO_G_1	ATHO_G_2	ATHO_G_3	ATHO_G_4	ATHO_G_5	**ATHO_G_5**		StHs6_1	StHs6_2	StHs6_3	StHs6_4
(%)	11/07/2018	11/07/2018	11/07/2018	12/07/2018	12/07/2018	12/07/2018	12/07/2018	12/07/2018	**Average**	**SD**	10/07/2018	10/07/2018	10/07/2018	10/07/2018
SiO_2	74.86	73.90	73.63	74.02	74.34	75.24	74.92	75.11	**74.53**	**0.55**	64.07	64.41	63.21	63.83
TiO_2	0.26	0.27	0.27	0.28	0.27	0.26	0.26	0.26	**0.27**	**0.01**	0.68	0.69	0.67	0.69
Al_2O_3	12.24	13.03	12.84	12.78	12.49	11.82	12.14	12.06	**12.40**	**0.39**	17.73	17.24	18.12	17.37
FeO	3.30	3.37	3.40	3.54	3.43	3.33	3.19	3.23	**3.35**	**0.11**	4.12	4.14	4.24	4.20
MnO	0.11	0.10	0.11	0.11	0.11	0.10	0.10	0.10	**0.10**	**0.00**	0.07	0.07	0.07	0.07
MgO	0.10	0.10	0.10	0.10	0.10	0.10	0.10	0.10	**0.10**	**0.00**	1.89	1.91	2.00	1.98
CaO	1.71	1.73	1.94	1.66	1.67	1.75	1.73	1.59	**1.71**	**0.10**	4.99	5.29	5.35	5.25
Na_2O	4.78	4.76	4.93	4.76	4.87	4.71	4.81	4.81	**4.81**	**0.07**	5.21	5.01	5.07	5.35
K_2O	2.59	2.70	2.74	2.74	2.70	2.66	2.70	2.69	**2.69**	**0.04**	1.12	1.13	1.15	1.15
P_2O_5	0.05	0.03	0.03	0.02	0.02	0.02	0.05	0.05	**0.03**	**0.01**	0.12	0.10	0.12	0.11
Total	100.00	100.00	100.00	100.00	100.00	100.00	100.00	100.00	**100.00**	**0.00**	100.00	100.00	100.00	100.00
CF	**1.96**	**2.04**	**1.98**	**2.19**	**1.98**	**1.99**	**1.98**	**2.03**	**2.04**	**0.08**	**3.46**	**3.32**	**3.35**	**3.25**
(ppm)														
Sc	7.44	7.90	9.34	6.07	6.44	10.25	6.39	5.69	**7.31**	**1.61**	6.99	9.31	15.97	12.79
V	2.05	2.24	3.92	3.88	5.65	4.81	3.11	4.32	**3.96**	**1.12**	77.38	76.19	77.23	78.91
Cr	29.01	13.20	4.16	23.45	1.47	24.37	-21.92	-16.44	**4.40**	**18.00**	39.46	35.09	52.56	9.18
Co	2.83	-0.31	0.90	-0.25	0.92	2.01	0.74	1.42	**1.09**	**1.02**	9.81	13.59	12.48	14.31
Ni	-7.58	-32.15	-1.94	1.66	26.17	14.72	-6.58	7.46	**1.59**	**15.36**	4.59	34.68	1.65	7.50
Cu	17.18	19.03	18.40	21.96	19.17	19.94	17.51	18.10	**19.03**	**1.48**	34.01	37.18	37.76	37.79
Zn	103.30	108.35	119.48	125.69	126.34	118.22	124.99	113.04	**118.69**	**7.17**	48.27	55.33	56.15	58.89
Ga	25.09	25.57	25.77	27.07	25.27	25.75	24.13	24.29	**25.49**	**1.00**	19.11	19.18	22.39	20.46
Rb	63.96	64.10	67.55	69.42	72.72	67.01	65.25	69.03	**67.79**	**2.77**	27.07	26.10	31.35	26.97
Sr	90.44	91.36	86.96	89.30	93.81	93.57	84.22	93.29	**90.68**	**3.45**	453.17	436.61	456.28	430.82
Y	101.03	101.07	105.74	104.72	107.02	103.63	96.00	106.13	**103.21**	**3.71**	12.85	9.05	11.62	12.40
Zr	510.64	541.07	533.82	528.23	554.34	518.20	514.93	523.62	**528.61**	**13.39**	121.45	116.24	124.86	119.14
Nb	58.83	61.70	62.56	63.48	65.74	61.68	57.93	57.27	**61.37**	**2.92**	6.59	6.33	6.35	6.45
Ba	525.83	518.98	563.64	537.39	563.43	521.81	506.65	522.25	**533.58**	**19.52**	268.05	264.00	274.10	273.93
La	51.33	54.54	57.69	54.80	55.65	53.24	52.05	52.61	**53.80**	**1.70**	11.35	12.07	10.65	10.43
Ce	114.11	120.57	121.33	125.78	127.88	123.79	112.14	120.80	**121.61**	**5.20**	23.93	22.50	24.14	24.62
Pr	13.71	14.10	13.97	14.26	14.83	13.60	14.21	14.66	**14.29**	**0.47**	2.96	2.46	2.96	2.89
Nd	58.01	55.93	57.04	58.90	63.52	54.20	56.29	59.97	**58.19**	**2.90**	10.37	12.43	13.80	10.96
Sm	12.35	13.42	14.68	14.78	15.66	16.20	14.75	12.18	**14.34**	**1.52**	2.42	5.62	3.20	2.14
Eu	2.80	1.97	2.75	2.79	2.68	2.26	2.45	2.62	**2.50**	**0.27**	1.68	0.37	0.43	0.81
Gd	17.78	17.09	14.03	17.17	16.85	13.05	17.66	17.24	**16.20**	**1.78**	2.12	6.78	0.28	6.78
Tb	2.07	2.52	2.68	3.12	2.49	3.03	2.45	2.48	**2.63**	**0.31**	0.27	0.49	0.59	0.51
Dy	14.89	16.80	16.31	16.86	17.18	16.24	15.71	14.89	**16.09**	**0.85**	1.84	2.76	2.76	3.70
Ho	3.19	3.37	3.94	4.09	3.86	3.52	2.96	3.11	**3.50**	**0.40**	0.45	0.27	0.06	0.46
Er	10.67	10.98	9.75	11.88	12.60	11.35	10.24	11.03	**11.14**	**0.83**	1.49	1.18	2.49	1.29
Tm	1.31	1.74	1.67	1.57	1.66	1.48	1.51	1.22	**1.54**	**0.21**	-0.02	0.39	0.30	0.28
Yb	9.55	9.13	11.40	11.57	9.89	9.69	9.68	10.56	**10.26**	**0.78**	1.67	0.31	1.24	1.20
Lu	1.60	1.58	1.92	1.70	1.56	1.59	1.41	1.72	**1.62**	**0.13**	0.05	0.29	0.35	0.11
Hf	12.95	14.64	15.21	13.86	14.21	14.20	14.39	14.40	**14.12**	**0.55**	3.11	4.68	2.66	2.73
Ta	4.08	3.78	3.76	4.34	4.26	3.63	3.64	3.62	**3.90**	**0.32**	0.32	0.63	0.14	0.44
Pb	4.91	3.98	4.91	5.34	5.07	4.77	4.76	3.99	**4.74**	**0.46**	10.90	7.93	10.65	11.38
Th	7.10	7.08	7.90	7.91	8.21	6.13	6.84	6.88	**7.27**	**0.68**	2.39	2.31	1.93	2.30
U	2.45	2.10	1.98	2.62	2.49	1.90	1.74	2.28	**2.25**	**0.33**	1.27	0.91	1.11	1.02

	StHs6_5	StHs6_1	StHs6_2	StHs6_3	StHs6_4	StHs6_5	StHs6_1	StHs6_2	StHs6_3	StHs6_4	StHs6_5	**StHs6_5**	
(%)	10/07/2018	11/07/2018	11/07/2018	11/07/2018	11/07/2018	11/07/2018	12/07/2018	12/07/2018	12/07/2018	12/07/2018	12/07/2018	**Average**	**SD**
SiO_2	63.51	63.57	62.31	62.82	62.27	62.03	64.07	64.41	63.21	63.83	63.51	**63.40**	**0.76**
TiO_2	0.72	0.75	0.75	0.75	0.78	0.75	0.68	0.69	0.67	0.69	0.72	**0.71**	**0.03**
Al_2O_3	18.12	17.70	18.63	18.24	18.47	18.81	17.73	17.24	18.12	17.37	18.12	**17.93**	**0.50**
FeO	4.23	4.21	4.48	4.35	4.26	4.48	4.12	4.14	4.24	4.20	4.23	**4.24**	**0.11**
MnO	0.07	0.07	0.08	0.08	0.07	0.08	0.07	0.07	0.07	0.07	0.07	**0.07**	**0.00**
MgO	2.00	1.95	2.02	2.07	2.04	2.08	1.89	1.91	2.00	1.98	2.00	**1.98**	**0.06**
CaO	5.14	5.25	5.14	5.45	5.68	5.33	4.99	5.29	5.35	5.25	5.14	**5.26**	**0.17**
Na_2O	4.94	5.19	5.21	4.90	5.15	5.16	5.21	5.01	5.07	5.35	4.94	**5.12**	**0.14**
K_2O	1.15	1.19	1.21	1.21	1.17	1.18	1.12	1.13	1.15	1.15	1.15	**1.16**	**0.03**
P_2O_5	0.12	0.13	0.17	0.13	0.12	0.10	0.12	0.10	0.12	0.11	0.12	**0.12**	**0.02**
Total	100.00	100.00	100.00	100.00	100.00	100.00	100.00	100.00	100.00	100.00	100.00	**100.00**	**0.00**
CF	**3.04**	**4.25**	**4.44**	**4.35**	**3.96**	**3.98**	**3.46**	**3.32**	**3.35**	**3.25**	**3.04**	**3.59**	**0.47**
(ppm)													
Sc	12.76	14.28	9.12	9.41	10.63	5.77	6.99	9.31	15.97	12.79	12.76	**10.99**	**3.21**
V	80.52	74.54	86.61	83.46	76.36	77.03	77.38	76.19	77.23	78.91	80.52	**78.56**	**3.14**
Cr	-6.90	15.84	-1.88	2.00	42.05	-7.69	39.46	35.09	52.56	9.18	-6.90	**20.61**	**22.49**
Co	10.64	11.68	10.06	11.70	11.15	11.12	9.81	13.59	12.48	14.31	10.64	**11.82**	**1.57**
Ni	3.32	33.76	-30.95	-11.05	31.87	21.74	4.59	34.68	1.65	7.50	3.32	**9.92**	**18.55**
Cu	38.11	34.64	33.23	37.63	33.61	33.50	34.01	37.18	37.76	37.79	38.11	**36.16**	**2.00**
Zn	48.59	46.07	59.61	-35.86	59.69	56.09	48.27	55.33	56.15	58.89	48.59	**48.00**	**23.68**
Ga	18.78	18.52	19.33	19.39	19.97	21.06	19.11	19.18	22.39	20.46	18.78	**19.87**	**1.24**
Rb	27.64	31.11	28.57	29.91	29.48	28.86	27.07	26.10	31.35	26.97	27.64	**28.41**	**1.85**
Sr	461.78	477.03	486.08	464.31	479.20	479.31	453.17	436.61	456.28	430.82	461.78	**457.55**	**18.06**
Y	14.42	10.65	15.29	11.43	13.81	16.10	12.85	9.05	11.62	12.40	14.42	**12.53**	**2.07**
Zr	122.77	118.40	133.50	131.96	126.49	126.93	121.45	116.24	124.86	119.14	122.77	**123.08**	**5.16**
Nb	6.26	6.44	7.27	6.55	7.17	6.25	6.59	6.33	6.35	6.45	6.26	**6.51**	**0.31**
Ba	276.70	279.16	298.37	279.63	286.59	301.43	268.05	264.00	274.10	273.93	276.70	**277.25**	**10.99**
La	10.80	12.80	13.47	11.81	11.72	12.03	11.35	12.07	10.65	10.43	10.80	**11.50**	**0.90**
Ce	24.96	26.03	23.81	25.88	27.38	26.48	23.93	22.50	24.14	24.62	24.96	**24.66**	**1.36**
Pr	3.10	3.27	3.39	2.81	3.43	3.69	2.96	2.46	2.96	2.89	3.10	**3.02**	**0.33**
Nd	13.55	9.57	14.26	13.69	12.54	11.41	10.37	12.43	13.80	10.96	13.55	**12.24**	**1.53**
Sm	4.10	2.86	1.73	1.38	2.56	3.41	2.42	5.62	3.20	2.14	4.10	**3.13**	**1.27**
Eu	1.55	1.02	1.67	1.04	1.01	0.78	1.68	0.37	0.43	0.81	1.55	**1.01**	**0.50**
Gd	4.77	5.88	2.52	4.62	-0.31	6.54	2.12	6.78	0.28	6.78	4.77	**4.05**	**2.64**
Tb	0.22	0.86	0.15	0.94	0.09	0.49	0.27	0.49	0.59	0.51	0.22	**0.45**	**0.25**
Dy	0.83	2.63	4.16	3.96	2.44	0.98	1.84	2.76	2.76	3.70	0.83	**2.53**	**1.10**
Ho	0.31	0.45	0.41	0.67	0.87	0.71	0.45	0.27	0.06	0.46	0.31	**0.41**	**0.22**
Er	1.33	0.31	1.48	0.99	1.02	1.26	1.49	1.18	2.49	1.29	1.33	**1.37**	**0.54**
Tm	0.17	-0.03	-0.04	0.11	0.08	0.20	-0.02	0.39	0.30	0.28	0.17	**0.17**	**0.15**
Yb	2.36	1.06	1.65	1.78	1.96	1.61	1.67	0.31	1.24	1.20	2.36	**1.44**	**0.61**
Lu	0.11	0.06	0.24	0.17	0.04	0.36	0.05	0.29	0.35	0.11	0.11	**0.18**	**0.12**
Hf	2.69	3.15	3.51	2.53	4.20	2.62	3.11	4.68	2.66	2.73	2.69	**3.18**	**0.75**
Ta	0.65	0.50	0.43	0.38	0.65	0.49	0.32	0.63	0.14	0.44	0.65	**0.46**	**0.17**
Pb	10.19	10.38	11.83	9.67	10.11	9.53	10.90	7.93	10.65	11.38	10.19	**10.24**	**1.13**
Th	2.30	2.17	2.30	2.59	2.31	2.66	2.39	2.31	1.93	2.30	2.30	**2.30**	**0.19**
U	0.89	0.86	1.06	0.91	1.12	0.98	1.27	0.91	1.11	1.02	0.89	**1.02**	**0.14**

Figure C5. OxCal phase model used to generate constrained eruption ages of the A-Ot, A-Fm and A-Kn ash deposits of Aira. The ^{14}C radiocarbon ages were generated from palaoesols that developed between the units, as reported by Nagakao et al. (2011). The Lake Suigetsu-derived eruption age of the AT tephra was also inserted wthin the model, which overlies these proximal units within the succession. The age of the Suigetsu cryptotephra layers known to have erupted from Aira lie outside the two-sigma uncertainty range for the modelled dates.



Appendix D: Supplementary Material for Article 4.

Table D1. Major element glass analyses of SG14-3216 (U-Ym; Ulleungdo) and SG14-3380 (B-Sg-42; Changbaishan)

SG Label	Run Date	SiO_2	TiO_2	Al_2O_3	FeOt	MnO	MgO	CaO	Na_2O	K_2O	P_2O_5	Cl	Analytical total
SG14-3216	11/06/2015	59.18	0.39	19.45	2.86	0.18	0.16	1.29	7.83	6.10	0.04	0.42	97.90
SG14-3216	11/06/2015	58.36	0.32	18.85	3.01	0.18	0.10	1.26	7.05	6.51	0.07	0.44	96.13
SG14-3216	11/06/2015	56.48	0.31	18.57	2.96	0.23	0.06	1.14	7.72	5.59	0.00	0.52	93.57
SG14-3216	11/06/2015	58.25	0.32	19.10	2.86	0.16	0.16	1.22	7.43	6.25	0.07	0.40	96.23
SG14-3216	11/06/2015	58.67	0.48	18.95	3.20	0.13	0.22	1.49	6.52	6.73	0.09	0.34	96.82
SG14-3216	11/06/2015	59.03	0.27	19.26	2.72	0.17	0.08	1.25	7.91	6.12	0.05	0.44	97.30
SG14-3216	11/06/2015	59.15	0.46	19.24	3.11	0.13	0.20	1.29	7.10	6.25	0.04	0.40	97.37
SG14-3216	11/06/2015	58.84	0.33	19.57	2.99	0.18	0.12	1.18	7.89	6.31	0.01	0.46	97.88
SG14-3216	11/06/2015	59.41	0.37	19.59	3.31	0.20	0.22	1.34	7.43	6.31	0.02	0.40	98.58
SG14-3216	11/06/2015	59.53	0.38	19.19	3.20	0.12	0.15	1.43	6.99	6.57	0.02	0.34	97.94
SG14-3216	11/06/2015	58.46	0.36	19.09	2.86	0.23	0.11	1.15	7.24	6.30	0.04	0.42	96.27
SG14-3216	11/06/2015	58.89	0.37	19.41	3.02	0.17	0.18	1.25	5.24	6.19	0.02	0.45	95.19
SG14-3216	11/06/2015	60.31	0.27	19.59	3.02	0.12	0.05	1.21	4.69	6.14	0.00	0.45	95.84
SG14-3216	11/06/2015	58.44	0.33	19.66	3.01	0.20	0.16	1.26	7.95	6.33	0.02	0.49	97.85
SG14-3216	11/06/2015	57.07	0.26	19.48	2.86	0.22	0.01	1.10	8.07	6.27	0.05	0.59	95.97
SG14-3216	11/06/2015	59.75	0.27	19.71	2.97	0.27	0.20	1.13	8.14	6.14	0.09	0.38	99.04
SG14-3216	11/06/2015	59.38	0.47	19.16	3.38	0.12	0.24	1.49	5.22	6.57	0.07	0.33	96.44
SG14-3216	11/06/2015	57.35	0.38	19.00	3.06	0.15	0.16	1.16	7.00	6.03	0.00	0.43	94.73
SG14-3216	11/06/2015	58.88	0.53	18.97	3.00	0.10	0.24	1.48	6.61	6.62	0.08	0.32	96.83
SG14-3216	11/06/2015	59.91	0.46	19.12	3.05	0.07	0.26	1.46	6.35	7.09	0.09	0.28	98.14
SG14-3216	11/06/2015	59.67	0.43	19.09	2.99	0.19	0.21	1.40	4.46	6.66	0.09	0.28	95.46

SG Label	Run Date	SiO_2	TiO_2	Al_2O_3	FeOt	MnO	MgO	CaO	Na_2O	K_2O	P_2O_5	Cl	Analytical total
SG14-3216	11/06/2015	59.49	0.35	19.08	2.83	0.22	0.20	1.26	7.42	6.29	0.09	0.25	97.48
SG14-3216	11/06/2015	59.82	0.44	19.00	3.05	0.16	0.17	1.40	7.34	6.33	0.05	0.22	97.98
SG14-3216	11/06/2015	59.89	0.45	19.11	3.19	0.23	0.22	1.42	7.20	6.44	0.08	0.23	98.47
SG14-3216	07/07/2010	58.57	0.27	19.81	3.02	0.12	0.06	1.15	8.78	5.75	0.05	0.41	98.00
SG14-3216	07/07/2010	56.93	0.49	18.35	3.16	0.20	0.26	1.38	6.32	6.33	0.06	0.28	93.76
SG14-3216	07/07/2010	60.41	0.41	19.68	3.14	0.15	0.21	1.53	7.10	6.46	0.02	0.28	99.37
SG14-3216	07/07/2010	55.80	0.41	18.43	2.82	0.14	0.15	1.27	7.06	5.61	0.03	0.38	92.10
SG14-3216	07/07/2010	58.99	0.40	19.47	3.09	0.15	0.16	1.33	7.49	5.93	0.02	0.33	97.36
SG14-3216	07/07/2010	58.98	0.28	19.97	2.86	0.32	0.06	1.14	8.38	5.68	0.02	0.47	98.15
SG14-3216	07/07/2010	59.67	0.43	19.31	3.20	0.12	0.26	1.38	6.73	6.66	0.09	0.26	98.12
SG14-3216	07/07/2010	60.00	0.42	19.41	3.15	0.13	0.23	1.31	7.01	6.57	0.00	0.24	98.48
SG14-3216	07/07/2010	59.59	0.34	19.72	2.98	0.24	0.13	1.22	8.02	6.09	0.02	0.34	98.69
SG14-3216	07/07/2010	59.40	0.39	19.33	3.09	0.15	0.20	1.36	7.14	6.39	0.12	0.24	97.82
SG14-3216	07/07/2010	59.57	0.48	19.50	3.23	0.24	0.22	1.38	6.92	6.76	0.06	0.28	98.64
SG14-3216	07/07/2010	59.03	0.36	19.50	3.19	0.14	0.19	1.19	7.25	6.16	0.00	0.29	97.30
SG14-3216	07/07/2010	59.50	0.41	18.75	2.71	0.15	0.22	1.31	6.49	6.88	0.09	0.21	96.72
SG14-3380	25/10/2017	63.65	0.48	14.26	4.92	0.11	0.21	1.06	5.62	5.22	0.04	0.13	95.69
SG14-3380	25/10/2017	64.33	0.71	15.18	4.97	0.11	0.36	1.31	5.82	5.22	0.15	0.13	98.29
SG14-3380	25/10/2017	64.81	0.54	14.15	5.07	0.21	0.21	1.12	5.71	5.31	0.06	0.16	97.37
SG14-3380	25/10/2017	62.83	0.66	14.20	5.16	0.17	0.33	1.50	5.50	5.19	0.11	0.13	95.80
SG14-3380	25/10/2017	64.40	0.64	14.77	5.19	0.11	0.32	1.37	5.59	5.46	0.08	0.15	98.09
SG14-3380	25/10/2017	61.67	0.62	14.10	4.84	0.13	0.25	1.21	5.55	5.15	0.13	0.12	93.77
SG14-3380	25/10/2017	65.00	0.67	14.80	4.76	0.15	0.27	1.33	3.27	5.18	0.09	0.15	95.66

SG Label	Run Date	SiO_2	TiO_2	Al_2O_3	FeOt	MnO	MgO	CaO	Na_2O	K_2O	P_2O_5	Cl	Analytical total
SG14-3380	25/10/2017	61.51	0.64	14.01	4.76	0.08	0.27	1.26	5.24	5.10	0.11	0.18	93.15
SG14-3380	20/10/2017	62.44	0.55	14.24	5.03	0.14	0.22	1.15	5.60	5.13	0.11	0.16	94.77
SG14-3380	20/10/2017	63.07	0.52	14.35	4.85	0.15	0.23	1.16	5.72	5.28	0.09	0.14	95.55
SG14-3380	20/10/2017	63.21	0.48	14.21	4.86	0.14	0.21	1.15	5.52	5.24	0.09	0.16	95.26
SG14-3380	20/10/2017	64.03	0.39	13.69	4.67	0.15	0.14	0.81	5.51	5.30	0.06	0.17	94.93
SG14-3380	20/10/2017	64.40	0.52	14.39	4.79	0.22	0.17	1.06	5.82	5.44	0.05	0.15	97.01
SG14-3380	20/10/2017	64.31	0.58	14.62	4.93	0.10	0.23	1.11	5.72	5.52	0.09	0.13	97.34

Table D1. Major element glass analyses of the MPI-DING reference glass (StHs6/80-G, GOR132-G and ATHO-G)

Reference Glass (Jochum et al., 2006)	Run Date	SiO_2	TiO_2	Al_2O_3	FeOt	MnO	MgO	CaO	Na_2O	K_2O	P_2O_5	Cl	Analytical total
StHs6/80-G_1	07/07/2010	63.19	0.62	17.94	4.55	0.12	1.90	5.16	4.64	1.29	0.18	0.00	99.59
StHs6/80-G_2	07/07/2010	63.48	0.69	17.67	4.40	0.12	1.92	5.73	4.51	1.29	0.17	0.00	99.97
StHs6/80-G_3	07/07/2010	63.55	0.69	18.03	4.63	0.00	1.97	5.24	4.55	1.24	0.13	0.01	100.06
StHs6/80-G_4	07/07/2010	63.43	0.66	17.87	4.40	0.13	1.96	5.72	4.55	1.26	0.17	0.01	100.17
StHs6/80-G_5	07/07/2010	63.73	0.71	17.94	4.59	0.07	1.95	5.06	4.39	1.26	0.13	0.03	99.85
StHs6/80-G_6	07/07/2010	61.82	0.69	17.48	4.66	0.05	1.94	5.51	4.55	1.24	0.17	0.01	98.11
StHs6/80-G_7	07/07/2010	63.19	0.66	17.86	4.29	0.03	1.92	5.02	4.68	1.32	0.23	0.01	99.20
StHs6/80-G_8	07/07/2010	63.70	0.72	18.06	4.29	0.00	1.95	5.62	4.48	1.26	0.22	0.00	100.29
StHs6/80-G_1	11/06/2015	63.41	0.80	17.67	4.30	0.12	1.85	5.41	4.55	1.30	0.11	0.02	99.54
StHs6/80-G_2	11/06/2015	63.65	0.69	17.53	4.27	0.09	2.02	5.22	4.43	1.27	0.02	0.00	99.19
StHs6/80-G_3	11/06/2015	63.47	0.69	17.61	4.34	0.03	2.02	5.31	4.62	1.35	0.08	0.01	99.53
StHs6/80-G_4	11/06/2015	63.60	0.67	17.57	4.36	0.15	2.02	5.17	4.71	1.29	0.05	0.00	99.59
StHs6/80-G_5	11/06/2015	63.86	0.75	17.67	4.21	0.07	1.89	5.27	4.61	1.30	0.10	0.01	99.74
StHs6/80-G_6	11/06/2015	63.85	0.74	17.62	4.29	0.09	2.02	5.26	4.33	1.36	0.12	0.02	99.70
StHs6/80-G_7	11/06/2015	63.73	0.67	17.74	4.35	0.07	1.86	5.27	4.74	1.32	0.13	0.00	99.88
StHs6/80-G_8	11/06/2015	63.98	0.73	17.63	4.40	0.06	1.95	5.25	4.17	1.28	0.10	0.00	99.55
StHs6/80-G_9	11/06/2015	63.89	0.75	17.93	4.24	0.04	1.90	5.28	4.78	1.41	0.11	0.01	100.34
StHs6/80-G_10	11/06/2015	63.07	0.73	17.59	4.29	0.04	1.91	5.22	4.25	1.28	0.13	0.00	98.51
StHs6/80-G_11	11/06/2015	63.02	0.65	17.84	4.12	0.00	2.01	5.23	4.52	1.36	0.15	0.05	98.95
StHs6/80-G_12	11/06/2015	63.30	0.66	17.78	4.50	0.07	1.98	5.15	4.75	1.28	0.21	0.02	99.70
StHs6/80-G_13	11/06/2015	63.30	0.64	17.75	4.24	0.06	1.97	5.18	4.61	1.27	0.18	0.01	99.21
StHs6/80-G_14	11/06/2015	62.86	0.73	17.60	4.29	0.06	1.94	5.19	4.60	1.32	0.11	0.00	98.70

Reference Glass (Jochum et al., 2006)	Run Date	SiO_2	TiO_2	Al_2O_3	FeOt	MnO	MgO	CaO	Na_2O	K_2O	P_2O_5	Cl	Analytical total
StHs6/80-G_15	11/06/2015	63.18	0.75	17.68	4.25	0.11	1.99	5.24	4.60	1.26	0.18	0.01	99.25
StHs6/80-G_16	11/06/2015	62.97	0.74	17.88	4.75	0.05	1.84	5.18	4.44	1.32	0.23	0.02	99.42
StHs6/80-G_17	11/06/2015	63.58	0.64	17.61	4.59	0.08	2.05	5.25	4.36	1.33	0.17	0.01	99.67
StHs6/80-G_18	11/06/2015	63.59	0.77	17.77	4.53	0.08	1.98	5.30	4.67	1.29	0.19	0.01	100.18
StHs6/80-G_19	11/06/2015	63.59	0.72	17.73	4.52	0.06	1.95	5.32	4.40	1.28	0.18	0.03	99.78
StHs6/80-G_20	11/06/2015	63.17	0.73	17.68	4.31	0.00	1.97	5.14	4.43	1.36	0.13	0.01	98.93
StHs6/80-G_22	11/06/2015	63.68	0.75	17.51	4.45	0.13	1.95	5.21	4.52	1.35	0.10	0.00	99.65
StHs6/80-G_1	20/10/2017	62.62	0.66	18.06	4.44	0.07	1.93	5.41	4.69	1.32	0.21	0.01	99.43
StHs6/80-G_2	20/10/2017	62.66	0.68	17.98	4.39	0.12	1.94	5.17	4.73	1.26	0.20	0.02	99.13
StHs6/80-G_3	20/10/2017	63.16	0.68	18.04	4.21	0.00	1.89	5.20	4.60	1.25	0.16	0.01	99.22
StHs6/80-G_4	20/10/2017	63.11	0.67	17.80	4.33	0.09	1.95	5.35	4.47	1.32	0.18	0.02	99.29
StHs6/80-G_5	20/10/2017	62.53	0.67	17.60	4.18	0.05	1.95	5.35	4.58	1.34	0.15	0.02	98.42
StHs6/80-G_6	20/10/2017	62.65	0.69	17.60	4.24	0.18	1.95	5.33	4.55	1.30	0.14	0.00	98.64
StHs6/80-G_7	20/10/2017	62.75	0.65	17.95	4.78	0.02	1.89	5.23	4.33	1.33	0.16	0.02	99.12
StHs6/80-G_8	20/10/2017	63.07	0.63	18.07	4.26	0.10	1.93	5.30	4.50	1.34	0.14	0.02	99.35
StHs6/80-G_9	20/10/2017	63.35	0.72	17.40	4.23	0.08	2.00	5.38	4.67	1.31	0.16	0.02	99.31
StHs6/80-G_10	20/10/2017	63.33	0.71	17.64	4.32	0.08	2.01	5.21	4.52	1.30	0.18	0.02	99.31
StHs6/80-G_11	20/10/2017	63.47	0.69	17.50	4.19	0.04	1.88	5.33	4.60	1.25	0.20	0.01	99.16
StHs6/80-G_12	20/10/2017	63.80	0.79	17.65	4.38	0.11	1.95	5.35	4.52	1.29	0.18	0.01	100.03
StHs6/80-G_13	20/10/2017	63.58	0.74	17.71	4.33	0.04	1.87	5.13	4.70	1.34	0.14	0.00	99.58
StHs6/80-G_14	20/10/2017	63.48	0.69	17.47	4.55	0.05	1.96	5.10	4.62	1.25	0.16	0.01	99.35
StHs6/80-G_15	20/10/2017	63.76	0.65	17.59	4.33	0.08	1.97	5.34	4.61	1.28	0.15	0.00	99.76
StHs6/80-G_16	20/10/2017	63.73	0.72	17.69	4.53	0.02	1.91	5.28	4.56	1.32	0.15	0.01	99.92

Reference Glass (Jochum et al., 2006)	Run Date	SiO_2	TiO_2	Al_2O_3	FeOt	MnO	MgO	CaO	Na_2O	K_2O	P_2O_5	Cl	Analytical total
StHs6/80-G_17	20/10/2017	63.85	0.69	17.28	4.39	0.07	1.88	5.23	4.51	1.31	0.13	0.00	99.35
StHs6/80-G_18	20/10/2017	63.88	0.69	17.32	4.36	0.08	1.97	5.21	4.71	1.33	0.11	0.00	99.66
StHs6/80-G_19	20/10/2017	63.58	0.70	17.44	4.39	0.01	2.00	5.31	4.49	1.30	0.07	0.01	99.31
StHs6/80-G_20	20/10/2017	63.33	0.70	17.33	4.49	0.07	1.92	5.22	4.61	1.38	0.09	0.00	99.13
StHs6/80-G_1	25/10/2017	63.56	0.76	17.94	4.41	0.06	1.90	5.13	4.54	1.27	0.13	0.00	99.70
StHs6/80-G_2	25/10/2017	63.54	0.66	17.84	4.20	0.08	1.88	5.11	4.50	1.36	0.13	0.00	99.30
StHs6/80-G_3	25/10/2017	63.56	0.70	17.62	4.05	0.11	1.88	5.22	4.45	1.27	0.11	0.00	98.96
StHs6/80-G_4	25/10/2017	63.36	0.71	17.72	4.41	0.01	1.91	5.40	4.74	1.32	0.15	0.01	99.76
StHs6/80-G_5	25/10/2017	63.94	0.73	17.79	4.53	0.07	1.92	5.21	4.40	1.32	0.11	0.01	100.04
StHs6/80-G_6	25/10/2017	63.61	0.69	17.86	4.56	0.04	1.92	5.27	4.63	1.34	0.07	0.00	100.00
StHs6/80-G_7	25/10/2017	63.74	0.65	17.39	4.37	0.12	1.90	5.30	4.48	1.27	0.09	0.01	99.31
ATHO-G_1	07/07/2010	75.38	0.25	12.53	3.31	0.12	0.08	1.68	3.97	2.76	0.07	0.05	100.20
ATHO-G_2	07/07/2010	75.58	0.23	12.45	3.32	0.03	0.09	1.82	4.11	2.61	0.02	0.03	100.28
ATHO-G_3	07/07/2010	76.02	0.25	12.33	3.52	0.12	0.08	1.82	4.21	2.66	0.03	0.03	101.06
ATHO-G_4	07/07/2010	75.58	0.28	12.34	3.19	0.14	0.10	1.64	4.08	2.76	0.04	0.02	100.19
ATHO-G_1	11/06/2015	74.17	0.23	12.35	3.06	0.07	0.04	1.77	3.97	2.77	0.00	0.04	98.47
ATHO-G_2	11/06/2015	74.86	0.25	12.24	3.04	0.08	0.04	1.67	4.21	2.78	0.00	0.05	99.22
ATHO-G_3	11/06/2015	74.61	0.31	12.42	3.35	0.11	0.12	1.74	4.32	2.74	0.01	0.07	99.80
ATHO-G_4	11/06/2015	74.84	0.21	12.28	3.19	0.12	0.06	1.68	4.14	2.75	0.02	0.04	99.33
ATHO-G_5	11/06/2015	74.77	0.20	12.25	3.40	0.04	0.05	1.63	4.00	2.78	0.00	0.04	99.16
ATHO-G_6	11/06/2015	75.07	0.28	12.32	3.23	0.08	0.10	1.71	4.29	2.72	0.02	0.05	99.87
ATHO-G_7	11/06/2015	74.90	0.27	12.13	3.15	0.04	0.05	1.69	4.18	2.77	0.02	0.03	99.23
ATHO-G_8	11/06/2015	74.89	0.23	12.38	3.15	0.12	0.12	1.62	4.28	2.71	0.04	0.06	99.60

Reference Glass (Jochum et al., 2006)	Run Date	SiO_2	TiO_2	Al_2O_3	FeOt	MnO	MgO	CaO	Na_2O	K_2O	P_2O_5	Cl	Analytical total
ATHO-G_9	11/06/2015	74.99	0.24	12.28	3.21	0.06	0.09	1.70	4.22	2.69	0.00	0.07	99.55
ATHO-G_10	11/06/2015	75.02	0.26	12.27	3.29	0.05	0.09	1.75	3.93	2.71	0.05	0.05	99.47
ATHO-G_11	11/06/2015	75.37	0.17	12.26	3.31	0.13	0.18	1.73	3.96	2.80	0.07	0.03	100.01
ATHO-G_12	11/06/2015	75.13	0.23	12.29	3.18	0.14	0.08	1.65	3.99	2.70	0.01	0.05	99.45
ATHO-G_13	11/06/2015	75.30	0.18	12.19	3.12	0.12	0.07	1.68	4.26	2.74	0.04	0.04	99.74
ATHO-G_14	11/06/2015	75.43	0.26	12.15	3.27	0.07	0.07	1.70	4.12	2.80	0.04	0.04	99.95
ATHO-G_15	11/06/2015	75.49	0.26	12.24	3.07	0.09	0.08	1.69	3.87	2.81	0.02	0.03	99.65
ATHO-G_16	11/06/2015	75.22	0.26	12.32	3.30	0.07	0.12	1.68	4.15	2.84	0.03	0.03	100.02
ATHO-G_18	11/06/2015	75.13	0.23	12.21	3.29	0.06	0.09	1.67	4.09	2.74	0.09	0.06	99.66
ATHO-G_19	11/06/2015	75.14	0.25	12.24	3.33	0.12	0.16	1.61	4.04	2.73	0.01	0.05	99.68
ATHO-G_20	11/06/2015	74.86	0.29	12.14	3.11	0.03	0.12	1.65	3.98	2.79	0.00	0.08	99.05
ATHO-G_21	11/06/2015	75.49	0.29	12.28	3.38	0.12	0.08	1.70	4.09	2.78	0.02	0.05	100.28
ATHO-G_1	20/10/2017	74.18	0.25	12.59	3.07	0.05	0.10	1.66	4.21	2.68	0.06	0.03	98.89
ATHO-G_2	20/10/2017	74.58	0.26	12.44	3.32	0.12	0.09	1.70	4.17	2.82	0.03	0.03	99.56
ATHO-G_3	20/10/2017	74.41	0.25	12.30	3.15	0.16	0.12	1.66	4.02	2.76	0.04	0.03	98.89
ATHO-G_4	20/10/2017	74.42	0.28	12.36	3.12	0.14	0.12	1.64	4.06	2.72	0.00	0.03	98.88
ATHO-G_5	20/10/2017	74.59	0.25	12.46	3.34	0.08	0.11	1.62	4.21	2.66	0.02	0.05	99.40
ATHO-G_6	20/10/2017	74.76	0.23	12.53	3.15	0.14	0.10	1.70	4.17	2.63	0.00	0.02	99.43
ATHO-G_7	20/10/2017	74.33	0.27	12.56	3.13	0.17	0.12	1.62	4.26	2.71	0.06	0.03	99.26
ATHO-G_8	20/10/2017	74.76	0.23	12.55	3.25	0.12	0.16	1.69	4.28	2.66	0.01	0.03	99.73
ATHO-G_9	20/10/2017	74.86	0.28	12.05	3.20	0.12	0.08	1.70	4.26	2.80	0.02	0.03	99.40
ATHO-G_10	20/10/2017	75.20	0.25	12.28	3.06	0.14	0.09	1.68	4.07	2.73	0.01	0.06	99.58
ATHO-G_11	20/10/2017	75.45	0.27	12.15	3.19	0.01	0.11	1.66	4.03	2.72	0.06	0.03	99.68

Reference Glass (Jochum et al., 2006)	Run Date	SiO_2	TiO_2	Al_2O_3	FeOt	MnO	MgO	CaO	Na_2O	K_2O	P_2O_5	Cl	Analytical total
ATHO-G_12	20/10/2017	75.57	0.29	11.97	3.05	0.10	0.10	1.68	4.23	2.74	0.02	0.04	99.80
ATHO-G_13	20/10/2017	75.10	0.22	12.22	3.18	0.13	0.09	1.70	4.21	2.79	0.02	0.02	99.70
ATHO-G_14	20/10/2017	75.01	0.23	12.22	3.37	0.11	0.10	1.72	3.92	2.76	0.05	0.01	99.49
ATHO-G_15	20/10/2017	75.58	0.19	12.34	3.28	0.06	0.09	1.65	4.16	2.73	0.02	0.04	100.15
ATHO-G_16	20/10/2017	75.28	0.27	12.38	3.51	0.04	0.11	1.72	4.17	2.82	0.04	0.02	100.37
ATHO-G_17	20/10/2017	75.69	0.23	12.30	3.58	0.10	0.11	1.64	4.19	2.75	0.02	0.04	100.64
ATHO-G_18	20/10/2017	75.39	0.22	12.32	3.39	0.15	0.06	1.67	4.09	2.71	0.00	0.03	100.02
ATHO-G_19	20/10/2017	75.53	0.25	12.13	3.61	0.14	0.09	1.59	3.90	2.70	0.02	0.04	100.00
ATHO-G_20	20/10/2017	75.24	0.31	12.31	3.13	0.09	0.09	1.68	4.20	2.68	0.03	0.05	99.81
ATHO-G_1	25/10/2017	75.16	0.24	12.54	3.24	0.08	0.11	1.72	4.44	2.68	0.00	0.03	100.24
ATHO-G_2	25/10/2017	74.91	0.23	12.50	3.17	0.00	0.11	1.66	3.92	2.76	0.06	0.04	99.36
ATHO-G_3	25/10/2017	75.14	0.25	12.22	3.41	0.02	0.09	1.71	4.08	2.79	0.06	0.04	99.80
ATHO-G_4	25/10/2017	75.16	0.26	12.31	3.36	0.05	0.07	1.64	4.19	2.69	0.05	0.02	99.81
ATHO-G_5	25/10/2017	75.51	0.32	12.21	3.26	0.07	0.09	1.66	3.88	2.77	0.00	0.03	99.81
ATHO-G_6	25/10/2017	75.24	0.27	12.39	3.42	0.14	0.12	1.69	4.18	2.63	0.07	0.02	100.18
ATHO-G_7	25/10/2017	75.02	0.24	12.45	3.39	0.16	0.12	1.77	4.20	2.71	0.02	0.02	100.09
GOR132-G_1	07/07/2010	45.77	0.32	11.14	9.86	0.17	22.50	8.14	0.76	0.00	0.07	0.02	98.75
GOR132-G_2	07/07/2010	45.88	0.31	11.21	10.37	0.21	22.08	8.88	0.60	0.04	0.07	0.01	99.65
GOR132-G_3	07/07/2010	45.79	0.26	11.10	10.25	0.10	22.25	7.93	0.83	0.03	0.07	0.02	98.65
GOR132-G_4	07/07/2010	45.93	0.28	11.02	10.55	0.14	22.24	8.96	0.83	0.04	0.00	0.00	99.99
GOR132-G_5	07/07/2010	45.88	0.27	10.95	10.61	0.28	22.39	8.94	0.92	0.04	0.04	0.00	100.33
GOR132-G_6	07/07/2010	45.72	0.33	11.13	10.24	0.15	22.06	9.01	0.76	0.03	0.07	0.02	99.52
GOR132-G_7	11/06/2015	45.69	0.33	11.00	10.18	0.15	22.09	8.58	0.69	0.01	0.05	0.02	98.79

Reference Glass (Jochum et al., 2006)	Run Date	SiO_2	TiO_2	Al_2O_3	FeOt	MnO	MgO	CaO	Na_2O	K_2O	P_2O_5	Cl	Analytical total
GOR132-G_8	11/06/2015	45.19	0.28	10.97	10.45	0.12	21.96	8.50	0.84	0.04	0.00	0.00	98.35
GOR132-G_9	11/06/2015	45.42	0.35	11.00	10.23	0.07	22.12	8.50	0.94	0.04	0.01	0.00	98.68
GOR132-G_10	11/06/2015	45.40	0.35	10.81	10.63	0.14	22.27	8.49	0.70	0.04	0.01	0.00	98.84
GOR132-G_11	11/06/2015	45.20	0.27	10.93	10.32	0.15	21.97	8.57	0.90	0.03	0.02	0.00	98.36
GOR132-G_12	11/06/2015	45.62	0.31	10.97	10.29	0.19	22.49	8.36	0.87	0.07	0.13	0.00	99.30
GOR132-G_13	11/06/2015	45.19	0.31	10.88	10.27	0.19	22.16	8.42	0.77	0.04	0.04	0.00	98.27
GOR132-G_14	11/06/2015	45.52	0.33	10.99	10.26	0.15	22.05	8.43	0.78	0.03	0.05	0.00	98.59
GOR132-G_15	11/06/2015	45.22	0.34	10.96	9.99	0.14	21.97	8.36	0.92	0.02	0.11	0.02	98.05
GOR132-G_16	11/06/2015	45.68	0.30	10.95	10.23	0.19	21.88	8.61	0.96	0.02	0.10	0.00	98.92
GOR132-G_18	11/06/2015	45.76	0.29	10.88	10.35	0.20	21.96	8.48	0.89	0.01	0.05	0.00	98.87
GOR132-G_19	11/06/2015	45.67	0.29	10.82	10.33	0.15	22.26	8.58	0.83	0.04	0.05	0.01	99.03
GOR132-G_20	11/06/2015	45.39	0.33	10.89	10.35	0.21	22.25	8.55	0.74	0.05	0.02	0.00	98.78
GOR132-G_21	11/06/2015	45.77	0.28	10.91	10.24	0.12	22.07	8.43	0.89	0.02	0.04	0.00	98.77
GOR132-G_22	11/06/2015	45.87	0.30	10.87	10.23	0.22	22.27	8.56	0.81	0.03	0.04	0.00	99.20
GOR132-G_1	20/10/2017	45.04	0.31	11.21	9.76	0.06	21.95	8.33	0.79	0.04	0.01	0.00	97.49
GOR132-G_2	20/10/2017	45.04	0.30	11.18	10.28	0.19	21.93	8.39	0.77	0.05	0.05	0.01	98.19
GOR132-G_3	20/10/2017	45.46	0.26	11.13	9.70	0.17	22.09	8.61	0.72	0.08	0.02	0.01	98.24
GOR132-G_4	20/10/2017	45.36	0.35	10.98	10.36	0.16	21.88	8.49	0.93	0.05	0.06	0.01	98.62
GOR132-G_5	20/10/2017	45.24	0.28	11.45	10.01	0.14	22.00	8.57	0.71	0.03	0.02	0.00	98.45
GOR132-G_6	20/10/2017	45.38	0.37	11.20	10.24	0.16	21.73	8.34	0.73	0.03	0.05	0.00	98.22
GOR132-G_7	20/10/2017	45.53	0.30	11.13	10.41	0.14	21.87	8.64	0.81	0.00	0.03	0.01	98.85
GOR132-G_8	20/10/2017	45.51	0.28	11.08	9.79	0.17	21.76	8.46	0.80	0.05	0.00	0.02	97.93
GOR132-G_9	20/10/2017	45.57	0.30	11.09	10.09	0.22	22.08	8.43	0.73	0.00	0.00	0.01	98.51

Reference Glass (Jochum et al., 2006)	Run Date	SiO_2	TiO_2	Al_2O_3	FeOt	MnO	MgO	CaO	Na_2O	K_2O	P_2O_5	Cl	Analytical total
GOR132-G_10	20/10/2017	45.63	0.27	11.03	10.07	0.13	21.83	8.49	0.74	0.06	0.06	0.00	98.30
GOR132-G_11	20/10/2017	45.60	0.28	11.07	9.96	0.17	21.98	8.62	0.70	0.01	0.06	0.00	98.45
GOR132-G_12	20/10/2017	45.45	0.29	11.09	10.11	0.14	21.96	8.50	0.79	0.02	0.00	0.01	98.37
GOR132-G_13	20/10/2017	45.78	0.35	10.91	9.68	0.16	21.96	8.43	0.68	0.03	0.04	0.00	98.02
GOR132-G_14	20/10/2017	45.70	0.26	11.05	9.98	0.21	22.00	8.39	0.80	0.03	0.07	0.00	98.51
GOR132-G_15	20/10/2017	45.98	0.29	11.19	10.25	0.14	22.06	8.55	0.80	0.05	0.04	0.00	99.35
GOR132-G_16	20/10/2017	45.95	0.30	10.94	10.59	0.09	21.98	8.53	0.69	0.03	0.04	0.00	99.14
GOR132-G_17	20/10/2017	45.62	0.25	10.90	10.27	0.13	22.09	8.65	0.74	0.05	0.05	0.00	98.75
GOR132-G_18	20/10/2017	45.62	0.29	11.20	10.30	0.09	22.09	8.55	0.81	0.03	0.00	0.00	99.00
GOR132-G_19	20/10/2017	45.75	0.31	11.12	10.30	0.13	22.38	8.41	0.78	0.03	0.03	0.00	99.25
GOR132-G_20	20/10/2017	45.84	0.28	11.11	10.78	0.22	22.39	8.31	0.83	0.04	0.01	0.01	99.83
GOR132-G_1	25/10/2017	45.31	0.26	11.08	10.06	0.15	22.16	8.63	0.79	0.03	0.01	0.00	98.46
GOR132-G_2	25/10/2017	45.59	0.30	11.05	10.07	0.11	21.76	8.38	0.92	0.04	0.01	0.01	98.23
GOR132-G_3	25/10/2017	45.43	0.32	11.29	10.52	0.17	21.75	8.50	0.85	0.04	0.05	0.02	98.94
GOR132-G_4	25/10/2017	45.86	0.29	10.96	9.96	0.11	22.03	8.41	0.77	0.03	0.08	0.01	98.51
GOR132-G_5	25/10/2017	45.34	0.32	10.95	10.24	0.19	22.05	8.26	0.65	0.05	0.09	0.01	98.14
GOR132-G_6	25/10/2017	45.61	0.28	10.86	10.40	0.23	21.97	8.29	0.78	0.01	0.05	0.00	98.49
GOR132-G_7	25/10/2017	45.48	0.30	11.00	10.24	0.09	22.00	8.37	0.74	0.03	0.02	0.00	98.28

Table D3. Trace element glass compositions of Changbaishan (SG14-0226; SG14-1058; SG14-3380) and Ulleungdo (SG14-1091 and SG14-3216) tephra layers using LA-ICP-MS

SG Label (SG14-)	Run Date	Rb	Sr	Y	Zr	Nb	Ba	La	Ce	Pr	Nd	Sm	Eu	Gd	Dy	Er	Yb	Hf	Ta	Th	U
0226	11/07/18	389.4	2.5	140.9	2362.3	274.5	6.0	136.1	281.1	29.9	107.2	27.7	0.3	26.7	23.9	13.5	11.0	55.4	15.4	47.2	9.9
0226	11/07/18	401.3	2.4	145.4	2402.4	294.2	6.9	140.7	301.9	33.7	117.4	26.9	0.3	26.2	23.7	13.9	10.9	55.6	18.4	47.8	10.9
0226	11/07/18	414.5	2.7	146.2	2472.7	289.9	5.2	139.9	288.3	31.6	117.8	29.6	0.3	27.0	26.5	15.1	11.5	57.5	18.3	52.0	11.0
0226	11/07/18	403.3	2.5	148.9	2565.3	300.5	6.8	141.7	292.7	31.6	116.1	28.2	0.2	26.0	26.9	13.8	11.7	58.6	17.1	50.8	10.9
0226	11/07/18	383.3	1.9	143.1	2414.5	277.0	5.2	141.4	301.0	33.0	123.2	28.6	0.3	29.1	27.2	13.7	12.2	55.9	17.2	54.3	11.5
0226	11/07/18	396.5	2.6	140.1	2367.4	289.2	7.1	138.8	288.5	32.3	118.7	27.2	0.5	27.1	26.6	13.8	11.7	54.7	17.4	52.5	11.3
0226	11/07/18	392.9	2.0	145.0	2437.0	281.1	7.7	143.4	282.5	32.3	114.2	26.5	0.2	27.7	25.4	14.8	11.6	56.5	16.6	49.2	11.3
0226	11/07/18	389.8	0.7	136.6	2300.3	282.3	6.4	129.0	259.5	30.6	111.8	25.9	0.4	24.0	22.4	13.8	10.9	50.7	15.8	45.3	9.6
1058	11/07/18	386.4	4.3	144.2	2291.2	241.6	8.7	117.2	229.1	26.7	93.8	24.7	0.6	24.6	25.2	13.6	10.4	54.4	13.6	49.1	8.4
1058	11/07/18	385.4	4.0	152.2	2428.7	261.5	3.0	134.9	242.7	28.6	109.6	28.4	-0.1	27.3	26.3	14.7	10.2	56.0	16.6	49.1	9.9
1058	11/07/18	390.5	6.0	150.1	2315.0	274.6	6.6	125.2	253.2	27.9	102.5	20.4	0.1	33.4	25.9	14.9	10.3	60.6	18.4	50.8	10.0
1058	11/07/18	411.6	3.9	166.8	2483.7	288.6	9.2	143.1	257.7	31.2	108.6	32.4	0.6	27.9	28.0	15.4	14.8	59.9	17.7	56.4	11.0
1058	11/07/18	345.6	3.9	135.9	1994.1	239.4	5.4	105.8	233.3	27.1	97.1	24.3	0.5	26.9	22.1	11.4	10.1	47.2	15.6	42.4	9.2
1091	09/07/18	204.2	4.2	20.8	735.3	183.6	4.6	93.6	146.3	12.0	34.6	4.7	0.8	3.7	3.5	2.2	2.4	13.4	9.3	27.7	6.0
1091	09/07/18	178.6	85.1	24.1	621.6	173.2	170.8	90.5	144.3	13.0	44.3	6.7	1.3	5.7	5.1	2.3	1.9	12.0	11.0	24.5	5.1
1091	09/07/18	198.6	22.0	23.8	689.6	184.3	14.0	86.9	146.2	12.1	39.7	6.2	1.4	6.5	4.0	2.6	2.0	11.2	10.7	23.6	5.0
1091	09/07/18	170.4	53.1	25.0	606.6	171.4	78.4	86.1	147.0	12.5	36.0	6.4	1.2	3.6	4.1	2.6	2.7	12.6	9.6	21.4	4.9
1091	17/07/18	183.5	46.6	22.7	617.6	158.6	69.5	84.2	145.7	12.4	35.4	4.0	1.3	2.5	3.6	3.0	2.7	12.8	9.6	23.9	4.8
1091	17/07/18	190.8	47.5	26.6	611.8	159.3	63.2	86.9	146.2	13.1	43.1	5.6	1.1	6.0	4.3	3.0	3.1	12.0	9.3	25.0	4.9
1091	17/07/18	188.5	152.1	20.0	557.2	145.3	331.3	77.6	126.9	11.3	35.2	4.8	1.8	4.9	3.8	2.7	2.8	11.0	8.9	20.6	4.3
1091	17/07/18	180.3	58.6	22.6	568.9	168.2	79.2	82.5	145.2	12.9	36.5	4.5	1.5	4.4	3.2	2.5	2.3	10.5	9.7	21.7	4.2

SG Label (SG14-)	Run Date	Rb	Sr	Y	Zr	Nb	Ba	La	Ce	Pr	Nd	Sm	Eu	Gd	Dy	Er	Yb	Hf	Ta	Th	U
1091	17/07/18	201.7	34.6	25.9	657.5	172.9	49.4	86.0	144.3	13.5	41.1	5.6	1.3	3.5	3.3	3.2	2.6	12.3	10.5	24.8	5.6
1091	17/07/18	189.8	72.6	22.9	578.0	162.7	115.4	84.0	139.8	13.4	39.7	5.4	1.8	5.9	2.7	1.8	2.3	12.6	9.1	22.8	4.5
1091	17/07/18	199.0	74.6	23.6	641.5	172.5	104.1	88.5	152.1	13.7	44.2	7.0	1.8	6.2	3.7	1.6	3.4	12.7	10.6	23.5	4.6
1091	17/07/18	180.3	79.4	22.0	587.9	169.3	140.7	84.6	141.2	12.1	39.9	6.8	1.8	7.0	4.3	2.2	2.4	9.7	9.4	22.3	4.3
1091	17/07/18	186.9	43.5	25.8	664.8	186.3	67.2	92.6	156.6	14.7	41.6	5.6	1.9	4.5	3.1	2.9	3.0	12.9	10.2	24.3	4.8
3216	10/07/18	200.2	31.9	28.4	823.9	193.9	44.3	99.0	172.4	14.3	48.1	5.2	0.4	3.4	4.7	2.8	2.7	15.9	10.7	25.5	5.8
3216	10/07/18	198.4	11.0	24.9	679.4	170.3	10.8	95.8	157.7	14.8	42.9	7.2	0.8	6.3	4.1	1.5	3.1	10.9	8.7	23.9	4.9
3216	10/07/18	219.3	27.6	29.3	847.1	200.0	25.3	106.2	177.5	16.1	48.7	7.2	0.3	5.0	4.6	2.5	4.5	15.2	10.9	27.8	6.3
3216	10/07/18	199.8	7.2	28.4	741.2	185.0	6.3	107.3	173.3	16.0	50.1	6.2	0.5	9.7	5.3	3.2	2.9	13.6	10.0	26.8	4.9
3216	10/07/18	193.8	7.7	27.1	684.8	170.5	8.4	99.8	159.0	14.0	43.8	6.7	0.4	5.6	5.0	2.7	3.6	14.1	9.4	24.9	5.2
3216	10/07/18	170.0	13.8	21.4	570.2	147.8	19.0	86.3	142.8	12.9	39.6	6.8	1.0	5.2	3.8	3.2	2.4	11.1	8.6	20.7	4.1
3216	10/07/18	215.8	2.8	26.6	760.8	190.8	3.2	107.0	174.9	14.9	41.1	5.9	0.5	4.0	4.5	3.5	3.1	15.2	11.0	30.6	6.6
3216	10/07/18	166.1	12.4	22.2	569.6	143.1	13.1	84.2	135.8	12.8	37.0	6.1	0.9	4.4	3.5	2.7	2.3	11.1	8.4	21.5	4.6
3380	10/07/18	138.3	11.0	47.8	723.8	95.9	53.2	72.7	152.2	16.4	65.0	11.9	0.6	11.3	9.4	4.8	4.3	17.4	5.6	12.6	2.6
3380	10/07/18	141.0	39.0	53.3	742.0	95.9	123.0	76.2	158.9	16.5	65.8	11.6	0.4	8.3	10.4	4.4	4.7	17.8	5.6	14.9	2.5
3380	10/07/18	148.6	8.9	53.7	767.8	105.3	37.9	78.5	159.6	17.4	59.4	15.0	0.6	10.2	10.4	4.6	4.8	16.7	5.8	15.1	2.9
3380	10/07/18	136.5	74.6	42.7	641.9	84.9	183.8	65.4	130.2	14.4	54.7	10.5	0.6	9.4	7.7	4.1	3.2	14.7	4.9	12.7	2.6
3380	10/07/18	145.9	4.5	49.7	740.3	99.3	23.9	76.1	156.2	18.1	66.8	12.6	0.5	10.4	9.2	5.2	4.0	16.4	5.7	14.7	3.0
3380	10/07/18	134.1	15.2	49.0	734.1	98.0	51.5	77.1	154.8	16.9	66.6	13.1	0.5	10.9	8.5	5.1	4.7	18.0	5.7	14.6	3.2
3380	10/07/18	155.1	14.6	54.9	763.4	98.2	50.2	80.9	156.2	18.2	73.0	12.6	0.6	12.5	8.3	6.3	4.7	15.0	5.4	13.5	2.3
3380	10/07/18	131.1	58.5	50.7	745.3	92.6	161.2	75.7	157.5	16.9	59.2	11.0	0.6	12.2	9.3	6.3	4.4	17.1	4.8	13.1	2.5
3380	10/07/18	158.2	2.9	55.4	826.6	102.4	29.1	82.1	166.8	18.1	74.8	16.7	0.7	12.4	10.0	5.0	4.8	18.1	6.3	15.2	3.2
3380	10/07/18	146.6	20.9	53.9	728.5	97.2	59.2	79.4	150.9	17.6	70.4	14.0	1.1	9.3	9.4	4.8	3.3	18.0	5.7	14.9	3.2

Table D4. Trace element glass compositions of BHVO-2G, LIP3 and the MPI-DING reference glass (StHs6/80-G and ATHO-G)

	BHVO-2G_1	BHVO-2G_2	BHVO-2G_3	BHVO-2G_4	BHVO-2G_5	BHVO-2G_6	BHVO-2G_7	BHVO-2G_8	BHVO-2G_9	BHVO-2G_10	BHVO-2G_1	BHVO-2G_2	BHVO-2G_3	BHVO-2G_4
(%)	09/07/2018	09/07/2018	09/07/2018	09/07/2018	09/07/2018	09/07/2018	09/07/2018	09/07/2018	09/07/2018	09/07/2018	09/07/2018	09/07/2018	09/07/2018	09/07/2018
SiO_2	47.96	47.82	48.04	48.38	48.32	48.57	47.78	48.73	48.12	48.36	48.75	49.15	48.51	48.09
TiO_2	2.90	3.01	3.00	3.01	2.99	2.94	2.99	2.94	3.01	2.88	2.83	2.88	2.89	2.93
Al_2O_3	14.03	13.92	13.88	13.98	14.17	14.15	14.05	13.85	14.07	13.81	13.98	13.76	13.75	14.13
FeO	11.55	12.19	11.61	11.58	11.56	11.28	11.90	11.86	11.67	11.91	11.10	11.19	11.20	11.12
MnO	0.18	0.19	0.18	0.19	0.18	0.18	0.18	0.18	0.18	0.18	0.17	0.17	0.17	0.17
MgO	7.87	7.57	7.76	7.74	7.70	7.64	7.53	7.41	7.78	7.62	7.76	7.67	7.73	7.77
CaO	12.18	12.09	12.23	11.81	11.83	12.09	12.48	12.00	12.13	12.12	12.00	11.77	12.34	12.38
Na_2O	2.53	2.41	2.49	2.47	2.41	2.41	2.33	2.30	2.30	2.34	2.44	2.45	2.44	2.44
K_2O	0.45	0.46	0.47	0.45	0.46	0.45	0.47	0.45	0.45	0.46	0.43	0.42	0.44	0.45
P_2O_5	0.37	0.35	0.35	0.38	0.38	0.29	0.30	0.29	0.28	0.31	0.54	0.52	0.52	0.52
Total	100.00	100.00	100.00	100.00	100.00	100.00	100.00	100.00	100.00	100.00	100.00	100.00	100.00	100.00
CF	1.57	1.62	1.66	1.70	1.71	1.42	1.47	1.49	1.59	1.50	**1.27**	**1.29**	**1.30**	**1.33**
(ppm)														
Sc	34.23	33.63	33.31	37.68	34.14	34.91	35.56	35.42	34.52	35.14	32.54	34.03	35.43	34.15
V	305.38	311.53	319.42	319.05	327.49	309.68	312.73	323.46	312.46	305.00	308.22	316.75	312.17	312.12
Cr	289.73	304.44	320.07	299.60	295.40	283.17	269.08	280.28	295.72	287.45	276.71	266.06	288.94	295.67
Co	45.64	46.44	48.08	45.41	45.89	45.45	45.87	45.89	44.77	44.45	44.72	44.12	44.57	44.47
Ni	109.98	113.01	115.56	107.62	119.09	98.13	108.64	107.87	109.82	109.53	105.58	108.11	104.87	110.17
Cu	116.28	115.00	118.85	119.80	120.60	120.47	123.09	118.59	118.37	113.63	113.87	112.84	107.19	116.32
Zn	102.70	107.54	112.82	111.85	106.93	109.52	114.40	108.17	113.12	111.05	105.76	105.30	96.65	98.76
Ga	21.21	22.33	22.34	21.27	22.90	22.53	22.61	23.90	21.95	22.06	20.08	20.63	20.49	21.61
Rb	8.94	9.78	9.43	8.60	9.22	9.47	9.44	8.58	9.17	9.44	8.62	9.12	8.27	10.25
Sr	395.50	403.75	386.10	388.67	396.64	402.04	408.29	399.22	411.06	395.63	355.00	369.34	362.38	390.18
Y	25.88	26.18	26.64	26.50	27.70	26.98	26.94	27.14	27.43	25.38	23.41	24.35	23.04	25.32
Zr	172.69	170.94	172.77	172.87	175.06	176.97	182.47	174.58	177.36	168.21	160.04	169.28	158.80	177.13
Nb	18.91	18.99	20.30	18.54	19.11	19.12	20.17	19.60	19.69	20.14	17.11	18.11	19.23	19.46
Ba	139.63	133.01	143.17	147.28	129.17	132.01	143.10	132.91	129.35	130.18	129.26	129.06	130.05	129.74
La	16.28	15.91	15.74	15.58	14.98	16.05	15.98	16.39	15.71	16.03	14.47	14.34	15.11	15.37
Ce	40.07	38.75	38.49	37.76	38.15	40.80	39.94	41.77	41.26	38.55	36.34	35.68	38.07	38.79
Pr	5.35	5.15	5.38	5.64	5.28	5.57	6.13	5.11	5.41	5.33	4.60	5.16	5.33	5.55
Nd	23.54	25.08	25.24	24.62	25.09	24.33	26.81	25.65	23.75	23.65	24.72	24.85	23.20	26.96
Sm	7.66	6.82	6.90	5.79	6.26	7.58	6.67	6.70	5.71	6.41	6.66	7.13	6.47	6.91
Eu	2.06	2.19	1.97	2.27	2.27	1.95	2.31	2.20	2.61	2.07	2.17	2.07	2.27	2.25
Gd	7.26	5.64	7.75	6.00	5.21	8.05	4.84	5.63	8.89	7.61	7.62	6.04	6.42	7.56
Tb	0.89	1.06	0.97	1.09	0.78	1.13	1.12	1.03	1.00	0.97	0.97	0.91	0.86	0.78
Dy	4.84	4.51	6.58	5.05	4.99	4.83	6.19	5.86	5.08	6.14	5.31	6.20	4.79	6.07
Ho	1.07	0.99	0.97	0.84	1.10	1.04	1.05	1.06	1.20	0.90	1.15	0.76	1.06	1.12
Er	2.56	2.14	2.88	2.57	2.92	3.55	3.44	2.60	3.37	2.74	2.81	2.69	2.61	2.74
Tm	0.34	0.34	0.33	0.42	0.30	0.33	0.30	0.31	0.25	0.36	0.42	0.32	0.33	0.41
Yb	2.14	1.86	1.52	2.17	1.93	2.26	2.42	1.86	1.73	1.74	1.90	2.15	1.62	1.80
Lu	0.27	0.42	0.34	0.37	0.22	0.22	0.45	0.29	0.26	0.38	0.29	0.26	0.21	0.24
Hf	3.95	4.29	4.69	4.48	4.84	4.75	5.01	4.75	3.97	3.02	4.50	4.06	4.60	4.53
Ta	1.30	1.31	1.28	1.17	1.38	1.24	1.11	1.14	1.10	1.19	1.10	1.43	1.25	1.21
Pb	2.00	1.31	1.59	2.07	1.35	1.65	2.18	2.34	1.81	1.92	1.99	1.98	1.52	1.79
Th	1.34	1.14	1.31	1.35	1.10	1.33	1.42	1.12	1.49	1.08	1.15	1.04	1.27	0.98
U	0.42	0.50	0.43	0.50	0.47	0.43	0.45	0.44	0.41	0.43	0.42	0.36	0.44	0.35

	BHVO-2G_5	BHVO-2G_6	BHVO-2G_1	BHVO-2G_2	BHVO-2G_3	BHVO-2G_4	BHVO-2G_5	BHVO-2G_6	BHVO-2G_7	BHVO-2G_8	BHVO-2G_9	BHVO-2G_10	BHVO-2G_1	BHVO-2G_2
(%)	09/07/2018	09/07/2018	09/07/2018	11/07/2018	11/07/2018	11/07/2018	11/07/2018	11/07/2018	11/07/2018	11/07/2018	11/07/2018	11/07/2018	11/07/2018	11/07/2018
SiO_2	47.76	49.06	49.62	48.67	49.21	48.97	48.41	49.39	49.41	48.83	48.41	49.87	47.72	48.09
TiO_2	2.93	2.96	2.80	3.04	2.91	3.00	2.93	2.88	2.87	2.90	2.84	2.80	2.98	2.97
Al_2O_3	13.95	14.32	14.45	14.05	14.28	14.09	14.33	14.02	14.04	13.87	14.20	13.58	14.28	13.70
FeO	11.40	11.04	10.75	11.52	11.26	11.51	11.78	11.17	11.19	11.44	11.78	11.14	11.43	11.76
MnO	0.17	0.18	0.18	0.18	0.17	0.18	0.18	0.17	0.18	0.18	0.18	0.17	0.17	0.18
MgO	7.80	7.38	7.65	7.70	7.44	7.60	7.52	7.39	7.45	7.43	7.60	7.25	7.51	7.42
CaO	12.52	12.19	11.48	11.79	11.69	11.56	11.84	11.96	11.86	12.29	11.95	12.14	12.86	12.89
Na_2O	2.48	2.29	2.44	2.40	2.40	2.44	2.36	2.34	2.32	2.38	2.39	2.38	2.39	2.34
K_2O	0.43	0.43	0.44	0.45	0.46	0.44	0.47	0.44	0.46	0.44	0.44	0.44	0.42	0.44
P_2O_5	0.55	0.16	0.19	0.19	0.18	0.20	0.19	0.24	0.22	0.23	0.22	0.22	0.22	0.22
Total	100.00	100.00	100.00	100.00	100.00	100.00	100.00	100.00	100.00	100.00	100.00	100.00	100.00	100.00
CF	**1.36**	**1.58**	**1.51**	**1.56**	**1.58**	**1.62**	**1.61**	**1.55**	**1.53**	**1.49**	**1.54**	**1.51**	1.59	1.61
(ppm)														
Sc	35.99	32.18	32.52	37.65	35.16	36.72	35.05	35.60	35.85	33.95	35.34	35.45	32.89	33.61
V	311.86	304.92	301.62	321.93	300.10	320.01	311.18	296.31	308.46	310.71	298.15	299.93	313.33	321.67
Cr	289.80	275.24	277.70	296.47	270.33	304.62	299.46	287.67	295.74	285.84	283.87	289.46	287.65	289.90
Co	43.69	45.66	42.53	44.06	43.22	44.70	46.13	45.42	44.69	45.11	45.50	43.86	43.71	46.02
Ni	113.45	106.99	100.58	93.75	99.59	120.95	95.86	107.52	95.40	103.45	107.01	99.64	109.08	112.88
Cu	116.26	118.77	112.98	105.46	112.35	118.30	111.97	105.70	113.15	110.70	108.16	108.19	110.61	115.40
Zn	103.16	103.93	104.07	98.24	98.31	101.32	108.52	97.90	106.04	103.51	98.39	94.24	106.81	103.27
Ga	21.37	21.90	20.45	19.62	20.48	22.49	21.11	20.78	20.15	20.80	21.59	19.61	20.61	22.58
Rb	9.90	8.26	8.55	8.55	8.67	8.83	10.31	8.84	9.70	8.83	8.39	8.52	9.26	8.63
Sr	402.63	375.81	373.66	380.43	386.45	373.41	386.67	364.00	387.29	379.42	375.73	360.39	371.17	388.02
Y	27.64	26.68	25.25	24.52	26.13	26.81	25.09	24.95	26.38	25.32	24.97	24.31	26.21	25.04
Zr	177.42	174.70	163.35	167.43	168.67	168.85	177.28	163.43	171.10	167.26	168.29	162.81	166.64	169.44
Nb	18.78	18.40	17.68	17.96	17.80	18.74	19.16	17.29	17.32	17.97	17.87	18.80	17.46	17.75
Ba	141.02	129.16	126.12	129.69	129.03	136.43	127.83	124.56	125.82	123.80	127.08	123.45	130.01	133.92
La	14.72	14.97	14.44	15.44	15.74	14.82	15.84	14.52	15.24	14.27	14.47	14.33	14.50	14.66
Ce	39.08	36.83	35.06	35.48	38.33	39.25	38.19	35.37	37.13	36.92	34.73	36.04	35.22	39.40
Pr	4.98	5.87	5.33	5.24	5.40	5.20	5.26	5.35	5.15	4.74	4.93	4.69	4.84	5.73
Nd	25.88	25.28	23.61	23.95	25.15	24.80	24.54	22.93	24.58	23.08	23.01	23.96	23.31	23.95
Sm	6.25	6.94	6.98	5.51	6.64	6.81	4.91	6.05	6.32	5.65	6.83	5.58	6.02	8.08
Eu	2.28	2.16	2.30	2.04	2.14	2.26	1.95	2.18	2.07	1.87	2.26	1.65	2.06	2.27
Gd	5.69	3.23	6.15	5.60	4.59	6.15	5.51	5.98	4.27	7.03	5.77	6.85	5.19	7.47
Tb	1.07	0.93	0.86	0.82	1.08	0.94	1.09	0.73	0.83	0.72	0.91	1.00	0.71	1.12
Dy	4.97	5.76	5.13	5.22	4.56	5.49	5.09	4.79	4.17	4.96	5.64	4.21	4.83	5.39
Ho	1.15	0.99	0.80	0.92	1.09	1.05	1.00	0.91	0.95	1.00	1.03	1.16	0.88	1.17
Er	2.43	3.15	2.42	2.35	2.02	2.29	2.99	2.06	2.37	2.04	2.67	2.39	3.33	2.61
Tm	0.40	0.39	0.40	0.29	0.43	0.41	0.33	0.19	0.28	0.31	0.26	0.30	0.25	0.36
Yb	2.04	2.05	1.82	2.15	1.84	1.73	2.55	1.46	2.01	2.60	1.83	2.28	2.32	1.95
Lu	0.47	0.36	0.23	0.29	0.33	0.25	0.29	0.37	0.33	0.21	0.30	0.19	0.35	0.36
Hf	4.43	5.08	4.96	4.13	4.66	3.89	4.40	3.71	4.75	4.78	4.78	3.64	4.51	4.76
Ta	1.19	0.91	1.00	0.92	1.21	1.10	1.21	1.34	1.17	0.92	1.07	1.06	1.17	1.23
Pb	1.40	1.99	1.67	1.72	1.39	1.11	1.53	1.56	1.81	2.57	1.86	1.86	1.75	1.37
Th	1.39	1.08	1.27	1.19	1.09	1.22	1.19	1.51	1.31	1.21	1.30	1.22	1.49	1.33
U	0.57	0.35	0.41	0.38	0.35	0.43	0.38	0.46	0.52	0.46	0.39	0.36	0.42	0.37

	BHVO-2G_3	BHVO-2G_4	BHVO-2G_5	BHVO-2G_6	BHVO-2G_7	BHVO-2G_8	BHVO-2G_9	BHVO-2G_10	**BHVO-2G**		LIP3_1	LIP3_2	LIP3_3	LIP3_4
(%)	11/07/2018	11/07/2018	11/07/2018	11/07/2018	17/07/2018	17/07/2018	17/07/2018	17/07/2018	**Average**	**SD**	09/07/2018	09/07/2018	09/07/2018	09/07/2018
SiO_2	47.69	47.87	45.94	50.43	49.24	49.47	49.04	49.35	**48.58**	**0.82**	74.00	74.38	74.03	74.02
TiO_2	3.00	3.01	3.12	2.74	2.84	2.91	2.79	2.80	**2.92**	**0.08**	0.08	0.09	0.08	0.09
Al_2O_3	14.43	14.13	14.80	14.00	13.95	13.83	14.41	14.24	**14.07**	**0.25**	13.86	13.42	13.85	13.90
FeO	11.62	11.70	11.99	10.35	11.08	10.91	11.16	11.03	**11.41**	**0.38**	1.60	1.55	1.54	1.57
MnO	0.18	0.18	0.19	0.16	0.16	0.17	0.17	0.16	**0.18**	**0.01**	0.06	0.07	0.06	0.06
MgO	7.72	7.65	8.09	7.46	7.48	7.43	7.57	7.63	**7.60**	**0.17**	0.04	0.04	0.04	0.04
CaO	12.36	12.47	12.89	11.98	12.40	12.39	11.96	11.92	**12.13**	**0.34**	0.76	0.96	0.68	0.69
Na_2O	2.32	2.31	2.30	2.28	2.27	2.28	2.28	2.26	**2.37**	**0.07**	4.15	4.13	4.45	4.29
K_2O	0.45	0.45	0.44	0.43	0.43	0.43	0.43	0.43	**0.45**	**0.01**	5.38	5.27	5.24	5.32
P_2O_5	0.23	0.23	0.25	0.17	0.16	0.18	0.19	0.18	**0.28**	**0.12**	0.07	0.10	0.02	0.02
Total	100.00	100.00	100.00	100.00	100.00	100.00	100.00	100.00	**100.00**	**0.00**	100.00	100.00	100.00	100.00
CF	1.62	1.63	1.73	1.63	1.58	1.59	1.53	1.64	**1.54**	**0.12**	**1.47**	**1.59**	**1.66**	**1.60**
(ppm)														
Sc	36.17	34.94	37.95	31.88	33.62	35.01	33.19	33.57	**34.69**	**1.51**	4.61	2.05	1.16	2.88
V	322.81	312.58	326.41	278.85	287.22	300.53	294.30	306.16	**309.57**	**10.79**	1.38	1.26	0.40	0.01
Cr	295.87	313.57	308.12	270.66	267.71	265.89	274.59	260.82	**287.31**	**14.18**	4.77	5.42	-18.97	-21.77
Co	45.37	45.29	45.59	41.62	44.71	41.82	44.29	42.23	**44.75**	**1.34**	0.85	0.56	-1.06	1.57
Ni	104.11	103.93	110.45	119.88	74.75	71.65	93.41	93.18	**104.60**	**10.56**	-5.43	-24.23	-9.09	-11.00
Cu	115.31	113.77	116.56	110.95	111.70	116.44	113.94	109.49	**114.20**	**4.35**	6.27	4.80	4.83	5.81
Zn	101.34	104.10	103.88	105.88	107.60	107.07	105.71	98.63	**104.63**	**4.95**	51.32	52.71	58.61	52.54
Ga	23.35	22.29	21.87	19.70	20.45	17.10	18.25	19.37	**21.16**	**1.42**	20.74	21.43	22.40	20.45
Rb	9.72	9.05	8.64	8.39	9.38	8.36	8.72	8.47	**9.01**	**0.56**	327.71	322.59	334.65	332.37
Sr	390.41	391.11	403.59	362.00	385.50	377.94	378.32	368.23	**384.06**	**14.60**	13.70	16.05	13.81	14.12
Y	25.78	24.75	28.00	26.44	26.04	26.05	26.56	24.00	**25.83**	**1.21**	42.11	46.03	43.24	43.43
Zr	171.78	169.60	179.77	165.23	168.23	164.11	165.31	159.44	**169.98**	**5.86**	188.75	194.42	200.26	187.95
Nb	18.40	19.17	19.01	17.35	17.77	17.86	17.86	16.49	**18.48**	**0.94**	38.35	41.45	42.06	38.04
Ba	135.77	131.90	128.20	119.92	123.89	123.56	126.78	132.09	**130.78**	**6.12**	18.35	19.00	17.22	15.78
La	14.87	14.57	15.73	13.16	14.21	14.48	14.42	14.70	**15.06**	**0.73**	63.40	65.20	68.64	64.93
Ce	39.40	37.52	40.31	35.15	38.77	38.58	36.31	34.69	**37.84**	**1.94**	125.90	127.96	131.78	124.28
Pr	5.18	5.39	5.34	5.66	5.11	4.91	5.20	5.11	**5.27**	**0.32**	13.20	13.13	14.40	12.27
Nd	22.74	23.02	25.07	22.58	25.93	24.25	23.42	21.44	**24.28**	**1.21**	39.68	44.09	45.41	46.05
Sm	6.65	6.24	6.11	5.40	5.25	7.19	6.17	5.02	**6.40**	**0.73**	7.97	8.54	8.98	9.03
Eu	1.79	2.61	1.95	1.95	2.31	2.10	2.26	2.06	**2.14**	**0.20**	0.28	0.08	0.22	0.26
Gd	5.33	6.34	7.78	8.48	6.36	7.38	8.12	6.93	**6.41**	**1.27**	9.07	7.70	7.23	8.57
Tb	1.01	0.70	1.06	0.86	0.91	0.83	0.90	0.83	**0.93**	**0.13**	1.15	1.12	1.29	0.99
Dy	5.06	4.74	5.85	4.91	5.51	4.88	4.77	4.70	**5.20**	**0.58**	6.16	6.97	7.14	6.96
Ho	1.10	0.97	1.08	1.14	0.79	0.83	0.90	0.78	**1.00**	**0.12**	1.47	1.44	1.60	1.45
Er	2.14	2.57	2.88	2.18	2.92	1.77	2.57	3.14	**2.64**	**0.43**	3.59	4.17	5.89	3.84
Tm	0.32	0.40	0.39	0.30	0.39	0.43	0.20	0.28	**0.34**	**0.06**	0.92	0.67	0.61	0.79
Yb	1.38	2.61	1.39	2.53	2.83	1.67	1.75	2.10	**2.00**	**0.36**	4.38	4.68	4.57	5.75
Lu	0.34	0.34	0.41	0.09	0.39	0.42	0.29	0.29	**0.31**	**0.08**	0.70	0.66	0.91	0.66
Hf	3.28	5.26	4.50	5.19	5.16	4.19	3.69	4.27	**4.43**	**0.53**	6.65	6.34	7.59	5.83
Ta	1.21	1.09	1.00	1.04	1.12	0.88	0.90	0.93	**1.14**	**0.14**	2.51	2.66	3.40	2.99
Pb	1.10	1.29	1.71	1.40	1.18	1.32	1.78	1.63	**1.68**	**0.34**	34.63	34.14	37.88	35.27
Th	1.45	1.24	1.42	1.47	1.45	1.06	1.14	1.24	**1.26**	**0.15**	55.16	52.62	55.48	52.25
U	0.36	0.44	0.44	0.46	0.33	0.30	0.40	0.40	**0.42**	**0.06**	16.00	16.31	16.81	16.21

	LIP3_5	LIP3_1	LIP3_2	LIP3_3	LIP3_4	LIP3_5	LIP3_2	LIP3_3	LIP3_4	LIP3_5	LIP3_1	**LIP3**		ATHO_G_1
(%)	09/07/2018	10/07/2018	10/07/2018	10/07/2018	10/07/2018	10/07/2018	11/07/2018	11/07/2018	11/07/2018	11/07/2018	17/07/2018	**Average**	**SD**	09/07/2018
SiO_2	74.10	74.48	74.53	74.97	74.54	74.15	74.95	74.76	74.80	74.61	74.13	**74.43**	**0.34**	75.67
TiO_2	0.08	0.08	0.08	0.08	0.08	0.08	0.08	0.08	0.07	0.08	0.08	**0.08**	**0.00**	0.23
Al_2O_3	13.72	13.44	13.21	13.52	13.63	13.60	13.30	13.22	13.02	13.43	13.86	**13.53**	**0.27**	11.65
FeO	1.70	1.57	1.67	1.51	1.53	1.54	1.29	1.47	1.47	1.51	1.30	**1.52**	**0.11**	3.14
MnO	0.07	0.07	0.07	0.06	0.06	0.06	0.05	0.06	0.06	0.06	0.06	**0.06**	**0.00**	0.10
MgO	0.04	0.04	0.04	0.04	0.04	0.04	0.03	0.04	0.04	0.04	0.03	**0.04**	**0.00**	0.09
CaO	0.74	0.80	0.89	0.35	0.80	0.85	0.78	0.74	0.91	0.85	0.63	**0.76**	**0.15**	1.41
Na_2O	4.25	4.32	4.23	4.14	4.19	4.29	4.17	4.31	4.32	4.21	4.36	**4.25**	**0.09**	4.96
K_2O	5.24	5.19	5.27	5.32	5.12	5.37	5.33	5.30	5.28	5.19	5.53	**5.29**	**0.10**	2.72
P_2O_5	0.06	0.02	0.01	0.01	0.01	0.01	0.02	0.02	0.03	0.02	0.02	**0.03**	**0.03**	0.03
Total	100.00	100.00	100.00	100.00	100.00	100.00	100.00	100.00	100.00	100.00	100.00	**100.00**	**0.00**	100.00
CF	**1.60**	**1.46**	**1.45**	**1.48**	**1.43**	**1.44**	1.49	1.39	1.36	1.40	1.49	**1.49**	**0.09**	3.68
(ppm)														
Sc	2.14	-0.03	1.35	1.75	1.23	1.34	2.35	0.60	2.82	2.33	1.20	**1.85**	**1.11**	5.28
V	0.05	0.22	0.47	-0.23	0.69	0.66	1.31	0.56	0.07	0.57	0.72	**0.54**	**0.49**	3.92
Cr	-4.88	12.47	15.46	-11.89	-10.91	7.45	8.00	7.57	24.32	-8.06	2.31	**0.75**	**13.08**	-11.15
Co	0.82	0.11	-0.01	-0.03	-0.53	-0.48	0.53	1.27	-0.01	0.22	-0.73	**0.21**	**0.74**	2.24
Ni	1.06	6.52	-6.86	1.98	-2.86	-8.03	11.90	-14.07	0.43	-7.38	3.20	**-4.26**	**8.94**	14.65
Cu	4.74	5.22	4.87	3.80	7.07	4.92	5.05	4.39	5.08	4.49	4.80	**5.08**	**0.79**	21.26
Zn	55.68	53.37	53.52	49.13	51.42	51.32	45.94	51.51	49.57	51.24	47.35	**51.68**	**3.11**	120.52
Ga	21.33	21.27	20.92	21.51	19.69	21.34	21.69	19.94	20.27	20.42	21.98	**21.03**	**0.77**	27.01
Rb	325.65	309.61	317.27	316.36	305.72	316.15	306.56	302.99	295.20	301.81	303.51	**314.54**	**12.11**	70.96
Sr	15.27	13.68	13.42	13.89	12.92	13.53	12.68	12.94	13.30	12.56	12.64	**13.63**	**0.97**	83.68
Y	46.70	43.35	43.80	42.13	40.21	45.07	40.79	40.42	39.25	39.81	40.34	**42.45**	**2.32**	99.10
Zr	203.33	184.90	192.26	186.62	181.89	190.45	191.18	173.11	172.44	174.28	180.91	**186.85**	**9.23**	534.19
Nb	40.78	38.04	39.95	37.83	39.14	38.64	38.52	36.59	35.00	34.62	37.57	**38.44**	**2.10**	55.83
Ba	18.92	16.42	16.90	15.74	15.84	15.67	12.52	17.29	15.06	16.64	17.13	**16.57**	**1.63**	486.57
La	62.59	59.79	62.97	62.54	60.11	59.74	54.29	55.33	55.57	55.17	56.38	**60.44**	**4.37**	52.33
Ce	128.10	120.21	122.42	121.26	120.65	120.70	107.98	110.88	109.40	112.25	111.04	**119.65**	**7.60**	114.88
Pr	13.00	12.54	11.72	12.66	11.80	12.30	11.68	11.84	11.12	11.04	11.42	**12.28**	**0.91**	13.08
Nd	44.37	42.01	42.25	41.82	41.67	39.85	35.95	39.68	35.68	36.73	34.64	**40.66**	**3.64**	58.61
Sm	7.88	6.98	8.79	7.54	8.10	9.45	7.79	7.96	7.31	8.85	8.50	**8.25**	**0.70**	15.62
Eu	0.12	-0.03	0.10	0.21	0.26	0.02	0.32	0.16	0.09	0.08	-0.14	**0.14**	**0.13**	2.63
Gd	6.06	6.70	5.71	6.62	6.79	7.13	6.57	6.47	4.93	6.17	6.73	**6.83**	**1.04**	14.24
Tb	1.22	1.05	0.88	1.04	1.12	0.91	1.29	0.81	0.94	0.99	1.10	**1.06**	**0.14**	2.15
Dy	7.79	6.39	6.43	6.66	6.23	7.20	6.75	6.14	6.09	5.80	6.09	**6.59**	**0.54**	18.57
Ho	1.35	1.50	1.64	1.25	1.25	1.46	1.30	1.30	1.40	1.44	1.50	**1.42**	**0.11**	3.81
Er	4.77	3.54	4.06	3.77	4.08	3.88	4.76	4.50	3.51	4.72	4.99	**4.27**	**0.66**	10.38
Tm	0.89	0.68	0.75	0.78	0.67	0.67	0.57	0.69	0.78	0.57	0.64	**0.71**	**0.10**	1.67
Yb	5.28	4.61	4.94	4.66	4.36	4.87	4.11	4.90	4.69	4.69	4.65	**4.74**	**0.39**	10.05
Lu	0.63	0.75	0.84	0.73	0.65	0.83	0.88	0.74	0.80	0.59	0.66	**0.74**	**0.10**	1.48
Hf	7.34	5.82	7.16	6.61	7.13	6.83	8.07	5.50	5.75	5.38	5.46	**6.50**	**0.85**	12.22
Ta	3.05	2.67	2.67	2.69	2.58	2.75	2.71	2.90	2.24	2.64	2.60	**2.74**	**0.27**	4.05
Pb	35.61	33.13	33.06	32.27	30.73	31.88	30.79	32.31	33.19	31.42	32.62	**33.26**	**1.96**	5.27
Th	51.66	52.71	52.87	52.85	51.15	52.80	61.84	54.83	54.47	52.65	54.34	**53.84**	**2.56**	6.54
U	16.11	15.15	15.76	15.64	15.56	16.34	16.63	15.67	14.74	14.88	15.40	**15.81**	**0.61**	2.27

	ATHO_G_2	ATHO_G_3	ATHO_G_4	ATHO_G_5	ATHO_G_1	ATHO_G_2	ATHO_G_3	ATHO_G_4	ATHO_G_5	ATHO_G_1	ATHO_G_2	ATHO_G_3	ATHO_G_4	ATHO_G_5
(%)	09/07/2018	09/07/2018	09/07/2018	09/07/2018	10/07/2018	10/07/2018	10/07/2018	10/07/2018	10/07/2018	11/07/2018	11/07/2018	11/07/2018	11/07/2018	11/07/2018
SiO_2	75.45	75.03	75.46	74.73	74.02	74.34	75.24	74.92	75.11	74.15	74.17	74.86	73.90	73.63
TiO_2	0.24	0.24	0.25	0.26	0.28	0.27	0.26	0.26	0.26	0.27	0.25	0.26	0.27	0.27
Al_2O_3	11.54	12.15	11.84	11.87	12.78	12.49	11.82	12.14	12.06	12.56	12.80	12.24	13.03	12.84
FeO	3.16	3.10	3.24	3.30	3.54	3.43	3.33	3.19	3.23	3.34	3.47	3.30	3.37	3.40
MnO	0.10	0.10	0.10	0.11	0.11	0.11	0.10	0.10	0.10	0.11	0.10	0.11	0.10	0.11
MgO	0.09	0.10	0.09	0.09	0.10	0.10	0.10	0.10	0.10	0.10	0.10	0.10	0.10	0.10
CaO	1.62	1.42	1.19	1.63	1.66	1.67	1.75	1.73	1.59	1.85	1.61	1.71	1.73	1.94
Na_2O	5.03	5.09	5.08	5.17	4.76	4.87	4.71	4.81	4.81	4.93	4.75	4.78	4.76	4.93
K_2O	2.74	2.76	2.71	2.78	2.74	2.70	2.66	2.70	2.69	2.67	2.71	2.59	2.70	2.74
P_2O_5	0.03	0.02	0.03	0.05	0.02	0.02	0.02	0.05	0.05	0.02	0.04	0.05	0.03	0.03
Total	100.00	100.00	100.00	100.00	100.00	100.00	100.00	100.00	100.00	100.00	100.00	100.00	100.00	100.00
CF	3.13	3.35	3.58	3.45	**2.19**	**1.98**	**1.99**	**1.98**	**2.03**	**2.11**	**2.13**	**1.96**	**2.04**	**1.98**
(ppm)														
Sc	5.77	8.91	7.83	8.23	6.07	6.44	10.25	6.39	5.69	8.86	6.44	7.44	7.90	9.34
V	4.12	4.08	4.56	3.89	3.88	5.65	4.81	3.11	4.32	2.87	4.84	2.05	2.24	3.92
Cr	7.49	19.21	16.09	-31.32	23.45	1.47	24.37	-21.92	-16.44	-0.84	-1.37	29.01	13.20	4.16
Co	1.28	1.99	0.49	-0.60	-0.25	0.92	2.01	0.74	1.42	0.42	2.90	2.83	-0.31	0.90
Ni	15.38	5.21	-6.51	7.72	1.66	26.17	14.72	-6.58	7.46	-8.26	-13.06	-7.58	-32.15	-1.94
Cu	18.48	20.10	18.47	21.98	21.96	19.17	19.94	17.51	18.10	17.82	19.63	17.18	19.03	18.40
Zn	128.07	124.91	130.17	132.60	125.69	126.34	118.22	124.99	113.04	117.93	114.80	103.30	108.35	119.48
Ga	24.81	24.62	26.87	25.59	27.07	25.27	25.75	24.13	24.29	26.27	26.68	25.09	25.57	25.77
Rb	66.03	65.17	71.67	67.86	69.42	72.72	67.01	65.25	69.03	65.37	69.08	63.96	64.10	67.55
Sr	84.65	82.85	88.80	89.84	89.30	93.81	93.57	84.22	93.29	88.91	94.15	90.44	91.36	86.96
Y	95.60	96.24	99.96	99.95	104.72	107.02	103.63	96.00	106.13	99.34	105.93	101.03	101.07	105.74
Zr	517.74	504.34	536.64	514.13	528.23	554.34	518.20	514.93	523.62	530.12	534.86	510.64	541.07	533.82
Nb	55.28	56.67	57.94	58.22	63.48	65.74	61.68	57.93	57.27	63.94	61.37	58.83	61.70	62.56
Ba	477.20	488.93	492.17	489.62	537.39	563.43	521.81	506.65	522.25	551.11	541.09	525.83	518.98	563.64
La	48.45	50.49	51.96	54.40	54.80	55.65	53.24	52.05	52.61	53.58	53.23	51.33	54.54	57.69
Ce	110.11	113.90	114.80	112.56	125.78	127.88	123.79	112.14	120.80	125.85	121.44	114.11	120.57	121.33
Pr	14.24	14.87	14.01	13.73	14.26	14.83	13.60	14.21	14.66	14.32	15.20	13.71	14.10	13.97
Nd	56.30	60.86	53.56	61.41	58.90	63.52	54.20	56.29	59.97	60.03	56.05	58.01	55.93	57.04
Sm	13.57	14.53	15.88	13.97	14.78	15.66	16.20	14.75	12.18	15.60	11.99	12.35	13.42	14.68
Eu	2.61	2.98	2.70	2.08	2.79	2.68	2.26	2.45	2.62	2.17	2.27	2.80	1.97	2.75
Gd	11.98	17.01	12.77	14.38	17.17	16.85	13.05	17.66	17.24	16.65	13.54	17.78	17.09	14.03
Tb	2.37	3.15	2.46	2.16	3.12	2.49	3.03	2.45	2.48	2.62	2.45	2.07	2.52	2.68
Dy	15.83	15.16	16.02	18.37	16.86	17.18	16.24	15.71	14.89	16.55	15.06	14.89	16.80	16.31
Ho	3.50	3.08	3.25	3.41	4.09	3.86	3.52	2.96	3.11	3.68	3.30	3.19	3.37	3.94
Er	11.59	10.11	10.74	10.45	11.88	12.60	11.35	10.24	11.03	11.00	10.53	10.67	10.98	9.75
Tm	1.56	1.60	1.57	1.36	1.57	1.66	1.48	1.51	1.22	2.05	1.40	1.31	1.74	1.67
Yb	10.74	12.13	10.56	10.43	11.57	9.89	9.69	9.68	10.56	10.24	10.78	9.55	9.13	11.40
Lu	1.96	1.63	1.91	1.28	1.70	1.56	1.59	1.41	1.72	1.63	1.67	1.60	1.58	1.92
Hf	11.00	14.17	12.99	13.38	13.86	14.21	14.20	14.39	14.40	13.72	13.19	12.95	14.64	15.21
Ta	3.38	4.20	3.26	2.98	4.34	4.26	3.63	3.64	3.62	3.60	4.29	4.08	3.78	3.76
Pb	5.12	4.90	4.47	4.51	5.34	5.07	4.77	4.76	3.99	4.38	5.03	4.91	3.98	4.91
Th	6.39	6.79	7.62	7.30	7.91	8.21	6.13	6.84	6.88	7.51	7.46	7.10	7.08	7.90
U	2.28	2.08	2.44	2.13	2.62	2.49	1.90	1.74	2.28	2.62	2.56	2.45	2.10	1.98

	ATHO_G_1	ATHO_G_2	ATHO_G_3	ATHO_G_4	ATHO_G_5	**ATHO_G**		StHs6_1	StHs6_2	StHs6_3	StHs6_4	StHs6_5	StHs6_1	StHs6_2
(%)	11/07/2018	11/07/2018	11/07/2018	11/07/2018	11/07/2018	**Average**	**SD**	09/07/2018	09/07/2018	09/07/2018	09/07/2018	09/07/2018	10/07/2018	10/07/2018
SiO_2	74.68	74.77	73.91	74.32	74.54	**74.65**	**0.58**	64.63	64.89	63.43	64.16	64.72	64.07	64.41
TiO_2	0.26	0.26	0.26	0.27	0.26	**0.26**	**0.01**	0.67	0.70	0.68	0.68	0.65	0.68	0.69
Al_2O_3	12.37	12.17	12.83	12.10	12.50	**12.29**	**0.43**	16.66	16.62	17.11	17.15	17.00	17.73	17.24
FeO	3.20	3.19	3.26	3.22	3.15	**3.28**	**0.12**	4.35	4.23	4.24	4.26	4.10	4.12	4.14
MnO	0.10	0.10	0.10	0.10	0.10	**0.10**	**0.00**	0.07	0.07	0.07	0.07	0.07	0.07	0.07
MgO	0.10	0.09	0.10	0.10	0.09	**0.10**	**0.00**	1.87	1.84	1.81	1.86	1.82	1.89	1.91
CaO	1.75	1.63	1.95	2.32	1.71	**1.69**	**0.23**	5.21	5.07	6.06	5.10	4.91	4.99	5.29
Na_2O	4.75	5.00	4.81	4.81	4.98	**4.89**	**0.13**	5.26	5.20	5.27	5.37	5.42	5.21	5.01
K_2O	2.62	2.67	2.63	2.59	2.56	**2.68**	**0.06**	1.17	1.23	1.20	1.22	1.20	1.12	1.13
P_2O_5	0.19	0.12	0.15	0.18	0.11	**0.06**	**0.05**	0.11	0.14	0.13	0.13	0.10	0.12	0.10
Total	100.00	100.00	100.00	100.00	100.00	**100.00**	**0.00**	100.00	100.00	100.00	100.00	100.00	100.00	100.00
CF	2.92	2.72	2.53	2.90	2.44	**2.55**	**0.61**	6.46	5.99	5.68	5.42	5.11	**3.46**	**3.32**
(ppm)														
Sc	6.81	7.29	5.67	9.46	7.42	**7.37**	**1.45**	6.76	7.04	9.18	12.22	13.02	6.99	9.31
V	2.65	3.74	5.41	3.43	2.54	**3.80**	**1.00**	76.58	82.97	85.19	81.14	75.08	77.38	76.19
Cr	14.39	-0.70	14.68	-21.08	-6.94	**2.79**	**16.99**	25.52	-10.69	42.91	38.89	8.36	39.46	35.09
Co	2.37	2.88	2.36	1.86	2.60	**1.45**	**1.12**	14.70	11.19	15.01	12.84	13.84	9.81	13.59
Ni	-22.09	-17.53	-26.62	16.45	-17.60	**-2.53**	**16.02**	9.63	1.22	-32.35	-10.57	17.62	4.59	34.68
Cu	18.94	19.44	14.69	16.93	18.96	**18.90**	**1.73**	37.15	44.43	42.33	37.56	37.29	34.01	37.18
Zn	94.89	103.31	102.67	116.18	104.91	**116.52**	**10.65**	63.39	65.97	64.53	60.64	53.04	48.27	55.33
Ga	25.76	23.97	24.46	26.48	24.58	**25.50**	**1.00**	22.80	21.53	21.72	21.65	20.54	19.11	19.18
Rb	62.85	64.17	65.35	65.67	62.95	**66.81**	**2.89**	32.82	32.38	29.89	30.12	30.15	27.07	26.10
Sr	87.58	82.83	86.17	86.80	85.49	**88.24**	**3.72**	450.05	421.72	443.09	428.29	442.30	453.17	436.61
Y	94.45	99.92	101.41	99.24	92.59	**100.45**	**4.15**	9.86	11.46	11.43	11.27	10.71	12.85	9.05
Zr	507.65	512.72	510.41	515.81	513.04	**522.83**	**13.18**	122.54	125.39	126.01	122.44	112.04	121.45	116.24
Nb	57.86	57.97	58.04	57.84	55.49	**59.28**	**3.02**	7.42	6.34	7.84	5.68	7.27	6.59	6.33
Ba	521.72	513.34	507.51	519.34	529.89	**518.92**	**24.73**	284.16	262.41	247.82	262.01	256.95	268.05	264.00
La	52.77	53.34	54.43	52.58	51.72	**53.06**	**1.97**	15.06	11.23	12.03	11.06	10.33	11.35	12.07
Ce	111.47	109.57	114.22	115.75	114.41	**117.27**	**5.64**	27.19	26.23	22.93	24.61	24.19	23.93	22.50
Pr	14.83	14.94	14.45	14.26	13.46	**14.24**	**0.55**	3.88	3.23	2.97	2.69	2.89	2.96	2.46
Nd	57.81	63.59	57.67	62.31	55.20	**58.36**	**2.93**	16.28	11.65	14.80	13.08	11.96	10.37	12.43
Sm	13.18	16.05	15.48	14.53	14.28	**14.43**	**1.31**	5.13	2.59	3.76	2.44	4.44	2.42	5.62
Eu	2.75	2.55	2.59	2.30	2.51	**2.52**	**0.27**	0.92	1.08	0.63	0.88	0.50	1.68	0.37
Gd	17.65	10.60	10.13	11.34	16.72	**14.89**	**2.59**	4.50	3.93	5.52	5.73	1.29	2.12	6.78
Tb	2.91	2.32	2.73	2.87	2.55	**2.58**	**0.31**	0.81	0.81	0.19	0.22	0.22	0.27	0.49
Dy	17.14	16.94	19.10	13.73	13.72	**16.25**	**1.46**	2.67	1.95	1.52	2.31	2.01	1.84	2.76
Ho	3.60	3.69	3.81	3.97	3.68	**3.54**	**0.33**	-0.04	0.67	0.28	0.32	0.37	0.45	0.27
Er	12.51	12.43	10.99	10.22	10.87	**11.02**	**0.82**	0.97	0.28	1.22	0.05	1.28	1.49	1.18
Tm	1.74	1.62	1.79	1.59	1.33	**1.57**	**0.19**	0.17	0.26	0.13	0.11	0.21	-0.02	0.39
Yb	11.56	10.77	9.22	9.96	9.56	**10.37**	**0.83**	1.80	2.58	1.19	1.29	1.16	1.67	0.31
Lu	1.56	1.48	1.56	1.69	1.77	**1.64**	**0.17**	0.31	0.15	0.12	0.08	-0.08	0.05	0.29
Hf	14.03	13.98	17.46	12.80	14.31	**13.86**	**1.27**	2.62	2.96	2.76	3.05	1.85	3.11	4.68
Ta	4.12	3.78	4.02	3.69	3.64	**3.81**	**0.36**	0.19	0.17	0.32	0.34	0.25	0.32	0.63
Pb	4.18	5.27	5.25	4.49	4.16	**4.74**	**0.44**	12.08	11.44	11.31	7.90	9.81	10.90	7.93
Th	7.49	8.14	8.33	7.81	7.31	**7.34**	**0.62**	2.17	2.05	2.49	2.34	2.16	2.39	2.31
U	2.34	2.44	2.12	2.25	2.12	**2.26**	**0.24**	0.76	0.96	0.99	0.90	1.08	1.27	0.91

	StHs6_3	StHs6_4	StHs6_5	StHs6_1	StHs6_2	StHs6_3	StHs6_4	StHs6_5	StHs6_1	StHs6_2	StHs6_3	StHs6_4	StHs6_5	**StHs6_5**	
(%)	10/07/2018	10/07/2018	10/07/2018	11/07/2018	11/07/2018	11/07/2018	11/07/2018	11/07/2018	17/07/2018	17/07/2018	17/07/2018	17/07/2018	17/07/2018	**Average**	**SD**
SiO_2	63.21	63.83	63.51	63.57	62.31	62.82	62.27	62.03	62.54	62.45	62.84	62.80	61.88	**63.32**	**0.94**
TiO_2	0.67	0.69	0.72	0.75	0.75	0.75	0.78	0.75	0.74	0.73	0.71	0.70	0.72	**0.71**	**0.03**
Al_2O_3	18.12	17.37	18.12	17.70	18.63	18.24	18.47	18.81	18.65	18.50	18.10	18.49	18.76	**17.87**	**0.72**
FeO	4.24	4.20	4.23	4.21	4.48	4.35	4.26	4.48	4.26	4.39	4.20	4.25	4.35	**4.27**	**0.10**
MnO	0.07	0.07	0.07	0.07	0.08	0.08	0.07	0.08	0.07	0.07	0.07	0.07	0.07	**0.07**	**0.00**
MgO	2.00	1.98	2.00	1.95	2.02	2.07	2.04	2.08	1.99	2.06	1.96	2.06	1.98	**1.96**	**0.09**
CaO	5.35	5.25	5.14	5.25	5.14	5.45	5.68	5.33	4.95	5.14	5.39	5.12	5.43	**5.26**	**0.26**
Na_2O	5.07	5.35	4.94	5.19	5.21	4.90	5.15	5.16	5.18	5.12	5.16	5.03	5.20	**5.17**	**0.13**
K_2O	1.15	1.15	1.15	1.19	1.21	1.21	1.17	1.18	1.19	1.14	1.17	1.12	1.16	**1.17**	**0.03**
P_2O_5	0.12	0.11	0.12	0.13	0.17	0.13	0.12	0.10	0.42	0.41	0.39	0.36	0.44	**0.19**	**0.13**
Total	100.00	100.00	100.00	100.00	100.00	100.00	100.00	100.00	100.00	100.00	100.00	100.00	100.00	**100.00**	**0.00**
CF	**3.35**	**3.25**	**3.04**	**4.25**	**4.44**	**4.35**	**3.96**	**3.98**	2.98	2.95	2.85	2.93	3.01	**4.04**	**1.14**
(ppm)															
Sc	15.97	12.79	12.76	14.28	9.12	9.41	10.63	5.77	9.36	11.00	10.03	8.51	9.14	**10.16**	**2.68**
V	77.23	78.91	80.52	74.54	86.61	83.46	76.36	77.03	81.44	83.24	81.17	76.58	76.43	**79.40**	**3.57**
Cr	52.56	9.18	-6.90	15.84	-1.88	2.00	42.05	-7.69	-11.30	26.34	44.20	-22.98	23.36	**17.21**	**22.80**
Co	12.48	14.31	10.64	11.68	10.06	11.70	11.15	11.12	11.04	12.24	12.96	11.02	11.22	**12.13**	**1.53**
Ni	1.65	7.50	3.32	33.76	-30.95	-11.05	31.87	21.74	-19.09	-19.07	26.84	4.20	-26.43	**2.45**	**21.29**
Cu	37.76	37.79	38.11	34.64	33.23	37.63	33.61	33.50	35.73	40.61	35.39	37.63	36.00	**37.08**	**2.88**
Zn	56.15	58.89	48.59	46.07	59.61	-35.86	59.69	56.09	52.64	56.25	64.26	55.34	54.11	**52.15**	**21.44**
Ga	22.39	20.46	18.78	18.52	19.33	19.39	19.97	21.06	20.30	19.36	18.80	20.70	19.02	**20.23**	**1.29**
Rb	31.35	26.97	27.64	31.11	28.57	29.91	29.48	28.86	30.06	29.22	28.24	27.25	27.49	**29.23**	**1.85**
Sr	456.28	430.82	461.78	477.03	486.08	464.31	479.20	479.31	475.41	482.97	455.54	453.11	465.41	**457.12**	**19.27**
Y	11.62	12.40	14.42	10.65	15.29	11.43	13.81	16.10	11.83	13.56	14.46	11.25	12.49	**12.30**	**1.83**
Zr	124.86	119.14	122.77	118.40	133.50	131.96	126.49	126.93	116.48	121.69	125.13	126.43	126.49	**123.32**	**5.19**
Nb	6.35	6.45	6.26	6.44	7.27	6.55	7.17	6.25	6.05	6.58	5.92	6.08	7.15	**6.60**	**0.57**
Ba	274.10	273.93	276.70	279.16	298.37	279.63	286.59	301.43	290.39	278.08	287.38	292.94	303.76	**278.39**	**15.19**
La	10.65	10.43	10.80	12.80	13.47	11.81	11.72	12.03	12.14	11.42	13.25	11.88	12.33	**11.89**	**1.14**
Ce	24.14	24.62	24.96	26.03	23.81	25.88	27.38	26.48	27.50	27.15	25.69	23.45	25.88	**25.23**	**1.53**
Pr	2.96	2.89	3.10	3.27	3.39	2.81	3.43	3.69	3.29	3.40	2.83	2.69	2.92	**3.09**	**0.36**
Nd	13.80	10.96	13.55	9.57	14.26	13.69	12.54	11.41	13.92	14.03	12.67	15.33	11.88	**12.91**	**1.69**
Sm	3.20	2.14	4.10	2.86	1.73	1.38	2.56	3.41	1.99	2.66	2.45	2.67	3.29	**3.04**	**1.10**
Eu	0.43	0.81	1.55	1.02	1.67	1.04	1.01	0.78	1.09	0.36	0.83	0.99	1.13	**0.94**	**0.39**
Gd	0.28	6.78	4.77	5.88	2.52	4.62	-0.31	6.54	-0.12	5.00	2.40	5.13	5.42	**3.94**	**2.31**
Tb	0.59	0.51	0.22	0.86	0.15	0.94	0.09	0.49	0.24	0.13	0.48	0.11	0.25	**0.40**	**0.27**
Dy	2.76	3.70	0.83	2.63	4.16	3.96	2.44	0.98	2.14	2.31	2.23	2.56	1.74	**2.38**	**0.86**
Ho	0.06	0.46	0.31	0.45	0.41	0.67	0.87	0.71	0.33	0.59	0.27	0.64	0.33	**0.42**	**0.22**
Er	2.49	1.29	1.33	0.31	1.48	0.99	1.02	1.26	2.00	1.10	1.14	0.50	1.00	**1.12**	**0.56**
Tm	0.30	0.28	0.17	-0.03	-0.04	0.11	0.08	0.20	0.21	0.22	0.10	0.08	0.23	**0.16**	**0.11**
Yb	1.24	1.20	2.36	1.06	1.65	1.78	1.96	1.61	1.39	1.01	1.59	1.60	0.51	**1.45**	**0.54**
Lu	0.35	0.11	0.11	0.06	0.24	0.17	0.04	0.36	0.24	0.05	0.10	0.17	0.16	**0.15**	**0.11**
Hf	2.66	2.73	2.69	3.15	3.51	2.53	4.20	2.62	3.19	2.84	3.03	2.37	2.47	**2.95**	**0.62**
Ta	0.14	0.44	0.65	0.50	0.43	0.38	0.65	0.49	0.54	0.23	0.33	0.23	0.54	**0.39**	**0.16**
Pb	10.65	11.38	10.19	10.38	11.83	9.67	10.11	9.53	9.82	10.43	10.05	10.54	11.41	**10.37**	**1.12**
Th	1.93	2.30	2.30	2.17	2.30	2.59	2.31	2.66	2.96	2.87	2.36	2.15	2.37	**2.36**	**0.25**
U	1.11	1.02	0.89	0.86	1.06	0.91	1.12	0.98	0.98	1.34	1.08	0.96	0.82	**1.00**	**0.14**